

2013

A Study of the Temporal and Spatial Distribution of Ichthyoplankton and Post-larval Penaeids Recruiting into a Louisiana Tidal Pass

Matthew John Kupchik

Louisiana State University and Agricultural and Mechanical College

Follow this and additional works at: https://digitalcommons.lsu.edu/gradschool_dissertations



Part of the [Oceanography and Atmospheric Sciences and Meteorology Commons](#)

Recommended Citation

Kupchik, Matthew John, "A Study of the Temporal and Spatial Distribution of Ichthyoplankton and Post-larval Penaeids Recruiting into a Louisiana Tidal Pass" (2013). *LSU Doctoral Dissertations*. 1604.
https://digitalcommons.lsu.edu/gradschool_dissertations/1604

This Dissertation is brought to you for free and open access by the Graduate School at LSU Digital Commons. It has been accepted for inclusion in LSU Doctoral Dissertations by an authorized graduate school editor of LSU Digital Commons. For more information, please contact gradetd@lsu.edu.

A STUDY OF THE TEMPORAL AND SPATIAL DISTRIBUTION OF
ICHTHYOPLANKTON AND POST-LARVAL PENAEIDS RECRUITING INTO
A LOUISIANA TIDAL PASS

A Dissertation

Submitted to the Graduate Faculty of the
Louisiana State University and
Agricultural and Mechanical College
in partial fulfillment of the
requirements for the degree of
Doctor of Philosophy

in

The Department of Oceanography and Coastal Sciences

by
Matthew John Kupchik
B.S., Richard Stockton College of New Jersey, 2004
May 2014

In Dedication to Dennis Kupchik;
a father, a friend, and a mentor.
1948-2008

ACKNOWLEDGEMENTS

The majority of this study was funded through a grant with the Northern Gulf Institute (NGI). Data and funding support for the first chapter of this dissertation, “Vertical Distribution of Ichthyoplankton and Commercially-Important Decapods in the Northcentral Gulf of Mexico”, was made possible from the Louisiana Department and Wildlife and Fisheries and the Conoco-Phillips Health and Environmental Management Division, respectively. I would first like to thank Dr. Richard F. Shaw who as my advisor shared his expertise, patience, and knowledge. I would also like to thank Dr. Redwood Nero, Dr. Chunyan Li, and Dr. Brian Marx for the invaluable help in their respective expertise of fisheries oceanography, physical oceanography, and statistics through the course of this study. In addition, I would like to thank Ms. Talat Farooqi for her expertise and knowledge in ichthyoplankton identification, Mr. Alvaro Armas for his help both in the field and in the lab during this study, and Mr. Wilton Delaune for his field help at the Fourchon Camp of the Louisiana University’s Marine Consortium. Thanks to Dr. Benfield, Dr. Lindau, Dr. Huang, and Dr. LaRock for their mentorship and expression of the joy of teaching while working as their assistant. Thanks also to Dr. Sutor for the discussions and insights on oceanography, and life in general. A special thanks to the many student workers who helped during this study, in particular, Mrs. Kate Lingoni, Dr. Weenan Wong, and Dr. Xi Chen. To my friend, Dr. Carey Gelpi, thanks for all the conversations on science and words of encouragement along the way. Emmy Hicks, you’re amazing! Finally, I would like to thank my mother, Lynn Kupchik, and my two brothers, Chris Kupchik and Andrew Kupchik Esq., for the love, support, and encouragement in my passion for oceanography and life.

TABLE OF CONTENTS

ACKNOWLEDGMENTS.....	iii
ABSTRACT.....	.xxvii
CHAPTER 1. GENERAL INTRODUCTION.....	1
1.1 General Study Background.....	1
1.2 Literature Cited.....	7
CHAPTER 2. VERTICAL DISTRIBUTION OF ICHTHYOPLANKTON AND COMMERCIALY-IMPORTANT DECAPODS IN THE NORTH- CENTRAL GULF OF MEXICO.....	13
2.1 Introduction.....	13
2.2 Materials and Methods.....	15
2.3 Results.....	21
2.3.1 Ichthyoplankton.....	21
2.3.2 Surface Oriented.....	22
2.3.3 Upper Water Column Orientation.....	55
2.3.4 Mid-Depth Oriented.....	57
2.3.5 Lower Water Column Orientation.....	58
2.3.6 Near-Bottom Oriented.....	58
2.3.7 Oblique Distribution.....	59
2.3.8 Commercially-Important Decapod Crustaceans.....	59
2.3.9 Day/Night Ratios.....	60
2.4 Discussion.....	61
2.5 Conclusions.....	63
2.6 Literature Cited.....	64
CHAPTER 3. EFFECT OF WINTER ATMOSPHERIC COLD FRONT PASSAGES ON DENSITIES OF ICHTHYOPLANKTON AND POST- LARVAL PENAEIDS IN A LOUISIANA TIDAL PASS.....	70
3.1 Introduction.....	70
3.2 Materials and Methods.....	77
3.2.1 Sampling Location.....	77
3.2.2 Field Sampling Methodology.....	77
3.2.3 Laboratory Methods.....	80
3.2.4 Statistical Analysis.....	80
3.3 Results.....	85
3.3.1 Hydrology.....	85
3.3.2 General Zoo-/Ichthyoplankton.....	100
3.3.3 <i>Brevoortia patronus</i> (gulf menhaden).....	102

3.3.4	<i>Micropogonias undulatus</i> (Atlantic croaker).....	117
3.3.5	<i>Anchoa hepsetus</i> (broad-striped anchovy).....	121
3.3.6	<i>Anchoa mitchilli</i> (bay anchovy).....	125
3.3.7	<i>Farfantepenaeus aztecus</i> (brown shrimp).....	129
3.3.8	<i>Pogonias cromis</i> (black drum).....	134
3.3.9	<i>Sciaenops ocellatus</i> (red drum).....	139
3.3.10	<i>Cynoscion arenarius</i> (sand seatrout).....	143
3.3.11	<i>Cynoscion nebulosus</i> (spotted seatrout).....	147
3.3.12	<i>Paralichthys lethostigma</i> (southern flounder).....	151
3.4	Discussion.....	151
3.4.1	Hydrography.....	151
3.4.2	General Zoo-/Ichthyoplankton.....	153
3.4.3	Species with High Atmospheric Forcing.....	154
3.4.4	Species with Moderate Atmospheric Forcing.....	157
3.4.5	Low Atmospheric Forcing – Inner Continental Shelf Spawners.....	159
3.4.6	Low Atmospheric Forcing – Shallow Water Spawners.....	161
3.4.7	Low Atmospheric Forcing – <i>Anchoa</i> Congenerics.....	161
3.4.8	Low Atmospheric Forcing – The Other Sciaenid.....	162
3.5	Conclusions.....	163
3.6	Literature Cited.....	167

CHAPTER 4. AGE, GROWTH, AND RECRUITMENT FROM OTOLITH

MICROSTRUCTURE FOR LARVAL <i>MICROPOGONIAS UNDULATUS</i>	181
4.1 Introduction.....	181
4.2 Materials and Methods.....	185
4.2.1 Sampling Location.....	185
4.2.2 Field Sampling Methodology.....	185
4.2.3 Laboratory Methodology.....	188
4.2.4 Otolith Removal, Preparation, and Interpretation.....	189
4.2.5 Otolith Ageing and Larval Hatch Dates.....	191
4.2.6 Growth and Estuarine Ingress.....	192
4.2.7 Statistical Analysis.....	194
4.3 Results.....	194
4.3.1 Hydrographic.....	194
4.3.2 Larval <i>Micropogonias undulatus</i> Catches.....	197
4.3.3 Length, Age, and Hatch Dates from Otolith Counts.....	199
4.3.4 Modeled Growth Rates and Estuarine Ingress Dates.....	202
4.3.5 Statistical Analysis.....	208
4.4 Discussion.....	211
4.5 Conclusions.....	215
4.6 Literature Cited.....	217

CHAPTER 5. AGE, GROWTH, AND RECRUITMENT FROM OTOLITH MICROSTRUCTURE FOR LARVAL <i>BREVOORTIA PATRONUS</i>	226
5.1 Introduction.....	226
5.2 Materials and Methods.....	229
5.2.1 Sampling Location.....	229
5.2.2 Field Sampling Methodology.....	230
5.2.3 Laboratory Methodology.....	232
5.2.4 Otolith Removal, Preparation, and Interpretation.....	233
5.2.5 Otolith Ageing and Spawning Dates.....	235
5.2.6 Growth Rates.....	236
5.3 Results.....	238
5.3.1 Hydrographic.....	238
5.3.2 Larval <i>Brevoortia patronus</i> Catches.....	240
5.3.3 Length, Age, and Spawning Dates.....	240
5.3.4 Modeled <i>Brevoortia patronus</i> Growth Rates.....	244
5.4 Discussion.....	250
5.5 Conclusions.....	254
5.6 Literature Cited.....	256

CHAPTER 6. LATERAL DIFFERENCES IN LARVAL DENSITY AND PROBABILITY OF ENCOUNTER USING A ZERO INFLATED NEGATIVE BINOMIAL MODEL WITHIN A VERTICALLY WELL- MIXED TIDAL PASS.....	264
6.1 Introduction.....	264
6.2 Materials and Methods.....	268
6.2.1 Sampling Location.....	268
6.2.2 Field Sampling Methodology.....	269
6.2.3 Laboratory Methods.....	272
6.2.4 Statistical Analysis.....	272
6.3 Results.....	274
6.3.1 General Hydrodynamics.....	274
6.3.2 Cross Channel Hydrodynamics – Northern Dock Edge.....	277
6.3.3 Cross Channel Hydrodynamics – Center Channel.....	278
6.3.4 Cross Channel Hydrodynamics – Southern Shore Edge.....	278
6.3.5 General Ichthyoplankton.....	279
6.3.6 <i>Anchoa hepsetus</i> (broad-striped anchovy).....	281
6.3.7 <i>Anchoa mitchilli</i> (bay anchovy).....	286
6.3.8 <i>Brevoortia patronus</i> (gulf menhaden).....	293
6.3.9 <i>Sciaenops ocellatus</i> (red drum).....	296
6.3.10 <i>Cynoscion arenarius</i> (sand seatrout).....	298
6.3.11 <i>Cynoscion nebulosus</i> (spotted seatrout).....	300
6.4 Discussion.....	302
6.4.1 Hydrography.....	302

6.4.2	<i>Anchoa</i> Congenerics.....	303
6.4.3	Other Species.....	305
6.5	Conclusions.....	307
6.6	Literature Cited.....	309
CHAPTER 7. GENERAL SUMMARY AND CONCLUSIONS.....		318
APPENDIX A: ATMOSPHERIC AND TIDAL CHARTS.....		324
APPENDIX B: WEATHER MAPS FOR COLD FRONTS.....		332
APPENDIX C: DERIVATION THE ZERO INFLATED NEGATIVE.....		351
BINOMIAL		
VITA.....		353

LIST OF TABLES

1. Table 2.1:	Louisiana Offshore Oil Platform (LOOP) sampling stations which met our depth criteria of approximately 8 m depth or greater, their latitudes and longitudes, and mean water column depth in meters. Through the course of the study (1978-1995), a number of these sampling sites were regrouped and/or combined into different sampling station numbers.....	17
2. Table 2.2:	Ichthyoplankton and economically-important decapod crustacean taxa which showed statistical differences between multiple depths in the analysis. Mean densities are given as individuals per 100 cubic meters of water filtered. Probabilities are from the Mixed ANOVA model, and were calculated for fish taxa and for decapods using Fisher's Least Significant Difference with a Bonferroni adjustment. Underlined depths indicate greater statistical densities. Surf = surface tows (0.5 and 1-m ring nets and surface 60-cm bongo net tows) ; Mid = mid-water bongo tows ; NB = near-bottom bongo tows ; UO = upper half water column oblique tow ; LO = lower half water column oblique tow ; VS or v= versus.....	23
3. Table 2.3:	All taxa with corresponding mean density (number of individuals per 100 cubic meters of water filtered), standard error, number of collections, and months analyzed. (Code: A=Taxa sampled throughout the water column that showed no statistical preference; B=Taxa which were sampled exclusively at the surface; C=Taxa which were sampled throughout the upper half water column; D=Taxa which were sampled exclusively in the mid-water; E=Taxa which were sampled exclusively near-bottom; F=Taxa sampled throughout the lower half water column; G=Some statistical difference; OM=Overall mean density for all depths; Surf=Discrete surface; Mid=Discrete mid-water; NB=Discrete near-bottom; UO=Upper half water column oblique; and LO=Lower half water column oblique).....	37
4. Table 2.4:	Day/night density ratios for ichthyoplankton and commercially-important decapods from all types of surface collections, and the near-bottom bongo net collections.....	61
5. Table 3.1:	Mean densities (indiv./15m ³ of water filtered) and standard deviations (S.D.) for all sampling efforts during each month for both years combined. Statistics for each species are provided, as well	

	as a total for each factor per species. Months where no larvae were collected under that designation are represented by an "x".....	103
6. Table 3.2:	Data and statistical results for Wilcoxon-Mann-Whitney (WMW) Rank Sum test for differences between ebb and flood tidal stages, and daytime and nocturnal sampling efforts. Mean and median densities are calculated per 15 cubic meters of water for all species. All metrics are based on the zero-truncated data set, and accounted for ties, for analysis under the assumptions of WMW. "*" Represents a statistically significant comparison ($\alpha=0.05$) with that group's density being the greater of the two.....	107
7. Table 3.3:	Mean densities (indiv./15m ³ of water filtered) and standard deviations (S.D.) for all sampling efforts during each month for both years combined. Statistics for each species are provided, as well as a total for each interaction per species. Months where no larvae were collected under that designation are represented by an "x".....	109
8. Table 3.4:	Data and statistical results for Kruskal-Wallis (KW) Rank Sum Test for differences between densities sampled during the interactions of tidal stage and circadian sampling efforts for both years combined. Mean and median densities are calculated per 15 cubic meters of water filtered. All metrics are based on the zero-truncated data set and accounting for ties to meet the assumptions of KW. Similarities and differences between each of the four groupings are presented as subscripted letters. The same letter shows similarity between those groups for each species. Different letters "A,B,C,D" represent statistically significant differences ($\alpha=0.05$) between groups.....	112
9. Table 3.5:	Model terms and associated significance levels for each species included for analysis. Terms in the models that were significant at $p \leq 0.05$ are in bold. Terms that upon stepwise model simplification were no longer necessary in the model are represented by an x. Those model terms that were able to have specification upon tidal stage have the significance values for each tidal stage, and the removed combined term is represented by a "~".....	114
10. Table 4.1:	Hatch dates for larval <i>M. undulatus</i> based on back-calculated otolith ages and collection dates after application of length frequency keys. Percentages and cumulative percentages are based on half month intervals.....	202

11. Table 4.2: Average growth rates and instantaneous growth rates for larval <i>M. undulatus</i> based on otolith data grouped by age blocks of ten days post hatch. Growth rates (g) and instantaneous growth rates (G) are provided for the October 2006 to March 2007 sampling period, the September 2007 to March 2008 sampling period, and the overall combined data.....	208
12. Table 5.1: Spawning dates for larval <i>B. patronus</i> based on back calculated otolith ages and collection dates after application of length frequency keys. Percentages and cumulative percentages are based on half month intervals.....	244
13. Table 5.2: Average growth rates and instantaneous growth rates for larval <i>B. patronus</i> based on otolith data, grouped by age blocks of ten days post spawning. Growth rates (g) and instantaneous growth rates (G) are provided for the October 2006 to March 2007 sampling period, the September 2007 to March 2008 sampling period, and the overall combined data.....	250
14. Table 6.1: Model terms and associated significance levels for general ichthyoplankton and each species included for the Zero Inflated Negative Binomial Model (ZINB). For all models, terms for both the logistic zero model (ZM) and the negative binomial model (NBM) are provided with the appropriate significance levels. Terms in the models that were significant at $p \leq 0.05$ (Chi-Square) are in bold. Terms that upon stepwise model building were no not significant in decreasing AIC, and subsequently excluded from the model, are represented by an x.....	283
15. Table 6.2: Larval fish mean densities (LD), probability of encounter (PE), and mean standard length (SL) for all species included in the analysis based on location across the tidal pass and by positive and negative net water transports. LD are provided as a mean and standard deviation in parenthesis, PE is presented as the percent chance of encounter, and SL are presented as the mean and standard deviation in parenthesis. Overall LD, PE, and SL are provided for each species across all locations for either all positive transports or all negative transports.....	287

LIST OF FIGURES

1. Figure 2.1:	Map of the study area and Louisiana Offshore Oil Platform (LOOP) sampling locations in coastal Louisiana, USA. Insert A is in the vicinity of the LOOP brine diffuser site (station 36) where more intensive sampling took place (scale=1:51,000; modified after Hanifen 1987; Figure 1.3). Zooplankton and ichthyoplankton sampling took place at a number of sampling sites, which through the course of the study (1978-1995) were regrouped and/or combined into different station numbers, so not all station numbers are represented on the maps, but all sampling sites are represented (See Table 2.1).....	20
2. Figure 3.1:	Map of the study location in relation to the Gulf of Mexico and coastal Louisiana. The points in black represent the sampling location, with the final panel being the sampling location from an aerial photograph of Bayou Tartellan. The X in the last panel marks the location of an extended dock used as a sampling platform and later destroyed by Hurricane Gustav.....	76
3. Figure 3.2:	Water temperature variations by month across the two years of field sampling, year 1 (red) and year 2(blue). Both years show a similar trend of decreased temperature from November through February, although 2008 shows the colder water lasting into March. The temperatures in 2006 and early 2007 were overall lower than late 2007 and 2008. In general, there was a higher degree of variability during the months with the coldest water temperatures.....	86
4. Figure 3.3:	Salinity variation by month across the two years of field sampling. There was more consistency across sampling efforts during year 1 (red) than year 2 (blue). The highest variability in salinities occurred from November through March for both years. April 2008 sampling efforts encountered extremely low salinities compared to all other efforts.....	87
5. Figure 3.4:	Boxplots comparing the dissolved oxygen concentration during sampling, based on sample depth and time of sample collection. Non-overlapping notches between any two boxplots represent “strong evidence” of statistically different median values (Chambers et al. 1983). Different colors represent statistically different (WMW) groups.....	89

6. Figure 3.5:	Expected and measured tidal height during September 2007 at the Port of Fourchon. The black sinusoidal line represents the expected tidal height. The light gray line represents the actual measured tidal height. The lower portion of the graph represents the difference between expected and measured (i.e., Expected - Measured). Sampling efforts are represented as the colored sections, where blue is the expected tidal height during sampling, red is the measured tidal height during sampling, and green is the difference of the two during sampling efforts. The black outlined rectangle represents passage of the atmospheric frontal events, but not duration.....	91
7. Figure 3.6:	Expected and measured tidal height during October 2006 and 2007 at the Port of Fourchon. The black sinusoidal line represents the expected tidal height. The light gray line represents the actual measured tidal height. The lower portion of the graph represents the difference between expected and measured (i.e., Expected - Measured). Sampling efforts are represented as the colored sections, where blue is the expected tidal height during sampling, red is the measured tidal height during sampling, and green is the difference of the two during sampling efforts. The black outlined rectangle represents the passage of atmospheric frontal events, but not duration.....	92
8. Figure 3.7:	Expected and measured tidal height during November 2006 and 2007 at the Port of Fourchon. The black sinusoidal line represents the expected tidal height. The light gray line represents the actual measured tidal height. The lower portion of the graph represents the difference between expected and measured (i.e., Expected - Measured). Sampling efforts are represented as the colored sections, where blue is the expected tidal height during sampling, red is the measured tidal height during sampling, and green is the difference of the two during sampling efforts. The black outlined rectangle represents the passage of atmospheric frontal events, but not duration.....	93
9. Figure 3.8:	Expected and measured tidal height during December 2006 and 2007 at the Port of Fourchon. The black sinusoidal line represents the expected tidal height. The light gray line represents the actual measured tidal height. The lower portion of the graph represents the difference between expected and measured (i.e., Expected - Measured). Sampling efforts are represented as the colored sections, where blue is the expected tidal height during sampling, red is the measured tidal height during sampling, and green is the difference of the two during sampling efforts. The black outlined rectangle represents passage of the atmospheric frontal events, but not duration.....	94

10. Figure 3.9: Expected and measured tidal height during January 2007 and 2008 at the Port of Fourchon. The black sinusoidal line represents the expected tidal height. The light gray line represents the actual measured tidal height. The lower portion of the graph represents the difference between expected and measured (i.e., Expected - Measured). Sampling efforts are represented as the colored sections, where blue is the expected tidal height during sampling, red is the measured tidal height during sampling, and green is the difference of the two during sampling efforts. The black outlined rectangle represents passage of the atmospheric events, but not duration..... 95
11. Figure 3.10: Expected and measured tidal height during February 2007 and 2008 at the Port of Fourchon. The black sinusoidal line represents the expected tidal height. The light gray line represents the actual measured tidal height. The lower portion of the graph represents the difference between expected and measured (i.e., Expected - Measured). Sampling efforts are represented as the colored sections, where blue is the expected tidal height during sampling, red is the measured tidal height during sampling, and green is the difference of the two during sampling efforts. The black outlined rectangle represents passage of the atmospheric frontal events, but not duration..... 96
12. Figure 3.11: Expected and measured tidal height during March 2007 and 2008 at the Port of Fourchon. The black sinusoidal line represents the expected tidal height. The light gray line represents the actual measured tidal height. The lower portion of the graph represents the difference between expected and measured (i.e., Expected - Measured). Sampling efforts are represented as the colored sections, where blue is the expected tidal height during sampling, red is the measured tidal height during sampling, and green is the difference of the two during sampling efforts. The black outlined rectangle represents passage of the atmospheric frontal events, but not duration..... 97
13. Figure 3.12: Expected and measured tidal height during April 2007 and 2008 at the Port of Fourchon. The black sinusoidal line represents the expected tidal height. The light gray line represents the actual measured tidal height. The lower portion of the graph represents the difference between expected and measured (i.e., Expected - Measured). Sampling efforts are represented as the colored sections, where blue is the expected tidal height during sampling, red is the measured tidal height during sampling, and green is the difference of the two during sampling efforts. The black outlined rectangle represents passage of the atmospheric frontal events, but not duration..... 98

14. Figure 3.13: Relationship between tidal prism, salinity, and water temperature during the interim or pre-frontal, passage of the front, and post-frontal phases of atmospheric cold front passage. The two vertical black lines bracket the passage of the actual front, with the time period beforehand representing the pre-frontal phase and the period after passage being the post-frontal phase. Trend lines are non-parametrically smoothed curves relating the parameter through time..... 99
15. Figure 3.14: Months where species of interest were encountered during sampling efforts. GAM models were truncated to exclude samples with no expectation of encountering a particular species..... 100
16. Figure 3.15: Comparison of densities by depth (Surface, N.Bottom) and time of day (Day, Night). The nocturnal samples had significantly more large outlying values, and greater variation, than those collected during the day. Despite these differences there were no statistically significant differences between the groups. Non-overlapping notches in the boxplot represent “strong evidence” of statistically different median values (Chambers et al. 1983)..... 101
17. Figure 3.16: Boxplots comparing the total density of larvae within a combination of depth (Surface, N.Bottom), time (Day, Night) and tidal stage (Ebb, Flood). Non-overlapping notches between any two boxplots represent “strong evidence” of statistically different median values (Chambers et al. 1983). Different colors represent statistically different groups (WMW), where secondary colors (i.e., green) represent similarities to both primary colored groups (i.e., yellow and blue). Densities are plotted on a log scale. Despite higher numbers of outlying larger values on ebb tides, flood tides have significantly greater densities..... 102
18. Figure 3.17: Density of *Brevoortia patronus* larvae as a function of tidal stage. Non-overlapping notches in the boxplots represent “strong evidence” of statistically different median values (Chambers et al. 1983). Different colors represent statistically different groups (WMW)..... 108
19. Figure 3.18: Density of *Brevoortia patronus* larvae as a function of tidal stage and time of day. There is a significant difference between those samples collected during flood and ebb tides; however, no difference is discernible in time of day. Non-overlapping notches in the boxplots represent “strong evidence” of statistically different median values (Chambers et al. 1983), which represents the equivalent of a “visual”

WMW. Different primary colors (yellow and blue) represent statistically different groups, while secondary colors (green) show similarities to both primary groups under Kruskal-Wallis test.....	113
20. Figure 3.19: Model fit for the 1-dimensional terms of the GAM model for larval <i>Brevoortia patronus</i> . Shaded areas represent 95% confidence intervals around the model fit represented by the black line. Tick marks on the x-axes represent actual observations. Only positive effects on density are shown to better illustrate the individual effects of model terms.	115
21. Figure 3.20: Larval <i>Brevoortia patronus</i> completed model and effect on density plotted as a contour map. Expected values are based on the complete model fit. Estimated density isolines as a function of barometric pressure and wind direction are shown in color. Areas where no plot is shown represent expected numbers of larvae within the tidal pass to be zero. The interaction is plotted individually for flood and ebb tidal stages. Histograms above contour plots represent frequency of wind directions during sampling.....	116
22. Figure 3.21: Density as a function of tidal stage for larval <i>Micropogonias undulatus</i> . Flood tides had a significantly higher median value than ebb tides. Ebb tides, however, had more large outliers. Non-overlapping notches in the boxplot represent “strong evidence” of statistically different median values (Chambers et al. 1983). Different colors represent statistically different groups (WMW).....	118
23. Figure 3.22: Model fit for the 1-dimensional terms of the GAM model for larval <i>Micropogonias undulatus</i> . Shaded areas represent 95% confidence intervals around the model fit represented by the black line. Tick marks on the x-axes represent actual observations. Only positive effects on density are shown to better illustrate the individual effects of model terms.....	119
24. Figure 3.23: Larval <i>Micropogonias undulatus</i> completed model and effect on density plotted as a contour map. Expected values are based on the complete model fit. Estimated density isolines as a function of barometric pressure and wind direction are shown in color. Areas where no plot is shown represent expected numbers of larvae within the tidal pass to be zero. The interaction is plotted individually for flood and ebb tidal stages. Histograms above contour plots represent percent frequency of wind direction during sampling.....	120

25. Figure 3.24: Model Fit for 1-dimensional terms of the GAM model for larval *Anchoa hepsetus*. Shaded areas represent 95% confidence intervals around the model fit represented by the black line. Tick marks on the x-axes represent actual observations. Only positive effects on density are shown to better illustrate the individual effects of model terms..... 123
26. Figure 3.25: Larval *Anchoa hepsetus* completed model and effect on density plotted as a contour map. Expected values are based on the complete model fit. Estimated density isolines as a function of wind direction and wind speed (left), and as a function of wind direction and barometric pressure (right), are shown in color. Areas where no plot is shown represent expected numbers of larvae within the tidal pass to be zero. Left histogram above contour maps shows percent frequency of wind speeds during sampling, while the histogram on the right shows wind direction percent frequency during sampling.....124
27. Figure 3.26: Density of *Anchoa mitchilli* larvae as a function of tidal stage and time of day. Flood tides had more of an effect on density estimates than day or night collections. Non-overlapping notches in the boxplots represent “strong evidence” of statistically different median values (Chambers et al. 1983), which represents the equivalent of a “visual” WMW. Different primary colors (yellow and blue) represent statistically different groups, while secondary colors (green) show similarities to both primary groups under Kruskal-Wallis test..... 126
28. Figure 3.27: Model fit for 1-dimensional terms of the GAM model for *Anchoa mitchilli* larvae. Shaded areas represent 95% confidence intervals around the model fit represented by the black line. Tick marks on the x-axes represent actual observations. Only positive effects on density are shown to better illustrate the individual effects of model terms.....127
29. Figure 3.28: Larval *Anchoa mitchilli* completed model and effect on density plotted as a contour map. Expected values are based on the complete model fit. Estimated density isolines as a function of wind speed and wind direction (left); as a function of barometric pressure and wind direction (right) are shown in color. Areas where no plot is shown represent expected numbers of larvae within the tidal pass to be zero. Left histogram above contour maps shows percent frequency of wind speeds during sampling, while the histogram on the right shows wind direction percent frequency during sampling.....128

30. Figure 3.29: Density by tidal stage for *Farfantepenaeus aztecus* postlarvae. Flood tides have significantly higher density values than ebb. Non-overlapping notches between boxplots provide “strong evidence” of difference in median values between the groups (Chambers et. al 1983). Different colors represent statistically different groups (WMW).....130
31. Figure 3.30: Density by tidal stage and day/night for *Farfantepenaeus aztecus* postlarvae. Flood tides, regardless of time of day, were significantly different from nocturnal collections on ebb tides. Different primary colors (yellow and blue) represent statistically different groups, while secondary colors (green) show similarities to both primary groupings under Kruskal-Wallis test.....131
32. Figure 3.31: Model fit for 1-dimensional terms of the GAM model for postlarval *Farfantepenaeus aztecus*. Shaded areas represent 95% confidence intervals around the model fit represented by the black line. Tick marks on the x-axes represent actual observations. Only positive effects on density are shown to better illustrate the individual effects of model terms.....132
33. Figure 3.32: Postlarval *Farfantepeanaeus aztecus* completed model and effect on density plotted as a contour map. Expected values are based on the complete model fit. Estimated density isolines as a function of barometric pressure and wind direction are shown in color. Areas where no plot is shown represent expected numbers of larvae within the tidal pass to be zero. The interaction is plotted individually for flood and ebb tidal stages. Histograms above contour plots represent percent frequency of wind directions during sampling.....133
34. Figure 3.33: Density by time of sample collection for *Pogonias cromis* larvae. Despite higher median densities collected during nocturnal sampling efforts there was no significant differences. Different colors represent differences under WMW test..... 135
35. Figure 3.34: Density by tidal stage and time of day for *Pogonias cromis* larvae. Samples collected during nocturnal flood tides were not significantly different from all other groups despite a much larger median value. Different colors represent differences between groups under Kruskal-Wallis test.....136
36. Figure 3.35: Model fit for 1-dimensional terms of the GAM model for larval *Pogonias cromis*. Shaded areas represent 95% confidence intervals around the model fit represented by the black line. Tick marks on

the x-axes represent actual observations. Only positive effects on density are shown to better illustrate the individual effects of model terms.....	137
37. Figure 3.36: Larval <i>Pogonias cromis</i> completed model and effect on density plotted as a contour map. Expected values are based on the complete model fit. Estimated density isolines as a function of barometric pressure and wind direction are shown in color. Areas where no plot is shown represent expected numbers of larvae within the tidal pass to be zero. The interaction is plotted individually for flood and ebb tidal stages. Histograms above contour maps represent percent frequency of wind directions during sampling.....	138
38. Figure 3.37: Density by tidal stage and time of day for <i>Sciaenops ocellatus</i> larvae. Nocturnal densities on flood tides had the largest median value, and were significantly different from samples collected during daytime ebb tides. Different colors represent differences between groups under Kruskal-Wallis test.....	140
39. Figure 3.38: Model fit for 1-dimensional terms of the GAM model for larval <i>Sciaenops ocellatus</i> . Shaded areas represent 95% confidence intervals around the model fit represented by the black line. Tick marks on the x-axes represent actual observations. Only positive effects on density are shown to better illustrate the individual effects of model terms.....	141
40. Figure 3.39: Larval <i>Sciaenops ocellatus</i> completed model and effect on density plotted as a contour map. Expected values are based on the complete model fit. Estimated density isolines as a function of barometric pressure and wind direction are shown in color. Areas where no plot is shown represent expected numbers of larvae within the tidal pass to be zero. Histogram above the contour map represents percent frequency of wind direction during sampling.....	142
41. Figure 3.40: Larval <i>Cynoscion arenarius</i> density by tidal stage and time of day. There is a lack of statistical difference between the groups. Samples collected on flood tides did, however, have higher median densities than those on ebb tides. Different primary colors (yellow and blue) represent statistically different groups, while secondary colors (green) show similarities to both primary groups under Kruskal-Wallis test.....	144

42. Figure 3.41: Model fit for 1-dimensional terms of the GAM model for larval <i>Cynoscion arenarius</i> . Shaded areas represent 95% confidence intervals around the model fit represented by the black line. Tick marks on the x-axes represent actual observations. Only positive effects on density are shown to better illustrate the individual effects of model terms.....	145
43. Figure 3.42: Larval <i>Cynoscion arenarius</i> completed model and effect on density plotted as a contour map. Expected values are based on the complete model fit. Estimated density isolines as a function of barometric pressure and wind direction are shown in color. Areas where no plot is shown represent expected numbers of larvae within the tidal pass to be zero. The interaction is plotted individually for flood and ebb tidal stages. Histograms above contour maps represent percent frequency of wind directions during sampling.....	146
44. Figure 3.43: Density by tidal stage and time of sample collection for <i>Cynoscion nebulosus</i> larvae. Median densities for flood tides were greater than those during ebb tides. Night flood densities were statistically greater than all other groups, despite second quartile overlap with daytime flood densities. Different colors represent differences between the groups under Kruskal-Wallis test.....	148
45. Figure 3.44: Model fit for the 1-dimensional terms of the GAM model for larval <i>Cynoscion nebulosus</i> . Shaded areas represent 95% confidence intervals around the model fit represented by the black line. Tick marks on the x-axes represent actual observations. Only positive effects on density are shown to better illustrate the individual effects of model terms.....	149
46. Figure 3.45: Larval <i>Cynoscion nebulosus</i> completed model and effect on density plotted as a contour map. Expected values are based on the complete model fit. Estimated density isolines as a function of wind speed and wind direction is shown in color. Areas where no plot is shown represent expected numbers of larvae within the tidal pass to be zero. The histogram above the contour map represents the percent frequency of wind directions during sampling.....	150
47. Figure 4.1: Map of the study location in relation to the Gulf of Mexico and coastal Louisiana. The points in black represent the sampling location, with the final panel being the sampling location from an aerial photograph of Bayou Tartellan. The X in the last panel marks the location of an extended dock used as a sampling platform and later destroyed by Hurricane Gustav.....	186

48. Figure 4.2:	Water temperature variations by month across the two years of field sampling, year 1 (red) and year 2 (blue). Both years show a similar trend of decreased temperature from November through early February. Year two was generally warmer, although cooler water lasted into March 2008. High variability occurred during the months with coldest water temperatures.....	195
49. Figure 4.3:	Salinity variation by month across the two years of field sampling. There was more variability across sampling efforts during year 1 (red) than year 2 (blue). Highest salinity variability occurred from November through March for both years.....	196
50. Figure 4.4:	Histograms showing <i>M. undulatus</i> collected by sampling trip for October 2006 to March 2007, and September 2007 to March 2008. Peak numbers of larvae collected occurred from late October through November for both years. February 2008 through March 2008 saw a higher percentage of the total number of larvae collected in that year than the same period within 2007.....	198
51. Figure 4.5:	Boxplots of standard length (SL- mm) for <i>M. undulatus</i> larvae by sampling effort for each month. October 2006 to March 2007 (red) and September 2007 to March 2008 (blue) are both provided.....	200
52. Figure 4.6:	Histograms of estimated hatch dates for <i>M. undulatus</i> larvae. Data include directly measured otoliths and those estimated from age at length frequency keys. Estimated number of larvae sampled and percentages of the total from half month increments are provided for October 2006 – March 2007, September 2007 – March 2008, and both years combined.	201
53. Figure 4.7:	Laird-Gompertz growth model of larval <i>M. undulatus</i> as standard length (SL - mm) versus age (days post hatch - dph). The model is artificially forced through the intercept at the estimated 1.5 mm SL at hatch to accurately reflect growth rates of ages in dph less than the minimum age calculated. Boxplots showing the median, 25% and 75% quantiles, 95 percent confidence intervals, and outliers are provided for each axis. The Laird-Gompertz model is parameterized as: $SL = 1.5 \cdot e^{2.613272(1-e^{-0.026186 \cdot Age})}$	203
54. Figure 4.8:	Laird-Gompertz growth models of larval <i>M. undulatus</i> as standard length (SL - mm) versus age (days post hatch - dph) for each of the two sample periods. The sample period from 10/06 to 03/07 is shown in black, and the Laird-Gompertz model had the following	

parameterization: $SL = 1.5 \cdot e^{2.77531(1-e^{-0.02300 \cdot Age})}$. The sample period from 09/07 to 03/08 is shown in red, and the Laird-Gompertz model had the following parameterization:
 $SL = 1.5 \cdot e^{2.422452(1-e^{-0.031297 \cdot Age})}$ 204

55. Figure 4.9: (A) Boxplots comparing larval *M. undulatus* otoliths with standard length (SL - mm) and age (days post hatch - dph) for the fall (blue) and spring (red) seasons in both sample years. Fall samples were similar in both age and length for both sample years, but were different from the spring in both age and length. Non-overlapping notches between any two boxplots represent “strong evidence” of statistically different median values (Chambers et al. 1983). (B) Laird-Gompertz growth models of larval *M. undulatus* otoliths as SL (mm) versus age (dph) for fall and spring from both sample years. The fall recruitment period from October to December, 2006, is shown in black, and the winter/spring recruitment period from January to March 2007 is shown in green. The fall recruitment period from September to December, 2007, is shown in red, and the winter/spring recruitment period from January to March 2008 is shown in blue. All models are forced through the intercept at the estimated 1.5 mm SL at hatch to accurately reflect growth rates of ages in dph less than the minimum otolith determined age.
 Model Parameterizations: Fall – Year 1: $SL = 1.5 \cdot e^{2.89159(1-e^{-0.02155 \cdot Age})}$;
 Fall – Year 2: $L = 1.5 \cdot e^{2.50594(1-e^{-0.02893 \cdot Age})}$;
 Spring – Year 1: $SL = 1.5 \cdot e^{2.54838(1-e^{-0.02512 \cdot Age})}$; and
 Spring – Year 2: $SL = 1.5 \cdot e^{2.11260(1-e^{-0.04726 \cdot Age})}$ 205

56. Figure 4.10: Maximum growth rates based on the derivative of the Laird-Gompertz growth model for larval *M. undulatus* otoliths. Daily growth rates ($\text{mm} \cdot \text{day}^{-1}$) are the slopes of the Laird-Gompertz models at any point in age (solid lines), and the maximum growth rates (dashed lines) are provided for fall 2006 (black), fall 2007 (red), spring 2007 (green), and spring 2008 (green). The maximum growth rate for the fall 2006 and 2007 was at 49 dph and 37 dph, respectively. The maximum growth rate for the spring 2007 and 2008 was at 32 dph and 16 dph, respectively..... 207

57. Figure 4.11: (A) Otolith ring mean distance (mm) from the core by season and sample year. Fall 2006 (black), fall 2007 (red), spring 2007 (green), and spring 2008 (blue), are all provided to show differences between year and season, and the estimated average ingress date is demarcated by the dashed orange line. Distance from the core as a proxy for the increased growth expected with the lower salinities of the estuaries

showed an average ingress date of 37 dph. (B) Mean ring width (mm) for individual daily rings from removed and imaged otoliths. Increases in ring width variability and increases from a regular ring width, of approximately 0.0005 mm for the fall 2006 (black) and the fall 2007 (red), and from a regular ring width of 0.0010 mm for the spring 2007 (green) and spring 2008 (blue), occurred for rings deposited after 37 dph.....	209
58. Figure 4.12: Mixed Model (MM) partial plots for growth rate ($\text{mm}\cdot\text{day}^{-1}$) data as a function of hydrodynamic parameters. Growth rate data are based on both directly measured otoliths and those ages provided from length frequency keys. All partial plots assume a static value for the other model terms in the graphical evaluation. (A) Growth rate as a function of water temperature ($^{\circ}\text{C}$), delineated by tide. (B) Growth rate as a function of salinity (ppt), delineated by tide. (C) Growth rate as a function of net water transport (NWT; $\text{m}^3\cdot\text{s}^{-1}$), delineated by tide.....	210
59. Figure 5.1: Map of the study location in relation to the Gulf of Mexico and coastal Louisiana. The points in black represent the sampling location, with the final panel being the sampling location from an aerial photograph of Bayou Tartellan. The X in the last panel marks the location of an extended dock used as a sampling platform and later destroyed by Hurricane Gustav.....	230
60. Figure 5.2: Water temperature variations by month across the two years of field sampling, year 1 (red) and year 2 (blue). Both years showed a similar trend of decreased temperature from November through early February. Year 2 was generally warmer, although cooler water lasted into March 2008. Higher variability occurred during the months with coldest water temperatures.....	239
61. Figure 5.3: Standard length (SL) data for all <i>B. patronus</i> larvae used for sagittal otolith analyses, presented as a histogram. (A) Contains all larvae between 5 and 16 mm SL, $\bar{x} = 10.8 \text{ mm}$, $sd = 2.51 \text{ mm}$. (B) Contains all larvae greater than 16 mm SL, $\bar{x} = 19.4 \text{ mm}$, $sd = 1.39 \text{ mm}$. Both histograms were normally distributed ($p > 0.05$, Shapiro-Wilk's test).....	241
62. Figure 5.4: Violin plots of larval <i>B. patronus</i> SL by month broken down by sampling period for each year and total. Violin plots show the kernel density of lengths as the shape, the mean for each month as the white point, and the 50% center quartile with the thick black bar. October	

2006 – March 2007 is provided in red, with $\bar{x} = 14.7 \text{ mm}$, and $sd = 4.61 \text{ mm}$. September 2007 – March 2008 is provided in blue, with $\bar{x} = 16.3 \text{ mm}$, and $sd = 4.83 \text{ mm}$. Pooled data are provided in green, with $\bar{x} = 15.4 \text{ mm}$, and $sd = 4.75 \text{ mm}$ 242

63. Figure 5.5: Violin plots of larval *B. patronus* age in days post spawning (dps) by month, broken down by sampling period for each year and total. Violin plots show the kernel density of ages as the shape, the mean for each month as the white point, and the 50% center quartile with the thick black bar. October 2006 – March 2007 is provided in red, with $\bar{x} = 30 \text{ dps}$, and $sd = 13.2 \text{ dps}$. September 2007 – March 2008 is provided in blue, with $\bar{x} = 29 \text{ dps}$, and $sd = 11.0 \text{ dps}$. Pooled data are provided in green, with $\bar{x} = 30 \text{ dps}$, and $sd = 12.4 \text{ dps}$ 243

64. Figure 5.6: Two cycle Laird-Gompertz growth models for each sample year and pooled total of larval *B. patronus* otoliths as SL (mm) versus age in days post spawning (dps). The models are hind casted through the estimated intercept to estimate growth rates of larvae at ages in dps less than the minimum age measured. Boxplots showing the median, 25% and 75% quantiles, 95 percent confidence intervals, and outliers are provided for each axis. The two cycle Laird-Gompertz models for each year are parameterized

$$\text{as: Year 1 } SL = 2.881552e^{\left[\frac{0.077875(1-e^{(-0.023201\Delta_1)})}{0.023201} + \frac{0.014877(1-e^{(-0.058754\Delta_1)})}{0.058754}\right]},$$

$$\Delta_1 = \text{MIN}(\text{Age}, 33.145155)$$

$$\Delta_2 = \text{MAX}(\text{Age} - 33.145155, 0)$$

$$\text{Year 2 } SL = 2.881552e^{\left[\frac{0.073058(1-e^{(-0.016744\Delta_1)})}{0.016744} + \frac{0.008855(1-e^{(-0.040660\Delta_1)})}{0.040660}\right]},$$

$$\Delta_1 = \text{MIN}(\text{Age}, 33.085634)$$

$$\Delta_2 = \text{MAX}(\text{Age} - 33.085634, 0).....246$$

65. Figure 5.7: Laird-Gompertz growth models of larval *B. patronus* otoliths as SL (mm) versus age (dps) for each of the two individual groupings. (A) In the age grouping, larvae with a measured age less than 33 dps are provided as points in black with the corresponding black model line, and larvae greater than 33 dps are provided as points in red with the corresponding red model line. (B) In the length grouping, larvae with a measured SL less than 16 mm are provided as points in black with the corresponding black model line, and larvae greater than 16 mm SL are provided as points in red with the corresponding red model line. The two Laird-Gompertz age models are parameterized as:

$$\text{Larvae} < 33 \text{ dps (Black) } SL = 2.881552e^{3.868674(1-e^{-0.019345\text{Age}})}$$

$$\text{Larvae} > 33 \text{ dps (Red) } SL = 6.54628e^{1.23864(1-e^{-0.05084\text{Age}})}$$

The two Laird-Gompertz length models are parameterized as:

$$\text{Larvae} < 16 \text{ mm SL (Black)} SL = 2.881552e^{2.298079(1-e^{-0.038964Age})}$$

$$\text{Larvae} > 16 \text{ mm SL (Red)} SL = 13.79161e^{0.74645(1-e^{-0.01480Age})} \dots\dots\dots 248$$

66. Figure 5.8: (A) Otolith ring mean distance (mm) from the core by sample year. October 2006 to March 2007 are provided in black, and September 2007 to March 2008 are provided in red. The blue dashed line represents the modeled developmental shift at 33 days post spawning (dps) from larvae into the beginning of the juvenile stage. (B) Mean ring width (mm) for individual daily rings from removed and imaged otoliths. October 2006 to March 2007 are provided in black, and September 2007 to March 2008 are provided in red. Decreases in ring width correspond to the modeled developmental shift (blue dashed line) occurring at 33 dps..... 249
67. Figure 6.1: Map of the study location in relation to the Gulf of Mexico and coastal Louisiana. The points in black represent the sampling location, with the final panel being the sampling locations from an aerial photograph of Bayou Tartellan..... 269
68. Figure 6.2: The upper graph provides predicted and measured tidal heights and overall net water transport for Bayou Tartellan during 18-22 April 2007. The lower graph provides the atmospheric data, including barometric pressure, air temperature, wet bulb temperature, and wind direction and magnitude for the same time period. For wind speed, every 2 degrees on the temperature scale corresponds to 1 m/s of wind speed..... 275
69. Figure 6.3: The upper graph provides predicted and measured tidal heights and net water transport for Bayou Tartellan during 16-20 September 2007. The lower graph provides the atmospheric data, including barometric pressure, air temperature, wet bulb temperature, and wind direction and magnitude for the same time period. For wind speed, every 2 degrees of temperature corresponds to 1 m/s of wind speed.....276
70. Figure 6.4: Frequency histograms of overall larval density during both positive and negative net water transports. Positive net water transports saw a higher frequency of zero collections, more positive collections overall, and higher maximum densities compared to negative transport events. Areas for the inserts are bounded by the rectangular box, and focus on densities less than 50 indiv./15m³ 280

71. Figure 6.5:	Mean density, standard error, and size-class percent frequency histograms for <i>A. hepsetus</i> larvae collected in 18-21 April and 16-19 September 2007. In April most of the larvae were greater than 12 mm SL. In September the highest densities of larvae were centered on the 9-10 mm SL size-class.....	281
72. Figure 6.6:	Surface plot showing the effect of net water transport and standard length (SL) on modeled densities of larval <i>A. hepsetus</i> at the northern dock edge, the center channel, and the southern shore edge. The highest larval densities at the northern dock occurred for larvae greater than 12 mm SL between positive net water transports of 0 and 50 m ³ /s, whereas at the center channel it occurred between 40 and 100 m ³ /s for larvae less than 10 mm SL, and at the southern shore net water transports of approximately -50 m ³ /s for larvae less than 8 mm SL.....	288
73. Figure 6.7:	Histogram showing the mean density, standard error, and percent frequency of size-classes of larval <i>A. hepsetus</i> at the three sampling locations across the tidal pass. Larvae greater than 15 mm SL were primarily found at the northern dock edge.....	289
74. Figure 6.8:	Mean density, standard error, and size-class frequency histograms of <i>A. mitchilli</i> larvae collected in April and September 2007. In April most of the larvae were between 6 and 8 mm SL. In September the highest densities of larvae were between 7 and 10 mm SL.....	290
75. Figure 6.9:	Surface plot for probability of encounter for <i>A. mitchilli</i> as a function of SL and net water transport. Across the range of SLs, the northern dock had high probability of encounter at net water transports greater than 35 m ³ /s and for smaller larvae at net water transports around -50m ³ /s, whereas the center channel had the highest probability of encounter at transports greater than 60 m ³ /s especially for larvae greater than 8 mm SL, and the southern shore at transports greater than 25 m ³ /s for larvae greater than 10 mm SL.....	292
76. Figure 6.10:	Histogram showing the mean density, standard error, and percent frequency of size classes of <i>A. mitchilli</i> at the three sampling locations across the tidal pass.....	293
77. Figure 6.11:	Mean density and size-class percent frequency histograms of <i>B. patronus</i> larvae collected in 18-21 April and 16-19 September	

2007. In April nearly all of the larvae were greater than 14 mm SL. In September all of the larvae were between 2 and 5 mm SL.....	294
78. Figure 6.12: Surface plot showing the effect of net water transport and SL on modeled densities for larval <i>B. patronus</i> for April (Plot A) and September (Plot B). Plot (A) shows peak densities for larvae with standard lengths from 12 to 14 mm, at positive net water transports greater than 100m ³ /s. Plot (B) shows peak densities for shorter larvae occurring between 50 and 100 m ³ /s.....	295
79. Figure 6.13: Mean density, standard error, and size-class frequency histograms of <i>S. ocellatus</i> larvae collected from 16-19 September 2007. The highest mean densities and greatest frequency of larvae were between 3 and 5 mm SL.....	296
80. Figure 6.14: Mean density, standard error, and size-class frequency histograms for <i>C. arenarius</i> larvae collected in 18-21 April and 16-19 September 2007. In April most larvae were less than 2 mm SL. In September most of the larvae were between 2 and 5 mm SL.....	298
81. Figure 6.15: Mean density, standard error, and size class frequency histograms of <i>C. nebulosus</i> larvae collected in 16-19 September 2007. The highest mean densities and greatest frequency of larvae were between 2 and 4 mm SL.....	301

ABSTRACT

This dissertation attempts to better understand astronomical, meteorological, and oceanographic forcing of offshore-spawned, estuarine-dependent species from continental shelf to estuarine waters through tidal passes. The vertical distribution of zoo-/ichthyoplankton within the inner continental shelf from the Louisiana Offshore Oil Platform monitoring project (1978-1995) provided an important offshore end member for the estuarine recruitment study, and is potentially useful in predicting vulnerabilities to past and future oil spills. The role that atmospheric cold front passages may have on densities and movement of zoo-/ichthyoplankton recruiting through the Bayou Tartellan tidal pass, Louisiana, were analyzed using a Generalized Additive Model. The pre-frontal phase, with dominant southern quadrant winds, leading to coastal setup, can enhance flood tides and increase larval recruitment. Post-frontal phase strong northerly winds can enhance ebb tides, which could have negative estuarine retention implications. Lateral differences across Bayou Tartellan at a bulkheaded northern edge, center channel, and a natural-sloping southern shore edge were analyzed using a Zero Inflated Negative Binomial model to determine if behaviorally-mediated, lateral movements by larger larvae could enhance estuarine recruitment/retention. During inflows, estuarine-dependent larvae generally utilized the surface of the center channel and had much lower densities towards the edges. During outflows, larger larvae were more numerous along the southern edge, where velocities were slower. Finally, otolith age and growth data for *Micropogonias undulatus* and *Brevoortia patronus* were analyzed for growth rates and microstructure differences associated with oceanographic variability along their recruitment corridors from offshore spawning grounds

through the coastal boundary layer, and into the tidal pass. Growth rates from a Laird-Gompertz model for *M. undulatus* were similar to previous studies. Otolith microstructure suggested ingress through the coastal boundary layer/estuarine waters occurred at approximately 40 days post hatch, and had a marked effect on growth. A two-cycle, Laird-Gompertz growth model for *B. patronus* suggested a growth stanza at 35 days post hatch, which most likely reflects changing oceanographic conditions during transport and biological consequences of a shift in ontogenetic feeding strategy from selective particulate feeder to an omnivorous filter feeder, with a strong initial growth rate decreasing rapidly after the beginning of the transition in feeding strategy.

CHAPTER 1. GENERAL INTRODUCTION

1.1 General Study Background

Successful estuarine recruitment of offshore-spawned zoo-/ichthyoplankton through tidal passes into estuarine nurseries is important, as exemplified by estuarine-dependent species comprising 75% to 95% of the commercial fisheries landings in the northern Gulf of Mexico (GOM; Chambers, 1992; Mann, 2000). Assemblages of these estuarine-dependent zoo-/ichthyoplankton in Louisiana estuaries vary across spatial and temporal scales (Mazzotti et al. 2008; Reyier et al. 2008). These early life history stages of zoo-/ichthyoplankton are expected to have limited ability to migrate horizontally. Therefore, their distribution and transport is likely determined by a combination of oceanographic flows, wind-driven currents and astronomical tides, which can exert strong effects on recruitment success (Joyeux 1999; Brown et al. 2004; Roegner et al. 2007; Lara-Lopez and Neira 2008). Understanding their capacity to vertically migrate within a water column that may have differential current flows may be ecologically important with respect to estuarine recruitment (Tankersley et al., 1998; Gibson et al. 2001; Criales et al., 2011). However, previous studies along the northern GOM have shown a lack of ichthyoplankton vertical stratification, which is most likely a reflection of the well-mixed nature of these estuaries and tidal passes (Lochmann et al., 1995; Holt and Holt, 2000; Kim et al., 2010).

Chapter 2: In many regions of the world with major fisheries, data are available on the vertical distributions of finfish and invertebrates abundances (Yatsu et al., 2005). In the GOM, however, there is a general lack of ichthyoplankton studies dealing with multi-species depth preferences over protracted time scales (Hernandez et al., 2003; Lindquist et al., 2005; Carassou

et al., 2012). This is somewhat surprising given that Louisiana ranks second in U.S. commercial fisheries landings and fourth in dockside value (Van Voorhees and Lowther, 2011). Furthermore, zoo-/ichthyoplankton vertical distribution data have ecological and environmental impact applications. For example, such vertical data would be helpful in determining potential vulnerabilities to oil spills such as the Deepwater Horizon Macondo blowout (20 April 2010) that occurred 66 km off the Louisiana coast in approximately 1600 m depth (Cleveland, 2011; Graham et al., 2012). Therefore, the overall objective of this chapter is to analyze zoo-/ichthyoplankton depth preferences in the water column utilizing the Louisiana Department of Wildlife and Fisheries' Louisiana Offshore Oil Port (LOOP) sampling program from 1978 to 1995, which had coastal sampling across a depth range of 7.6 to 37 m.

Chapter 3: Many species of fish in the northern GOM spawn on the inner continental shelf or near the mouths of estuaries, and utilize estuaries as nursery habitat for larval, postlarval and juvenile life history stages. This chapter of the dissertation, however, focuses on several commercially- and recreationally-important species which spawn during fall through spring (Able 2005; Hare and Govoni 2005; Glass et al. 2008; Vinagre et al. 2009). During this time interval, winter storm events, i.e., atmospheric cold front passages, can exert either a negative or positive force on recruitment and retention, since these energetic meteorological events have been shown to temporarily override the effects of astronomical tides (Reyes et al. 2002; Stone et al. 2004; Li et al. 2011). To remove the tidal and inertial effects, a 6th-order 40-hr Butterworth low-pass filter was applied to the raw volume transport to produce a **net water transport** (m^3/s ; NWT). These net transport data effectively show the lower-frequency subtidal oscillations associated with cold front events and other wind forcing, while filtering out the higher frequency

diurnal tidal oscillations (Li et al. 2009). This is particularly true given Louisiana's micro-tides and generally north/south oriented estuaries, which align with the prevailing north/south wind fields of winter frontal events. These cold fronts have been shown to cause extreme changes in estuarine water levels, with volume transport up to six times greater than the average normal tidal flux, and water level variations of 1.2 m or more (Swenson and Chuang 1983; Perez et al. 2000; Walker and Hammack 2000). Therefore, the timing and densities of transported larvae at any given moment along their recruitment corridor may be controlled by a varying combination of oceanographic flows, astronomical tides, and meteorological forces (Joyeux 1999; Brown et al. 2004; Comyns and Lyczkowski-Shultz 2004; Johnson et al. 2009). The objective of this chapter is the evaluation of the relative contributions of these high-energy, atmospheric cold front passages and astronomical tides to the successful estuarine recruitment of winter-spawned, estuarine-dependent fisheries species in a Louisiana tidal pass.

Chapter 4: Atlantic croaker (*Micropogonias undulatus*) is a commercially- and ecologically-important species in the GOM, but the stock has been historically drawn down as bycatch from other fisheries. The amount of Atlantic croaker harvested commercially has been cyclic, ranging from 1,100 metric tons (t) to over 15,000 t per year, which does not include the extremely high levels of bycatch, i.e., from 100,000 to 400,000 t annually (NMFS, 2009; NMFS, 2012). Under such fishing mortality pressures, hydrologic variability at large and small spatial and temporal scales can greatly affect the successful recruitment of *M. undulatus* into estuarine nursery grounds (Norcross, 1983; Shaw et al., 1988; Raynie, 1991; Raynie and Shaw, 1994). Once in the estuary, survival during their first winter is primarily effected by lower temperatures increasing mortality, as verified in both the field (Norcross and Austin, 1981; Hare and Able,

2007), and laboratory (Lankford and Targett, 2001a/b). Modeling larval growth during their transport along the recruitment corridor, therefore, can prove to be a useful tool. Analyzing otolith microstructure can be used to estimate approximate times of larval ingress (Hoover et al., 2012), and illuminate growth responses to changes in hydrologic conditions. Differences in ring width at length have also been used to determine within season cohorts, based on variable growth between seasons in the same recruitment year (Brophy and Danilowicz, 2002). The primary objectives of this chapter are to determine the length at age for *M. undulatus* larvae, estimate estuarine/coastal boundary zone ingress times through the tidal pass, and determine the effect of hydrodynamic patterns associated with the differences between continental shelf and estuarine waters on growth.

Chapter 5: *Brevoortia patronus*, gulf menhaden, represents both a commercially-important fishery in the GOM (Pritchard, 2005; Vaughn et al., 2010; McCrea-Strub et al., 2011), and an ecologically-important prey item for commercially- and recreationally-important species (Del Rio et al., 2010; Nelson et al., 2012; Simonsen and Cowan, 2013). The *B. patronus* fishery is the second largest United States fishery by weight and fourth in value (Pritchard, 2005), harvesting an average of 400-600 kilotons annually with 92% of the annual landings occurring in Louisiana in recent years (Vaughn et al., 2010). Possible population limitations for *B. patronus* include food availability, habitat limitations, and successful recruitment of larvae into estuarine nursery areas, with declining recruitment being more of a concern based on a recent decrease in population fecundity (Vaughn et al., 2007). Recruitment from the more oligotrophic continental shelf spawning grounds through tidal passes into more productive estuarine waters represents an ecologically important change (Raynie and Shaw, 1994). This time period also corresponds to

when *B. patronus* larvae transform from selective particulate feeding to omnivorous filter feeding as juveniles (Stoecker and Govoni, 1984; Deegan 1990; Chen et al. 1992; Lozano et al., 2012). Analysis of otolith microstructure can provide information to calculate growth rates and to document metabolic responses to changing environments and to metamorphic changes, through variability in otolith ring width (Maillet and Checkley 1990; Chambers and Miller, 1995). The primary objectives of chapter 5 are to determine the length at age of *B. patronus* larvae, determine at what age there is a shift in growth rate consistent with the expected shift in feeding strategy from a selective particulate feeder to an omnivorous filter feeder, and determine the distribution of the spawning period using back calculation of spawning dates from age frequency keys

Chapter 6: Other than the Mississippi and Atchafalya Rivers, most of the embayments and estuaries in the northcentral GOM have relatively small drainage basins with little freshwater head. In addition, most of these estuaries are very shallow (< 2 m deep) and have a diurnal micro-tidal regime which limits their potential for vertical haline stratification (Smith, 1977; Moeller et al., 1993; Cahoon and Reed, 1995; Wang, 1997; Li et al., 2009; Li et al., 2011). Under the vertically well-mixed conditions prevalent in the northcentral GOM, the shape of the tidal pass and resultant hydrodynamics created from bathymetric variability, branches, and eddies can create micro-environments where flow velocity may vary laterally during either tidal stage (Kjerfve, 1978; Boon and Byrne, 1981; Wang and Craig, 1993; Li and O'Donnell, 1997). This is in contrast to the deep, more often vertically-stratified, drowned river valley estuaries of the east coast of the U.S.A., where behaviorally-mediated recruitment strategies involve moving vertically, such as selective tidal stream transport (STST), are predominate (Arnold and Cook,

1984; Boehlert and Mundy, 1988; Tankersley et al., 1998; Gibson et al. 2001; Criales et al., 2011). Chapter six analyzed lateral differences across Bayou Tartellan, at a bulkheaded northern edge, center channel, and a natural, gently sloping southern shore edge to determine if behaviorally-mediated, lateral movements by larger larvae could enhance estuarine recruitment/retention. To counter the typically large number of zeroes in this fisheries dataset, a Zero Inflated Negative Binomial (ZINB) model was used to analyze ichthyoplankton densities, fish standard lengths, and NWTs using both the logistic (i.e., probability of encounter) and negative binomial (i.e., larval density) portion of the model.

Summary: The overall focus of this dissertation is on ichthyoplankton estuarine recruitment dynamics across varying spatial and temporal scales, incorporating both environmental and organismal analyses, allowed for the investigation of estuarine recruitment processes in the highly variable environment along a recruitment corridor from the coastal ocean to a Louisiana tidal pass. This dissertation had a systematic and sequential research approach. First, determine general vertical structure for zoo-/ichthyoplankton within the Louisiana inner continental shelf. Second, investigate the effect of winter cold front passages have on estuarine recruitment dynamics for winter spawning species using a Generalized Additive Model (GAM). Third, to use non-linear growth modeling and fine-scale measurement of otolith microstructure to investigate the effects the transition from more oligotrophic continental shelf waters experienced along the recruitment corridor may have on larval *Micropogonias undulatus* and *Brevoortia patronus*. Finally, investigate differences in lateral cross channel probability of encounter and larval densities utilizing a Zero Inflated Negative Binomial (ZINB) model to help account for patchy distributions of larvae in the tidal pass.

1.2 Literature Cited

- Able, K.W. 2005. A re-examination of fish estuarine dependence: evidence for connectivity between estuarine and ocean habitats. *Est., Coast. Shelf Sci.*, 64(1): 5-17.
- Brophy, D., and B.S. Danilowicz. 2002. Tracing populations of Atlantic herring (*Clupea harangus* L.) in the Irish and Celtic Seas using otolith microstructure. *ICES J. Mar. Sci.*, 59: 1305-1313.
- Brown, C., S. Holt, G. Jackson, D. Brooks, and G. Holt. 2004. Simulating larval supply to estuarine nursery areas: how important are physical processes to the supply of larvae to the Aransas Pass Inlet? *Fish. Oce.*, 13(3): 181-196.
- Cahoon, D.R., and D.J. Reed. 1995. Relationships among marsh surface topography, hydroperiod, and soil accretion in a deteriorating Louisiana salt marsh. *J. Coast. Res.*, 11: 357-369.
- Carassou, L., F.J. Hernandez, S.P. Powers, and W.M. Graham. 2012. Cross-shore, seasonal, and depth-related structure of ichthyoplankton assemblages in coastal Alabama. *Trans. Amer. Fish. Soc.* 141(4): 1137-1150.
- Chambers, J.R. 1992. Coastal degradation and fish population losses. *Stemming the Tide of Coastal Fish Habitat Loss. Mar. Rec. Fish. Pub.*, 14: 45-52.
- Chambers, R.C. and T.J. Miller. 1995. Evaluating fish growth by means of otolith increment analysis: special properties of individual-level longitudinal data. *Recent Developments in Fish Otolith Research. J.D.Secor & S.E.Campana (eds): University of South Carolina Press, Columbia, SC*: 155-175.
- Chen, W., J.J. Govoni, and S. Wavlen. 1992. Comparison of feeding and growth of larval round herring (*Etrumeus teres*) and gulf menhaden (*Brevoortia patronus*). *Fish. Bull.*, 90:183-189.
- Comyns, B.H., and J. Lyczkowski-Shultz. 2004. Diel vertical distribution of Atlantic croaker, *Micropogonias undulatus*, larvae in the northcentral Gulf of Mexico with comparisons to red drum, *Sciaenops ocellatus*. *Bull. Mar. Sci.*, 74(1): 69-80.
- Deegan, L.A. 1990. Effects of estuarine environmental conditions on population dynamics of young-of-the-year gulf menhaden. *Mar. Eco. Prog. Ser.. Oldendorf* 68:195-205.
- Del Rio, R., S. Bargu, D. Baltz, S. Fire, G. Peterson, and Z. Wang. 2010. Gulf menhaden (*Brevoortia patronus*): A potential vector of domoic acid in coastal Louisiana food webs. *Harm. Al.*, 10(1): 19-29.

- Glass, L.A., J.R. Rooker, R.T. Kraus, and G.J. Holt. 2008. Distribution, condition, and growth of newly settled southern flounder (*Paralichthys lethostigma*) in the Galveston Bay Estuary, TX. *J. Sea Res.*, 59(4): 259-268.
- Graham, B., W.K. Reilly, F. Beinecke, D.F. Boesch, T.D. Garcia, C.A. Murray, and F. Ulmer. 2012. Deep Water Horizon: The Gulf oil disaster and the future of offshore drilling. Report to the President. National Commission on the BP Deepwater Horizon Oil Spill and Offshore Drilling. Cleveland, C.J. (ed.) pp. 1-398.
- Hare, J.A., and J.J. Govoni. 2005. Comparison of average larval fish vertical distributions among species exhibiting different transport pathways on the southeast United States continental shelf. *Fish. Bull.*, 103: 728-736.
- Hare, J.A., and K.W. Able. 2007. Mechanistic links between climate and fisheries along the east coast of the United States: explaining population outbursts of Atlantic croaker (*Micropogonias undulatus*). *Fish. Oce.*, 16(1): 31-45.
- Hernandez, F.J., R.F. Shaw, J.S. Cope, J.G. Ditty, T.W. Farooqi, and M.C. Benfield. 2003. The across-shelf larval, post-larval and juvenile fish community associated with offshore oil and gas platforms west of the Mississippi River delta. *Amer. Fish. Soc. Spec. Symp. Ser.* 36: 39 – 72.
- Holt, G.J., and S.A. Holt. 2000. Vertical distribution and the role of physical processes in the feeding dynamics of two larval sciaenids *Sciaenops ocellatus* and *Cynoscion nebulosus*. *Mar. Eco. Prog. Ser.*, 193: 181-190.
- Hoover, R.R., C.M. Jones, and C.E. Grosch 2012. Estuarine ingress timing as revealed by spectral analysis of otolith life history scans. *Can. J. Fish. Aq. Sci.*, 69(8), 1266-1277.
- Johnson, D.R., H.M. Perry, J. Lyczkowski-Shultz, and D. Hanisko. 2009. Red snapper larval transport in the northern Gulf of Mexico. *Tran. Am. Fish. Soc.*, 138: 458-470.
- Joyeux, J. 1999. The abundance of fish larvae in estuaries: Within-tide variability at inlet and immigration. *Est. Coast.*, 22(4): 889-904.
- Kim, C.K., K. Park, S.P. Powers, W.M. Graham, and K.M. Bayha. 2010. Oyster larval transport in coastal Alabama: Dominance of physical transport over biological behavior in a shallow estuary. *J. Geo. Res.: Oceans* (1978–2012) 115.
- Lankford Jr, T.E., and T.E. Targett. 2001a. Low-temperature tolerance of age-0 Atlantic croakers: recruitment implications for US mid-Atlantic estuaries. *Tran. Am. Fish. Soc.*, 130(2), 236-249.

- Lankford Jr, T.E., & T.E. Targett. 2001b. Physiological performance of young-of-the-year Atlantic croakers from different Atlantic coast estuaries: implications for stock structure. *Trans. Am. Fish. Soc.*, 130(3), 367-375.
- Lara-Lopez, A., and F.J. Neira. 2008. Synchronicity between zooplankton biomass and larval fish concentrations along a highly flushed Tasmanian estuary: assessment using net and acoustic methods. *J. Plank. Res.*, 30(9): 1061-1073.
- Li, C., E. Weeks, and J.L. Rego. 2009. In situ measurements of saltwater flux through tidal passes of Lake Pontchartrain estuary by Hurricanes Gustav and Ike in September 2008. *Geo. Res. Lett.*, 36:L19609.
- Li, C., H. Roberts, G.W. Stone, E. Weeks, and Y. Luo. 2011. Wind surge and saltwater intrusion in Atchafalaya Bay during onshore winds prior to cold front passage. *Hydrobiologia* 658(1): 1-13.
- Lindquist, D.C., R.F. Shaw, and F.J. Hernandez, Jr. 2005. Distributional patterns of larval and juvenile fishes at offshore petroleum platforms in the north-central Gulf of Mexico. *Estu. Coast. Shelf Sci.* 62(4): 655-665.
- Lochmann, S.E., R.M. Darnell, and J.D. McEachran. 1995. Temporal and vertical distribution of crab larvae in a tidal pass. *Estuaries* 18: 255-263.
- Lozano, C., E. Houde, R. Wingate, and D. Secor. 2012. Age, growth and hatch dates of ingressing larvae and surviving juveniles of Atlantic menhaden *Brevoortia tyrannus*. *J. Fish Bio.*, 81:1665-1685.
- Mann, K.H. 2000. Ecology of the coastal waters with implications for management. 2nd Edition. John Wiley and Sons, Hoboken, NJ. 410 pp.
- Maillet, G.L. and D.M. Checkley Jr. 1990. Effects of starvation on the frequency of formation and width of growth increments in sagittae of laboratory-reared Atlantic menhaden *Brevoortia tyrannus* larvae. *Fish. Bull.*, 88: 155–165.
- Mazzotti, F.J., L.G. Pearlstine, T. Barnes, S.A. Bortone, K. Chartier, A.M. Weinstein, and D. DeAngelis. 2008. Stressor Response Model for the Spotted Seatrout (*Cynoscion nebulosus*). University of Florida IFAS Extension. University of Florida, Gainesville, Florida.
- McCrea-Strub, A., K. Kleisner, U. Sumaila, W. Swartz, R. Watson, D. Zeller, and D. Pauly. 2011. Potential impact of the Deepwater Horizon oil spill on commercial fisheries in the Gulf of Mexico. *Fisheries* 36:332-336.

- Moeller, C.C., O.K. Huh, H.H. Roberts, L.E. Gumley, and W.P. Menzel. 1993. Response of Louisiana coastal environments to a cold front passage. *J. Coast. Res.*, 9(2): 434-447.
- National Marine Fisheries Service, NMFS. 2009. Our living oceans. Report on the status of U.S. living marine resources, 6th edition. U.S. Dep. Commerce, NOAA Tech. Memo. NMFS-F/SPO-80, 369 p.
- National Marine Fisheries Service, NMFS. 2012. Fisheries of the United States. Lowther, A.(ed.). U.S. Dep. Commerce, NOAA. 124 p.
- Nelson, J., R. Wilson, F. Coleman, C. Koenig, D. DeVries, C. Gardner, and J. Chanton. 2012. Flux by fin: fish-mediated carbon and nutrient flux in the northeastern Gulf of Mexico. *Mar. Bio.*, 159:365-372.
- Norcross, B.L. 1983. Climate scale environmental factors affecting year-class fluctuations of Atlantic croaker (*Micropogonias undulatus*) in the Chesapeake Bay. Ph.D. Dissertation. College of William & Mary. 388 p.
- Norcross, B.L., and H.M. Austin. 1988. Middle Atlantic Bight meridional wind component effect on bottom water temperatures and spawning distribution of Atlantic croaker. *Cont. Shelf Res.*, 8: 69-88.
- Perez, B., J. Day, L. Rouse, R. Shaw, and M. Wang. 2000. Influence of Atchafalaya River discharge and winter frontal passage on suspended sediment concentration and flux in Fourleague Bay, Louisiana. *Est., Coast. Shelf Sci.*, 50(2): 271-290.
- Pritchard, E.S. 2005. Fisheries of the United States 2004. Silver Spring, MD: National Marine Fisheries Service, Office of Science and Technology, pp. 1-19.
- Raynie, R.C. 1991. Study of the spatial and temporal ichthyoplankton abundance along a recruitment corridor from offshore to estuarine nursery. Master's thesis. Louisiana State University, Baton Rouge, Louisiana.
- Raynie, R.C., and R.F. Shaw. 1994. Ichthyoplankton abundance along a recruitment corridor from offshore spawning to estuarine nursery ground. *Est., Coast. Shelf Sci.* 39(6): 421-450.
- Reyes, E., I. Georgiou, D. Reed, and A. McCorquodale. 2002. Using models to evaluate the effects of barrier islands on estuarine hydrodynamics and habitats: A numerical experiment. *J. Coast. Res.*, 44: 176-185.

- Reyier, E.A., J.M. Shenker, and D. Christian. 2008. Role of an estuarine fisheries reserve in the production and export of ichthyoplankton. *Mar. Eco. Prog. Ser.*, 359: 249-260.
- Roegner, G.C., D.A. Armstrong, and A.L. Shanks. 2007. Wind and tidal influences on larval crab recruitment to an Oregon estuary. *Mar. Eco. Prog. Ser.*, 351: 177-188.
- Shaw, R.F., B.D. Rogers, J.H. Cowan, and W.H. Herke. 1988. Ocean-estuary coupling of ichthyoplankton and nekton in the Northern Gulf of Mexico. *Am. Fish. Soc. Symp.*, 3: 77-89.
- Simonsen, K.A. and J.H. Cowan. 2013. Effects of an inshore artificial reef on the trophic dynamics of three species of estuarine fish. *Bull. Mar. Sci.*, 89:657-676.
- Smith, N.P. 1977. Meteorological and tidal exchanges between Corpus Christi Bay, Texas, and the northwestern Gulf of Mexico. *Est. Coast. Mar. Sci.*, 5: 511-520.
- Stoecker, D. and J. Govoni. 1984. Food selection by young larval gulf menhaden (*Brevoortia patronus*). *Mar. Bio.*, 80:299-306.
- Stone, G.W., B. Liu, D.A. Pepper, and P. Wang. 2004. The importance of extratropical and tropical cyclones on the short-term evolution of barrier islands along the northern Gulf of Mexico, USA. *Mar. Geo.*, 210(1-4): 63-78.
- Swenson, E.M., and W.S. Chuang. 1983. Tidal and subtidal water volume exchange in an estuarine system. *Est., Coast. Shelf Sci.*, 16(3): 229-240.
- Van Voorhees, D., and A. Lowther. (ed). 2011. Fisheries of the United States, 2003. U.S. Dept. of Commerce, Nat. Mar. Fish. Serv., Silver Springs, MD, Current Fisheries Statistics 2011. 107 pp.
- Vaughan, D.S., K.W. Shertzer, and J.W. Smith. 2007. Gulf menhaden (*Brevoortia patronus*) in the U.S. Gulf of Mexico: fishery characteristics and biological reference points for management. *Fish. Res.*, 83:263-275.
- Vaughan, D.S., J.W. Smith, and A.M. Schueller. 2010. Age, growth, and reproduction of gulf menhaden. Southeast data, assessment, and Review SEDAR 27-DW02. 34 pp.
- Vinagre, C., F.D. Santos, H.N. Cabral, and M.J. Costa. 2009. Impact of climate and hydrology on juvenile fish recruitment towards estuarine nursery grounds in the context of climate change. *Est., Coast. Shelf Sci.*, 85(3): 479-486.

- Walker, N.D., and A.B. Hammack. 2000. Impacts of winter storms on circulation and sediment transport: Atchafalaya-Vermilion Bay region, Louisiana, USA. *J. Coast. Res.*, 16(4): 996-1010.
- Wang, F. 1997. Dynamics of intertidal marshes near shallow estuaries in Louisiana. *Wetlands Ecol. Man.*, 5: 131-143.
- Yatsu, A., C. Sassa, M. Moku, and T. Kinoshita. 2005. Night-time vertical distribution and abundance of small epipelagic and mesopelagic fishes in the upper 100m layer of the Kuroshio-Oyashio Transition Zone in spring. *Fish. Sci.* 71: 1280 – 1286.

CHAPTER 2. VERTICAL DISTRIBUTION OF ICHTHYOPLANKTON AND COMMERCIALY-IMPORTANT DECAPODS IN THE NORTH-CENTRAL GULF OF MEXICO

Ichthyoplankton and commercially-important decapod vertical distribution patterns were analyzed from the Louisiana Department of Wildlife and Fisheries' Louisiana Offshore Oil Port (LOOP) sampling program across a depth range of 7.6 to 37 m from 1978 to 1995. Analyses used sampling gear and protocol to divide the water column into horizontally-stratified depth bins, i.e., surface tows, surface, mid-water and near-bottom bongo tows, and two, half-water-column, oblique tows. Of the 321 taxa identified for analysis, 125 were found to have statistically significant depth differences. In addition to these statistically significant findings, 75 taxa were found distributed exclusively in horizontal surface tows only; three taxa were collected exclusively at mid-depth; and three in near-bottom horizontal bongo net tows. In general, within the horizontally-stratified samples, species richness, i.e., total taxa collected, total density, and mean variability declined with water depth.

2.1 Introduction

Understanding the vertical distributional pattern of larval fish and invertebrates in the marine environment has long been recognized as being important for ecological and fisheries analyses (Ahlstrom, 1959; Finucane et al., 1977; Lang, 2012). In many regions of the world with major fisheries, data are available on the vertical distributions of finfish and invertebrates abundances (Yatsu et al., 2005). In the Gulf of Mexico (GOM), however, there is a general lack of ichthyoplankton studies dealing with multi-species depth preferences over protracted time scales (Hernandez et al., 2003; Lindquist et al., 2005; Carassou et al., 2012). What little that is known about the vertical distribution of ichthyoplankton in the northern GOM has recently been reviewed by Shaw (unpublished manuscript in review). This is somewhat surprising given that Louisiana ranks second in U.S. commercial fisheries landings and fourth in

dockside value (Van Voorhees and Lowther, 2011). The absence of such empirical data in association with a high number of confounding biotic interactions and abiotic forcing functions makes modeling the vertical distribution of zoo-/ichthyoplankton very difficult. Some of those confounding factors include: the high variability associated with water column physics (e.g., thermohaline stratification, wind mixing, presence or absence of river plumes and associated convergence and divergence zones/fronts, coastal boundary layers, etc. (Auth and Brodeur, 2006; Muhling and Beckley, 2007; Carassou et al., 2012); the resultant spatial variation associated with motile, feeding or diel migratory behavior (Braztikovich, 1988); and plankton patchiness.

Obviously zoo-/ichthyoplankton vertical distribution data have ecological and environmental impact applications. For example, such vertical data would be helpful in determining potential vulnerabilities to oil spills such as the Deepwater Horizon Macondo blowout (20 April 2010) that occurred 66 km off the Louisiana coast in approximately 1600 m depth (Cleveland, 2011; Graham et al., 2012). In addition, normal production at offshore oil and gas platforms as well as proposed offshore Liquefied Natural Gas (LNG) port facilities can use ambient seawater for a number of different purposes, and can have authorized and/or accidental discharges at the surface and at depth. In the case of LNG facilities, it has been estimated that 76 million to 176 million gallons·day⁻¹ per facility of ambient seawater could be taken at depth for use in their proposed, radiator-like open-loop (i.e., single pass through) re-gasification systems (Helvarg, 2006). Clearly such vertical distribution data would facilitate more accurate prediction of oil spill vulnerability and could significantly reduce offshore, platform-related potential impingement, entrainment and discharge mortalities of commercially-, recreationally-, or ecologically-important planktonic organisms.

2.2 Materials and Methods

The Louisiana Offshore Oil Port (LOOP) is located off central Louisiana (98° 53' 06.06" N, 90° 01' 30.18" W) and is the only U.S. superport for off-loading deep draft oil tankers. The entire facility stretches from the continental shelf port platform 30 kilometers offshore across the coast and then across 50 kilometers of terrestrial landscape until it reaches the inshore storage facility, Clovelly Storage Dome, near Galliano, Louisiana. Oil is transported through a large diameter pipeline that receives a flow boost from a pumping station near the port of Fourchon (Shaw et al., 1998).

The initial environmental assessment and subsequent monitoring program for the LOOP project provided an environmental data set from 1978 to 1995 and incorporated sampling for both ichthyoplankton and zooplankton. This is the most comprehensive, vertically-stratified, sampling effort in the northern GOM to date.

For the purposes of this inner continental shelf analysis, only station locations with a water depth greater than 7.6 meters (m) were included (range 7.6 m – 37 m). Of the complete suite of LOOP sampling sites, which also included freshwater and estuarine locations, 78 sampling sites (92 stations) were included in this shelf plankton analysis (Table 2.1; Figure 2.1). Through time a number of these sampling sites were regrouped and/or combined into different sampling station numbers making it somewhat difficult to continually trace the sampling history at a given location. Therefore, we took the approach of trying to determine the vertical distributions of plankton within the depth zone selected (7.6 m – 37 m station depth) regardless of the actual location. For most of the collection sites, sampling was conducted monthly and mostly during daylight hours. A number of stations through time had a combination of monthly,

quarterly, and nocturnal sampling, while a few others were only sampled quarterly. Therefore, no effort was made herewithin to analyze the vertical distribution results by seasons, and there were also no available data on fish eggs. However, monthly densities for both zooplankton and combined into different station numbers, so not all station numbers are represented on the maps, but all sampling sites are represented (See Table 2.1). ichthyoplankton have been reported for the 0.5 and 1.0 m ring nets and the 60-centimeter (cm) bongo net collections for all LOOP stations combined within the final environmental impact report of the LOOP Marine and Estuarine Monitoring Program, 1978 - 1995 (Shaw et al., 1998; tables II-A to II-F7).

Plankton collections were taken using a number of different sampling gears and protocols. Surface plankton collections were taken with 0.5 m ring nets that used both 80 and 0.153-millimeter (mm) net mesh and had tow durations of one minute. The surface was also sampled with 1 m ring nets with 0.363 mm mesh. In addition, 60 cm, hinged, opening and closing, bongo nets with 0.363 mm mesh were also used to discretely sample the surface, mid-depth, and near-bottom. At deeper sampling stations, opening and closing bongo nets were also used to obliquely sample two halves of the water column discretely, i.e., from near-bottom to mid-depth and from mid-depth to surface. With the exception of the 0.5 m ring net, all other horizontally stratified and all obliquely towed collections had tow durations of approximately 3-5 minutes.

All samples were identified to the lowest taxonomic level possible, i.e., at least to the family level, with most being identified to genus and/or species. Identifications were based on the following literature: Miller and Jorgenson (1973); Fritzsche (1978); Hardy (1978a, 1978b);

Table 2.1: Louisiana Offshore Oil Platform (LOOP) sampling stations which met our depth criteria of approximately 8 m depth or greater, their latitudes and longitudes, and mean water column depth in meters. Through the course of the study (1978-1995), a number of these sampling sites were regrouped and/or combined into different sampling station numbers.

Station No.	Latitude (N)	Longitude (W)	Depth (m)
4	29.1833	89.9000	12.2
35, 335, 435, 535, 829	29.1228	90.0833	10.8
36	29.1000	90.1150	11.0
44	28.9317	90.5250	9.2
50	28.8089	90.0764	37.0
51	28.9450	90.0308	28.0
52, 482	28.9133	89.9847	34.0
53, 481	28.8850	90.0250	34.0
54, 479	28.9367	90.0686	27.0
55	28.8633	90.0253	34.5
306, 472	29.0967	90.1108	10.0
318	29.1044	90.1131	11.0
319	29.0950	90.1608	7.6
336, 470, 825	29.0906	90.1231	10.4
337, 469	29.0964	90.1267	9.5
467	29.1047	90.1292	8.8
468, 830	29.0997	90.1217	9.8
471, 828	29.0872	90.1161	12.2
473	29.1003	90.1133	8.8
474	29.0978	90.1147	8.8
475	29.1003	90.1167	9.5
476	29.1031	90.1153	8.5
477	29.0358	90.0967	15.2
478	29.0358	90.0867	15.2
480	28.9361	90.0597	27.0
484	28.8511	90.0717	34.0
485	28.8661	90.0153	37.0
486	28.8792	90.0025	34.0
487	29.0903	90.1056	12.8
500	29.1039	90.1183	9.0
501	29.0964	90.1183	9.0
502	29.0972	90.1114	10.0
505	29.0956	90.0861	11.0
506	29.0872	90.1178	10.0

Table 2.1 *Continued*:

Station No.	Latitude (N)	Longitude (W)	Depth (m)
507	29.0894	90.1022	11.0
557, 857	29.1017	90.1236	8.8
701	29.0967	90.1117	9.7
702	29.0672	90.1056	12.7
703	29.0367	90.0950	15.2
704	28.9961	90.0831	19.4
705	28.9742	90.0794	22.4
706	28.9417	90.0694	26.1
707	28.9092	90.0456	30.6
708	28.8842	90.0250	33.0
709	29.1067	90.1183	8.4
710	29.1119	90.1242	7.7
711	28.7847	90.1461	33.5
713	28.8492	90.1650	27.4
715	28.9150	90.1833	21.3
717	28.9797	90.2011	15.5
719	29.0428	90.2186	9.1
788	28.8947	90.0283	32.6
798	28.8756	90.0197	34.4
801	29.1047	90.1078	9.8
802	29.1031	90.1097	9.9
803	29.1022	90.1119	10.1
804	29.1011	90.1142	9.9
805	29.0994	90.1161	10.1
806	29.0978	90.1178	9.4
807	29.0961	90.1197	9.3
808	29.1033	90.1156	9.1
809	29.1006	90.1144	10.0
810	29.0989	90.1131	10.1
811	29.0967	90.1114	10.1
812	29.0978	90.1103	9.5
813	29.0994	90.1119	9.2
814	29.1100	90.1136	9.5
815	29.1028	90.1147	10.4
816	29.0933	90.1219	11.2
817	29.0947	90.1097	9.7

Table 2.1 *Continued*:

Station No.	Latitude (N)	Longitude (W)	Depth (m)
818	29.0956	90.1086	9.5
819	29.1064	90.1056	9.8
820	29.1047	90.1167	9.3
821	29.1042	90.1175	9.1
822	29.1064	90.1183	9.2
823	29.1056	90.1189	9.2
824	29.1044	90.1044	11.0
826	29.1131	90.1267	9.5

Johnson (1978); Jones et al. (1978); Martin and Drewry (1978); Colton et al. (1979); Leak (1981); Houde (1982); Stuck and Perry (1982); Fahay (1983); Moser (1984); and Ruple (1984).

Individual taxa counts from net collections were converted to density, i.e., the number of individuals per volume (m^3) of water filtered was standardized to a volume of 100 m^3 , and log-transformed, i.e., $\log_{10}(\text{density} + 1)$, for the purposes of meeting the assumptions of the Analysis of Variance (ANOVA). The depth bins used in the analysis were determined by the sampling gear's trajectory in the water column. The statistical model used in the analyses was a mixed effects analysis of variance (Mixed ANOVA; SAS, version 9.3, SAS Inst., Inc., Cary, NC) with depth as the fixed effect. The linear model has the following form:

$$y_{ijk} = \mu + \alpha_i + \beta_j + \varepsilon_{ijk}$$

where y_{ijk} is the dependent response of $\log_{10}(\text{density} + 1)$, μ is the overall response mean, α_i is the fixed main effect of level i of the factor of interest, depth, subject to the constraint $\sum \alpha_i = 0$, β_j is the main effect of level j of the random effect time, with $\beta_j \sim N(0, \sigma_\beta^2)$, and ε_{ij} is the overall

error term $\sim N(0, \sigma^2)$, including the interaction term to boost power. The model was applied to each taxa for all portions of the water column. All LOOP sampling efforts that fit within the

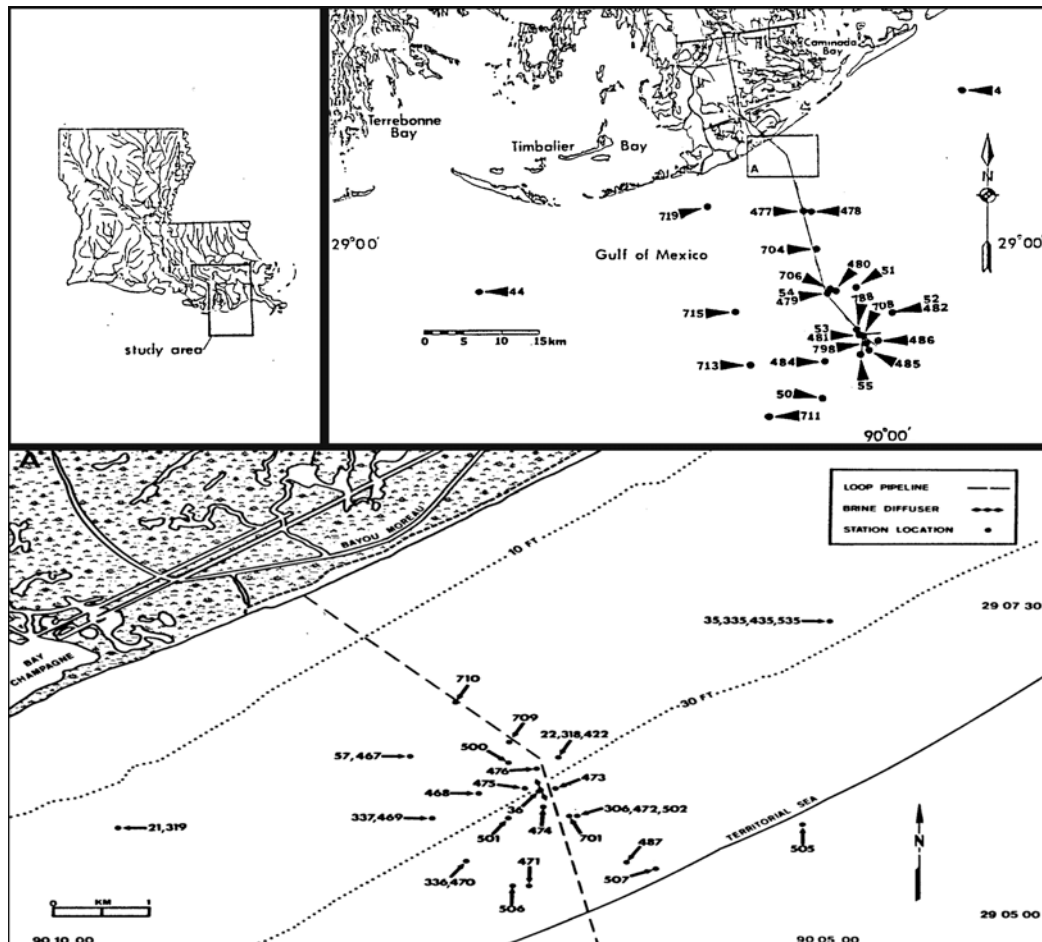


Figure 2.1: Map of the study area and Louisiana Offshore Oil Platform (LOOP) sampling locations in coastal Louisiana, USA. Insert A is in the vicinity of the LOOP brine diffuser site (station 36) where more intensive sampling took place (scale=1:51,000; modified after Hanifen 1987; Figure 1.3). Zooplankton and ichthyoplankton sampling took place at a number of sampling sites, which through the course of the study (1978-1995) were regrouped and/or combined into different station numbers, so not all station numbers are represented on the maps, but all sampling sites are represented (See Table 2.1).

depth range were used in the analysis. Seasonal encounter was computed for each taxa, and only those months where there was an expectation of encountering the taxa during sampling were

included in the analysis. Comparisons among the surface tows and the three, discrete, horizontal, bongo net tows as well as contrasts between the two (half water column) stepped-oblique tows were done using Fisher's Least Significant Difference (SAS, version 9.3, SAS Inst., Inc., Cary, NC) where appropriate. When considering multiple comparisons, critical values were adjusted with a Bonferroni correction ($p = 0.0167$) to compensate for experiment-wise error rate.

Day night catch ratios (D/N) were computed using the mean density during the day at the surface, divided by the mean density at night. Day was defined as any sampling conducted from 11:00 to 22:59 GMT (6:00 to 17:59 CST) and night as occurring from 23:00 to 10:59 GMT (18:00 to 5:59 CST). Only taxa sampled in both time categories were included in the day/night ratio analysis. There was, however, a noticeable lack of sampling at night, especially in the near-bottom depth bin, which made it impossible to distinguish between daytime visual gear avoidance in surface waters and diel vertical migration from depth.

2.3 Results

2.3.1 Ichthyoplankton

Of the 314 fish taxa identified which were sampled at some combination of depths (i.e., surface tows, surface, mid-water and near-bottom opening-closing bongo tows, or some surface collection and either the upper or lower oblique, half water column tows), 122 had statistically significant vertical distribution patterns after Bonferroni adjustment (Table 2.2 and Table 2.3, code G). In addition to these statistically significant findings, 75 fish taxa were exclusively sampled with horizontal surface gears only, yet, were not statistically analyzed against the other zero values (Table 2.3, code B). There were also three taxa, *Anchoa nasuta*, *Ophichthus ophis*, and *Serraniculus pumilio*, which were exclusively collected within mid-depth horizontal tows

(Table 2.3, code D), and three taxa, *Lestrolepis intermedia*, *Paraconger caudilmbatus*, and *Trachinocephalus myops*, in near-bottom horizontal bongo tows (Table 2.3, code E). Fifty-one taxa were sampled throughout the upper half of the water column, i.e., in the surface and mid-water depth bins and/or the upper oblique, half water column tows (Table 2.3, code C). Finally, there were only 5 taxa *Chaunax* spp., *Gadus* spp., Lampridae, *Scomberomorus regalis*, and *Scopelarchus* spp., that were sampled exclusively in the bottom half of the water column, i.e., the mid-water, near-bottom and/or lower oblique depth bins (Table 2.3, code F). In general, within the horizontally stratified sampling, species richness (i.e., total taxa collected), total density, and mean variability declined with depth.

The 122 taxa, which showed some statistical preference for a portion of the water column, comprised six general vertical functional groups: surface oriented; mid-depth oriented; near-bottom oriented; upper water column oriented; lower water column oriented; and obliquely distributed (i.e., vertically ubiquitous). Inclusion in any vertical group does not denote zero collections in any other group; rather it simply shows affinity for a particular portion of the water column with respect to all others sampled within the LOOP sampling protocols. There were 51 families of fish and the family Portunidae that showed some statistical difference in our analysis.

2.3.2 Surface Oriented

Overall there were twelve taxa which showed statistically significant preferences for the surface. There were five taxa which showed statistical preferences for surface waters in relation to the other depth bins. Leatherjacket fish, *Oligoplites saurus*, showed the most affinity towards the surface with surface densities statistically greater than all other depth bins. Four taxa had surface tow mean densities that were statistically greater, but showed no preference for any other

Table 2.2: Ichthyoplankton and economically-important decapod crustacean taxa which showed statistical differences between multiple depths in the analysis. Mean densities are given as individuals per 100 cubic meters of water filtered. Probabilities are from the Mixed ANOVA model, and were calculated for fish taxa and for decapods using Fisher's Least Significant Difference with a Bonferroni adjustment. Underlined depths indicate greater statistical densities. Surf = surface tows (0.5 and 1-m ring nets and surface 60-cm bongo net tows) ; Mid = mid-water bongo tows ; NB = near-bottom bongo tows ; UO = upper half water column oblique tow ; LO = lower half water column oblique tow ; VS or v= versus.

Family	Fish Taxa	Depth	Density	VS	Prob.	Additional VS of Note	Prob.
Achiridae	<i>Trinectes maculatus</i> (hogchoacker)	Surf	0.0009	Surf v Mid	1.0000	Surf v <u>LO</u>	<0.0001
		Mid	0	Surf v NB	1.0000	Mid v <u>LO</u>	0.0006
		NB	0	Mid v NB	1.0000	NB v <u>LO</u>	0.0007
						UO v <u>LO</u>	0.0026
Ariommatidae	<i>Ariomma</i> spp. (butterfishes)	Surf	0.0762	Surf v Mid	1.0000	Surf v <u>UO</u>	0.0211
		Mid	0.0302	Surf v NB	0.5210	Mid v <u>UO</u>	0.0096
		NB	0.0094	Mid v NB	1.0000	NB v <u>UO</u>	0.0016
Atherinidae	Atherinidae (silversides)	Surf	0.0074	Surf v Mid	0.0974	<u>Surf</u> v UO	0.0163
		Mid	0	Surf v NB	0.0580		
		NB	0.0143	Mid v NB	1.0000		
Blenniidae	Blenniidae (blennies)	Surf	3.3614	<u>Surf</u> v Mid	<0.0001	<u>Surf</u> v UO	0.0023
		Mid	0.9107	<u>Surf</u> v NB	<0.0001	<u>Surf</u> v LO	<0.0001
		NB	0.3546	Mid v NB	0.1918	Mid v <u>UO</u>	<0.0001
						NB v <u>UO</u>	<0.0001
						<u>UO</u> v LO	<0.0001
Bothidae	Bothidae (left-eye flounders)	Surf	0.0323	Surf v <u>Mid</u>	0.0016	Surf v <u>LO</u>	0.0047
		Mid	0.1983	Surf v NB	1.0000		
		NB	0.0524	Mid v NB	0.3390		
	<i>Bothus</i> spp. (left-eye flounder)	Surf	0.0058	Surf v Mid	1.0000	Surf v <u>UO</u>	<0.0001
		Mid	0	Surf v NB	1.0000	Mid v <u>UO</u>	<0.0001
		NB	0	Mid v NB	1.0000	NB v <u>UO</u>	<0.0001
						<u>UO</u> v LO	0.0003
	<i>Engyophrys senta</i> (American spiny flounder)	Surf	0.0025	Surf v Mid	1.0000	Surf v <u>UO</u>	<0.0001
		Mid	0.0111	Surf v NB	1.0000	Surf v <u>LO</u>	<0.0001
		NB	0.0189	Mid v NB	1.0000	Mid v <u>UO</u>	<0.0001
						Mid v <u>LO</u>	<0.0001
						NB v <u>UO</u>	<0.0001
						NB v <u>LO</u>	0.0003
	<i>Trichopsetta ventralis</i> (sash flounder)	Surf	0.0139	Surf v Mid	1.0000	Surf v <u>UO</u>	<0.0001
		Mid	0	Surf v NB	1.0000	Mid v <u>UO</u>	<0.0001
		NB	0	Mid v NB	1.0000	NB v <u>UO</u>	<0.0001
						<u>UO</u> v LO	0.0050

Table 2.2 *Continued*:

Family	Fish Taxa	Depth	Density	VS	Prob.	Additional VS of Note	Prob.
Bregmacerotidae	<i>Bregmaceros</i> spp. (codlets)	Surf	0.0266	Surf v Mid	0.8238	<u>NB</u> v <u>UO</u>	<0.0001
		Mid	0.1362	Surf v <u>NB</u>	<0.0001	<u>NB</u> v <u>LO</u>	<0.0001
		NB	1.622	Mid v <u>NB</u>	<0.0001		
	<i>Bregmaceros atlanticus</i> (antenna codelt)	Surf	0.0112	Surf v Mid	1.0000	Surf v <u>UO</u>	<0.0001
		Mid	0.0397	Surf v NB	1.0000	Surf v <u>LO</u>	0.0030
		NB	0.0094	Mid v NB	1.0000	Mid v <u>UO</u>	0.0460
						NB v <u>UO</u>	0.0003
						NB v <u>LO</u>	0.0468
	<i>Bregmaceros cantori</i> (striped codelt)	Surf	0.301	Surf v Mid	1.0000	Surf v <u>UO</u>	<0.0001
		Mid	0.8978	Surf v NB	1.0000	Surf v <u>LO</u>	<0.0001
		NB	0.1157	Mid v NB	1.0000	Mid v <u>UO</u>	<0.0001
						Mid v <u>LO</u>	<0.0001
						NB v <u>UO</u>	<0.0001
						NB v <u>LO</u>	<0.0001
						UO v <u>LO</u>	<0.0001
Carangidae	Carangidae (jacks)	Surf	0.6866	Surf v Mid	1.0000	<u>Surf</u> v <u>UO</u>	0.0464
		Mid	3.5086	Surf v NB	0.9916	<u>Surf</u> v <u>LO</u>	0.0010
		NB	0.3337	Mid v NB	0.8946	<u>Mid</u> v <u>LO</u>	0.0093
	<i>Caranx</i> spp. (jacks)	Surf	0.0792	Surf v Mid	0.9851	Surf v <u>UO</u>	<0.0001
		Mid	0	Surf v NB	1.0000	Mid v <u>UO</u>	<0.0001
		NB	0	Mid v NB	1.0000	NB v <u>UO</u>	<0.0001
						<u>UO</u> v <u>LO</u>	<0.0001
	<i>Chloroscombrus chrysurus</i> (Atlantic bumper)	Surf	8.1095	Surf v <u>Mid</u>	<0.0001	Surf v <u>UO</u>	0.0028
		Mid	83.9297	Surf v NB	1.0000	<u>Mid</u> v <u>LO</u>	<0.0001
		NB	16.9541	<u>Mid</u> v NB	0.0007	UO v <u>LO</u>	0.0077
	<i>Decapterus punctatus</i> (round scad)	Surf	0.1077	Surf v Mid	0.8178	Surf v <u>UO</u>	0.0445
		Mid	0	Surf v NB	0.8698	Mid v <u>UO</u>	0.0044
		NB	0	Mid v NB	1.0000	NB v <u>UO</u>	0.0051
						<u>UO</u> v <u>LO</u>	0.0453
	<i>Oligoplites saurus</i> (leatherjack)	Surf	0.3741	<u>Surf</u> v Mid	0.0089	<u>Surf</u> v <u>UO</u>	0.0032
		Mid	0	<u>Surf</u> v NB	0.0134	<u>Surf</u> v <u>LO</u>	0.0053
		NB	0	Mid v NB	1.0000		
	<i>Selar crumenophthalmus</i> (bigeye scad)	Surf	0.0652	Surf v Mid	1.0000	NB v <u>UO</u>	0.0077
		Mid	0.0238	Surf v NB	0.7577		
		NB	0.0038	Mid v NB	1.0000		
	<i>Selene setapinnis</i> (Atlantic moonfish)	Surf	0	Surf v Mid	1.0000	Surf v <u>UO</u>	0.0032
		Mid	0	Surf v NB	1.0000		
		NB	0	Mid v NB	1.0000		

Table 2.2 *Continued*:

Family	Fish Taxa	Depth	Density	VS	Prob.	Additional VS of Note	Prob.
Carangidae	<i>Selene vomer</i> (lookdown)	Surf	0	Surf v Mid	1.0000	Surf v <u>UO</u>	< 0.0001
		Mid	0	Surf v NB	1.0000	Mid v <u>UO</u>	0.0024
		NB	0	Mid v NB	1.0000	NB v <u>UO</u>	0.0027
	<i>Trachurus lathami</i> (rough scad)	Surf	0.0276	Surf v Mid	1.0000	Surf v <u>UO</u>	< 0.0001
		Mid	0.0543	Surf v NB	1.0000	Surf v <u>LO</u>	0.0037
		NB	0.0132	Mid v NB	1.0000	Mid v <u>UO</u>	0.0390
	<i>Trichiurus lepturus</i> (largehead hairtail)	Surf	1.9195	Surf v Mid	1.0000	NB v <u>UO</u>	0.0012
						Surf v <u>UO</u>	< 0.0001
						Surf v <u>LO</u>	< 0.0001
						Mid v <u>UO</u>	< 0.0001
						Mid v <u>LO</u>	< 0.0001
						NB v <u>UO</u>	< 0.0001
Caulophrynidae	Caulophrynidae (anglerfishes)	Surf	0.0005	Surf v Mid	1.0000	NB v <u>LO</u>	< 0.0001
		Mid	0	Surf v NB	1.0000	UO v <u>LO</u>	0.0009
		NB	0	Mid v NB	1.0000		0.0016
							0.0031
Centriscidae	<i>Macrorhamphosus scolopax</i> (longspine snipefish)	Surf	0.1004	Surf v Mid	0.8014	Surf v <u>UO</u>	0.0002
		Mid	0	Surf v NB	1.0000	Mid v <u>UO</u>	< 0.0001
		NB	0	Mid v NB	1.0000	NB v <u>UO</u>	0.0002
						UO v <u>LO</u>	0.0106
Clupeidae	<i>Brevoortia gunteri</i> (finescale menhaden)	Surf	0.231	Surf v Mid	1.0000	Surf v <u>UO</u>	0.0021
		Mid	0.0324	Surf v NB	1.0000	Mid v <u>UO</u>	0.0008
		NB	0.9968	Mid v NB	0.2992	UO v <u>LO</u>	0.0086
	<i>Brevoortia patronus</i> (Gulf menhaden)	Surf	17.921	Surf v Mid	0.3311	Surf v <u>UO</u>	< 0.0001
		Mid	14.0732	Surf v NB	0.0003	Mid v <u>UO</u>	< 0.0001
		NB	12.5076	Mid v NB	1.0000	NB v <u>UO</u>	< 0.0001
	<i>Brevoortia</i> spp. (menhaden)	Surf	0.4278	Surf v Mid	0.7922	UO v <u>LO</u>	< 0.0001
		Mid	0.6014	Surf v NB	1.0000	Mid v <u>UO</u>	0.0491
		NB	1.3844	Mid v NB	1.0000	Mid v <u>LO</u>	0.0228
	<i>Harengula pensacolatae</i> (scaled herring)	Surf	1.821	Surf v Mid	1.0000	Mid v <u>UO</u>	< 0.0001
		Mid	2.3823	Surf v NB	0.1029	Surf v <u>LO</u>	< 0.0001
		NB	0.3222	Mid v NB	0.0313	Mid v <u>UO</u>	< 0.0001
	<i>Opisthonema oglinum</i> (Atlantic thread herring)	Surf	7.8547	Surf v Mid	< 0.0001	Mid v <u>LO</u>	0.0001
						Surf v <u>LO</u>	< 0.0001
						Mid v <u>UO</u>	< 0.0001
						Mid v <u>LO</u>	< 0.0001
		Mid	37.2805	Surf v NB	0.0006	NB v <u>LO</u>	< 0.0001
		NB	18.4867	Mid v NB	0.0269	UO v <u>LO</u>	0.0064

Table 2.2 *Continued*:

Family	Fish Taxa	Depth	Density	VS	Prob.	Additional VS of Note	Prob.
Congridae	Congridae (conger eels)	Surf	0.0014	Surf v Mid	1.0000	Surf v <u>UO</u>	< 0.0001
		Mid	0	Surf v NB	1.0000	Mid v <u>UO</u>	0.0023
		NB	0	Mid v NB	1.0000	NB v <u>UO</u>	0.0027
Cynoglossidae	<i>Symphurus</i> spp. (tonguefish)	Surf	0.7243	Surf v <u>Mid</u>	0.0215	Surf v <u>UO</u>	< 0.0001
		Mid	1.5083	Surf v NB	1.0000	Surf v <u>LO</u>	< 0.0001
		NB	1.3495	Mid v NB	1.0000	Mid v <u>UO</u>	< 0.0001
						Mid v <u>LO</u>	< 0.0001
						NB v <u>UO</u>	< 0.0001
						NB v <u>LO</u>	< 0.0001
						<u>UO</u> v LO	0.0235
	<i>Symphurus plagiusa</i> (blackcheek tonguefish)	Surf	0.0092	Surf v Mid	1.0000	Surf v <u>UO</u>	0.0344
		Mid	0	Surf v NB	1.0000		
		NB	0	Mid v NB	1.0000		
Dussumieriidae	<i>Etrumeus teres</i> (round herring)	Surf	0.3317	Surf v Mid	1.0000	Surf v <u>UO</u>	< 0.0001
		Mid	0.0236	Surf v NB	1.0000	Surf v <u>LO</u>	< 0.0001
		NB	0.0433	Mid v NB	1.0000	Mid v <u>UO</u>	< 0.0001
						Mid v <u>LO</u>	< 0.0001
						NB v <u>UO</u>	< 0.0001
						NB v <u>LO</u>	< 0.0001
Elopidae	<i>Elops saurus</i> (ladyfish)	Surf	0	Surf v Mid	1.0000	Surf v <u>LO</u>	0.0056
		Mid	0	Surf v NB	1.0000		
		NB	0	Mid v NB	1.0000		
Engraulidae	Engraulidae (anchovies)	Surf	47.7949	Surf v Mid	1.0000	Surf v <u>UO</u>	< 0.0001
		Mid	108.229	<u>Surf</u> v NB	0.0021	<u>Mid</u> v <u>UO</u>	0.0187
		NB	18.0221	<u>Mid</u> v NB	0.0005	NB v <u>UO</u>	< 0.0001
						<u>UO</u> v LO	< 0.0001
	<i>Anchoa</i> spp. (anchovies)	Surf	14.6403	Surf v Mid	1.0000	<u>Surf</u> v UO	0.0008
		Mid	6.394	Surf v NB	1.0000	<u>Surf</u> v LO	0.0010
		NB	3.1229	Mid v NB	1.0000	<u>Mid</u> v UO	0.0230
						<u>Mid</u> v LO	0.0248
	<i>Anchoviella</i> spp. (anchovies)	Surf	0.0065	Surf v Mid	1.0000	Surf v <u>UO</u>	0.0284
		Mid	0	Surf v NB	1.0000		
		NB	0	Mid v NB	1.0000		
	<i>Anchoviella perfasciata</i> (Poey's anchovy)	Surf	0.0108	Surf v <u>Mid</u>	< 0.0001	<u>Mid</u> v UO	0.0011
		Mid	0.1073	Surf v NB	1.0000	<u>Mid</u> v LO	0.0002
		NB	0	<u>Mid</u> v NB	0.0013		
Ehippidae	<i>Chaetodipterus faber</i> (Atlantic spadefish)	Surf	0.1747	Surf v <u>Mid</u>	< 0.0001	Surf v <u>UO</u>	0.0187
		Mid	5.6436	Surf v NB	1.0000	<u>Mid</u> v <u>UO</u>	0.0001
		NB	0.248	<u>Mid</u> v NB	< 0.0001	<u>Mid</u> v LO	< 0.0001
						<u>UO</u> v LO	0.0452

Table 2.2 *Continued*:

Family	Fish Taxa	Depth	Density	VS	Prob.	Additional VS of Note	Prob.
Ephippidae	Ephippidae (batfishes)	Surf	0.0035	Surf v Mid	1.0000	Surf v <u>UO</u>	< 0.0001
		Mid	0	Surf v NB	1.0000	Mid v <u>UO</u>	0.0032
		NB	0	Mid v NB	1.0000	NB v <u>UO</u>	0.0041
						<u>UO</u> v LO	0.0013
Gadidae	Gadidae (cod/haddock/whiting/pollock)	Surf	0.01	Surf v Mid	1.0000	Surf v <u>UO</u>	0.0139
		Mid	0	Surf v NB	1.0000	Mid v <u>UO</u>	0.0331
		NB	0	Mid v NB	1.0000	NB v <u>UO</u>	0.0410
Gempylidae	Gempylidae (snake mackerels)	Surf	0.0071	Surf v Mid	1.0000	Surf v <u>UO</u>	< 0.0001
		Mid	0	Surf v NB	1.0000	Mid v <u>UO</u>	< 0.0001
		NB	0	Mid v NB	1.0000	NB v <u>UO</u>	0.0001
						<u>UO</u> v LO	< 0.0001
	<i>Diplospinus multistriatus</i> (striped escolar)	Surf	0.0122	Surf v Mid	1.0000	Surf v <u>UO</u>	0.0018
		Mid	0	Surf v NB	1.0000	Mid v <u>UO</u>	0.0029
		NB	0	Mid v NB	1.0000	NB v <u>UO</u>	0.0031
Gobiidae	Gobiidae (gobies)	Surf	0.7604	Surf v Mid	1.0000	Surf v <u>UO</u>	< 0.0001
		Mid	0.2768	Surf v NB	0.1773	Surf v <u>LO</u>	< 0.0001
		NB	1.3685	Mid v NB	0.1955	Mid v <u>UO</u>	< 0.0001
						Mid v <u>LO</u>	< 0.0001
						NB v <u>UO</u>	< 0.0001
						NB v <u>LO</u>	< 0.0001
Gobiesocidae	Gobiesocidae (clingfishes)	Surf	0.0026	Surf v Mid	1.0000	Surf v <u>UO</u>	0.0038
		Mid	0	Surf v NB	1.0000	Mid v <u>UO</u>	0.0323
		NB	0	Mid v NB	1.0000	NB v <u>UO</u>	0.0382
						<u>UO</u> v LO	0.0234
	<i>Gobiesox strumosus</i> (skilletfish)	Surf	0.1653	<u>Surf</u> v Mid	0.0049		
		Mid	0	<u>Surf</u> v NB	0.0204		
		NB	0.0095	Mid v NB	1.0000		
Gonostomatidae	Gonostomatidae (bristlemouths)	Surf	0.0936	Surf v Mid	0.6414	Surf v <u>UO</u>	< 0.0001
		Mid	0	Surf v NB	1.0000	Mid v <u>UO</u>	< 0.0001
		NB	0.0043	Mid v NB	1.0000	NB v <u>UO</u>	< 0.0001
						<u>UO</u> v LO	< 0.0001
Haemulidae	<i>Orthopristis chrysoptera</i> (pigfish)	Surf	0.11	Surf v Mid	1.0000	<u>NB</u> v UO	0.0091
		Mid	0	Surf v <u>NB</u>	0.0328	<u>NB</u> v LO	0.0091
		NB	0.4994	Mid v NB	0.0637		
Labridae	Labridae (wrasses)	Surf	0.0176	Surf v Mid	1.0000	Surf v <u>UO</u>	0.0005
		Mid	0.0292	Surf v NB	1.0000	NB v <u>UO</u>	0.0146
		NB	0.0078	Mid v NB	1.0000	<u>UO</u> v LO	0.0137

Table 2.2 *Continued*:

Family	Fish Taxa	Depth	Density	VS	Prob.	Additional VS of Note	Prob.
Lutjanidae	Lutjanidae (snappers)	Surf	0.0011	Surf v Mid	1.0000	Surf v <u>UO</u>	< 0.0001
		Mid	0	Surf v NB	1.0000	Mid v <u>UO</u>	0.0010
		NB	0	Mid v NB	1.0000	NB v <u>UO</u>	0.0014
	<i>Lutjanus</i> spp. (snapper)	Surf	0.0592	Surf v Mid	1.0000	Surf v <u>UO</u>	0.0006
		Mid	0.02	Surf v NB	1.0000	Mid v <u>UO</u>	0.0010
		NB	0.097	Mid v NB	1.0000		
	<i>Lutjanus campechanus</i> (red snapper)	Surf	0.0051	Surf v Mid	1.0000	Surf v <u>UO</u>	0.0179
		Mid	0	Surf v NB	1.0000	Mid v <u>LO</u>	0.0476
		NB	0	Mid v NB	1.0000		
Microdesmidae	<i>Microdesmus</i> spp. (wormfish)	Surf	0.0941	Surf v Mid	1.0000	Surf v <u>UO</u>	< 0.0001
		Mid	0.0814	Surf v NB	1.0000	Mid v <u>UO</u>	< 0.0001
		NB	0.057	Mid v NB	1.0000	NB v <u>UO</u>	< 0.0001
	<i>Microdesmus lanceolatus</i> (lancetail wormfish)					<u>UO</u> v <u>LO</u>	< 0.0001
		Surf	0.044	Surf v Mid	1.0000		
		Mid	0	Surf v <u>NB</u>	0.0427		
Moringuidae	<i>Neoconger mucronatus</i> (ridged eel)	NB	0.2574	Mid v NB	0.1575		
		Surf	0.0072	Surf v Mid	1.0000	Surf v <u>LO</u>	0.0005
		Mid	0	Surf v NB	1.0000	Mid v <u>LO</u>	0.0045
Mugilidae	<i>Mugil</i> spp. (mullet)	NB	0.0071	Mid v NB	1.0000	NB v <u>LO</u>	0.0128
		Surf	0.0057	Surf v Mid	1.0000	Surf v <u>UO</u>	< 0.0001
		Mid	0	Surf v NB	1.0000	Surf v <u>LO</u>	0.0003
		NB	0	Mid v NB	1.0000	Mid v <u>UO</u>	0.0007
						Mid v <u>LO</u>	0.0125
						NB v <u>UO</u>	0.0009
	<i>Mugil cephalus</i> (flathead mullet)					NB v <u>LO</u>	0.0149
		Surf	0.889	Surf v Mid	0.0663	Surf v <u>UO</u>	< 0.0001
		Mid	0.0658	<u>Surf</u> v NB	0.0093	Mid v <u>UO</u>	< 0.0001
		NB	0.0061	Mid v NB	1.0000	NB v <u>UO</u>	< 0.0001
						<u>UO</u> v <u>LO</u>	< 0.0001
Mullidae	Mullidae (goat fishes)	Surf	0.0818	Surf v Mid	0.0952	<u>Surf</u> v <u>LO</u>	0.0071
		Mid	0.0106	<u>Surf</u> v NB	0.0329		
		NB	0	Mid v NB	1.0000		
Muraenidae	Muraenidae (moray eels)	Surf	0.0024	Surf v Mid	1.0000	Surf v <u>UO</u>	< 0.0001
		Mid	0.2176	Surf v NB	1.0000	Surf v <u>LO</u>	< 0.0001
		NB	0	Mid v NB	1.0000	Mid v <u>UO</u>	< 0.0001
						Mid v <u>LO</u>	0.0001
						NB v <u>UO</u>	< 0.0001
						NB v <u>LO</u>	< 0.0001

Table 2.2 *Continued*:

Family	Fish Taxa	Depth	Density	VS	Prob.	Additional VS of Note	Prob.
Myctophidae	Myctophidae (lanternfishes)	Surf	1.0168	Surf v Mid	0.1903	Surf v <u>UO</u>	< 0.0001
		Mid	0.368	<u>Surf</u> v NB	0.0014	Surf v <u>LO</u>	< 0.0001
		NB	0.1926	Mid v NB	1.0000	Mid v <u>UO</u>	< 0.0001
						Mid v <u>LO</u>	< 0.0001
						NB v <u>UO</u>	< 0.0001
						NB v <u>LO</u>	< 0.0001
						<u>UO</u> v LO	< 0.0001
	<i>Hygophum</i> spp. (lanternfish)	Surf	0.0734	Surf v Mid	1.0000	Surf v <u>UO</u>	< 0.0001
		Mid	0.0656	Surf v NB	1.0000	Mid v <u>UO</u>	0.0219
		NB	0	Mid v NB	1.0000	NB v <u>UO</u>	0.0005
						<u>UO</u> v LO	0.0009
	<i>Hygophum taaningi</i> (Tåning's lanternfish)	Surf	0	Surf v <u>Mid</u>	0.0094	<u>Mid</u> v UO	0.0411
		Mid	0.0884	Surf v NB	1.0000	<u>Mid</u> v LO	0.0411
		NB	0	Mid v NB	0.2679		
Nettastomatidae	Nettastomatidae (duckbill/witch eels)	Surf	0.0046	Surf v Mid	1.0000	Surf v <u>UO</u>	0.0037
		Mid	0.0217	Surf v NB	1.0000		
		NB	0	Mid v NB	1.0000		
Ophichthidae	Ophichthidae (snake eels)	Surf	0.0303	Surf v Mid	1.0000	Surf v <u>UO</u>	< 0.0001
		Mid	0	Surf v NB	1.0000	Surf v <u>LO</u>	< 0.0001
		NB	0.0371	Mid v NB	1.0000	Mid v <u>UO</u>	< 0.0001
						Mid v <u>LO</u>	< 0.0001
						NB v <u>UO</u>	< 0.0001
						NB v <u>LO</u>	< 0.0001
	<i>Myrophis punctatus</i> (speckled worm eel)	Surf	0.0983	Surf v Mid	1.0000	Surf v <u>LO</u>	< 0.0001
		Mid	0.0804	Surf v NB	1.0000	Mid v <u>LO</u>	< 0.0001
		NB	0.1658	Mid v NB	1.0000	NB v <u>LO</u>	0.0001
						UO v <u>LO</u>	0.0005
	<i>Ophichthus</i> spp. (snake eel)	Surf	0.0106	Surf v Mid	1.0000	Surf v <u>UO</u>	< 0.0001
		Mid	0	Surf v NB	1.0000	Surf v <u>LO</u>	< 0.0001
		NB	0.0481	Mid v NB	1.0000	Mid v <u>UO</u>	< 0.0001
						Mid v <u>LO</u>	< 0.0001
						NB v <u>UO</u>	0.0011
						NB v <u>LO</u>	0.0004
Ophidiidae	Ophidiidae (cusk eels)	Surf	0.0428	Surf v Mid	1.0000	Surf v <u>UO</u>	< 0.0001
		Mid	0.1594	Surf v NB	1.0000	Surf v <u>LO</u>	< 0.0001
		NB	0.047	Mid v NB	1.0000	Mid v <u>UO</u>	< 0.0001
						Mid v <u>LO</u>	< 0.0001
						NB v <u>UO</u>	< 0.0001
						NB v <u>LO</u>	< 0.0001

Table 2.2 *Continued*:

Family	Fish Taxa	Depth	Density	VS	Prob.	Additional VS of Note	Prob.
Ophidiidae	<i>Brotula barbata</i> (Atlantic bearded brotula)	Surf	0.0031	Surf v Mid	1.0000	Surf v <u>UO</u>	< 0.0001
		Mid	0.0279	Surf v NB	1.0000	Surf v <u>LO</u>	< 0.0001
		NB	0	Mid v NB	1.0000	Mid v <u>UO</u>	0.0023
						Mid v <u>LO</u>	0.0002
						NB v <u>UO</u>	0.0002
						NB v <u>LO</u>	< 0.0001
	<i>Lepophidium</i> spp. (cusk eel)	Surf	0.026	Surf v Mid	1.0000	Surf v <u>UO</u>	< 0.0001
		Mid	0.095	Surf v NB	0.5013	Surf v <u>LO</u>	< 0.0001
		NB	0.7605	Mid v NB	1.0000	Mid v <u>UO</u>	< 0.0001
						Mid v <u>LO</u>	< 0.0001
						NB v <u>UO</u>	< 0.0001
						NB v <u>LO</u>	< 0.0001
	<i>Ophidion</i> spp. (cusk eel)	Surf	0.0153	Surf v <u>Mid</u>	0.0001	Surf v <u>UO</u>	0.0005
		Mid	0.1961	Surf v NB	1.0000		
		NB	0.0708	Mid v NB	0.2307		
	<i>Ophidion selenops</i> (mooneye cusk eel)	Surf	0.0004	Surf v Mid	1.0000	Surf v <u>UO</u>	< 0.0001
		Mid	0	Surf v NB	1.0000	Surf v <u>LO</u>	0.0069
		NB	0	Mid v NB	1.0000	Mid v <u>UO</u>	0.0004
						NB v <u>UO</u>	0.0005
Paralepididae	Paralepididae (barracudinas)	Surf	0.014	Surf v Mid	1.0000	Surf v <u>UO</u>	< 0.0001
		Mid	0.0047	Surf v NB	1.0000	Mid v <u>UO</u>	< 0.0001
		NB	0	Mid v NB	1.0000	NB v <u>UO</u>	< 0.0001
						<u>UO</u> v <u>LO</u>	< 0.0001
	<i>Lestidiops affinis</i> (barracudina)	Surf	0.0014	Surf v Mid	1.0000	<u>NB</u> v <u>UO</u>	0.0159
		Mid	0	Surf v <u>NB</u>	0.0071	<u>NB</u> v <u>LO</u>	0.0163
Paralichthyidae	<i>Citharichthys</i> spp. (sanddab)	Surf	0.0093	Surf v <u>Mid</u>	0.0291		
		Mid	0.0652	Surf v NB	1.0000		
		NB	0.0228	Mid v NB	0.8562		
	<i>Citharichthys spilopterus</i> (bay whiff)	Surf	0.0643	Surf v Mid	1.0000	Surf v <u>UO</u>	< 0.0001
		Mid	0.1031	Surf v NB	0.0645	Surf v <u>LO</u>	< 0.0001
		NB	0.4089	Mid v NB	1.0000	Mid v <u>UO</u>	< 0.0001
						Mid v <u>LO</u>	< 0.0001
						NB v <u>UO</u>	< 0.0001
						NB v <u>LO</u>	< 0.0001
	<i>Cyclopsetta</i> spp. (flounder)	Surf	0.0037	Surf v Mid	1.0000	Surf v <u>UO</u>	0.0004
		Mid	0	Surf v NB	1.0000	Mid v <u>UO</u>	0.0104
		NB	0	Mid v NB	1.0000	<u>UO</u> v <u>LO</u>	0.0480

Table 2.2 *Continued*:

Family	Fish Taxa	Depth	Density	VS	Prob.	Additional VS of Note	Prob.
Paralichthyidae	<i>Etropus crossotus</i> (fringed flounder)	Surf	0.2863	Surf v <u>Mid</u>	<0.0001	Surf v <u>UO</u>	<0.0001
		Mid	1.5129	Surf v <u>NB</u>	0.0001	Surf v <u>LO</u>	<0.0001
		NB	1.4984	Mid v NB	1.0000	Mid v <u>UO</u>	<0.0001
						Mid v <u>LO</u>	<0.0001
						NB v <u>UO</u>	<0.0001
						NB v <u>LO</u>	<0.0001
	<i>Etropus rimosus</i> (gray flounder)	Surf	0	Surf v <u>Mid</u>	0.0144	<u>Mid</u> v UO	0.4140
		Mid	0.0784	Surf v NB	1.0000	<u>Mid</u> v LO	0.0407
		NB	0	Mid v NB	0.2188		
	<i>Paralichthys</i> spp. (flounder)	Surf	0.0164	Surf v <u>Mid</u>	0.0074		
		Mid	0.125	Surf v NB	1.0000		
		NB	0	<u>Mid</u> v NB	0.0171		
	<i>Paralichthys lethostigma</i> (southern flounder)	Surf	0	Surf v <u>Mid</u>	0.0069		
		Mid	0.3619	Surf v NB	1.0000		
		NB	0	Mid v NB	0.0984		
	<i>Syacium</i> spp. (flounder)	Surf	0.0289	Surf v Mid	1.0000	Surf v <u>UO</u>	<0.0001
		Mid	0.0318	Surf v NB	1.0000	Surf v <u>LO</u>	<0.0001
		NB	0.3943	Mid v NB	1.0000	Mid v <u>UO</u>	<0.0001
						Mid v <u>LO</u>	<0.0001
						NB v <u>UO</u>	<0.0001
						NB v <u>LO</u>	<0.0001
	<i>Syacium gunteri</i> (shoal flounder)	Surf	0	Surf v Mid	1.0000	<u>UO</u> v LO	0.0005
		Mid	0.0102	Surf v NB	1.0000		
		NB	0.0302	Mid v NB	1.0000		
Phycidae	<i>Urophycis</i> spp. (codling/hake)	Surf	0.4231	Surf v Mid	0.0503	<u>Surf</u> v LO	0.0079
		Mid	0.0328	<u>Surf</u> v NB	0.0153		
		NB	0	Mid v NB	1.0000		
Pomatomidae	<i>Pomatomus saltatrix</i> (bluefish)	Surf	0.1216	Surf v Mid	0.1613	Surf v <u>UO</u>	0.0006
		Mid	0	Surf v NB	0.2115	Mid v <u>UO</u>	<0.0001
		NB	0	Mid v NB	1.0000	NB v <u>UO</u>	<0.0001
						<u>UO</u> v LO	<0.0001
Rachycentridae	<i>Rachycentron canadum</i> (cobia)	Surf	0.014	Surf v Mid	1.0000	Surf v <u>UO</u>	0.0398
		Mid	0	Surf v NB	1.0000		
		NB	0	Mid v NB	1.0000		
Sciaenidae	Sciaenidae (drums)	Surf	0.1996	Surf v Mid	0.3747	<u>NB</u> v LO	0.0174
		Mid	1.7319	Surf v <u>NB</u>	0.0030		
		NB	1.3633	Mid v NB	1.0000		
	<i>Bairdiella chrysoura</i> (silver perch)	Surf	0.0288	Surf v Mid	0.5314	Surf v <u>UO</u>	0.0055
		Mid	0.0923	Surf v NB	1.0000	<u>UO</u> v LO	0.0047
		NB	0.052	Mid v NB	1.0000		

Table 2.2 *Continued*:

Family	Fish Taxa	Depth	Density	VS	Prob.	Additional VS of Note	Prob.
Sciaenidae	<i>Cynoscion</i> spp. (seatrout)	Surf	0.2805	Surf v <u>Mid</u>	<0.0001	<u>Mid</u> v UO	<0.0001
		Mid	3.2832	Surf v <u>NB</u>	<0.0001	<u>Mid</u> v LO	<0.0001
		NB	4.1911	Mid v NB	0.2800	<u>NB</u> v UO	<0.0001
						<u>NB</u> v LO	<0.0001
	<i>Cynoscion arenarius</i> (sand seatrout)	Surf	2.8607	Surf v <u>Mid</u>	<0.0001	Surf v <u>UO</u>	<0.0001
		Mid	125.976	Surf v <u>NB</u>	<0.0001	Surf v <u>LO</u>	<0.0001
		NB	22.4209	Mid v NB	1.0000	<u>Mid</u> v LO	0.0234
						<u>NB</u> v LO	0.0058
	<i>Cynoscion nothus</i> (silver seatrout)	Surf	0.0401	Surf v Mid	0.0665	<u>NB</u> v UO	0.0285
		Mid	0.1436	Surf v <u>NB</u>	<0.0001	<u>NB</u> v LO	0.0092
		NB	0.5148	Mid v NB	0.3241		
	<i>Larimus fasciatus</i> (banded drum)	Surf	0.0394	Surf v <u>Mid</u>	0.0006	Surf v <u>UO</u>	0.0004
		Mid	0.1407	Surf v NB	1.0000		
		NB	0.0649	Mid v NB	0.3819		
	<i>Leiostomus xanthurus</i> (spot croaker)	Surf	0.231	Surf v <u>Mid</u>	0.0010	Surf v <u>UO</u>	<0.0001
		Mid	0.7412	Surf v NB	1.0000	Surf v <u>LO</u>	<0.0001
		NB	0.2811	Mid v NB	0.2940	Mid v <u>UO</u>	<0.0001
						NB v <u>UO</u>	<0.0001
						NB v <u>LO</u>	0.0496
						<u>UO</u> v LO	<0.0001
	<i>Menticirrhus</i> spp. (kingcroaker)	Surf	0.3443	Surf v <u>Mid</u>	<0.0001	<u>Mid</u> v UO	<0.0001
		Mid	2.4801	Surf v NB	0.2543	<u>Mid</u> v LO	<0.0001
		NB	0.5273	<u>Mid</u> v NB	<0.0001		
	<i>Micropogonias undulatus</i> (Atlantic croaker)	Surf	1.0696	Surf v <u>Mid</u>	<0.0001	Surf v <u>UO</u>	<0.0001
		Mid	25.7908	Surf v <u>NB</u>	<0.0001	Surf v <u>LO</u>	<0.0001
		NB	37.4229	Mid v <u>NB</u>	0.0172	<u>NB</u> v UO	0.0137
						<u>NB</u> v LO	0.0163
	<i>Sciaenops ocellatus</i> (red drum)	Surf	17.3481	Surf v <u>Mid</u>	0.0113	<u>Surf</u> v LO	0.0042
		Mid	59.3986	Surf v NB	1.0000	<u>Mid</u> v LO	<0.0001
		NB	47.7319	Mid v NB	0.2130	<u>NB</u> v LO	0.0304
	<i>Stellifer lanceolatus</i> (American stardrum)	Surf	0.0297	Surf v <u>Mid</u>	<0.0001	<u>Mid</u> v UO	<0.0001
		Mid	3.6117	Surf v <u>NB</u>	<0.0001	<u>Mid</u> v LO	<0.0001
		NB	1.568	Mid v NB	1.0000	<u>NB</u> v UO	<0.0001
						<u>NB</u> v LO	<0.0001
Scombridae	Scombridae (mackerels)	Surf	0.0778	Surf v Mid	0.0774	Surf v <u>UO</u>	0.0213
		Mid	0.4851	Surf v NB	1.0000		
		NB	0.2116	Mid v NB	0.8473		

Table 2.2 *Continued*:

Family	Fish Taxa	Depth	Density	VS	Prob.	Additional VS of Note	Prob.
Scombridae	<i>Auxis</i> spp. (tuna)	Surf	0.3305	Surf v Mid	1.0000	Mid v <u>UO</u>	0.0370
		Mid	0.0916	Surf v NB	0.1289	NB v <u>UO</u>	0.0024
		NB	0.02	Mid v NB	1.0000		
	<i>Euthynnus</i> spp. (kawakawa/tunny/tuna)	Surf	0	Surf v Mid	1.0000	Surf v <u>UO</u>	0.0175
		Mid	0	Surf v NB	1.0000		
		NB	0	Mid v NB	1.0000		
	<i>Euthynnus alletteratus</i> (little tunny)	Surf	0.1015	Surf v Mid	1.0000	Surf v <u>UO</u>	<0.0001
		Mid	0.0582	Surf v NB	1.0000	Surf v <u>LO</u>	0.0036
		NB	0.045	Mid v NB	1.0000	Mid v <u>UO</u>	<0.0001
						Mid v <u>LO</u>	0.0185
						NB v <u>UO</u>	<0.0001
						NB v <u>LO</u>	0.0111
	<i>Scomberomorus cavalla</i> (king mackerel)	Surf	0.0137	Surf v Mid	1.0000	Surf v <u>UO</u>	<0.0001
		Mid	0.0645	Surf v NB	0.0015	Mid v <u>UO</u>	0.0009
		NB	0.4909	Mid v NB	0.1228	<u>UO</u> v LO	0.0013
	<i>Scomberomorus maculatus</i> (Spanish mackerel)	Surf	1.9911	Surf v Mid	<0.0001	Surf v <u>UO</u>	0.0001
		Mid	5.6147	Surf v NB	1.0000	Mid v LO	<0.0001
		NB	1.3733	Mid v NB	<0.0001	<u>UO</u> v LO	0.0019
	<i>Thunnus</i> spp. (tuna)	Surf	0.0016	Surf v Mid	1.0000	Surf v <u>UO</u>	0.0009
		Mid	0	Surf v NB	1.0000	Mid v <u>UO</u>	0.0291
		NB	0	Mid v NB	1.0000	NB v <u>UO</u>	0.0361
						<u>UO</u> v LO	0.0106
Scorpaenidae	Scorpaenidae (scorpionfishes)	Surf	0.0022	Surf v Mid	1.0000	Surf v <u>UO</u>	<0.0001
		Mid	0	Surf v NB	1.0000	Surf v <u>LO</u>	<0.0001
		NB	0	Mid v NB	1.0000	Mid v <u>UO</u>	0.0008
						Mid v <u>LO</u>	0.0008
						NB v <u>UO</u>	0.0012
						NB v <u>LO</u>	0.0013
	<i>Scorpaena</i> spp. (scorpionfish)	Surf	0.0168	Surf v Mid	1.0000	Surf v <u>UO</u>	<0.0001
		Mid	0.0063	Surf v NB	1.0000	Surf v <u>LO</u>	0.0001
		NB	0	Mid v NB	1.0000	Mid v <u>UO</u>	<0.0001
						Mid v <u>LO</u>	0.0037
						NB v <u>UO</u>	<0.0001
						NB v <u>LO</u>	0.0017
						<u>UO</u> v LO	0.0363
Serranidae	Serranidae (groupers)	Surf	0.0584	Surf v Mid	1.0000	Surf v <u>UO</u>	<0.0001
		Mid	0.072	Surf v NB	1.0000	Surf v <u>LO</u>	<0.0001
		NB	0.059	Mid v NB	1.0000	Mid v <u>UO</u>	<0.0001
						Mid v <u>LO</u>	<0.0001
						NB v <u>UO</u>	<0.0001
						NB v <u>LO</u>	<0.0001

Table 2.2 *Continued*:

Family	Fish Taxa	Depth	Density	VS	Prob.	Additional VS of Note	Prob.
Serranidae	<i>Anthias</i> spp. (basslets)	Surf	0.0074	Surf v Mid	1.0000	Surf v <u>UO</u>	0.0297
		Mid	0.0094	Surf v NB	1.0000		
		NB	0	Mid v NB	1.0000		
	<i>Centropristis</i> spp. (seabass)	Surf	0.0024	Surf v Mid	1.0000	Surf v <u>UO</u>	0.0049
		Mid	0	Surf v NB	1.0000	Surf v <u>LO</u>	0.0430
		NB	0.0289	Mid v NB	1.0000		
	<i>Diplectrum</i> spp. (sand perch)	Surf	0.003	Surf v Mid	1.0000	Surf v <u>LO</u>	0.0099
		Mid	0	Surf v NB	1.0000		
		NB	0	Mid v NB	1.0000		
	<i>Serranus</i> spp. (grouper)	Surf	0.0134	Surf v Mid	1.0000	Surf v <u>LO</u>	0.0016
		Mid	0	Surf v NB	1.0000	Mid v <u>LO</u>	0.0104
		NB	0	Mid v NB	1.0000	NB v <u>LO</u>	0.0134
Sparidae	<i>Archosargus probatocephalus</i> (sheepshead)	Surf	0.3648	Surf v Mid	0.1624	<u>Surf</u> v LO	0.0130
		Mid	0.0167	Surf v NB	0.1641		
		NB	0	Mid v NB	1.0000		
	<i>Lagodon rhomboides</i> (pinfish)	Surf	0.3045	Surf v Mid	0.0561	<u>Surf</u> v LO	0.0419
		Mid	0.069	Surf v NB	0.0022	Mid v <u>UO</u>	0.0085
		NB	0.0219	Mid v NB	1.0000	NB v <u>UO</u> <u>UO</u> v LO	0.0004 0.0066
Sphyraenidae	<i>Sphyraena</i> spp. (barracuda)	Surf	0.1074	Surf v Mid	1.0000	Surf v <u>UO</u>	<0.0001
		Mid	0.0764	Surf v NB	1.0000	Mid v <u>UO</u>	<0.0001
		NB	0.0911	Mid v NB	1.0000	NB v <u>UO</u>	<0.0001
						<u>UO</u> v LO	<0.0001
Stomiidae	<i>Stomias</i> spp. (dragonfish/boafish)	Surf	0.0112	Surf v Mid	1.0000	<u>UO</u> v LO	0.0386
		Mid	0	Surf v NB	1.0000		
		NB	0	Mid v NB	1.0000		
Stromateidae	<i>Peprilus burti</i> (gulf butterfish)	Surf	0.359	Surf v <u>Mid</u>	0.0008	Surf v <u>UO</u>	<0.0001
		Mid	0.8283	Surf v NB	1.0000	Surf v <u>LO</u>	<0.0001
		NB	0.1944	<u>Mid</u> v NB	0.0018	Mid v <u>UO</u>	0.0016
						NB v <u>UO</u>	<0.0001
						NB v <u>LO</u>	<0.0001
	<i>Peprilus paru</i> (American harvestfish)	Surf	0.1194	Surf v <u>Mid</u>	<0.0001	Surf v <u>UO</u>	0.0016
		Mid	32.4019	Surf v <u>NB</u>	0.0013	<u>Mid</u> v UO	0.0394
		NB	0.6869	Mid v NB	0.1486	<u>Mid</u> v LO	0.0011
	<i>Peprilus</i> spp. (butterfish)	Surf	0.0057	Surf v Mid	1.0000	Surf v <u>UO</u>	0.0276
		Mid	0	Surf v NB	1.0000		
		NB	0	Mid v NB	1.0000		

Table 2.2 *Continued*:

Family	Fish Taxa	Depth	Density	VS	Prob.	Additional VS of Note	Prob.
Syngnathidae	<i>Syngnathus</i> spp. (pipefish)	Surf	0.0165	Surf v Mid	1.0000	Surf v <u>UO</u>	0.0003
		Mid	0.0326	Surf v NB	1.0000	NB v <u>UO</u>	0.0005
		NB	0	Mid v NB	1.0000		
Synodontidae	Synodontidae (lizardfishes)	Surf	0.0396	Surf v Mid	1.0000	Surf v <u>UO</u>	0.0043
		Mid	0.0581	Surf v NB	0.4574	Surf v <u>LO</u>	<0.0001
		NB	0.9848	Mid v NB	1.0000	Mid v <u>LO</u>	0.0470
	<i>Synodus</i> spp. (lizardfish)	Surf	0.0582	Surf v Mid	1.0000	Surf v <u>UO</u>	<0.0001
		Mid	0.0059	Surf v NB	1.0000	Surf v <u>LO</u>	<0.0001
		NB	0.3623	Mid v NB	1.0000	Mid v <u>UO</u>	<0.0001
						Mid v <u>LO</u>	<0.0001
						NB v <u>UO</u>	<0.0001
						NB v <u>LO</u>	<0.0001
						UO v <u>LO</u>	0.0048
Tetraodontidae	<i>Sphoeroides</i> spp. (puffer)	Surf	0.0709	Surf v Mid	0.7831	Surf v <u>UO</u>	<0.0001
		Mid	0.0087	Surf v NB	1.0000	Surf v <u>LO</u>	<0.0001
		NB	0.0362	Mid v NB	1.0000	Mid v <u>UO</u>	<0.0001
						Mid v <u>LO</u>	<0.0001
						NB v <u>UO</u>	<0.0001
						NB v <u>LO</u>	0.0002
Triglidae	Triglidae (sea robins)	Surf	0.0013	Surf v Mid	1.0000	Surf v <u>UO</u>	0.0031
		Mid	0	Surf v NB	1.0000		
		NB	0	Mid v NB	1.0000		
	<i>Prionotus</i> spp. (searobin)	Surf	0.0583	Surf v Mid	1.0000	Surf v <u>UO</u>	<0.0001
		Mid	0.0545	Surf v NB	1.0000	Surf v <u>LO</u>	<0.0001
		NB	0.0207	Mid v NB	1.0000	Mid v <u>UO</u>	<0.0001
						Mid v <u>LO</u>	0.0002
						NB v <u>UO</u>	<0.0001
						NB v <u>LO</u>	<0.0001
Family	Decapod Taxa	Depth	Density	VS	Prob.	Additional VS of Note	Prob.
Portunidae	<i>Callinectes</i> spp. (decapod crab)	Surf	0.3714	Surf v Mid	0.1440	<u>Mid</u> v UO	0.0412
		Mid	0.5816	Surf v <u>NB</u>	0.0005	<u>Mid</u> v LO	0.0438
		NB	1.0134	Mid v NB	1.0000	<u>NB</u> v UO	0.0005
	<i>Callinectes sapidis</i> (blue crab)					<u>NB</u> v LO	0.0006
		Surf	97.9460	Surf v Mid	0.6708	<u>Surf</u> v UO	<0.0001
		Mid	23.0575	Surf v NB	1.0000	<u>Surf</u> v LO	<0.0001
		NB	25.1321	Mid v NB	1.0000		
	<i>Callinectes similis</i> (lesser blue crab)	Surf	14.1663	<u>Surf</u> v Mid	<0.0001	Surf v <u>UO</u>	0.0260
		Mid	10.6156	<u>Surf</u> v NB	0.0001	Mid v <u>UO</u>	<0.0001
		NB	6.5536	Mid v NB	1.0000	Mid v <u>LO</u>	<0.0001
						NB v <u>UO</u>	<0.0001
						NB v <u>LO</u>	<0.0001

Table 2.2 *Continued*:

Family	Decapod Taxa	Depth	Density	VS	Prob.	Additional VS of Note	Prob.
Penaeidae	<i>Penaeus spp.</i> (shrimps)	Surf	1.0798	Surf v Mid	1.0000		
		Mid	0.1446	Surf v NB	1.0000		
		NB	0.1807	Mid v NB	1.0000		
	<i>Farfantepenaeus aztecus</i> (brown shrimp)	Surf	2.1832	Surf v Mid	1.0000		
		Mid	3.7310	Surf v NB	0.8001		
		NB	1.3872	Mid v NB	0.2509		
	<i>Farfantepenaeus duorarum</i> (pink shrimp)	Surf	0.1427	Surf v Mid	1.0000		
		Mid	0.0901	Surf v NB	1.0000		
		NB	0.2160	Mid v NB	0.7561		
	<i>Litopenaeus setiferus</i> (white shrimp)	Surf	1.0065	Surf v Mid	1.0000		
		Mid	0.5046	Surf v NB	1.0000		
		NB	1.2878	Mid v NB	1.0000		

depth. *Gobiesox strumosus* (skilletfish), *Urophycis* spp. (hakes), and Mullidae (goat fishes) showed surface densities being significant over two depth bins, the near-bottom and either the lower-oblique or mid-water tow. *Archosargus probatocephalus* (sheepshead) densities were only significantly greater than the lower oblique tow densities.

Four taxa still showed affinity towards the surface, but upper oblique tow densities were also statistically greater than most or all other depth bins, i.e., Blennidae (blennies), *Brevoortia patronus* (gulf menhaden), *Lagodon rhomboides* (pinfish), and *Mugil cephalus* (flathead mullet). Both Myctophidae (lanternfish) and *Trichiurus lepturus* (Atlantic cutlassfish) also showed statistical preference for the surface, but densities for both oblique tows were significantly greater than all the other horizontal depth bins. Finally, Atherinidae (silversides) had a surprisingly weak association with the surface waters. Also, as mentioned previously, in addition

Table 2.3: All taxa with corresponding mean density (number of individuals per 100 cubic meters of water filtered), standard error, number of collections, and months analyzed. (Code: A=Taxa sampled throughout the water column that showed no statistical preference; B=Taxa which were sampled exclusively at the surface; C=Taxa which were sampled throughout the upper half water column; D=Taxa which were sampled exclusively in the mid-water; E=Taxa which were sampled exclusively near-bottom; F=Taxa sampled throughout the lower half water column; G=Some statistical difference; OM=Overall mean density for all depths; Surf=Discrete surface; Mid=Discrete mid-water; NB=Discrete near-bottom; UO=Upper half water column oblique; and LO=Lower half water column oblique).

Fish Taxa	Code	OM	Surf	Mid	NB	UO	LO
<i>Scientific Name</i>	<i>Code</i>	<i>Mean Density</i>					
<i>Common Name</i>		<i>Standard Error</i>					
<i>Months Analyzed</i>		<i>Number of Collections</i>					
<i>Achirus lineatus</i>	C	0.065	0.0835	0.1465	0	0.0191	0
lined sole		0.0463	0.0766	0.0755	0	0.0191	0
Jun-Aug		699	417	62	61	82	77
Acropomatidae	B	0.0058	0.0095	0	0	0	0
lanternbellies/ temp. ocean basses		0.0058	0.0095	0	0	0	0
Dec		207	126	27	24	16	14
<i>Anchoa</i> spp.	G	9.4327	14.6403	6.394	3.1229	0.0175	0.0179
anchovies		5.02	8.6204	2.7589	1.3435	0.0175	0.0179
Mar-Dec		2180	1267	214	204	251	244
<i>Anchoa hepsetus</i>	A	0.3361	0.5345	0.1217	0.1678	0.0026	0
broad-striped anchovy		0.1653	0.2847	0.0478	0.1252	0.0026	0
Feb-Dec		2634	1525	250	231	318	310
<i>Anchoa mitchilli</i>	A	0.775	1.3314	0	0.0343	0.0089	0
bay anchovy		0.7008	1.2104	0	0.0156	0.0089	0
Jan-Dec		2634	1525	250	231	318	310
<i>Anchoa nasuta</i>	D	0.0122	0	0.1123	0	0	0
shortfinger anchovy		0.0122	0	0.1123	0	0	0
Sep		285	153	31	30	36	35
<i>Anchoviella</i> spp.	G	0.0129	0.0065	0	0	0.0719	0.0065
anchovies		0.0061	0.0037	0	0	0.048	0.0046
Jun-Feb		2108	1212	210	198	248	240
<i>Anchoviella perfasciata</i>	G	0.0169	0.0108	0.1073	0	0.0105	0
Poey's anchovy		0.006	0.0065	0.0509	0	0.0105	0
Jan-Sep		1964	1141	169	151	255	248
Anguillidae	C	0.0089	0	0	0	0.063	0
fresh-water eels		0.0089	0	0	0	0.063	0
Jun		233	144	13	12	33	31
Antennariidae	A	0.0074	0.0074	0	0.0143	0	0.0159
frog fishes		0.0027	0.0033	0	0.0143	0	0.0113
Aug-Apr		1973	1125	194	189	234	231
<i>Anthias</i> spp.	G	0.0123	0.0074	0.0094	0	0.0511	0.0083
basslets		0.0044	0.0042	0.0094	0	0.0285	0.0083
Jul-Apr		2219	1272	215	204	267	261
Apogonidae	C	0.0092	0	0	0	0.0725	0
cardinalfishes		0.0092	0	0	0	0.0725	0
Sep		285	153	31	30	36	35
<i>Archosargus</i> spp.	B	0.0264	0.0449	0	0	0	0
porgies		0.0264	0.0449	0	0	0	0
Apr		219	129	12	11	33	34
<i>Archosargus probatocephalus</i>	G	0.2593	0.3648	0.0167	0	0.2921	0.0142
sheepshead		0.052	0.0791	0.0167	0	0.1618	0.0142
Jan-Jul		1459	862	110	87	203	197
<i>Arionmma</i> spp.	G	0.0769	0.0762	0.0302	0.0094	0.1524	0.0907
butterfishes		0.0117	0.0169	0.0183	0.0094	0.0446	0.0241
Jan-Dec		2634	1525	250	231	318	310

Table 2.3 *Continued*:

Fish Taxa	Code	OM	Surf	Mid	NB	UO	LO
Atherinidae		0.1429	0.2369	0.0073	0	0.0433	0
silversides	G	0.0564	0.0974	0.0073	0	0.0207	0
Aug-Apr		1916	1108	180	169	233	226
<i>Auxis</i> spp.		0.3369	0.3305	0.0916	0.02	0.3049	0.8352
tuna	G	0.1046	0.101	0.0483	0.0144	0.0668	0.733
Apr-Jan		2634	1525	250	231	318	310
<i>Auxis thazard</i>		0.035	0	0	0	0.2769	0
frigate tuna	A	0.035	0	0	0	0.2769	0
Sep		285	153	31	30	36	35
<i>Bairdiella chrysoura</i>		0.0449	0.0288	0.0923	0.052	0.1212	0.0027
silver perch	G	0.011	0.0129	0.0551	0.0266	0.0461	0.0027
Jan-Dec		2634	1525	250	231	318	310
<i>Balistes</i> spp.		0.0025	0.0043	0	0	0	0
triggerfish	B	0.0025	0.0043	0	0	0	0
Nov		275	158	24	26	33	34
Balistidae		0.0132	0.0161	0.0186	0	0.02	0
triggerfish	C	0.0075	0.0125	0.0186	0	0.02	0
Sep-Nov		748	411	85	86	83	83
<i>Bascanichthys</i> spp.		0.005	0	0	0	0.0394	0
sand-eel	C	0.005	0	0	0	0.0394	0
Sep		285	153	31	30	36	35
<i>Bascanichthys bascanium</i>		0.0016	0.0027	0	0	0	0
sooty eel	B	0.0012	0.002	0	0	0	0
Jun-Sep		984	570	93	91	118	112
<i>Bathophilus</i> spp.		0.0048	0.0017	0	0	0.026	0
dragonfish	C	0.0028	0.0012	0	0	0.0184	0
Jan-Apr		798	462	54	45	119	118
Belonidae		0.0012	0.0022	0	0	0	0
needlefish	B	0.0009	0.0017	0	0	0	0
Sep-Nov		748	411	85	86	83	83
Blenniidae		2.3825	3.3614	0.9107	0.3546	2.2552	0.3952
blennies	G	0.7102	1.2246	0.1867	0.1141	0.2183	0.0984
Jan-Dec		2634	1525	250	231	318	310
Bothidae		0.0696	0.0323	0.1983	0.0524	0.0811	0.1508
left-eye flounders	G	0.012	0.0092	0.0832	0.0233	0.0308	0.0504
Jan-Dec		2634	1525	250	231	318	310
<i>Bothus</i> spp.		0.0187	0.0058	0	0	0.0935	0.0346
left-eye flounders	G	0.0043	0.0029	0	0	0.0264	0.0192
Jan-Dec		2634	1525	250	231	318	310
<i>Bothus ocellatus</i>		0.0175	0.031	0	0	0	0
left-eye flounder	B	0.0162	0.0287	0	0	0	0
Jan		236	133	19	12	36	36
Bramidae		0.0025	0	0	0	0.0117	0.0078
sea breams	A	0.0018	0	0	0	0.0117	0.0078
Apr & Nov		1280	746	105	95	168	166
<i>Bregmaceros</i> spp.		0.2974	0.0266	0.1362	1.622	0.1318	0.942
codlets	G	0.0931	0.0099	0.0631	0.6342	0.0723	0.6227
Jan-Dec		2634	1525	250	231	318	310
<i>Bregmaceros atlanticus</i>		0.035	0.0112	0.0397	0.0094	0.1075	0.0923
antenna codlet	G	0.0067	0.0029	0.018	0.0094	0.0298	0.0424
Jan-Dec		2634	1525	250	231	318	310
<i>Bregmaceros cantori</i>		3.234	0.301	0.8978	0.1157	4.1406	20.9407
striped codlet	G	0.6065	0.262	0.5959	0.0473	0.5515	4.8194
Jan-Dec		2634	1525	250	231	318	310

Table 2.3 *Continued*:

Fish Taxa	Code	OM	Surf	Mid	NB	UO	LO
<i>Bregmaceros houdei</i>		0.0112	0.0195	0	0	0	0
stellate codlet	B	0.008	0.0139	0	0	0	0
Feb		218	125	17	15	31	30
<i>Bregmaceros maclellandii</i>		0.0061	0.0105	0	0	0	0
spotted codlet	B	0.0043	0.0074	0	0	0	0
Jan-Apr		798	462	54	45	119	118
Bregmacerotidae		0.0095	0	0	0	0.0673	0
codlets	C	0.0095	0	0	0	0.0673	0
Jun		233	144	13	12	33	31
<i>Brevoortia gunteri</i>		0.329	0.231	0.0324	0.9968	0.6101	0.2517
finestale menhaden	G	0.0752	0.069	0.0324	0.599	0.1959	0.1952
Oct-Mar		1249	717	123	114	149	146
<i>Brevoortia patronus</i>		19.4031	17.921	14.0732	12.5076	41.5453	13.4174
gulf menhaden	G	1.3109	1.7919	3.4596	3.9351	4.4805	2.6563
Jan-Dec		2634	1525	250	231	318	310
<i>Brevoortia</i> spp.		0.4199	0.4278	0.6014	1.3844	0.0335	0
menhaden	G	0.1334	0.1322	0.3372	1.2933	0.0335	0
Oct-Jun		1883	1099	170	152	233	229
<i>Brotula</i> spp.		0.0087	0	0	0	0.0724	0
brotula	C	0.0087	0	0	0	0.0724	0
Nov		275	158	24	26	33	34
<i>Brotula barbata</i>		0.0474	0.0031	0.0279	0	0.1598	0.2398
Atlantic bearded brotula	G	0.0137	0.0027	0.0279	0	0.0542	0.112
Jun-Dec		1654	954	174	171	181	174
Callionymidae		0.0015	0.0016	0	0	0	0.0048
dragonets	A	0.0009	0.0012	0	0	0	0.0048
Apr & Nov		1280	746	105	95	168	166
<i>Callionymus</i> spp.		0.0033	0.0007	0	0	0.0249	0
dragonets	C	0.003	0.0007	0	0	0.0249	0
Feb & Sep		1409	795	148	137	166	163
<i>Callionymus bairdi</i>		0.0031	0.0057	0	0	0	0
lancer dragonet	B	0.0031	0.0057	0	0	0	0
Sep		285	153	31	30	36	35
(<i>Callionymus</i>) <i>Diplogrammus pauciradiatus</i>		0.0116	0.0131	0.013	0.0099	0.013	0.003
spotted dragonet	A	0.0033	0.0046	0.013	0.0099	0.0093	0.003
Sep-Feb		1409	795	148	137	166	163
Carangidae		0.7869	0.6866	3.5086	0.3337	0.2093	0.015
jacks	G	0.3189	0.1676	3.191	0.1886	0.1382	0.0088
Jan-Dec		2634	1525	250	231	318	310
<i>Caranx</i> spp.		0.1126	0.0792	0	0	0.4333	0.1199
jacks	G	0.0204	0.0235	0	0	0.1024	0.0705
Feb-Oct		1916	1108	180	169	233	226
<i>Caranx chrysos</i>		0.0152	0.0166	0	0	0.0381	0.0103
blue runner	A	0.005	0.0072	0	0	0.022	0.0083
Apr-Jan		2291	1325	227	209	268	262
<i>Caranx hippos</i>		0.0028	0.0024	0	0	0	0.0133
crevalle jack	A	0.002	0.0024	0	0	0	0.0133
Jul-Sep		751	426	80	79	85	81
<i>Caranx latus</i>		0.0049	0	0	0	0.0364	0
horse-eye jack	C	0.0049	0	0	0	0.0364	0
Jul		246	147	21	15	33	30
Carapidae		0.0069	0.0123	0	0	0	0
pearlfishes	B	0.0053	0.0093	0	0	0	0
Jan		236	133	19	12	36	36

Table 2.3 *Continued*:

Fish Taxa	Code	OM	Surf	Mid	NB	UO	LO
Caulophrynidae		0.0062	0.0005	0	0	0.039	0.0066
anglerfishes	G	0.0023	0.0005	0	0	0.0161	0.0066
Jan-Sep		1964	1141	169	151	255	248
Centriscidae		0.0159	0.016	0	0	0.0082	0.0401
snipefishes	A	0.0109	0.016	0	0	0.0082	0.0401
Feb & Jul		1223	729	91	75	167	161
<i>Centrobranchus nigroocellatus</i>		0.0019	0.0032	0	0	0	0
roundnose lanternfish	B	0.0019	0.0032	0	0	0	0
Dec		207	126	27	24	16	14
<i>Centropristis</i> spp.		0.0578	0.0024	0	0.0289	0.2671	0.1378
seabasses	G	0.0295	0.0024	0	0.0289	0.1993	0.0833
Feb-Jul		1223	729	91	75	167	161
<i>Centropristis striata</i>		0.0076	0	0	0	0.0567	0
black seabass	C	0.0076	0	0	0	0.0567	0
Jul		246	147	21	15	33	30
<i>Chaetodipterus faber</i>		0.7695	0.1747	5.6436	0.248	0.4027	0.124
Atlantic spadefish	G	0.3614	0.045	3.458	0.1295	0.1048	0.0774
May-Jan		2072	1196	215	198	235	228
<i>Chaunax</i> spp.		0.0034	0	0	0	0	0.028
sea toads	F	0.0034	0	0	0	0	0.028
Jul		246	147	21	15	33	30
<i>Chloroscombrus chrysurus</i>		17.328	8.1095	83.9297	16.9541	8.8739	17.9163
Atlantic bumper	G	4.7885	1.1035	46.8071	7.8445	1.5659	12.5283
Jan-Dec		2634	1525	250	231	318	310
<i>Citharichthys</i> spp.		0.0231	0.0093	0.0652	0.0228	0.0149	0.066
sanddab	G	0.006	0.0038	0.0333	0.0172	0.0088	0.0353
Jan-Dec		2634	1525	250	231	318	310
<i>Citharichthys gymnorhinus</i>		0.0019	0.0032	0	0	0	0
angelfin whiff	B	0.0019	0.0032	0	0	0	0
Dec		207	126	27	24	16	14
<i>Citharichthys spilopterus</i>		0.3507	0.0643	0.1031	0.4089	0.728	1.5289
bay whiff	G	0.0915	0.0144	0.0333	0.2008	0.1106	0.7479
Jan-Dec		2634	1525	250	231	318	310
Clupeidae		1.7493	1.7718	2.317	2.3414	0.6974	1.8183
herrings/shads/menhadens	A	0.3339	0.4966	0.8502	0.9435	0.306	1.0103
Jan-Dec		2634	1525	250	231	318	310
Congridae		0.0142	0.0014	0	0	0.0939	0.0265
conger eels	G	0.0066	0.001	0	0	0.0546	0.0215
May-Nov		1629	937	169	162	183	178
<i>Coryphaena</i> spp.		0.0022	0.0018	0	0	0	0.0104
dolphinfish	A	0.0013	0.0011	0	0	0	0.0104
May-Nov		1629	937	169	162	183	178
<i>Coryphaena equisetis</i>		0.0022	0.0038	0	0	0	0
pompano	B	0.001	0.0017	0	0	0	0
Apr-Oct		1573	908	157	147	183	178
<i>Coryphaena hippurus</i>		0.004	0	0	0	0.0317	0
common dolphinfish	C	0.004	0	0	0	0.0317	0
Sep		285	153	31	30	36	35
Coryphaenidae		0.0086	0.0144	0	0	0	0
dolphinfish	B	0.004	0.0067	0	0	0	0
Apr-Aug		1100	655	96	87	133	129
<i>Cryptopsaras</i> spp.		0.0028	0.0046	0	0	0	0
seadevils	B	0.0028	0.0046	0	0	0	0
Dec		207	126	27	24	16	14

Table 2.3 *Continued*:

Fish Taxa	Code	OM	Surf	Mid	NB	UO	LO
<i>Cryptosaras couesi</i>		0.0033	0.0058	0	0	0	0
triplewart seadevil	B	0.0033	0.0058	0	0	0	0
Feb		218	125	17	15	31	30
<i>Cubiceps pauciradiatus</i>		0.021	0.0205	0.0122	0.0237	0.0378	0.0111
longfin fathead	A	0.0048	0.0066	0.0122	0.0124	0.019	0.0079
Feb-Dec		2398	1392	231	219	282	274
<i>Cyclopsetta</i> spp.		0.0095	0.0037	0	0	0.0583	0.0067
flounder	G	0.0044	0.0037	0	0	0.0329	0.0067
Jun-Nov		1447	828	147	147	165	160
<i>Cyclopsetta chittendeni</i>		0.0053	0.0032	0	0	0.0242	0.0099
Mexican flounder	A	0.0027	0.0032	0	0	0.0172	0.0099
Jul-Oct		939	526	110	109	99	95
<i>Cyclopsetta fimbriata</i>		0.0174	0	0	0	0.1375	0
spotfin flounder	C	0.0109	0	0	0	0.0844	0
Sep		285	153	31	30	36	35
<i>Cyclothone</i> spp.		0.0663	0.0808	0.028	0.0043	0.1186	0.0183
bristlemouth	A	0.0178	0.0276	0.0127	0.0043	0.0628	0.0109
Aug-May		2634	1525	250	231	318	310
<i>Cyclothone braueri</i>		0.0221	0.0225	0.0169	0.0238	0.0452	0
light fish	A	0.0088	0.0124	0.0169	0.0238	0.0354	0
Nov-Feb		936	542	87	77	116	114
Cynoglossidae		0.0137	0.0096	0	0	0.0407	0.0295
tonguefishes	A	0.0072	0.0082	0	0	0.0407	0.0228
Nov-Jun		1848	1066	181	173	216	212
<i>Cynoscion</i> spp.		0.8421	0.2805	3.2832	4.1911	0	0.0039
weakfish	G	0.169	0.0702	1.2655	1.2418	0	0.0039
Jan-Dec		2634	1525	250	231	318	310
<i>Cynoscion arenarius</i>		17.495	2.8607	125.9764	22.4209	8.0467	8.0232
sand weakfish	G	7.343	0.5966	76.9423	4.2026	1.1813	1.4084
Jan-Dec		2634	1525	250	231	318	310
<i>Cynoscion nebulosus</i>		0.6354	0.8717	0.9061	0.1791	0.1334	0.11
spotted weakfish	A	0.1884	0.3186	0.3848	0.097	0.0344	0.03
Feb-Nov		2634	1525	250	231	318	310
<i>Cynoscion nothus</i>		0.1055	0.0401	0.1436	0.5148	0.1068	0.0556
silver seatrout	G	0.0342	0.0305	0.0664	0.2884	0.0561	0.0242
May-Jan		2072	1196	215	198	235	228
<i>Cypselurus</i> spp.		0.0018	0.0029	0	0	0	0
flyingfish	B	0.0018	0.0029	0	0	0	0
Jun		233	144	13	12	33	31
Dactylopteridae		0.005	0	0	0	0.0328	0
flying gurnards	C	0.005	0	0	0	0.0328	0
Jan		236	133	19	12	36	36
<i>Dactylopterus volitans</i>		0.0024	0.0011	0	0	0.0151	0
flying gurnard	C	0.0019	0.0011	0	0	0.0151	0
May & Sep		1166	679	115	106	136	130
<i>Decapterus</i> spp.		0.0058	0	0	0	0.0461	0
scad	C	0.0058	0	0	0	0.0461	0
Sep		285	153	31	30	36	35
<i>Decapterus punctatus</i>		0.0945	0.1077	0	0	0.2627	0.028
round scad	G	0.0341	0.0556	0	0	0.1044	0.0162
May-Nov		1629	937	169	162	183	178
<i>Diaphus</i> spp.		0.0071	0.0009	0.0758	0	0	0
lanternfish	C	0.0066	0.0009	0.0758	0	0	0
Nov		275	158	24	26	33	34

Table 2.3 *Continued*:

Fish Taxa	Code	OM	Surf	Mid	NB	UO	LO
<i>Diogenichthys atlanticus</i>		0.0445	0.0776	0	0	0	0
longfin lanternfish	B	0.0288	0.05	0	0	0	0
Feb		218	125	17	15	31	30
<i>Diplectrum formosum</i>		0.0057	0	0	0	0.0453	0
sand seabass	C	0.0057	0	0	0	0.0453	0
Sep		285	153	31	30	36	35
<i>Diplectrum</i> spp.		0.0199	0.003	0	0	0.0208	0.131
sand perch	G	0.0114	0.003	0	0	0.0208	0.0917
May-Jun		415	253	35	27	51	49
<i>Diplospinus multistriatus</i>		0.0182	0.0122	0	0	0.075	0.0241
striped escolar	G	0.0049	0.0039	0	0	0.0341	0.0172
Aug-Mar		1754	996	182	178	201	197
<i>Elagatis bipinnulata</i>		0.0112	0.0105	0	0.0247	0.0069	0.0181
rainbow runner	A	0.0038	0.0044	0	0.0247	0.0069	0.0129
Apr-Oct		1573	908	157	147	183	178
Elopidae		0.0012	0.0022	0	0	0	0
ladyfishes	B	0.0012	0.0022	0	0	0	0
Jan		236	133	19	12	36	36
<i>Elops saurus</i>		0.0094	0	0	0	0	0.068
ladyfish	G	0.0066	0	0	0	0	0.0473
Feb		218	125	17	15	31	30
Engraulidae		49.6677	47.7949	108.2289	18.0221	52.3238	32.5098
anchovies	G	5.2159	6.1457	35.1989	4.9703	6.0978	13.5273
Jan-Dec		2634	1525	250	231	318	310
<i>Engyophrys senta</i>		0.0367	0.0025	0.0111	0.0189	0.1583	0.1434
American spiny flounder	G	0.0072	0.0016	0.0111	0.0133	0.0452	0.0443
May-Dec		1836	1063	196	186	199	192
Ephippidae		0.0106	0.0035	0	0	0.0706	0
batfishes	G	0.0049	0.0028	0	0	0.0377	0
Feb-Oct		1916	1108	180	169	233	226
<i>Epinephelus</i> spp.		0.0026	0.0048	0	0	0	0
grouper	B	0.0026	0.0048	0	0	0	0
Sep		285	153	31	30	36	35
<i>Etropus</i> spp.		0.014	0.017	0.0146	0.0267	0	0
flounder	A	0.0066	0.0101	0.0146	0.0267	0	0
May-Oct		1354	779	145	136	150	144
<i>Etropus crossotus</i>		1.6463	0.2863	1.5129	1.4984	4.5952	5.5294
fringed flounder	G	0.1788	0.175	0.448	0.3985	0.5837	0.9417
Jan-Dec		2634	1525	250	231	318	310
<i>Etropus rimosus</i>		0.0063	0	0.0784	0	0	0
gray flounder	G	0.0063	0	0.0784	0	0	0
Jan		236	133	19	12	36	36
<i>Etrumeus teres</i>		0.8983	0.3317	0.0236	0.0433	2.2466	3.6449
round herring	G	0.1938	0.2143	0.012	0.0252	0.6258	1.0741
Jan-Dec		2634	1525	250	231	318	310
<i>Eucinostomus</i> spp.		0.001	0.0017	0	0	0	0
mojarra	B	0.0008	0.0013	0	0	0	0
Apr-Jul		880	529	68	53	117	113
<i>Eucinostomus gula</i>		0.0013	0.0004	0	0	0.0079	0
Jenny mojarra	C	0.0011	0.0004	0	0	0.0079	0
Mar & Jul		1005	604	74	60	136	131
<i>Eustomias</i> spp.		0.0071	0.0126	0	0	0	0
lightfish & dragonfish	B	0.0042	0.0075	0	0	0	0
Jan		236	133	19	12	36	36

Table 2.3 *Continued*:

Fish Taxa	Code	OM	Surf	Mid	NB	UO	LO
<i>Euthynnus</i> spp.		0.05	0	0	0	0.4199	0.0227
kawakawa/tunny/tuna	G	0.0459	0	0	0	0.4052	0.0227
Jul-Sep		751	426	80	79	85	81
<i>Euthynnus alletteratus</i>		0.1862	0.1015	0.0582	0.045	0.5524	0.4359
little tunny	G	0.0266	0.0218	0.0277	0.0253	0.1315	0.1411
Jan-Oct		2634	1525	250	231	318	310
<i>Euthynnus pelamis</i>		0.0504	0.0052	0	0.4494	0.0368	0
skipjack tuna	A	0.0432	0.0032	0	0.4494	0.0261	0
Feb-Oct		1973	1125	194	189	234	231
Exocoetidae		0.0091	0.0127	0	0	0.0147	0
flying fishes	C	0.0028	0.0043	0	0	0.0107	0
Jan-Dec		2634	1525	250	231	318	310
<i>Exocoetus volitans</i>		0.0042	0.0068	0	0	0	0
tropical two-wing flyingfish	B	0.0042	0.0068	0	0	0	0
Jun		233	144	13	12	33	31
<i>Fistularia</i> spp.		0.0043	0	0	0	0.0324	0
trumpetfish/cornetfish	C	0.0043	0	0	0	0.0324	0
Jul		246	147	21	15	33	30
<i>Fistularia tabacaria</i>		0.0012	0.0021	0	0	0	0
cornet fish	B	0.0012	0.0021	0	0	0	0
Apr		219	129	12	11	33	34
Gadidae		0.0138	0.01	0	0	0.0542	0.0108
cod/haddock/whiting/pollock	G	0.0044	0.005	0	0	0.0246	0.0108
Oct-Apr		1468	846	135	125	182	180
<i>Gadus</i> spp.		0.0056	0	0	0	0	0.0367
cod/pollock	F	0.0056	0	0	0	0	0.0367
Jan		236	133	19	12	36	36
Gempylidae		0.0111	0.0071	0	0	0.0553	0.0026
snake mackerels	G	0.0028	0.0023	0	0	0.0199	0.0026
Sep-Jun		2634	1525	250	231	318	310
<i>Gempylus</i> spp.		0.0076	0.0133	0	0	0	0
mackerel	B	0.0076	0.0133	0	0	0	0
Feb		218	125	17	15	31	30
Gerreidae		0.0081	0.0126	0	0	0	0.0063
mojarras	A	0.0026	0.0043	0	0	0	0.0063
Apr-Jan		2634	1525	250	231	318	310
Gigantactinidae		0.0021	0.0035	0	0	0	0
anglerfishes	B	0.0021	0.0035	0	0	0	0
May		182	109	22	15	18	18
<i>Gnathanodon</i> spp.		0.0276	0.0447	0	0	0	0
trevally	B	0.0276	0.0447	0	0	0	0
Jun		233	144	13	12	33	31
Gobiesocidae		0.0051	0.0026	0	0	0.0304	0
clingfishes	G	0.0023	0.0019	0	0	0.0175	0
Apr-Oct		1573	908	157	147	183	178
<i>Gobiesox strumosus</i>		0.1202	0.1653	0	0.0095	0.1165	0.0788
skilletfish	G	0.0283	0.0483	0	0.0095	0.0317	0.024
Jan-Dec		2427	1399	223	207	302	296
Gobiidae		2.3219	0.7604	0.2768	1.3685	5.7943	8.8014
gobies	G	0.2486	0.1962	0.0631	0.394	0.6305	1.6751
Jan-Dec		2634	1525	250	231	318	310
<i>Gobionellus hastatus</i>		0.0042	0.0009	0.0153	0.0148	0.008	0
highfin goby	A	0.0017	0.0005	0.0108	0.0106	0.008	0
Jan-Oct		2634	1525	250	231	318	310

Table 2.3 *Continued*:

Fish Taxa	Code	OM	Surf	Mid	NB	UO	LO
<i>Gonichthys</i> spp. lanternfish Feb	B	0.0035 0.0035 218	0.0061 0.0061 125	0 0 17	0 0 15	0 0 31	0 0 30
Gonostomatidae bristlemouths Jan-Dec	G	0.2421 0.1057 2634	0.0936 0.0235 1525	0 0 250	0.0043 0.0043 231	1.4308 0.8654 318	0.1261 0.0368 310
<i>Gymnothorax</i> spp. moray eels Apr-Dec	A	0.0081 0.0027 2055	0.0066 0.0028 1192	0 0 208	0 0 197	0.029 0.0178 232	0.009 0.0064 226
Haemulidae grunts and sweetlips Jan-Feb & Jul	A	0.0029 0.0017 1459	0.0017 0.0017 862	0.0136 0.0136 110	0 0 87	0 0 203	0.007 0.007 197
<i>Halieutichthys aculeatus</i> Pancake batfish Oct	B	0.0076 0.0076 188	0.0142 0.0142 100	0 0 30	0 0 30	0 0 14	0 0 14
<i>Harengula jaguana</i> scaled herring Mar-Nov	A	1.3969 0.2423 1973	1.6631 0.3402 1141	0.0104 0.0104 187	0 0 180	3.5533 1.1719 235	0.0937 0.0366 230
<i>Harengula pensacolae</i> scaled herring Apr-Oct	G	1.3243 0.2198 1573	1.821 0.3208 908	2.3823 1.1631 157	0.3222 0.1348 147	0 0 183	0.0463 0.0463 178
<i>Hemanthias leptus</i> longtail bass Apr	B	0.0134 0.0134 219	0.0227 0.0227 129	0 0 12	0 0 11	0 0 33	0 0 34
<i>Hippocampus erectus</i> lined seahorse Apr	B	0.0026 0.0026 219	0.0044 0.0044 129	0 0 12	0 0 11	0 0 33	0 0 34
<i>Hirundichthys</i> spp. flyingfish May	B	0.0044 0.0044 182	0.0073 0.0073 109	0 0 22	0 0 15	0 0 18	0 0 18
<i>Hirundichthys rondeleti</i> black wing flyingfish Jun	B	0.0034 0.0034 233	0.0056 0.0056 144	0 0 13	0 0 12	0 0 33	0 0 31
<i>Histrio histrio</i> sargassumfish Feb-Jun	B	0.0019 0.0012 977	0.0032 0.0021 582	0 0 70	0 0 60	0 0 134	0 0 131
Holocentridae squirrelfishes and soldierfishes Jun-Sep	B	0.0055 0.0051 984	0.0095 0.0088 570	0 0 93	0 0 91	0 0 118	0 0 112
<i>Holocentrus</i> spp. grouper/squirrelfish May	B	0.0021 0.0021 182	0.0035 0.0035 109	0 0 22	0 0 15	0 0 18	0 0 18
<i>Hoplunnis</i> spp. pink-conger Jan & Aug	A	0.0013 0.0008 1629	0.0014 0.001 921	0 0 176	0.0053 0.0053 171	0 0 182	0 0 179
<i>Hygophum</i> spp. lanternfish Nov-Jun	G	0.1574 0.0583 1695	0.0734 0.0372 999	0.0656 0.0356 140	0 0 122	0.7813 0.4134 219	0.0613 0.0419 215
<i>Hygophum taaningi</i> Tåning's lanternfish Jan	G	0.0071 0.0071 236	0 0 133	0.0884 0.0884 19	0 0 12	0 0 36	0 0 36
<i>Hypleurochilus</i> spp. blenny Jun	C	0.0167 0.0167 233	0 0 144	0 0 13	0 0 12	0.1176 0.1176 33	0 0 31

Table 2.3 *Continued*:

Fish Taxa	Code	OM	Surf	Mid	NB	UO	LO
<i>Hyporhamphus unifasciatus</i>		0.0027	0.0028	0	0	0.0091	0
common halfbeak	C	0.0015	0.0019	0	0	0.0091	0
Jun-Nov		1447	828	147	147	165	160
<i>Hypsoblennius</i> spp.		0.0081	0.0135	0	0	0	0
blenny	B	0.0059	0.01	0	0	0	0
Mar-Aug		1225	730	102	94	152	147
<i>Hypsoblennius hentzi</i>		0.004	0.0065	0	0	0	0
feather blenny	B	0.004	0.0065	0	0	0	0
Jun		233	144	13	12	33	31
<i>Istiophorus</i> spp.		0.002	0.0032	0	0	0	0
sailfish	B	0.002	0.0032	0	0	0	0
Jun		233	144	13	12	33	31
<i>Istiophorus platypterus</i>		0.0019	0.0036	0	0	0	0
Indo-Pacific sailfish	B	0.0019	0.0036	0	0	0	0
Sep		285	153	31	30	36	35
Labridae		0.0391	0.0176	0.0292	0.0078	0.1951	0.0147
wrasses	G	0.0136	0.0067	0.0168	0.0078	0.1053	0.0104
Sep-May		1935	1108	188	170	236	233
<i>Lagodon rhomboids</i>		0.2447	0.3045	0.069	0.0219	0.3919	0.1071
pinfish	G	0.0327	0.0497	0.0264	0.0165	0.1176	0.0431
Jan-Dec		2634	1525	250	231	318	310
<i>Lampanyctus</i> spp.		0.1082	0.0864	0	0	0.3467	0.0486
lanternfish	A	0.0328	0.0302	0	0	0.1799	0.0486
Jan-Mar		579	333	42	34	86	84
Lampridae		0.0032	0	0	0	0	0.0262
opahs	F	0.0032	0	0	0	0	0.0262
Nov		275	158	24	26	33	34
<i>Larimus fasciatus</i>		0.0678	0.0394	0.1407	0.0649	0.1394	0.0793
banded drum	G	0.0094	0.0113	0.0381	0.0285	0.0357	0.0235
Jan-Dec		2398	1392	231	219	282	274
<i>Leiostomus xanthurus</i>		0.86	0.231	0.7412	0.2811	4.0088	1.2514
spot croaker	G	0.1781	0.0635	0.1741	0.0805	1.3366	0.5038
Jan-Dec		2634	1525	250	231	318	310
<i>Lepidopus</i> spp.		0.0061	0	0	0	0.0397	0
scabbardfish	C	0.0061	0	0	0	0.0397	0
Jan		236	133	19	12	36	36
<i>Lepophidium</i> spp.		0.4708	0.026	0.095	0.7605	1.1403	2.0595
cuskeel	G	0.1069	0.0069	0.0585	0.5176	0.2797	0.7616
Apr-Jan		2634	1525	250	231	318	310
<i>Lepophidium graellsii</i>		0.0014	0.0023	0	0	0	0
shortbeard cuskeel	B	0.0014	0.0023	0	0	0	0
Jul		246	147	21	15	33	30
<i>Lepophidium staurophor</i>		0.0168	0.0143	0	0	0.0367	0.0345
barred cuskeel	A	0.0073	0.0105	0	0	0.0204	0.0279
Jan-Dec		2634	1525	250	231	318	310
<i>Leptostomias gladiator</i>		0.0111	0.0035	0	0	0.0639	0
scaleless dragonfish	C	0.0093	0.0035	0	0	0.0639	0
Feb		218	125	17	15	31	30
<i>Lestidiops</i> spp.		0.0303	0	0	0	0.1986	0
barracudina	C	0.0303	0	0	0	0.1986	0
Jan		236	133	19	12	36	36
<i>Lestidiops affinis</i>		0.003	0.0014	0	0.0363	0	0
barracudina	G	0.0023	0.0014	0	0.0363	0	0
Jan-Feb		454	258	36	27	67	66

Table 2.3 *Continued*:

Fish Taxa	Code	OM	Surf	Mid	NB	UO	LO
<i>Lestrolepis intermedia</i>		0.0039	0	0	0.0253	0	0
barracudina antifaz	E	0.0039	0	0	0.0253	0	0
Aug		220	126	28	34	16	16
<i>Liopropoma</i> spp.		0.0192	0.0083	0	0	0.0572	0.0614
basslet	A	0.0113	0.0083	0	0	0.0572	0.0614
Sep		285	153	31	30	36	35
<i>Liopropoma eukrines</i>		0.0017	0.0029	0	0	0	0
wrasse bass	B	0.0017	0.0029	0	0	0	0
Jul		246	147	21	15	33	30
Lophiidae		0.0052	0.0086	0	0	0	0
goosefishes	B	0.0052	0.0086	0	0	0	0
May		182	109	22	15	18	18
Lutjanidae		0.016	0.0011	0	0	0.0975	0.0304
snappers	G	0.0063	0.0008	0	0	0.0476	0.0203
Jan-Dec		2634	1525	250	231	318	310
<i>Lutjanus</i> spp.		0.1045	0.0592	0.02	0.097	0.2785	0.2224
snapper	G	0.0224	0.0133	0.02	0.0598	0.0913	0.1442
Jan-Dec		2634	1525	250	231	318	310
<i>Lutjanus campechanus</i>		0.0085	0.0051	0	0	0.0415	0.0087
red snapper	G	0.0033	0.0025	0	0	0.0249	0.0087
Jun-Oct		1172	670	123	121	132	126
<i>Macrorhamphosus scolopax</i>		0.1171	0.1004	0	0	0.3192	0.1412
longspine snipefish	G	0.0237	0.0262	0	0	0.1042	0.0957
Nov-May		1462	855	127	110	186	184
<i>Melamphaes</i> spp.		0.012	0.0089	0	0	0	0.0456
bigscale	A	0.0079	0.0066	0	0	0	0.0456
Jan		236	133	19	12	36	36
<i>Melamphaes polylepis</i>		0.0022	0.0039	0	0	0	0
melanfido	B	0.0022	0.0039	0	0	0	0
Feb		218	125	17	15	31	30
Melanostomiidae		0.003	0.0052	0	0	0	0
scaleless dragonfishes	B	0.0018	0.0031	0	0	0	0
Jan-Apr		798	462	54	45	119	118
<i>Membras martinica</i>		0.0415	0.0652	0	0	0.0282	0
rough silverside	C	0.0136	0.023	0	0	0.0162	0
Apr-Sep		1385	808	127	117	169	164
<i>Menidia</i> spp.		0.0045	0.0076	0	0	0	0
silverside	B	0.0035	0.0059	0	0	0	0
Mar-Apr		344	204	18	18	52	52
<i>Menticirrhus</i> spp.		0.5378	0.3443	2.4801	0.5273	0.3164	0.1578
kingcroaker	G	0.0983	0.1088	0.7704	0.1325	0.0624	0.0323
Jan-Dec		2634	1525	250	231	318	310
Microdesmidae		0.0053	0.0052	0	0	0	0.0191
wormfishes	A	0.0031	0.0035	0	0	0	0.0191
May & Oct		1650	955	157	140	200	198
<i>Microdesmus</i> spp.		0.1698	0.0941	0.0814	0.057	0.6497	0.2051
wormfish	G	0.0225	0.0194	0.0452	0.0272	0.1452	0.0524
Jan-Dec		2634	1525	250	231	318	310
<i>Microdesmus lanceolatus</i>		0.065	0.044	0	0.2574	0	0
lancetail wormfish	G	0.0327	0.044	0	0.131	0	0
Aug		220	126	28	34	16	16
<i>Microdesmus longipinnis</i>		0.0125	0	0	0	0.0882	0
pink wormfish	C	0.0125	0	0	0	0.0882	0
Jun		233	144	13	12	33	31

Table 2.3 *Continued*:

Fish Taxa	Code	OM	Surf	Mid	NB	UO	LO
<i>Micropogonias undulatus</i>		8.3628	1.0696	25.7908	37.4229	8.5415	8.3479
Atlantic Croaker	G	1.2148	0.2138	8.3903	9.3356	2.4269	1.33
Jan-Dec		2634	1525	250	231	318	310
<i>Monacanthus</i> spp.		0.0015	0.0027	0	0	0	0
filefish	B	0.0011	0.002	0	0	0	0
Jul-Sep		751	426	80	79	85	81
<i>Monacanthus hispidus</i>		0.0056	0.0097	0	0	0	0
planehead filefish	B	0.0034	0.0059	0	0	0	0
Jun-Nov		1447	828	147	147	165	160
<i>Monacanthus setifer</i>		0.0093	0.0162	0	0	0	0
pygmy filefish	B	0.005	0.0087	0	0	0	0
Sep-Jun		2168	1252	201	182	269	264
<i>Monolene sessilicauda</i>		0.0062	0	0	0	0.0435	0
deepwater flounder	C	0.0062	0	0	0	0.0435	0
Feb		218	125	17	15	31	30
Moringuidae		0.0273	0.0011	0	0	0.0691	0.1704
worm/spaghetti eels	A	0.0113	0.0011	0	0	0.0359	0.0947
May-Jan		2072	1196	215	198	235	228
<i>Mugil</i> spp.		0.3262	0.0057	0	0	1.1668	1.6312
mullet	G	0.1661	0.0033	0	0	0.5736	1.3308
Jun-Feb		2108	1212	210	198	248	240
<i>Mugil cephalus</i>		0.7706	0.889	0.0658	0.0061	1.7637	0.3077
flathead mullet	G	0.2043	0.3394	0.041	0.0061	0.4497	0.0842
Jan-Dec		2634	1525	250	231	318	310
<i>Mugil curema</i>		0.0143	0.0157	0.0288	0	0.0204	0
white mullet	A	0.0041	0.0057	0.0216	0	0.012	0
Apr-Nov		1848	1066	181	173	216	212
Mugilidae		0.0115	0.0126	0	0	0.0185	0.0183
mulletts	A	0.0048	0.007	0	0	0.0134	0.0183
Apr-Oct		1573	908	157	147	183	178
Mullidae		0.0582	0.0818	0.0106	0	0.082	0
goat fishes	G	0.0103	0.016	0.0106	0	0.0355	0
Jan-Dec		2634	1525	250	231	318	310
Muraenidae		0.098	0.0024	0.2176	0	0.3575	0.2784
moray eels	G	0.0265	0.0011	0.2176	0	0.1049	0.089
Jan-Dec		2634	1525	250	231	318	310
Myctophidae		1.4797	1.0168	0.368	0.1926	5.0352	1.9646
lanternfishes	G	0.1134	0.1306	0.1093	0.0943	0.5488	0.3676
Jan-Dec		2634	1525	250	231	318	310
<i>Myctophum</i> spp.		0.0116	0.0015	0	0	0.0293	0.0437
lanternfish	A	0.0055	0.0015	0	0	0.0206	0.0309
Jan-Mar		579	333	42	34	86	84
<i>Myrophis</i> spp.		0.0124	0.0233	0	0	0	0
worm eel	B	0.0124	0.0233	0	0	0	0
Oct		188	100	30	30	14	14
<i>Myrophis punctatus</i>		0.1719	0.0983	0.0804	0.1658	0.1686	0.616
speckled worm eel	G	0.0298	0.0198	0.0236	0.0755	0.0629	0.2153
Jan-Dec		2634	1525	250	231	318	310
<i>Naucrates ductor</i>		0.0016	0.0028	0	0	0	0
pilotfish	B	0.0016	0.0028	0	0	0	0
Jan		236	133	19	12	36	36
<i>Neoconger mucronatus</i>		0.021	0.0072	0	0.0071	0.0324	0.1247
ridged eel	G	0.008	0.0043	0	0.0071	0.0229	0.0704
Aug-Nov		968	537	113	120	99	99

Table 2.3 *Continued*:

Fish Taxa	Code	OM	Surf	Mid	NB	UO	LO
<i>Nesiarchus nasutus</i>		0.0032	0.0056	0	0	0	0
black gemfish	B	0.0032	0.0056	0	0	0	0
Jan		236	133	19	12	36	36
Nettastomatidae		0.0155	0.0046	0.0217	0	0.0536	0.0323
duckbill/witch eels	G	0.0042	0.0019	0.0154	0	0.0262	0.0136
Nov-Jul		1941	1146	161	137	252	245
Nomeidae		0.0096	0.0167	0	0	0	0
driftfishes	B	0.0042	0.0073	0	0	0	0
Oct-Apr		1468	846	135	125	182	180
<i>Nomeus gronovii</i>		0.0018	0.003	0	0	0	0
man-of-war fish	B	0.0013	0.0022	0	0	0	0
Dec-Jan & Jun		1420	841	116	96	186	181
<i>Notoscopelus resplendens</i>		0.0097	0.0082	0	0.0844	0	0
patchwork lampfish	A	0.0058	0.0053	0	0.0844	0	0
Jan-Feb		454	258	36	27	67	66
Ogcocephalidae		0.0066	0	0.0359	0	0.028	0
batfishes	C	0.0047	0	0.0359	0	0.028	0
Nov-Dec		482	284	51	50	49	48
<i>Oligoplites</i> spp.		0.0041	0.0069	0	0	0	0
leatherjack	B	0.0031	0.0052	0	0	0	0
Jul		246	147	21	15	33	30
<i>Oligoplites saurus</i>		0.2204	0.3741	0	0	0.0062	0.0122
leatherjack	G	0.0447	0.076	0	0	0.0062	0.0122
Apr-Sep		1385	808	127	117	169	164
Ophichthidae		0.1936	0.0303	0	0.0371	0.5154	0.9392
snake eels	G	0.0325	0.0087	0	0.0371	0.0917	0.2492
Jan-Dec		2634	1525	250	231	318	310
<i>Ophichthus</i> spp.		0.0782	0.0106	0	0.0481	0.2839	0.3223
snake eel	G	0.0186	0.0056	0	0.0384	0.1109	0.1142
Apr-Dec		2055	1192	208	197	232	226
<i>Ophichthus gomesi</i>		0.057	0.031	0.0131	0.1354	0.114	0.1003
shrimp eel	A	0.017	0.019	0.0131	0.092	0.0618	0.0444
Jul-Nov		1214	684	134	135	132	129
<i>Ophichthus ophis</i>		0.0134	0	0.1026	0	0	0
spotted snake eel	D	0.0134	0	0.1026	0	0	0
Dec		207	126	27	24	16	14
Ophidiidae		0.2365	0.0428	0.1594	0.047	1.0769	0.531
cusk eels	G	0.0653	0.008	0.1063	0.0383	0.5176	0.119
Jan-Dec		2634	1525	250	231	318	310
<i>Ophidion</i> spp.		0.063	0.0153	0.1961	0.0708	0.1466	0.0997
blenny/cusk eel	G	0.0111	0.0043	0.0685	0.039	0.0516	0.0405
Feb-Jun & Sep-Nov		1973	1141	187	180	235	230
<i>Ophidion nocomis</i>		0.0056	0	0	0	0.0373	0
letter opener	C	0.0056	0	0	0	0.0373	0
Apr		219	129	12	11	33	34
<i>Ophidion selenops</i>		0.0116	0.0004	0	0	0.067	0.0356
mooneye cusk eel	G	0.0038	0.0004	0	0	0.029	0.0162
May-Nov		1629	937	169	162	183	178
<i>Ophioblennius</i> spp.		0.0034	0.0057	0	0	0	0
blenny	B	0.0018	0.003	0	0	0	0
Jan & Jun-Jul		1459	862	110	87	203	197
<i>Opisthonema oglinum</i>		10.9557	7.8547	37.2805	18.4867	8.1354	2.2622
Atlantic thread herring	G	1.7845	2.1489	12.0412	4.9973	2.6651	0.7693
Jan-Dec		2634	1525	250	231	318	310

Table 2.3 *Continued*:

Fish Taxa	Code	OM	Surf	Mid	NB	UO	LO
<i>Orthopristis</i> spp.		0.0049	0.0081	0	0	0	0
grunt	B	0.0049	0.0081	0	0	0	0
Mar		125	75	6	7	19	18
<i>Orthopristis chrysoptera</i>		0.0913	0.11	0	0.4994	0	0
pigfish	G	0.037	0.0544	0	0.3398	0	0
Mar-Apr		344	204	18	18	52	52
<i>Oxyporhamphus micropterus</i>		0.0027	0.0047	0	0	0	0
bigwing halfbeak	B	0.0016	0.0028	0	0	0	0
Jun-Sep		984	570	93	91	118	112
<i>Paraconger caudilimbatus</i>		0.0077	0	0	0.05	0	0
margintail conger	E	0.0077	0	0	0.05	0	0
Aug		220	126	28	34	16	16
Paralepididae		0.0233	0.014	0.0047	0	0.1094	0.0137
barracudinas	G	0.0047	0.0049	0.0047	0	0.0292	0.0079
Sep-Jun		2634	1525	250	231	318	310
<i>Paralichthys</i> spp.		0.0329	0.0164	0.125	0	0.0411	0.0555
flounder	G	0.0088	0.0066	0.0752	0	0.0179	0.0242
Jan-Dec		2634	1525	250	231	318	310
<i>Paralichthys lethostigma</i>		0.0472	0	0.3619	0	0	0
southern flounder	G	0.0388	0	0.2952	0	0	0
Dec		207	126	27	24	16	14
<i>Peprilus alepidotus</i>		0.0433	0.0756	0	0	0	0
harvestfish	B	0.0294	0.0513	0	0	0	0
Aug		220	126	28	34	16	16
<i>Peprilus burti</i>		0.6811	0.359	0.8283	0.1944	1.7359	1.4272
Gulf butterfish	G	0.0566	0.047	0.1728	0.0567	0.2772	0.2621
Jan-Dec		2634	1525	250	231	318	310
<i>Peprilus paru</i>		3.4006	0.1194	32.4019	0.6869	0.4856	0.3231
American harvestfish	G	2.8599	0.03	29.1826	0.2068	0.1175	0.0847
Apr-Nov		1848	1066	181	173	216	212
<i>Peprilus</i> spp.		0.0171	0.0057	0	0	0.1081	0.018
butterfish	G	0.0103	0.0057	0	0	0.0865	0.018
Sep-Nov		748	411	85	86	83	83
<i>Photostomias</i> spp.		0.0042	0.0068	0	0	0	0
barbeled dragonfish	B	0.0042	0.0068	0	0	0	0
Dec		207	126	27	24	16	14
Pleuronectidae		0.0455	0.058	0	0	0.1089	0
right-eye flounders	C	0.0318	0.05	0	0	0.1089	0
May		182	109	22	15	18	18
<i>Pogonias cromis</i>		0.2736	0.3159	0.2107	0.7326	0.0576	0.0135
black drum	A	0.0705	0.1029	0.1048	0.4234	0.0326	0.0096
Sep-Apr		1753	999	166	155	218	215
Pomatomidae		0.0139	0.0228	0	0	0	0.0069
bluefishes	A	0.0079	0.0138	0	0	0	0.0069
Sep-Apr		1753	999	166	155	218	215
<i>Pomatomus saltatrix</i>		0.1259	0.1216	0	0	0.4277	0.0211
bluefish	G	0.0228	0.0266	0	0	0.1336	0.0111
Sep-Jun		2168	1252	201	182	269	264
Priacanthidae		0.0073	0	0	0	0.0272	0.0238
bigeyes	A	0.0052	0	0	0	0.0272	0.0238
Feb-Mar & Sep		343	200	23	22	50	48
<i>Prionotus</i> spp.		0.1197	0.0583	0.0545	0.0207	0.3299	0.3323
searobin	G	0.0218	0.0292	0.0252	0.0207	0.0726	0.0848
Jan-Dec		2634	1525	250	231	318	310

Table 2.3 *Continued*:

Fish Taxa	Code	OM	Surf	Mid	NB	UO	LO
<i>Pronotogrammus aureorubens</i>		0.0059	0.0105	0	0	0	0
streamer bass	B	0.0059	0.0105	0	0	0	0
Jan		236	133	19	12	36	36
<i>Pseudogramma</i> spp.		0.0054	0	0	0	0.0356	0
podge	C	0.0054	0	0	0	0.0356	0
Jan		236	133	19	12	36	36
<i>Pseudomyrophis</i> spp.		0.0049	0.0015	0	0	0	0.0398
worm eel	A	0.0041	0.0015	0	0	0	0.0398
Nov-Dec		482	284	51	50	49	48
<i>Rachycentron canadum</i>		0.0331	0.014	0	0	0.1536	0.027
cobia	G	0.0154	0.0097	0	0	0.0996	0.027
Jun-Jul		479	291	34	27	66	61
<i>Rypticus</i> spp.		0.008	0	0	0	0.0567	0
soapfish	C	0.008	0	0	0	0.0567	0
Jun		233	144	13	12	33	31
<i>Rypticus maculatus</i>		0.0007	0.0012	0	0	0	0
whitespotted soapfish	B	0.0007	0.0012	0	0	0	0
Jul		246	147	21	15	33	30
<i>Sarda sarda</i>		0.0083	0	0	0	0.0584	0
Atlantic bonito	C	0.0083	0	0	0	0.0584	0
Feb		218	125	17	15	31	30
<i>Sardinella</i> spp.		0.006	0.0084	0	0	0.0096	0
sardinella	C	0.0026	0.0041	0	0	0.0096	0
Apr-Oct		1573	908	157	147	183	178
<i>Sardinella anchovia</i>		0.0265	0.0462	0	0	0	0
round sardinella	B	0.0265	0.0462	0	0	0	0
Feb		218	125	17	15	31	30
Scaridae		0.0069	0.0015	0.0576	0	0	0
parrot fishes	C	0.006	0.0015	0.0576	0	0	0
Dec-Jan		443	259	46	36	52	50
<i>Scartella cristata</i>		0.0033	0.0044	0	0	0	0.0065
molly miller	A	0.002	0.0032	0	0	0	0.0065
Apr-Nov		1848	1066	181	173	216	212
Sciaenidae		0.4498	0.1996	1.7319	1.3633	0.269	0.151
drums	G	0.1436	0.0587	1.2749	0.7634	0.1236	0.0832
Jan-Dec		2634	1525	250	231	318	310
<i>Sciaenops ocellatus</i>		22.3987	17.3481	59.3986	47.7319	5.453	0.5469
red drum	G	5.183	6.66	22.6764	22.2163	1.7554	0.2954
Aug-Jan		1411	796	159	156	151	149
<i>Scomber</i> spp.		0.016	0	0	0	0.1064	0
mackerel/tuna	C	0.016	0	0	0	0.1064	0
Apr		219	129	12	11	33	34
<i>Scomber japonicus</i>		0.0076	0.0101	0	0	0.0146	0
chub mackerel	C	0.0029	0.0044	0	0	0.0112	0
Sep-Jun		2634	1525	250	231	318	310
<i>Scomberomorus</i> spp.		0.1636	0.2484	0.0305	0.0748	0.0785	0
mackerel	A	0.1277	0.2187	0.0305	0.0577	0.0561	0
May-Sep		1166	679	115	106	136	130
<i>Scomberomorus cavalla</i>		0.2849	0.0137	0.0645	0.4909	1.8755	0.0638
king mackerel	G	0.1399	0.0058	0.0481	0.225	1.1799	0.0269
May-Sep		1166	679	115	106	136	130
<i>Scomberomorus maculatus</i>		2.1022	1.9911	5.6147	1.3733	1.6987	0.5878
Spanish mackerel	G	0.4831	0.7652	1.8406	0.5268	0.2912	0.1463
Mar-Oct		1573	908	157	147	183	178

Table 2.3 *Continued*:

Fish Taxa	Code	OM	Surf	Mid	NB	UO	LO
<i>Scomberomorus regalis</i>		0.007	0	0	0	0	0.0526
cero	F	0.007	0	0	0	0	0.0526
Jun		233	144	13	12	33	31
Scombridae		0.1632	0.0778	0.4851	0.2116	0.3505	0.095
mackerels/bonitos/tunas	G	0.0343	0.0184	0.2621	0.156	0.1226	0.0504
Jan-Dec		2634	1525	250	231	318	310
Scopelarchidae		0.0024	0.0043	0	0	0	0
pearleyes	B	0.0024	0.0043	0	0	0	0
Jan		236	133	19	12	36	36
<i>Scopelarchus</i> spp.		0.0094	0	0	0	0	0.068
pearleye	F	0.0094	0	0	0	0	0.068
Feb		218	125	17	15	31	30
Scopelosauridae		0.0091	0	0	0	0.0594	0
waryfishes	C	0.0091	0	0	0	0.0594	0
Jan		236	133	19	12	36	36
<i>Scorpaena</i> spp.		0.0482	0.0168	0.0063	0	0.2074	0.1092
scorpionfish	G	0.0088	0.0068	0.0063	0	0.0569	0.0315
Jan-Dec		2634	1525	250	231	318	310
Scorpaenidae		0.0214	0.0022	0	0	0.0787	0.0908
scorpionfishes	G	0.0056	0.0011	0	0	0.0285	0.0368
Sep-Jun		2634	1525	250	231	318	310
<i>Selar crumenophthalmus</i>		0.067	0.0652	0.0238	0.0038	0.171	0.0514
bigeye scad	G	0.0129	0.0163	0.0137	0.0038	0.0678	0.023
Jan-Dec		2634	1525	250	231	318	310
<i>Selene</i> spp.		0.0523	0.0821	0.05	0	0	0
moonfish	C	0.0274	0.0472	0.0322	0	0	0
Apr-Nov		1848	1066	181	173	216	212
<i>Selene setapinnis</i>		0.0031	0	0	0	0.0255	0
Atlantic moonfish	G	0.0023	0	0	0	0.0192	0
Jun-Sep		984	570	93	91	118	112
<i>Selene vomer</i>		0.0134	0	0	0	0.0875	0.0254
lookdown	G	0.0059	0	0	0	0.0452	0.0189
Jun-Sep		984	570	93	91	118	112
<i>Seriola</i> spp.		0.0215	0.0286	0	0	0.0412	0
jack/amberjack	C	0.0072	0.0119	0	0	0.018	0
Jan-Dec		2634	1525	250	231	318	310
<i>Serraniculus pumilio</i>		0.0112	0	0.07	0	0	0
pygmy sea bass	D	0.0112	0	0.07	0	0	0
Oct		188	100	30	30	14	14
Serranidae		0.2533	0.0584	0.072	0.059	0.8434	0.898
groupers/sea basses	G	0.0267	0.0095	0.0281	0.0301	0.1318	0.1642
Jan-Dec		2634	1525	250	231	318	310
<i>Serranus</i> spp.		0.0228	0.0134	0	0	0.041	0.0858
grouper	G	0.007	0.0076	0	0	0.0261	0.038
Jan-Dec		2634	1525	250	231	318	310
Soleidae		0.0107	0.0082	0	0	0.0406	0.0053
true soles	A	0.0033	0.0029	0	0	0.0208	0.0053
Jan-Sep		1964	1141	169	151	255	248
Sparidae		0.0524	0.0695	0	0	0.0713	0.0306
breams/porgies	A	0.0115	0.0189	0	0	0.0254	0.0149
Jan-Dec		2634	1525	250	231	318	310
<i>Sphoeroides</i> spp.		0.1154	0.0709	0.0087	0.0362	0.3294	0.26
puffer	G	0.0156	0.0148	0.0087	0.0206	0.0803	0.07
Jan-Dec		2634	1525	250	231	318	310

Table 2.3 *Continued*:

Fish Taxa	Code	OM	Surf	Mid	NB	UO	LO
<i>Sphyraena</i> spp. barracuda Jan-Dec	G	0.135 0.0188 2634	0.1074 0.0218 1525	0.0764 0.0415 250	0.0911 0.0429 231	0.4093 0.1025 318	0.0695 0.0223 310
<i>Sphyraena borealis</i> northern sennet Mar-Apr	B	0.0036 0.0021 344	0.006 0.0036 204	0 0 18	0 0 18	0 0 52	0 0 52
<i>Sphyraena guachancho</i> Guachanche barracuda Aug	A	0.0043 0.0039 220	0.0008 0.0008 126	0 0 28	0.025 0.025 34	0 0 16	0 0 16
Sphyraenidae barracuda Jun-Oct	B	0.0057 0.0042 1172	0.01 0.0073 670	0 0 123	0 0 121	0 0 132	0 0 126
<i>Stellifer lanceolatus</i> American stardrum Apr-Jan	G	0.5295 0.1938 2634	0.0297 0.0075 1525	3.6117 1.9653 250	1.568 0.4972 231	0.2188 0.1878 318	0.0475 0.0207 310
<i>Stemonosudis intermedia</i> baracudilla Jan-Apr	A	0.0022 0.0018 798	0.0008 0.0008 462	0 0 54	0 0 45	0 0 119	0.0117 0.0117 118
<i>Stomias</i> spp. dragonfish/boafish Oct-May	G	0.0104 0.0027 1650	0.0112 0.0033 955	0 0 157	0 0 140	0.0323 0.0153 200	0 0 198
Stomiidae barbeled dragonfishes/streeters Jan-Apr	A	0.0062 0.0027 798	0.0083 0.0039 462	0 0 54	0 0 45	0 0 119	0.0097 0.0097 118
Stromateidae butterfishes Sep-Apr	C	0.0063 0.0046 1753	0.0099 0.0079 999	0 0 166	0 0 155	0.0054 0.0054 218	0 0 215
<i>Syacium</i> spp. flounder Jan-Dec	G	0.3259 0.0482 2634	0.0289 0.0086 1525	0.0318 0.016 250	0.3943 0.3351 231	1.3287 0.2109 318	0.9447 0.2258 310
<i>Syacium gunteri</i> shoal flounder Jun-Nov	G	0.0254 0.0196 1654	0 0 954	0.0102 0.0102 174	0.0302 0.0302 171	0.1937 0.1766 181	0 0 174
<i>Syacium papillosum</i> dusky flounder Jul-Sep	C	0.0039 0.0021 751	0.0043 0.0026 426	0 0 80	0 0 79	0.0127 0.0127 85	0 0 81
<i>Symphurus</i> spp. tonguefish Jan-Dec	G	2.3618 0.2781 2634	0.7243 0.3499 1525	1.5083 0.7147 250	1.3495 0.8218 231	8.5061 1.0215 318	5.5571 0.7862 310
<i>Symphurus plagiusa</i> blackcheek tonguefish Apr-May & Sep	G	0.09 0.055 1385	0.0092 0.0061 808	0 0 127	0 0 117	0.5293 0.4383 169	0.1691 0.1037 164
Syngnathidae seahorses/pipefishes/sea dragons Jul-Dec	A	0.0065 0.003 1421	0.0051 0.0033 810	0 0 161	0 0 159	0.0197 0.0197 148	0.0154 0.0114 143
<i>Syngnathus</i> spp. pipefish Jan-Dec	G	0.027 0.0043 2634	0.0165 0.0037 1525	0.0326 0.0205 250	0 0 231	0.0714 0.0202 318	0.0482 0.0175 310
<i>Syngnathus louisianae</i> chain pipefish Apr-Oct	A	0.0285 0.0082 1573	0.0291 0.012 908	0.0122 0.0122 157	0 0 147	0.0703 0.0326 183	0.0203 0.0144 178
<i>Syngnathus scovelli</i> Gulf pipefish Jun	B	0.001 0.001 233	0.0016 0.0016 144	0 0 13	0 0 12	0 0 33	0 0 31

Table 2.3 *Continued*:

Fish Taxa	Code	OM	Surf	Mid	NB	UO	LO
Synodontidae		0.1681	0.0396	0.0581	0.9848	0.1739	0.2747
lizardfishes	G	0.0751	0.0111	0.0268	0.8411	0.0471	0.0914
Jan-Dec		2634	1525	250	231	318	310
<i>Synodus</i> spp.		0.4616	0.0582	0.0059	0.3623	1.0275	2.3073
lizardfish	G	0.0988	0.0243	0.0059	0.2183	0.1929	0.7817
Jan-Dec		2634	1525	250	231	318	310
<i>Synodus foetens</i>		0.0075	0.0126	0	0	0	0
inshore lizardfish	B	0.0075	0.0126	0	0	0	0
May		182	109	22	15	18	18
Tetragonuridae		0.0198	0	0	0	0.139	0
squaretails	C	0.0198	0	0	0	0.139	0
Feb		218	125	17	15	31	30
<i>Tetragonurus</i> spp.		0.0035	0.0062	0	0	0	0
squaretail	B	0.0035	0.0062	0	0	0	0
Jan		236	133	19	12	36	36
<i>Tetragonurus atlanticus</i>		0.0083	0.0023	0	0	0.0476	0
bigeye squaretail	C	0.0071	0.0023	0	0	0.0476	0
Feb-Mar		343	200	23	22	50	48
Tetraodontidae		0.0039	0.0036	0	0	0.013	0
pufferfishes	C	0.0028	0.0036	0	0	0.013	0
Apr-Jun		634	382	47	38	84	83
<i>Thunnus</i> spp.		0.006	0.0016	0	0	0.04	0
tuna	G	0.003	0.0008	0	0	0.0236	0
Feb-Sep		1728	1008	150	139	219	212
<i>Thunnus albacares</i>		0.1286	0.1559	0.0834	0	0.3002	0.0263
yellowfin tuna	A	0.0435	0.0737	0.0834	0	0.1374	0.0263
Sep-Oct		473	253	61	60	50	49
<i>Thunnus atlanticus</i>		0.0123	0.0142	0.0104	0	0.0141	0.0103
blackfin tuna	A	0.0043	0.0064	0.0104	0	0.0141	0.0073
Jan-May & Sep		1964	1141	169	151	255	248
<i>Thunnus thynnus</i>		0.0162	0.0277	0	0	0	0
northern bluefin tuna	B	0.0083	0.0142	0	0	0	0
Apr-May & Sep		1385	808	127	117	169	164
<i>Trachinocephalus myops</i>		0.0078	0	0	0.0506	0	0
snakefish	E	0.0078	0	0	0.0506	0	0
Aug		220	126	28	34	16	16
<i>Trachinotus</i> spp.		0.0033	0.0056	0	0	0	0
pompano	B	0.0033	0.0056	0	0	0	0
Apr		219	129	12	11	33	34
<i>Trachinotus carolinus</i>		0.0296	0.0494	0	0	0	0
Florida pompano	B	0.0296	0.0494	0	0	0	0
May		182	109	22	15	18	18
<i>Trachipterus</i> spp.		0.0029	0.005	0	0	0	0
ribbonfish	B	0.0029	0.005	0	0	0	0
Feb		218	125	17	15	31	30
<i>Trachurus</i> spp.		0.0029	0.0051	0	0	0	0
scad	B	0.0018	0.0031	0	0	0	0
Jan-Apr		798	462	54	45	119	118
<i>Trachurus lathami</i>		0.0626	0.0276	0.0543	0.0132	0.222	0.1151
rough scad	G	0.014	0.0141	0.0284	0.0094	0.0822	0.0389
Sep-Jun		2634	1525	250	231	318	310
Trichiuridae		0.0053	0.0071	0	0	0.0115	0
cutlassfishes	C	0.0029	0.0045	0	0	0.0115	0
Jun & Oct-Dec		1654	954	174	171	181	174

Table 2.3 *Continued*:

Fish Taxa	Code	OM	Surf	Mid	NB	UO	LO
<i>Trichiurus lepturus</i>		1.4744	1.9195	0.0624	0.3934	0.8233	1.9382
largehead hairtail	G	1.0997	1.8912	0.0402	0.1315	0.1375	0.5528
Jan-Dec		2398	1392	231	219	282	274
<i>Trichopsetta ventralis</i>		0.0378	0.0139	0	0	0.2103	0.0453
sash flounder	G	0.0119	0.0083	0	0	0.0891	0.027
Apr-Nov		1848	1066	181	173	216	212
Triglidae		0.0123	0.0013	0	0	0.0521	0.0445
sea robins	G	0.0059	0.0007	0	0	0.0349	0.0346
Jan-Dec		2634	1525	250	231	318	310
<i>Trinectes maculatus</i>		0.012	0.0009	0	0	0.0104	0.0897
hogchoaker	G	0.0054	0.0009	0	0	0.0104	0.0457
Jun-Sep		984	570	93	91	118	112
Uranoscopidae		0.0044	0.0033	0	0	0.0188	0
stargazers	C	0.0024	0.0027	0	0	0.0137	0
Nov-Apr		1280	746	105	95	168	166
<i>Urophycis</i> spp.		0.2929	0.4231	0.0328	0	0.2915	0.0419
codling/hake	G	0.0634	0.1033	0.0233	0	0.1459	0.0221
Nov-Apr		1280	746	105	95	168	166
<i>Urophycis regia</i>		0.0096	0.0124	0	0	0.0176	0
spotted codling	C	0.0053	0.0081	0	0	0.0176	0
Jan-Feb		454	258	36	27	67	66
<i>Verasper variegatus</i>		0.002	0.0032	0	0	0	0
spotted halibut	B	0.002	0.0032	0	0	0	0
Jun		233	144	13	12	33	31
<i>Vinciguerria</i> spp.		0.0354	0.0398	0.0274	0	0.0762	0.0044
lightfish	A	0.0116	0.0187	0.0202	0	0.0293	0.0044
Oct-May		1650	955	157	140	200	198
<i>Vinciguerria nimbaria</i>		0.0235	0.0297	0	0	0.0359	0.0108
oceanic lightfish	A	0.0067	0.0101	0	0	0.0232	0.0076
Nov-Jun		1695	999	140	122	219	215
<i>Zu cristatus</i>		0.0057	0.0049	0	0	0.0227	0
scalloped ribbonfish	C	0.0033	0.0028	0	0	0.0227	0
Dec-Feb		661	384	63	51	83	80
Decapod Taxa	Code	OM	Surf	Mid	NB	UO	LO
<i>Callinectes</i> spp.		0.4044	0.3715	0.5816	1.0134	0	0
crabs	G	0.1593	0.2501	0.2586	0.3703	0	0
Jan-Dec		2104	1269	250	231	179	175
<i>Callinectes sapidus</i>		66.447	97.946	23.057	25.132	9.5709	12.734
blue crab	G	15.553	25.727	3.3061	4.4096	1.3991	3.3512
Jan-Dec		2104	1269	250	231	179	175
<i>Callinectes similis</i>		12.985	14.166	10.616	6.5536	16.279	12.923
lesser blue crab	G	1.0919	1.522	4.3501	1.2372	2.3097	1.8482
Jan-Dec		2104	1269	250	231	179	175
<i>Penaeus</i> spp.		0.6959	1.0798	0.1446	0.1807	0.0741	0.0162
shrimps	A	0.2636	0.4363	0.0461	0.0597	0.0658	0.0096
Jan-Dec		2104	1269	250	231	179	175
<i>Farfantepenaeus aztecus</i>		2.2488	2.1832	3.731	1.3872	2.3841	1.6062
brown shrimp	A	0.2444	0.2153	1.6036	0.3084	0.8133	0.3014
Jan-Dec		2104	1269	250	231	179	175
<i>Farfantepenaeus duorarum</i>		0.1393	0.1427	0.0901	0.216	0.1634	0.0584
pink shrimp	A	0.0206	0.0268	0.0426	0.078	0.0923	0.0231
Jan-Dec		2104	1269	250	231	179	175
<i>Litopenaeus setiferus</i>		0.8806	1.0065	0.5046	1.2878	0.4818	0.3751
white shrimp	A	0.2236	0.3433	0.1949	0.718	0.2009	0.1008
Jan-Dec		2104	1269	250	231	179	175

to these statistically significant findings, 75 taxa were found distributed exclusively in horizontal surface tows only, yet were not statistically analyzed against the other zero values (Table 2.3, code B).

2.3.3 Upper Water Column Orientation

The largest statistically tested group of taxa ($N = 58$) showed a combination of either statistical significance in surface and mid-water horizontal tows, or upper water column oblique, or a combination of the two groupings. There were 18 taxa whose upper oblique densities were significantly greater than other depths, including: *Bothus* spp. (left-eye flounders), *Caranx* spp. (jacks), Caulophrynidae (fanfins/anglerfishes), *Decapterus punctatus* (round scad), Ephippidae (batfishes), Gempylidae (snake mackerels), Gobiesocidae (clingfishes), Gonostomatidae (bristlemouths), *Hygophum* spp. (lanternfish), *Macrorhamphosus scolopax* (longspine snipefish), *Microdesmus* spp. (wormfish), Paralepididae (barracudinas), *Pomatomus saltatrix* (bluefish), Scorpaenidae (scorpionfishes), *Sphyræna* spp. (barracuda), *Thunnus* spp. (tuna), *Trichopsetta ventralis* (sash flounder), and *Syacium* spp. (flounder).

There were ten taxa that showed a statistically greater difference between the upper water column oblique tows and each of the three distinct horizontal tows, i.e., *Ariomma* spp. (driftfish), *Brotula barbata* (Atlantic bearded brotula), Congridae (conger/garden eels), *Diplospinus multistriatus* (striped escolar), Gadidae (cods/haddock), Lutjanidae (snapper), Muraenidae (moray eels), *Selene vomer* (lookdown), and *Trachurus lathami* (rough scad), with only *Trachurus lathami* showing a difference between the lower oblique mean density and any of the three horizontal sampling efforts. There were also five taxa that showed upper oblique densities to be greater than two of the horizontal depths, and also the lower oblique tows, i.e., *Brevoortia*

gunteri (finescale menhaden), *Cyclopsetta* spp. (flounder), Labridae (wrasses), *Lutjanus* spp. (snapper), and *Scomberomorus cavalla* (king mackerel).

Of those species which only had one or two significant comparisons involving the upper oblique tow, all but three were significant when compared against the surface. There were eleven taxa where the only comparison that was significant was the upper oblique densities being greater than the surface, i.e., *Anchoviella* spp. (anchovy), *Anthias* spp. (basslets), *Euthynnus* spp. (mackerel), Nettastomatidae (duckbill eels), *Peprilus* spp. (butterfish), *Rachycentron canadum* (cobia), Scombridae (mackerels), *Selene setapinnis* (Atlantic moonfish), *Syacium gunteri* (shoal flounder), *Symphurus plagiusa* (blackcheek tonguefish), and Triglidae (searobins). Interestingly, only three taxa had upper oblique densities greater than horizontal near-bottom densities, i.e., *Auxis* spp. (tuna), *Selar crumenophthalmus* (bigeye scad), and *Syngnathus* spp. (pipefish), but the upper oblique was also significantly greater when compared to the mid-water in the case of *Auxis* spp. and surface tow densities in case for pipefish. Finally, *Bairdiella chrysoura* (silver perch) and *Stomias* spp. (lightfishes/dragonfishes) were similar in that the upper oblique was significantly greater than the lower oblique depth bin, but *B. chrysoura* upper oblique densities were also significantly greater than surface densities.

An upper water column orientation was also seen when both the surface and mid-water exhibited significantly greater densities over other depth bins. Despite some comparisons where surface and mid-depth were different against each other, the overall number of comparisons with other depths along with these taxa generally having higher overall mean densities in the surface, mid-depth, and upper oblique tows led to their overall upper water column orientation, i.e., *Anchoa* spp. (anchovy), Carangidae (jacks/pompanos), Engraulidae (anchovies), *Harengula*

pensacolae (scaled sardine), *Scomberomorus maculatus* (Spanish mackerel), and to a lesser extent *Sciaenops ocellatus* (red drum). Finally, three taxa showed an affinity for not only the upper water column, but also for the mid-depth, i.e., *Larimus fasciatus* (banded drum), *Leiostomus xanthurus* (spot), and *Ophidion* spp. (cusk eels).

2.3.4 Mid-Depth Oriented

Sixteen taxa showed statistically greater densities within the mid-water depth bin. In particular, nine taxa showed significant comparisons among depth bins with the mid-depth having the highest density. With both *Anchoviella perfasciata* (Poey's anchovy) and *Menticirrhus* spp. (kingcroakers), the mid-depth was significantly greater in all possible comparisons including both upper and lower oblique tows. With *Chaetodipterus faber* (Atlantic spadefish), *Etropus rimosus* (gray flounder), and *Hygophum taaningi* (lanternfish), the mid-depth comparisons were still highly significant. Mid-depth dominance was weaker for *Brevoortia* spp. (menhaden), *Citharichthys* spp. (lefteye flounders), *Paralichthys lethostigma* (southern flounder), and *Paralichthys* spp. (flounders).

The final seven taxa within this mid-depth category had as a common trait a somewhat mixed signal of not only statistically greater densities at mid-depth, but since the upper and lower water column half oblique tows overlapped coverage at mid-depth, they often had greater densities as well. *Cynoscion arenarius* (sand weakfish), *Opisthonema oglinum* (Atlantic thread herring), and *Peprilus paru* (American harvestfish) also showed statistically higher densities in the near-bottom tows, while Bothidae (lefteye flounders), *Chloroscombrus chrysurus* (Atlantic bumper), *Peprilus burti* (Gulf butterfish), and *Symphurus* spp. (tonguefish) showed statistically greater densities in lower oblique tows. As mentioned previously, in addition to these statistically

significant findings, three taxa were found distributed exclusively in horizontal mid-depth tows only, yet were not statistically analyzed against the other zero values (Table 2.3, code D), i.e., *Anchoa nasuta* (shortfinger anchovy), *Ophichthus ophis* (spotted snake eel), and *Serriculus pumilio* (pygmy sea bass).

2.3.5 Lower Water Column Orientation

Those taxa determined to have a preference for the lower portion of the water column ($N = 12$) exhibited statistically greater densities for the lower oblique or combinations of results involving lower oblique, mid-depth, and near-bottom suggesting a preference for the lower half of the water column. Four of these taxa showed significantly higher lower oblique densities than all other depth bins, i.e., *Bregmaceros cantori* (striped codlet), *Myrophis punctatus* (speckled worm eel), *Synodus* spp. (lizardfish), and *Trinectes maculatus* (hogchocker). The remaining eight taxa showed statistical combinations suggesting the dominance of the mid to lower half of the water column, i.e., *Cynoscion* spp. (trout/weakfish), *Diplectrum* spp. (sand perch), *Elops saurus* (ladyfish), *Micropogonias undulatus* (Atlantic croaker), *Neoconger mucronatus* (ridged eel), *Serranus* spp. (bass), *Stellifer lanceolatus* (American stardrum), and Synodontidae (lizardfishes).

2.3.6 Near-Bottom Oriented

Six taxa showed only statistically greater densities with the near-bottom horizontal tows. Of these, *Bregmaceros* spp. (codlets) and *Lestidiops affinis* (barracudina) showed statistical significance in every comparison with any other depth-bin. The other four taxa had statistically greater near-bottom densities over at least one depth bin, i.e., *Cynoscion nothus* (silver seatrout), *Microdesmus lanceolatus* (lancetail wormfish), *Orthopristis chrysoptera* (pigfish), and Sciaenidae (drums). As mentioned previously, in addition to these statistically significant

findings, three taxa were found distributed exclusively in horizontal near-bottom tows only, yet were not statistically analyzed against the other zero values (Table 2.3, code E), i.e., *Lestrolepis intermedia* (barracudina antifaz), *Paraconger caudilimbatus* (margintail conger), and *Trachinocephalus myops* (snakefish).

2.3.7 Oblique Distribution

There were 21 taxa which displayed statistically greater densities for both the lower and upper oblique tows. Seventeen of these taxa had significantly greater densities for both oblique tows versus the three horizontal depth bins, i.e., *Citharichthys spilopterus* (bay whiff), *Engyophrys senta* (American spiny flounder), *Etropus crossotus* (fringed flounder), *Etrumeus teres* (round herring), *Euthynnus alletteratus* (little tunny), Gobiidae (gobies), *Mugil* spp. (mullet), Muraenidae (moray eels), *Lepophidium* spp. (cusk eels), Ophichthidae (snake eels), *Ophichthus* spp. (snake eels), Ophidiidae (cusk eels), *Prionotus* spp. (searobin), *Scorpaena* spp. (scorpionfish), Scorpaenidae (scorpionfishes), Serranidae (groupers), and *Sphoeroides* spp. (puffer fishes). The statistical dominance of lower and upper oblique densities versus other depth bins decreased with *Bregmaceros atlanticus* (antenna codlet) and *Ophidion selenops* (mooneye cusk-eel), but especially for *Centropristis* spp. (sea basses/grouper) and *Lutjanus campechanus* (red snapper).

2.3.8 Commercially-Important Decapod Crustaceans

Of the seven, commercially-important decapod taxa analyzed, the three *Callinectes* species had statistical differences by depth after Bonferroni adjustment, while penaeids appeared to be more ubiquitously distributed throughout the water column (Table 2.2). *Callinectes* spp. (crab) appeared to prefer the lower portion of the water column, based on significantly greater

densities associated with both the mid-water and near-bottom horizontal depth bins. Both *Callinectes sapidis* (blue crab) and *Callinectes similis* (lesser blue crab), however, generally had densities associated with the upper portion of the water column.

2.3.9 Day/Night Ratios

Only a few taxa ($N = 19$) were effectively sampled within the LOOP program during both day and night. Approximately half of the ichthyoplankton and commercially-important decapod taxa with adequate coverage were seen to have fairly low day/night ratios, i.e., less than one, in surface related collections (Table 2.4). Such surface catch ratios indicate either visual gear avoidance during daylight hours or diel vertical migration. In general, the noticeable lack of sampling in the near-bottom depth bin made distinguishing between these two possible explanations of behavior difficult. Those taxa, which had day/night ratios greater than one, are most probably highly visual predators, which is likely the case for the carangid *Oligoplites saurus* (leatherjacket) and the scombrid *Scomberomorus maculatus* (Spanish mackerel). Both *C. similis* and *F. setiferus* were also found to have day/night ratios greater than one, possibly denoting reverse vertical migration.

Table 2.4: Day/night density ratios for ichthyoplankton and commercially-important decapods from all types of surface collections, and the near-bottom bongo net collections.

Fish Taxa	D/N Density Ratio
<i>Achirus lineatus</i>	0.0001
Blenniidae	0.2297
<i>Chloroscombrus chrysurus</i>	0.3447
<i>Cynoscion arenarius</i>	0.1035
<i>Cynoscion nebulosus</i>	0.0304
Engraulidae	0.0169
Gobiidae	0.0305
<i>Harengula jaguana</i>	0.0331
<i>Menticirrhus</i> spp.	0.1733
<i>Microdesmus</i> spp.	0.0105
<i>Mugil curema</i>	0.0098
<i>Oligoplites saurus</i>	0.0109
<i>Opisthonema oglinum</i>	0.1633
<i>Scomberomorus maculatus</i>	0.1475
Serranidae	0.0283
<i>Symphurus</i> spp.	2.1964

Decapod Taxa	D/N Density Ratio
<i>Callinectes sapidis</i>	1.4196
<i>Callinectes similis</i>	0.4341
<i>Farfantepenaeus aztecus</i>	1.0729

2.4 Discussion

The largest majority of statistically significant fish taxa were associated with the surface and upper half of the water column. Moreover, the single largest grouping of fish taxa ($N = 75$) not statistically analyzed were found exclusively in surface waters during horizontal tows. When expanded to include the upper half of the water column 40% of all fish taxa collected were found to have significantly higher densities in these upper waters, consistent with previous studies on the northern GOM shelf (Richards et al. 1993; Lindo-Atichati et al., 2012). Two of the three

statistically significant decapod taxa were also found in the upper water column, and the *Callinectes* congeners are typically found in the upper portion of the water column during their planktonic stages (Rabalais et al., 1995; Heck et al., 2001).

The smallest number of taxa were found to be associated with the mid-depth, near-bottom, or lower half of the water column and comprised approximately 4% of all taxa collected and identified (i.e., both fish and decapods). The species richness of zoo-/ichthyoplankton normally found in these lower depths has been reported to be low along the GOM shelf (Rabalais et al., 2001; Lindo-Atichati et al., 2012). The high degree of estuarine-dependent, offshore-spawned larvae that need to be transported to estuarine nursery grounds in the coastal waters of the GOM (Chambers, 1992; Mann, 2000) suggests that being in the lower portion of the water column may not be a beneficial transport and survival behavior (Able, 2005; Hare and Govoni, 2005; Glass et al., 2008; Vinagre et al., 2009).

There were 59 taxa, composed of 55 fish taxa and 4 decapod taxa that were found to be distributed throughout the entire water column, with no statistical preference for depth. This may not be as surprising as it first appears given the high degree of temporal and spatial variability in water column stability exhibited on the inner continental shelf of the northcentral GOM (Carassou et al., 2012). The inner shelf is extremely responsive to forcing by wind-driven vertical mixing (Swenson and Chuang, 1983; Perez et al., 2000; Walker and Hammack, 2000) and is also heavily influenced by riverine inputs associated with both the Mississippi River and Atchafalaya River plumes (Alexander et al., 2000; Carassou et al., 2012). Also, shelf ichthyoplankton and zooplankton communities are often characterized by high temporal and spatial variability and patchiness (Shaw et al. 1988; Leffler and Shaw 1992; Comyns et al. 2003).

The lack of nocturnal plankton collections in general, and at near-bottom in particular, made it difficult to illuminate diel vertically migrating taxa or to interpret our taxa groupings with respect to D/N ratios. The low D/N ratios probably reflect reactionary movements, i.e., a function of daytime gear avoidance in surface waters or a possible attempt to reduce exposure to mortality from visual predators (Pearre, 1979). The second type of movement, as suggested by day/night ratios greater than one, may indicate reverse vertical migration. This movement pattern usually occurs in taxa that are strong visual predators, or are photopositive, or in the general absence of extensive fish predation dependent upon adequate light fields.

2.5 Conclusions

The importance of a high percentage of zoo-/ichthyoplankton having an affinity for surface waters on the continental shelf is even more relevant when considering the potential that oil and gas industry environmental impacts, either authorized or accidental, may have within the upper water column. With authorized or licensed actions such as the use of ambient seawater associated with the normal activities of offshore oil and gas production or possible activities associated with proposed offshore LNG facilities needing to utilize large quantities of warm surface water for regasification, entrainment of surface or upper water column-oriented zoo-/ichthyoplankton could become a significant source of mortality. Accidental industrial effects, like those of the Deepwater Horizon oil spill (2010) and other events, e.g., Taylor Energy Wells Platform 23051 oil spill/leak (ongoing since 1994) and the gas blowout at the Hercules 265 Rig (2013), could represent significant additional mortality effects on early life history stages already experiencing up to 99% natural mortality (Hjort 1914; Hjort, 1926; Cushing, 1975; Houde, 1987; Cowan et al., 1996).

Further work should focus on more discrete depth resolution across shelf and into the deep GOM to more precisely delineate the vertical biological structure of the water column. Such detailed empirical data would allow for a more complete modeling of the structure of zoo-/ichthyoplankton in both the vertical and horizontal, to better predict vertical distributions and subsequent vulnerabilities to potential environmental impacts.

2.6 Literature Cited

- Able, K.W. 2005. A re-examination of fish estuarine dependence: evidence for connectivity between estuarine and ocean habitats. *Est. Coast. Shelf Sci.* 64(1): 5-17.
- Ahlstrom, E.H. 1959. Vertical distribution of pelagic fish eggs and larvae off California and Baja California. *Fish. Bull. NOAA* 60: 107 – 146.
- Alexander, R.B., R.A. Smith, and G.E. Schwarz. 2000. Effect of stream channel size on the delivery of nitrogen to the Gulf of Mexico. *Nature*, 403(6771): 758-761.
- Auth, T.D., and R.D. Brodeur. 2006. Distribution of community structure of ichthyoplankton of the coast of Oregon, USA, in 2000 and 2002. *Mar. Eco. Prog. Ser.* 319: 199-213.
- Brazitikovich, A. 1988. The use of planktonic organism distributions as an indicator of physical variability in marine environments. pp. 13 – 34. In: D.F. Soule and G.S. Kleppel (eds.), *Marine Organisms as Indicators*. Springer-Verlag, New York, NY, USA.
- Carassou, L., F.J. Hernandez, S.P. Powers, and W.M. Graham. 2012. Cross-shore, seasonal, and depth-related structure of ichthyoplankton assemblages in coastal Alabama. *Trans. Amer. Fish. Soc.* 141(4): 1137-1150.
- Chambers, J.R. 1992. Coastal degradation and fish population losses. *Stemming the Tide of Coastal Fish Habitat Loss*. *Mar. Recr. Fish. Pub.* 14:45-52.
- Cleveland, C.J. 2011. Deep Water: the gulf oil disaster and the future of offshore drilling. Report to the President. National Commission on the BP Deepwater Horizon Oil Spill and Offshore Drilling. Environmental Information Coalition, National Council for Science and the Environment, Washington, D.C.

- Colton, J.B., W.G. Smith Jr., A.W. Kendall, Jr., P.L. Berrien, and M.L. Fahay. 1979. Principal spawning areas and times of marine fishes, Cape Sable to Cape Hatteras. Fish. Bull. NOAA 76: 911 – 916.
- Cowan Jr., J.H., E.D. Houde, and K.A. Rose. 1996. Size-dependent vulnerability of marine fish larvae to predation: an individual-based numerical experiment. ICES J. of Mar. Sci. 53: 23-37.
- Cushing, D.H. 1975. Fisheries resources of the sea and their management. Vol. 1975, Oxford: Oxford University Press. pp. 1-75.
- Comyns, B.H., R.F. Shaw, and J. Lyczkowski-Shultz. 2003. Small-scale spatial and temporal variability in growth and maturity of fish larvae in the subtropical northcentral Gulf of Mexico: Implications for assessing recruitment success. Fish. Bull. NOAA 101: 10 – 21.
- Fahay, M.P. 1983. Guide to the early stages of marine fishes occurring in the western North Atlantic Ocean, Cape Hatteras to the south Scotian Shelf. North. Atl. Fish. Sci. 4: 1 – 423.
- Finucane, J.H., L.A. Collins, and J.D. McEachran. 1977. Ichthyoplankton/mackerel eggs and larvae. In: W.B. Jackson (ed.), Environmental studies of the south Texas outer continental shelf 1976. NOAA Final Report to BLM, Contract No. AA550-TA7-3. 183 pp.
- Fritzche, R.A. 1978. Development of Fishes of the Mid-Atlantic Bight: An Atlas of Egg, Larval and Juvenile Stages. Volume 5, Chaetodontidae through Ophidiidae. FWS/OBS-78/12, U.S. Fish and Wildlife Service, Washington, D.C., 237 pp.
- Glass, L.A., J.R. Rooker, R.T. Kraus, and G.J. Holt. 2008. Distribution, condition, and growth of newly settled southern flounder (*Paralichthys lethostigma*) in the Galveston Bay Estuary, TX. J. of Sea Res. 59(4): 259-268.
- Graham, B., W.K. Reilly, F. Beinecke, D.F. Boesch, T.D. Garcia, C.A. Murray, and F. Ulmer. 2012. Deep Water: The Gulf oil disaster and the future of offshore drilling. Report to the President. National Commission on the BP Deepwater Horizon Oil Spill and Offshore Drilling, pp. 1-398.
- Hanifen, J.G. 1987. Introduction, pp 1-1 to 1-65. In: K.J. Foote, J.G. Hamilton, and B.B. Barette (eds.). Environmental analysis and monitoring results of the Louisiana Offshore Oil Port (LOOP) and related facilities. Chapter 1. LDWF, Baton Rouge, LA.

- Hardy Jr., J.D. 1978a. Development of Fishes of the Mid-Atlantic Bight: An Atlas of Egg, Larval and Juvenile Stages. Volume 2, Anguillidae through Syngnathidae. FWS/OBS-78/12, U.S. Fish and Wildlife Service, Washington, D.C., 229 pp.
- Hardy Jr., J.D. 1978b. Development of Fishes of the Mid-Atlantic Bight: An Atlas of Egg, Larval and Juvenile Stages. Volume 3, Aphredoderidae through Rachycentridae. FWS/OBS-78/12, U.S. Fish and Wildlife Service, Washington, D.C., 249 pp.
- Hare, J.A., and J.J. Govoni. 2005. Comparison of average larval fish vertical distributions among species exhibiting different transport pathways on the southeast United States continental shelf. Fish. Bull. 103: 728-736.
- Heck Jr, K., L.D. Coen, and S.G. Morgan. 2001. Pre-and post-settlement factors as determinants of juvenile blue crab *Callinectes sapidus* abundance: results from the north-central Gulf of Mexico. Mar. Ecol. Prog. Ser., 222: 163-176.
- Helvarg, D. 2006. Blue Frontier: Saving America's Living Seas. Henry Holt and Company, New York, NY, USA. 320 pp.
- Hernandez, F.J., R.F. Shaw, J.S. Cope, J.G. Ditty, T.W. Farooqi, and M.C. Benfield. 2003. The across-shelf larval, post-larval and juvenile fish community associated with offshore oil and gas platforms west of the Mississippi River delta. Amer. Fish. Soc. Spec. Symp. Ser. 36: 39 – 72.
- Hjort, J. 1914. Fluctuations in the great fisheries of northern Europa. Rapp. Conseil Expl. Mer. XX. Copenhagen.
- Hjort, J. 1926. Fluctuations in the year classes of important food fishes. J. du Con., 1(1): 5-38.
- Houde, E.D. 1982. Kinds, distributions and abundances of sea bass larvae (Pisces:Serranidae) from the eastern Gulf of Mexico. Bull. Mar. Sci. 32: 511 – 522.
- Houde, E.D. 1987. Fish early life dynamics and recruitment variability. Am. Fish. Soc. Symp. 2: 17-29.
- Johnson, G.D. 1978. Development of Fishes of the Mid-Atlantic Bight: An Atlas of Egg, Larval and Juvenile Stages. Volume 4, Carangidae through Ephippidae. FWS/OBS-78/12, U.S. Fish and Wildlife Service, Washington, D.C., 189 pp.
- Jones, P.W., F.D. Martin, and J.D. Hardy. 1978. Development of Fishes of the Mid-Atlantic Bight: An Atlas of Egg, Larval and Juvenile Stages. Volume 1, Acipenseridae through Ictaluridae. FWS/OBS-78/12, U.S. Fish and Wildlife Service, Washington, D.C., 224 pp.

- Lang, L. 2012. The effects of hypoxia and other environmental factors on the vertical distribution of larval fishes in the northern Gulf of Mexico. Doctoral Dissertation, University of South Alabama, AL, USA.
- Leak, J.C. 1981. Distribution and abundance of carangid fish larvae in the eastern Gulf of Mexico, 1971-1974. *Biol. Ocean.* 1(1): 1 – 28.
- Leffler, D.L., and R.F. Shaw. 1992. Age validation, growth, and mortality of larval Atlantic bumper, (Carangidae: *Chloroscombrus chrysurus*) in the northern Gulf of Mexico. *Fish. Bull. NOAA* 90: 711 – 719.
- Lindo-Atichati, D., F. Bringas, G. Goni, B. Muhling, F.E. Muller-Karger, and S. Habtes, 2012. Varying mesoscale structures influence larval fish distribution in the northern Gulf of Mexico. *Mar. Eco. Prog. Ser.*, 463: 245-257.
- Lindquist, D.C., R.F. Shaw, and F.J. Hernandez, Jr. 2005. Distributional patterns of larval and juvenile fishes at offshore petroleum platforms in the north-central Gulf of Mexico. *Estu. Coast. Shelf Sci.* 62(4): 655-665.
- Mann, K.H. 2000. Ecology of the coastal waters with implications for management. 2nd Edition. John Wiley and Sons, Hoboken, NJ. 410 pp.
- Martin, F.D., and G.E. Drewry. 1978. Development of Fishes of the Mid-Atlantic Bight: An Atlas of Egg, Larval and Juvenile Stages. Volume 6, Stromateidae through Ogococephalidae. FWS/OBS-78/12, U.S. Fish and Wildlife Service, Washington, D.C., 176 pp.
- Miller, G.L., and S.C. Jorgenson. 1973. Meristic characters of some marine fishes of the western Atlantic Ocean. *Fish. Bull. NOAA* 71: 301 – 312.
- Moser, H.G. 1984. Ontogeny and systematics of fishes. American Society of Ichthyologists and Herpetologists Special Publication No. 1. Allen Press, Lawrence, KS. 760 pp.
- Muhling, B.A., and L.E. Beckley. 2007. Seasonal variation in horizontal and vertical structure of larval fish assemblages off south-western Australia, with implications for larval transport. *J. Plank. Res.* 29: 967-983.
- Pearre, S. 1979. Problems of detection and interpretation of vertical migration. *J. Plank. Res.*, 1(1): 29-44.
- Perez, B., J. Day, L. Rouse, R.F. Shaw, and M. Wang. 2000. Influence of Atchafalaya River discharge and winter frontal passage on suspended sediment concentration and flux in Fourleague Bay, Louisiana. *Estu. Coast Shelf Sci.* 50(2): 271-290.

- Rabalais, N.N., J. Burditt, F. Raymond, L.D. Coen, B.E. Cole, C. Eleuterius, R. Heck, R., L. Kenneth, T.A. McTigue, S.G. Morgan, H.M. Perry, F.M. Truesdale, R.K. Zimmer-Faust, and R.J. Zimmerman. 1995. Settlement of *Callinectes sapidus* megalopae on artificial collectors in four Gulf of Mexico estuaries. *Bull. Mar. Sci.*, 57(3): 855-876.
- Rabalais, N.N., R.E. Turner, and W.J. Wiseman. 2001. Hypoxia in the Gulf of Mexico. *J. . Envi. Qual.*, 30(2): 320-329.
- Richards, W.J., M.F. McGowan, T. Leming, J.T. Lamkin, and S. Kelley. 1993. Larval fish assemblages at the Loop Current boundary in the Gulf of Mexico. *Bull. Ma. Sci.*, 53(2): 475-537.
- Ruple, D.L. 1984. Occurrences of larval fishes in the surf zone of a northern Gulf of Mexico barrier island. *Estu. Coastal Shelf Sci.* 18: 191 – 208.
- SAS Institute Inc. 2011. Base SAS® 9.3 Procedures Guide. Cary, NC: SAS Institute Inc.
- Shaw, R.F. (In Review). Vertical distribution of ichthyoplankton within the northern Gulf of Mexico: A Review. Submitted to *Estu. Coastal Shelf Sci.*
- Shaw, R.F., J.S. Cope, and K.A. Edds. 1998. Volume IV: Zooplankton and ichthyoplankton. LOOP Marine and Estuarine Monitoring Program, 1978 – 1995. Center for Coastal, Energy and Environmental Resources, Louisiana State University, Baton Rouge, LA 70803. Prepared for the Louisiana Transportation Research Center (Proj. No. 97 – 3 IMP). Res. Rept. No. 316. 262 pp.
- Shaw, R.F., D.L. Drullinger, K.A. Edds, and D.L. Leffler. 1988. Fine-scale spatial distribution of red-drum, *Sciaenops ocellatus*, larvae. *Contr. Mar. Sci.* 30 (Supplement): 109-116.
- Stuck, K.C., and H.M. Perry.. 1982. Ichthyoplankton community structure in Mississippi coastal waters. pp. VI-I-1 to VI-I-53. In: Fishery monitoring and assessment completion report, 1 January 1977 to 31 December 1981. GCRL, Project No. 2- 296-R.
- Swenson, E.M., and W.S. Chuang. 1983. Tidal and subtidal water volume exchange in an estuarine system. *Estu. Coastal Shelf Sci.* 16(3): 229-240.
- Van Voorhees, D., and A. Lowther. (ed). 2011. Fisheries of the United States, 2003. U.S. Dept. of Commerce, Nat. Mar. Fish. Serv., Silver Springs, MD, Current Fisheries Statistics 2011. 107 pp.

- Vinagre, C., F.D. Santos, H.N. Cabral, and M.J. Costa. 2009. Impact of climate and hydrology on juvenile fish recruitment towards estuarine nursery grounds in the context of climate change. *Estu. Coastal Shelf Sci.* 85(3): 479-486.
- Walker, N.D., and A.B. Hammack. 2000. Impacts of winter storms on circulation and sediment transport: Atchafalaya-Vermilion Bay region, Louisiana, USA. *J. Coastal Res.* 16(4): 996-1010.
- Yatsu, A., C. Sassa, M. Moku, and T. Kinoshita. 2005. Night-time vertical distribution and abundance of small epipelagic and mesopelagic fishes in the upper 100m layer of the Kuroshio-Oyashio Transition Zone in spring. *Fish. Sci.* 71: 1280 – 1286.

CHAPTER 3. EFFECT OF WINTER ATMOSPHERIC COLD FRONT PASSAGES ON DENSITIES OF ICTHYOPLANKTON AND POST-LARVAL PENAIDS IN A LOUISIANA TIDAL PASS

One source of the temporal heterogeneity in estuarine recruitment and retention of offshore-spawned, estuarine-dependent ichthyoplankton in the northcentral Gulf of Mexico is the passage of atmospheric cold fronts. These energetic weather events are characterized by strong southerly and northerly winds, which are in alignment with the predominantly north/south oriented estuaries, and have been shown to temporarily override astronomical tides. Tidal pass densities of larval *Brevoortia patronus*, *Micropogonias undulatus*, *Pogonias cromis*, *Anchoa hepsetus*, *A. mitchilli*, *Sciaenops ocellatus*, *Cynoscion arenarius*, *C. nebulosus*, *Paralichthys lethostigma*, and the post-larval penaid *Farfantepenaeus aztecus*, collected in Bayou Tartellan, Louisiana, were calculated for October through April 2006-2007 and September through April 2007-2008, the time period of highest cold front occurrence. Surface and near-bottom samples were collected every four hours during flood and ebb tides over 72 hour periods, twice monthly. A Generalized Additive Model (GAM) was used to investigate the effect of net water transport resulting from astronomical and meteorological forcing on larval densities in the tidal pass, allowing for the non-linear response expected by the temporal heterogeneity. Results indicate that estuarine ichthyoplankton densities had a strong correlation to these winter frontal events, with high flood densities associated with southerly winds and coastal setup during the pre-frontal phase and up until passage of the fronts during westerly winds, producing favorable recruitment and retention conditions. Elevated larval densities on ebb tides were associated with northwesterly to northerly winds indicating that cold fronts can negatively impact estuarine retention.

3.1 Introduction

Assemblages of zooplankton and ichthyoplankton (zoo-/ichthyoplankton) in Louisiana estuaries are variable across spatial and temporal scales (Mazzotti et al., 2008; Reyier et al., 2008). In addition, the early life history stages of zoo-/ichthyoplankton have limited ability to move horizontally in the water column. Therefore, their distribution and transport is structured by a combination of oceanographic wind-driven currents and astronomical tides which can exert

strong effects on recruitment success (Joyeux, 1999; Brown et al., 2004; Roegner et al., 2007; Lara-Lopez and Neira, 2008). The recruitment of estuarine-dependent larvae spawned offshore may rely even more heavily on these physical factors, since they require a transport mechanism for their larvae to reach the estuary (Shaw et al., 1988; Raynie and Shaw, 1994; Cowen et al., 2000; Hines et al., 2008). Along the northern coast of the Gulf of Mexico, periodic winter storm events, i.e., atmospheric cold front passages, can be particularly important, since they have been shown to override the effects of astronomical tides (Reyes et al., 2002; Stone et al., 2004; Li et al., 2011). Therefore, the timing and densities of larvae being transported through a tidal pass at any given moment may be controlled by a varying combination of oceanographic flows, astronomical tides, and meteorological forces (Joyeux, 1999; Brown et al., 2004; Comyns and Lyczkowski-Shultz, 2004; Johnson et al., 2009).

Although many species in the Gulf of Mexico (GOM) spawn offshore during the winter months, there are several fisheries species which spawn on the inner continental shelf or near the mouths of estuaries, which utilize estuaries as nursery habitat for larval, postlarval and juvenile life history stages (Able, 2005; Hare and Govoni, 2005; Glass et al., 2008; Vinagre et al., 2009). Estuaries are thought to be important to these vulnerable life stages because they may provide increased food resources, reduced numbers of predator species, or complex habitat structure which can reduce exposure to predation (Nordlie, 2003; Sheaves, 2005). Several zoo-/ichthyoplankton species utilize estuaries in this manner, and their distributions may provide valuable insights into these physical factors that can facilitate successful estuarine recruitment. For example, *Brevoortia patronus* (gulf menhaden) and *Micropogonias undulates* (Atlantic croaker) are found in high numbers in tidal passes during many winter months (Ditty et al., 1988;

Deegan, 1990; Barbieri et al., 1994; Nixon and Jones, 1997; Hare and Able, 2007; Vaughan et al., 2007; Schaffler et al., 2009; Taylor et al., 2009; Hernandez et al., 2010). Other species which have more truncated spawning seasons, such as *Sciaenops ocellatus* (red drum) or *Pogonias cromis* (black drum), may only comprise a portion of the ichthyoplankton community in a tidal pass during certain specific months (Nieland and Wilson, 1993; Saucier and Baltz, 1993; Wilson and Nieland, 1994; Holt, 2008; Arnott et al., 2010; Ojanguren and Fuiman, 2010). Still other species, such as *Farfantepenaeus aztecus* (brown shrimp) and *Cynoscion arenarius* (sand seatrout), may become predominant members of the zooplankton assemblage while displaying a bimodal recruitment peak from late fall through early spring (Zein-Eldin and Renaud, 1986; Ditty et al., 1988; Minello et al., 1989; Rogers et al., 1993). Some species have minimal recruitment potential during the winter with increasing densities during spring, which builds towards more dominant summer recruitment, such as *Cynoscion nebulosus*, spotted seatrout (Moffett et al., 1979; Holt et al., 1985; Saucier et al., 1992). Still other species, for example, *Paralichthys lethostigma* (southern flounder) seem to have variable estuarine recruitment associated with a protracted spawning season from late fall through February (Warlen and Burke, 1990; Miller et al., 1991). Finally there are estuarine residents which are fairly constant members of ichthyoplankton assemblages, such as the congeneric *Anchoa hepsetus* (broad-striped anchovy) and *Anchoa mitchilli* (bay anchovy), which traditionally start spawning in spring, peak during the summer, and then taper off during late summer or early fall (Ruple, 1984; Castro and Cowen, 1991; Lapolla, 2001; Fahay, 2007).

Since a commonly held premise is that offshore spawning species rely upon favorable currents or circulation patterns to transport larvae to estuarine nursery grounds (Norcross and

Shaw, 1984; Shaw et al., 1985; Cowen et al., 2000; Bailey et al., 2008; Brochier et al., 2008; Bolle et al., 2009), their successful estuarine recruitment should be intimately coupled to favorable, on-shore oceanographic transport patterns including astronomical and meteorological forcing (Joyeux, 1998; Joyeux, 1999; Brown et al., 2004). Estuaries along the northern GOM, and in particular Louisiana, typically have a microtidal range associated with a prevailing diurnal tidal regime. Tidal ranges for these estuaries are on the order of tens of centimeters ($\bar{x} = 32 \text{ cm}$), and do not represent a very strong pulsing force for water movement into and out of an estuary (Smith, 1977; Moeller et al., 1993; Cahoon and Reed, 1995; Wang, 1997). However, those areas west of 91°W have shown relatively high semidiurnal tides (Feng, 2009). Advective currents and flows on the inner continental shelf, such as Ekman transport, have been shown to be important factors in estuarine recruitment (Lee et al., 1992; Govoni and Pietrafesa, 1994; Myers, 1998). In addition, as mentioned earlier, winter frontal events have been shown to cause extreme changes in water depth in Louisiana estuaries, with volume transport up to six times greater than the average normal tidal flux, and water level variation ranging 1.2 m or more (Swenson and Chuang, 1983; Chesney et al., 2000; Perez and Day, 2000; Walker and Hammack, 2000). As a result, meteorological forces, which have the ability to override the astronomical tidal cycle, may at times become dominant factors in water and zooplankton transport. Determining the relative contributions of these forces is important to understanding the transport mechanisms responsible for successful estuarine recruitment of these offshore-spawned species with complex life cycles (Roughgarden et al., 1988; Fogarty et al., 1991; Brown et al., 2000; Costa et al., 2002; Reese et al., 2008).

Zoo-/ichthyoplankton estuarine recruitment along the northern GOM, despite being well studied, is often attributed to a variety of forces (Rooker et al., 1998; Joyeux, 1999; Brown et al., 2004; Comyns and Lyczkowski-Shultz, 2004). This difficulty in determining the operative recruitment forces for winter-spawning species in the northern GOM may have more to do with the difficulties associated with trying to sample estuarine recruitment associated with periodic meteorological events operating on different temporal, spatial and strength/duration scales, than our inability to demonstrate significant transport events linked to local astronomical tides and/or vertical migration (Joyeux, 1999; Brown et al., 2004; Roegner et al., 2007; Lara-Lopez and Neira, 2008). Despite their variable periodicity, winter storm events are seasonally regular with approximately 40 cold fronts per year occurring across the northern GOM from October through April (Moeller et al., 1993). Although the actual passage of individual frontal events may last only 12 to 24 hours, the prevailing northwesterly to northeasterly winds of the postfrontal phase may remain for several days (Roberts et al., 1987). The type of frontal event further determines the extent of the spatial effect on Louisiana coastal estuaries. For example, arctic surges, which tend to come down the Mississippi River valley, have a weak prefrontal phase with strong northeasterly winds dominant after frontal passage simultaneously effecting larger areas due to the orientation of the front to the coastline (Roberts et al., 1987; Pepper and Stone, 2004). While migrating cyclones, which tend to migrate from the northwest to the southeast, initially have strong southerly prefrontal winds associated with strong northwestern winds after front passage (Roberts et al., 1987; Moeller et al., 1993; Pepper and Stone, 2004). With estuarine recruitment transit times reported as being 40 to 73 days for species such as *Brevoortia patronus*, the effect of these variable (in strength, duration, time and space) and periodic frontal events may

strongly influence the number of larvae that can successfully recruit to the estuary (Shaw et al., 1988).

Other than the Mississippi, Atchafalaya, and Mobile river systems, most estuaries and coastal embayments along the northern GOM do not have much freshwater input or haline stratification. These coastal water bodies are generally north-south trending and are relatively shallow. All of these characteristics make them very responsive to wind forcing and helps further explain why they are also well mixed and turbid (Holt et al., 1985; Lyczkowski-Shultz et al., 1990; Bianchi et al., 1997; Chesney et al., 2000; Lipp et al., 2001; Brown et al., 2004). These characteristics are especially relevant during high-energy, winter storm events with their prevailing wind conditions being primarily from the southern and northern quadrants, which strengthens their influence on **net water transport** (defined as the effective water movement into or out of an estuary after filtering the diurnal tidal cycle effects from measured velocities and calculated volume estimates) within these estuaries (Lee et al., 1990; Wang, 1997; Wiseman et al., 1998; Reyes et al., 2002; Swenson, 2003; Stone et al., 2004; Li et al., 2011). These northern GOM characteristics are in contrast to the deep, drowned-river-valley, estuarine systems along the Canadian-U.S. Atlantic coast, where large tidal ranges, large riverine inputs, and stratified two-layered flow usually dominate over wind-dominated transport (Henri et al., 1985; Epifanio, 1995; Wong and Munchow, 1995; Werner et al., 1999). Selective tidal stream transport (STST) involving vertical migration of larval fish linked to astronomical tidal flows has been shown to be the more prevalent recruitment and retention mechanism for offshore-spawned, estuarine-dependent ichthyoplankton in these Atlantic estuaries (Brewer and Kleppel, 1986; Rogers and Herke, 1987; Selden Burke et al., 1995; Cowen et al., 2000; Hare and Govoni, 2005).

Therefore, in the northern GOM, the geomorphic and hydrologic structure of the estuary may facilitate the role that atmospheric cold front passages play in effecting the densities of zoo-/ichthyoplankton within estuaries and their potential recruitment success (Rogers et al., 1993; Parker et al., 1995; Wood, 2000).

The objective of this study is the evaluation of the relative contribution of these high-energy, atmospheric cold front passages and astronomical tides to the successful estuarine recruitment of winter-spawned, estuarine-dependent fisheries species in a Louisiana estuary.

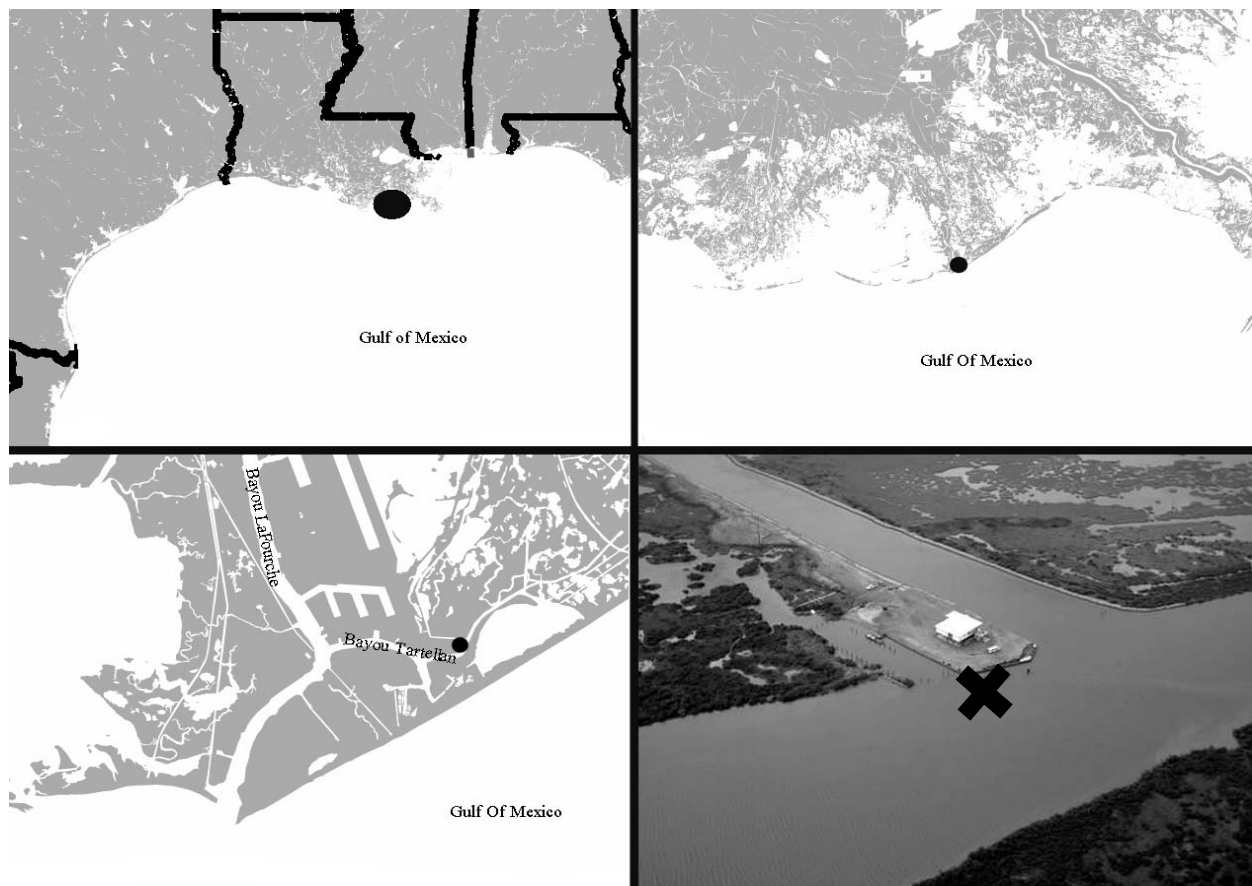


Figure 3.1: Map of the study location in relation to the Gulf of Mexico and coastal Louisiana. The points in black represent the sampling location, with the final panel being the sampling location from an aerial photograph of Bayou Tartellan. The X in the last panel marks the location of an extended dock used as a sampling platform and later destroyed by Hurricane Gustav.

3.2 Materials and Methods

3.2.1 Sampling Location

Zoo-/ichthyoplankton sampling was conducted in Bayou Tartellan, near the Port of Fourchon, Fourchon, Louisiana (Figure 3.1). Bayou Tartellan and Bayou LaFourche are the first major inland channel bifurcations from the connection with the Gulf of Mexico at Belle Pass (29° 5' 53.9" N, 90° 13' 17.8" W). The area represents a well-mixed tidal pass (i.e., little temperature, salinity or dissolved oxygen stratification) having high turbidity, and a relatively small drainage basin contributing a low volume of freshwater input. The sampling site (29° 6' 49" N, 90° 11' 4" W) consisted of a single location where passive plankton net sampling was conducted in approximately 10 meters of water from a dock extending 12 feet from the northern bank into a 72 meter wide tidal pass.

3.2.2 Field Sampling Methodology

Zooplankton sampling was conducted using a fixed davit at the end of the dock, which suspended a stainless steel cable from above the sampling deck to the channel bottom. Passive plankton samples were taken using a 60-cm ring net (333 μ m mesh, 2 meter length, dyed dark green) attached to a gimbal with a vane for orientation into the current. A plastic vinyl coated cod-end with 333 μ m mesh drainage ports was attached to the end of the net to facilitate sample collection. A General Oceanics flowmeter (model no. 2030 with slow velocity rotor) was positioned just off center of the ring to determine volume of water filtered and subsequent calculation of zoo-/ichthyoplankton densities (number of organisms / 15 m³ of water).

Zooplankton samples were collected every four hours over a 72 hour period, twice monthly between the months of October and April over a two year period (2006 – 2008), except

for December and January, which were only sampled monthly. In addition there were two sampling efforts made in September 2007. The sampling season was chosen to maximize encounters of wind-dominant meteorological events (i.e., atmospheric cold front passages) from late fall to early spring. Individual sampling dates were chosen to maximize astronomical tidal ranges. During sampling, both a surface and a near-bottom, passive, zooplankton collection was taken in random order. Surface collections were six minutes long, and near-bottom collections were ten minutes to compensate for vertical differences in current speed and ultimately volume of water filtered (i.e., sampling effort). For near-bottom collections the net mouth was closed on deployment until in position, opened for sampling, and subsequently closed for retrieval to prevent vertical contamination of the sample during transit through the water column. Nets were rinsed and washed down using a freshwater source to avoid contamination.

Zoo-/ichthyoplankton samples were initially preserved in 10% buffered (sodium phosphate, dibasic $\text{NaH}_2\text{PO}_4 \cdot \text{H}_2\text{O}$ and monobasic Na_2HPO_4) formalin for approximately 3.5 hours as a short-exposure, long-term fixative. Samples were then rinsed and switched into a 70% ethanol solution for long-term storage, and later access for larval fish otolith work.

Meteorological data were collected using a handheld temperature/pressure integrated anemometer and by accessing an on-site meteorological station that continuously recorded wind speed, wind gust strength, wind direction, barometric pressure, and air temperature. The meteorological station was located approximately 20 meters from the net sampling site, and was at a height of 20 meters to avoid confounding interactions with ground structures.

Meteorological data were also incorporated from a weather station located on Grand Isle (29° 15.8' N, 89° 57.4' W, Station ID: 87161724), approximately 27 kilometers away from the

sample site and maintained by the National Oceanographic and Atmospheric Administration (NOAA). The meteorological data was used to determine passage of the fronts as described by Moeller et al. (1993; Appendix A). United States surface frontal maps were also downloaded from the archive of NOAA's Hydrometeorological Prediction Center (HPC; www.hpc.ncep.noaa.gov). These maps are produced in 3 hour increments and are used to confirm passage of the fronts (Appendix B).

Estuarine hydrographic parameters were measured during each plankton sample using a portable YSI (model no. 85) to record temperature, conductivity (salinity) and dissolved oxygen. A continuously sampling YSI (model no. 600R) moored offshore of the dock, also measured the same parameters. Meteorological and hydrographic data were periodically downloaded as necessary and archived for storage. Data concerning predicted diurnal tides, measured tide height, and the resulting difference in tidal prism were from the tide gauge station (Station ID: 8762075) at the Port of Fourchon, Fourchon, Louisiana (29° 6.8' N, 90° 11.9' W).

A bottom-mounted, upward-looking Acoustic Doppler Current Profiler (ADCP, RDI 1200 KHz Broadband Workhorse) was placed in the center of Bayou Tartellan to measure the vertical profile of current velocity and direction. Boat surveys along Bayou Tartellan and Bayou LaFourche out to Belle Pass were also conducted using downward-looking ADCPs to provide a correction factor for the mid-channel stationary upward-facing ADCP. A volume transport (m^3/s) was calculated for Bayou Tartellan from these data. To remove the tidal and inertial effects, a 6th-order 40-hr Butterworth low-pass filter was applied to the raw volume transport to produce a **net water transport** (m^3/s ; NWT). These net transport data effectively show the

lower-frequency subtidal oscillations associated with cold front events and other wind forcing, while filtering out the higher frequency diurnal tidal oscillations (Li et al., 2009).

3.2.3 Laboratory Methods

In the lab, zoo-/ichthyoplankton collections with a volume of material greater than 200 mL were split in half using a box plankton splitter, and those with a volume greater than 400 mL were split into quarters. Samples were sorted under a dissecting stereoscope and all ichthyoplankton and postlarval penaeids were removed for identification, measurement and analyzed. A subset of sorted samples was checked for completeness of zooplankton removal by a second party.

Ichthyoplankton and postlarval penaeids were identified to the lowest taxonomic level possible, depending on size of the organism and physical condition. Standard Length (SL) of each specimen was measured and recorded for analysis. Some larval fish that were difficult to identify were stained using Alizarin blue and Alizarin red to facilitate meristic counts.

Identifications were based on the following literature: Miller and Jorgenson (1973); Fritzsche (1978); Hardy (1978a, 1978b); Johnson (1978); Jones et al. (1978); Martin and Drewry (1978); Colton et al. (1979); Leak (1981); Houde (1982); Stuck and Perry (1982); Fahay (1983); Moser (1984); Ruple (1984); Richards (2006); and Fahay (2007).

3.2.4 Statistical Analysis

The statistical approaches applied make use of both parametric and nonparametric techniques. The intent of the various statistical methodologies is to illuminate the relative contributions of physical forcing, such as astronomical tides (i.e., tidal state), wind speed, wind direction, barometric pressure, air temperature (i.e., atmospheric cold front passages and other

meteorological forcing), and net water transport (i.e., wind-driven transport) had on estuarine recruitment. Although the distributions of these data sets violated certain assumptions of parametric analysis (i.e., normality and homogeneity of variance), the structure and robustness of these types of analyses often makes them far more illuminating and interpretable than nonparametric techniques. Utilizing a combination of both approaches, while remaining mindful of their limitations, allows for the most informed interpretation of results. These considerations can be best applied using a semi-nonparametric methodology. For the purposes of utilizing nonparametric methodologies, allowing the collected data to determine the function about the mean allows for more flexibility than a specified distribution driven estimation typical in parametric techniques. The variability and periodicity of winter meteorological events on larval recruitment supports a model where the relationship is determined from the relationship within the data, instead of specified a priori. Further, the nature of several of the measured meteorological variables to co-vary supports a modeling structure that can explain their relationship using a single function.

The effects of the explanatory factors of tidal state, surface versus near-bottom collections, and day versus night on zoo-/ichthyoplankton densities were analyzed separately to investigate the effects these regular, and in the case of tidal state, high-frequency, events have on larval densities sampled in the estuary. Log transformation of the response variable, zoo-/ichthyoplankton density, was attempted, but did not yield a normal distribution or homogeneous variance structure, violating assumptions for an ANOVA type analysis. Comparisons between individual factor levels (i.e., Ebb vs Flood) were conducted nonparametrically using a Wilcoxon Mann Whitney Test (WMW), after accounting for presence/absence to avoid misinterpretation

from zero inflation. Tukey critical values were computed based on the number of comparisons to be made overall, and used for comparison against individual Wilcoxon critical values to preserve overall experiment-wise error rate. There were two levels for the factor tidal state (Ebb and Flood), two levels for surface versus near-bottom collections (Surface and Near-Bottom), and two levels for day versus night (Day and Night). Further, sample collections based on tidal state, surface/near-bottom, and day/night were analyzed collectively using Kruskal Wallis tests for significant differences (KW). The length of the data sets for individual species included in these analyses was based on their expected spawning and recruitment period (i.e., their larval stage seasonality).

The effects of oceanographic flows on recruitment are driven by a combination of tidal state (mass balance in the estuary) and meteorological effects, such as Ekman transport. Traditional models attempt to meet the assumption of normality, allowing for a Gaussian distribution of the error, after a log transformation of the response variable (i.e., density of zoo-/ichthyoplankton) of the structure:

$$\tau = \log_{10}(\delta + 1)$$

where τ represents the log transformed density estimate (number of organisms / 15 m³ of water), and δ represents the original untransformed density estimate. However, log transformation of the response variable does not address the assumption of homogeneity of variance. Further, it alters the inherent structure created by the patchy distributions common to plankton surveys.

Therefore, the analyses focus on a combination of singular main effects and interaction effects using estimation of the nonparametrically-smoothed, curvilinear relationship of the effects using the statistical package MGCV in R (R Development Core Team 2008).

Even nonparametric models become difficult to quantify when there are a number of predictor variables, as in our case with the continuous variables of wind speed, wind direction, barometric pressure and net transport. Further, the relationship between each of the predictor variables and the response variable (i.e., density of zoo-/ichthyoplankton) becomes difficult to discern for analytical purposes (Eubank, 1988, Fox, 2002). The analysis on zoo-/ichthyoplankton densities presented here has several meteorological variables to be included in the model. In this case, a generalized additive model becomes useful, despite being more restrictive than the general case nonparametric regression model:

$$g(E(Y)) = \mu + f_1(x_1) + f_2(x_2) + \cdots + f_n(x_n)$$

where $g(E(Y))$ represents the response variable of zoo-/ichthyoplankton density with an identifiable mean under an exponential family through the link function, and the x variables represent the explanatory variables to be included into the model. The overall mean is represented by μ , the smoothing functions for each variable are represented by f .

Although the model appears to be similar to the linear parametric case, the functions here are estimated to be smooth curves determined from the structure of the data. These partial regression functions are also able to accommodate interactions, using tensor products, between the measured variables (Hastie, 1990). In application of the regression, we are attempting to smooth a scatterplot of some multiple dimensions (Eubank and Spiegelman, 1990). The generalized additive model (GAM) function used in our analyses estimates the number of kernels, or the weighting functions determining the structure of the spline (Wood, 2001). Since we have no *a priori* choice for the estimation of the number of kernels, the software will estimate using a penalized sum of squares approach:

$$Penalized\ SS = \varphi \int (s(x))^2 dx + \sum_{i=1}^n (y_i - s(x_i))^2.$$

In this approach, the amount of smoothing where the spline function is represented by $s()$, is controlled by the φ parameter, using generalized cross validation. As this estimate begins to approach zero, the spline function begins to follow every point in the original data (Golubev 1993). Reinsch (1967) showed that by fixing that estimation, there is a natural spline created through minimizing the penalized sum of squares and fixing the number of kernels. Although this solution to the kernel density utilizes a smoothing spline for each x_i , it allows for a great deal of flexibility in model fitting (Fox, 2002).

The non-linear nature of explanatory variables (i.e., wind speed, wind direction, barometric pressure, and net transport), which were used to elucidate the effects of winter frontal passage, were explored using a GAM in relation to a model fit against the response variable of zoo-/ichthyoplankton density. More specifically, the explanatory variables of wind speed, wind direction, barometric pressure and net transport were fit as individual variables, and the interaction of barometric pressure and wind direction was fit as a proxy for winter frontal passage. This model took the form of:

$$g(\mu_i) = b_0 + s_1(WS_i) + s_2(NWT_i) + s_3(WD_i) + s_4(BARO_i) + ti_5(BARO_i, WD_i)$$

where $g(\mu_i)$ represents the mean from the negative binomial distribution of the response through the logit link, WS represents wind speed, WD represents wind direction, $BARO$ represents barometric pressure, and NWT represents net water transport. The function $s()$ is the penalized smooth response of the explanatory variable that best fits residuals within the model, and $ti()$ is a tensor product smooth that accounts for the smooth functions of the main effects for the interaction term under the assumption that the identifiability constraints for the main effects

(i.e., sum to zero) have already been applied. Individual model terms are evaluated against a Chi-Square (Chisq) Distribution for significance. Determination of final model structure varied by species and probably represents a combination of life history strategy, spawning/planktonic season, and prevailing meteorological and oceanographic conditions. Further, interactions between other variables such as salinity, water temperature and dissolved oxygen were included to help distinguish particular characteristics of the water masses. Therefore, the statistical methodology utilized a combination of factorial component levels on continuous explanatory variables in complex nonparametric models for elucidating structure of the relationships between the explanatory variables of wind speed, wind direction, barometric pressure, net transport, the associated interactions, and the response variable as density of zoo-/ichthyoplankton sampled.

3.3 Results

3.3.1 Hydrology

Observed water temperature measurements were consistent with a well-mixed tidal pass. Water temperature ($\bar{x} = 20.51$ °C) generally had low variability during any sampling effort. However, the November and December 2006 efforts and the January 2007 effort, recorded temperature fluctuations that were significantly greater than the other sampling efforts. In particular, the January 2007 sampling effort showed 10.2 °C in temperature fluctuation during the 72 hour sampling period (Figure 3.2). Comparison of temperature based on sampling depth yielded no statistical differences. Water temperature variations during the first sampling year (Oct. 2006 – Apr. 2007) had much lower median water temperatures with greater variation, than during the same months in year two. Generally, the water was warmer during the early fall (i.e.,

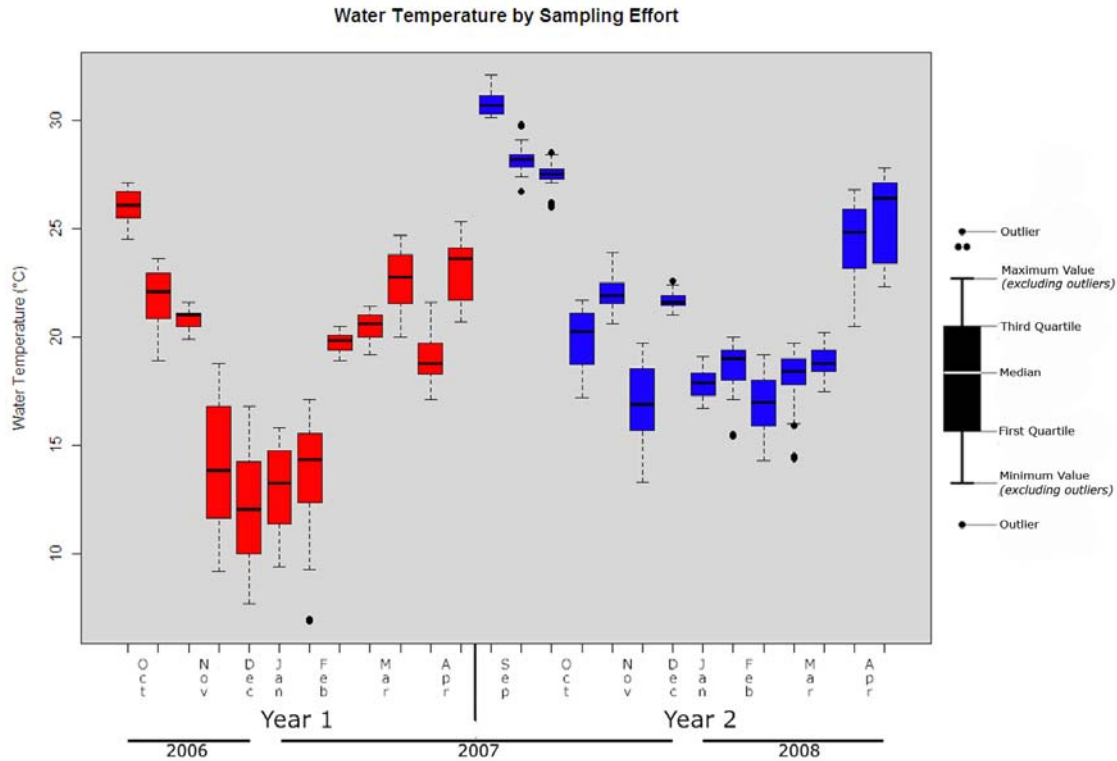


Figure 3.2: Water temperature variations by month across the two years of field sampling, year 1 (red) and year 2 (blue). Both years show a similar trend of decreased temperature from November through February, although 2008 shows the colder water lasting into March. The temperatures in 2006 and early 2007 were overall lower than late 2007 and 2008. In general, there was a higher degree of variability during the months with the coldest water temperatures.

September and October) and cooled into the winter before rising again during March and April.

There was a noticeable dropoff in temperature during November 2006, and median water temperature remained below 15°C through early February 2007. The sharp decline in water temperature coincides with the passage of a large frontal event on November 15th 2006.

Although there was also a decrease in water temperature in November 2007, the median water temperature did not fall below 17°C during the remaining year. Moreover, the median water

temperature remained fairly constant from November 2007 through March 2008, with little variation through late March 2008.

Monthly patterns of salinity were less consistent than water temperature between year one and two of the study period. In general, 95% of all measured salinity values fell between 21.5 and 31.4 ppt with a total salinity range of 14.5 to 33.2 ppt and a mean of 27.32 ppt (Figure 3.3). Median salinity values dropped more than 5 ppt between December 2006 and January 2007.

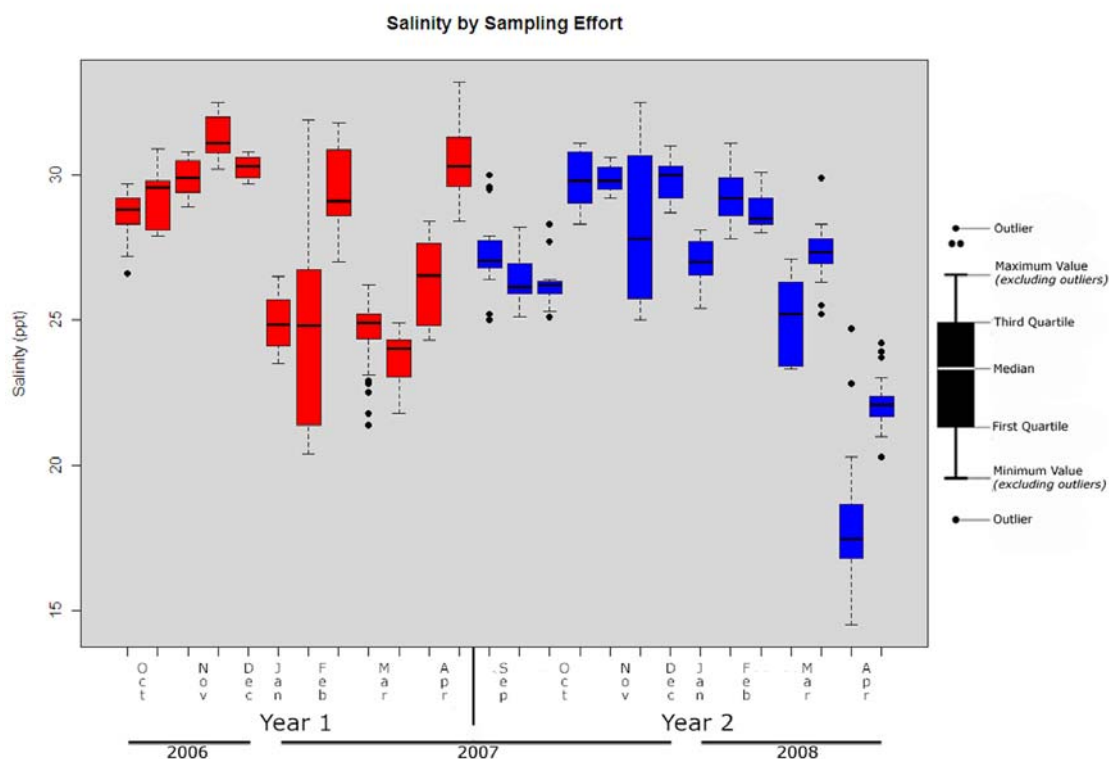


Figure 3.3: Salinity variation by month across the two years of field sampling. There was more consistency across sampling efforts during year 1(red) than year 2(blue). The highest variability in salinities occurred from November through March for both years. April 2008 sampling efforts encountered extremely low salinities compared to all other efforts.

Early February 2007 had a similar median value as January 2007, but had salinity ranges from as high as 32 ppt to nearly 20 ppt over the 4 day sampling. Aside from median salinities in late

February 2007 of approximately 28 ppt, the median salinity in Bayou Tartellan remained below 25 ppt until early April 2007. Salinities during late 2007 and early 2008, with the exception of early March, showed less variation and were generally higher than the previous sample year. However, early April 2008 samples had an extreme drop in salinity, with a minimum value less than 15 ppt, and extreme outlying values as high as 25 ppt. Sampling efforts in March (both years) and April 2007 had the lowest salinities, possibly indicating increased precipitation. There were no statistically significant differences between surface or near-bottom salinities, further supporting a well-mixed estuary.

Variability was seen with dissolved oxygen ($\bar{x} = 6.35 \text{ mg/L}$) measurements, which reflected differences between surface/bottom and day/night sampling and the associated oxygen cycling within the water column. Surface dissolved oxygen concentrations were significantly higher than near-bottom measurements ($p < 0.001$, WMW), and surprisingly, nocturnal samples had higher levels of dissolved oxygen than day ($p < 0.001$, WMW). Daytime surface samples had median dissolved oxygen concentration of 6.4 mg/L, but there was little difference from the nocturnal surface samples (*median* = 6.7 mg/L). Nocturnal surface samples had the highest mean value, while daytime, near-bottom samples were statistically lowest (Figure 3.4).

The tidal regime for the area around Bayou Tartellan and Bayou LaFourche is typically diurnal; however, deviations from the expected tidal range and periodicity were encountered. During any individual sampling trip, tidal ranges were as small as 40 cm or as large as 75 cm. However, tidal ranges recorded outside of our normal sampling efforts were as high as 1.2 meters (Figures 3.5-3.12). The mean tidal range was approximately 60 cm, and was not significantly different from the mean expected astronomical tidal range ($p = 0.21$, WMW).

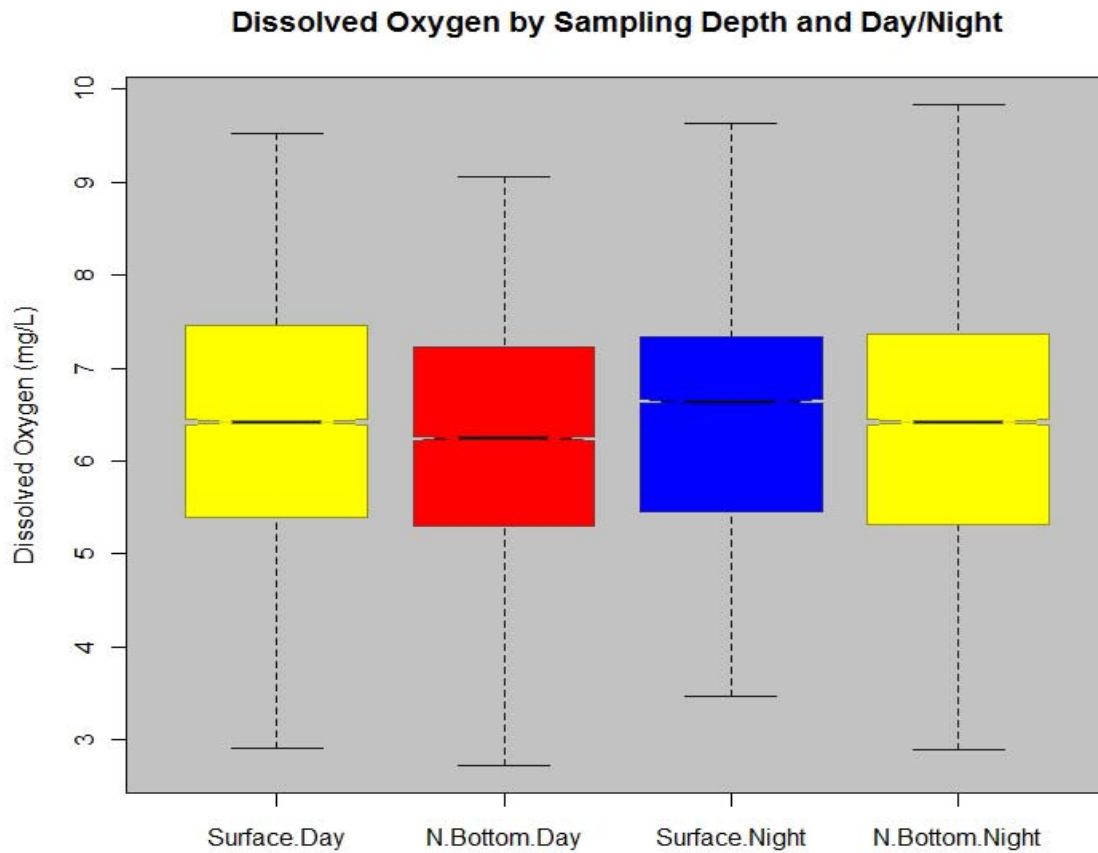


Figure 3.4: Boxplots comparing the dissolved oxygen concentration during sampling, based on sample depth and time of sample collection. Non-overlapping notches between any two boxplots represent “strong evidence” of statistically different median values (Chambers et al. 1983). Different colors represent statistically different (WMW) groups.

Initial observation of tidal direction conducted during sampling efforts indicated that 43% of plankton sampling occurred during flood tides and 57% during ebb tides. However, when factoring in a slack tide category, defined as those tides with water velocities less than 0.312 cm/s at the net mouth, the resultant distribution of tidal sampling effort became heavily favored towards ebb tides which account for 51% of the sampling, flood tides 33% of the time and slack tides 15%.

Passage of meteorological cold fronts occurred before, during and after sampling efforts. As a result, some sampling efforts encountered increased water volume within the tidal pass from coastal setup caused by the southerly winds during the pre-frontal passage phase. This is evident as an increase in the positive difference between observed and predicted water levels immediately before front passage (Figures 3.5-3.12). Passage of the front was marked by a sharp increase in barometric pressure, a decrease in air temperature coupled with a similar decrease in dew point temperature, and a switch in wind direction from southerly to northerly winds through the western quadrant. The post-frontal phase is represented by a decrease in water levels well below expected levels, including similar decreases in salinity and water temperature, resulting from the effect of cold, northerly winds and preceding rainfall within this shallow estuary (Figure 3.13). In particular, the time periods immediately following passage of the front experienced sharp declines in tidal prism, up to 44 cm and in some cases occurring in less than a day. The actual passages of the fronts varied in length from 10 hours to 30 hours, and were more numerous from November through February.

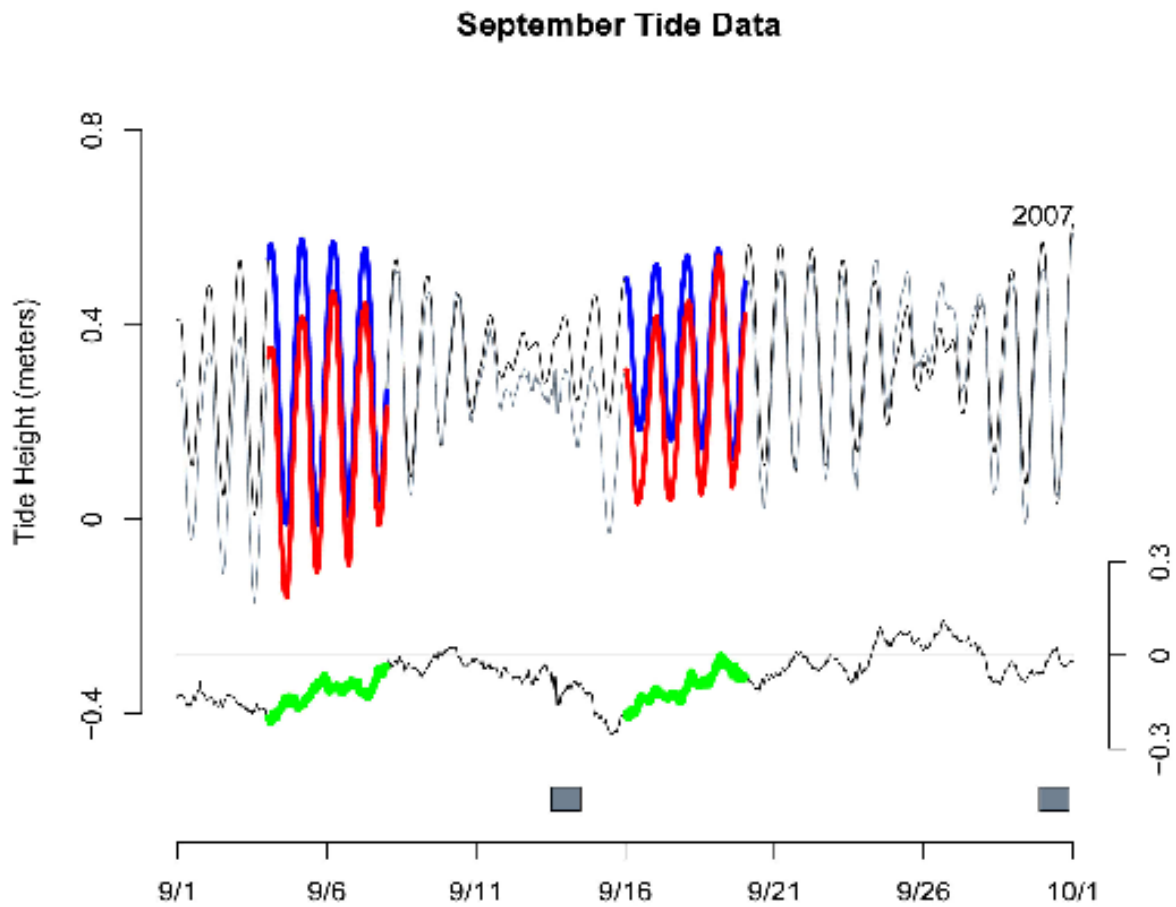


Figure 3.5: Expected and measured tidal height during September 2007 at the Port of Fourchon. The black sinusoidal line represents the expected tidal height. The light gray line represents the actual measured tidal height. The lower portion of the graph represents the difference between expected and measured (i.e., Expected - Measured). Sampling efforts are represented as the colored sections, where blue is the expected tidal height during sampling, red is the measured tidal height during sampling, and green is the difference of the two during sampling efforts. The black outlined rectangle represents passage of the atmospheric frontal events, but not duration.

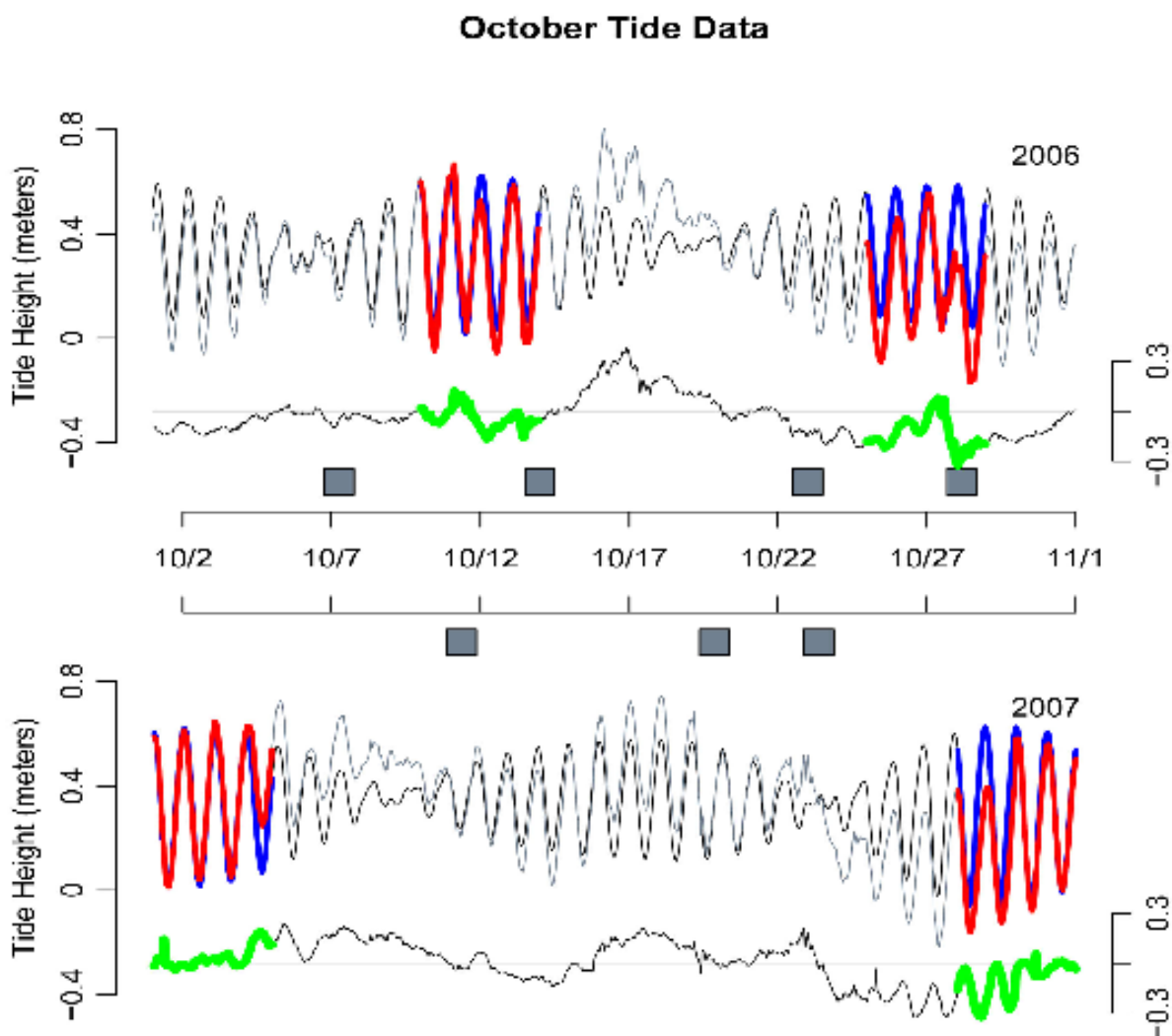


Figure 3.6: Expected and measured tidal height during October 2006 and 2007 at the Port of Fourchon. The black sinusoidal line represents the expected tidal height. The light gray line represents the actual measured tidal height. The lower portion of the graph represents the difference between expected and measured (i.e., Expected - Measured). Sampling efforts are represented as the colored sections, where blue is the expected tidal height during sampling, red is the measured tidal height during sampling, and green is the difference of the two during sampling efforts. The black outlined rectangle represents the passage of atmospheric frontal events, but not duration.

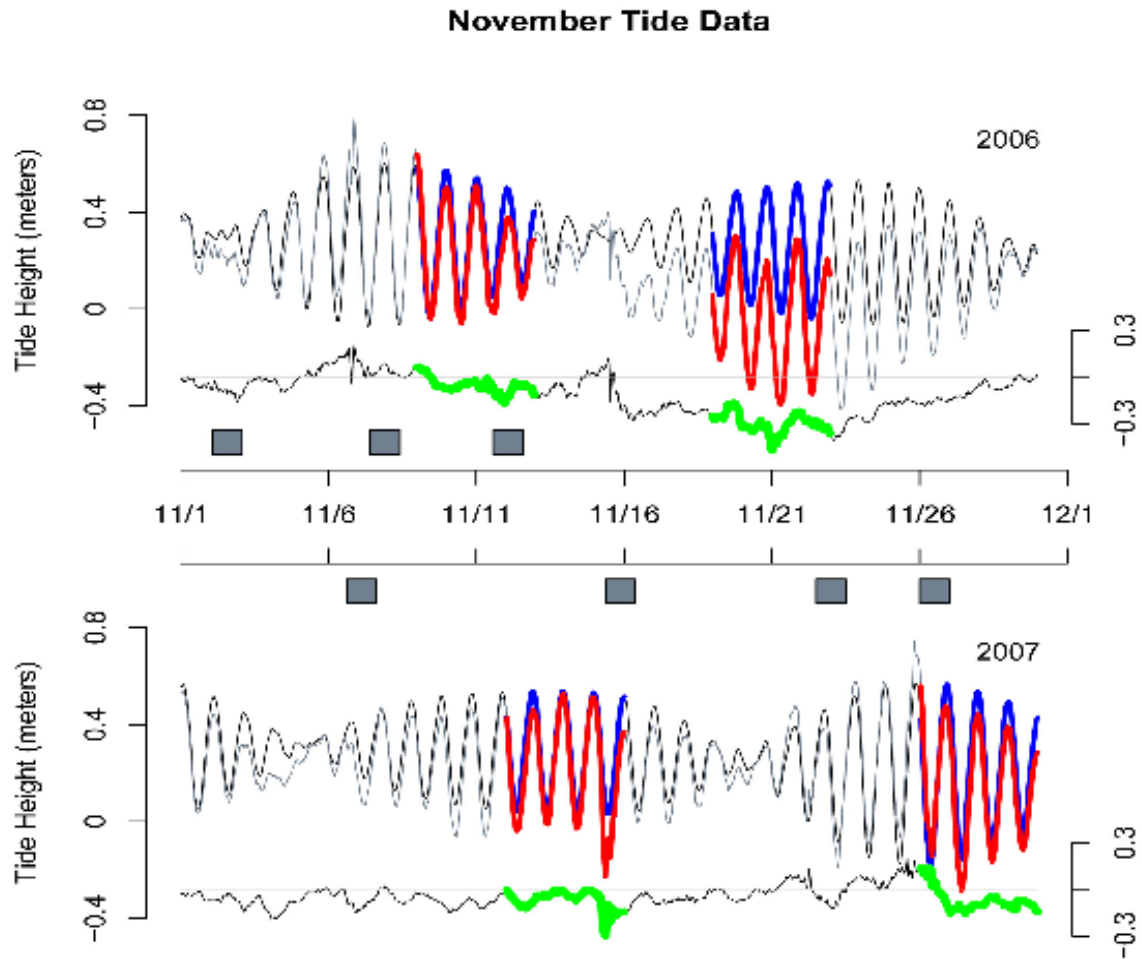


Figure 3.7: Expected and measured tidal height during November 2006 and 2007 at the Port of Fourchon. The black sinusoidal line represents the expected tidal height. The light gray line represents the actual measured tidal height. The lower portion of the graph represents the difference between expected and measured (i.e., Expected - Measured). Sampling efforts are represented as the colored sections, where blue is the expected tidal height during sampling, red is the measured tidal height during sampling, and green is the difference of the two during sampling efforts. The black outlined rectangle represents the passage of atmospheric frontal events, but not duration.

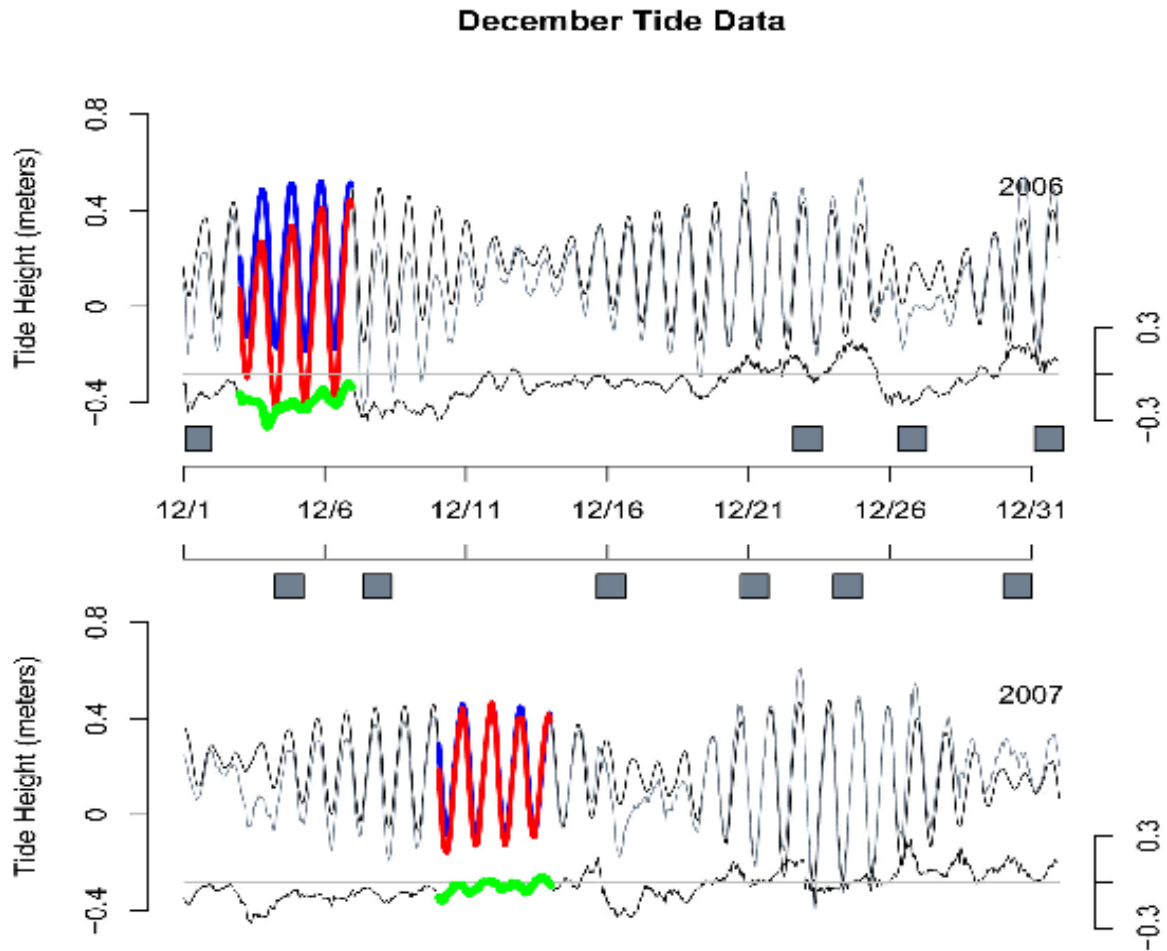


Figure 3.8: Expected and measured tidal height during December 2006 and 2007 at the Port of Fourchon. The black sinusoidal line represents the expected tidal height. The light gray line represents the actual measured tidal height. The lower portion of the graph represents the difference between expected and measured (i.e., Expected - Measured). Sampling efforts are represented as the colored sections, where blue is the expected tidal height during sampling, red is the measured tidal height during sampling, and green is the difference of the two during sampling efforts. The black outlined rectangle represents passage of the atmospheric frontal events, but not duration.

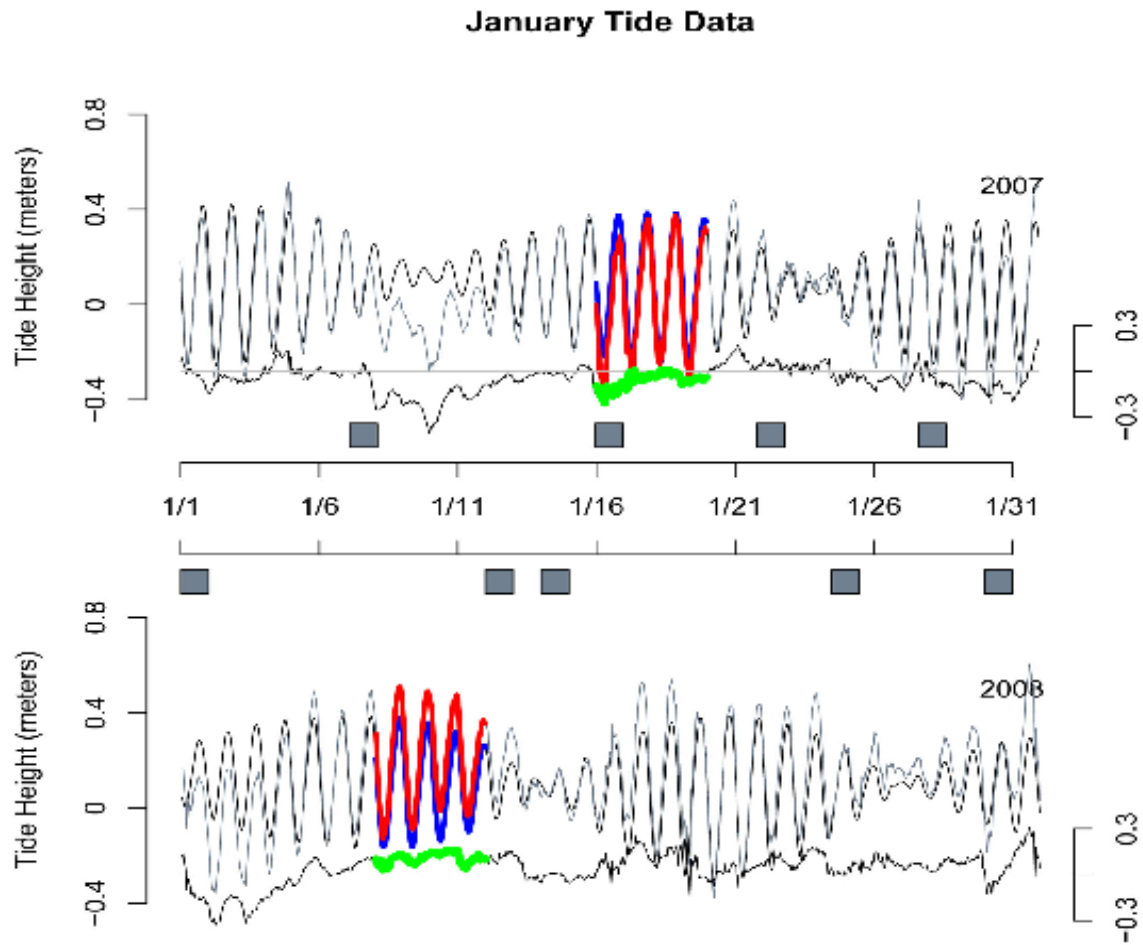


Figure 3.9: Expected and measured tidal height during January 2007 and 2008 at the Port of Fourchon. The black sinusoidal line represents the expected tidal height. The light gray line represents the actual measured tidal height. The lower portion of the graph represents the difference between expected and measured (i.e., Expected - Measured). Sampling efforts are represented as the colored sections, where blue is the expected tidal height during sampling, red is the measured tidal height during sampling, and green is the difference of the two during sampling efforts. The black outlined rectangle represents passage of the atmospheric events, but not duration.

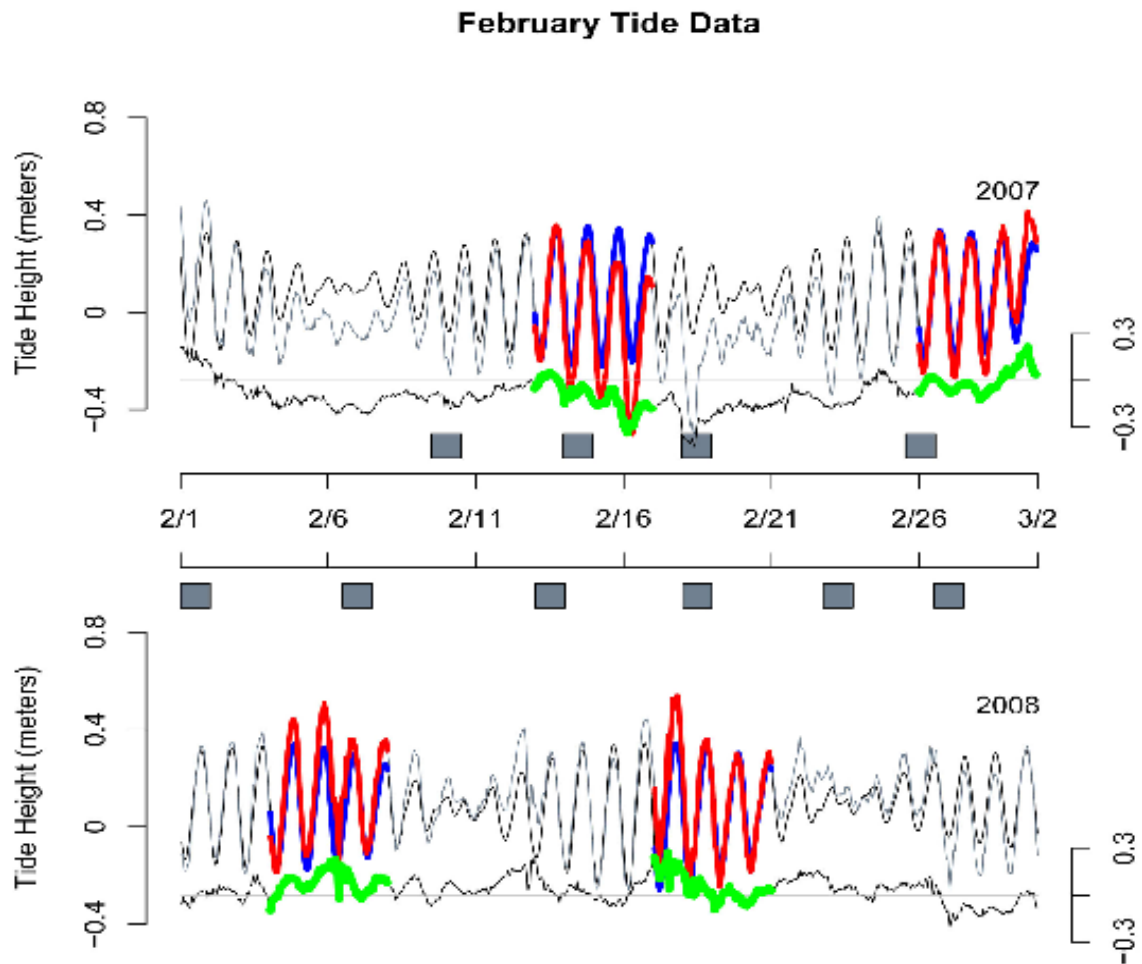


Figure 3.10: Expected and measured tidal height during February 2007 and 2008 at the Port of Fourchon. The black sinusoidal line represents the expected tidal height. The light gray line represents the actual measured tidal height. The lower portion of the graph represents the difference between expected and measured (i.e., Expected - Measured). Sampling efforts are represented as the colored sections, where blue is the expected tidal height during sampling, red is the measured tidal height during sampling, and green is the difference of the two during sampling efforts. The black outlined rectangle represents passage of the atmospheric frontal events, but not duration.

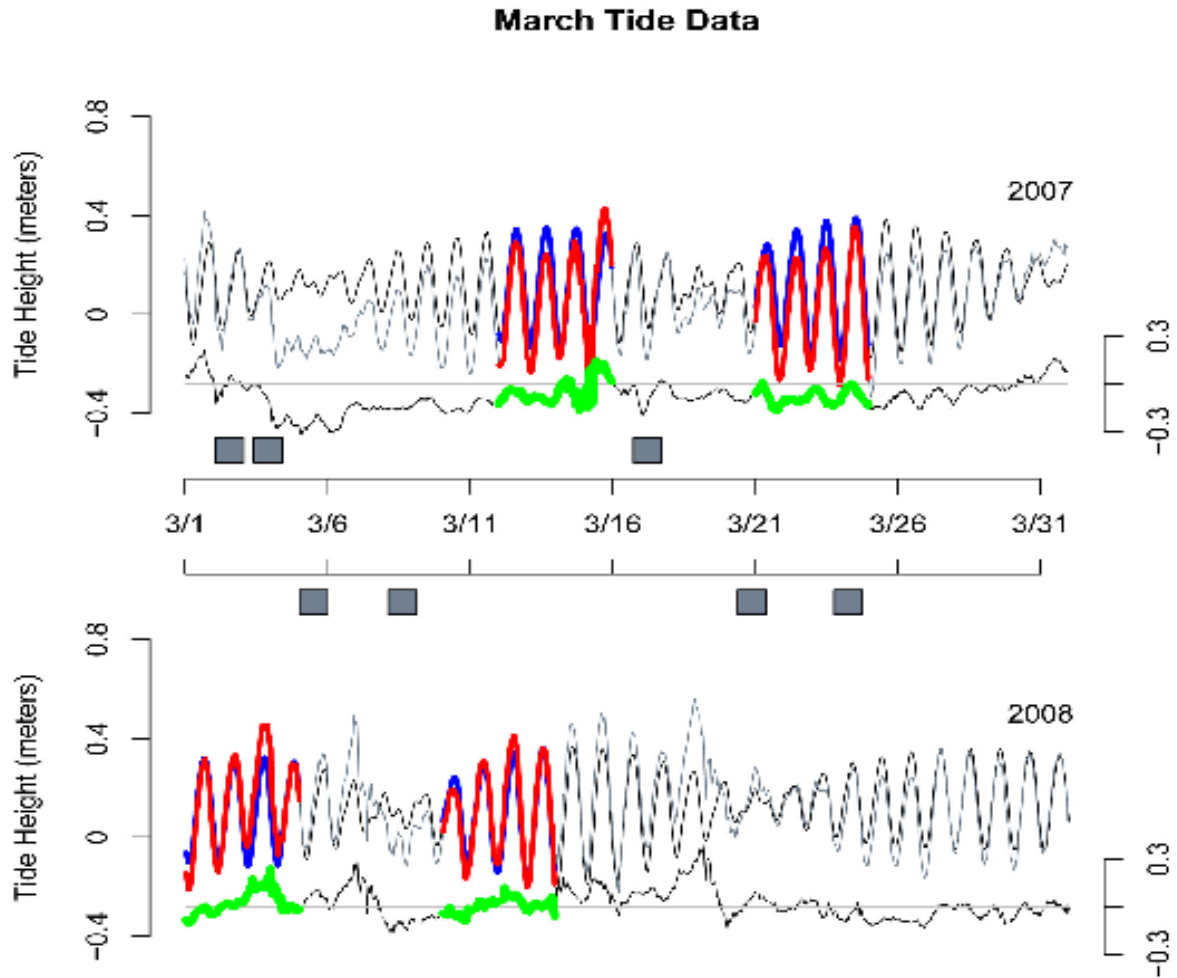


Figure 3.11: Expected and measured tidal height during March 2007 and 2008 at the Port of Fourchon. The black sinusoidal line represents the expected tidal height. The light gray line represents the actual measured tidal height. The lower portion of the graph represents the difference between expected and measured (i.e., Expected - Measured). Sampling efforts are represented as the colored sections, where blue is the expected tidal height during sampling, red is the measured tidal height during sampling, and green is the difference of the two during sampling efforts. The black outlined rectangle represents passage of the atmospheric frontal events, but not duration.

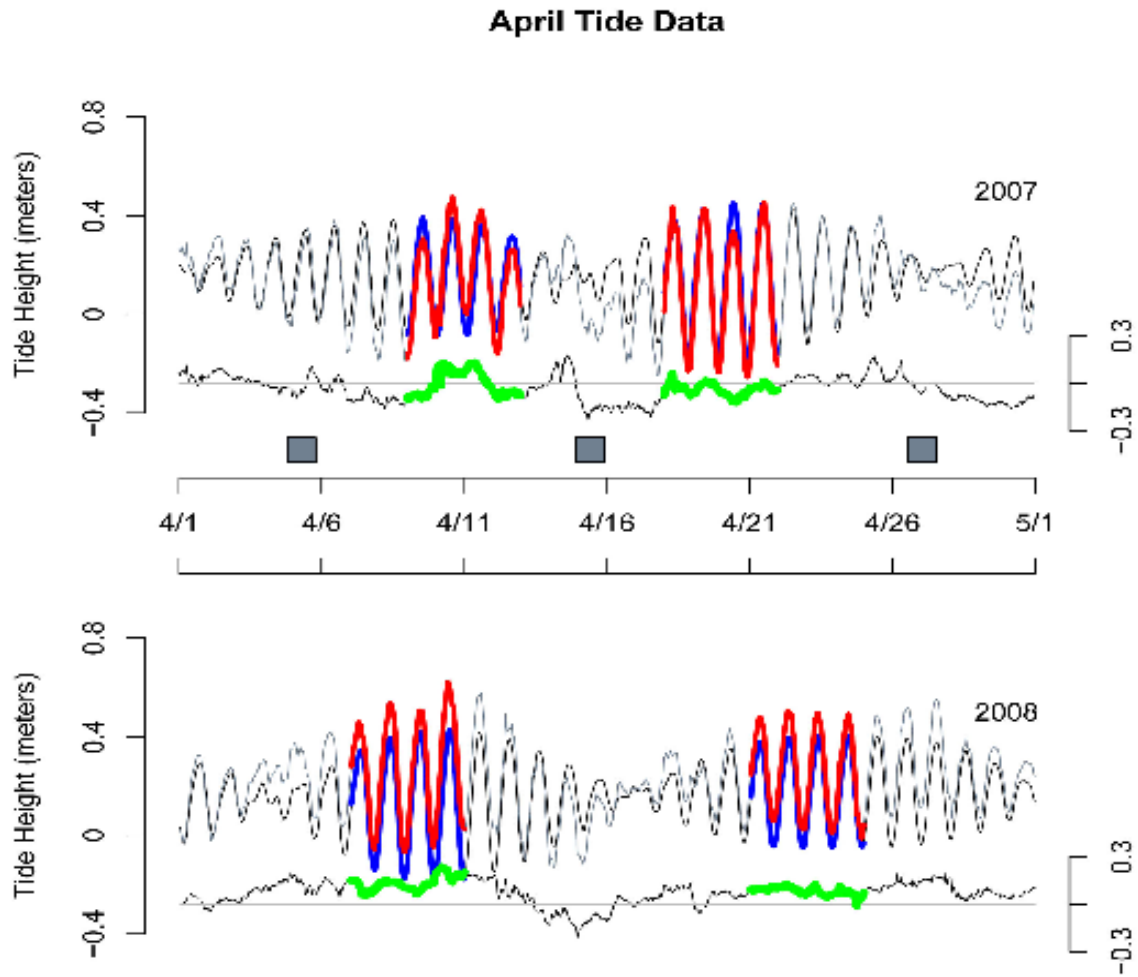


Figure 3.12: Expected and measured tidal height during April 2007 and 2008 at the Port of Fourchon. The black sinusoidal line represents the expected tidal height. The light gray line represents the actual measured tidal height. The lower portion of the graph represents the difference between expected and measured (i.e., Expected - Measured). Sampling efforts are represented as the colored sections, where blue is the expected tidal height during sampling, red is the measured tidal height during sampling, and green is the difference of the two during sampling efforts. The black outlined rectangle represents passage of the atmospheric frontal events, but not duration.

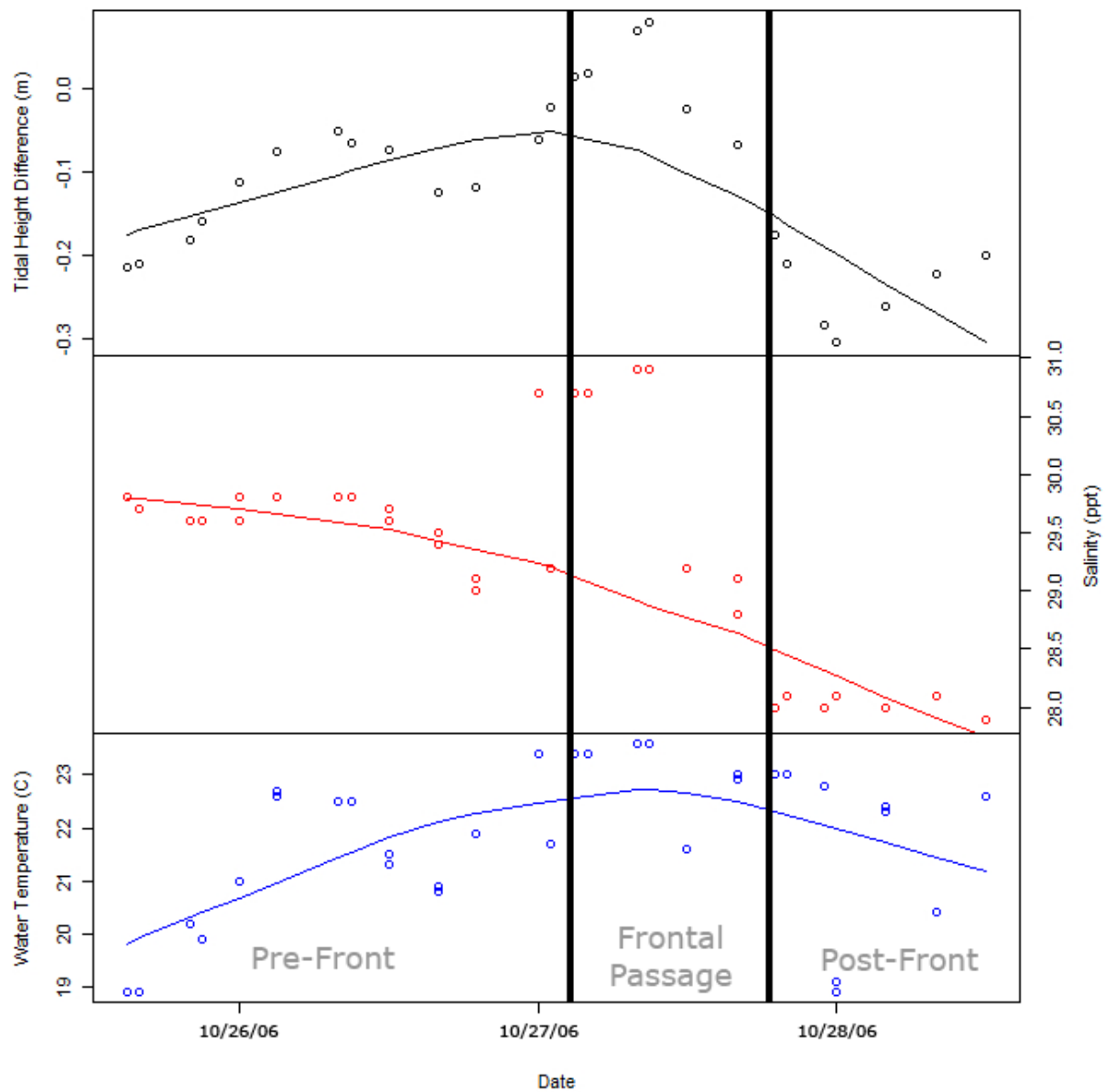


Figure 3.13: Relationship between tidal prism, salinity, and water temperature during the interim or pre-frontal, passage of the front, and post-frontal phases of atmospheric cold front passage. The two vertical black lines bracket the passage of the actual front, with the time period beforehand representing the pre-frontal phase and the period after passage being the post-frontal phase. Trend lines are non-parametrically smoothed curves relating the parameter through time.

3.3.2 General Zoo-/Ichthyoplankton

Over the course of the two years of sampling, 103 taxa were collected, with most of those being identified down to the species level. Probability of encountering a particular species was expected to be zero outside of their expected spawning and larval recruitment season, and this was checked by analyzing the numbers of larvae collected during each sampling trip so as not to exclude either early or late recruitment by any species (Figure 3.14). Densities of larvae sampled

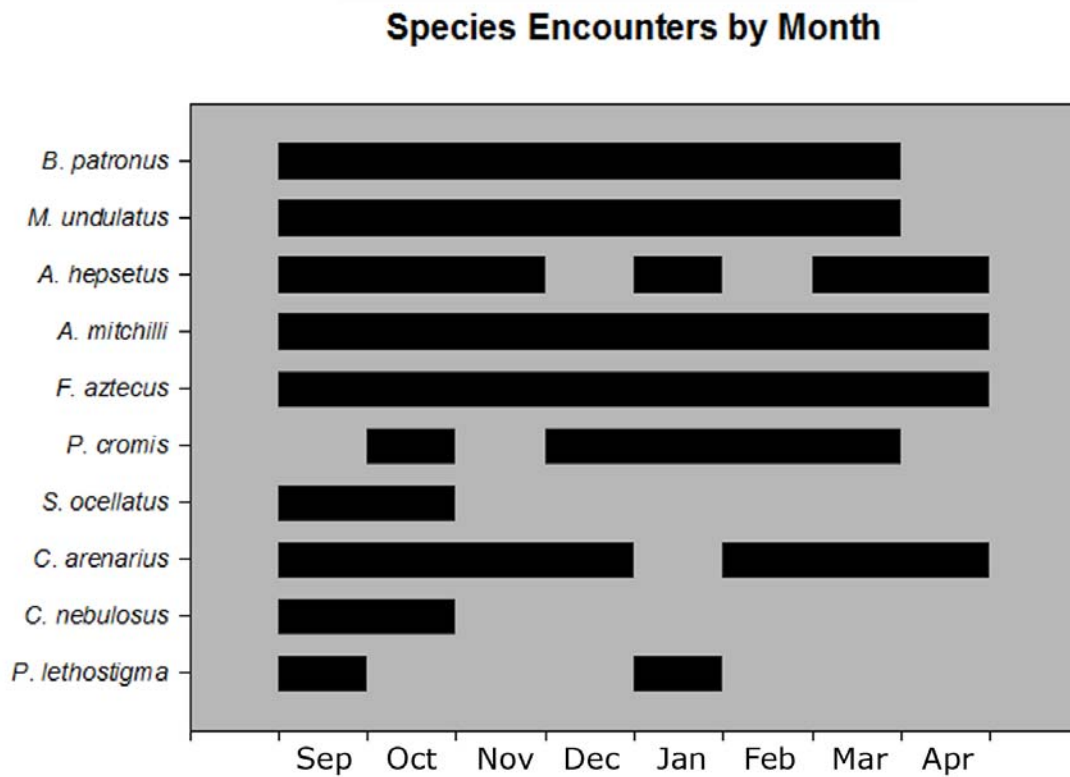


Figure 3.14: Months where species of interest were encountered during sampling efforts. GAM models were truncated to exclude samples with no expectation of encountering a particular species.

were Negative Binomial distributed, with over-dispersion, having low mean values relative to very large densities for a small number of particular sampling efforts. Ichthyoplankton were

collected in 79% of all samples taken over the course of the two year period. When controlling for a patchy distribution, surface samples had a mean density of 55 indiv./15m³ ($sd = 4.3e^2$), with a median value an order of magnitude smaller at 4 indiv./15m³; and mean near-bottom densities were 33.3 indiv./15m³ ($sd = 1.5e^2$; *median* = $1.5e^2$ indiv./15m³).

Surface collections had higher total densities than bottom collections ($p = 0.053$, WMW) and both had extremely high variances likely due to patchy and/or pulsed recruitment. Significantly more larvae were collected during daylight sampling ($\bar{x} = 58.5$ indiv./15m³, $sd = 5.3e^2$) than at night ($\bar{x} = 38.8$ indiv./15m³, $sd = 1.8e^2$; $p = 0.038$, WMW). There was

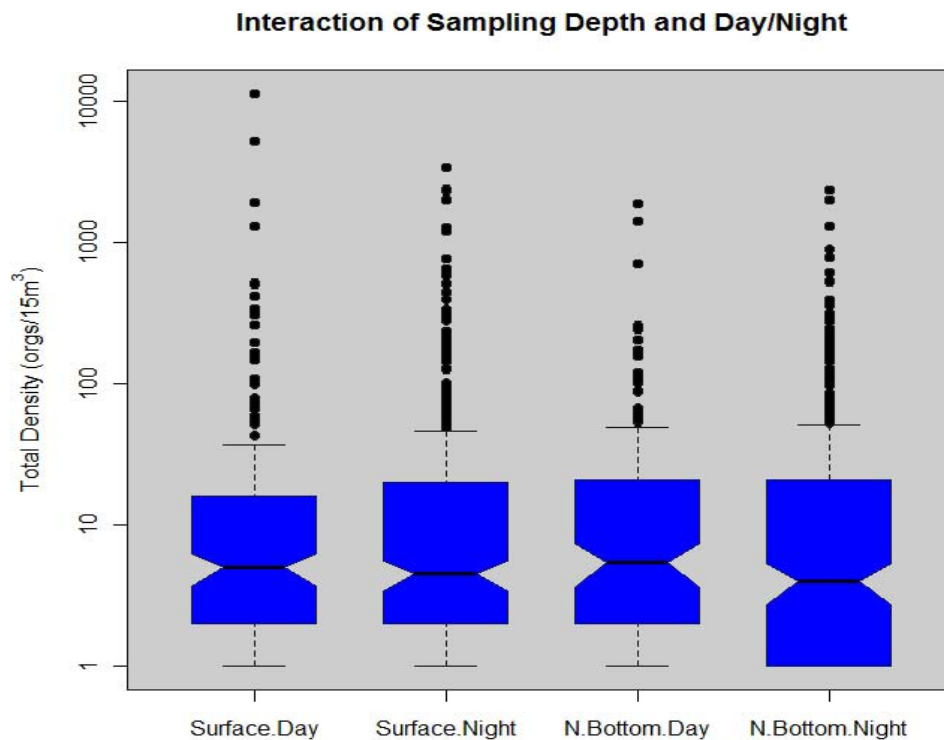


Figure 3.15: Comparison of densities by depth (Surface, N.Bottom) and time of day (Day, Night). The nocturnal samples had significantly more large outlying values, and greater variation, than those collected during the day. Despite these differences there were no statistically significant differences between the groups. Non-overlapping notches in the boxplot represent “strong evidence” of statistically different median values (Chambers et al. 1983).

little difference between daytime surface and near-bottom samples, and these were not significantly different from nocturnal surface efforts. However, nocturnal near-bottom collections had lower median and first quartile densities than the other three groups (Figure 3.15). Further, there is a net transport of larvae into the estuary, with significantly higher numbers of larvae collected during flood tides ($p < 0.001$, WMW; Figure 3.16).

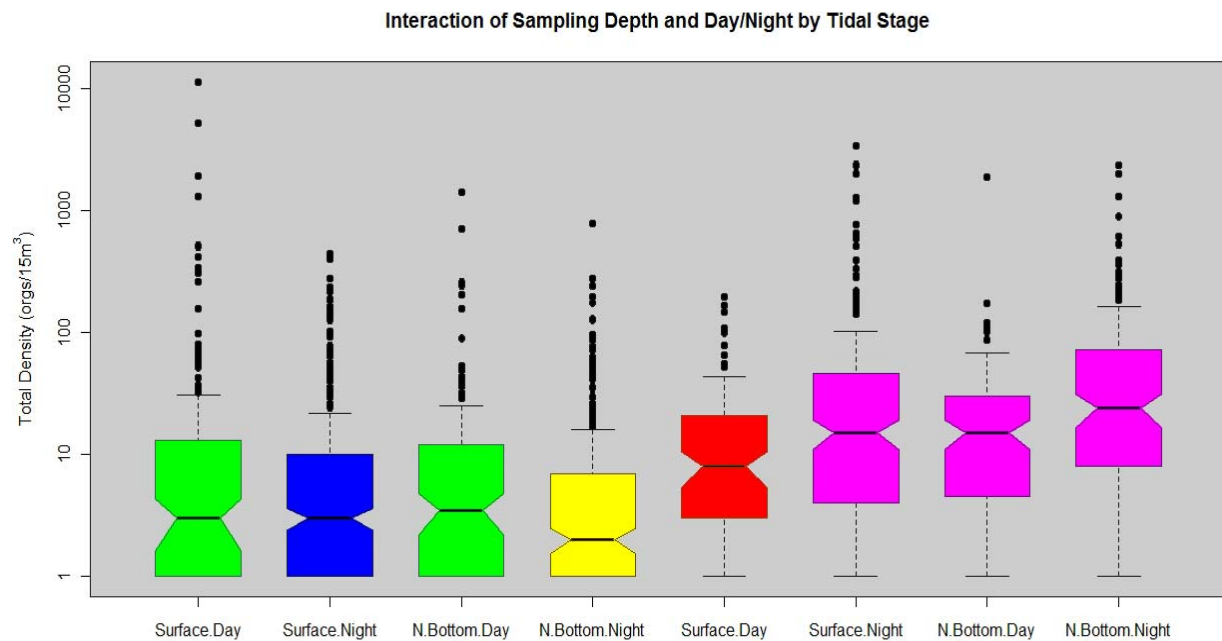


Figure 3.16: Boxplots comparing the total density of larvae within a combination of depth (Surface, N.Bottom), time (Day, Night) and tidal stage (Ebb, Flood). Non-overlapping notches between any two boxplots represent “strong evidence” of statistically different median values (Chambers et al. 1983). Different colors represent statistically different groups (WMW), where secondary colors (i.e., green) represent similarities to both primary colored groups (i.e., yellow and blue). Densities are plotted on a log scale. Despite higher numbers of outlying larger values on ebb tides, flood tides have significantly greater densities.

3.3.3 *Brevoortia patronus* (gulf menhaden)

Brevoortia patronus, gulf menhaden, larvae were sampled during all months except for April (Table 3.1; Figure 3.14). October and November had the highest overall mean densities,

Table 3.1: Mean densities (indiv./15m³ of water filtered) and standard deviations (S.D.) for all sampling efforts during each month for both years combined. Statistics for each species are provided, as well as a total for each factor per species. Months where no larvae were collected under that designation are represented by an "x".

	Month								
	Mean Density (S.D.)								
<i>Brevoortia patronus</i>									
<i>Factor</i>	Sept.	Oct.	Nov.	Dec.	Jan.	Feb.	Mar.	Apr.	Total
<i>Ebb Tidal Stage</i>	x	8.7 (34.9)	5.5 (3.6)	3.6 (7.6)	9.4 (14.7)	1.6 (3.7)	5.4 (12.7)	x	5.1 (18.4)
<i>Flood Tidal Stage</i>	0.9 (5.2)	11.6 (49.2)	16.3 (55.5)	2.4 (7.6)	1.9 (4.9)	0.6 (4.3)	6.8 (45.4)	x	6.6 (36.6)
<i>Daytime Sampling</i>	1.3 (6.3)	1.5 (4.6)	9.9 (23.8)	1.0 (4.5)	0.9 (2.1)	0.8 (4.6)	0.8 (2.4)	x	2.7 (11.5)
<i>Nocturnal Sampling</i>	0.1 (0.4)	15.7 (52.8)	9.7 (43.7)	4.7 (8.7)	8.6 (13.9)	1.3 (3.6)	9.3 (40.1)	x	7.7 (34.4)
<i>Total</i>	0.5 (3.7)	9.9 (41.2)	9.8 (36.9)	3.2 (7.6)	5.4 (11.3)	1.1 (4.0)	6.0 (31.6)	x	
<i>Micropogonias undulatus</i>									
<i>Factor</i>	Sept.	Oct.	Nov.	Dec.	Jan.	Feb.	Mar.	Apr.	Total
<i>Ebb Tidal Stage</i>	x	8.3 (31.7)	32.6 (94.4)	17.0 (76.2)	2.9 (5.4)	0.2 (0.5)	1.7 (6.4)	x	10.5 (52.3)
<i>Flood Tidal Stage</i>	0.6 (3.7)	10.3 (38.5)	56.2 (257.5)	6.0 (25.2)	2.4 (8.7)	x	0.1 (0.4)	x	12.2 (109.3)
<i>Daytime Sampling</i>	x	3.5 (11.6)	63.7 (266.4)	27.5 (101.2)	1.7 (6.5)	x	0.9 (5.7)	x	15.6 (121.5)
<i>Nocturnal Sampling</i>	0.5 (3.2)	13.0 (43.5)	27.3 (69.3)	4.3 (8.6)	3.3 (7.8)	0.2 (0.5)	1 (4.3)	x	8.4 (36.7)
<i>Total</i>	0.3 (2.6)	9.1 (34.5)	42.0 (177.4)	13.5 (64.3)	2.7 (7.3)	0.1 (0.4)	1.0 (4.9)	x	
<i>Anchoa hepsetus</i>									
<i>Factor</i>	Sept.	Oct.	Nov.	Dec.	Jan.	Feb.	Mar.	Apr.	Total
<i>Ebb Tidal Stage</i>	0.2 (0.8)	1.2 (7.6)	0.6 (5.3)	x	x	x	1.1 (5.4)	13.8 (45.1)	0.9 (8.7)
<i>Flood Tidal Stage</i>	10.8 (41.2)	0.5 (3.4)	0.5 (3.4)	x	0.03 (0.2)	x	x	8.3 (22.4)	1.5 (14.3)
<i>Daytime Sampling</i>	3.3 (11.1)	1.1 (8.4)	0.4 (3.4)	x	0.03 (0.2)	x	0.02 (0.1)	20.3 (55.3)	1.1 (10.1)
<i>Nocturnal Sampling</i>	6.6 (35.6)	0.6 (5.3)	0.6 (5.3)	x	x	x	1.0 (5.1)	6.1 (18.9)	1.2 (12.3)
<i>Total</i>	5.5 (29.7)	0.7 (5.9)	0.5 (4.6)	x	0.01 (0.1)	x	0.6 (4.0)	11.3 (35.9)	

Table 3.1 *Continued*: Mean densities (indiv./15m³ of water filtered) and standard deviations (S.D.) for all sampling efforts during each month for both years combined. Statistics for each species are provided, as well as a total for each factor per species. Months where no larvae were collected under that designation are represented by an "x".

	Month								
	Mean Density (S.D.)								
<i>Anchoa mitchilli</i>									
<i>Factor</i>	Sept.	Oct.	Nov.	Dec.	Jan.	Feb.	Mar.	Apr.	Total
<i>Ebb Tidal Stage</i>	4.8 (12.6)	3.3 (12.9)	0.1 (0.3)	0.8 (2.2)	0.2 (1.0)	0.4 (1.7)	4.1 (10.9)	109.8 (378.0)	4.8 (62.2)
<i>Flood Tidal Stage</i>	10.9 (28.9)	36.3 (169.5)	0.04 (0.3)	x	0.1 (0.3)	1.1 (6.5)	0.1 (0.5)	x	7.5 (71.2)
<i>Daytime Sampling</i>	8.8 (24.2)	5.0 (14.7)	0.03 (0.3)	0.4 (2.3)	0.1 (0.4)	x	0.3 (1.1)	164.6 (462.8)	5.9 (74.3)
<i>Nocturnal Sampling</i>	7.4 (21.6)	24.6 (140.7)	0.1 (0.3)	0.6 (1.5)	0.2 (0.9)	1.3 (5.9)	3.6 (10.5)	x	6.0 (60.4)
<i>Total</i>	7.9 (22.3)	16.6 (108.7)	0.1 (0.3)	0.5 (1.8)	0.1 (0.7)	0.7 (4.5)	2.3 (8.4)	59.9 (279.2)	
<i>Farfantepenaeus aztecus</i>									
<i>Factor</i>	Sept.	Oct.	Nov.	Dec.	Jan.	Feb.	Mar.	Apr.	Total
<i>Ebb Tidal Stage</i>	0.3 (0.7)	1.1 (6.2)	0.02 (0.2)	1.7 (7.8)	1.2 (2.1)	0.7 (2.0)	9.9 (35.9)	0.3 (0.9)	2.1 (14.7)
<i>Flood Tidal Stage</i>	4.7 (10.8)	0.7 (2.0)	1.1 (5.1)	0.4 (1.2)	28.7 (75.2)	8.6 (22.6)	33.5 (75.4)	x	10.2 (40.1)
<i>Daytime Sampling</i>	3.8 (11.7)	0.3 (1.4)	0.2 (1.0)	0.3 (1.2)	0.1 (0.3)	3.6 (15.9)	6.6 (16.6)	0.1 (0.4)	2.4 (10.4)
<i>Nocturnal Sampling</i>	1.8 (5.2)	1.2 (5.7)	0.7 (4.3)	1.8 (7.9)	21.2 (63.9)	4.8 (16.2)	28.7 (70.8)	0.2 (0.8)	7.7 (35.4)
<i>Total</i>	2.5 (8.0)	0.9 (4.8)	0.5 (3.6)	1.3 (6.5)	14.2 (52.7)	4.4 (16.0)	21.2 (59.1)	0.2 (0.7)	
<i>Pogonias cromis</i>									
<i>Factor</i>	Sept.	Oct.	Nov.	Dec.	Jan.	Feb.	Mar.	Apr.	Total
<i>Ebb Tidal Stage</i>	x	0.01 (0.1)	x	2.1 (6.2)	0.3 (1.2)	7.5 (31.9)	2.5 (19.8)	x	2.1 (16.5)
<i>Flood Tidal Stage</i>	x	0.5 (3.7)	x	9.0 (43.4)	0.9 (4.4)	1.9 (11.0)	x	x	1.3 (13.3)
<i>Daytime Sampling</i>	x	x	x	2.4 (6.9)	1.3 (5.0)	0.2 (1.1)	0.1 (0.3)	x	0.4 (2.8)
<i>Nocturnal Sampling</i>	x	0.3 (3.0)	x	5.6 (31.8)	0.1 (0.4)	8.4 (32.1)	2.2 (18.9)	x	2.7 (19.5)
<i>Total</i>	x	0.2 (2.3)	x	4.4 (25.0)	0.6 (3.3)	5.0 (24.8)	1.4 (14.8)	x	

Table 3.1 *Continued*: Mean densities (indiv./15m³ of water filtered) and standard deviations (S.D.) for all sampling efforts during each month for both years combined. Statistics for each species are provided, as well as a total for each factor per species. Months where no larvae were collected under that designation are represented by an "x".

	Month								
	Mean Density (S.D.)								
<i>Sciaenops ocellatus</i>									
<i>Factor</i>	Sept.	Oct.	Nov.	Dec.	Jan.	Feb.	Mar.	Apr.	Total
<i>Ebb Tidal Stage</i>	1.1 (4.8)	0.2 (1.1)	x	x	x	x	x	x	0.4 (2.8)
<i>Flood Tidal Stage</i>	98.8 (393.1)	1.8 (6.3)	x	x	x	x	x	x	38.9 (245.8)
<i>Daytime Sampling</i>	1.4 (5.3)	0.1 (0.5)	x	x	x	x	x	x	0.5 (2.9)
<i>Nocturnal Sampling</i>	74.3 (342.0)	1.3 (5.4)	x	x	x	x	x	x	27.6 (207.1)
<i>Total</i>	50.0 (280.4)	0.8 (4.2)	x	x	x	x	x	x	
<i>Cynoscion arenarius</i>									
<i>Factor</i>	Sept.	Oct.	Nov.	Dec.	Jan.	Feb.	Mar.	Apr.	Total
<i>Ebb Tidal Stage</i>	3.5 (5.8)	0.4 (1.5)	0.02 (0.2)	0.02 (0.1)	x	0.4 (1.0)	4.1 (9.0)	1.1 (2.5)	1.2 (4.5)
<i>Flood Tidal Stage</i>	33.1 (56.2)	3.2 (10.9)	x	x	x	0.2 (1.5)	1.9 (10.3)	14.4 (23.4)	5.4 (23.1)
<i>Daytime Sampling</i>	7.0 (9.1)	0.5 (1.8)	0.02 (0.1)	x	x	0.2 (1.6)	5.8 (14.5)	1.1 (2.8)	1.8 (7.2)
<i>Nocturnal Sampling</i>	24.0 (50.8)	2.2 (9.1)	0.01 (0.1)	0.02 (0.2)	x	0.3 (0.9)	1.4 (3.5)	10.6 (20.9)	3.7 (19.1)
<i>Total</i>	18.3 (42.4)	1.5 (7.1)	0.01 (0.1)	0.01 (0.1)	x	0.3 (1.2)	3.1 (9.6)	7.1 (17.2)	
<i>Cynoscion nebulosus</i>									
<i>Factor</i>	Sept.	Oct.	Nov.	Dec.	Jan.	Feb.	Mar.	Apr.	Total
<i>Ebb Tidal Stage</i>	0.8 (2.2)	0.03 (0.2)	x	x	x	x	x	x	0.3 (1.3)
<i>Flood Tidal Stage</i>	2.0 (8.4)	0.3 (1.5)	x	x	x	x	x	x	0.9 (5.3)
<i>Daytime Sampling</i>	1.8 (3.5)	0.3 (1.5)	x	x	x	x	x	x	0.7 (2.4)
<i>Nocturnal Sampling</i>	1.2 (7.1)	0.02 (0.2)	x	x	x	x	x	x	0.4 (4.3)
<i>Total</i>	1.4 (6.1)	0.1 (1.0)	x	x	x	x	x	x	

with 9.9 and 9.8 fish per 15m³ of water, respectively. There was a second peak in mean density in March ($\bar{x} = 6.0$ indiv./15m³, $sd = 31.6$; Table 3.1), with slightly smaller densities sampled during December ($\bar{x} = 3.2$ indiv./15m³, $sd = 7.6$) and January ($\bar{x} = 5.4$ indiv./15m³, $sd = 11.3$). Despite some samples with extremely high densities of gulf menhaden, nearly 47% of all samples contained zero larvae, indicating pulsed recruitment events.

This concept of pulsed recruitment is also evident when looking at catch differences by tidal stage. When controlling for the binomial (i.e., catch, no-catch) nature of encountering larvae (i.e., resulting metrics are based on the zero-truncated data set), flood tide densities ($\bar{x} = 52.0$ indiv./15m³, $sd = 97.4$) were significantly greater than ebb ($\bar{x} = 21.2$ indiv./15m³, $sd = 38.0$, $p < 0.006$, WMW, Table 3.2; Figure 3.17). Without controlling for presence/absence, the greatest densities occurred on nocturnal flood tides ($\bar{x} = 9.5$ indiv./15m³, $sd = 49.6$, Table 3.3). Additional noteworthy comparisons, when controlling for zeros, include Kruskal-Wallis testing showing nocturnal flood densities having far greater chance of non-zero densities and the highest overall peak densities ($\bar{x} = 56.9$, $sd = 111.0$ indiv./15m³, Table 3.4; Figure 3.18). Difference between night densities ($\bar{x} = 34.0$, $sd = 71.6$ indiv./15m³, Table 3.2) versus day ($\bar{x} = 20.0$, $sd = 26.4$ indiv./15m³), although large, was not significant.

In analyzing for the effects of meteorological variables on the variation in gulf menhaden densities, significant non-linear relationships were exhibited by net water transport, wind direction ($p < 0.051$, Chisq), wind speed, barometric pressure, and the interaction of barometric pressure and wind direction (Adj. $R^2 = 0.92$, Table 3.5). The interaction of wind direction and barometric pressure was accounted for based on tidal stage, as differences were expected between flood and ebb tides. Net water transport and wind speed exerted only small-scale

Table 3.2: Data and statistical results for Wilcoxon-Mann-Whitney (WMW) Rank Sum test for differences between ebb and flood tidal stages, and daytime and nocturnal sampling efforts. Mean and median densities are calculated per 15 cubic meters of water for all species. All metrics are based on the zero-truncated data set, and accounted for ties, for analysis under the assumptions of WMW. "*" Represents a statistically significant comparison ($\alpha=0.05$) with that group's density being the greater of the two.

Species	Ebb Tidal Stage			Flood Tidal Stage			WMW
	Mean	Median	S.D.	Mean	Median	S.D.	$P_{H_0}(Z \geq W)$
<i>B. patronus</i>	21.2	8.0	38.0	52.0	23.0*	97.4	<0.006
<i>M. undulatus</i>	44.8	6.0	117.2	126.8	28.5*	337.6	<0.001
<i>A. hepsetus</i>	20.8	3.0	38.1	55.6	27.0	77.6	0.057
<i>A. mitchilli</i>	35.2	5.0	167.1	92.1	34.5*	281.8	<0.001
<i>F. aztecus</i>	11.4	2.0	32.9	61.5	17.0*	108.0	<0.001
<i>P. cromis</i>	31.9	4.0	60.5	48.9	27.5	69.3	0.203
<i>S. ocellatus</i>	6.8	2.5	9.8	203.4	25.0*	564.4	<0.003
<i>C. arenarius</i>	9.1	4.0	13.8	65.7	36.0*	82.4	<0.001
<i>C. nebulosus</i>	3.1	1.0	4.4	14.7	9.0*	17.0	<0.009

Species	Daytime Sampling			Nocturnal Sampling			WMW
	Mean	Median	S.D.	Mean	Median	S.D.	$P_{H_0}(Z \geq W)$
<i>B. patronus</i>	20.0	9.0	26.4	34.0	9.0	71.6	0.321
<i>M. undulatus</i>	122.4	11.0	333.7	40.6	8.0	84.7	0.381
<i>A. hepsetus</i>	41.6	30.5	51.8	28.2	6.5	57.0	0.327
<i>A. mitchilli</i>	63.9	10.5	241.5	47.9	7.0	195.1	0.516
<i>F. aztecus</i>	20.0	8.5	25.7	37.2	4.0	88.6	0.415
<i>P. cromis</i>	9.4	3.0	10.8	51.3	21.0	73.9	0.283
<i>S. ocellatus</i>	6.3	3.0	9.7	183.9	18.5	537.2	0.087
<i>C. arenarius</i>	17.5	9.0	21.1	32.6	5.5	65.6	0.744
<i>C. nebulosus</i>	6.7	6.0	4.8	8.4	1.0	17.9	0.157

fluctuations on density estimation when compared to the scale of effect from the other variables (Figure 3.21). Significant increases in the number of larvae expected (i.e., recruitment events) were associated with wind directions from the northeast and northwest quadrants and high and

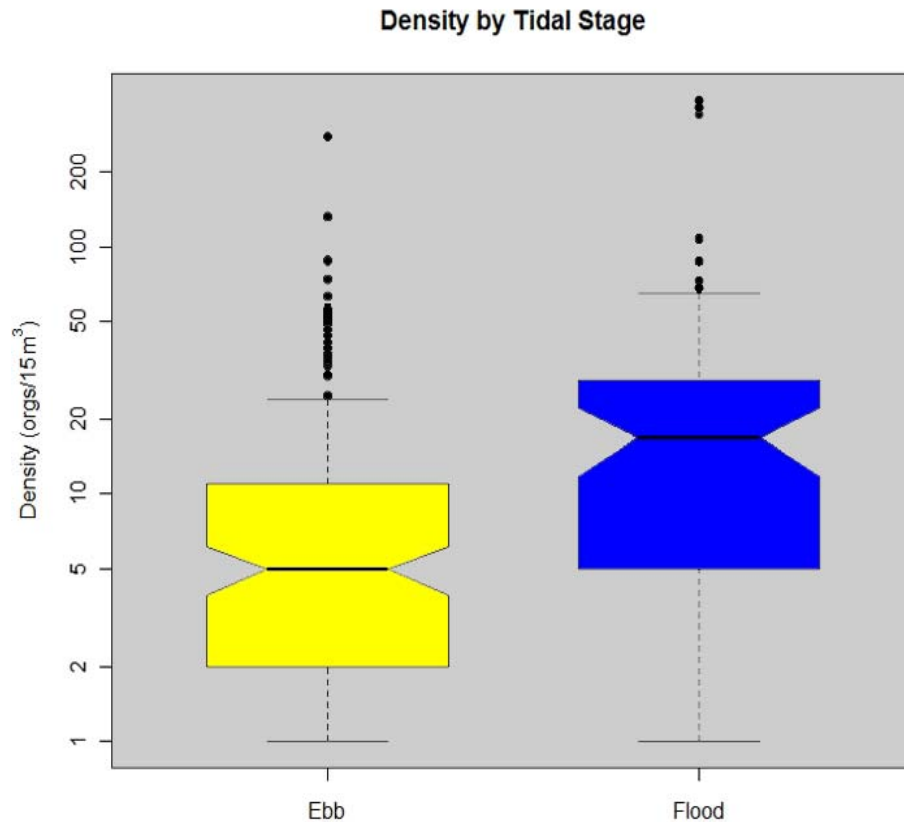


Figure 3.17: Density of *Brevoortia patronus* larvae as a function of tidal stage. Non-overlapping notches in the boxplots represent “strong evidence” of statistically different median values (Chambers et al. 1983). Different colors represent statistically different groups (WMW).

low barometric pressures (Barometric Pressure: $p < 0.027$, Chisq), when looking at each factor individually. Analyzing the interaction of barometric pressure and wind direction by tide, two sets of conditions appear favorable for recruitment during flood tides (Figure 3.22). High estuarine catch rates primarily occurred during low to mid atmospheric pressure events associated with westerly and northwesterly winds (i.e., 270° and 325° , respectively), and to a lesser extent during a range of atmospheric pressures and southerly winds. Ebb tides show

Table 3.3: Mean densities (indiv./15m³ of water filtered) and standard deviations (S.D.) for all sampling efforts during each month for both years combined. Statistics for each species are provided, as well as a total for each interaction per species. Months where no larvae were collected under that designation are represented by an "x".

	Month								
	Mean Density (S.D.)								
<i>Brevoortia patronus</i>									
Interaction	Sept.	Oct.	Nov.	Dec.	Jan.	Feb.	Mar.	Apr.	Total
Daytime Ebb	x	0.8 (2.1)	5.2 (17.4)	x	0.1 (0.4)	0.7 (1.9)	1.8 (3.4)	x	1.8 (8.5)
Nocturnal Ebb	x	15.6 (46.9)	5.7 (13.0)	4.6 (8.3)	11.7 (15.7)	1.8 (4.1)	7.2 (15.0)	x	6.7 (21.5)
Daytime Flood	2.6 (8.9)	2.9 (7.4)	15.4 (28.8)	1.6 (5.8)	1.1 (2.3)	0.9 (5.4)	x	x	3.6 (13.5)
Nocturnal Flood	0.1 (0.6)	15.8 (59.6)	17.2 (72.1)	4.8 (11.8)	3 (7.3)	x	12.8 (62.3)	x	9.5 (49.6)
<i>Micropogonias undulatus</i>									
Interaction	Sept.	Oct.	Nov.	Dec.	Jan.	Feb.	Mar.	Apr.	Total
Daytime Ebb	x	0.6 (1.8)	42.3 (140.8)	57.5 (157.1)	x	x	2.1 (8.3)	x	14.2 (80.2)
Nocturnal Ebb	x	15.1 (42.4)	27.3 (55.1)	5.0 (9.1)	3.6 (5.9)	0.3 (0.6)	1.6 (5.4)	x	8.8 (31.0)
Daytime Flood	x	9.6 (19.2)	88.4 (362.7)	8.2 (29.2)	2.3 (7.4)	x	x	x	16.7 (148.3)
Nocturnal Flood	0.9 (1.5)	10.6 (45.2)	27.3 (91.3)	x	2.7 (10.6)	x	x	x	7.8 (45.1)
<i>Anchoa hepsetus</i>									
Interaction	Sept.	Oct.	Nov.	Dec.	Jan.	Feb.	Mar.	Apr.	Total
Daytime Ebb	x	1.6 (10.3)	x	x	x	x	0.04 (0.2)	32.4 (69.7)	1.6 (14.0)
Nocturnal Ebb	0.3 (1.0)	0.7 (4.3)	0.9 (6.5)	x	x	x	1.6 (6.5)	0.4 (1.1)	0.6 (4.2)
Daytime Flood	6.5 (15.3)	x	1.0 (5.0)	x	0.04 (0.2)	x	x	x	0.6 (4.7)
Nocturnal Flood	13.0 (50.0)	x	x	x	x	x	x	11.9 (26.5)	2.3 (19.5)

Table 3.3 *Continued*: Mean densities (indiv./15m³ of water filtered) and standard deviations (S.D.) for all sampling efforts during each month for both years combined. Statistics for each species are provided, as well as a total for each interaction per species. Months where no larvae were collected under that designation are represented by an "x".

	Month								
	Mean Density (S.D.)								
<i>Anchoa mitchilli</i>									
Interaction	Sept.	Oct.	Nov.	Dec.	Jan.	Feb.	Mar.	Apr.	Total
Daytime Ebb	8.6 (19.6)	1.0 (2.1)	x	1.1 (3.6)	x	x	0.4 (1.5)	263.4 (585.1)	10.1 (108.1)
Nocturnal Ebb	2.9 (6.8)	5.3 (17.3)	0.1 (0.4)	0.7 (1.6)	0.3 (1.1)	0.6 (2.0)	5.9 (13.0)	x	2.2 (9.0)
Daytime Flood	9 (29.0)	13.5 (24.0)	0.1 (0.4)	x	0.1 (0.4)	x	0.1 (0.8)	x	2.2 (11.8)
Nocturnal Flood	12.0 (29.4)	47.4 (206.0)	x	x	x	3.0 (10.6)	x	x	12.7 (99.1)
<i>Farfantepenaeus aztecus</i>									
Interaction	Sept.	Oct.	Nov.	Dec.	Jan.	Feb.	Mar.	Apr.	Total
Daytime Ebb	x	x	x	x	0.2 (0.4)	1.0 (3.5)	6.6 (13.8)	0.2 (0.4)	1.3 (6.1)
Nocturnal Ebb	0.4 (0.9)	1.7 (7.6)	0.04 (0.2)	2.2 (8.9)	1.6 (2.5)	0.5 (0.8)	11.8 (44.6)	0.4 (1.1)	2.5 (17.5)
Daytime Flood	7.7 (15.9)	0.8 (2.2)	0.5 (1.6)	0.7 (1.7)	x	6.1 (21.9)	6.5 (20.6)	x	3.6 (13.8)
Nocturnal Flood	3.3 (7.1)	0.6 (2.0)	1.3 (6.0)	x	44.4 (91.0)	10.1 (23.4)	44.8 (86.9)	x	13.7 (47.8)
<i>Pogonias cromis</i>									
Interaction	Sept.	Oct.	Nov.	Dec.	Jan.	Feb.	Mar.	Apr.	Total
Daytime Ebb	x	x	x	6.2 (10.2)	1.3 (2.6)	0.6 (1.9)	0.2 (0.5)	x	0.7 (3.4)
Nocturnal Ebb	x	0.02 (0.1)	x	0.9 (3.8)	0.1 (0.3)	9.7 (36.3)	3.6 (24.1)	x	2.8 (19.9)
Daytime Flood	x	x	x	x	1.3 (5.6)	x	x	x	0.2 (2.2)
Nocturnal Flood	x	0.7 (4.5)	x	34.7 (85.0)	0.1 (0.5)	5.3 (18.0)	x	x	2.5 (18.9)

Table 3.3 *Continued*: Mean densities (indiv./15m³ of water filtered) and standard deviations (S.D.) for all sampling efforts during each month for both years combined. Statistics for each species are provided, as well as a total for each interaction per species. Months where no larvae were collected under that designation are represented by an "x".

	Month								
	Mean Density (S.D.)								
<i>Sciaenops ocellatus</i>									
Interaction	Sept.	Oct.	Nov.	Dec.	Jan.	Feb.	Mar.	Apr.	Total
Daytime Ebb	0.6 (0.9)	x	x	x	x	x	x	x	0.1 (0.5)
Nocturnal Ebb	1.4 (5.9)	0.3 (1.5)	x	x	x	x	x	x	0.7 (3.7)
Daytime Flood	2.2 (7.5)	0.3 (0.9)	x	x	x	x	x	x	1.0 (4.7)
Nocturnal Flood	147.1 (477.3)	2.5 (7.6)	x	x	x	x	x	x	57.6 (299.3)
<i>Cynoscion arenarius</i>									
Interaction	Sept.	Oct.	Nov.	Dec.	Jan.	Feb.	Mar.	Apr.	Total
Daytime Ebb	7.8 (6.1)	0.6 (2.1)	0.03 (0.2)	x	x	0.1 (0.3)	7.9 (14.1)	0.2 (0.4)	2.2 (6.8)
Nocturnal Ebb	1.4 (4.5)	0.2 (0.6)	0.01 (0.1)	0.03 (0.2)	x	0.5 (1.1)	2.3 (4.2)	1.7 (3.1)	0.7 (2.4)
Daytime Flood	6.2 (11.6)	0.2 (0.7)	x	x	x	0.3 (1.9)	4.0 (14.8)	2.7 (4.6)	1.4 (7.5)
Nocturnal Flood	46.6 (64.6)	4.6 (13.1)	x	x	x	x	x	19.4 (27.5)	9.0 (30.8)
<i>Cynoscion nebulosus</i>									
Interaction	Sept.	Oct.	Nov.	Dec.	Jan.	Feb.	Mar.	Apr.	Total
Daytime Ebb	2.0 (3.6)	0.02 (0.2)	x	x	x	x	x	x	0.5 (1.9)
Nocturnal Ebb	0.2 (0.5)	0.04 (0.2)	x	x	x	x	x	x	0.1 (0.3)
Daytime Flood	1.5 (3.5)	0.9 (2.6)	x	x	x	x	x	x	1.1 (3.0)
Nocturnal Flood	2.2 (10.0)	x	x	x	x	x	x	x	0.8 (6.2)

Table 3.4: Data and statistical results for Kruskal-Wallis (KW) Rank Sum Test for differences between densities sampled during the interactions of tidal stage and circadian sampling efforts for both years combined. Mean and median densities are calculated per 15 cubic meters of water filtered. All metrics are based on the zero-truncated data set and accounting for ties to meet the assumptions of KW. Similarities and differences between each of the four groupings are presented as subscripted letters. The same letter shows similarity between those groups for each species. Different letters "A,B,C,D" represent statistically significant differences ($\alpha=0.05$) between groups.

Species	Ebb Tidal Stage Daytime Sampling			Ebb Tidal Stage Nocturnal Sampling			Flood Tidal Stage Daytime Sampling			Flood Tidal Stage Nocturnal Sampling			K-W
	Mean	Median	S.D.	Mean	Median	S.D.	Mean	Median	S.D.	Mean	Median	S.D.	$P_{H_0}(\chi^2 \geq H)$
<i>B. patronus</i>	8.3	3.5 ^A	17.1	15.2	5.0 ^{AB}	30.4	23.6	16.0 ^{AB}	27.4	56.9	20.5 ^B	111.0	0.0084
<i>M. undulatus</i>	91.5	4.0 ^A	215.2	32.1	6.0 ^A	67.8	162.4	34.0 ^B	447.9	86.4	27.0 ^{AB}	140.6	0.0081
<i>A. hepsetus</i>	57.0	35.0	72.8	11.2	2.0	16.0	26.3	30.5	18	79.0	27.0	101.2	0.1049
<i>A. mitchilli</i>	87.1	4.0 ^A	315.6	15.2	5.5 ^A	21.4	31.0	16.5 ^{AB}	39.8	137.9	40.5 ^B	369.6	<0.0005
<i>F. aztecus</i>	13.4	7.5 ^{AB}	16.2	10.9	2.0 ^A	35.7	25.3	8.5 ^B	31.2	76.0	27.0 ^B	124.1	<0.0001
<i>P. cromis</i>	9.1	4.5	10.4	45.2	4.0	73.2	10.3	3.0	14.5	72.0	45.0	80.8	0.2516
<i>S. ocellatus</i>	2.3	2.0 ^A	1.5	9.4	3.0 ^A	12.0	10.3	4.0 ^A	13.7	242.0	26.0 ^A	614.1	0.0832
<i>C. arenarius</i>	14.4	7.0 ^A	19.6	5.8	3.0 ^A	6.5	25.8	12.0 ^{AB}	23.9	84.5	45.0 ^B	93.6	<0.0001
<i>C. nebulosus</i>	5.0	3.0 ^A	5.8	1.2	1.0 ^A	0.4	8.8	9.0 ^A	2.2	26.5	26.5 ^B	31.2	0.0317

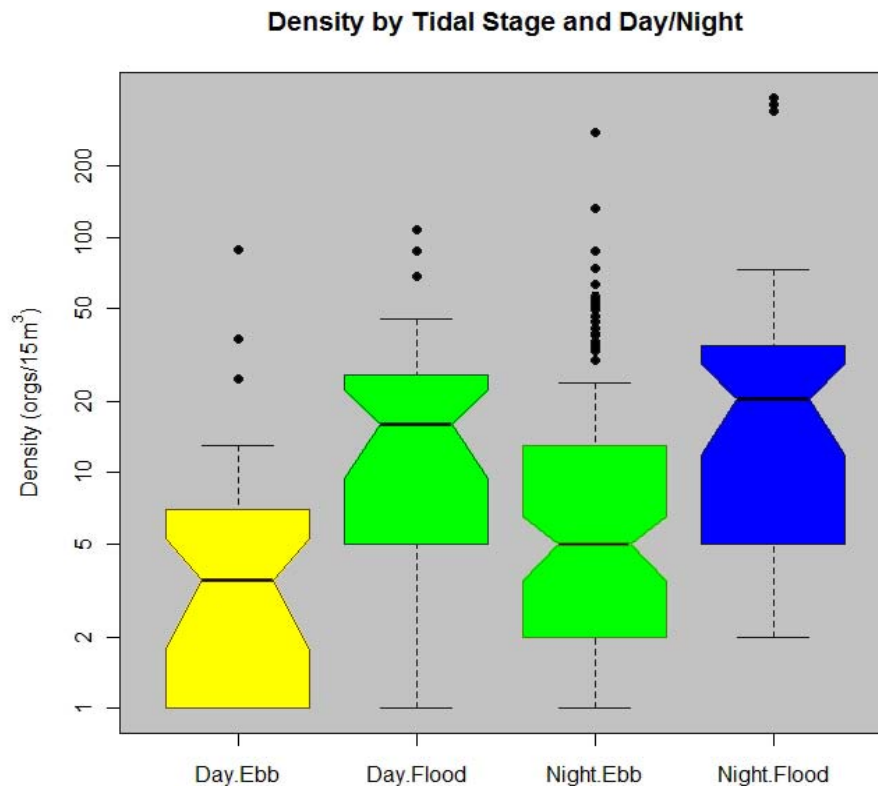


Figure 3.18: Density of *Brevoortia patronus* larvae as a function of tidal stage and time of day. There is a significant difference between those samples collected during flood and ebb tides; however, no difference is discernible in time of day. Non-overlapping notches in the boxplots represent “strong evidence” of statistically different median values (Chambers et al. 1983), which represents the equivalent of a “visual” WMW. Different primary colors (yellow and blue) represent statistically different groups, while secondary colors (green) show similarities to both primary groups under Kruskal-Wallis test.

medium numbers of larvae within the tidal pass associated with northerly winds and extremely high or low atmospheric pressures. Overall, the most favorable conditions for high catch rates of *B. patronus* were associated with passage of the front (i.e., low pressures associated with westerly winds), and the period immediately after frontal passage with climbing barometric

Table 3.5: Model terms and associated significance levels for each species included for analysis. Terms in the models that were significant at $p \leq 0.05$ are in bold. Terms that upon stepwise model simplification were no longer necessary in the model are represented by an x. Those model terms that were able to have specification upon tidal stage have the significance values for each tidal stage, and the removed combined term is represented by a "~".

Model Terms	Species								
	<i>B. patronus</i>	<i>M. undulatus</i>	<i>A. hepsetus</i>	<i>A. mitchilli</i>	<i>F. aztecus</i>	<i>P. cromis</i>	<i>S. ocellatus</i>	<i>C. arenarius</i>	<i>C. nebulosus</i>
Net Water Transport	0.0002	<0.0001	0.0014	0.0099	x	x	x	0.0005	x
Wind Direction	0.0508	0.2529	0.0361	0.0383	~	~	<0.0001	~	0.0514
Flood					0.0007	<0.0001		0.0053	
Ebb					0.0227	0.0014		0.0005	
Wind Speed	0.0022	x	0.0153	0.0867	0.0003	x	x	0.0074	0.0029
Flood									
Ebb									
Barometric Pressure	0.0265	0.0019	0.0395	0.0001	~	~	0.0052	~	x
Flood					0.0058	<0.0001		0.0049	
Ebb					0.0057	0.0012		0.0018	
Interaction	~	~	x	x	x	x	x	x	x
Flood	0.0016	0.0207							
Ebb	<0.0001	<0.0001							
Adj. R ²	0.92	0.91	0.34	0.32	0.34	0.49	0.39	0.37	0.38
Deviance Explained	84.80%	95.30%	67.70%	66.50%	62.90%	85.20%	72.30%	71.60%	59.00%

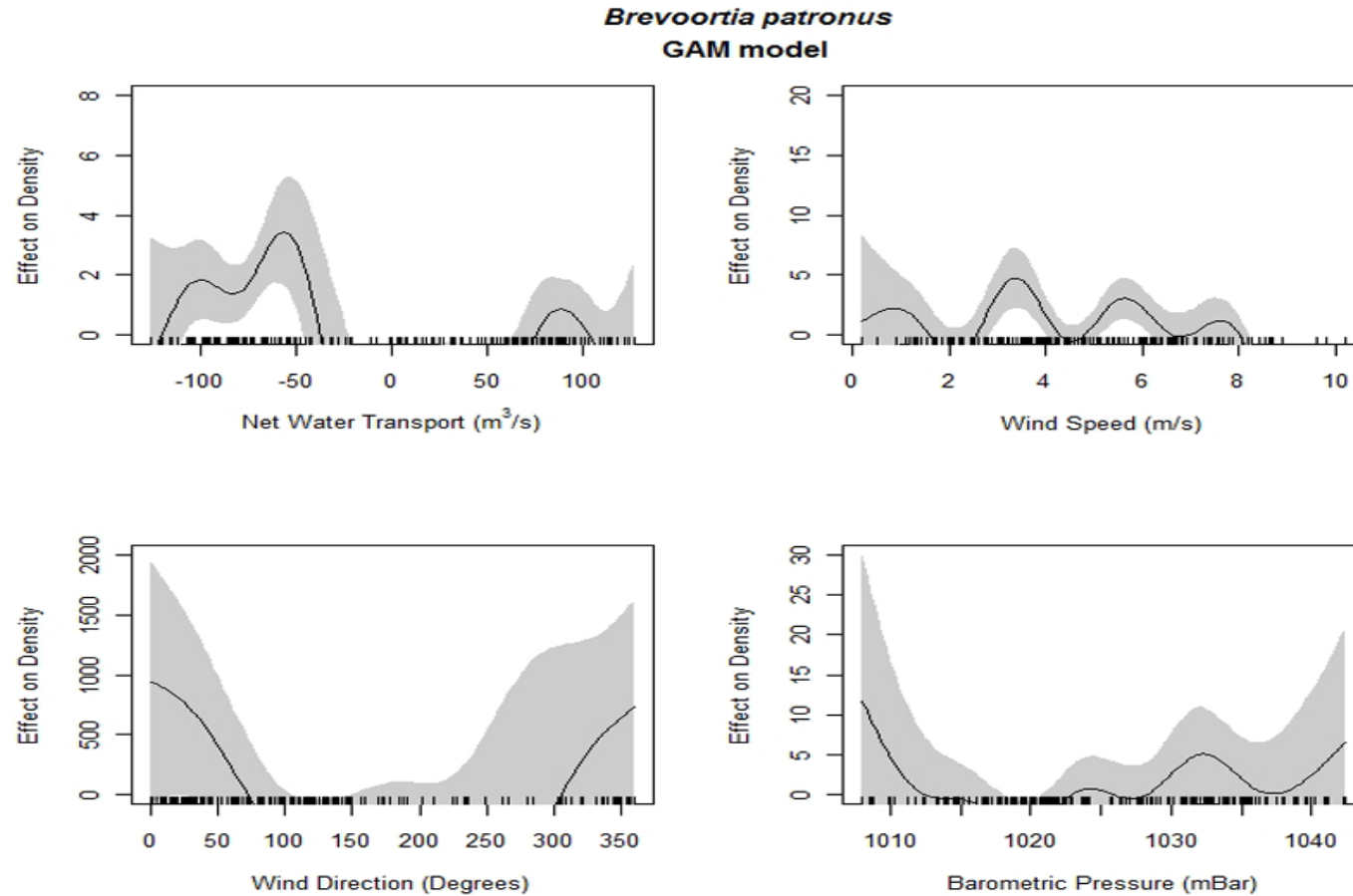


Figure 3.19: Model fit for the 1-dimensional terms of the GAM model for larval *Brevoortia patronus*. Shaded areas represent 95% confidence intervals around the model fit represented by the black line. Tick marks on the x-axes represent actual observations. Only positive effects on density are shown to better illustrate the individual effects of model terms.

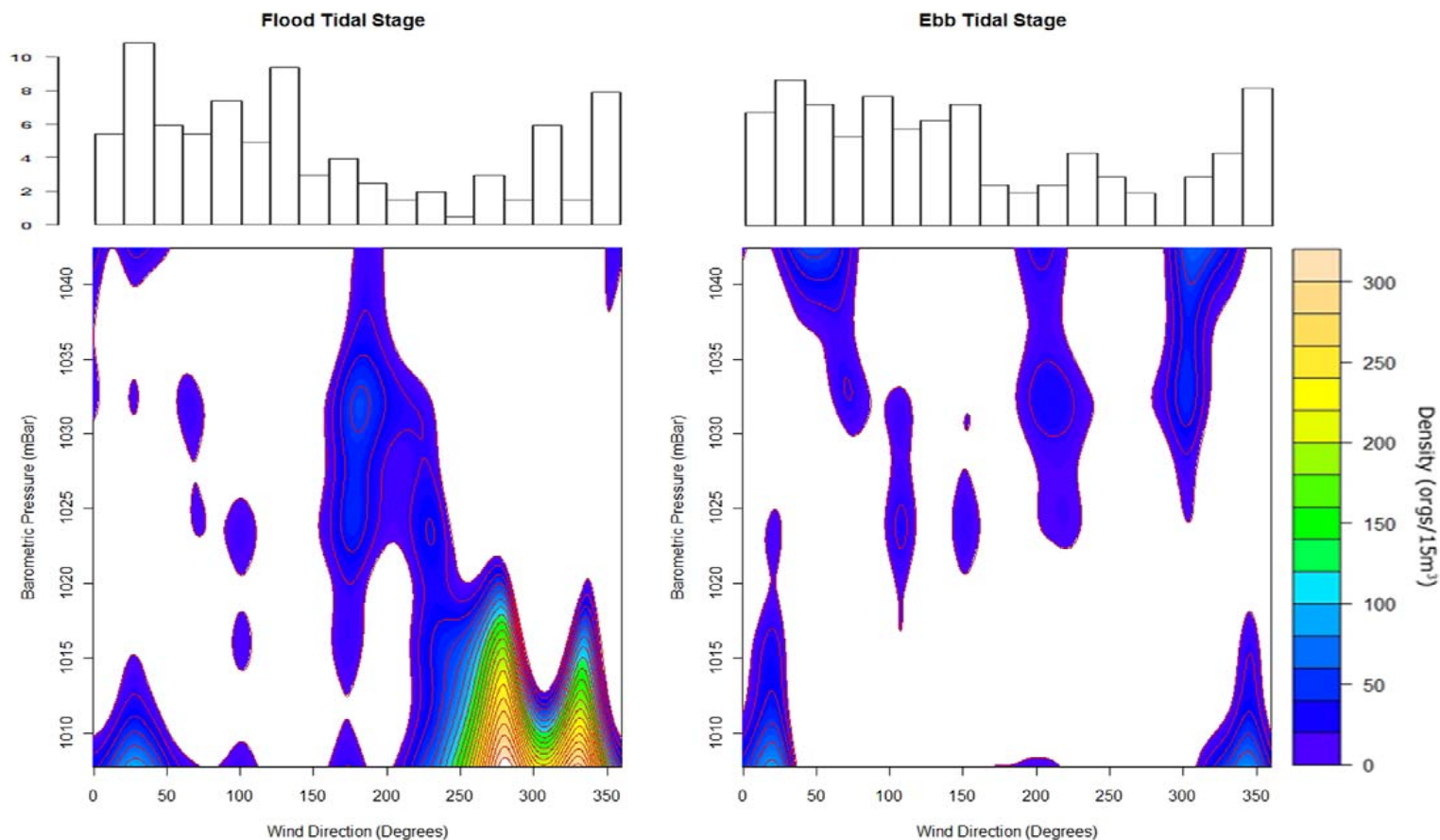


Figure 3.20: Larval *Brevoortia patronus* completed model and effect on density plotted as a contour map. Expected values are based on the complete model fit. Estimated density isolines as a function of barometric pressure and wind direction are shown in color. Areas where no plot is shown represent expected numbers of larvae within the tidal pass to be zero. The interaction is plotted individually for flood and ebb tidal stages. Histograms above contour plots represent frequency of wind directions during sampling.

pressures and northerly winds. Interestingly, easterly winds across a range of atmospheric pressures, usually associated with Ekman transport inshore, showed no positive effect on densities.

3.3.4 *Micropogonias undulatus* (Atlantic croaker)

Atlantic croaker, *Micropogonias undulatus*, larvae were collected in all months except for April over the course of the two year study (Table 3.1; Figure 3.14). There was a distinct peak in the mean density of Atlantic croaker in November ($\bar{x} = 42.0$ indiv./15m³, $sd = 177.4$), which decreased sharply through December ($\bar{x} = 13.5$ indiv./15m³, $sd = 64.3$) and January ($\bar{x} = 2.7$ indiv./15m³, $sd = 7.3$; Table 3.1). Despite encounters during all of the sample months except April, and particularly high densities sampled from October through December, nearly 74% of the samples taken had no larvae. The above observations plus the general relationships between flood or ebb and day or night collections again yielded results indicative of pulsed recruitment into a well-mixed estuary.

Controlling for presence/absence, flood tides had significantly higher densities ($\bar{x} = 126.8$ indiv./15m³, $sd = 337.6$, Table 3.2) when compared with ebb ($\bar{x} = 44.8$ indiv./15m³, $sd = 117.2$, $p < 0.001$, WMW; Figure 3.21), regardless of time of day. Nocturnal densities (Ebb: $\bar{x} = 8.8$ indiv./15m³, $sd = 31.0$; Flood: $\bar{x} = 7.8$ indiv./15m³, $sd = 45.1$) were smaller than day densities (Ebb: $\bar{x} = 14.2$ indiv./15m³, $sd = 80.2$; Flood: $\bar{x} = 16.7$ indiv./15m³, $sd = 148.3$, Table 3.3). However, when controlling for the presence or absence of larvae, there is no statistical difference between the nocturnal and daytime distributions (Table 3.2). Atlantic croaker daytime flood catches ($\bar{x} = 162.4$ indiv./15m³, $sd = 447.9$), were statistically greatest followed by nocturnal flood catches ($\bar{x} = 86.4$ indiv./15m³, $sd = 140.6$, $p = 0.0081$, K-W,

Table 3.4). Recruitment events for Atlantic croaker, therefore, seem to be more associated with tidal stage rather than circadian (i.e., day/night) cycles.

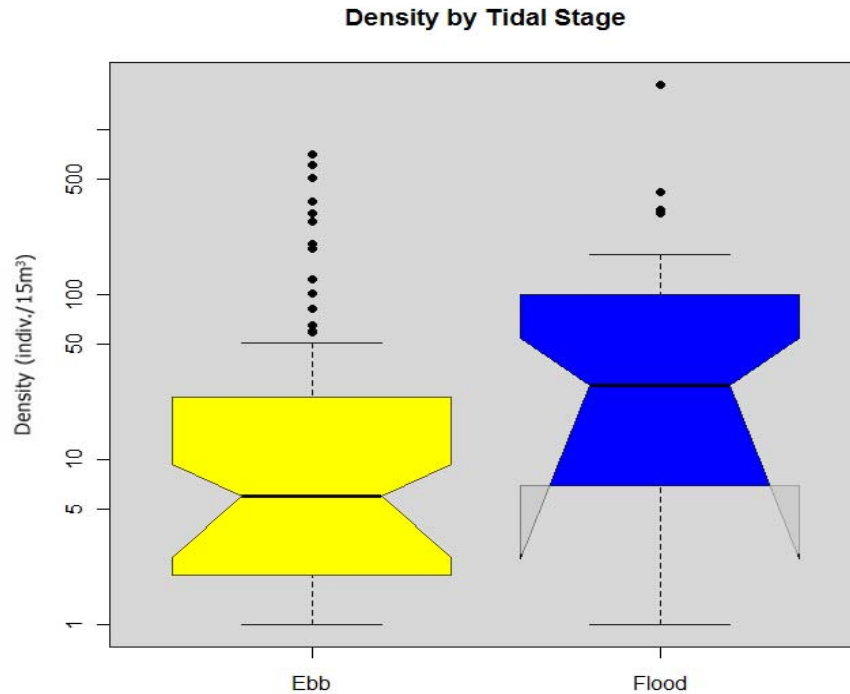


Figure 3.21: Density as a function of tidal stage for larval *Micropogonias undulatus*. Flood tides had a significantly higher median value than ebb tides. Ebb tides, however, had more large outliers. Non-overlapping notches in the boxplot represent “strong evidence” of statistically different median values (Chambers et al. 1983). Different colors represent statistically different groups (WMW).

With respect to meteorological variables, such as net water transport, barometric pressure, and the interaction of barometric pressure and wind direction, all appear to have strong non-linear effects on Atlantic croaker density (Adj. $R^2 = 0.91$, Table 3.5; Figure 3.22). Although net water transport appeared to affect the Atlantic croaker baseline mean density in the tidal pass, as with *B. patronus*, large scale variations in density were more a function of barometric pressure and wind direction. The interaction of wind direction and barometric pressure was controlled for

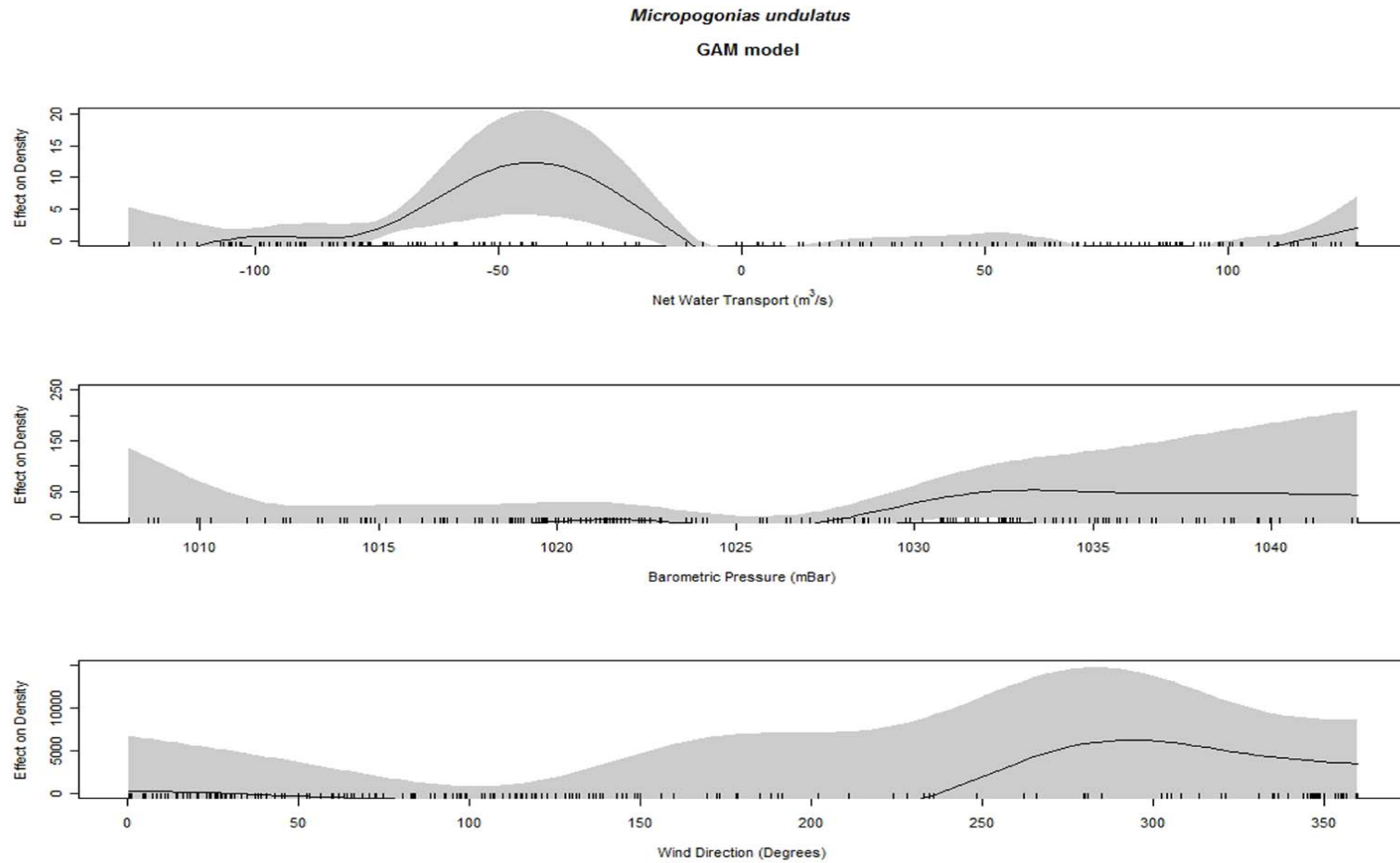


Figure 3.22: Model fit for the 1-dimensional terms of the GAM model for larval *Micropogonias undulatus*. Shaded areas represent 95% confidence intervals around the model fit represented by the black line. Tick marks on the x-axes represent actual observations. Only positive effects on density are shown to better illustrate the individual effects of model terms.

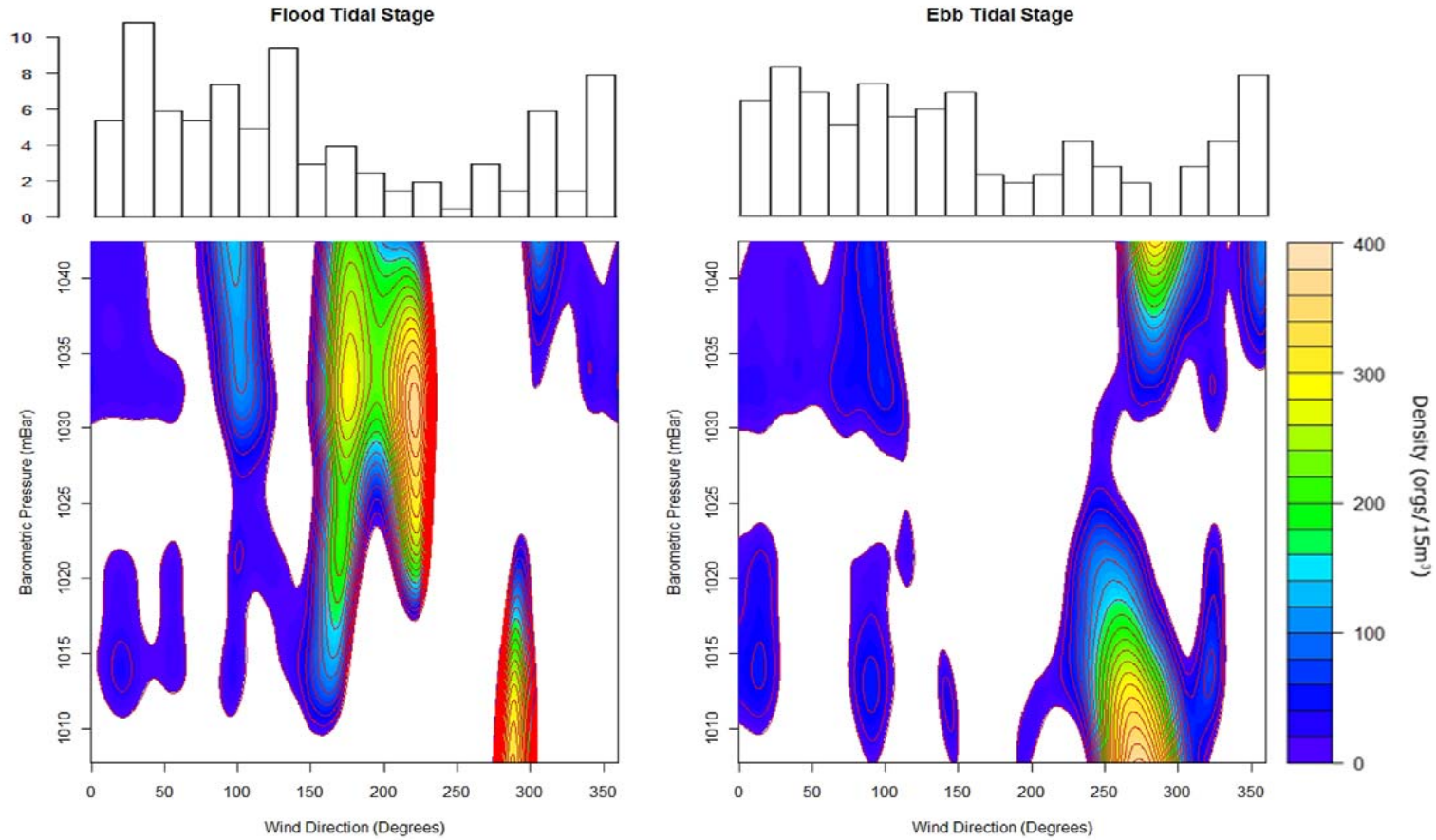


Figure 3.23: Larval *Micropogonias undulatus* completed model and effect on density plotted as a contour map. Expected values are based on the complete model fit. Estimated density isolines as a function of barometric pressure and wind direction are shown in color. Areas where no plot is shown represent expected numbers of larvae within the tidal pass to be zero. The interaction is plotted individually for flood and ebb tidal stages. Histograms above contour plots represent percent frequency of wind direction during sampling.

differences expected between flood and ebb tidal stages. This interaction was significant ($p < 0.05$, Chisq) for both tidal stages. During flood tides, large estuarine densities were mostly driven by southerly winds and coastal setup, particularly associated with mid to high barometric pressures (Figure 3.23). Flood tides also had high predicted Atlantic croaker densities during westerly winds and low barometric pressures associated with the early passage of frontal events. The primary effect on densities during ebb tides was most notable during westerly winds, at either low or high barometric pressures. To a much lesser extent, easterly and southeasterly winds associated with the late post-frontal and interim periods, were also influential during ebb tides.

3.3.5 *Anchoa hepsetus* (broad-striped anchovy)

Broad-striped anchovy, *Anchoa hepsetus*, larvae are estuarine dependent and were collected during all months except for December and February (Table 3.1; Figure 3.14). However, densities were generally extremely small with only two months with relatively high densities in spring (April, $\bar{x} = 11.3$ indiv./15m³, $sd = 35.9$, Table 3.1) and early fall (September, $\bar{x} = 5.5$ indiv./15m³, $sd = 29.7$). This observed seasonality coincides with the expected summer spawning peak, with densities gradually increasing during spring and waning during fall. Although several collection densities were greater than 150 larvae per 15m³, most samples (93%) contained no broad-striped anchovy larvae.

Mean densities of broad-striped anchovy were greater during flood ($\bar{x} = 1.5$ indiv./15m³, $sd = 14.3$, Table 3.1) than ebb tides ($\bar{x} = 0.9$ indiv./15m³, $sd = 8.7$; $p = 0.057$, WMW, Table 3.2). Although night collection mean densities ($\bar{x} = 1.2$ indiv./15m³, $sd = 12.3$, Table 3.1) were similar to day ($\bar{x} = 1.1$ indiv./15m³, $sd = 10.1$), there were more positive collections during day

when controlling for presence/absence (Table 3.2). Interaction between time of day and tidal stage was not significant (Table 3.4), however, nocturnal floods had the highest densities ($\bar{x} = 2.3 \text{ indiv./15m}^3$, $sd = 19.5$, Table 3.3). Further, nighttime collections occasionally had singular, extremely high densities, regardless of the prevailing tidal stage. In addition, there was also no discernible difference between surface and near-bottom densities.

When accounting for the atmospheric/meteorological variables, the significant non-linear relationships were with net water transport, wind direction, wind speed, and barometric pressure (Table 3.5). These variables, while describing the meteorological effect from passage of winter fronts, generally were insufficient to describe a large portion of the variation in sampled densities of broad-striped anchovy (Adj. $R^2 = 0.34$; Figure 3.24). High atmospheric pressures resulted in complete lack of any larvae, regardless of wind direction. Coupling wind speed with wind direction, peak density effects were associated with relatively rare high wind speeds, perhaps with a weak central tendency towards southerly wind patterns and mid to high barometric pressures (Figure 3.25).

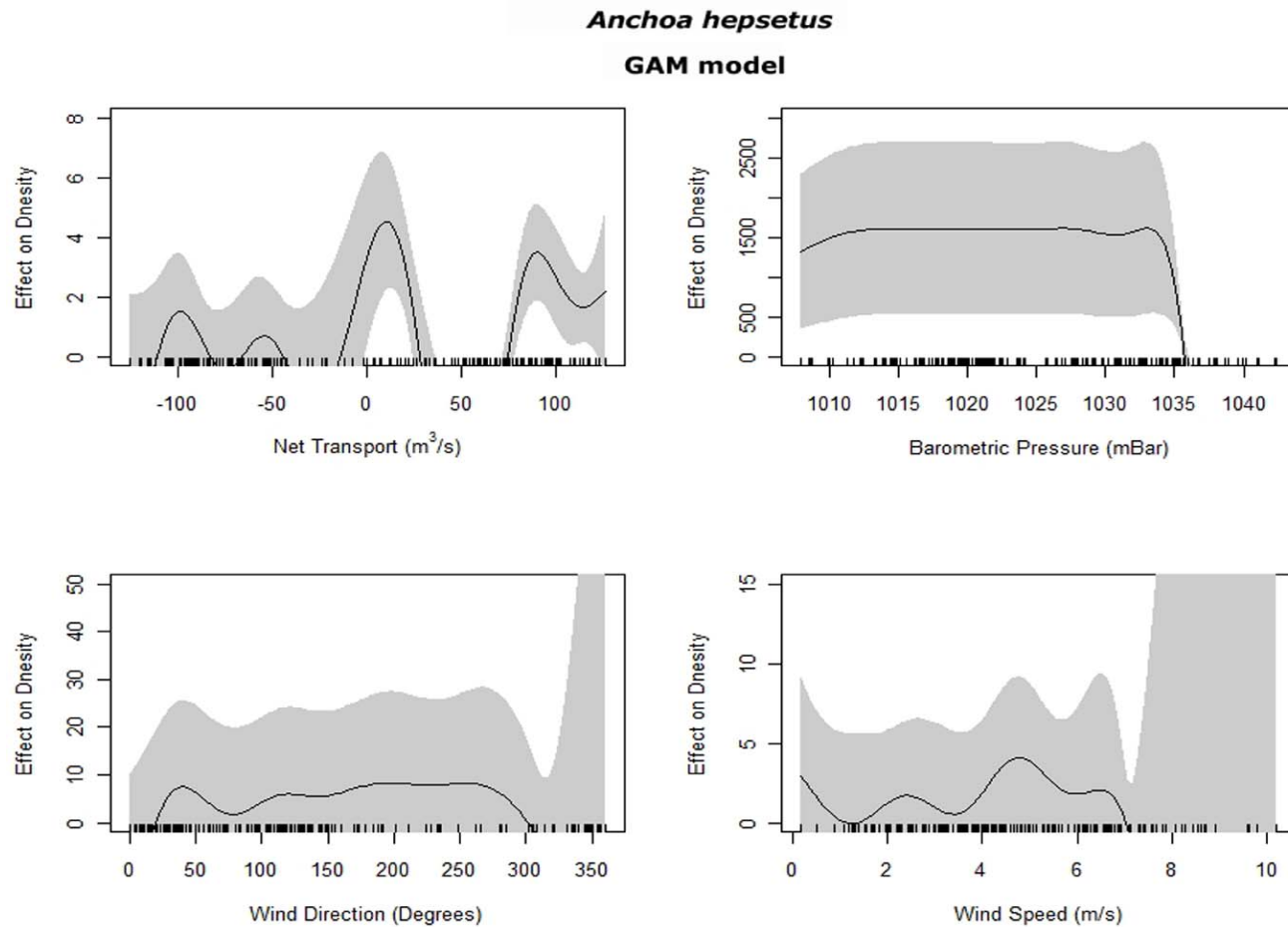


Figure 3.24: Model Fit for 1-dimensional terms of the GAM model for larval *Anchoa hepsetus*. Shaded areas represent 95% confidence intervals around the model fit represented by the black line. Tick marks on the x-axes represent actual observations. Only positive effects on density are shown to better illustrate the individual effects of model terms.

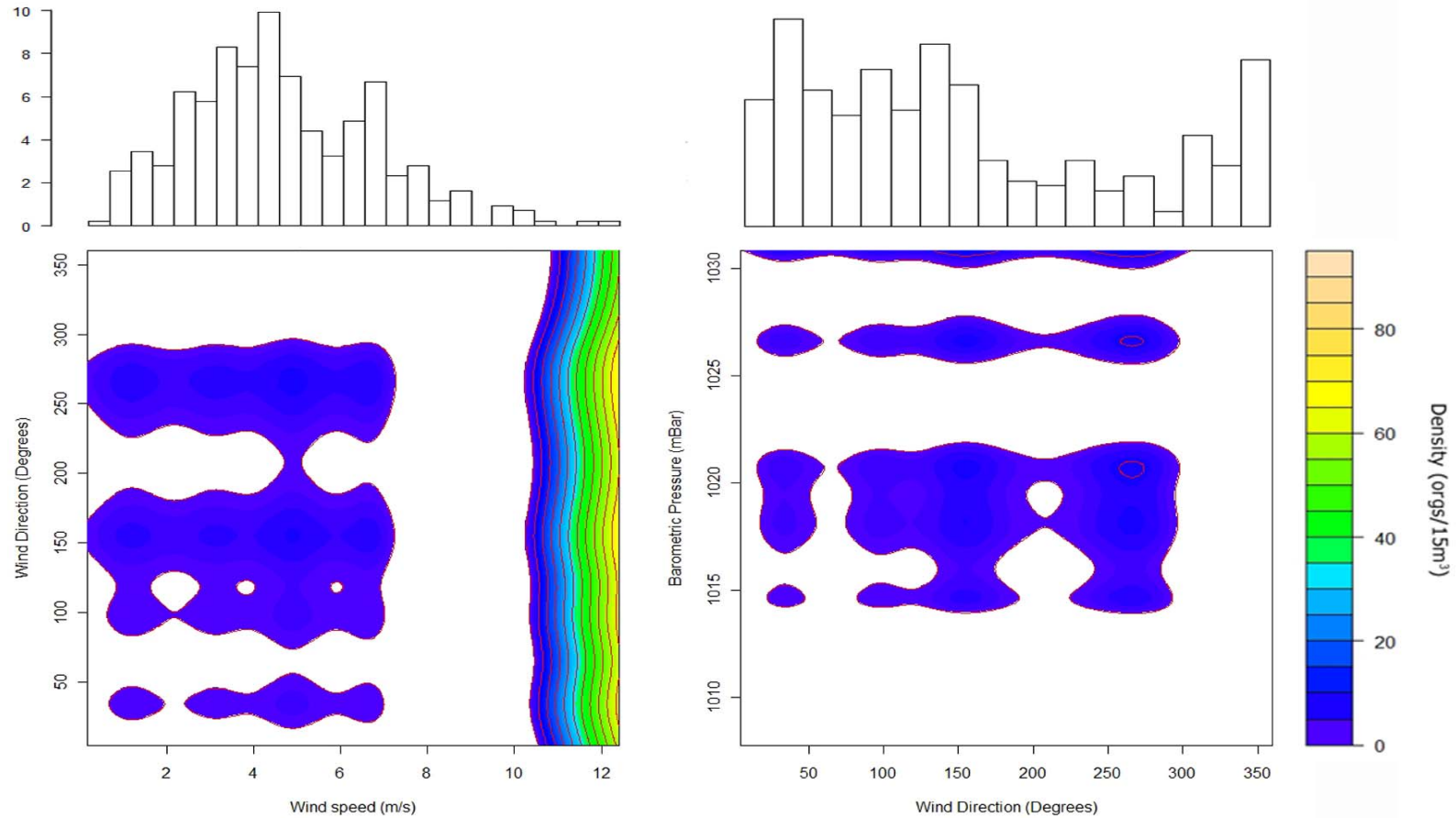


Figure 3.25: Larval *Anchoa hepsetus* completed model and effect on density plotted as a contour map. Expected values are based on the complete model fit. Estimated density isolines as a function of wind direction and wind speed (left), and as a function of wind direction and barometric pressure (right), are shown in color. Areas where no plot is shown represent expected numbers of larvae within the tidal pass to be zero. Left histogram above contour maps shows percent frequency of wind speeds during sampling, while the histogram on the right shows wind direction percent frequency during sampling.

3.3.6 *Anchoa mitchilli* (bay anchovy)

In contrast to *A. hepsetus*, *Anchoa mitchilli*, bay anchovy, is an estuarine-obligate species, whose spawning peak also occurs over the summer months (Table 3.1; Figure 3.14). Densities were generally large, and positive collections more numerous during the months of April ($\bar{x} = 59.9$ indiv./15m³, $sd = 279.2$, Table 3.1), September ($\bar{x} = 7.9$ indiv./15m³, $sd = 22.3$), and October ($\bar{x} = 16.6$ indiv./15m³, $sd = 108.7$). However, there were collections of bay anchovy during all sample months with decreasing numbers of positive collections during winter, and 83% of all samples collected contained no bay anchovies.

Surprisingly, flood tides collected significantly higher bay anchovy densities especially on the zero-truncated dataset ($\bar{x} = 92.1$ indiv./15m³, $sd = 281.8$) than ebb ($\bar{x} = 35.2$ indiv./15m³, $sd = 167.1$, $p < 0.001$, WMW, Table 3.2). There was no significant difference between night and day densities (Table 3.2). Controlling for presence/absence, nocturnal flood density estimates ($\bar{x} = 137.9$ indiv./15m³, $sd = 369.6$, Table 3.4) were statistically higher than either ebb, but statistically indistinguishable from daytime flood densities ($\bar{x} = 31.0$ indiv./15m³, Figure 3.26).

The same suite of meteorological terms (i.e., net water transport, wind direction, wind speed, and barometric pressure) was significant for *A. mitchilli* as for *A. hepsetus* (Table 3.5). Net water transport was highly significant ($p < 0.01$, Chisq), but the density effects were generally muted (i.e., density effects < 5 ; Adj. $R^2 = 0.32$, Table 3.5), with minimal changes in density resulting from net water transport, and large peaks in expected density for specific conditions were absent (Figure 3.27). Considering the interactions of wind direction with wind speed and barometric pressure, multiple peaks of relatively high densities were associated with

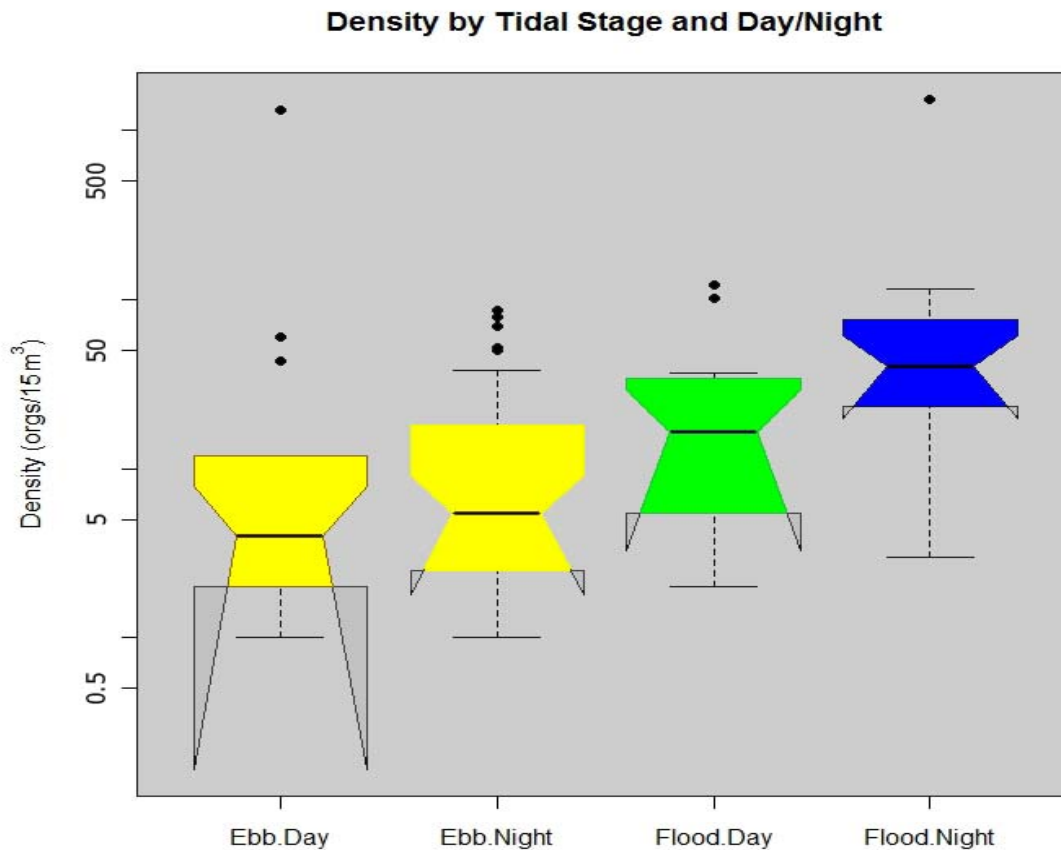


Figure 3.26: Density of *Anchoa mitchilli* larvae as a function of tidal stage and time of day. Flood tides had more of an effect on density estimates than day or night collections. Non-overlapping notches in the boxplots represent “strong evidence” of statistically different median values (Chambers et al. 1983), which represents the equivalent of a “visual” WMW. Different primary colors (yellow and blue) represent statistically different groups, while secondary colors (green) show similarities to both primary groups under Kruskal-Wallis test.

both high and low barometric pressure; particularly with relatively high wind speeds (9 – 11 m/s) from the northwesterly through northeasterly quadrant. These wind directions correlate well with the end of declining tidal prism during the post-frontal phase (Figure 3.28). Expectedly, due to the estuarine obligate nature of bay anchovies, these values correspond more with negative net transport events.

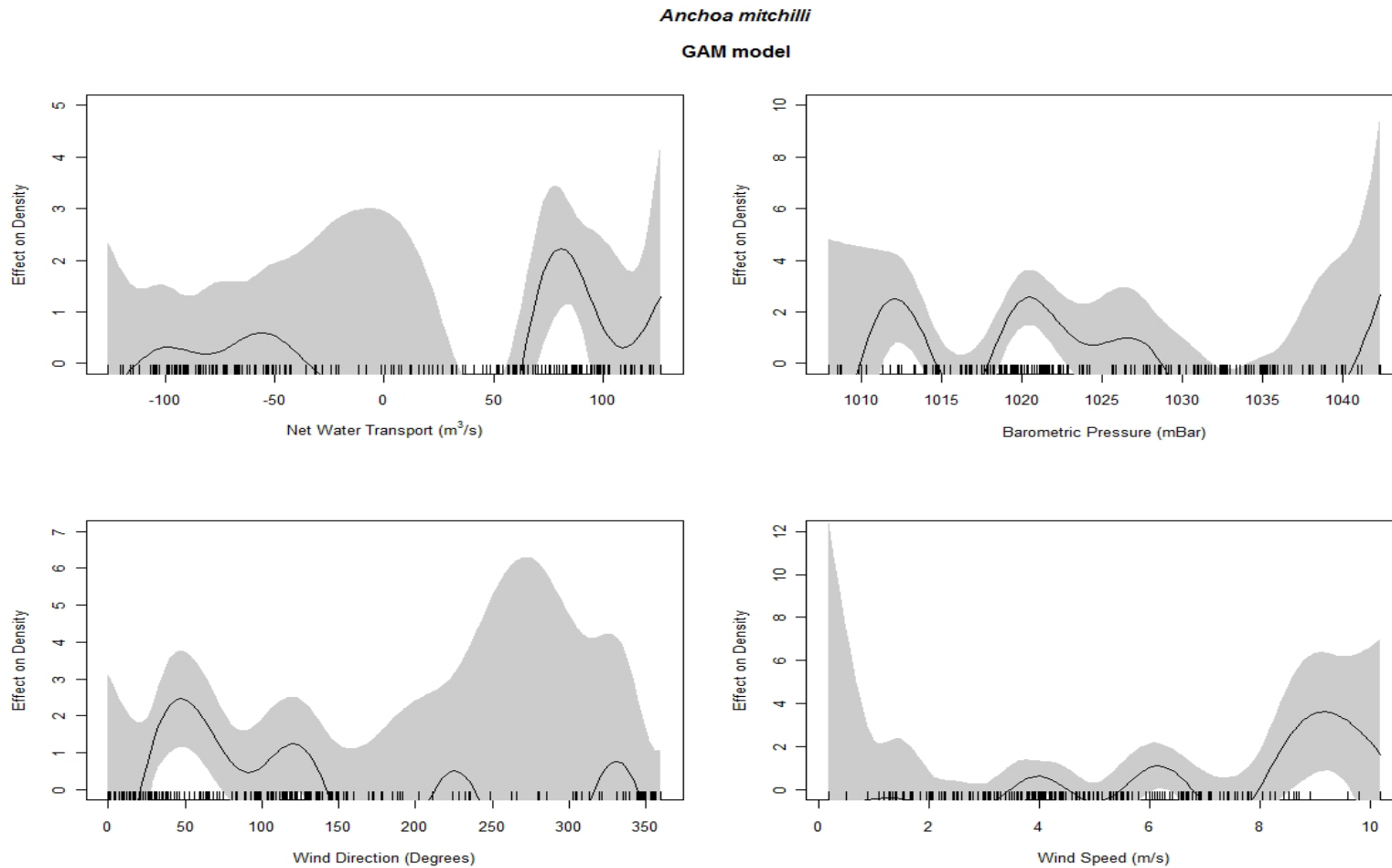


Figure 3.27: Model fit for 1-dimensional terms of the GAM model for *Anchoa mitchilli* larvae. Shaded areas represent 95% confidence intervals around the model fit represented by the black line. Tick marks on the x-axes represent actual observations. Only positive effects on density are shown to better illustrate the individual effects of model terms.

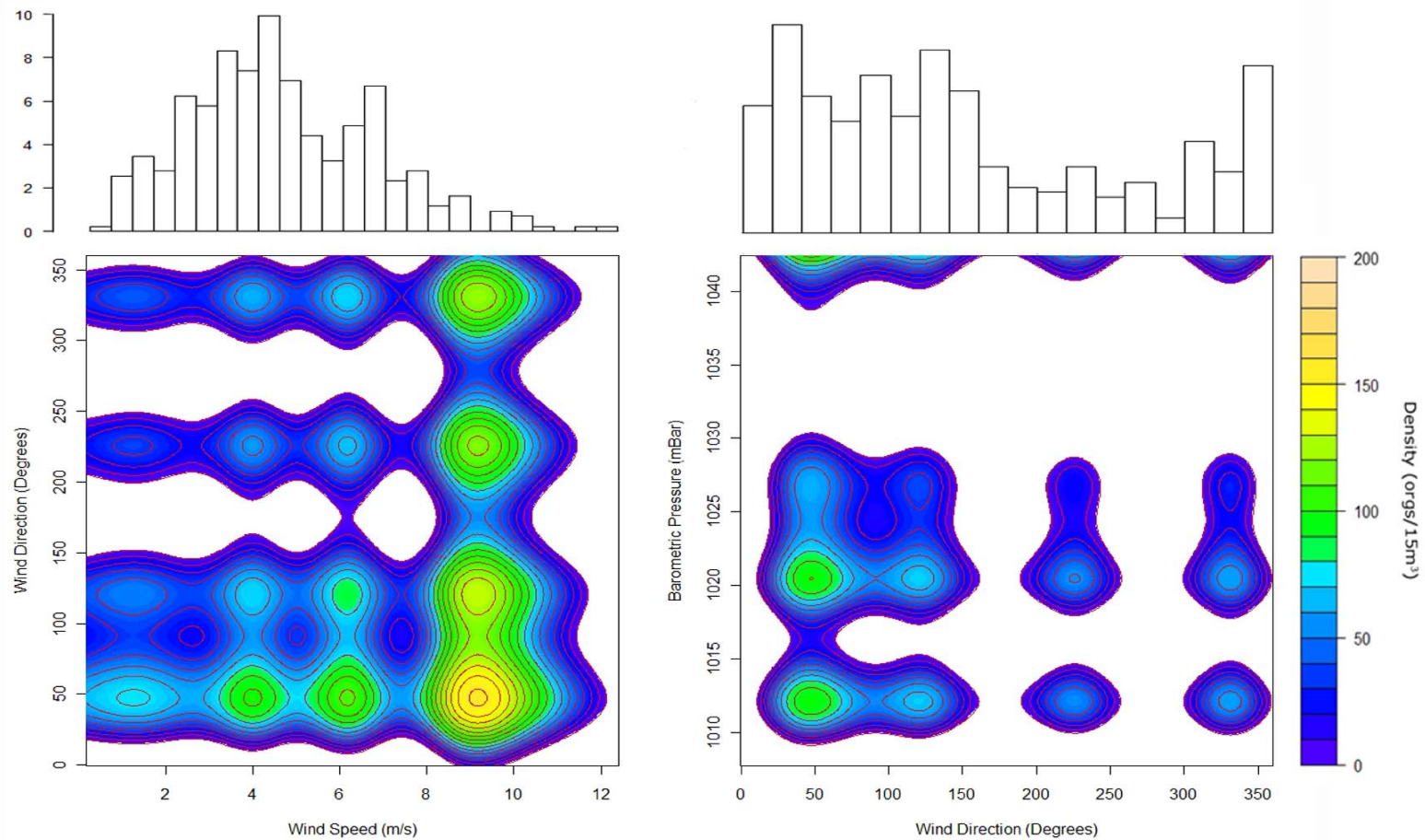


Figure 3.28: Larval *Anchoa mitchilli* completed model and effect on density plotted as a contour map. Expected values are based on the complete model fit. Estimated density isolines as a function of wind speed and wind direction (left); as a function of barometric pressure and wind direction (right) are shown in color. Areas where no plot is shown represent expected numbers of larvae within the tidal pass to be zero. Left histogram above contour maps shows percent frequency of wind speeds during sampling, while the histogram on the right shows wind direction percent frequency during sampling.

3.3.7 *Farfantepenaeus aztecus* (brown shrimp)

Postlarval brown shrimp were sampled during all months of the study period (Table 3.1; Figure 3.14), having an expected peak from January ($\bar{x} = 14.2$ indiv./15m³, $sd = 52.7$, Table 3.1) through February ($\bar{x} = 4.4$ indiv./15m³, $sd = 16.0$) and March ($\bar{x} = 21.2$ indiv./15m³, $sd = 59.1$) with a sharp drop off in both the number of positive collections and mean densities during the month of April ($\bar{x} = 0.2$ indiv./15m³, $sd = 0.7$). Notably, there was a second, smaller recruitment peak seen during September ($\bar{x} = 2.5$ indiv./15m³, $sd = 8.0$, Table 3.1) which tailed off through November. Across both sample years, 77% of the samples contained no postlarval brown shrimp.

Densities collected during flood tides ($\bar{x} = 10.2$ indiv./15m³, $sd = 40.1$, Table 3.1), were greater than those collected during ebb tides ($\bar{x} = 2.1$ indiv./15m³, $sd = 14.7$), and when controlling for presence/absence the difference was highly significant (Ebb: $\bar{x} = 11.4$ indiv./15m³, $sd = 32.9$; Flood: $\bar{x} = 61.5$ indiv./15m³, $sd = 108.0$, $p < 0.001$, WMW, Table 3.2). The graphical methodology proposed by Chambers et al. (1983) also supports the difference between flood and ebb densities (Figure 3.29). Further, greater brown shrimp densities occurred during night ($\bar{x} = 7.7$ indiv./15m³, $sd = 35.4$, Table 3.1) than day ($\bar{x} = 2.4$ indiv./15m³, $sd = 10.4$), but the difference was non-significant (Table 3.2). The interaction between tidal stage and day/night was significant ($p < 0.0001$, K-W, Table 3.4), with flood densities dominant in the comparisons, despite some smaller differences between median densities for night and day samples (Figure 3.30). Night time ebb samples had some particularly high densities, but these were only a few singular events.

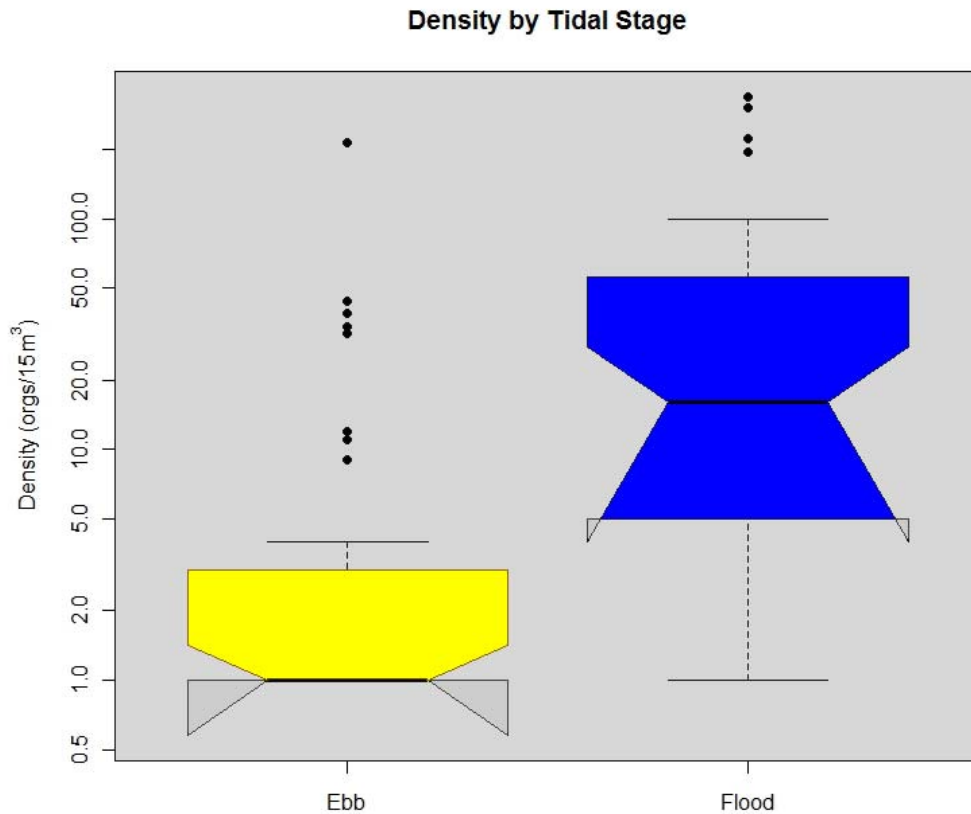


Figure 3.29: Density by tidal stage for *Farfantepenaeus aztecus* postlarvae. Flood tides have significantly higher density values than ebb. Non-overlapping notches between boxplots provide “strong evidence” of difference in median values between the groups (Chambers et. al 1983). Different colors represent statistically different groups (WMW).

Wind direction, wind speed, and barometric pressure all had significant non-linear relationships for *F. aztecus* density estimation (Table 3.5). During ebb tides, density appeared to be most affected by low and high barometric pressures, and by winds from the northern quadrant (Figure 3.31). During flood tides, densities were most affected by low to mid-range atmospheric pressures. Winds from the southerly quadrant possibly associated with coastal setup during the pre-frontal phase showed the greatest effect on increases in density, again however, these fluctuations were small (i.e., $n < 5$). In general, stronger wind speeds ($> 8 \text{ m/s}$) were shown to

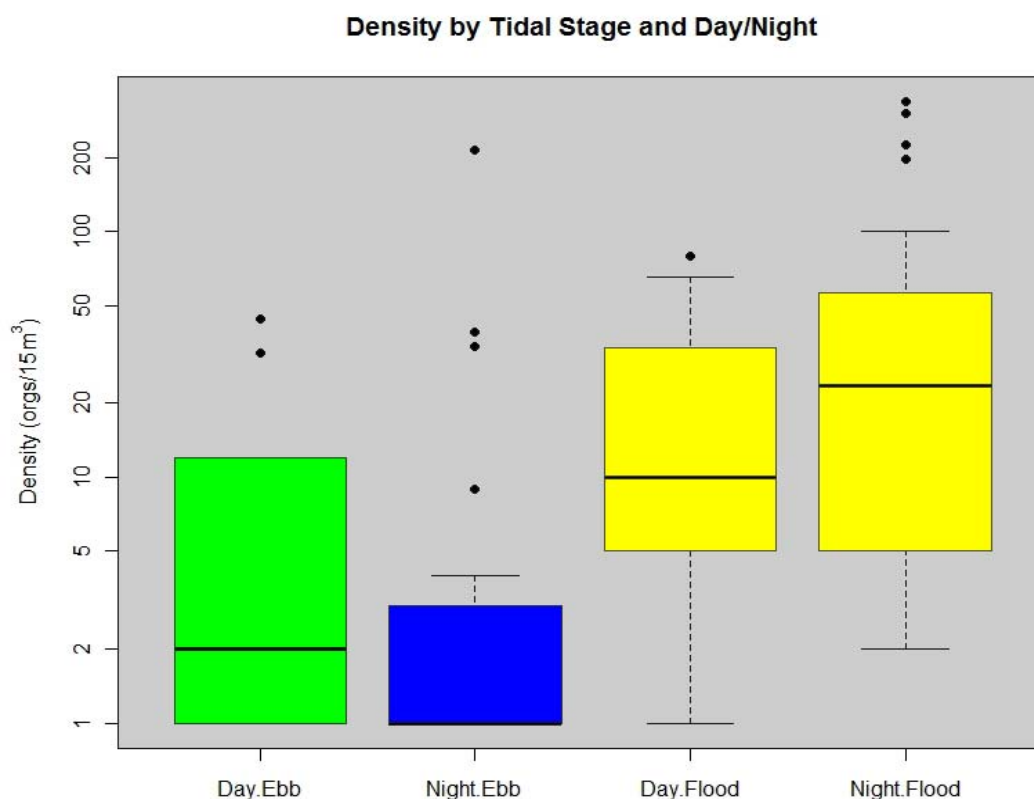


Figure 3.30: Density by tidal stage and day/night for *Farfantepenaeus aztecus* postlarvae. Flood tides, regardless of time of day, were significantly different from nocturnal collections on ebb tides. Different primary colors (yellow and blue) represent statistically different groups, while secondary colors (green) show similarities to both primary groupings under Kruskal-Wallis test.

have the most potential for greater densities ($5 - 10/15\text{m}^3$). Looking at the interaction of wind direction and barometric pressure, there were distinct frontal passage trends evident for both flood and ebb tides (Figure 3.32). During flood tides the greatest positive densities were correlated with northerly winds, and to a lesser extent southerly winds. These effects were more pronounced at lower and mid-range pressures, suggestive of pre-frontal and post-frontal periods. Ebb tide export saw the highest densities associated with northwesterly to northeasterly winds at both high and low pressures. Model fit, however, was generally insufficient to describe a large

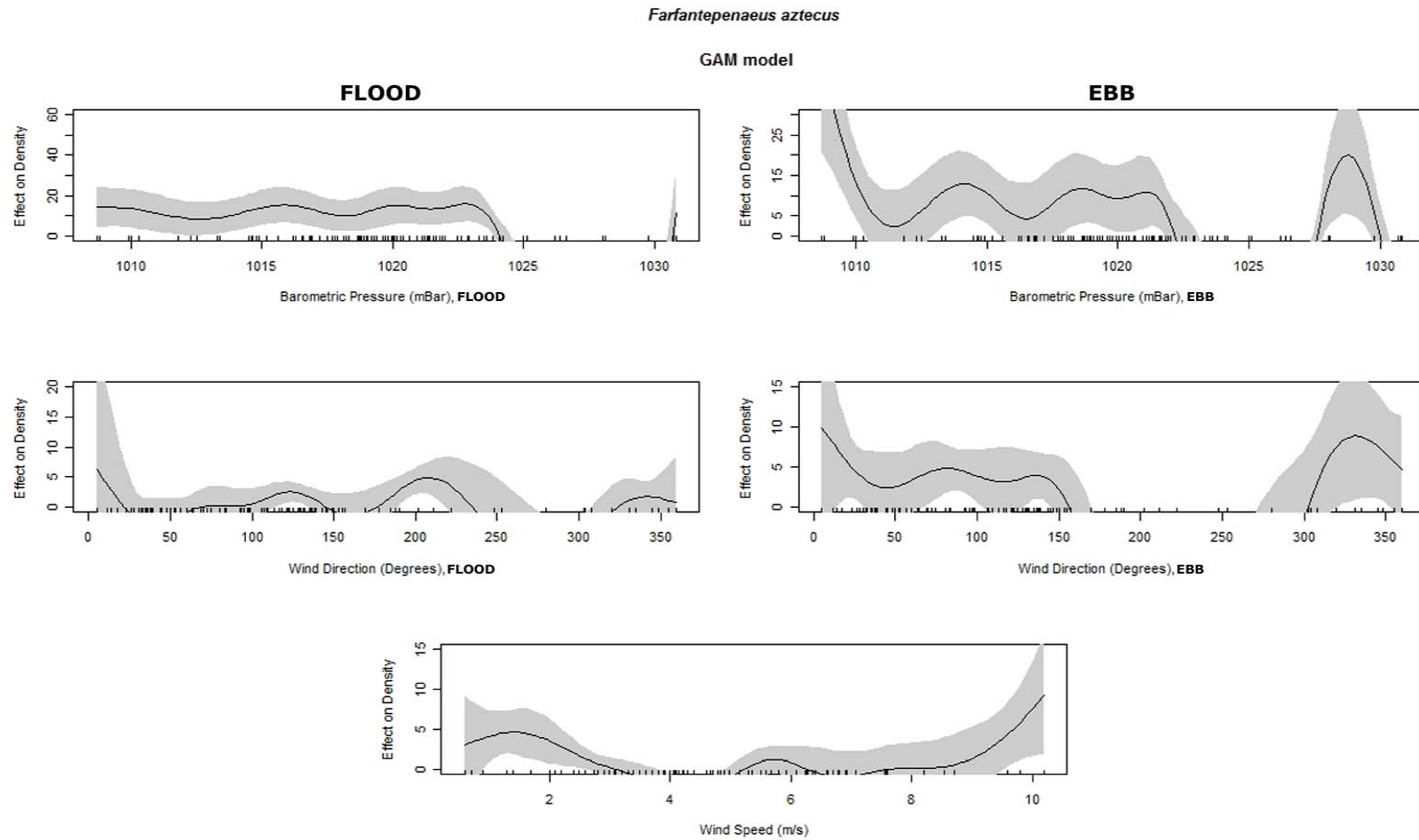


Figure 3.31: Model fit for 1-dimensional terms of the GAM model for postlarval *Farfantepenaeus aztecus*. Shaded areas represent 95% confidence intervals around the model fit represented by the black line. Tick marks on the x-axes represent actual observations. Only positive effects on density are shown to better illustrate the individual effects of model terms.

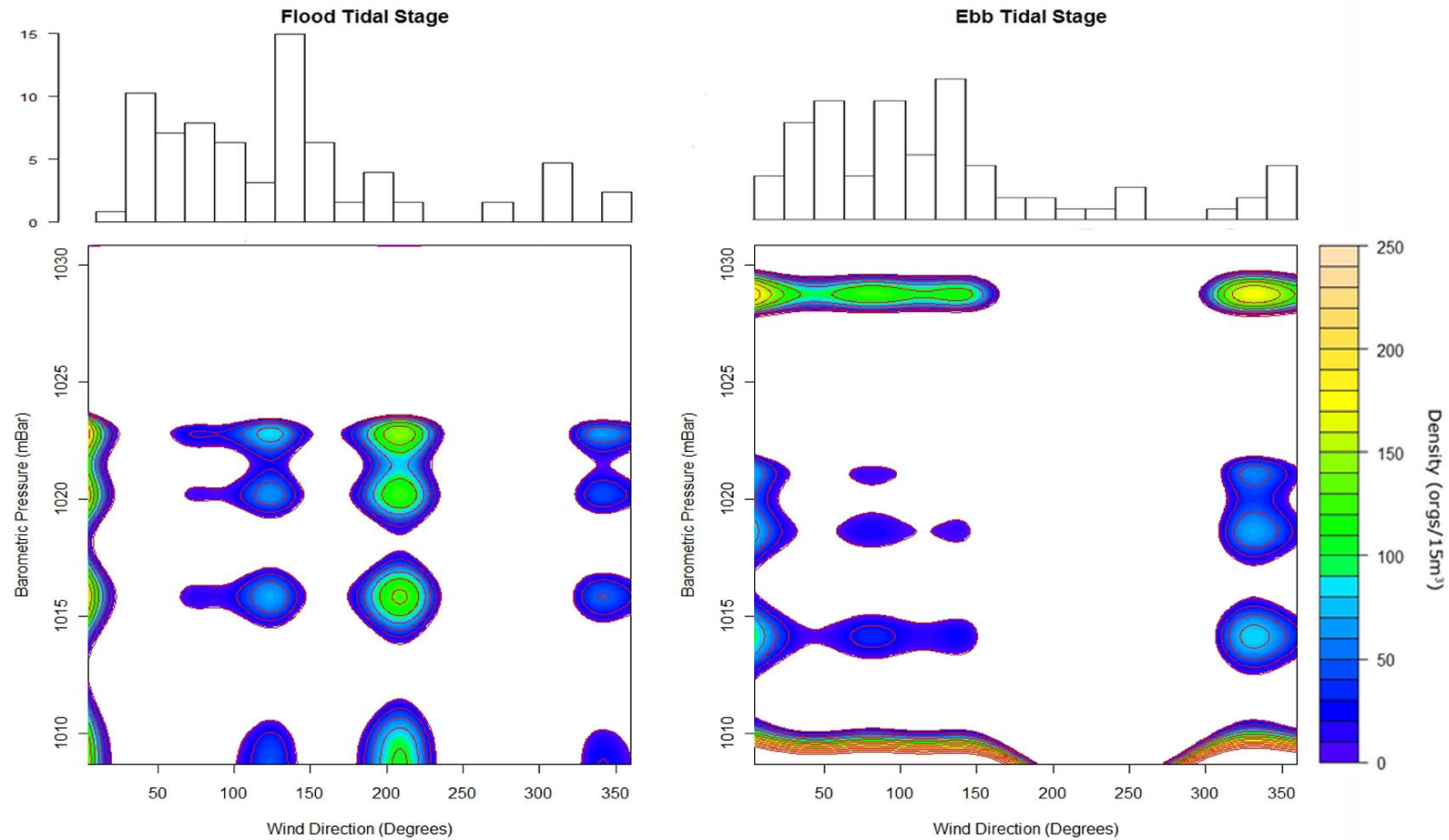


Figure 3.32: Postlarval *Farfantepeanaeus aztecus* completed model and effect on density plotted as a contour map. Expected values are based on the complete model fit. Estimated density isolines as a function of barometric pressure and wind direction are shown in color. Areas where no plot is shown represent expected numbers of larvae within the tidal pass to be zero. The interaction is plotted individually for flood and ebb tidal stages. Histograms above contour plots represent percent frequency of wind directions during sampling.

amount of density differences (Adj. $R^2 = 0.34$, Table 3.5), suggesting that other mechanisms besides winter frontal events may be influencing the recruitment of postlarval brown shrimp.

3.3.8 *Pogonias cromis* (black drum)

Black drum, *Pogonias cromis*, larvae were generally collected from December through March, with the highest densities taken in December ($\bar{x} = 4.4$ indiv./15m³, $sd = 25.0$, Table 3.1) and February ($\bar{x} = 5.0$ indiv./15m³, $sd = 24.8$). Low densities were collected during October ($\bar{x} = 0.02$ indiv./15m³, $sd = 2.3$, Table 3.1) and January ($\bar{x} = 0.6$ indiv./15m³, $sd = 3.3$) which suggests either pulsed recruitment or patchiness issues perhaps confounded by only sampling January once per year. In particular during March, there was one event with a density in excess of 1000 individuals per 15m³ of water. There were no black drum taken during September, November, or April in either year of the study period (Table 3.1; Figure 3.14), and 94% of all samples during the expected recruitment season contained zero larvae.

In general, diurnal or tidal differences including their interactions did not elucidate any particular patterns or structure. Black drum, *Pogonias cromis*, showed no significant differences in density between flood ($\bar{x} = 1.3$ indiv./15m³, $sd = 13.3$, Table 3.1) and ebb tides ($\bar{x} = 2.1$ indiv./15m³, $sd = 16.5$) when accounting for presence/absence in sampled densities (Table 3.2). There was a similar lack of statistical difference between day and night densities (Table 3.2); however, zero inflated nocturnal collections ($\bar{x} = 2.7$ indiv./15m³, $sd = 19.5$, Table 3.1) were almost seven times higher than during day ($\bar{x} = 0.4$ indiv./15m³, $sd = 2.8$; Figure 3.33). The interaction of tidal stage and time of day showed the same trend, albeit non-significant when controlling for a patchy distribution, where larger densities occurred during nocturnal floods ($\bar{x} = 72.0$ indiv./15m³, $sd = 80.8$, Table 3.4) and ebbs ($\bar{x} = 45.2$ indiv./15m³, $sd = 73.2$). However,

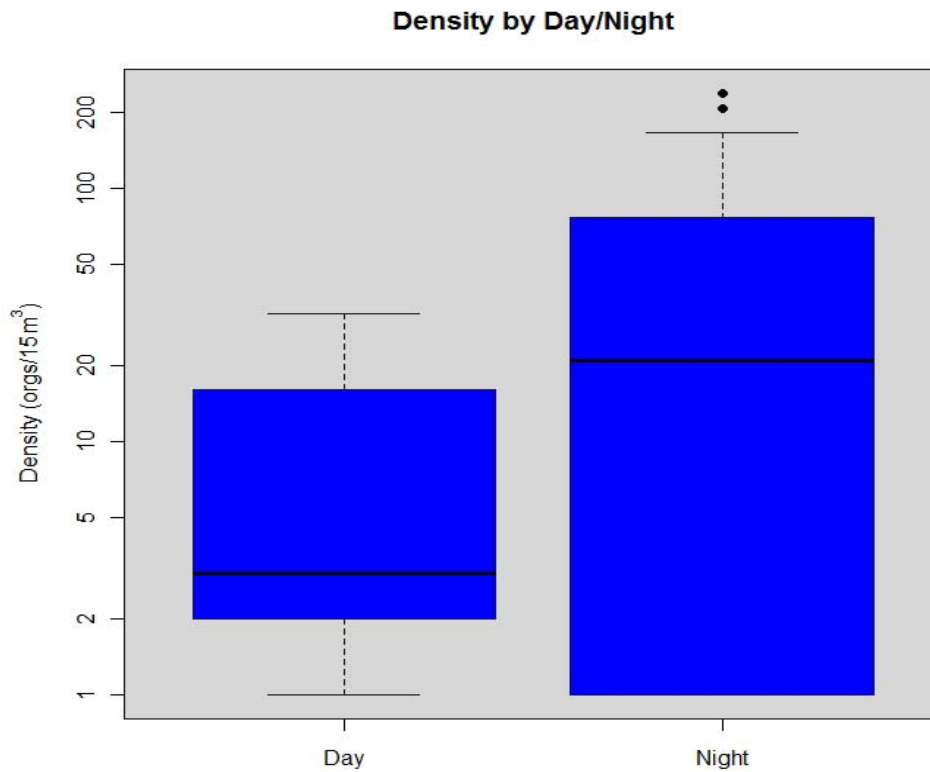


Figure 3.33: Density by time of sample collection for *Pogonias cromis* larvae. Despite higher median densities collected during nocturnal sampling efforts there was no significant differences. Different colors represent differences under WMW test.

visual inspection of the medians suggested that higher probabilities of encountering large densities occurred only during nighttime floods with little differences between the other tidal/day-night stages (Figure 3.34).

Although initial GAM model building determined net water transport to be significant, inclusion of wind direction and barometric pressure, both terms constrained by tidal stage, suggested the removal of net water transport from the model (Adj. $R^2 = 0.49$, Table 3.5). Winter storm fronts are a likely force controlling estuarine recruitment of black drum, since density peaked during the middle of winter and meteorological terms (i.e., wind direction and barometric

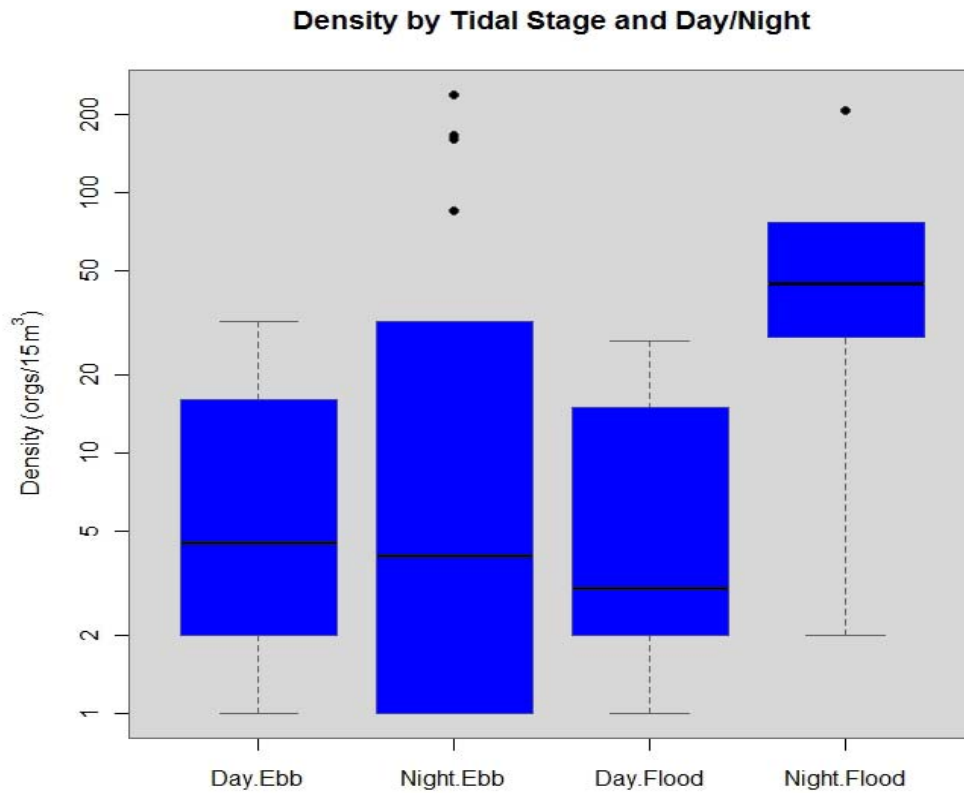


Figure 3.34: Density by tidal stage and time of day for *Pogonias cromis* larvae. Samples collected during nocturnal flood tides were not significantly different from all other groups despite a much larger median value. Different colors represent differences between groups under Kruskal-Wallis test.

pressure) were significant in the final model. Low to mid-level atmospheric pressures, regardless of tidal stage, showed the highest increases in black drum density (Figure 3.35). For ebb tides, modest densities appeared to only be associated with winds from the southern and northern quadrants, whereas for flood tides and almost all wind directions showed strong density increases of approximately 25 - 30 larvae per 15m³ of water. Interaction of barometric pressure and wind direction (Figure 3.36) during flood tides showed a relatively strong linear prediction with lower atmospheric pressures across almost all wind directions. The increase in flood density is

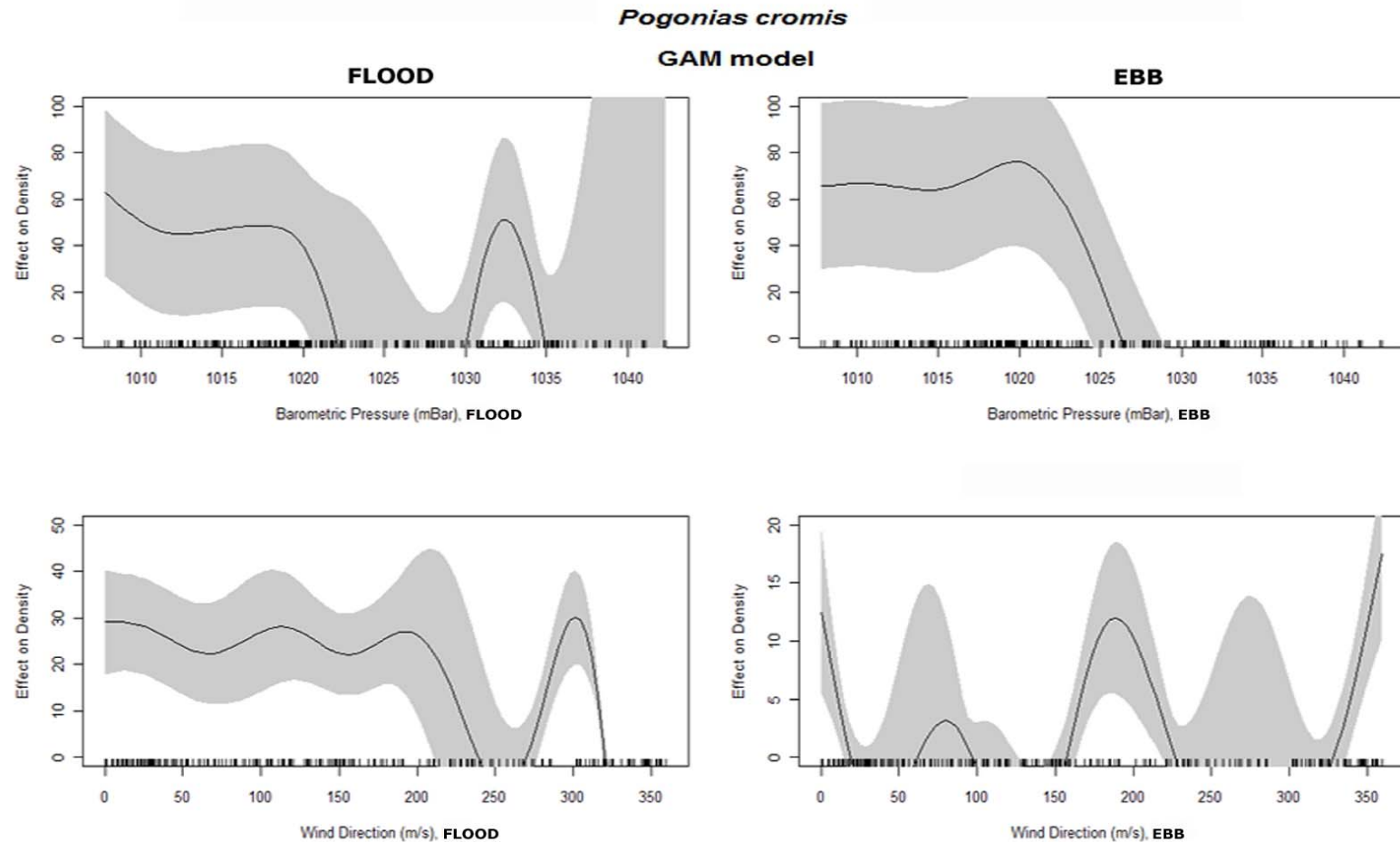


Figure 3.35: Model fit for 1-dimensional terms of the GAM model for larval *Pogonias cromis*. Shaded areas represent 95% confidence intervals around the model fit represented by the black line. Tick marks on the x-axes represent actual observations. Only positive effects on density are shown to better illustrate the individual effects of model terms.

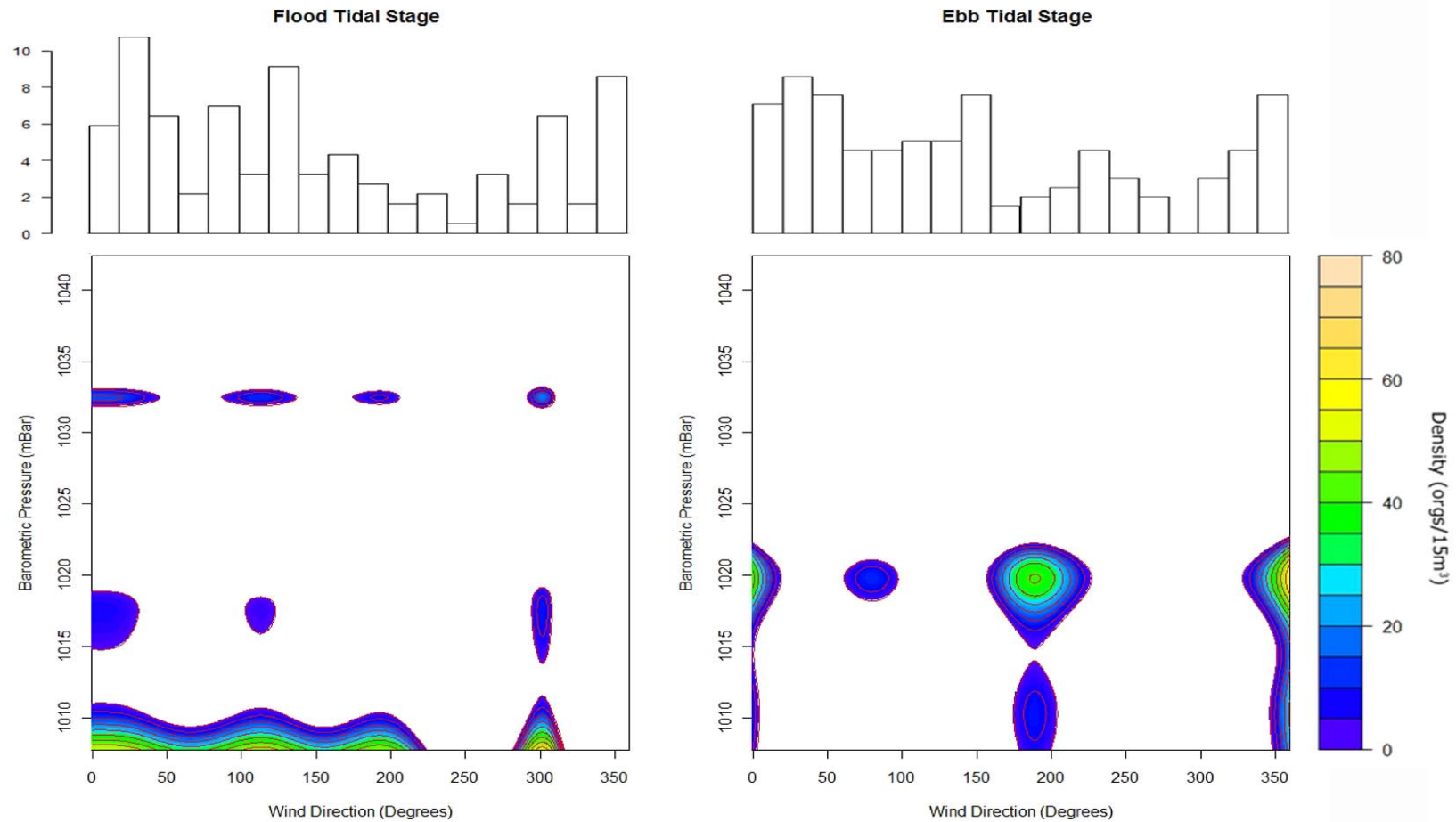


Figure 3.36: Larval *Pogonias cromis* completed model and effect on density plotted as a contour map. Expected values are based on the complete model fit. Estimated density isolines as a function of barometric pressure and wind direction are shown in color. Areas where no plot is shown represent expected numbers of larvae within the tidal pass to be zero. The interaction is plotted individually for flood and ebb tidal stages. Histograms above contour maps represent percent frequency of wind directions during sampling.

most pronounced during low pressures and winds out of the eastern and southern quadrants associated with coastal setup during the pre-frontal phase of winter frontal passage, and also during passage of the actual front with the associated westerly and northerly winds. During ebb tides, the structure of the interaction between barometric pressure and wind direction supported higher densities associated with post-frontal northerly winds, and to a lesser extent the coastal setup caused by southerly winds.

3.3.9 *Sciaenops ocellatus* (red drum)

Red drum larvae were only sampled during the early fall months, September and October (Table 3.1; Figure 3.14). The reduction in average density from September ($\bar{x} = 50.0$ indiv./15m³, $sd = 280.4$, Table 3.1) to October ($\bar{x} = 0.8$ indiv./15m³, $sd = 4.2$) was exceptionally large, indicative of their truncated spawning season (i.e., Aug. – Sept.). September also had a much higher range of densities, and very few non-zero collections. The bulk of the empty collections (84%) occurred during October, particularly during the second sampling trip.

For *S. ocellatus*, effective estuarine recruitment was seen with the highly significant greater differences ($p < 0.003$, WMW, Table 3.2) in flood densities ($\bar{x} = 38.9$ indiv./15m³, $sd = 245.8$, Table 3.1) versus ebb ($\bar{x} = 0.4$ indiv./15m³, $sd = 2.8$). In addition, nocturnal red drum densities ($\bar{x} = 27.6$ indiv./15m³, $sd = 207.1$, Table 3.1) were greater, and had a higher degree of dispersion than day ($\bar{x} = 0.5$ indiv./15m³, $sd = 2.9$, Table 3.1; $p = 0.087$, WMW, Table 3.2). There was also a near-significant interaction of tidal stage and day/night, where nocturnal, flood densities were far greater (i.e., two orders of magnitude) than any other diurnal-tidal category ($\bar{x} = 242.0$ indiv./15m³, $sd = 614.1$, $p = 0.0832$, K-W, Table 3.4; Figure 3.37). There was no significant difference between surface and near-bottom collections.

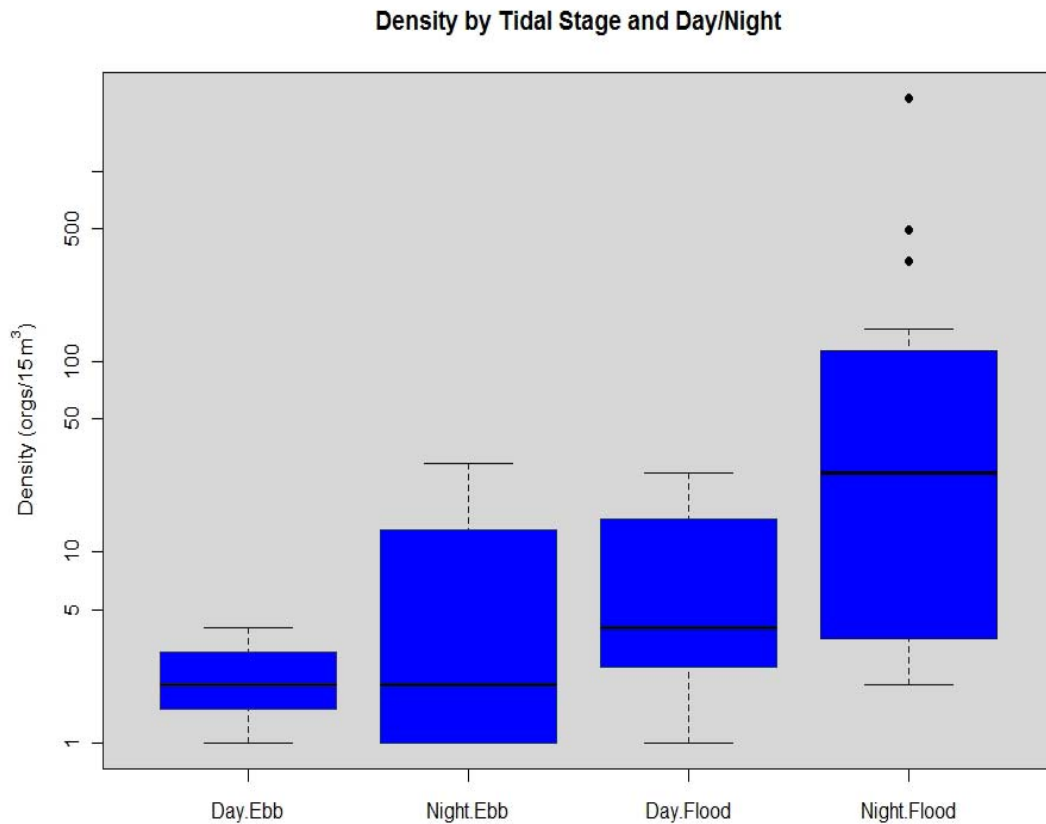


Figure 3.37: Density by tidal stage and time of day for *Sciaenops ocellatus* larvae. Nocturnal densities on flood tides had the largest median value, and were significantly different from samples collected during daytime ebb tides. Different colors represent differences between groups under Kruskal-Wallis test.

Both wind direction and barometric pressure were significant non-linear parameters in density estimation for red drum (Table 3.5). Red drum densities, however, were not wholly driven by meteorological forces, as the model only explained a moderate to low amount of the variation ($\text{Adj. } R^2 = 0.39$). A wide range of low-mid barometric pressures, 1011 through 1024 mBar, showed expected increases in density of approximately 50 larvae per 15m³ of water filtered (Figure 3.38). Further, wind directions associated with the western quadrant, and to a

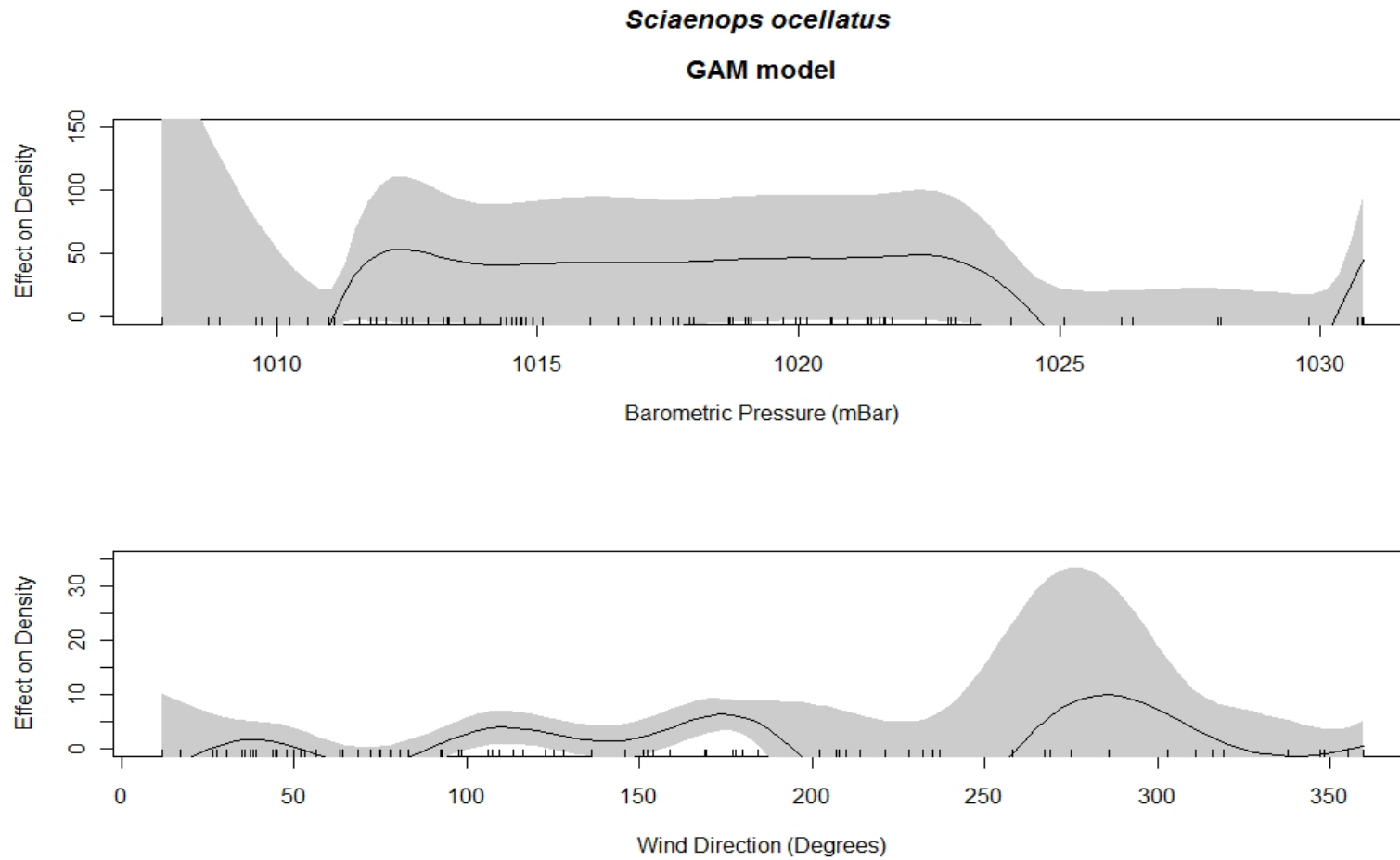


Figure 3.38: Model fit for 1-dimensional terms of the GAM model for larval *Sciaenops ocellatus*. Shaded areas represent 95% confidence intervals around the model fit represented by the black line. Tick marks on the x-axes represent actual observations. Only positive effects on density are shown to better illustrate the individual effects of model terms.

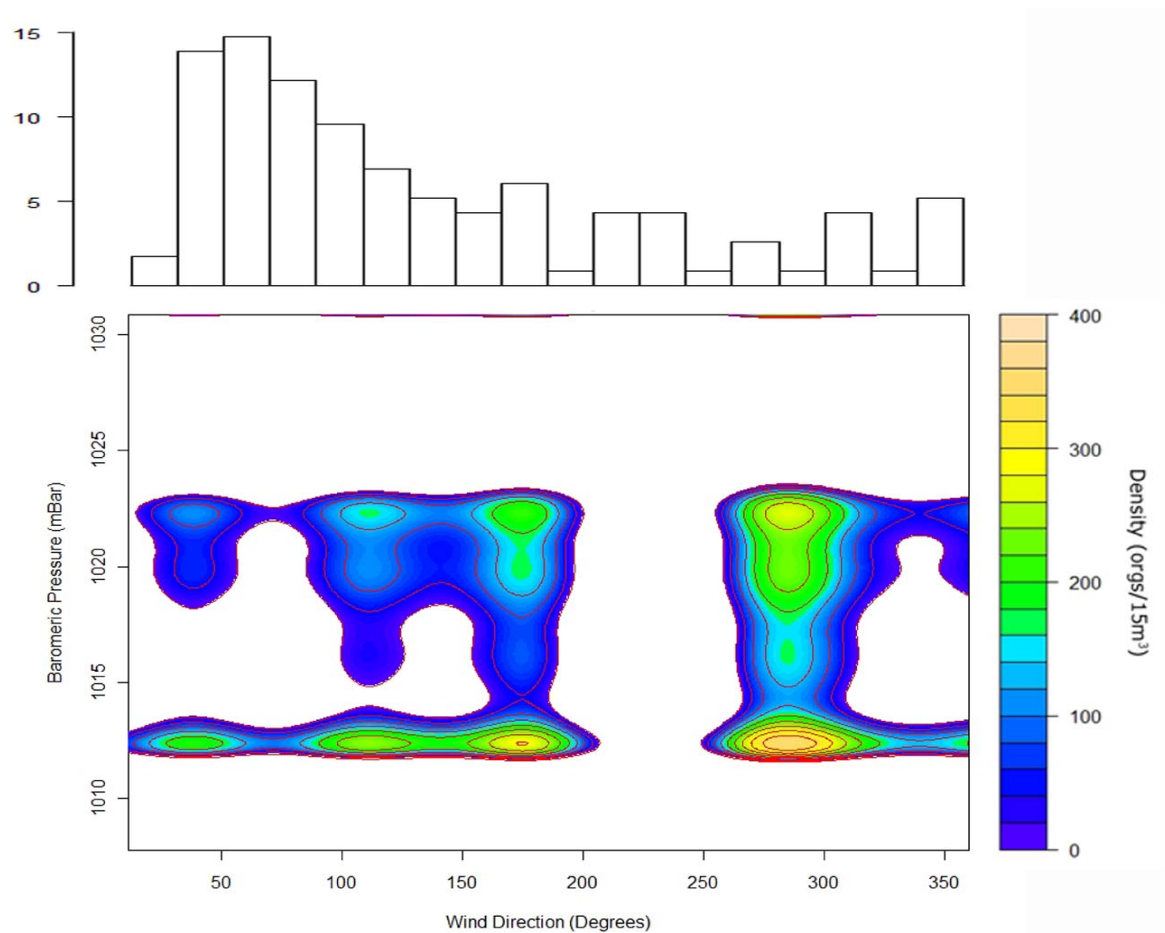


Figure 3.39: Larval *Sciaenops ocellatus* completed model and effect on density plotted as a contour map. Expected values are based on the complete model fit. Estimated density isolines as a function of barometric pressure and wind direction are shown in color. Areas where no plot is shown represent expected numbers of larvae within the tidal pass to be zero. Histogram above the contour map represents percent frequency of wind direction during sampling.

lesser extent the southern quadrant modestly affected expected densities. The interplay between atmospheric pressure and wind direction predicted increased density along similar trends (Figure 3.39). During both low and mid-range atmospheric pressures, increases in expected density were primarily associated with westerly winds as well as winds out of the southeast to southern quadrants. When taking into account the large disparity in flood versus ebb densities, it appears that peak densities of larvae entering the estuary associated with westerly winds across a range of pressures suggests that early passage of fronts and southeasterly and southerly winds associated with coastal setup during the normal (interim) or prefrontal phases appear to represent the best opportunity for estuarine recruitment of red drum.

3.3.10 *Cynoscion arenarius* (sand seatrout)

Sand seatrout, *Cynoscion arenarius*, larvae were collected during all months except for January (Table 3.1; Figure 3.14). Densities in September were the largest ($\bar{x} = 18.3$ indiv./15m³, $sd = 42.4$, Table 3.1) and sharply dropped off in October ($\bar{x} = 1.5$ indiv./15m³, $sd = 7.1$), but there was an indication of spawning onset in the spring starting in March ($\bar{x} = 3.1$ indiv./15m³, $sd = 9.6$) and April ($\bar{x} = 7.1$ indiv./15m³, $sd = 17.2$). All other months had very low densities in comparison, and overall, 84% of the samples contained zero sand seatrout larvae.

There were significant differences between flood ($\bar{x} = 5.4$ indiv./15m³, $sd = 23.1$) and ebb densities ($\bar{x} = 1.2$ indiv./15m³, $sd = 4.5$, Table 3.1; $p < 0.001$, WMW, Table 3.2).

Although there were apparent differences between nocturnal densities ($\bar{x} = 3.7$ indiv./15m³, $sd = 19.1$, Table 3.1) and those collected during the day ($\bar{x} = 1.8$ indiv./15m³, $sd = 7.2$), the differences were not significant when controlling for the patchy distribution (Table 3.2). The interaction of the diurnal-tidal factors showed a similar trend, where flood tides were more likely

to encounter extremely high densities, regardless of time of day (Tables 3.3 and 3.4; Figure 3.40).

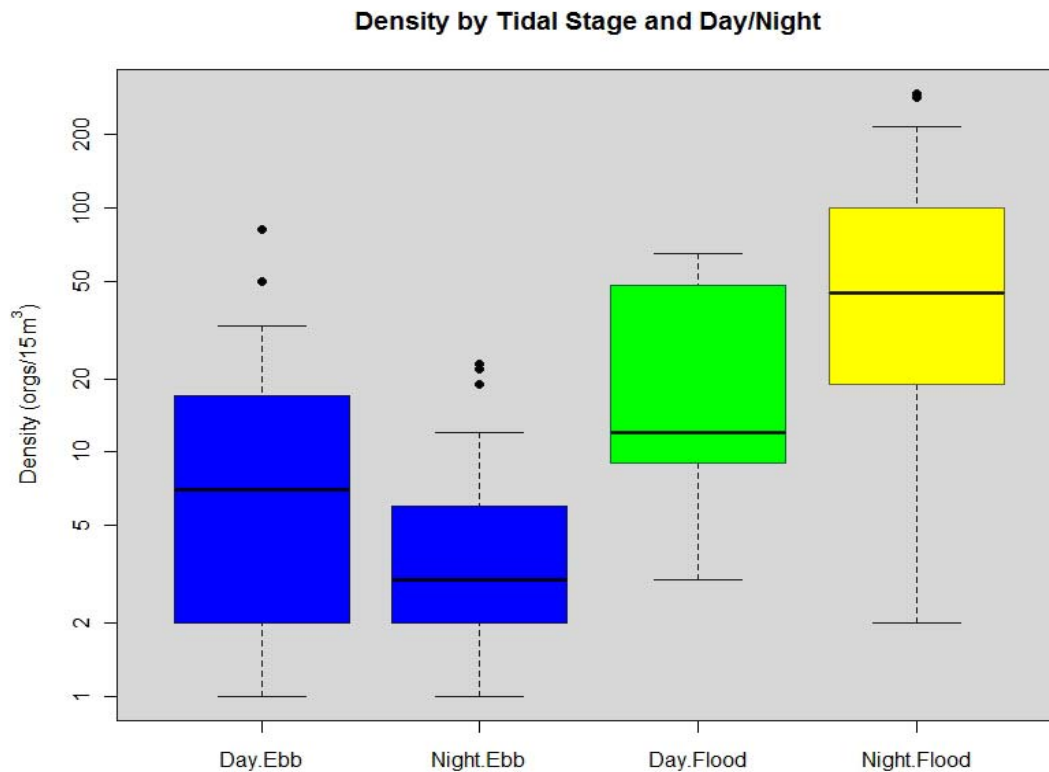


Figure 3.40: Larval *Cynoscion arenarius* density by tidal stage and time of day. There is a lack of statistical difference between the groups. Samples collected on flood tides did, however, have higher median densities than those on ebb tides. Different primary colors (yellow and blue) represent statistically different groups, while secondary colors (green) show similarities to both primary groups under Kruskal-Wallis test.

Net water transport, wind direction, wind speed and barometric pressure were highly significant ($p < 0.008$, Chisq) in the GAM model describing sand seatrout densities (Table 3.5). Controlling for tidal stage was significant in explaining the effects wind direction and barometric pressure had on density, however, the model accounted for little variability based on meteorological terms (Adj. $R^2 = 0.37$). Higher net water transport and winds exerted minor

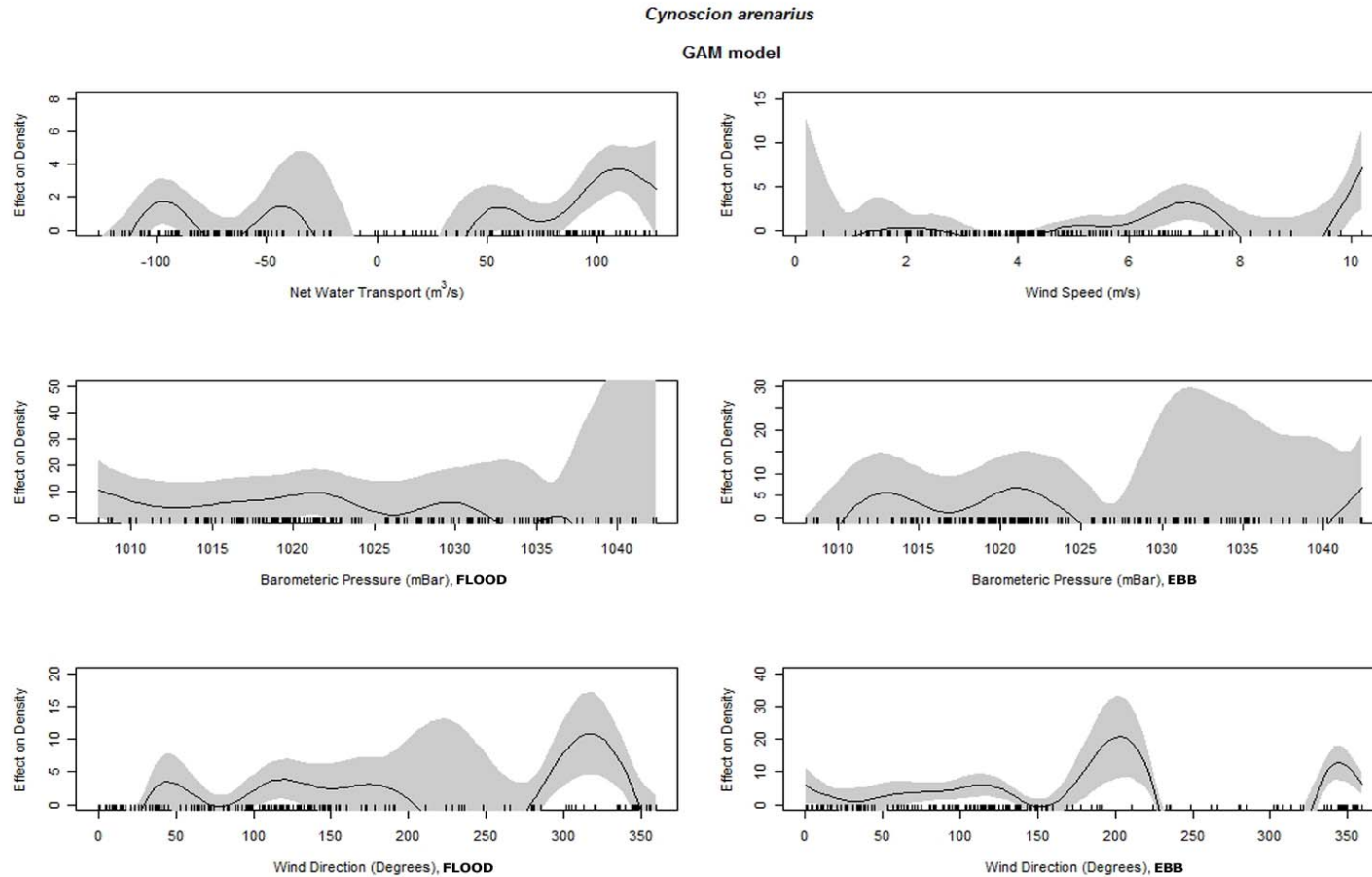


Figure 3.41: Model fit for 1-dimensional terms of the GAM model for larval *Cynoscion arenarius*. Shaded areas represent 95% confidence intervals around the model fit represented by the black line. Tick marks on the x-axes represent actual observations. Only positive effects on density are shown to better illustrate the individual effects of model terms.

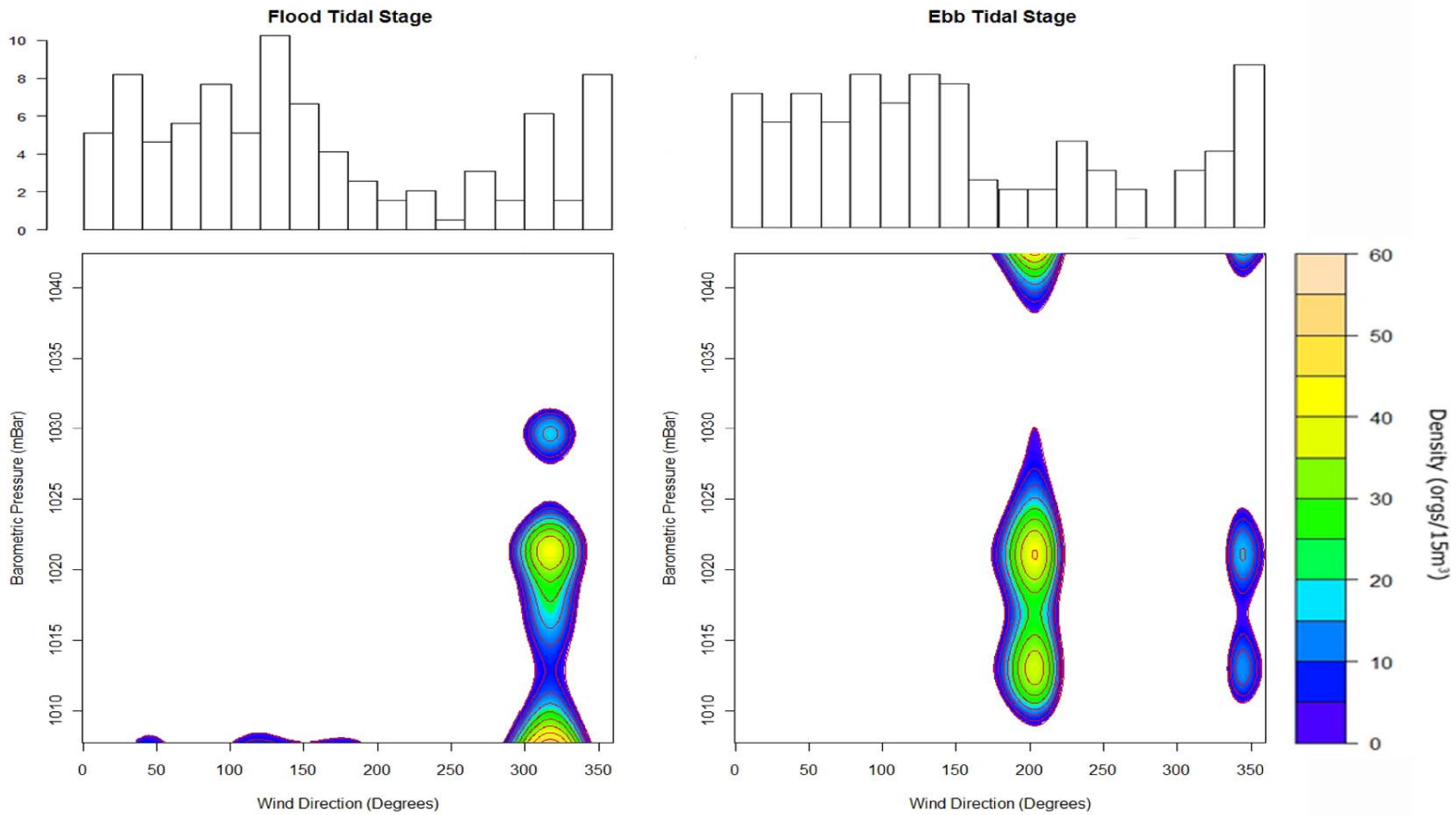


Figure 3.42: Larval *Cynoscion arenarius* completed model and effect on density plotted as a contour map. Expected values are based on the complete model fit. Estimated density isolines as a function of barometric pressure and wind direction are shown in color. Areas where no plot is shown represent expected numbers of larvae within the tidal pass to be zero. The interaction is plotted individually for flood and ebb tidal stages. Histograms above contour maps represent percent frequency of wind directions during sampling.

influences on sand seatrout densities (Figure 3.41). Wind direction showed the greatest effect on density, in particular during ebb tides when southerly winds associated with coastal setup showed high densities (20 indiv./15m³) with generally low variability around the estimates. During flood tides, densities increased when winds were in the western quadrant. Low to mid-level barometric pressures supported slight increases in density as well. Looking at the interaction of barometric pressure and wind direction (Figure 3.42), southerly winds during ebb tides with low and high barometric pressures appear to have the greatest effect on density. Flood tides had slightly smaller increases in density, associated with northwesterly winds, with low (and to a lesser degree medium) atmospheric pressures, which correlate to periods immediately after passages of fronts.

3.3.11 *Cynoscion nebulosus* (spotted seatrout)

Cynoscion nebulosus, spotted seatrout, have a traditional spawning season during the summer with a recruitment peak in late summer and early fall (Table 3.1; Figure 3.14). As a result, spotted seatrout were collected only during September ($\bar{x} = 1.4$ indiv./15m³, $sd = 6.1$, Table 3.1) and October ($\bar{x} = 0.1$ indiv./15m³, $sd = 1.0$). Overall, 91% of the samples during the expected recruitment season contained zero larvae. In contrast to *C. arenarius*, the lack of *C. nebulosus* larvae during spring sampling indicated onset of spawning season occurring after mid to late April.

Spotted seatrout densities for flood tides ($\bar{x} = 0.9$ indiv./15m³, $sd = 5.3$, Table 3.1) were significantly greater ($p < 0.009$, WMW, Table 3.2), than those for ebb ($\bar{x} = 0.3$ indiv./15m³, $sd = 1.3$). Day mean densities ($\bar{x} = 0.7$ indiv./15m³, $sd = 2.4$, Table 3.1) were slightly higher than nocturnal densities ($\bar{x} = 0.4$ indiv./15m³, $sd = 4.3$), which displayed high variances and

more zero collections. The interaction of tidal stage and day/night was significant ($p < 0.032$, Table 3.4), and lent support to the importance of tidal stage, regardless of time of collection (Table 3.3). In particular, night flood densities had the highest median value, and were significantly different from all other groups (Figure 3.43).

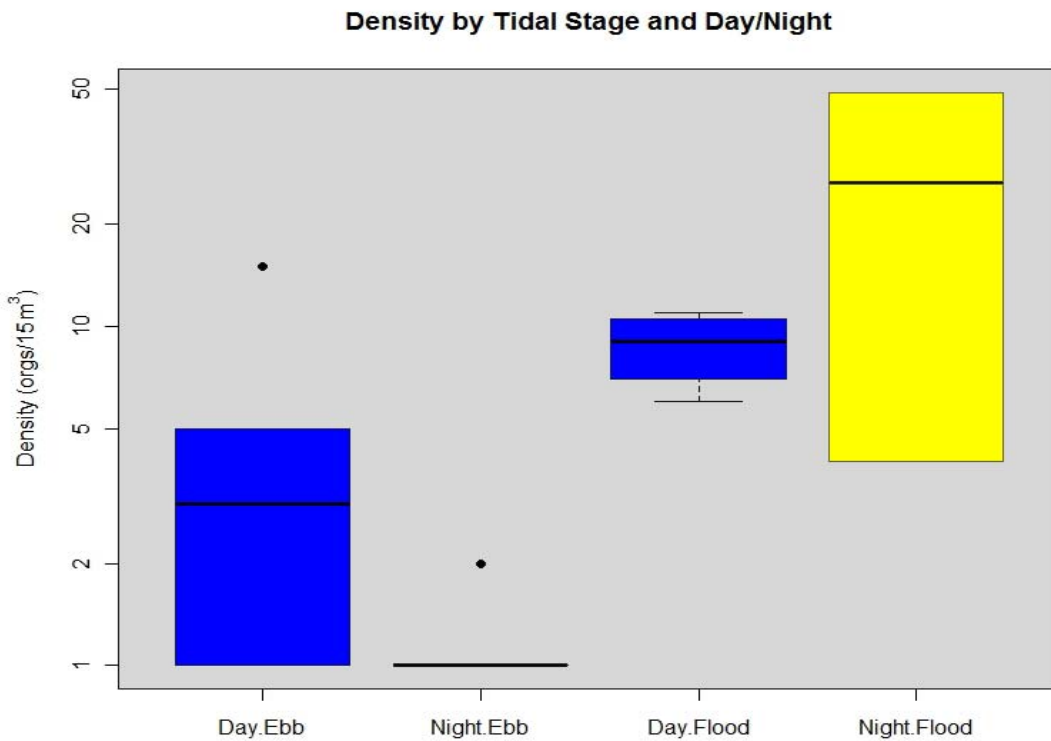


Figure 3.43: Density by tidal stage and time of sample collection for *Cynoscion nebulosus* larvae. Median densities for flood tides were greater than those during ebb tides. Night flood densities were statistically greater than all other groups, despite second quartile overlap with daytime flood densities. Different colors represent differences between the groups under Kruskal-Wallis test.

Spotted seatrout did not have a significant model that included much evidence of the influence of winter frontal passages, since the significant terms did not include barometric pressure. The simplest model, which explained the low density variation, however, did include

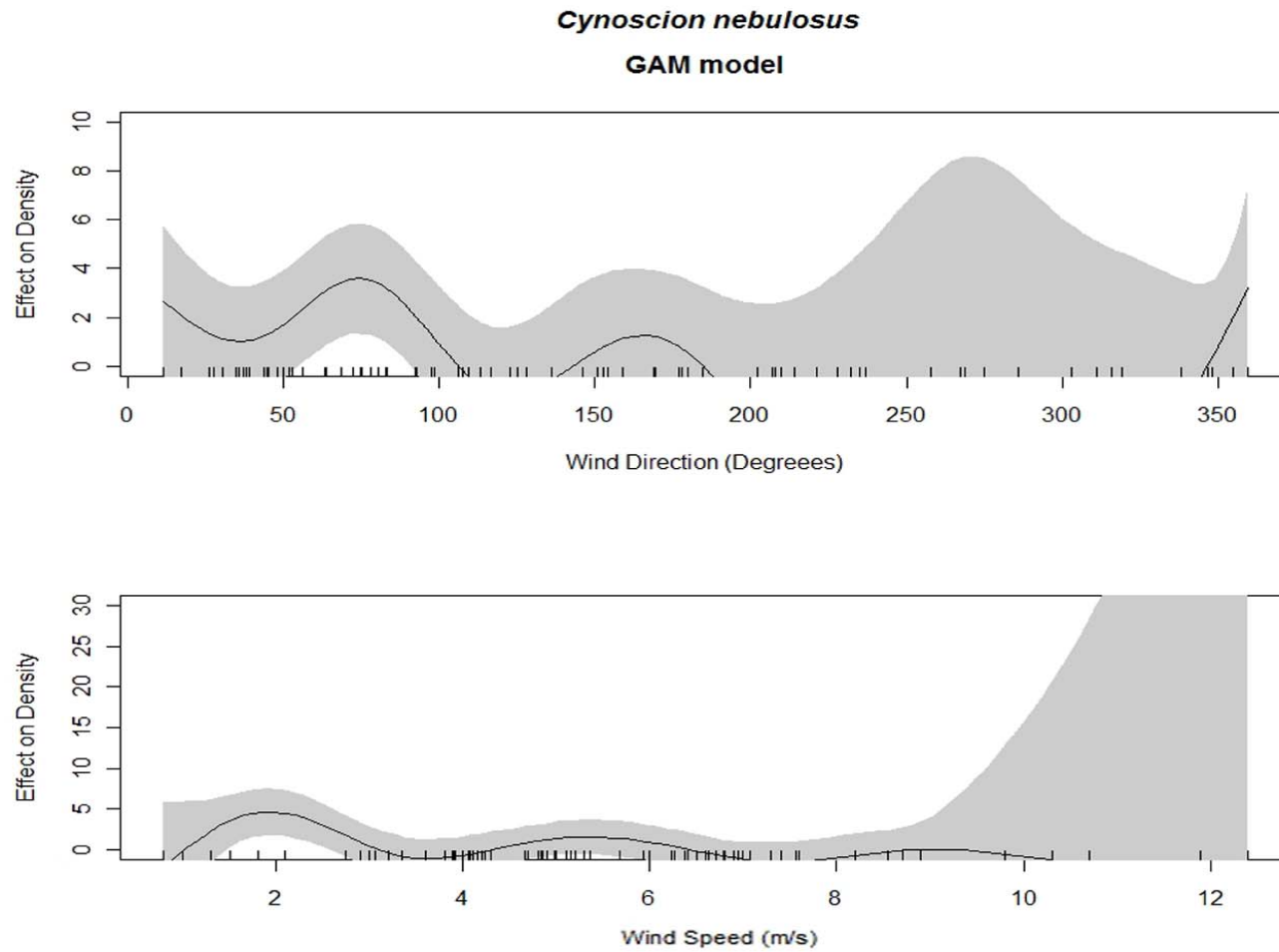


Figure 3.44: Model fit for the 1-dimensional terms of the GAM model for larval *Cynoscion nebulosus*. Shaded areas represent 95% confidence intervals around the model fit represented by the black line. Tick marks on the x-axes represent actual observations. Only positive effects on density are shown to better illustrate the individual effects of model terms.

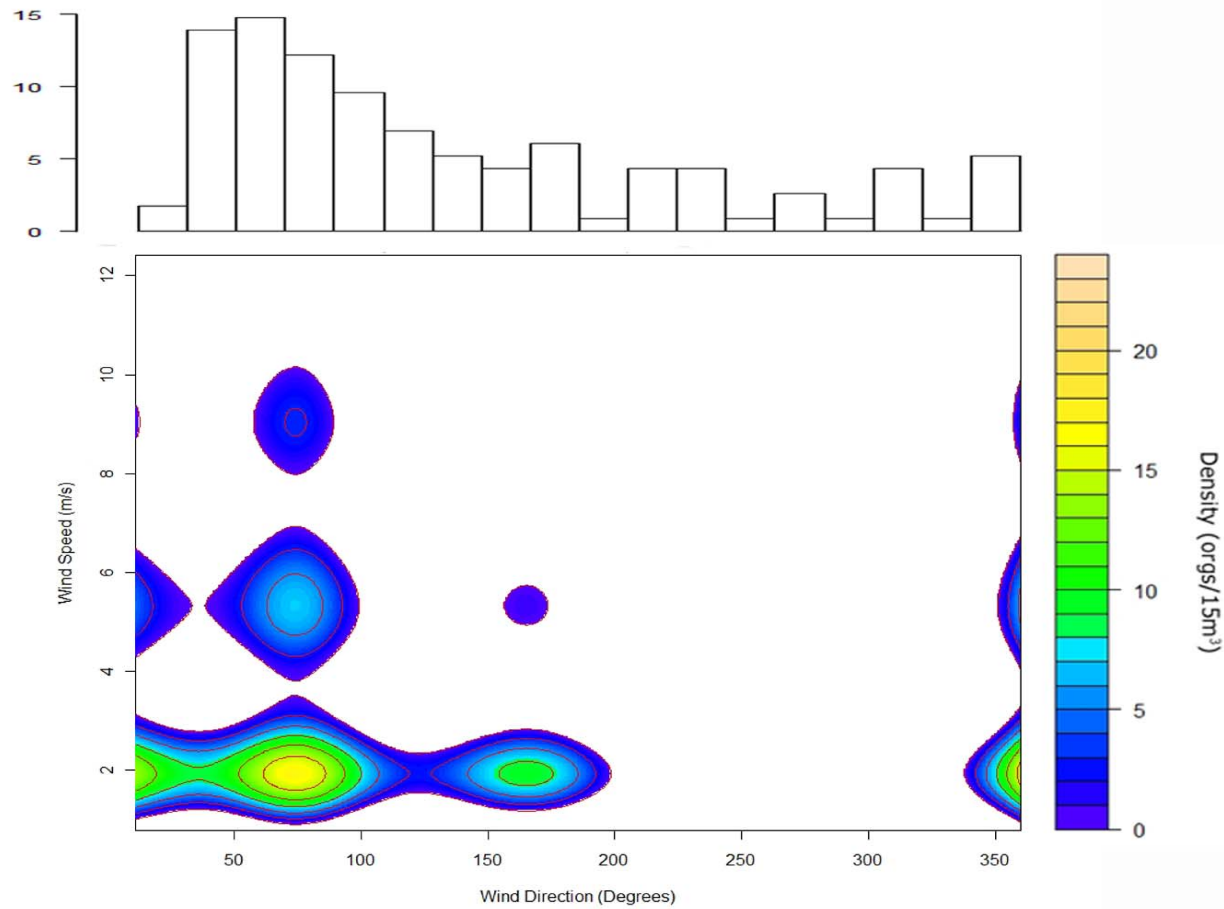


Figure 3.45: Larval *Cynoscion nebulosus* completed model and effect on density plotted as a contour map. Expected values are based on the complete model fit. Estimated density isolines as a function of wind speed and wind direction is shown in color. Areas where no plot is shown represent expected numbers of larvae within the tidal pass to be zero. The histogram above the contour map represents the percent frequency of wind directions during sampling.

wind direction ($p < 0.052$, Chisq) and wind speed ($p < 0.003$, Chisq; Adj. $R^2 = 0.38$, Table 3.5). Very small sand seatrout density increases (< 5), occurred with low winds from the north and northeasterly quadrants, and to even a lesser extent from the south (Figure 3.44). Looking at wind speed and wind direction interactions (Figure 3.45), the same weak trend appeared, where low density affects occurred during postfrontal and interim periods with very low wind speeds and a shifting wind field from the northerly to easterly, and ultimately to southerly winds early in the cold front season.

3.3.12 *Paralichthys lethostigma* (southern flounder)

Southern flounder were only encountered once in September and January (Figure 3.14). The one January collection contained only one fish ($\bar{x} < 1$ indiv./15m³). The September collection was composed of a single sample having a density of 587 individuals per 15m³ ($N = 80$) and taken during a nocturnal flood tide. The January individual was also collected on a flood tide, but during daylight. No attempt was made to model this species.

3.4 Discussion

3.4.1 Hydrography

Bayou Tartellan tidal pass was well-mixed having no statistical difference between surface and near-bottom measured water temperature or salinity; however, there were significantly lower dissolved oxygen concentrations near-bottom. Water temperature and salinity variation depended on the tidal cycle, suggesting a horizontally stratified system similar to other estuaries along the northern Gulf coast (Turner et al., 1987; Li et al., 2009). Frontal events occurring during our four-day sampling period produced more variability in water temperature. This suggests atmospheric events may have a considerable small-scale temporal effect, which

supports results from previous studies, i.e., although the passage of winter cold fronts can rapidly increase vertical mixing, their cold air temperatures can also rapidly decrease water temperatures in these shallow estuaries (Walker and Hammack, 2000; Kineke et al., 2006). Low daytime, near-bottom dissolved oxygen measurements have been also reported for estuaries from Florida to Texas along the northern GOM (Engle et al., 1999).

Generally throughout most of the year, the northern GOM is dominated by winds out of the SE-S-SW quadrant, which leads to coastal setup and higher seasonal estuarine water levels especially during the late spring and summer. During our study, increases in measured tidal height compared to the expected diurnal tidal cycle were generally associated with the interim or pre-frontal phase of winter cold fronts and predominant southerly winds, mirroring results from previous studies (Moeller et al., 1993; Li et al., 2011). Longer time periods between fronts resulted in more coastal setup during the interim or pre-frontal phase, and subsequent larger positive differences between measured and expected tidal heights. For example, during the 25th - 29th October 2006 sampling effort, tidal height increased nearly 35 cm, water temperature increased from 18.9 °C to 23.9 °C, and salinity increased from 29.7 ppt to 30.9 ppt (Figure 3.15). Moreover, the pre-frontal phase of winter cold fronts had warmer air temperatures, warmer water temperatures, increased water levels in the estuary, and higher salinities more indicative of GOM coastal shelf waters (Pitts, 1989; Moeller et al., 1993; Li et al., 2011). With the exception of April 2008, salinities at our sampling station remained relatively high due to the proximity of the sampling location to the GOM and the normal lack of freshwater head in the estuarine system above Bayou Tartellan.

The decreasing water temperature, air temperature, and salinity during the post-frontal phase correlate to atmospheric cooling and flushing of the rain-engorged shallow, north/south oriented estuarine waters above Bayou Tartellan. During cold front passage, differences between measured and expected tidal height were negative 67% of the time, indicating that the expected mass balance of normal astronomical tides was temporarily overrode by the NW-N-NE wind field disproportionately driving water out of the estuary. During the post-frontal phase encountered during 25th- 29th October 2006, tidal height decreased nearly 40 cm, water temperature decreased almost 3 °C, and salinities decreased to less than 28 ppt (Figure 3.15). Although temperature and salinity continued to rise during the initial passage of the front due to continued transport momentum from the previous coastal setup, it decreased after the rotation in wind direction had enough time to reverse the system. Previous studies have also shown northerly winds during the post-frontal phase having similar effects of increased flushing on estuarine tidal prisms (Moeller et al., 1993; Li et al., 2009).

3.4.2 General Zoo-/Ichthyoplankton

The lack of difference between surface and near-bottom zoo-/ichthyoplankton densities is supported by the lack of difference in vertical hydrographic structure within this well-mixed tidal pass. Observed total densities were dependent on tidal stage and source waters, with little difference in total density resulting from depth or time of day (or depth). The effect of tidal stage, and associated directional flows, controlling the accumulation of larvae within the estuary has been previously reported (Lyczkowski-Shultz et al., 1990; Joyeux, 1999; Stunz and Reese, 2008; Flores-Coto et al., 2010). Recruitment was pulsed, and although a large majority of the samples contained zoo-/ichthyoplankton, individual species experienced much lower positive

encounter rates (i.e., *range* = 53% – 7%, excluding southern flounder). Recruitment pulsing being a function of individual species spawning preference, differing recruitment corridor lengths, coastal current variability, density fronts, connectivity between environments, climate forcing, tidal mixing, and multiple other factors (Shaw et al., 1988; Parker et al., 1995; Quinlan et al., 1999; Able, 2005).

Coastal setup driven by southerly winds during the interim or pre-frontal phase, conditions expected to be favorable for recruitment (Shaw et al., 1988; Joyeux, 1999; Brown et al., 2004; Comyns and Lyczkowski-Shultz, 2004), were irregular, periodic, and less numerous than unfavorable conditions (i.e., extended ebb tides or flushing during the post-frontal phase). For example, southeasterly and southerly winds during the interim or pre-frontal phases showed favorable recruitment conditions for *B. patronus* and *M. undulatus* larvae spawned offshore, but accounted for approximately only 18% of all wind directions measured during sampling within this study. The net recruitment of larvae exhibited by significantly larger densities collected on flood tides, particularly associated with southerly winds, may indicate the significance of these irregularly periodic (i.e., pulsed) events positively effecting overall recruitment potential. Previous studies have also shown that recruitment is strongly influenced by winds and environmental conditions, which drive circulation of water masses along the coast and within tidal passes (Checkley et al., 1988; Hare et al., 1999).

3.4.3 Species with High Atmospheric Forcing

B. patronus and *M. undulatus* spawn further offshore than most other species analyzed, which creates a longer larval recruitment corridor, and perhaps increasing their reliance on atmospheric forcing to transport their larvae from spawning grounds to tidal passes (Shaw et al.,

1988; Comyns and Lyczkowski-Shultz, 2004). In this study, *B. patronus* and *M. undulatus* showed the highest transport model fit of all species analyzed (0.92 and 0.91 Adjust R^2 , respectively), with mostly pulsed recruitment being indicated by the relatively low number of zero catches (47% and 74%, respectively). Spawning depth for *B. patronus* is reported to be 90 meters and shallower (Whitehead, 1985), and that depth may become deeper (i.e, spawning location moving further offshore) the longer the season progresses (Vaughan et al., 2007). *M. undulatus* typically has a spawning depth of 54 meters or shallower, with some portion of the population moving inshore towards the estuaries to complete spawning at the end of the season (Barbieri et al., 1994). The longer recruitment corridor for these two species may lead to some homogenization of their spawning/recruitment pulses by averaging out some of the variable and cumulative effects of hydrographic flows across temporal and spatial patchiness (Sclafani et al., 1993), therefore, leading to the higher encounter rates within the tidal pass.

Transport model results indicated passage of winter cold fronts to be highly important for successful estuarine recruitment of *B. patronus* and *M. undulatus*. The late October/November peak densities for both species had a minimum of four front passages occurring in each month for each year of the study (Figures 3.4, 3.5). Although both showed similar density peaks during October and November, with densities gradually decreasing through the spring, *B. patronus* had a secondary, smaller density peak in March. While sampling on the western Louisiana continental shelf, Shaw et al. (1985) indicated a density peak in *B. patronus* larvae during February with highest egg densities found in December, but sampling only encompassed December through April. Notably, the collection of *B. patronus* larvae during September is an earlier estuarine recruitment than previously indicated (Ruple, 1984). Sampled densities of *M.*

undulatus larvae, with an October/November peak, correspond well to the reported July through December spawning season, and late summer or fall peak in recruitment (Warlen and Burke, 1990; Barbieri et al., 1994). The lack of April estuarine samples for both species may be a reflection of winter frontal events weakening at the end of the storm season.

There was net recruitment of *B. patronus* and *M. undulatus* larvae through the tidal pass as flood collections were significantly greater than ebb. However, there were no statistical differences between surface and near-bottom densities for either species, possibly reflecting the effects of a well-mixed tidal pass, which would likely negate vertical movement under selective tidal stream transport (STST) as a recruitment mechanism. The lack of vertical stratification and STST evidence have been reported for other well-mixed estuaries along the northern GOM (Lyczkowski-Shultz et al., 1990; Bianchi et al., 1997; Chesney et al., 2000; Lipp et al., 2001; Brown et al., 2004). However, *B. patronus* larvae did show some evidence of diel vertical migration with greatest densities taken during nocturnal floods which has been reported previously (Shaw et al., 1988; Raynie, 1991; Govoni, 1997). Although no diel vertical migration was found for *M. undulatus* within the tidal pass, such vertical movement has been seen offshore (Comyns and Lyczkowski-Shultz, 2004).

Coastal setup from the prefrontal phase is the probable dominant force for recruitment of *B. patronus* and *M. undulatus* through the tidal pass. Density peaks were evident for both species at mid-high barometric pressure during southerly winds on flood tides, but *M. undulatus* had a much stronger signal (Figures 3.20, 3.23). Interestingly, density peaks during passage of winter cold fronts, with low to mid-barometric pressures and winds switching from southerly to westerly, were also indicative of both species. The lack of parity in density peaks for *M.*

undulatus between flood and ebb tides and day vs. night may also allude to a tidal recruitment cue triggering larval vertical movement in the water column as suggested in estuaries along the U.S. East Coast (Hare and Able, 2007; Love et al., 2009), and differs from previous work where significantly more larvae were found during flood tides (Raynie, 1991). There was no indication of high flood densities associated with easterly winds and onshore Ekman transport for either species.

Negative estuarine recruitment from wind-forced estuarine flushing during the post-frontal phase, with high barometric pressure and northerly winds was not great for both species. *B. patronus* showed near zero densities for these wind events, except during ebb tides. *M. undulatus* density peaks associated with the post-frontal phase, however, were evident on both flood and ebb tides, with flood tides having smaller density peaks than the corresponding ebb tides. The flood tide peak for *M. undulatus* at barometric pressures above 1035 mBar for northerly winds suggested stronger fronts may have a disproportionate effect by stacking up larvae in Bayou Tartellan. Stronger fronts have been shown to cause more severe reductions in the tidal prism, limiting the chance for larvae to recruit far enough up estuary to avoid strong outflows (Whitfield, 1989; Schultz et al., 2003), and larger larvae may be more able to move horizontally to facilitate retention by utilizing flow differentials at channel edges due to boundary conditions (Beckley, 1985; Whitfield, 1989; Schultz et al., 2003).

3.4.4 Species with Moderate Atmospheric Forcing

During this study, black drum recruitment was heavily pulsed, with no larvae taken in 94% of the samples collected during the expected recruitment season. Black drum traditionally spawn between coastal depths of approximately 10 to 50 feet in areas with high water movement,

or occasionally near or within estuarine mouths provided depth requirements can be met (Nieland and Wilson, 1993; Saucier and Baltz, 1993; Able and Fahay, 1998). Although *P. cromis* was sampled in all months except September, November, and April, densities peaked during December and February, with a relatively quick drop-off in mean density during March. Saucier and Baltz (1993) found *P. cromis* larvae densities to be less pulsed, with more regular recruitment of larvae during the spring months. However, the spawning season for black drum has been reported to be highly variable, with large differences in peak spawning months (Murphy and Taylor, 1989; Peters and McMichael, 1990; Fitzhugh et al., 1993; Saucier and Baltz, 1993).

This protracted spawning season increases the likelihood of encounters with winter cold front passages, which may account for a transport model fit greater than the remainder of the other species analyzed (Adj. $R^2 = 0.49$). Atmospheric forcing had some demonstrative effects on predicted densities of *P. cromis*. Wind direction and barometric pressure were significant, and depended on tidal stage as individual factors. During ebb tides, densities associated with southerly winds at approximately 1020 mBar, indicative of the pre-frontal phase, likely stacked up larvae in the face of the astronomical tidal signal. In addition, modest densities during ebb tides were also associated with northerly winds at around the same barometric pressures, likely a result of larvae being flushed from the estuary.

During flood tides, *P. cromis* densities appeared to respond to barometric pressures less than 1020 mBar and northeasterly, easterly, and southerly winds, suggesting Ekman transport and coastal setup after the post-frontal phase may be an important recruitment mechanism. The difference between flood and ebb tidal density patterns implies partial decoupling of black drum

recruitment from atmospheric forcing, when normal hydrographic flows such as any flood tide, or other wind-driven forcing can overcome outwelling during ebb tides.

3.4.5 Low Atmospheric Forcing – Inner Continental Shelf Spawners

Two sciaenids, *C. arenarius* and *S. ocellatus*, and *F. aztecus* had similar transport model results, with red drum having slightly higher model fit (Adj. $R^2 = 0.39$) than either sand seatrout (Adj. $R^2 = 0.37$) or postlarval brown shrimp (Adj. $R^2 = 0.34$). In Louisiana, *S. ocellatus* spawn in shallow waters on the inner continental shelf or within the estuarine mouth (Wilson and Nieland, 1994; Nieland et al., 2002). For the other two species within this category, *F. aztecus* and *C. arenarius*, there was a degree of overlap between the spawning depths. Most brown shrimp typically spawn in depths less than 40 meters, but spawning can range from 25 and 110 meters (Cook and Lindner, 1970; Ditty et al., 1988). *Cynoscion arenarius* spawn at wide range of depths, i.e., 7 to 90 meters, however, the highest percentages of older gravid females are found at depths between 50 and 70 meters (Sutter and McIlwain, 1987). These offshore depths lead to a longer recruitment corridor, which is evident in the shelf-to-estuary transit time for *C. arenarius* larvae being 30-94 days and subject to cross-shelf transport similar to *B. patronus* and *M. undulatus* (Shaw et al., 1988).

The recruitment season for both *C. arenarius*, *S. ocellatus*, and *F. aztecus* differ in the timing of peak densities and the structure of the dominant atmospheric forces across their respective seasons. Although *F. aztecus* was sampled during all months of the study, there were two density peaks, the primary one during winter with highs in January and March and a much smaller, secondary peak in September. This second minor peak may not always be present as it is in Texas waters (Benefield, 1982) and like other shrimp species could be brought on by

variations in offshore water temperature (Boddeke, 1982). Lack of model fit for *S. ocellatus* is probably a result of its truncated spawning and recruitment season, typically from August through early October (Wilson and Nieland, 1994; Rooker and Holt, 1997; Holt, 2008; Arnott et al., 2010), when the chance of strong, regular atmospheric events are minimal. The major density peak for *S. ocellatus* (~ 300 indiv./ 15m^3) related to normal coastal setup caused by southerly winds, from approximately 160° to 200° , along a range of barometric pressures, between 1012 and 1024 mBar (Figure 3.33, 3.34). In contrast, *C. arenarius* displayed protracted spawning with peak densities coming in late summer/early fall (Ditty et al., 1988). The rising densities during March and April, with still high densities in September, represent the beginning and end of this recruitment season, respectively. While the waning, extremely low, and zero collections during the winter (i.e., November – February) for *C. arenarius* provide an explanation for lack of model fit, the increased numbers of postlarval *F. aztecus* that were collected during interim periods between winter frontal events (i.e., variable slow winds, medium barometric pressures) likely led to its decreased model fit, i.e., explained variability.

Although atmospheric effects for both species during flood tides had some similarity, differences existed in the magnitude and number of density impacts. In light of low model fits, *C. arenarius* during flood tides had a single modest density peak associated with northwesterly winds correlating to the period during the prefrontal phase, when the normal tidal prism is beginning to decrease, and the pending outwelling is likely to begin stacking up larvae recruited into the tidal pass (Figure 3.40, 3.41). The major difference in flood tide for *F. aztecus* was the presence of multiple density impacts associated with southerly as well as northerly winds across a range of barometric pressures, showing the importance of both astronomical and atmospheric

forces working in concert (Horton, 1998). This utilization of the flood tidal stage correlates well to established endogenous tidal activity rhythms for postlarval brown shrimp (Hughes 1972; Matthews et al., 1991). The ebb tide density peak for *C. arenarius* related to coastal setup from southerly winds, likely overriding the astronomical tidal regime. This result for *C. arenarius* is not dissimilar from other species in the analysis with similar seasonal recruitment peaks and spawning depths.

3.4.6 Low Atmospheric Forcing – Shallow Water Spawners

The degree of variability explained within transport models for *A. hepsetus* (Adj. $R^2 = 0.34$), *A. mitchilli* (Adj. $R^2 = 0.32$), and *C. nebulosus* (Adj. $R^2 = 0.38$), was also relatively low. Along with traditional spawning peaks that would have limited encounter with winter cold front events, *A. hepsetus*, *S. ocellatus*, and *C. nebulosus* spawn near-shore in approximately 10 meters of water or less (Ditty et al., 1988; Whitehead et al., 1988; Lapolla, 2001). *Anchoa mitchilli*, being estuarine obligate, represents a specific case (Zastrow et al., 1991). The shallow depths, proximal location to the tidal pass, and spawning seasons with weak or no atmospheric frontal events partially explain the low degree of frontal forcing for these species.

3.4.7 Low Atmospheric Forcing – *Anchoa* Congenerics

Although both *A. hepsetus* and *A. mitchilli* were sampled during most months of the study, samples collected during April and September/October had the greatest densities and the most non-zero collections. In particular, peak broad-striped anchovy densities during September flood tides, and peak bay anchovy densities during April ebb tides, show the estuarine dependent and estuarine obligate nature of the two species, respectively. Furthermore, they also illustrate

the low probability of the importance of atmospherically-driven hydrographic flows as indicated by the low strength and limited number of winter frontal events during these months.

Despite low model fits for *A. hepsetus* (Adj. $R^2 = 0.34$) and *A. mitchilli* (Adj. $R^2 = 0.32$), the effects of wind direction on estuarine obligate versus estuarine dependent strategies were apparent. For example, coastal setup during southerly winds, and to a lesser extent Ekman transport from southeasterly winds, had a greater predicted influence on *A. hepsetus* densities (Figure 3.24). The estuarine-dependent nature of broad striped anchovy, with the need for estuarine recruitment from coastal spawning grounds suggested that easterly to southerly and northeasterly winds might be an important mechanism. *A. mitchilli* also exhibited greater densities associated with northeasterly and northwesterly winds, but southerly winds had a very limited expectation of encountering larvae (Figure 3.27). Being estuarine obligate, the expectation would be to only see bay anchovy larvae in the tidal pass during the flushing of these north/south trending estuaries by wind fields from the northern quadrant (Lyczkowski-Schultz et al., 1990). Differences in barometric pressure and wind speed on *A. mitchilli* larval densities also highlighted the dichotomy of estuarine obligate, where high densities of *A. mitchilli* were predicted at much lower and higher atmospheric pressures and moderate wind speeds (Figures 3.23, 3.24).

3.4.8 Low Atmospheric Forcing – The Other Sciaenid

Limited encounters due to spawning season and low atmospheric forcing existed for the other sciaenid, *C. nebulosus*. Spotted seatrout traditionally spawn during the summer (Holt et al., 1985; Saucier et al., 1992) which did not overlap very much with our sampling period. However,

the months of encounter (September and October) were the same as *S. ocellatus*, yet presented a lower model fit and a different explanation.

Southerly winds produced low density predictions for *C. nebulosus* at extremely low wind speeds. The necessity for spawning locations with higher current velocities for *C. nebulosus* (Saucier and Baltz, 1993), suggest normal tidal regimes occasionally enhanced by coastal setup may be an important driver for species with small to virtually no recruitment corridors. This parallels similar findings for other species with short recruitment corridors in this analysis, such as *A. hepsetus*. Life history characteristics for *C. nebulosus*, however, suggest the larvae are more developed at the time of recruitment into the tidal pass than *S. ocellatus* larvae (Baltz et al., 1998). If this is the case, *C. nebulosus* may be more likely to resist the relatively short lived out going flows, due to low percentages of westerly winds, during Ekman transport offshore.

3.5 Conclusions

The passage of winter frontal events was demonstrated to have variable effects on the larval recruitment of estuarine-dependent larvae and the retention of estuarine-obligate larvae with their ultimate fate being controlled by a combination of astronomical and meteorological forces (Brown et al. 2004; Lyczkowski-Shultz 2004; Johnson et al. 2009). Differences occurred not only between family and genera, but there were also differences within congenics. In general, similarities within life history strategy, recruitment dynamics associated with the length of the transport corridor (i.e., spawning depth or distance from shore), and species- specific responses to atmospheric forcing within this microtidal, northern GOM tidal pass were determinant in predicting the importance of meteorological forcing. For most species analyzed, atmospheric

factors appeared to be only minimally important and not overly determinant in successful recruitment.

The lack of significant differences between surface and bottom zoo-/ichthyoplankton densities and similarities in hydrographic parameters between surface and near-bottom measurements suggests vertical movement under STST as an ineffective strategy for transport through and retention within this well-mixed tidal pass. Virtually all species in the analysis (the exceptions being gulf menhaden and Atlantic croaker) exhibited a very high degree of recruitment pulsing, as evidenced by the very large portion of zero collections. This pulsing partially accounts for low model fits where the probability of encounter with larvae in the tidal pass is dependent on specific variables such as spawning location, patch dynamics along density fronts, and other factors not included in the model analysis. Individual based models (IBMs) or zero inflated models (ZIMs) may help to account for this variation in pulsing and provide greater stability by reducing unexplained or immeasurable variability in future analyses.

Those species with similar life history patterns tended to have similar degrees of model fits and predicted density responses to atmospheric forcing within the transport model. While having the highest model fits, both *B. patronus* and *M. undulatus* have somewhat protracted, over winter spawning and recruitment seasons, and spawn in deeper continental shelf waters than other species analyzed. The moderate level of model fit for *P. cromis* is likely bolstered from its protracted, over-winter spawning season, which provided increased encounters with winter cold fronts, but is perhaps decreased somewhat by the seasonal variability in spawning depth or distance from shore. Although *F. aztecus* and *C. arenarius* have relatively similar spawning depths and locations with respect to the tidal pass as compared to *B. patronus* and *M. undulatus*,

their peak spawning and recruitment seasons offer at least a partial explanation for the lack of highly significant atmospheric forcing. All other species in the analysis that had low model fits spawn in shallow coastal waters, some even within the estuary or tidal pass itself, and have traditional spawning peaks that would limit interaction with strong winter frontal events.

The strong atmospheric forcing leading to a reduced or negative tidal prism during the postfrontal phases of winter frontal events within these shallow, well-mixed estuaries was important for many species. The westerly wind fields and low atmospheric pressures, despite their rarity during sampling, modeled density peaks for most species analyzed. The occurrence of these peaks even during flood tides is perhaps a function of atmospheric forces overriding the prevailing microtidal regime. Most species showed density peaks associated with northerly winds resulting in flushing of the estuary even during flood tides. The density peaks for *B. patronus* and *M. undulatus* at low barometric pressures during westerly and northwesterly winds, and high barometric pressures during northerly winds highlight the effect of passage of a front and the post frontal phase on these negative estuarine recruitment issues.

The increasing tidal prism of the pre-frontal phase during coastal setup with its dominate southerly wind fields, appeared to be an important offshore to inshore transport mechanism for successful estuarine recruitment for species (i.e., *B. patronus* and *M. undulatus*) which spawn in deeper waters farther from shore. All other species in the analysis, except for *A. mitchilli*, show density peaks associated with southerly winds and the resultant coastal setup for the tidal pass at Bayou Tartellan, which doesn't have a large freshwater head. Astronomical cues may be evident for species such as *F. aztecus*, which rely on the coastal setup during flood tides, while some species appear to decouple the astronomical from the atmospheric signal, such as *P. cromis*. The

astronomical micro-tides, shallow nature of the estuaries and their cardinal alignment with the general path of the winter frontal events reinforces the importance of the north and south winds in predicting zoo-/ichthyoplankton densities for estuaries in Louisiana.

In conclusion, the relative contribution of these high-energy, atmospheric cold front passages and astronomical tides to the successful estuarine recruitment of winter-spawned, estuarine-dependent fisheries is species specific and dependent upon a number of factors. Generally, those species with similarities within life history strategy and recruitment dynamics associated with the length of the transport corridor showed similar effects with respect to atmospheric forcing. In particular, those species with longer recruitment corridors and protracted, over-winter spawning and recruitment showed a high degree of atmospheric forcing from winter cold front passages and reduced patchiness. Those species with lower encounters of winter cold front passage due to spawning season or shortened recruitment corridors showed minimal effects from atmospheric forcing and increased heterogeneity of distribution. Some of these differences are explained by the differences in life history strategy, as is the case between estuarine-dependent *A. hepsetus* and estuarine-obligate *A. mitchilli*. Further research into the variability of these specific weather patterns, inclusion of the recruitment corridor into the sampling design, and a sampling protocol which specifically targets atmospheric cold front passage encounter exclusively, may lead to a better understanding of the potential effects changes in the periodicity, frequency, and strength of winter frontal events have on recruitment for commercially and ecologically important species in the northern GOM.

3.6 Literature Cited

- Able, K.W. 2005. A re-examination of fish estuarine dependence: evidence for connectivity between estuarine and ocean habitats. *Estuarine, Coastal and Shelf Science* 64(1): 5-17.
- Able, K.W., and M.P. Fahay. 1998. The first year in the life of estuarine fishes in the middle Atlantic bight. Rutgers University Press, New Brunswick, New Jersey.
- Arnott, S.A., Roumillat, W.A., Archambault, J.A., Wenner, C.A., Gerhard, J.I., Darden, T. L., and M.R. Denson. 2010. Spatial synchrony and temporal dynamics of juvenile red drum *Sciaenops ocellatus* populations in South Carolina, USA. *Marine Ecology Progress Series* 415: 221-236.
- Bailey, K.M., Abookire, A.A., and J.T. Duffy Anderson. 2008. Ocean transport paths for the early life history stages of offshore spawning flatfishes: a case study in the Gulf of Alaska. *Fish and Fisheries* 9(1): 44-66.
- Baltz, D.M., Fleeger, J.W., Rakocinski, C.F., and J.N. McCall. 1998. Food, density, and microhabitat: factors affecting growth and recruitment potential of juvenile saltmarsh fishes. *Environmental Biology of Fishes* 53:89-103.
- Barbieri, L.R., Chittenden Jr, M., and S.K. Lowerre-Barbieri. 1994. Maturity, spawning, and ovarian cycle of Atlantic croaker, *Micropogonias undulatus*, in the Chesapeake Bay and adjacent coastal waters. *Fishery Bulletin* 92(4): 671-685.
- Beckley, L.E. 1985. Tidal exchanges of ichthyoplankton in the Swartkops estuary mouth, South Africa. *South African Journal of Zoology* 20(1): 15-20.
- Benefield, R.L. 1982. Studies of shrimp populations in selected coastal bays of Texas. Texas Parks and Wildlife Department, Coastal Fisheries Board, Management and Data Services 41, i-ii, 1-9, i-ii, 1-34, A-I-A-90.
- Bianchi, T.S., Baskaran, M., DeLord, J., and M. Ravichandran. 1997. Carbon cycling in a shallow turbid estuary of southeast Texas: The use of plant pigment biomarkers and water quality parameters. *Estuaries and Coasts* 20(2): 404-415.
- Boddeke, R. 1982. The occurrence of winter and summer eggs in the brown shrimp (*Crangon crangon*) and the pattern of recruitment. *Netherlands Journal of Sea Research* 16:151-162.

- Bolle, L.J., Dickey-Collas, M., Van Beek, J.K.L., Erftemeijer, P.L.A., Witte, J.I.J., Van der Veer, H.W., and A.D. Rijnsdorp. 2009. Variability in transport of fish eggs and larvae. III. Effects of hydrodynamics and larval behaviour on recruitment in plaice. *Marine Ecology Progress Series* 390: 195-211.
- Brewer, G.D., and G. Kleppel. 1986. Diel vertical distribution of fish larvae and their prey in nearshore waters of southern California. *Marine Ecology Progress Series* 27(3): 217–226.
- Brochier, T., Ramzi, A., Lett, C., Machu, E., Berraho, A., Fréon, P., and S. Hernández-León. 2008. Modeling sardine and anchovy ichthyoplankton transport in the Canary Current System. *Journal of Plankton Research* 30(10): 1133-1146.
- Brown, C., Holt, S., Jackson, G., Brooks, D., and G. Holt. 2004. Simulating larval supply to estuarine nursery areas: how important are physical processes to the supply of larvae to the Aransas Pass Inlet? *Fisheries Oceanography* 13(3): 181-196.
- Brown, C.A., Jackson, G.A., and D.A. Brooks. 2000. Particle transport through a narrow tidal inlet due to tidal forcing and implications for larval transport. *Journal of Geophysical Research* 105(C10): 24141-24124, 24156.
- Cahoon, D.R., and D.J. Reed. 1995. Relationships among marsh surface topography, hydroperiod, and soil accretion in a deteriorating Louisiana salt marsh. *Journal of Coastal Research* 11(2): 357-369.
- Castro, L.R., and R.K. Cowen. 1991. Environmental factors affecting the early life history of bay anchovy *Anchoa mitchilli* in Great South Bay, New York. *Marine Ecology Progress Series* 76(3): 235-247.
- Chambers, J.M., Cleveland, W.S., Kleiner, B., and P.A. Tukey. 1983. *Graphical Methods for Data Analysis*. Wadsworth, Belmont, California.
- Checkley Jr., D.M., Ramen, S., Maillet, G.L., and K.M. Mason. 1988. Winter storm effects on the spawning and larval drift of a pelagic fish. *Nature* 335: 346-348.
- Chesney, E.J., Baltz, D.M., and R.G. Thomas. 2000. Louisiana estuarine and coastal fisheries and habitats: Perspectives from a fish's eye view. *Ecological Applications* 10(2): 350-366.
- Colton, J.B., Smith, W.G., Kendall Jr., A.W., Berrien, P.L., and M.L. Fahay. 1979. Principal spawning areas and times of marine fishes, Cape Sable to Cape Hatteras. *Fisheries Bulletin*, NOAA 76: 911-916.

- Comyns, B.H., and J. Lyczkowski-Shultz. 2004. Diel vertical distribution of Atlantic croaker, *Micropogonias undulatus*, larvae in the northcentral Gulf of Mexico with comparisons to red drum, *Sciaenops ocellatus*. *Bulletin of Marine Science* 74(1): 69-80.
- Cook, H.L., and M.J. Lindner. 1970. Synopsis of biological data on the brown shrimp *Penaeus aztecus* Ives. *FAO Fisheries Report* 57, 4:1471-1497.
- Costa, M., Cabral, H., Drake, P., Economou, A., Fernandez Delgado, C., Gordo, L., Marchand, J., and R. Thiel. 2002. Recruitment and production of commercial species in estuaries. Pages 54-123 in Elliott M., and K. Hemingway editors. *Fishes in Estuaries*. Blackwell Science, Oxford.
- Cowen, R.K., Lwiza, K.M M., Sponaugle, S., Paris, C.B., and D.B. Olson. 2000. Connectivity of marine populations: open or closed? *Science* 287(5454): 857-859.
- Deegan, L.A. 1990. Effects of estuarine environmental conditions on population dynamics of young-of-the-year gulf menhaden. *Marine Ecology Progress Series* 68(1): 195-205.
- Ditty, J., Zieske, G., and R. Shaw. 1988. Seasonality and depth distribution of larval fishes in the northern Gulf of Mexico above latitude 26 degree 00'N. *Fishery Bulletin* 86(4): 811-823.
- Engle, V.D., Summers, J.K., and J.M. Macauley. 1999. Dissolved oxygen conditions in northern Gulf of Mexico estuaries. *Environmental Monitoring and Assessment* 57(1): 1-20.
- Epifanio, C. 1995. Transport of blue crab (*Callinectes sapidus*) larvae in the waters off mid-Atlantic states. *Bulletin of Marine Science* 57(3): 713-725.
- Eubank, R.L. and C.H. Spiegelman. 1990. Testing the goodness of fit of a linear model via nonparametric regression techniques. *Journal of the American Statistical Society* 85(410):387-392
- Fahay, M.P. 1983. Guide to the early stages of marine fishes occurring in the western North Atlantic Ocean, Cape Hatteras to the south Scotian Shelf. *North Atlantic Fisheries Science* 4: 1-423.
- Fahay, M.P. 2007. Early Stages of Fishes in the Western North Atlantic Ocean: Davis Strait, Southern Greenland and Flemish Cap to Cape Hatteras. *Scorpaeniformes Through Tetraodontiformes*, Volume 2: Northwest Atlantic Fisheries Organization. 1696 pp.
- Feng, Z. 2009. Hydrodynamic Response to Cold Fronts along the Louisiana Coast. Master's thesis. Louisiana State University, Baton Rouge, Louisiana.

- Fitzhugh, G.R., Thompson, B.A., and T.G. Snider. 1993. Ovarian development, fecundity, and spawning frequency of black drum *Pogonias cromis* in Louisiana. Fisheries Bulletin 91: 244-253.
- Flores-Coto, C., Becerril-Martinez, J.A., Zavala-Garcia, F., Garcia, A. and J.S. Burke. 2010. Shrimp postlarvae immigration during the high velocity period of the flood tide in the southern Gulf of Mexico. Hydrobiologica 20(1): 1-12.
- Fogarty, M.J., Sissenwine, M.P., and E.B. Cohen. 1991. Recruitment variability and the dynamics of exploited marine populations. Trends in Ecology & Evolution 6(8): 241-246.
- Fox, J. 2002. Introduction to Nonparametric Regression. ESRC, Oxford University Press. Oxford.
- Fritzsche, R.A. 1978. Development of Fishes of the Mid-Atlantic Bight: An Atlas of Egg, Larval and Juvenile Stages. Volume 5, Chaetodontidae through Ophidiidae. FWS/OBS-78/12, U.S. Fish and Wildlife Service, Washington D.C. 237 pp.
- Glass, L.A., Rooker, J.R., Kraus, R.T., and G.J. Holt. 2008. Distribution, condition, and growth of newly settled southern flounder (*Paralichthys lethostigma*) in the Galveston Bay Estuary, TX. Journal of Sea Research 59(4): 259-268.
- Golubev, G.K. 1993. Adaptive spline estimates for nonparametric regression models. Theory of Probability and its Applications 37:521-529.
- Govoni, J.J. 1997. The association of the population recruitment of Gulf menhaden, *Brevoortia patronus*, with Mississippi River discharge. Journal of Marine Systems 12(1-4): 101-108.
- Govoni, J.J., and L.J. Pietrafesa. 1994. Eulerian views of layered water currents, vertical distribution of some larval fishes, and inferred advective transport over the continental shelf off North Carolina, USA, in winter. Fisheries Oceanography 3(2): 120-132.
- Hardy Jr., J.D. 1978a. Development of Fishes of the Mid-Atlantic Bight: An Atlas of Egg, Larval and Juvenile Stages. Volume 2, Anguillidae through Syngnathidae. FWS/OBS-78/12, U.S. Fish and Wildlife Service, Washington D.C. 229 pp.
- Hardy Jr., J.D. 1978b. Development of Fishes of the Mid-Atlantic Bight: An Atlas of Egg, Larval and Juvenile Stages. Volume 3, Aphredoderidae through Rachycentridae. FWS/OBS-78/12, U.S. Fish and Wildlife Service, Washington, D.C. 249 pp.
- Hare, J.A., and K.W. Able. 2007. Mechanistic links between climate and fisheries along the east coast of the United States: explaining population outbursts of Atlantic croaker (*Micropogonias undulatus*). Fisheries Oceanography 16(1): 31-45.

- Hare, J.A., and J.J. Govoni. 2005. Comparison of average larval fish vertical distributions among species exhibiting different transport pathways on the southeast United States continental shelf. *Fisheries Bulletin* 103: 728-736.
- Hare, J.A., Quinlan, J.A., Werner, F.E., Blanton, B.O., Govoni, J.J., Forward, R.B., Settle, L.R., and D.E. Hoss. 1999. Larval transport during winter in the SABRE study area: results of a coupled vertical larval behavior-three-dimensional circulation model. *Fisheries Oceanography* 8(2): 57-76.
- Hastie, T.J. and R.J. Tibshirani. 1990. *Generalized Additive Models*. Chapman and Hill, London. 333 pp.
- Henri, M., Dodson, J., and H. Powles. 1985. Spatial configurations of young herring (*Clupea harengus harengus*) larvae in the St. Lawrence Estuary: importance of biological and physical factors. *Canadian Journal of Fisheries and Aquatic Sciences* 42(S1): 91-104.
- Hernandez Jr, F.J., Powers, S.P., and W.M. Graham. 2010. Detailed examination of ichthyoplankton seasonality from a high-resolution time series in the northern Gulf of Mexico during 2004-2006. *Transactions of the American Fisheries Society* 139(5): 1511-1525.
- Hines, A.H., Johnson, E.G., Young, A.C., Aguilar, R., Kramer, M.A., Goodison, M., Zmora, O., and Y. Zohar. 2008. Release strategies for estuarine species with complex migratory life cycles: Stock enhancement of Chesapeake blue crabs (*Callinectes sapidus*). *Reviews in Fisheries Science* 16(1): 175-185.
- Holt, G.J., Holt, S.A., and C.R. Arnold. 1985. Diel periodicity of spawning in sciaenids. *Marine Ecology Progress Series* 27: 1-7.
- Holt, S.A. 2008. Distribution of red drum spawning sites identified by a towed hydrophone array. *Transactions of the American Fisheries Society* 137(2): 551-561.
- Horton, R. 1998. Atmospheric and hydrographic effects on postlarval brown shrimp (*Penaeus aztecus* Ives) estuarine recruitment. Master's thesis. Louisiana State University, Baton Rouge, Louisiana.
- Houde, E.D. 1982. Kinds, distributions and abundances of sea bass larvae (Pisces:Serranidae) from the eastern Gulf of Mexico. *Bulletin of Marine Science* 32: 511-522.
- Hughes, D.A. 1972. On the endogenous control of tide-associated displacements of pink shrimp, *Penaeus duorarum* Burkenroad. *Biological Bulletin* 142: 271-280.

- Johnson, D.R., Perry, H.M., Lyczkowski-Shultz, J., and D. Hanisko. 2009. Red snapper larval transport in the northern Gulf of Mexico. *Transactions of the American Fisheries Society* 138: 458-470.
- Johnson, G.D. 1978. Development of Fishes of the Mid-Atlantic Bight: An Atlas of Egg, Larval and Juvenile Stages. Volume 4, Carangidae through Ehippidae. FWS/OBS-78/12, U.S. Fish and Wildlife Service, Washington D.C. 189 pp.
- Jones, P.W., Martin, F.D., and J.D. Hardy. 1978. Development of Fishes of the Mid-Atlantic Bight: An Atlas of Egg, Larval and Juvenile Stages. Volume 1, Acipenseridae through Ictaluridae. FWS/OBS-78/12, U.S. Fish and Wildlife Service, Washington D.C. 224 pp.
- Joyeux, J. 1998. Spatial and temporal entry patterns of fish larvae into North Carolina estuaries: comparisons among one pelagic and two demersal species. *Estuarine, Coastal and Shelf Science* 47(6): 731-752.
- Joyeux, J. 1999. The abundance of fish larvae in estuaries: Within-tide variability at inlet and immigration. *Estuaries and Coasts* 22(4): 889-904.
- Kineke, G.C., Higgins, E.E., Hart, K. and D. Velasco. 2006. Fine-sediment transport associated with cold front passages on the shallow shelf, Gulf of Mexico. *Continental Shelf Research* 26: 2073-2091.
- Lapolla, A.E. 2001. Bay anchovy *Anchoa mitchilli* in Narragansett Bay, Rhode Island. II. Spawning season, hatch-date distribution and young-of-the-year growth. *Marine Ecology Progress Series* 217: 103-109.
- Lara-Lopez, A., and F.J. Neira. 2008. Synchronicity between zooplankton biomass and larval fish concentrations along a highly flushed Tasmanian estuary: assessment using net and acoustic methods. *Journal of Plankton Research* 30(9): 1061-1073.
- Leak, J.C. 1981. Studies on recruitment process focusing on early life history of the Japanese sardine, *Sardinops melanostictus* (Schlegel). *Bulletin of Natural Resources, Institute of Fisheries Science* 3: 25-278.
- Lee, J., Wiseman, W., and F. Kelly. 1990. Barotropic, subtidal exchange between Calcasieu Lake and the Gulf of Mexico. *Estuaries and Coasts* 13(3): 258-264.
- Lee, T.N., Rooth, C., Williams, E., McGowan, M., Szmant, A.F., and M. Clarke. 1992. Influence of Florida Current, gyres and wind-driven circulation on transport of larvae and recruitment in the Florida Keys coral reefs. *Continental Shelf Research* 12(7-8): 971-1002.

- Li, C., Roberts, H., Stone, G.W., Weeks, E., and Y. Luo. 2011. Wind surge and saltwater intrusion in Atchafalaya Bay during onshore winds prior to cold front passage. *Hydrobiologia* 658(1): 1-13.
- Li, C., Weeks, E., and J.L. Rego. 2009. In situ measurements of saltwater flux through tidal passes of Lake Pontchartrain estuary by Hurricanes Gustav and Ike in September 2008. *Geophysical Research Letters* 36(19): L19609.
- Lipp, E. K., Rodriguez-Palacios, C., and J.B. Rose. 2001. Occurrence and distribution of the human pathogen *Vibrio vulnificus* in a subtropical Gulf of Mexico estuary. *Hydrobiologia* 460(1): 165-173.
- Love, J.W., Luers, D.F., & Williams, B.D. 2009. Spatio-temporal patterns of larval fish ingress to Chincoteague Bay, Maryland, USA during winter and spring 2004 to 2007. *Marine Ecology Progress Series* 377: 203-212.
- Lyczkowski-Shultz, J., Ruple, D.L., Richardson, S.L., Cowan, J., and H. James. 1990. Distribution of fish larvae relative to time and tide in a Gulf of Mexico barrier island pass. *Bulletin of marine science* 46(3): 563-577.
- Martin, F.D., and G.E. Drewery. 1978. Development of Fishes of the Mid-Atlantic Bight: An Atlas of Egg, Larval and Juvenile Stages. Volume 6, Stromateidae through Ogococephilidae. FWS/OBS-78/12, U.S. Fish and Wildlife Service, Washington D.C. 176 pp.
- Matthews, T.R., Schroeder, W.M. and D.E. Stearns. 1991. Endogenous rhythm, light and salinity effects on postlarval brown shrimp *Penaeus aztecus* Ives recruitment to estuaries. *Journal of Experimental Marine Biology and Ecology* 154(2):177-189.
- Mazzotti, F.J., Pearlstine, L.G., Barnes, T., Bortone, S.A., Chartier, K., Weinstein, A.M., and D. DeAngelis. 2008. Stressor Response Model for the Spotted Seatrout (*Cynoscion nebulosus*). University of Florida IFAS Extension. University of Florida, Gainesville, Florida.
- Miller, G.L., and S.C. Jorgenson. 1973. Meristic characters of some marine fishes of the western Atlantic Ocean. *Fisheries Bulletin*, NOAA 71: 301-312.
- Miller, J., Burke, J., and G. Fitzhugh. 1991. Early life history patterns of Atlantic North American flatfish: likely (and unlikely) factors controlling recruitment. *Netherlands Journal of Sea Research* 27(3-4): 261-275.

- Minello, T.J., Zimmerman, R.J., and E.X. Martinez. 1989. Mortality of young brown shrimp *Penaeus aztecus* in estuarine nurseries. Transactions of the American Fisheries Society 118(6): 693-708.
- Moeller, C.C., Huh, O.K., Roberts, H.H., Gumley, L.E., and W.P. Menzel. 1993. Response of Louisiana coastal environments to a cold front passage. Journal of Coastal Research 434-447.
- Moffett, A., McEachron, L., and J. Key. 1979. Observations on the biology of sand seatrout (*Cynoscion arenarius*) in Galveston and Trinity Bays, Texas. Contributions to Marine Science 22: 163-172.
- Moser, H.G. 1984. Ontogeny and Systematics of Fishes. American Society of Ichthyologists and Herpetologists Special Publication No. 1. Allen Press, Lawrence, Kansas. 760 pp.
- Murphy, M.D., and R.G. Taylor. 1989. Reproduction and growth of black drum, *Pogonias cromis* in northeast Florida. Northeast Gulf Science 10: 127-137.
- Myers, R. A. 1998. When do environment–recruitment correlations Work? Reviews in Fish Biology and Fisheries 8(3): 285-305.
- Nieland, D.L., and C.A. Wilson. 1993. Reproductive biology and annual variation of reproductive variables of black drum in the northern Gulf of Mexico. Transactions of the American Fisheries Society 122(3): 318-327.
- Nieland, D.L., Thomas, R.G., and C.A. Wilson. 2002. Age, growth, and reproduction of spotted seatrout in Barataria Bay, Louisiana. Transactions of the American Fisheries Society 131(2): 245-259.
- Nixon, S., and C. Jones. 1997. Age and growth of larval and juvenile Atlantic croaker, *Micropogonias undulatus*, from the Middle Atlantic Bight and estuarine waters of Virginia. Fishery Bulletin 95(4): 773-784.
- Norcross, B.L., and R.F. Shaw. 1984. Oceanic and estuarine transport of fish eggs and larvae: a review. Transactions of the American Fisheries Society 113(2): 153-165.
- Nordlie, F.G. 2003. Fish communities of estuarine salt marshes of eastern North America, and comparisons with temperate estuaries of other continents. Reviews in Fish Biology and Fisheries 13(3): 281-325.
- Ojanguren, A.F., and L.A. Fuiman. 2010. Seasonal variability in antipredator performance of red drum larvae. Marine Ecology Progress Series 413: 117-123.

- Parker, K.S., Royer, T.C., and R.B. Deriso. 1995. High latitude climate forcing and tidal mixing by the 18.6 year lunar nodal cycle and low frequency recruitment trends in Pacific halibut (*Hippoglossus stenolepis*). *Climate change and northern fish populations* 447-459.
- Pepper, D.A., and G.W. Stone. 2004. Hydrodynamic and sedimentary responses to two contrasting winter storms on the inner shelf of the northern Gulf of Mexico. *Marine Geology* 210(1-4): 43-62.
- Peters, K.M., and R.H. McMichael. 1990. Early life history of the black drum *Pogonias cromis* (Pisces: Sciaenidae) in Tampa Bay, Florida. *Northeast Gulf Science* 11(1): 39-58.
- Perez, B., Day J., Rouse, L. Shaw, R., and M. Wang. 2000. Influence of Atchafalaya River discharge and winter frontal passage on suspended sediment concentration and flux in Fourleague Bay, Louisiana. *Estuarine, Coastal and Shelf Science* 50(2): 271-290.
- Pitts, P.A. 1989. Upwind return flow in a coastal lagoon: Seasonal-scale barotropic transport. *Estuaries* 12: 92-97.
- Quinlan, J.A., Blanton, B.O., Miller, T.J., and F.E. Werner. 1999. From spawning grounds to the estuary: using linked individual-based and hydrodynamic models to interpret patterns and processes in the oceanic phase of Atlantic menhaden *Brevoortia tyrannus* life history. *Fisheries Oceanography* 8(2): 224-246.
- R Development Core Team. 2008. R: A language and environment for statistical computing. R Foundation for Statistical Computing, Vienna, Austria. ISBN 3-900051-07-0, URL <http://www.R-project.org>.
- Raynie, R.C. 1991. Study of the spatial and temporal ichthyoplankton abundance along a recruitment corridor from offshore to estuarine nursery. Master's thesis. Louisiana State University, Baton Rouge, Louisiana.
- Raynie, R.C., and R.F. Shaw. 1994. Ichthyoplankton abundance along a recruitment corridor from offshore spawning to estuarine nursery ground. *Estuarine, Coastal and Shelf Science* 39(6): 421-450.
- Reese, M.M., Stunz, G.W., and A.M. Bushon. 2008. Recruitment of estuarine-dependent nekton through a new tidal inlet: the opening of Packery Channel in Corpus Christi, Texas, USA. *Estuaries and Coasts* 31(6): 1143-1157.
- Reisch, C.H. 1967. Smoothing by Spline Functions. *Numerical Mathematics* 10:177-183.
- Reyes, E., Georgiou, I., Reed, D., and A. McCorquodale. 2002. Using models to evaluate the effects of barrier islands on estuarine hydrodynamics and habitats: A numerical experiment. *Journal of Coastal Research* 44: 176-185.

- Reyier, E.A., Shenker, J. M., and D. Christian. 2008. Role of an estuarine fisheries reserve in the production and export of ichthyoplankton. *Marine Ecology Progress Series* 359: 249-260.
- Richards, W.J. 2006. *Early Stages of Atlantic Fishes: An Identification Guide for the Western Central North Atlantic. Volume I & II.* CRC Press, Boca Raton, FL. 2640 pp.
- Roberts, H., Huh, O., Hsu, S., Rouse, L., and D. Rickman. 1987. Impact of cold-front passages on geomorphic evolution and sediment dynamics of the complex Louisiana coast. In: *Coastal Sediments 1987, Proceedings of a Specialty Conference, American Society of Civil Engineers 1950-1963.*
- Roegner, G.C., Armstrong, D.A., and A.L. Shanks. 2007. Wind and tidal influences on larval crab recruitment to an Oregon estuary. *Marine Ecology Progress Series* 351: 177-188.
- Rogers, B., and W. Herke. 1987. Diel otter trawl catch of Atlantic croaker, *Micropogonias undulatus*, in a Louisiana estuary. *Northeast Gulf Science* 9(2): 147-152.
- Rogers, B.D., Shaw, R.F., Herke, W.H., and R.H. Blanchet. 1993. Recruitment of postlarval and juvenile brown shrimp (*Penaeus aztecus* Ives) from offshore to estuarine waters of the northwestern Gulf of Mexico. *Estuarine, Coastal and Shelf Science* 36(4): 377-394.
- Rooker, J.R., and S.A. Holt. 1997. Utilization of sub-tropical seagrass meadows by newly settled red drum, *Sciaenops ocellatus*: patterns of distribution and growth. *Marine Ecology Progress Series* 158: 139-149.
- Rooker, J.R., Holt, S.A., Soto, M.A., and G. Joan Holt. 1998. Postsettlement patterns of habitat use by sciaenid fishes in subtropical seagrass meadows. *Estuaries and Coasts* 21(2): 318-327.
- Roughgarden, J., Gaines, S., and H. Possingham. 1988. Recruitment dynamics in complex life cycles. *Science* 241(4872): 1460-1466.
- Ruple, D. L. 1984. Occurrence of larval fishes in the surf zone of a northern Gulf of Mexico barrier island. *Estuarine, Coastal and Shelf Science* 18(2): 191-208.
- Saucier, M., Baltz, D., and W. Roumillat. 1992. Hydrophone identification of spawning sites of spotted seatrout, *Cynoscion nebulosus* (Osteichthys: Sciaenidae), near Charleston, South Carolina. *Northeast Gulf Science* 12(2): 141-145.
- Saucier, M.H., and D.M. Baltz. 1993. Spawning site selection by spotted seatrout, *Cynoscion nebulosus*, and black drum, *Pogonias cromis*, in Louisiana. *Environmental Biology of Fishes* 36(3): 257-272.

- Schaffler, J.J., Reiss, C.S., and C.M. Jones. 2009. Spatial variation in otolith chemistry of Atlantic croaker larvae in the Mid-Atlantic Bight. *Marine Ecology Progress Series* 23: 18-35.
- Schultz, E.T., Lwiza, K.M.M., Fencil, M.C., and J.M. Martin. 2003. Mechanisms promoting upriver transport of two species in the Hudson River estuary. *Marine Ecology Progress Series* 251: 263-277.
- Sclafani, M., Taggart, C.T., and K.R. Thompson. 1993. Condition, buoyancy and the distribution of larval fish: implications for vertical migration and retention. *Journal of Plankton Research* 15(4): 413-435.
- Selden Burke, J., Tanaka, M., and T. Seikai. 1995. Influence of light and salinity on behaviour of larval Japanese flounder (*Paralichthys olivaceus*) and implications for inshore migration. *Netherlands Journal of Sea Research* 34(1-3): 59-69.
- Shaw, R.F., Cowan, J.H., and T.L. Tillman. 1985. Distribution and density of *Brevoortia patronus* (gulf menhaden) eggs and larvae in the continental shelf waters of western Louisiana. *Bulletin of Marine Science* 36(1): 96-103.
- Shaw, R.F., Rogers, B.D., Cowan, J., and W.H. Herke. 1988. Ocean-estuary coupling of ichthyoplankton and nekton in the Northern Gulf of Mexico. *American Fisheries Society Symposium* 3: 77-89.
- Shaw, R.F., Wiseman JR, W.J., Turner, R.E., Rouse Jr, L.J., Condrey, R.E., and F.J. Kelly Jr. 1985. Transport of larval gulf menhaden *Brevoortia patronus* in continental shelf waters of western Louisiana: a hypothesis. *Transactions of the American Fisheries Society* 114(4): 452-460.
- Sheaves, M. 2005. Nature and consequences of biological connectivity in mangrove systems. *Marine Ecology Progress Series* 302: 293-305.
- Smith, N.P. 1977. Meteorological and tidal exchanges between Corpus Christi Bay, Texas, and the northwestern Gulf of Mexico. *Estuarine and Coastal Marine Science* 5(4): 511-520.
- Stone, G.W., Liu, B., Pepper, D.A., and P. Wang. 2004. The importance of extratropical and tropical cyclones on the short-term evolution of barrier islands along the northern Gulf of Mexico, USA. *Marine Geology* 210(1-4): 63-78.
- Stuck, K.C. and H.M. Perry. 1982. Ichthyoplankton community structure in Mississippi coastal waters. Pp. VI-I-1 to VI-I-53. *In: Fishery monitoring and assessment completion report, 1 January 1977 to 31 December 1981. Gulf Coast Research Lab, Project No. 2-296-R.*

- Stunz, G., and M. Reese. 2008. Impacts of a new tidal inlet on estuarine nekton: Fisheries recruitment assessment of Packery Channel post-opening in Corpus Christi, Texas. Coastal Bend Bays & Estuaries Program, CBBEP Publication 57, Project No. 0720. 30 pp.
- Sutter, F.C. and T.D. McIlwain. 1987. Species profiles: Life histories and environmental requirements of coastal fishes and invertebrates (Gulf of Mexico): Sand seatrout and silver seatrout. [*Cynoscion arenarius*; *Cynoscion nothus*]. TR-EL-82-4/82-11-72; OSTI ID: 6221321; Legacy ID: TI87900645
- Swenson, E.M. 2003. Assessing the potential climate change impact on salinity in the northern Gulf of Mexico estuaries: A test case in the Barataria estuarine system. Integrated Assessment of the Climate Change Impacts on the Gulf Coast Region. GCRCC & LSU Graphic Series, Baton Rouge, LA: 131-150.
- Swenson, E.M., and W.S. Chuang. 1983. Tidal and subtidal water volume exchange in an estuarine system. Estuarine, Coastal and Shelf Science 16(3): 229-240.
- Taylor, J.C., Mitchell, W.A., Buckel, J.A., Walsh, H.J., Shertzer, K.W., Martin, G.B., and J. A. Hare. 2009. Relationships between larval and juvenile abundance of winter-spawned fishes in North Carolina, USA. Marine and Coastal Fisheries: Dynamics, Management, and Ecosystem Science 1: 12-21.
- Turner, R.E., Schroeder, W.W. and W.J. Wiseman Jr. 1987. The role of stratification in the deoxygenation of Mobile Bay and Adjacent Shelf Bottom Waters. Estuaries 10(1): 13-19.
- Vaughan, D.S., Shertzer, K.W., and J.W. Smith. 2007. Gulf menhaden (*Brevoortia patronus*) in the US Gulf of Mexico: Fishery characteristics and biological reference points for management. Fisheries research 83(2-3): 263-275.
- Vinagre, C., Santos, F.D., Cabral, H.N., and M.J. Costa. 2009. Impact of climate and hydrology on juvenile fish recruitment towards estuarine nursery grounds in the context of climate change. Estuarine, Coastal and Shelf Science 85(3): 479-486.
- Walker, N.D., and A.B. Hammack. 2000. Impacts of winter storms on circulation and sediment transport: Atchafalaya-Vermilion Bay region, Louisiana, USA. Journal of Coastal Research 16(4): 996-1010.
- Wang, F. 1997. Dynamics of intertidal marshes near shallow estuaries in Louisiana. Wetlands Ecology and Management 5(2): 131-143.

- Warlen, S.M., and J.S. Burke. 1990. Immigration of larvae of fall/winter spawning marine fishes into a North Carolina estuary. *Estuaries and Coasts* 13(4): 453-461.
- Werner, F.E., Blanton, B.O., Quinlan, J.A., and R.A. Luettich Jr. 1999. Physical oceanography of the North Carolina continental shelf during the fall and winter seasons: implications for the transport of larval menhaden. *Fisheries Oceanography* 8(2): 7-21.
- Whitehead, P.J.P., 1985. FAO Species Catalogue. Clupeoid fishes of the world (Suborder Clupeoidei). An annotated and illustrated catalogue of the herrings, sardines, pilchards, sprats, shads, anchovies and wolf-herrings. Part 1 – Chriocentridae, Clupeidae and Pristigasteridae. FAO Fisheries Synopsis, Rome 125(7/2); 305-579.
- Whitehead, P.J.P., Nelson, G.J., and T. Wongratana. 1988. FAO Species Catalogue. Vol 7. Clupeoid fishes of the world (Suborder Clupeoidei). An annotated and illustrated catalogue of the herrings, sardines, pilchards, sprats, shads, anchovies and wolf-herrings. Part 2 – Engraulidae. FAO Fisheries Synopsis, Rome 125(7/2); 305-579.
- Whitfield, A.K. 1989. Ichthyoplankton interchange in the mouth of a southern African estuary. *Marine Ecology Progress Series* 54(1-2): 25-33.
- Wilson, C.A., and D.L. Nieland. 1994. Reproductive biology of red drum, *Sciaenops ocellatus*, from the neritic waters of the northern Gulf of Mexico. *Fishery Bulletin* 92(4): 841-850.
- Wiseman Jr, W.J., Grymes III, J.M., and W.W. Schroeder. 1998. Coastal wind stress variability along the northern Gulf of Mexico. In: Editors Dronkers, J. et al. 1988. Physics of estuaries and coastal areas: Proceedings of the 8th International Biennial Conference on physics of estuaries and coastal seas. The Hague, Netherlands, 9-12 September 1996. pp. 55-61.
- Wong, K.C., and A. Münchow. 1995. Buoyancy forced interaction between estuary and inner shelf: Observation. *Continental Shelf Research* 15(1): 59-88.
- Wood, R.J. 2000. Synoptic scale climatic forcing of multispecies fish recruitment patterns in Chesapeake Bay. Doctoral dissertation. The College of William and Mary, Williamsburg, Virginia.
- Wood, S.N. 2001. mgcv: GAMs and Generalized Ridge Regression for R. *R News* 1(2):20-25.
- Zastrow, C.E., Houde, E.D., and L.G. Morin. 1991. Spawning, fecundity, hatch-date frequency and young-of-the-year growth of bay anchovy, *Anchoa mitchilli*, in mid-Chesapeake Bay. *Marine Ecological Progress Series* 73:161-171.

Zein-Eldin, Z.P., and M.L. Renaud. 1986. Inshore environmental effects on brown shrimp, *Penaeus aztecus*, and white shrimp, *P. setiferus*, populations in coastal waters, particularly of Texas. Marine Fisheries Review 48(3): 9-19.

CHAPTER 4. AGE, GROWTH, AND RECRUITMENT FROM OTOLITH MICROSTRUCTURE FOR LARVAL *MICROPOGONIAS UNDULATUS*

Atlantic croaker (*Micropogonias undulatus*) is an important commercial species in the Gulf of Mexico, but the stock has been historically drawn down as bycatch from other fisheries. Atlantic croaker collected within a tidal pass in Louisiana over a two year period, from October 2006 to March 2007 and from September 2007 to March 2008, had the sagittal otoliths (N=190) removed and analyzed using digital imaging and Fast Fourier Transformations for age and growth analyses. Standard length (SL) at age in days post hatch (dph) was estimated using a Laird-Gompertz growth model on the pooled data ($SL = 1.5 \cdot e^{\{2.61372[1 - e^{(-0.026186 \cdot dph)}]\}}$) over both years. Laird-Gompertz growth models were also fit separately to year and season to determine if different spawning subgroups exist. In both years, the maximum growth rate with respect to dph in the spring occurred approximately 20 days earlier than the fall. Digital image measurements were used to investigate fine-scale otolith microstructure to determine if offshore spawned larvae may have experienced growth discontinuities as they transgressed different water masses along their recruitment corridor to their estuarine nursery. The approximate age at which the larvae encounter differing water mass characteristics was determined to be 37 dph. Length frequency at age keys were used to determine temporal variability in *M. undulatus* spawning, with the highest frequency of hatch dates occurring during November in 2006 and 2007. Growth rates are similar to previous studies in the northern Gulf of Mexico, and growth rate increases occurred upon encountering lower salinity waters indicative of the coastal boundary zone and estuary.

4.1 Introduction

Micropogonias undulatus (Linnaeus, 1776), Atlantic croaker, have a distribution ranging in the Western Atlantic from the Gulf of Maine to the northern Gulf of Mexico (GOM). In addition, their range may potentially extend into the southern GOM, the Lesser Antilles and southern Caribbean, and from Brazil through southern Argentina (Smith, 1997). *Micropogonias undulatus* stock status is unknown (NMFS, 2009; NMFS, 2012), although it is expected to be

below the maximum sustainable yield. The amount of Atlantic croaker harvested commercially has been cyclic, ranging from 1,100 metric tons (t) to over 15,000 t per year, with current levels at approximately 9,000 t, with a value of approximately eight million US dollars (NMFS, 2009; NMFS, 2012). One source of this catch variability is the high variability in their recruitment patterns, which have been shown to be driven by environmental conditions on both small and large spatial and temporal scales, such as wind field patterns, storm frequency, salinity, temperature, hypoxic zones, and GOM basin circulations (Norcross, 1983; Norcross and Austin, 1988; Able 2005; Eby et al., 2005; Montane and Austin, 2005).

Further compounding the status of the commercial stock is the amount of *M. undulatus* caught as bycatch, principally through shrimp trawling. Within the shrimp trawl fishery of the GOM and South Atlantic Bight (SAB), 60% to 80% of the catch by weight is comprised of bycatch (NMFS, 2009; NMFS, 2012). Annually this can total from 100,000 to 400,000 t, with data from the 1990s suggesting *M. undulatus* may have made up almost 73% of the total bycatch of short-lived demersal species (NMFS, 2009; NMFS, 2012). Southeast Area Monitoring and Assessment Program (SEAMAP) samples from 1986-2006 showed Atlantic croaker to be the dominant bycatch species by weight at depths less than the 30 m isobath for the area off the Louisiana coast, regardless of sampling period during the year. At greater than 30 m depths, *M. undulatus* is either the second or third highest bycatch by weight, depending on the time period of sampling (Helies and Jamison, 2009). Because of these high mortality pressures from bycatch and directed fishing, survival in the larval stage is believed to be critically important in stock success because minor variation in mortality in the early life history stages can greatly affect recruitment rates (Norcross, 1983; Diamond et al., 2000).

Atlantic croaker larvae have a spawning peak from July through December and an estuarine recruitment peak in October/November (Cowan, 1988; Ditty et al., 1988; Warlen and Burke, 1990; Barbieri et al., 1994). Atlantic croaker spawn over a wide range of inner continental shelf depths, i.e., 54 meters or shallower, with a portion of the population moving inshore towards the estuaries to complete spawning in the winter and early spring months (Barbieri et al., 1994). Hydrologic variability at large and small spatial and temporal scales can greatly affect the numbers of *M. undulatus* larvae able to successfully recruit to estuarine nursery grounds (Norcross, 1983; Shaw et al., 1988; Raynie, 1991; Raynie and Shaw, 1994). Once in the estuary, survival during their first winter is primarily effected by lower temperatures increasing mortality, as verified in both the field (Norcross and Austin, 1981; Hare and Able, 2007), and laboratory (Lankford and Targett, 2001a/b).

Previous studies on *M. undulatus* age and growth have generally focused on the Mid-Atlantic Bight (MAB) and the southeastern United States, with limited studies occurring in the GOM. These studies have utilized linear growth rate models from otoliths aged using visual techniques, and have found growth rates between 0.16 and 0.27 mm day⁻¹ (Warlen, 1982; Thorrold et al., 1997), while in the GOM growth rate was determined to be 0.19 mm day⁻¹ (Cowan, 1988). Differing growth rates for larval *M. undulatus* during the spawning and estuarine recruitment peak in the late summer and early fall, and lower larval growth rates occurring during the over-winter period and into the spring have led to the suggestion that different spawning subgroups may exist (Warlen, 1982). This is further supported by differing growth rates and recruitment dynamics based on latitude along the estuaries of the MAB and SAB (Chittendbn and Jones, 1994; Thorrold et al., 1997).

Otolith daily growth increments, first described by Pannella (1971, 1974), have been confirmed in the genus *Micropogonias* (Campana, 1984; Cowan, 1988; Albuquerque et al., 2009). Otolith daily rings can not only provide information on growth rates, but they can also be used to estimate approximate times of larval ingress, i.e., transport from offshore spawning grounds to estuarine nurseries (Hoover et al., 2012). For example, previous studies have found that the timing for ingress of *M. undulatus* larvae along the western Atlantic estuaries varies between 30 and 60 days after hatch (Warlen, 1982; Warlen and Burke, 1990; Hettler and Hare, 1998; Hoskin, 2002; Hoover et al., 2012). The daily periodicity of larval otolith rings has also been used to help determine the structure of environmental parameters affecting growth and survivorship (Campana, 1999; Campana and Thorrold, 2001). Differences in ring width at length have also been used to determine within season cohorts for *Clupea harangus*, based on variable growth between seasons in the same year (Brophy and Danilowicz, 2002).

Analysis of larval otolith structure was initially done by visual inspection; however, video and digital methodologies have become prevalent with the increase in computing resolution and digital imaging (Ralston and Williams, 1989; Campana, 1992; Morales-Nin et al., 1998). Regardless of what ring counting methodology is being used, the ring structure must be verified because the shape and relative size of otoliths are under genetic regulation and thus species specific (Schmitt, 1969; Gaemers, 1976; Nolf, 1985; Lombarte and Morales-Nin, 1995; EFAN, 1997; Morales-Nin et al., 1998).

The objectives of this study were as follows. First, define and determine an iterative digital filtering mechanism for accurate determination of daily increments in *M. undulatus* larval otoliths. Second, determine the length at age of *M. undulatus* larvae collected in a tidal pass in

the northern GOM from fall through spring over a two year recruitment period. Third, compare observed larval growth rates determined from linear and non-linear growth models to previous studies. Fourth, to estimate coastal boundary zone/estuarine ingress times through the tidal pass based on daily counts corrected for hatching date and time of first ring formation. Finally, to determine the effect of hydrodynamic patterns associated with the differences between continental shelf and estuarine waters on larval *M. undulatus* growth.

4.2 Materials and Methods

4.2.1 Sampling Location

Ichthyoplankton sampling was conducted in Bayou Tartellan, near the Port of Fourchon, Fourchon, Louisiana (Figure 4.1). Bayou Tartellan and Bayou LaFourche are the first major inland channel bifurcations from the connection with the Gulf of Mexico at Belle Pass (29° 5' 53.9" N, 90° 13' 17.8" W). The area represents a well-mixed tidal pass (i.e., little temperature, salinity or dissolved oxygen stratification) having high turbidity, and a relatively small drainage basin contributing a low volume of freshwater input. The sampling site (29° 6' 49" N, 90° 11' 4" W) consisted of a single location where passive plankton net sampling was conducted in approximately 10 meters of water from a dock extending 3.7 meters from the northern bank into an approximately 73 meter wide tidal pass.

4.2.2 Field Sampling Methodology

Ichthyoplankton sampling was conducted using a fixed davit at the end of the dock, which suspended a stainless steel cable from above the sampling deck to the channel bottom. Passive plankton samples were taken using a 60-cm ring net (333 μ m mesh, 2 meter length) dyed dark green to minimize visual avoidance and attached to a gimbal with a vane for orientation into

the current. A plastic vinyl coated cod-end with 333 μm mesh drainage ports was attached to the end of the net to facilitate sample collection. A General Oceanics flowmeter (model no. 2030 with slow velocity rotor) was positioned just off center of the ring to determine volume of water filtered.

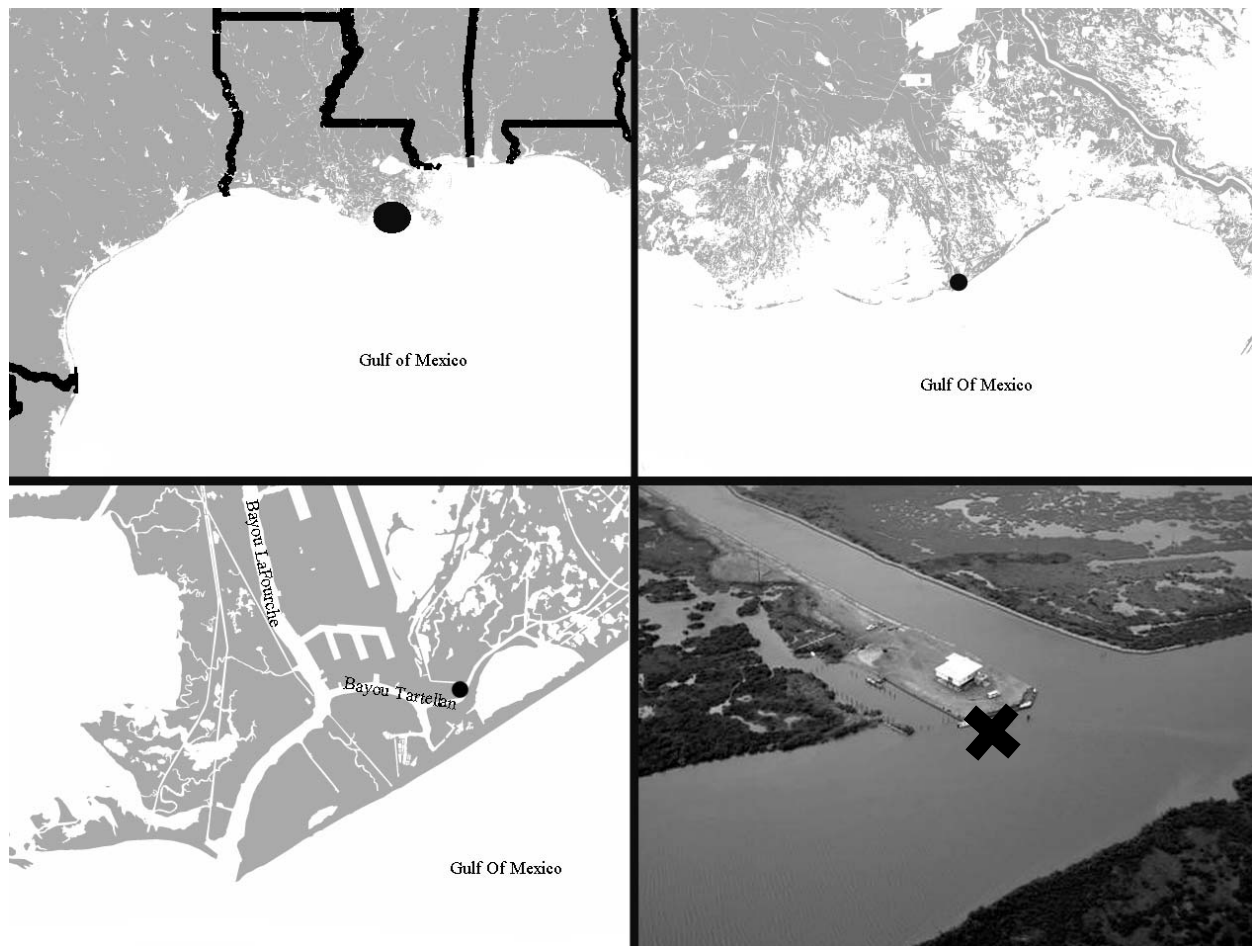


Figure 4.1: Map of the study location in relation to the Gulf of Mexico and coastal Louisiana. The points in black represent the sampling location, with the final panel being the sampling location from an aerial photograph of Bayou Tartellan. The X in the last panel marks the location of an extended dock used as a sampling platform and later destroyed by Hurricane Gustav.

Ichthyoplankton samples were collected every four hours over a 72-hour period, twice monthly between the months of October and April over a two year period (2006 – 2008), except

for December and January, which were only sampled monthly. In addition, there were two sampling efforts made in September 2007. The sampling season was chosen to maximize encounters of wind-dominant meteorological events (i.e., atmospheric cold front passages) from late fall to early spring. Individual sampling dates were chosen to maximize astronomical tidal ranges. During sampling, both a surface and a near-bottom, passive, zooplankton collection was randomly taken. Surface collections were six minutes long, and near-bottom collections were ten minutes to compensate for vertical differences in current speed and ultimately volume of water filtered (i.e., sampling effort). For near-bottom collections, the net mouth was closed on deployment until in position, opened for sampling, and subsequently closed for retrieval to prevent vertical contamination of the sample during transit through the water column. Nets were rinsed and washed down using a freshwater source to avoid contamination.

Ichthyoplankton samples were initially preserved in 10% buffered (sodium phosphate, dibasic $\text{NaH}_2\text{PO}_4 \cdot \text{H}_2\text{O}$ and monobasic Na_2HPO_4) formalin for approximately 3.5 hours as a short-exposure, long-term fixative. Samples were then rinsed and switched into a 70% ethanol solution for long-term storage, and later access for larval fish otolith work.

Estuarine hydrographic parameters were measured dockside during each plankton sample using a portable YSI (model no. 85) to record temperature, conductivity (salinity) and dissolved oxygen. A continuously sampling YSI (model no. 600R) moored on the bottom offshore of the dock, also measured the same parameters. Hydrographic data were periodically downloaded as necessary and archived for storage. Data concerning predicted diurnal tides, measured tide height, and the resulting alteration in the expected tidal prism were from a nearby tide gauge

station (Station ID: 8762075) at the Port of Fourchon, Fourchon, Louisiana (29° 6.8' N, 90° 11.9' W).

A bottom-mounted, upward-looking Acoustic Doppler Current Profiler (ADCP, RDI 1200 KHz Broadband Workhorse) was placed in the center of Bayou Tartellan (offshore of the dock) to measure the vertical profile of current velocity and direction. Boat surveys along Bayou Tartellan and Bayou LaFourche out to Belle Pass were also conducted using downward-looking ADCPs to provide a channel-wide correction factor for the mid-channel stationary upward-facing ADCP. A volume transport (m^3/s) was calculated for Bayou Tartellan from these data. To remove the tidal and inertial effects, a 6th-order 40-hr Butterworth low-pass filter was applied to the raw volume transport to produce a **net water transport** (m^3/s). These net transport data effectively show the lower-frequency subtidal oscillations associated with cold front events and other wind forcing, while filtering out the higher frequency diurnal tidal oscillations (Li et al., 2009).

4.2.3 Laboratory Methodology

In the lab, ichthyoplankton collections with a volume of material greater than 200 mL were split in half using a box plankton splitter, and those with a volume greater than 400 mL were split into quarters. Samples were sorted under a dissecting stereoscope and all ichthyoplankton were removed. A subset of sorted samples was checked for completeness of ichthyoplankton removal by a second party.

Ichthyoplankton were identified to the lowest taxonomic level possible, depending on size of the organism and physical condition. Some larval fish that were difficult to identify were stained using Alizarin blue and Alizarin red to facilitate meristic counts. *Micropogonias*

undulatus larvae were separated and stored for otolith analysis. Identifications were based on the following literature: Miller and Jorgenson (1973); Fritzsche (1978); Hardy (1978a, 1978b); Johnson (1978); Jones et al. (1978); Martin and Drewry (1978); Colton et al. (1979); Leak (1981); Houde (1982); Stuck and Perry (1982); Fahay (1983); Moser (1984); Ruple (1984); Richards (2006); Fahay (2007).

Micropogonias undulatus larvae were subsampled for otolith analysis based on a normal distribution of standard length (SL) of all *M. undulatus* larvae collected. Measurement of SL to the nearest 0.1 mm was conducted using a Leica MZ6 stereoscope calibrated against a stage micrometer. *M. undulatus* larvae were subsampled from every sampling effort that contained the target species. In samples where three or less *M. undulatus* larvae were collected, all larvae were scheduled for otolith removal. In samples that contained greater than three *M. undulatus* larvae, three were selected so that the longest SL, shortest SL, and a SL from the normal distribution were scheduled for otolith removal.

4.2.4 Otolith Removal, Preparation, and Interpretation

Removal and preparation of sagittal otoliths from *M. undulatus* larvae selected for dissection followed the methodology described by Barbieri et al. (1994a/b). All dissections were conducted using an Olympus SZX12 stereoscope with a 1x objective. Both left and right sagittal otoliths were removed and placed on a slide using Permount[®], with the left otolith cusp side up, and the right otolith cusp side down. Otoliths were polished using 0.3 µm alumina paste and microcloth to reveal the core. Otoliths were etched using a 0.1 N HCL acid for between 10 and 20 s to facilitate reading under a compound stereoscope. Digital images were taken using an

Olympus BX41 compound stereoscope, with a phase contrast filter to highlight light and dark ring discontinuity zones, under magnification from 500x to 1250x under oil immersion.

Images were post-processed using Adobe Photoshop CS4[®] (v11.0) to convert the image from color to gray scale, and to enhance differences between light and dark rings by means of increasing the image contrast and improving the illumination. Otolith radii and measurements of grey scale values for each radius were conducted using ImageJ[®] (v1.44p) photo software. Measurement of any radii produces a calibrated length and corresponding grey scale values ranging from 0 (black) to 255 (white) along that radius. A central radius and two radii to the left and right of the central radii, offset by a single pixel each, were measured. All five radii were averaged to produce the grey scale values used for filter analysis, to avoid the bias that could be introduced by choice of the reading radius and making a reading radius that becomes the average of a 5 pixel radius for any point along the radius (Morales-Nin et al., 1998). Radius length and grey scale data were collected for each otolith that was imaged.

Image data were imported into MATLAB (v7.6.0.324 R2008a) for filtering and age determination. Initial radii measurements were treated as being in the time domain for the purposes of filtering due to the growth of increments being directly related to age in days. Filtering was done using a Fast Fourier Transform (FFT) to determine the appropriate low pass filter structure to exclude high frequency sub-daily discontinuities on the otolith radius. Filter design was based on a low pass filter fit iteratively to the individual otoliths based on the understanding that the nyquist frequency is the daily otolith ring accreted by the larvae. As noted by Morales-Nin et al. (1998) this iterative fitting is done for each otolith due to increments of varying radius length between otoliths, differences in magnification, and variable growth rates

for individuals. An Inverse FFT was then done to transform the signal back into the time domain for determination of the location of the sinusoidal peaks, and thus the position and width of the respective rings along the reading radius. There were ten otoliths that were selected at random and ran using this methodology twice, independently, to compare against a traditional eye reading for error and difference in ring count. All ten otoliths showed the same number of rings after both FFT methodology, and only one differed by one ring based on a visual reading of the otolith.

4.2.5 Otolith Ageing and Larval Hatch Dates

Larval age recorded in days post hatch (dph) was determined from the increment counts for each otolith radius using the methodology previously described. Daily increment deposition has been confirmed to have a positive relationship to larval *M. undulatus* growth (Searcy, 2005). Following the methodology used by Cowan (1988), we applied a four day lag for first increment formation post-hatch for *M. undulatus* larvae, based on laboratory work (Peters et al., 1978, Warlen and Chester, 1985, University of Texas Mariculture Program Rep., 1982-1983). This resulted in a calculation of total age that follows an equation of the form:

$$Age_{dph} = Increments_{total} + \varphi, \quad \text{where } \varphi = 4$$

where Age_{dph} represents the age in days from hatch to collection, $Increments_{total}$ represents the number of increments determined from the digital analysis, and the value of φ is the applied number of days from hatch to the deposition of the initial growth increment. Ages were estimated for larvae not selected for dissection by use of frequency of age at length keys utilizing the FSA package for R Software (v2.14.0).

Determination of hatch dates were calculated for all *M. undulatus* larvae, direct calculation was done for those larvae where otolith radii were analyzed and also for those where the age was estimated in the methodology described previously. The hatch date was determined using the following equation:

$$Date_{hatch} = Date_{capture} - Age_{dph}$$

where $Date_{hatch}$ represents the hatch date for that particular larvae, $Date_{capture}$ represents the sample date when that larvae was collected, and Age_{dph} represents the age in days from hatch to collection.

4.2.6 Growth and Estuarine Ingress

For comparison to previous studies of larval *M. undulatus* growth, a linear model was applied to allow direct comparison of our results. A non-parametric smoother was also applied to determine the applicability of selecting a non-linear model for growth rate. Since larval growth is slowest near the hatch date, increases thereafter, and slows again as the larvae settles and begins further organ and sensory development, a derivative of the Gompertz model was selected as the non-linear model as it highlights this specific pattern of growth (Gompertz, 1815).

Micropogonias undulatus larval somatic growth was modeled using only the directly analyzed otolith data by a Laird-Gompertz growth model (Laird et al., 1965; Zweifel and Lasker, 1976; Lozano et al., 2012). The model had a set intercept of $L_{null} = 1.5 \text{ mm SL}$ to accurately represent the hatching length (dph=0; Warlen, 1981, Cowan, 1988, Barbieri et al., 1994). The Laird-Gompertz growth model is represented by the following equation:

$$L_t = L_{null} e^{k(1-e^{-at})}$$

where L_t represents the SL (mm) at an age t (days), L_{null} represents the SL at hatch for *M. undulatus*, a is the rate of exponential decay, and k is a dimensionless parameter so that ka represents the instantaneous growth rate at hatching. Hind-casting to estimate growth rates for larvae at ages not sampled, due to larvae being offshore at these early ages, can be accomplished using the Laird-Gompertz growth model (Lozano et al., 2012).

Instantaneous growth rates, i.e., the rate of growth at a particular time in dph, were estimated using the maximum growth rates calculated from both the first derivative of the Laird-Gompertz modeled equation, and mean growth rates based on a 10 day interval. The first derivative of the Laird-Gompertz equation has the following equation:

$$G_{DI} = L_{null} e^{k(1-e^{-at})} * (kae^{-at})$$

where G_{DI} represents the instantaneous daily growth rate through the first derivative of the Laird-Gompertz model, and all other parameters have the same distinction as in the Laird-Gompertz growth model previously described. Mean growth rates for the 10 day interval were calculated with the following equation:

$$G_{10} = \frac{(L_{t2} - L_{t1})}{\Delta t}, \quad \text{where } t2 > t1$$

where G_{10} represents the average growth rate for that 10 day interval, L_{t2} represents the modeled SL at some point $t2$, and L_{t1} represents the modeled SL at some point $t1$. Instantaneous growth rates were then determined from the natural log of the lengths in the mean growth equation described above.

Estuarine recruitment date was determined from a difference in the width of the daily increments and variation in ring distance from the otolith core. Recruitment date was determined

as the point in dph where there was an increase in the ring diameter, and an increase in ring distance from the core. Movement by the larvae into the estuary, where there is lower salinity, increased nutrient loads, and higher primary production, has been shown to cause a rapid increase in growth for larvae and young-of-the-year juveniles (Hoss et al., 1988; Moser and Gerry, 1989).

4.2.7 Statistical Analysis

Distributions of lengths and calculated ages based on otolith extraction were tested for normality using a Shapiro-Wilk's test. A Mixed Model (MM) was applied using R Software (v2.14.0) to look at growth rates of individual larvae with respect to salinity, temperature, and net water transport in the tidal pass. The model used in the analysis had the following general form:

$$y_{ij} = \beta_0 + \beta_1 \text{Salinity}_{ij} + \beta_2 \text{WaterTemp}_{ij} + \beta_3 \text{NWT}_{ij} + \beta_4 \text{Tide}_{ij} + \tau_i + \varepsilon_{ij}$$

where y_i is the response variable of growth rate, β_0 is the intercept term, the β parameters represent the effect for each of the variables (i.e., salinity, water temperature, and NWT), with tide being a binary dummy variable for each of the tide states (i.e., flood or ebb), the τ_i term represents the random effect of sampling month when larvae were collected, and ε_{ij} is the random error term for the model.

4.3 Results

4.3.1 Hydrographic

Water temperatures based on sampling depth yielded no statistical differences, which is consistent with a vertically well-mixed tidal pass. Water temperatures ($\bar{x} = 20.51^\circ\text{C}$) generally had low variability during any sampling effort (Figure 4.2). However, from late November 2006

to early February 2007, recorded temperatures were colder and fluctuations were greater than other sampling efforts. In particular, the January 2007 sampling effort had a range of 10.2°C during the 72-hour sampling period. Generally, water temperatures followed the normal seasonal trends, i.e., water was warmer during the early fall (i.e., September and October) and cooled into the winter before rising again during March and April. There was a noticeable drop in

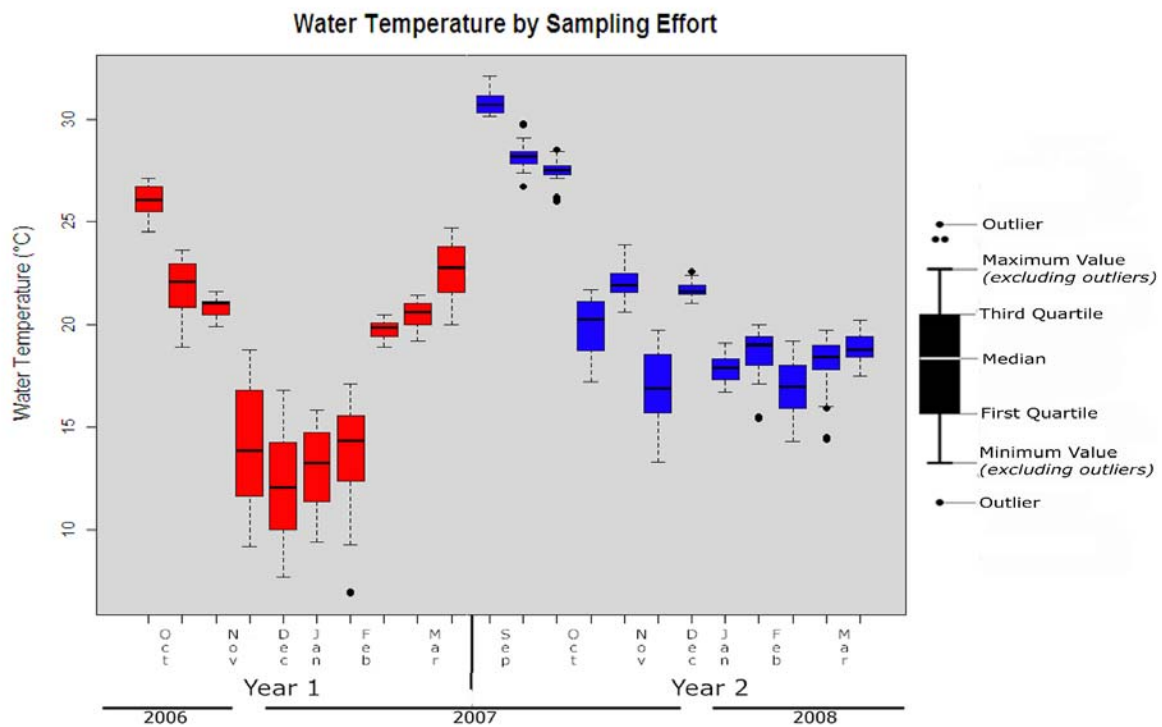


Figure 4.2: Water temperature variations by month across the two years of field sampling, year 1 (red) and year 2 (blue). Both years show a similar trend of decreased temperature from November through early February. Year two was generally warmer, although cooler water lasted into March 2008. High variability occurred during the months with coldest water temperatures.

temperature during November 2006, and median water temperature remained below 15°C through early February 2007. Although there was also a decrease in water temperature in

November 2007, the median water temperature did not fall below 17°C during the remaining year.

There were no statistically significant differences between surface or near-bottom salinities, once again supporting a well-mixed estuary. In general, 95% of all measured salinity values fell between 21.5 and 31.4 ppt with a total salinity range of 14.5 to 33.2 ppt and a mean of 27.32 ppt (Figure 4.3). Median salinity values dropped more than 5 ppt between December 2006

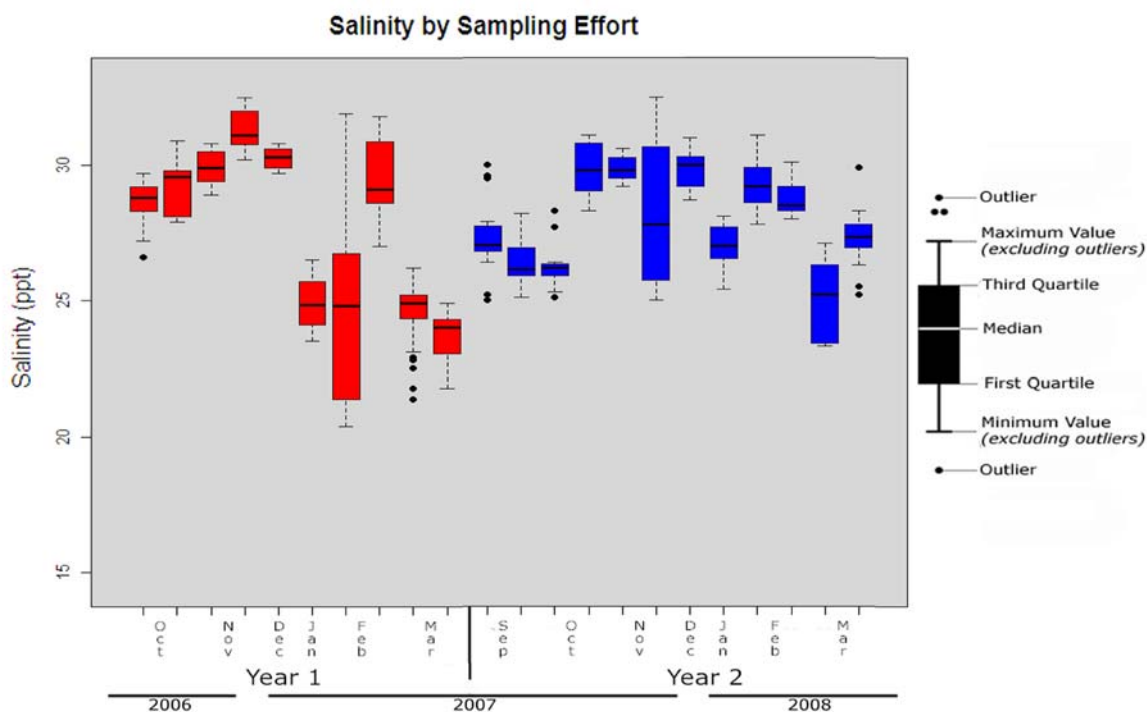


Figure 4.3: Salinity variation by month across the two years of field sampling. There was more variability across sampling efforts during year 1 (red) than year 2 (blue). Highest salinity variability occurred from November through March for both years.

and January 2007. Early February 2007 had a similar median value as January 2007, but had salinity ranges from as high as 32 ppt to nearly 20 ppt over a four day period. Aside from median salinities in late February 2007 of approximately 28 ppt, the median salinity in Bayou Tartellan

remained below 25 ppt until early April 2007. Salinities during late 2007 and early 2008, with the exception of early March, showed less variation and were generally higher than the previous sample year. However, early April 2008 samples had an extreme drop in salinity, with a minimum value less than 15 ppt, and extreme outlying values as high as 25 ppt. Sampling efforts in March (both years) and April 2007 had the lowest salinities, probably reflecting increased precipitation.

4.3.2 Larval *Micropogonias undulatus* Catches

There were 3,543 *M. undulatus* larvae collected in Bayou Tarellan during the sampling efforts from October 2006 to March 2008, 3,118 larvae collected in the period from October 2006 to March 2007, and 425 larvae collected from September 2007 to March 2008 (Figure 4.4). November 2006 accounted for 53.5% of the total number of *M. undulatus* larvae collected over both years. November 2007 collections had the greatest number of larvae again, but there was a second peak in March 2008.

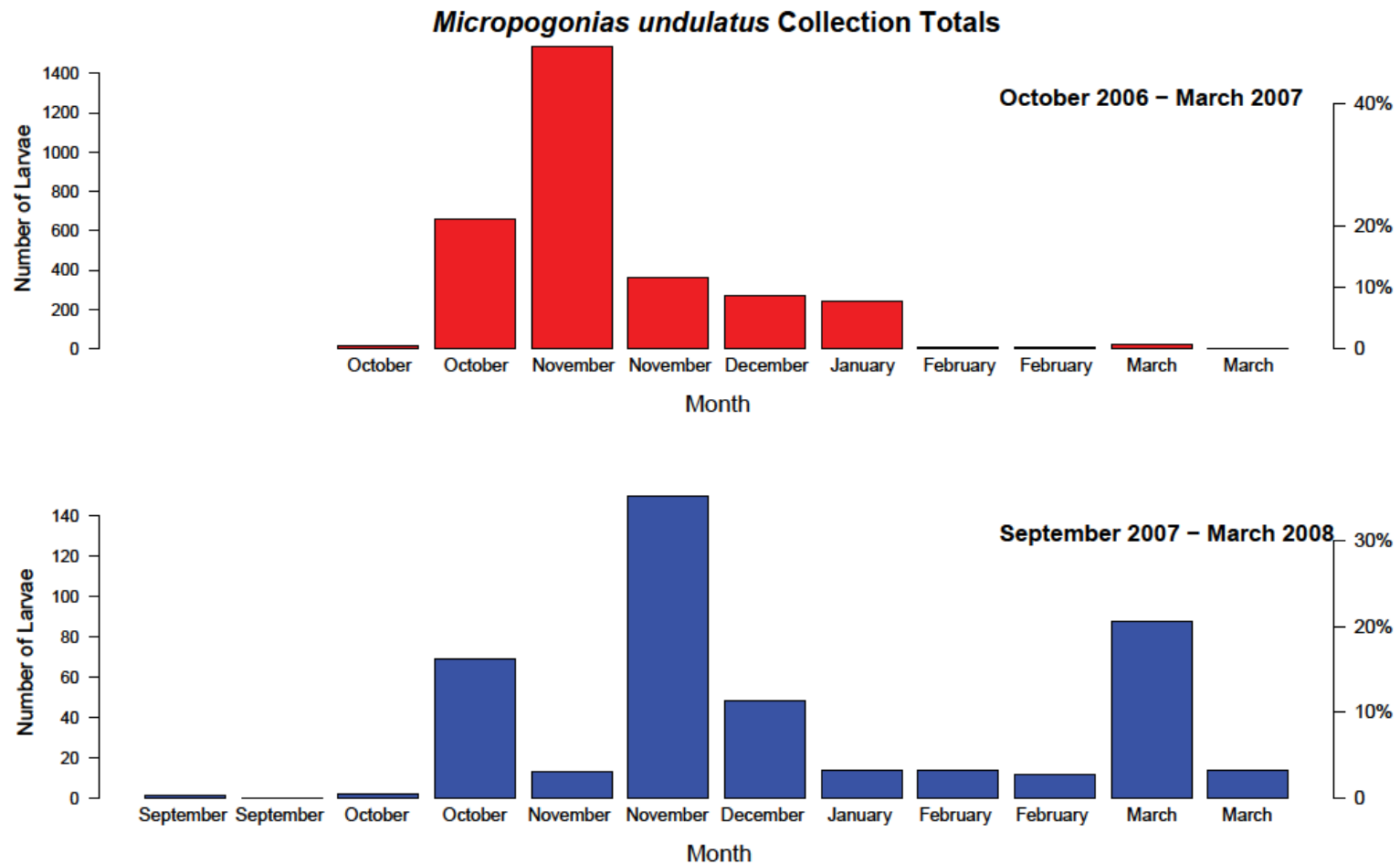


Figure 4.4: Histograms showing *M. undulatus* collected by sampling trip for October 2006 to March 2007, and September 2007 to March 2008. Peak numbers of larvae collected occurred from late October through November for both years. February 2008 through March 2008 saw a higher percentage of the total number of larvae collected in that year than the same period within 2007.

4.3.3 Length, Age, and Hatch Dates from Otolith Counts

There were a total of 203 *M. undulatus* larvae that had sagittal otoliths removed for analysis. Thirteen otoliths did not produce readable radii and were excluded. The length frequency plot of all larval *M. undulatus* that were aged ($N = 190$) followed a normal distribution (Shapiro-Wilk: $p = 0.4347$), with a mean of 8.3 mm SL ($sd = 5.4$ mm; range from 3.5 to 15.3 mm). During both sampling periods, i.e., October 2006 – March 2007 and September 2007 – March 2008, the mean length was 8.3 mm SL, but the distribution was flatter in year one ($sd = 2.5$ mm) than in year two ($sd = 2.0$ mm).

All of the larval *M. undulatus* ages also followed a normal distribution (Shapiro-Wilk: $p = 0.1066$) with a mean age of 41 dph ($sd = 10.14$), a median of 39 dph, and a range of 20 dph to 70 dph. Ages from the October 2006 to March 2007 sampling period had a strongly peaked distribution with a maximum density between 35 and 40 dph. Despite a similar peak in numbers of larvae between 35 and 40 dph, year two had generally higher densities between 30 and 45 dph.

In general, SL increased as the spawning and recruitment season progressed. Smaller larvae were more prevalent in September and/or October for both years (Figure 4.5). The median SL of larvae sampled began to stabilize in late November and early December for both years and remained relatively constant through the spring. In both sample years, the highest density of hatch dates occurred between 16th September and 31st October, with far lower numbers occurring in the rest of the months (Figure 4.6; Table 4.1). In year one, cumulatively, more than 95% of all estimated hatch dates had occurred before 15th January 2007, while during year two, the 95%

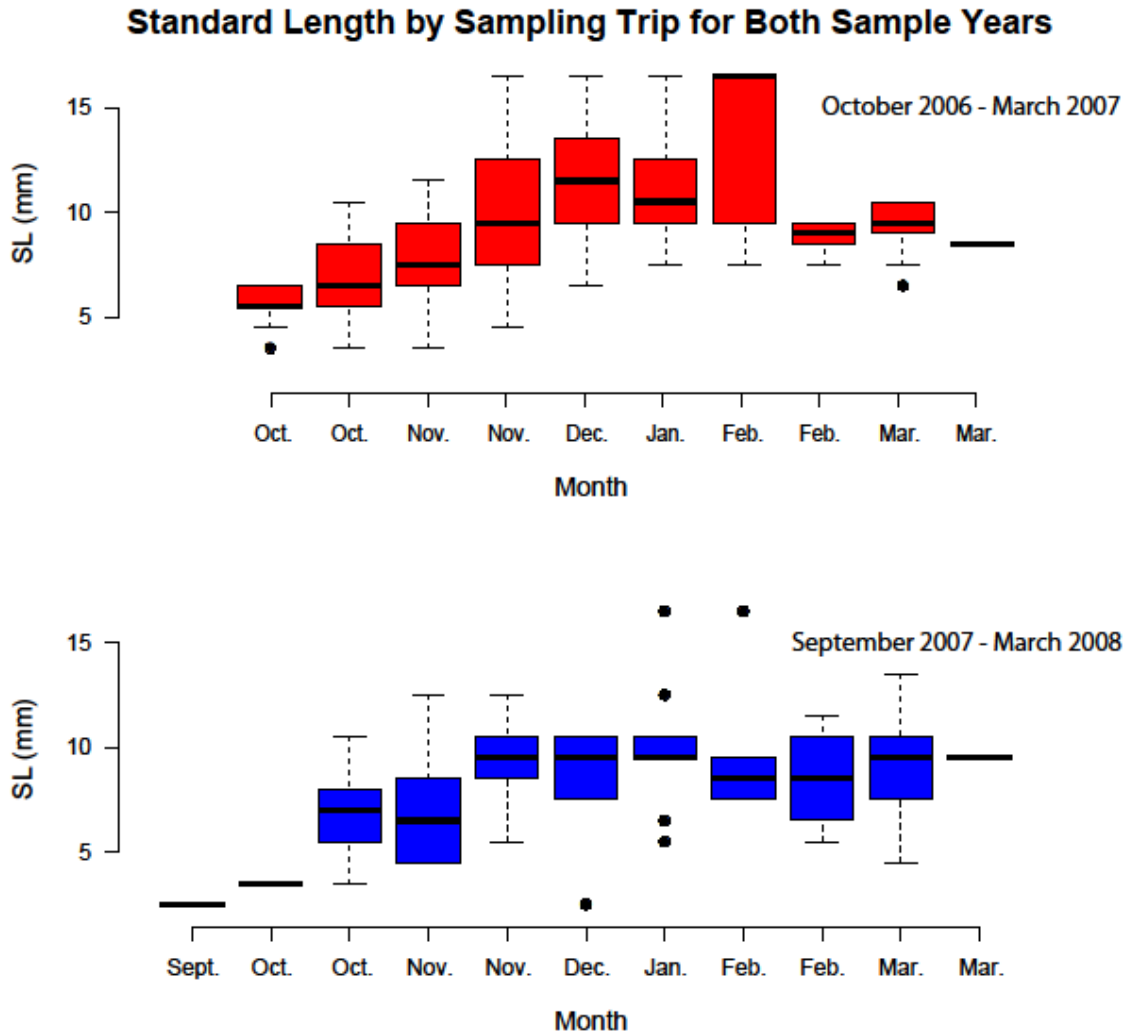


Figure 4.5: Boxplots of standard length (SL- mm) for *M. undulatus* larvae by sampling effort for each month. October 2006 to March 2007 (red) and September 2007 to March 2008 (blue) are both provided.

cumulative distribution was not reached until early February 2008, after a small, secondary peak in late January.

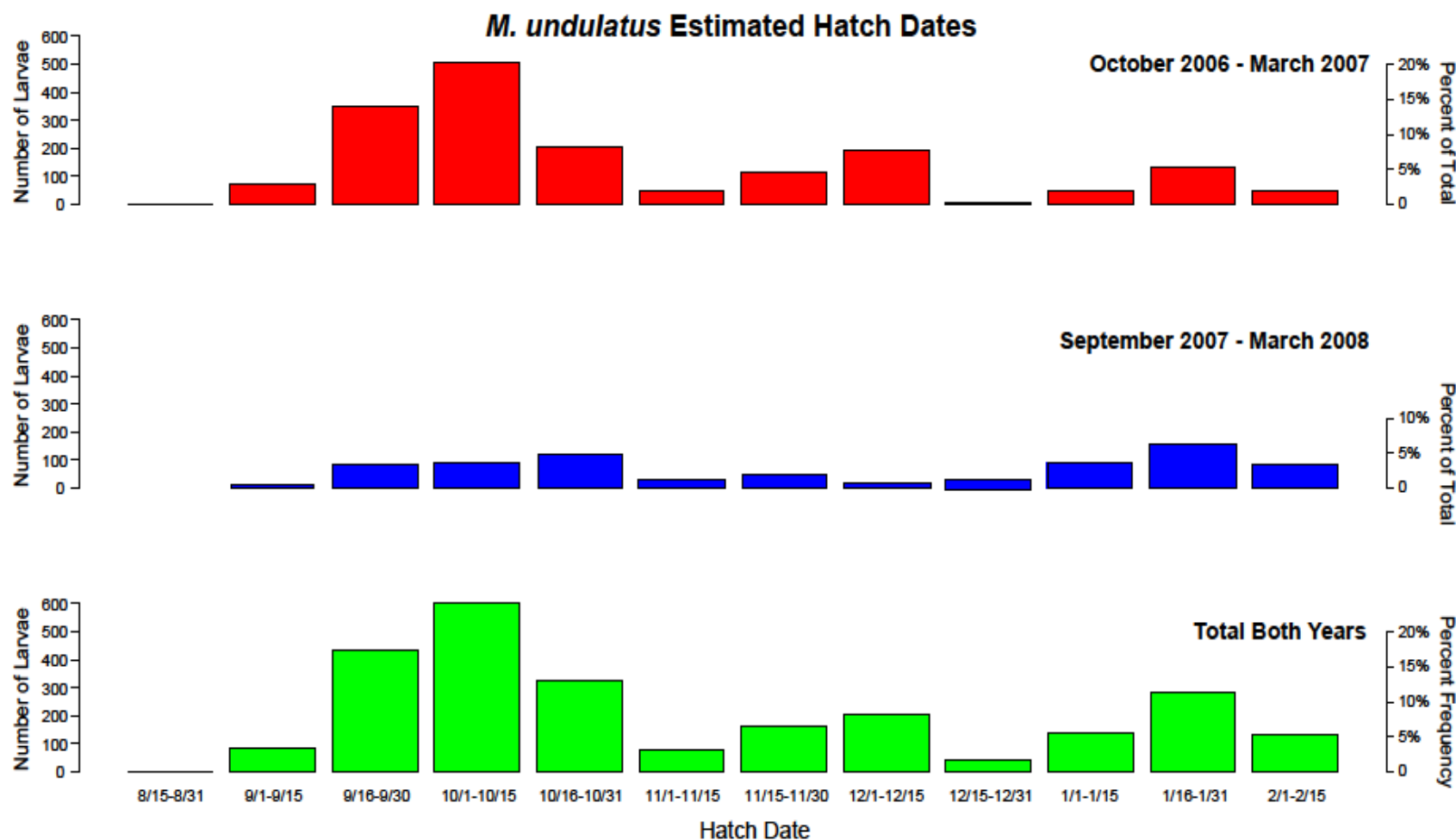


Figure 4.6: Histograms of estimated hatch dates for *M. undulatus* larvae. Data include directly measured otoliths and those estimated from age at length frequency keys. Estimated number of larvae sampled and percentages of the total from half month increments are provided for October 2006 – March 2007, September 2007 – March 2008, and both years combined.

Table 4.1: Hatch dates for larval *M. undulatus* based on back-calculated otolith ages and collection dates after application of length frequency keys. Percentages and cumulative percentages are based on half month intervals.

Interval	2006 - 2007		2007 - 2008	
	%	Cumulative %	%	Cumulative %
08/15 - 08/31	0.26	0.26	0.00	0.00
09/01 - 09/15	8.97	9.23	4.65	4.65
09/16 - 09/30	29.74	38.97	21.71	26.36
10/01 - 10/15	32.56	71.54	17.83	44.19
10/16 - 10/31	10.51	82.05	18.60	62.79
11/01 - 11/15	2.05	84.10	3.88	66.67
11/16 - 11/30	4.10	88.21	5.43	72.09
12/01 - 12/15	6.15	94.36	1.55	73.64
12/16 - 12/31	0.26	94.62	3.10	76.74
01/01 - 01/15	1.28	95.90	6.98	83.72
01/16 - 01/31	3.08	98.97	10.85	94.57
02/01 - 02/15	1.03	100.00	5.43	100.00
02/16 - 02/28	0.00	100.00	0.00	100.00

4.3.4 Modeled Growth Rates and Estuarine Ingress Dates

There was a significant linear relationship between measured lengths and ages for larval *M. undulatus* ($p < 0.0001$; $R^2 = 0.76$). The linear model had an average rate of growth of $0.198 \text{ mm} \cdot \text{d}^{-1}$, and an underestimation of the hatch length, with an intercept of 0.97 mm SL . The Laird-Gompertz growth model forced through the 1.5 mm hatch length provided a better model fit accounting for the slower initial growth rate, and for changes in growth rate due to sensory and organ development as length increased (Figure 4.7). There were slight differences in the Laird-Gompertz models of length by age for each of the two sample periods. The sampling period from

Length Versus Age for *Micropogonias undulatus*

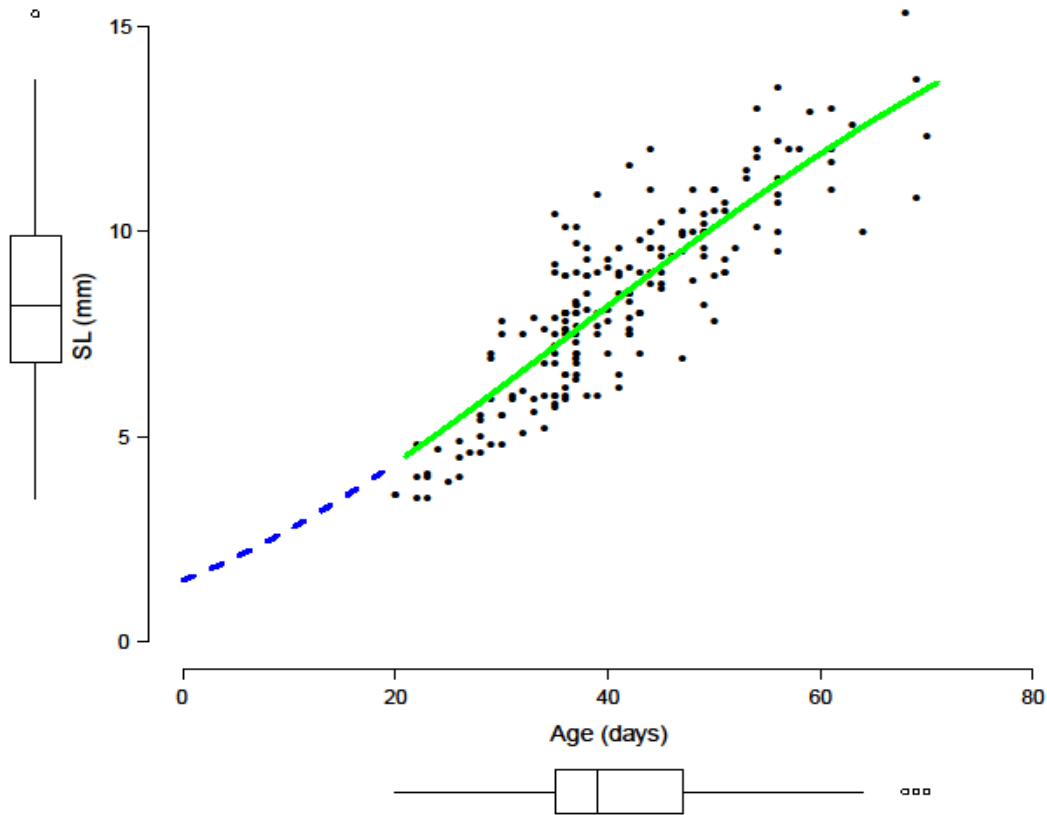


Figure 4.7: Laird-Gompertz growth model of larval *M. undulatus* as standard length (SL - mm) versus age (days post hatch - dph). The model is artificially forced through the intercept at the estimated 1.5 mm SL at hatch to accurately reflect growth rates of ages in dph less than the minimum age calculated. Boxplots showing the median, 25% and 75% quantiles, 95 percent confidence intervals, and outliers are provided for each axis. The Laird-Gompertz model is parameterized as: $SL = 1.5 \cdot e^{2.613272(1-e^{-0.026186 \cdot Age})}$.

September 2007 to March 2008 had larvae with a faster initial growth rate, but that growth rate leveled off and dropped below the October 2006 to March 2007 growth rates at lengths greater than 11 mm and ages greater than 55 dph (Figure 4.8).

***Micropogonias undulatus* Length Versus Age by Year**

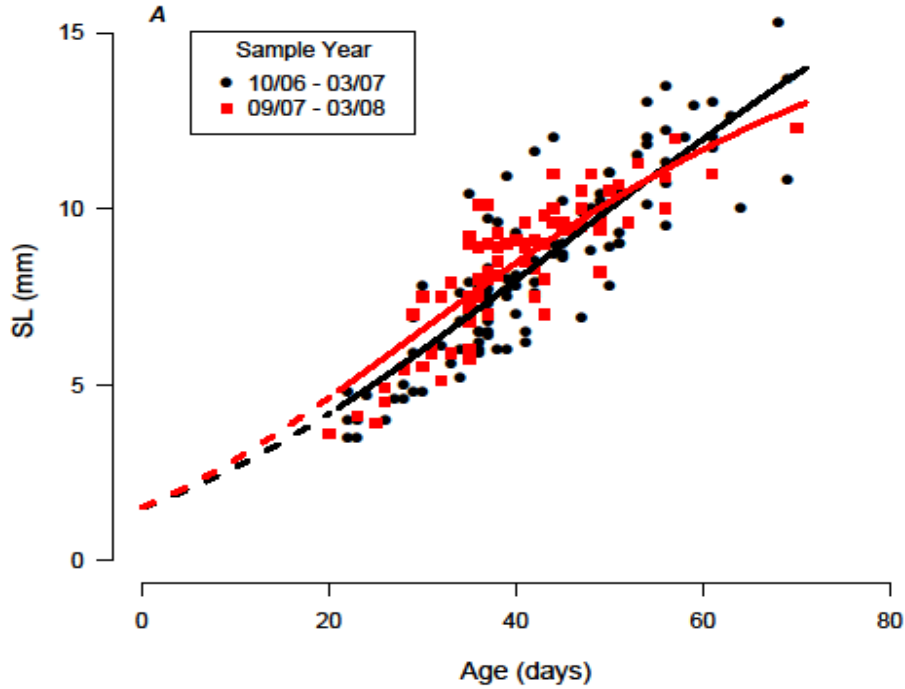


Figure 4.8: Laird-Gompertz growth models of larval *M. undulatus* as standard length (SL - mm) versus age (days post hatch - dph) for each of the two sample periods. The sample period from 10/06 to 03/07 is shown in black, and the Laird-Gompertz model had the following parameterization: $SL = 1.5 \cdot e^{2.77531(1-e^{-0.02300 \cdot Age})}$. The sample period from 09/07 to 03/08 is shown in red, and the Laird-Gompertz model had the following parameterization: $SL = 1.5 \cdot e^{2.422452(1-e^{-0.031297 \cdot Age})}$.

There were differences between the fall and spring in each year for length, age, and growth. Larvae collected during the peak spawning and recruitment season during the fall (i.e., September through December) of 2006 and 2007 were shorter and younger than those collected in the spring of 2007 and 2008 (Figure 4.9a). The fall of 2006 and 2007 had lower initial growth rates, but continued to increase and did not level off at older ages. In contrast, the spring of 2007

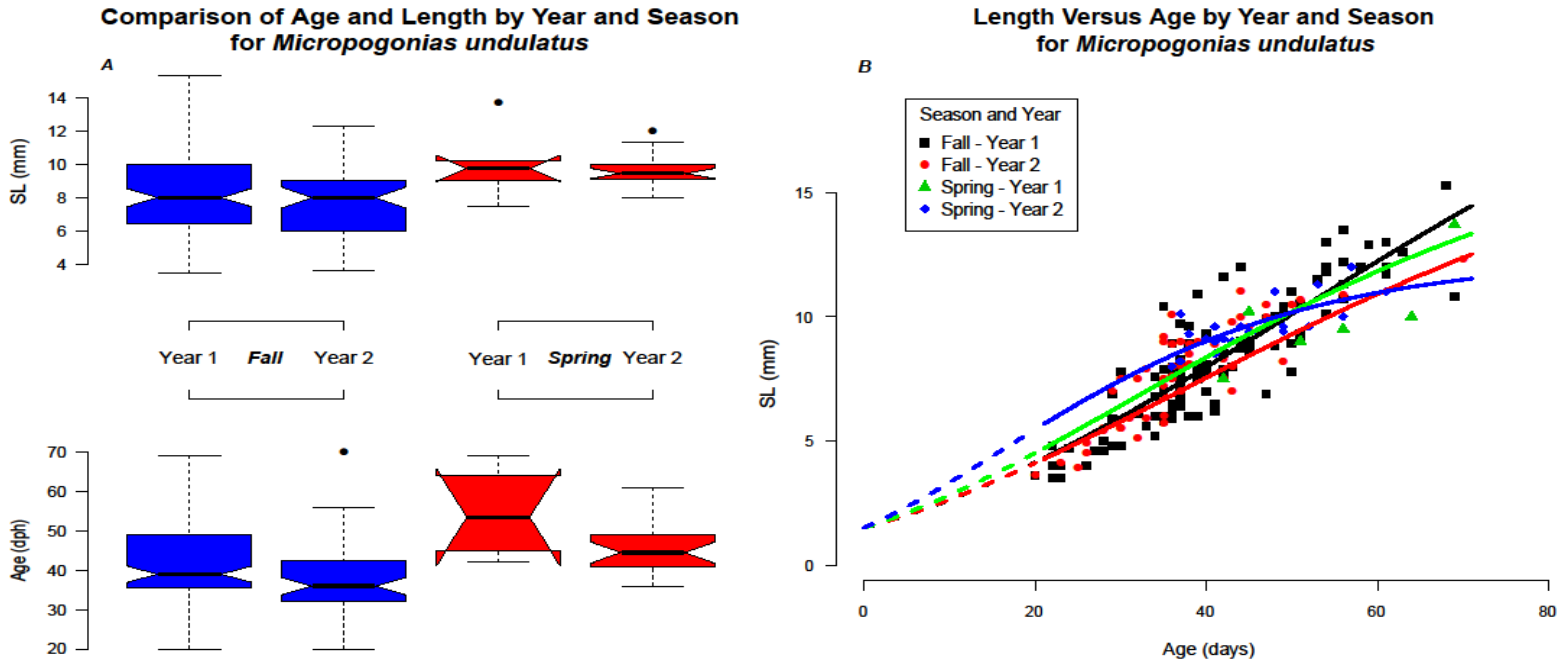


Figure 4.9: (A) Boxplots comparing larval *M. undulatus* otoliths with standard length (SL - mm) and age (days post hatch - dph) for the fall (blue) and spring (red) seasons in both sample years. Fall samples were similar in both age and length for both sample years, but were different from the spring in both age and length. Non-overlapping notches between any two boxplots represent “strong evidence” of statistically different median values (Chambers et al. 1983). (B) Laird-Gompertz growth models of larval *M. undulatus* otoliths as SL (mm) versus age (dph) for fall and spring from both sample years. The fall recruitment period from October to December, 2006, is shown in black, and the winter/spring recruitment period from January to March 2007 is shown in green. The fall recruitment period from September to December, 2007, is shown in red, and the winter/spring recruitment period from January to March 2008 is shown in blue. All models are forced through the intercept at the estimated 1.5 mm SL at hatch to accurately reflect growth rates of ages in dph less than the minimum otolith determined age. Model Parameterizations:

Fall – Year 1: $SL = 1.5 \cdot e^{2.89159(1-e^{-0.02155 \cdot Age})}$; Fall – Year 2: $SL = 1.5 \cdot e^{2.50594(1-e^{-0.02893 \cdot Age})}$;
 Spring – Year 1: $SL = 1.5 \cdot e^{2.54838(1-e^{-0.02512 \cdot Age})}$; and Spring – Year 2: $SL = 1.5 \cdot e^{2.11260(1-e^{-0.04726 \cdot Age})}$.

and 2008 had higher initial growth, but both leveled off quickly, and resulted in shorter fish at greater than 50 dph and 60 dph, respectively (Figure 4.9b). The difference in fall versus spring growth rate patterns was more pronounced in year two, when there were generally warmer water temperatures and lower salinities.

The age and magnitude of maximum growth rate for larval *M. undulatus* differed for the sampling year by season Laird-Gompertz models. Overall, the Laird-Gompertz models by year and season showed maximum rates with respect to dph in the fall occur approximately 20 dph later than in the spring. Fall 2006 and 2007 had a similar minimum growth rate of $0.093 \text{ mm} \cdot \text{day}^{-1}$, but fall 2006 had a higher maximum growth rate ($0.214 \text{ mm} \cdot \text{day}^{-1}$; 49 dph) than fall 2007 ($0.177 \text{ mm} \cdot \text{day}^{-1}$; 37dph; Figure 4.10). Spring 2008 had a greater initial instantaneous growth rate ($0.150 \text{ mm} \cdot \text{day}^{-1}$) compared to spring 2007 ($0.113 \text{ mm} \cdot \text{day}^{-1}$). Although, the maximum growth rate in spring 2008 ($0.216 \text{ mm} \cdot \text{day}^{-1}$) was greater than spring 2007 ($0.196 \text{ mm} \cdot \text{day}^{-1}$), it occurred at an earlier age (16 dph and 32 dph, respectively) and decreased rapidly thereafter. The ten day averages for the two sample years were slightly different, with year one having the highest average growth rate at $0.203 \text{ mm} \cdot \text{day}^{-1}$ between 40 to 50 dph (Table 4.2) correlating to a peak at 49 dph, and year two having the maximum growth rate of $0.193 \text{ mm} \cdot \text{day}^{-1}$ occurring between 20 and 30 dph, which is consistent with the larger relative peak at 16 dph during the spring of year two (Figure 4.10).

Overall similarities in the estimated average estuarine ingress date existed for both fall and spring seasons in both years, but there were differences between seasons in the mean ring distance from the otolith core. Regardless of season or year, otolith ring mean distance from the

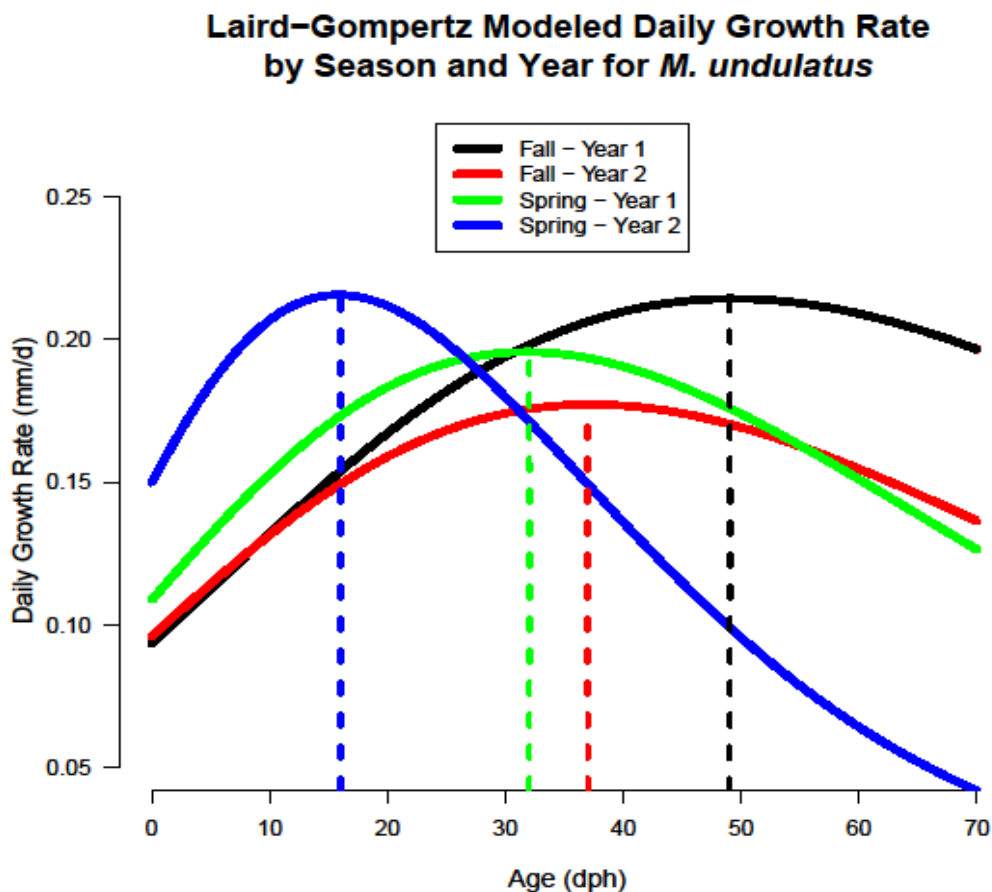


Figure 4.10: Maximum growth rates based on the derivative of the Laird-Gompertz growth model for larval *M. undulatus* otoliths. Daily growth rates ($\text{mm} \cdot \text{day}^{-1}$) are the slopes of the Laird-Gompertz models at any point in age (solid lines), and the maximum growth rates (dashed lines) are provided for fall 2006 (black), fall 2007 (red), spring 2007 (green), and spring 2008 (green). The maximum growth rate for the fall 2006 and 2007 was at 49 dph and 37 dph, respectively. The maximum growth rate for the spring 2007 and 2008 was at 32 dph and 16 dph, respectively.

core, as a proxy for growth, is fairly stable before 40 dph, and increased more rapidly and became more variable after that point (Figure 4.11a). In particular, spring 2007 and spring 2008 distances from the core were greater than the distances for the same age for the fall 2006 and fall 2007. Mean otolith ring width was somewhat constant at approximately $0.5 \mu\text{m}$ for the fall of

Table 4.2: Average growth rates and instantaneous growth rates for larval *M. undulatus* based on otolith data grouped by age blocks of ten days post hatch. Growth rates (g) and instantaneous growth rates (G) are provided for the October 2006 to March 2007 sampling period, the September 2007 to March 2008 sampling period, and the overall combined data.

Blocks (dph)	2006 - 2007		2007 - 2008		Overall	
	g (mm·day ⁻¹)	G (day ⁻¹)	g (mm·day ⁻¹)	G (day ⁻¹)	g (mm·day ⁻¹)	G (day ⁻¹)
0 - 10	0.115	0.057	0.138	0.065	0.124	0.060
10 - 20	0.152	0.045	0.175	0.048	0.161	0.046
20 - 30	0.181	0.036	0.193	0.035	0.187	0.036
30 - 40	0.198	0.029	0.190	0.025	0.196	0.027
40 - 50	0.203	0.023	0.173	0.019	0.192	0.021
50 - 60	0.198	0.018	0.149	0.014	0.178	0.016
60 - 70	0.185	0.014	0.122	0.010	0.158	0.013

both years and 1.1 μm for the spring of both years until 40 dph, when mean ring width became very much more variable, and generally increased with ring count thereafter (Figure 4.11b).

4.3.5 Statistical Analysis

The MM fit water temperature, salinity, and net water transport, by tide, to the estimated growth rate of all individuals collected during both study years with significant model terms for all continuous variables. The only model terms which were not significant at the *a priori* 0.05 alpha level were tidal stage, and salinity as a function of tidal stage. The non-significance of the tidal stage term is likely a function of masking due to the higher level interaction terms in the model.

The individual model terms generally showed a trend of increased growth rate with ingress through the tidal pass, supporting the otolith ring width and growth rate increases at

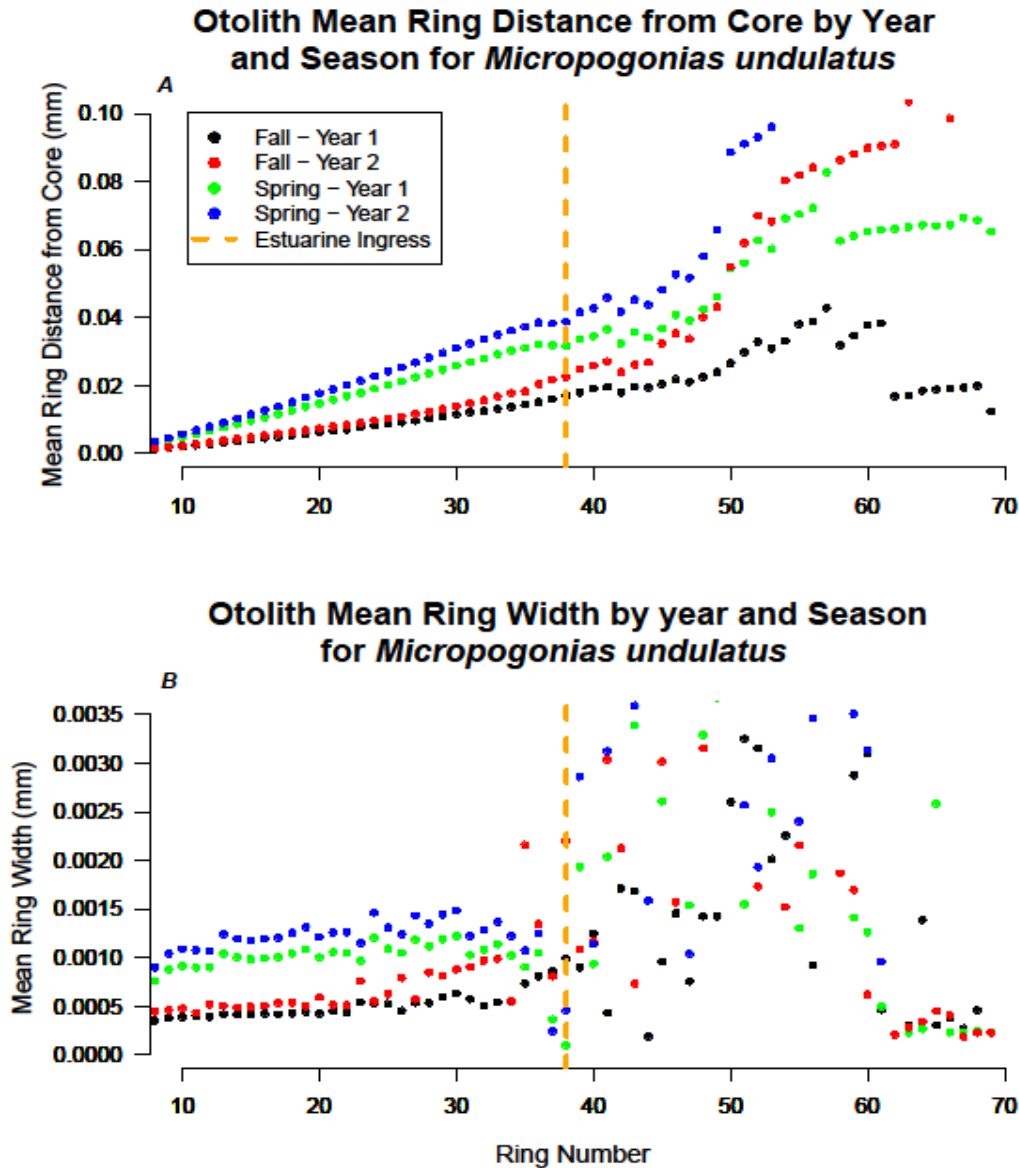


Figure 4.11: (A) Otolith ring mean distance (mm) from the core by season and sample year. Fall 2006 (black), fall 2007 (red), spring 2007 (green), and spring 2008 (blue), are all provided to show differences between year and season, and the estimated average ingress date is demarcated by the dashed orange line. Distance from the core as a proxy for the increased growth expected with the lower salinities of the estuaries showed an average ingress date of 37 dph. (B) Mean ring width (mm) for individual daily rings from removed and imaged otoliths. Increases in ring width variability and increases from a regular ring width, of approximately 0.0005 mm for the fall 2006 (black) and the fall 2007 (red), and from a regular ring width of 0.0010 mm for the spring 2007 (green) and spring 2008 (blue), occurred for rings deposited after 37 dph.

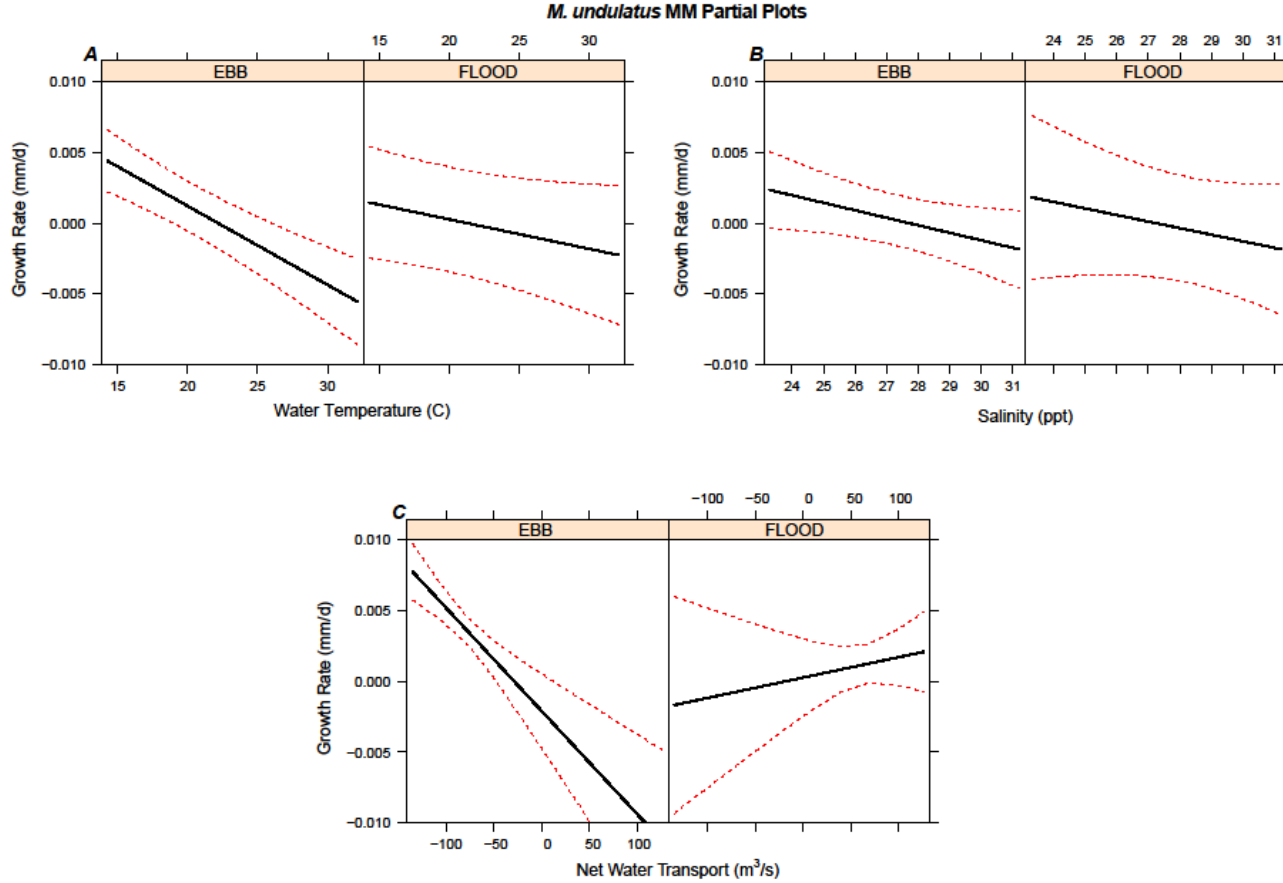


Figure 4.12: Mixed Model (MM) partial plots for growth rate ($\text{mm} \cdot \text{day}^{-1}$) data as a function of hydrodynamic parameters. Growth rate data are based on both directly measured otoliths and those ages provided from length frequency keys. All partial plots assume a static value for the other model terms in the graphical evaluation. (A) Growth rate as a function of water temperature ($^{\circ}\text{C}$), delineated by tide. (B) Growth rate as a function of salinity (ppt), delineated by tide. (C) Growth rate as a function of net water transport (NWT; $\text{m}^3 \cdot \text{s}^{-1}$), delineated by tide.

ingress, regardless of year or season. The interaction of flood tides with water temperature showed higher growth associated with colder temperatures indicative of estuarine waters during late fall-winter ($p = 0.0395$; Figure 4.12a). The flood tide interaction with water temperature shows a similar trend, although more muted, likely due to the more oligotrophic and higher temperatures of the inner continental shelf-coastal waters. Salinity showed a similar trend of increasing growth with decreasing salinity regardless of tidal stage, resulting in a non-significant interaction ($p = 0.9006$), although the 95% confidence interval was much larger at lower salinities during flood tides (Figure 4.12b). Similar to water temperature, salinities more consistent with estuarine conditions had higher modeled growth rates ($p = 0.0458$). Partial effects show a general trend with higher growth rates at large negative net water transport during ebb tides ($p = 0.0005$; Figure 4.12c). However, during flood tides, higher growth rates were associated with strong positive net water transport values, although the 95% confidence interval showed the ability for higher individual growth rates at large negative net water transports on flood tides.

4.4 Discussion

Successful estuarine recruitment of *M. undulatus* larvae through tidal passes along the northern GOM depends on a highly variable spawning regime, advantageous environmental conditions including hydrographic, tide, and wind forcing factors, and ultimately larval growth (Norcross and Austin, 1988; Eby et al., 2005; Montane and Austin, 2005). Hind-casting of the Laird-Gompertz growth model to 0 dph allows for inferences on growth rates of larvae along the recruitment corridor across the continental shelf and coastal zone. The bottleneck nature of a tidal pass and the highly variable hydrodynamic environment of a well-mixed tidal pass at Bayou

Tartellan, with associated increase of larval growth with ingress into the estuarine nursery ground (Searcy et al., 2007), illustrate the challenges and rewards of successful recruitment for larval *M. undulatus* spawned offshore.

The highest frequency of hatch dates occurred between late September and early October for both years, but hatching continued through the late winter and early spring (Figure 4.6) indicating an overwinter spawning and recruitment period. The peak hatch dates correspond well with previously described July through December peak spawning and recruitment (Warlen and Burke, 1990; Barbieri et al., 1994b), and an overall spawning and recruitment period from August through May (Hettler and Chester, 1990). Differences in the distribution of hatch dates between year one and year two of the study highlight the variability in yearly *M. undulatus* spawning due to factors on various spatial (Miller and Able, 2002) and temporal scales (Norcross, 1983). For example, year two had a less peaked distribution of hatch dates than year one, with a higher percentage of larvae recruiting in the months after December 2007, indicating a more protracted spawning season (Barbieri et al., 1994a). The second peak in hatch dates in late January and early February for both sample years suggests a second spawning sub-group (Figure 6; Warlen, 1982; Thorrold et al., 1997). Warmer water temperatures during winter sampling efforts in year two were more similar to temperatures during the fall months in sampling year one, potentially explaining the protracted 2007-2008 spawning season (Figure 2; Lankford and Targett, 2001a/b; Hare and Able, 2007).

Larval *M. undulatus* collected in Bayou Tartellan showed increased and variable growth rates after encountering lower salinity coastal boundary and estuarine waters (Nixon and Jones, 2000). The linear growth rate of $0.2 \text{ mm} \cdot \text{day}^{-1}$ compared favorably with the growth rate of 0.19

mm·day⁻¹ from larvae collected from inner continental shelf waters offshore of Sabine Pass, Texas, and the Mermentau River, Louisiana (Cowan, 1988). The Laird-Gompertz model daily maximum growth rates for the fall and spring of both sample years falls within the range of growth rates reported for coastal waters off North Carolina, i.e., 0.16 to 0.27 mm·day⁻¹ (Warlen, 1982). The differences in seasonal growth rates within the Laird-Gompertz models showed evidence of spawning/recruitment subgroups with maximum growth rates occurring later in the fall than in the spring, similar to subgroups determined by seasonal growth rate differences in North Carolina waters (Warlen, 1982) and the MAB (Thorrold et al., 1997), which were based on food availability and salinity differences. Within this study, maximum growth rates were approximately 20 dph later in the fall than in the spring, suggesting a more productive and potentially more suitable essential fish habitat during the spring (Searcy et al., 2007; Sponagle, 2010). Lower salinities indicative of estuarine waters have been shown to increase somatic growth rates of larval *M. undulatus* (Peterson et al., 1999). While all growth analyses showed similar growth rates, the use of the Laird-Gompertz model allowed for accurate hind-casting of the low growth rates of larvae in the recruitment corridor on the continental shelf, since it used the true estimate of hatch length, whereas the linear models failed to accurately reflect/account for length at hatch.

The mean age in dph of larval *M. undulatus* transgressing these lower salinity waters of the coastal boundary layer and/or ingressing into the estuary was estimated to be approximately 40 dph, based upon changes in otolith ring width and ring distance from the core (Figures 4.11a/b). Studies of ingress into Chesapeake Bay, Delaware Bay, and Pamlico Sound have shown ingress dates to be between 30 and 60 dph (Warlen, 1982, Miller et al., 2003, Schaffler et

al., 2009a/b), which compare favorably with the directly aged larvae in Bayou Tartellan tidal pass being between 22 and 70 dph. The role of periodic atmospheric winter frontal passages on larval *M. undulatus* densities was shown to be significant in this system (Kupchik, 2014), suggesting that patterns such as inlet geomorphology and wind-forcing can play a large role in the timing of ingress for *M. undulatus* (Raynie and Shaw, 1994, Joyeaux, 1998, Wood, 2000). Larval ingress can be driven by active mechanisms like selective tidal stream transport (STST), but the vertically, well-mixed nature of tidal passes in the northern GOM, and in particular our study site of Bayou Tartellan, suggests passive recruitment/retention mechanisms such as residual bottom-flow (Joyeux, 1999, Shultz et al., 2003), wind-driven transport (Shaw et al., 1985, Joyeaux, 1999, Hare et al., 1999, Hare and Govoni, 2005), or flow differentials laterally across the channel due to boundary conditions and marsh edge effects may be the driving forces (Lyczkowski-Shultz et al., 1990; Raynie, 1991; Raynie and Shaw, 1994; Kupchik, 2014). The variability in otolith distance from the core for larger larvae from the overall trend (Figures 4.11a/b) supported within year variability in batch spawning leading to different cohorts with potentially variable recruitment corridor lengths (Brophy and Danilowicz, 2002; Sponaugle and Pinkard, 2004; Searcy et al., 2007).

Lower growth rates associated with continental shelf waters, and higher growth rates associated with estuarine or coastal boundary waters. The effect of salinity on growth rate is further exemplified by the steep increase in growth rate during low salinities on ebb tides, waters that would represent the upper estuarine nursery ground. Increased larval *M. undulatus* growth based on lower salinities has been previously documented in other estuaries (Peterson et al., 1999). Growth rate as a function of water temperature showed no difference associated with tide,

and higher growth rates were associated with lower water temperatures which probably reflect the higher productivity of estuaries which at this time of year have cooler temperatures and lower salinities than warmer more saline GOM waters. The notable exception to this pattern was the growth rate increase during positive net transports associated with flood tides, which may be a function of interim or pre-frontal conditions associated with southerly winds and coastal setup reestablishing the tidal prism after flushing from northerly winds of the post-frontal phase. The MM for larval *M. undulatus* confirmed the importance of salinity on larval and juvenile fish growth (Sogard, 1992; Rooker and Holt, 1997; Lankford and Targett, 2001a), and the variability associated with differences between estuarine waters and continental shelf waters which vary on temporal and spatial scales (Searcy et al. 2007) .

4.5 Conclusions

Digital analysis of larval *M. undulatus* daily saccular otolith rings, collected in Bayou Tartellan from October 2006 to March 2007 and September 2007 to March 2008, provided a fast, reliable method for analyzing otolith rings, growth rate, and estuarine ingress. The digital image filters removed the need for human interpretation, and allowed for direct measurement and averaging of multiple readings to avoid aliasing. Furthermore, the digital analysis allowed for methods involving exact measurement of otolith ring width and distance from the core to confirm the estimated estuarine ingress date determined from growth rate changes. This estimated growth rate from the multiple analyses facilitated through the digital image process thereby allowed for a confident estimation of the age that larval *M. undulatus* leave the continental shelf and encounter the more hydrodynamically variable coastal boundary zone and lower salinity estuarine waters.

The linear growth model, although useful for comparison to previous studies, was less effective than the Laird-Gompertz growth curve in detailing accurate larval fish growth rates. The Laird-Gompertz growth models were hind-casted to represent the SL at hatch and rate of growth more effectively in the dph before sampling, and provided more detail in relation to *M. undulatus* ingress into estuaries where growth rate was expected to increase. The model allowed for expression of the limited somatic growth of larvae before recruitment into the lower salinity estuarine system of Bayou Tartellan. Moreover, the nature of the growth model allowed for calculation of instantaneous growth rates that reflect small scale daily changes effected by spatial location within the recruitment corridor without the bias introduced from overall averages expressed in a linear relationship with a singular rate of $0.2 \text{ mm} \cdot \text{day}^{-1}$, or from bias introduced from groupings of larvae in dph. The model also allowed for an estimation of maximum growth rate, showing the difference of later occurring maximum fall growth rates with respect to dph versus spring. Evidence based on differing growth rates between the fall traditional peak spawning and recruitment season and the spring recruitment season suggested for the first time that in the northern GOM similar potential spawning subgroups were identified as have been found from North Carolina waters and the MAB. This result was confirmed with differences in otolith microstructure between the fall and spring for both years, and the microstructure analysis was able to show within year variability in batch spawning producing different cohorts with variable recruitment corridor lengths. The highly significant salinity component in the MM relating growth rate to the hydrodynamics in Bayou Tartellan supported the importance of the low salinity and high productivity of estuarine waters for maximizing growth for larval and, ultimately, juvenile *M. undulatus*.

4.6 Literature Cited

- Albuquerque, C.Q.D., Muelbert, J.H., and L.A.N.D. Sampaio. 2009. Early developmental aspects and validation of daily growth increments in otoliths of *Micropogonias furnieri* (Pisces, Sciaenidae) larvae reared in laboratory.
- Adobe Photoshop CS4® (v11.0). 2008. Adobe Systems Incorporated.
- Able, K.W. 2005. A re-examination of fish estuarine dependence: evidence for connectivity between estuarine and ocean habitats. *Estuarine, Coastal and Shelf Science* 64(1): 5-17.
- Barbieri, L.R., Chittenden Jr, M., and S.K. Lowerre-Barbieri. 1994a. Maturity, spawning, and ovarian cycle of Atlantic croaker, *Micropogonias undulatus*, in the Chesapeake Bay and adjacent coastal waters. *Fishery Bulletin* 92(4): 671-685.
- Barbieri, L.R., Chittenden Jr, M., and S.K. Lowerre-Barbieri. 1994b. Age, growth and mortality of Atlantic croaker, *Micropogonias undulatus*, in the Chesapeake Bay region, with a discussion of apparent geographical changes in population dynamics. *Fishery Bulletin* 92(4): 1-12.
- Beamish, R.J., and C. Mahnken. 2001. A critical size and period hypothesis to explain natural regulation of salmon abundance and the linkage to climate and climate change. *Progress in Oceanography* 49(1-4): 423-437.
- Brophy, D., and B.S. Danilowicz. 2002. Tracing populations of Atlantic herring (*Clupea harengus* L.) in the Irish and Celtic Seas using otolith microstructure. *ICES journal of Marine Science* 59: 1305-1313.
- Brown, C., Holt, S., Jackson, G., Brooks, D., and G. Holt. 2004. Simulating larval supply to estuarine nursery areas: how important are physical processes to the supply of larvae to the Aransas Pass Inlet? *Fisheries Oceanography* 13(3): 181-196.
- Campana, S.E. 1984. Interactive effects of age and environmental modifiers on the production of daily growth increments in otoliths of plainfin midshipman, *Porichthyes notatus*. *Fisheries Bulletin* 82: 165-177.
- Campana, S.E. 1992. Measurement and interpretation of the microstructure of fish otoliths. In: D.K. Stevenson and S.E. Campana, eds., *Otolith microstructure examination and analysis*. Canadian Special Publication on Fisheries and Aquatic Sciences 117: 59-71.
- Campana, S.E. 1999. Chemistry and composition of fish otoliths: pathways, mechanisms and applications. *Marine Ecology Progress Series* 199: 263-297.

- Campana, S.E., and S.R. Thorrold. 2001. Otoliths, increments, and elements: a key to the understanding of fish populations? *Canadian Journal of Fisheries & Aquatic Sciences* 58: 30-38.
- Chittenden JR, M.E., and C.M. Jones 1994. Age, growth, and mortality of Atlantic croaker, *Micropogonias undulatus*, in the Chesapeake Bay region, with a discussion of apparent geographic changes in population dynamics. *Fisheries Bulletin* 92, 1-12.
- Colton, J.B., Smith, W.G., Kendall Jr., A.W., Berrien, P.L., and M.L. Fahay. 1979. Principal spawning areas and times of marine fishes, Cape Sable to Cape Hatteras. *Fisheries Bulletin*, NOAA 76: 911-916.
- Cowan, J.H. 1988. Age and growth of Atlantic croaker, *Micropogonias undulatus*, larvae collected in the coastal waters of the northern Gulf of Mexico as determined by increments in saccular otoliths. *Bulletin of Marine Science* 42(3): 349-357.
- Diamond, S.L., Cowell, L.G., and L.B. Crowder 2000. Population effects of shrimp trawl bycatch on Atlantic croaker. *Canadian Journal of Fisheries and Aquatic Sciences* 57(10), 2010-2021.
- Ditty, J., Zieske, G., and R. Shaw. 1988. Seasonality and depth distribution of larval fishes in the northern Gulf of Mexico above latitude 26 degree 00'N. *Fishery Bulletin* 86(4): 811-823.
- Eby, L.A., Crowder, L.B., McClellan, C.M., Peterson, C.H., and M.J. Powers. 2005. Habitat degradation from intermittent hypoxia: impacts on demersal fishes. *Marine Ecology Progress Series* 291: 249-261.
- European Fish Ageing Network (EFAN). 1997. Report of the first plenary meeting. Brest, Belarus, May 1997: 12 p.
- Fahay, M.P. 1983. Guide to the early stages of marine fishes occurring in the western North Atlantic Ocean, Cape Hatteras to the south Scotian Shelf. *North Atlantic Fisheries Science* 4: 1-423.
- Fahay, M.P. 2007. Early Stages of Fishes in the Western North Atlantic Ocean: Davis Strait, Southern Greenland and Flemish Cap to Cape Hatteras. *Scorpaeniformes Through Tetraodontiformes*, Volume 2: Northwest Atlantic Fisheries Organization. 1696 pp.
- Fritzsche, R.A. 1978. Development of Fishes of the Mid-Atlantic Bight: An Atlas of Egg, Larval and Juvenile Stages. Volume 5, Chaetodontidae through Ophidiidae. FWS/OBS-78/12, U.S. Fish and Wildlife Service, Washington D.C. 237 pp.
- Gaemers, P.A.M. 1976. New concepts in the evolution of the Gadidae (Vertebrata, Pisces), based on their otoliths. *Mededelingen van der Werkgroep voor Tertiaire en Kwartaire Geologie* 13: 3-22.

- Gompertz, B. 1815. On the nature of the function expressive of the law of human mortality, and on a new mode of determining the value of life contingencies. *Philosophical Transactions of the Royal Society of London* 115: 513–585.
- Hardy Jr., J.D. 1978a. Development of Fishes of the Mid-Atlantic Bight: An Atlas of Egg, Larval and Juvenile Stages. Volume 2, Anguillidae through Syngnathidae. FWS/OBS-78/12, U.S. Fish and Wildlife Service, Washington D.C. 229 pp.
- Hardy Jr., J.D. 1978b. Development of Fishes of the Mid-Atlantic Bight: An Atlas of Egg, Larval and Juvenile Stages. Volume 3, Aphredoderidae through Rachycentridae. FWS/OBS-78/12, U.S. Fish and Wildlife Service, Washington, D.C. 249 pp.
- Hare, J.A., and K.W. Able. 2007. Mechanistic links between climate and fisheries along the east coast of the United States: explaining population outbursts of Atlantic croaker (*Micropogonias undulatus*). *Fisheries Oceanography* 16(1): 31-45.
- Hare, J.A., and J.J. Govoni. 2005. Comparison of average larval fish vertical distributions among species exhibiting different transport pathways on the southeast United States continental shelf. *Fisheries Bulletin* 103: 728-736.
- Hare, J.A., Quinlan, J.A., Werner, F.E., Blanton, B.O., Govoni, J.J., Forward, R.B., Settle, L.R., and D.E. Hoss. 1999. Larval transport during winter in the SABRE study area: results of a coupled vertical larval behavior-three-dimensional circulation model. *Fisheries Oceanography* 8(2): 57-76.
- Heintz, R.A., and J.J. Vollenweider. 2010. Influence of size on the sources of energy consumed by overwintering walleye pollock (*Theragra chalcogramma*). *Journal of Experimental Marine Biology and Ecology* 393(1): 43-50.
- Helies, F.C., and J.L. Jamison. 2009. Reduction rates, species composition, and effort: Assessing bycatch within the Gulf of Mexico shrimp trawl fishery. NOAA/NMFS Cooperative Agreement Number NA07NMF4330125 (101). Final Report. 183 pp.
- Hettler, W.F., and A.J. Chester. 1990 Temporal distribution of ichthyoplankton near Beaufort inlet, North Carolina. *Marine Ecology Progress Series* 68(1-2): 157-168.
- Hettler, W.F., and J.A. Hare. 1998. Abundance and size of larval fishes outside the entrance to Beaufort Inlet, North Carolina. *Estuaries* 21(3), 476-499.
- Hoover, R. R., Jones, C. M., and C.E. Grosch 2012. Estuarine ingress timing as revealed by spectral analysis of otolith life history scans. *Canadian Journal of Fisheries and Aquatic Sciences*, 69(8), 1266-1277.

- Hoskin, S. 2002. Recruitment variability of Atlantic croaker, *Micropogonias undulatus*, with observations on environmental factors. Master's thesis, Old Dominion University, Norfolk, Virginia.
- Hoss, D.E., Coston-Clements, L., Peters, D.S., and P.A. Tester. 1988. Metabolic responses of spot, *Leiostomus xanthurus*, and Atlantic croaker, *Micropogonias undulatus*, larvae to cold temperatures encountered following recruitment to estuaries. *Fishery Bulletin* 86(3): 483-488.
- Houde, E.D. 1982. Kinds, distributions and abundances of sea bass larvae (Pisces:Serranidae) from the eastern Gulf of Mexico. *Bulletin of Marine Science* 32: 511-522.
- Johnson, G.D. 1978. Development of Fishes of the Mid-Atlantic Bight: An Atlas of Egg, Larval and Juvenile Stages. Volume 4, Carangidae through Ehippidae. FWS/OBS-78/12, U.S. Fish and Wildlife Service, Washington D.C. 189 pp.
- Jones, P.W., Martin, F.D., and J.D. Hardy. 1978. Development of Fishes of the Mid-Atlantic Bight: An Atlas of Egg, Larval and Juvenile Stages. Volume 1, Acipenseridae through Ictaluridae. FWS/OBS-78/12, U.S. Fish and Wildlife Service, Washington D.C. 224 pp.
- Joyeux, J. 1998. Spatial and temporal entry patterns of fish larvae into North Carolina estuaries: comparisons among one pelagic and two demersal species. *Estuarine, Coastal and Shelf Science* 47(6): 731-752.
- Joyeux, J. 1999. The abundance of fish larvae in estuaries: Within-tide variability at inlet and immigration. *Estuaries and Coasts* 22(4): 889-904.
- Kupchik, M.J. 2014. A study of the temporal and spatial distribution of ichthyoplankton and post-larval penaeids recruiting into a Louisiana tidal pass. PhD Dissertation. Louisiana State University, Baton Rouge, LA, USA. 384 pp.
- Laird, A.K., Tyler, S.A., and A.D. Barton. 1965. Dynamics of normal growth. *Growth* 29: 233-248.
- Lankford Jr, T.E., and T.E. Targett. 2001a. Low-temperature tolerance of age-0 Atlantic croakers: recruitment implications for US mid-Atlantic estuaries. *Transactions of the American Fisheries Society* 130(2), 236-249.
- Lankford Jr, T.E., & T.E. Targett. 2001b. Physiological performance of young-of-the-year Atlantic croakers from different Atlantic coast estuaries: implications for stock structure. *Transactions of the American Fisheries Society* 130(3), 367-375.

- Leak, J.C. 1981. Studies on recruitment process focusing on early life history of the Japanese sardine, *Sardinops melanostictus* (Schlegel). Bulletin of Natural Resources, Institute of Fisheries Science 3: 25-278.
- Li, C., Weeks, E., and J.L. Rego. 2009. In situ measurements of saltwater flux through tidal passes of Lake Pontchartrain estuary by Hurricanes Gustav and Ike in September 2008. Geophysical Research Letters 36(19): L19609.
- Linnaeus, C. (1766). Systema naturae sive regna tria naturae, secundum classes, ordines, genera, species, cum characteribus, differentiis, synonymis, locis. Laurentii Salvii, Holmiae. 12th ed. v. 1 (pt 1): 532 p.
- Lozano, C., Houde, E.D., Wingate, R.L., and D.H. Secor. 2012. Age, growth and hatch dates of ingressing larvae and surviving juveniles of Atlantic menhaden *Brevoortia tyrannus*. Journal of Fish Biology 81: 1665-1685.
- Lombarte, A., and B. Morales-Nin. 1995. Morphology and ultrastructure of saccular otoliths from five species of the genus *Coelorincus* (Gadiformes: Macrouridae) from the southeast Atlantic. Journal of Morphology 225: 179-192.
- Lyczkowski-Shultz, J., Ruple, D.L., Richardson, S.L., Cowan, J., and H. James. 1990. Distribution of fish larvae relative to time and tide in a Gulf of Mexico barrier island pass. Bulletin of marine science 46(3): 563-577.
- Martin, F.D., and G.E. Drewery. 1978. Development of Fishes of the Mid-Atlantic Bight: An Atlas of Egg, Larval and Juvenile Stages. Volume 6, Stromateidae through Ogococephilidae. FWS/OBS-78/12, U.S. Fish and Wildlife Service, Washington D.C. 176 pp.
- Miller, M.J., and K.W. Able. 2002. Movements and growth of tagged young-of-the-year Atlantic croaker (*Micropogonias undulatus* L.) in restored and reference marsh creeks in Delaware Bay, USA. Journal of Experimental Marine Biology and Ecology 267(1): 15-33.
- Miller, G.L., and S.C. Jorgenson. 1973. Meristic characters of some marine fishes of the western Atlantic Ocean. Fisheries Bulletin, NOAA 71: 301-312.
- Miller, M.J., Nemerson, D.M., and K.W. Able. 2003. Seasonal distribution, abundance, and growth of young-of-the-year Atlantic croaker (*Micropogonias undulatus*) in Delaware Bay and adjacent marshes. Fishery Bulletin 101(1): 100-115.

- Montane, M.M., & Austin, H.M. (2005). Effects of hurricanes on Atlantic croaker (*Micropogonias undulatus*) recruitment to Chesapeake Bay. Hurricane Isabel in Perspective, Chesapeake Research Consortium, CRC Publication, 05-160.
- Morales-Nin, B., Lombarte, A., and B. Japon. 1998. Approaches to otolith age determination: image signal treatment and age attribution. *Scientia Marina* 62(3): 247-256.
- Moser, H.G. 1984. Ontogeny and Systematics of Fishes. American Society of Ichthyologists and Herpetologists Special Publication No. 1. Allen Press, Lawrence, Kansas. 760 pp.
- Moser, M.L., and L.R. Gerry. 1989. Differential effects of salinity changes on two estuarine fishes, *Leiostomus xanthurus* and *Micropogonias undulatus*. *Estuaries* 12(1): 35-41.
- Nixon, S., and C. Jones. 1997. Age and growth of larval and juvenile Atlantic croaker, *Micropogonias undulatus*, from the Middle Atlantic Bight and estuarine waters of Virginia. *Fishery Bulletin* 95(4): 773-784.
- National Marine Fisheries Service, NMFS. 2009. Our living oceans. Report on the status of U.S. living marine resources, 6th edition. U.S. Dep. Commerce, NOAA Tech. Memo. NMFS-F/SPO-80, 369 p.
- National Marine Fisheries Service, NMFS. 2012. Fisheries of the United States. Lowther, A.(ed.). U.S. Dep. Commerce, NOAA. 124 p.
- Nolf, D. 1985. Otolithi piscium. In: M. P. Schultze, (ed), *Handbook of Paleoichthyology* Vol. 10. Gustav Fisher Verlag, Stugart, Germany, and New York, USA.
- Norcross, B.L. 1983. Climate scale environmental factors affecting year-class fluctuations of Atlantic Croaker (*Micropogonias undulatus*) in the Chesapeake Bay. Ph.D. Dissertation. College of William & Mary. 388 p.
- Norcross, B.L., and H.M. Austin. 1988. Middle Atlantic Bight meridional wind component effect on bottom water temperatures and spawning distribution of Atlantic croaker. *Continental Shelf Research* 8: 69-88.
- Pannella, G. 1971. Fish otoliths: daily growth layers are periodical patterns. *Science* 173: 1124-1127.
- Pannella, G. 1974. Otolith growth patterns: an aid in age determination in temperate and tropical fishes. *The Ageing of Fish*, T.B. Bagenel, ed. Unwin Brothers, Ltd., Surrey, England. 28-39.

- Peters, D.S., Devane Jr., J.C., Boyd, M.T., Clements, L.C., and A.B. Powell. 1978. Preliminary observations of feeding, growth, and energy budget of larval spot (*Leiostomus xanthurus*). Annual Report NMFS. Beaufort Lab, Beaufort, North Carolina. 377-397.
- Peterson, M.S., Comyns, B.H., Rakocinski, C.F., and G.L. Fulling. 1999. Does salinity affect somatic growth in early juvenile Atlantic croaker, *Micropogonias undulatus* (L.)?. Journal of Experimental Marine Biology and Ecology 238(2), 199-207.
- R Development Core Team (v.2.14.0). 2008. R: A language and environment for statistical computing. R Foundation for Statistical Computing, Vienna, Austria. ISBN 3-900051-07-0, URL <http://www.R-project.org>.
- Ralston, S. and H. Williams. 1989. Numerical integration of daily growth increments: An efficient means of aging tropical fishes for stock assessment. Fisheries Bulletin 87: 1-16.
- Rasband WS. ImageJ, U.S. National Institutes of Health, Bethesda, Maryland, USA, imagej.nih.gov/ij/, 1997—2012.
- Raynie, R.C. 1991. Study of the spatial and temporal ichthyoplankton abundance along a recruitment corridor from offshore to estuarine nursery. Master's thesis. Louisiana State University, Baton Rouge, Louisiana.
- Raynie, R.C., and R.F. Shaw. 1994. Ichthyoplankton abundance along a recruitment corridor from offshore spawning to estuarine nursery ground. Estuarine, Coastal and Shelf Science 39(6): 421-450.
- Richards, W.J. 2006. Early Stages of Atlantic Fishes: An Identification Guide for the Western Central North Atlantic. Volume I & II. CRC Press, Boca Raton, FL. 2640 pp.
- Rooker, J.R., and S.A. Holt. 1997. Utilization of sub-tropical seagrass meadows by newly settled red drum, *Sciaenops ocellatus*: patterns of distribution and growth. Marine Ecology Progress Series 158: 139-149.
- Ruple, D. L. 1984. Occurrence of larval fishes in the surf zone of a northern Gulf of Mexico barrier island. Estuarine, Coastal and Shelf Science 18(2): 191-208.
- Schaffler, J.J., Reiss, C.S., and C.M. Jones. 2009a. Spatial variation in otolith chemistry of Atlantic croaker larvae in the Mid-Atlantic Bight. Marine Ecology Progress Series 23: 18-35.
- Schaffler, J.J., Reiss, C.S., and C.M. Jones. 2009b. Patterns of larval Atlantic croaker ingress into Chesapeake Bay, USA. Marine Ecology Progress Series 378: 187-197.

- Schmitt, W. 1969. The otoliths as a mean for differentiation between species of very similar appearance. Procedural Symposium on Oceanic Fishes. Resources of Sea Tropical Atlantic. FAO. 393-396.
- Schultz, E.T., Lwiza, K.M.M., Fencil, M.C., and J.M. Martin. 2003. Mechanisms promoting upriver transport of two species in the Hudson River estuary. Marine Ecology Progress Series 251: 263-277. 97 pp.
- Searcy, S.P. 2005. Is growth a reliable indicator of essential fish habitat. PhD Dissertation. Marine, Earth, and Atmospheric Sciences, North Carolina State University, Raleigh, North Carolina, USA.
- Searcy, S.P., Eggleston, D.B., and J.A. Hare. 2007. Is growth a reliable indicator of habitat quality and essential fish habitat for a juvenile estuarine fish? Canadian Journal of Fisheries and Aquatic Science 64: 681-691.
- Shaw, R.F., Cowan, J.H., and T.L. Tillman. 1985. Distribution and density of *Brevoortia patronus* (gulf menhaden) eggs and larvae in the continental shelf waters of western Louisiana. Bulletin of Marine Science 36(1): 96-103.
- Shaw, R.F., Rogers, B.D., Cowan, J.H., and W.H. Herke. 1988. Ocean-estuary coupling of ichthyoplankton and nekton in the Northern Gulf of Mexico. American Fisheries Society Symposium 3: 77-89.
- Smith, C.L. 1997. National Audubon Society field guide to tropical marine fishes of the Caribbean, the Gulf of Mexico, Florida, the Bahamas, and Bermuda. Alfred A. Knopf, INC., New York, NY, USA. 720 p.
- Sogard, S.M. 1992. Variability in growth rates of juvenile fishes in different estuarine habitats. Marine Ecology progress Series 85: 35-53.
- Sogard, S.M. 1997. Size-selective mortality in the juvenile stage of teleost fishes: a review. Bulletin of Marine Science 60(3), 1129-1157.
- Sponaugle, S. 2010. Otolith microstructure reveals ecological and oceanographic processes important to ecosystem-based management. Environmental Biology of Fishes 89(3-4): 221-238.
- Sponaugle, S., and D. Pinkard. 2004. Impact of variable pelagic environments on larval growth and recruitment of the reef fish *Thalassoma bifasciatum*. Journal of Fish Biology 64: 34-54.

- Stuck, K.C. and H.M. Perry. 1982. Ichthyoplankton community structure in Mississippi coastal waters. Pp. VI-I-1 to VI-I-53. *In*: Fishery monitoring and assessment completion report, 1 January 1977 to 31 December 1981. Gulf Coast Research Lab, Project No. 2-296-R.
- Thorrold, S.R., Jones, C.M., and S.E. Campana. 1997. Response of otolith microchemistry to environmental variations experienced by larval and juvenile Atlantic croaker (*Micropogonias undulatus*). *Limnology and Oceanography*, 42(1), 102-111.
- University of Texas Mariculture Program Report. 1982-1983. Marine Science Institute, University of Texas, Port Aransas, Texas 78373, USA. 36 pp.
- Walker, N.D., and A.B. Hammack. 2000. Impacts of winter storms on circulation and sediment transport: Atchafalaya-Vermilion Bay region, Louisiana, USA. *Journal of Coastal Research* 16(4): 996-1010.
- Warlen, S.M. 1982. Age and growth of larvae and spawning time of Atlantic croaker larvae in North Carolina. *Proc. Annual Conference, Southeast Association of Fish and Wildlife Agencies* 34: 204-214.
- Warlen, S.M., and A.J. Chester. 1985. Age, growth, and distribution of larval spot, *Leiostomus xanthurus*, off North Carolina. *Fisheries Bulletin* 83: 587-599.
- Warlen, S.M., and J.S. Burke. 1990. Immigration of larvae of fall/winter spawning marine fishes into a North Carolina estuary. *Estuaries* 13(4): 453-461.
- Wood, R.J. 2000. Synoptic scale climatic forcing of multispecies fish recruitment patterns in Chesapeake Bay. Doctoral dissertation. The College of William and Mary, Williamsburg, Virginia.
- Zweifel, J.R., and R. Iasker. 1976. Prehatch and post-hatch growth of fishes – a general model. *Fishery Bulletin* 74: 609-621.

CHAPTER 5. AGE, GROWTH, AND RECRUITMENT FROM OTOLITH MICROSTRUCTURE FOR LARVAL *BREVOORTIA PATRONUS*

Gulf menhaden (*Brevoortia patronus*) is an ecologically- and commercially-important species supporting the largest fishery by weight in the Gulf of Mexico. Sagittal otoliths (N=208) were removed from gulf menhaden collected over a two year period, from October 2006 to March 2007 and from September 2007 to March 2008, and analyzed using digital imaging and Fast Fourier Transformations for age and growth estimation. Length at age was estimated using a two cycle, Laird-Gompertz growth model to determine growth rates. Laird-Gompertz growth models were also fit separately to age and length groupings to confirm if the ontogenetic shift in stage was correlated to age or length. Digital image measurements were used to conduct fine-scale otolith microstructure analyses. Length frequencies at age keys were used to determine temporal variability in *B. patronus* spawning and to document earlier spawning and estuarine recruitment (i.e., September), and shorter recruitment corridors than previously reported. Results indicated that growth rates were similar to previous studies in the northern Gulf of Mexico, with small variation between years probably a result of water temperature differences. The ontogenetic shift in feeding strategy was estimated from the model to begin 33 days post spawning.

5.1 Introduction

Brevoortia patronus (Goode, 1878), gulf menhaden, is both a commercially-important fishery in the Gulf of Mexico (GOM; Pritchard, 2005; Vaughn et al., 2010; McCrea-Strub et al., 2011) and an ecologically-important prey item for commercially- and recreationally-important species (Del Rio et al., 2010; Nelson et al., 2012; Simonsen and Cowan, 2013). Gulf menhaden have an established range from the Western Central Atlantic to the GOM, and specifically within the GOM from Florida Bay to the Bay of Campeche (Whitehead, 1985). The *Brevoortia patronus* fishery is the second largest United States fishery by weight and fourth in value (Pritchard, 2005), with this reduction fishery harvesting an average of 400-600 kilotons annually.

In recent years, 92% of the annual landings occurred in Louisiana (Vaughn et al., 2010). There is also a second and minor component of annual landings comprising a small bait fishery in the GOM (VanderKooy and Smith, 2002). Although the stock is relatively healthy with lower than target fishing mortality over the long term, recent years have shown increasing fishing mortality and decreasing population fecundity (Vaughn et al., 2007). Possible population limitations for *B. patronus* include food availability, habitat limitations, and successful recruitment of larvae into estuarine nursery areas, with declining recruitment being more of a concern based on a recent decrease in population fecundity (Vaughn et al., 2007).

Gulf menhaden are estuarine dependent and reportedly spawn from October through February (Whitehead, 1985; Nelson and Ahrenholz, 1986; Vaughn et al., 2000), with the peak estuarine recruitment occurring in late January and early February (Lewis and Roithmayer, 1981; Shaw et al., 1988). Spawning depth for *B. patronus* is reported to be 90 meters and shallower (Whitehead, 1985; Powell, 1994), with spawning location moving further offshore as the season progresses (Vaughan et al., 2007). Mean egg diameter has been reported as 1.61 mm, with a length at hatch of approximately 3mm total length (Dahlberg, 1970; Lewis and Roithmayr, 1981; Shaw et al., 1985). The pelagic eggs take two to three days to hatch and another two to three days until yolk absorption is complete, yielding first feeding and first increment formation occurring approximately five days post spawning (Warlen, 1988). Offshore larval drift and cross shelf transport has been reported to take between 4 and 10 weeks (Shaw et al., 1988). The variability in transport times is tied to the limited swimming capacity of larval fishes (Shanks and Eckert 2005) resulting in successful estuarine recruitment being driven more by oceanographic flows (Guillory et al., 1983; Epifanio and Garvine, 2001; Gillianders et al., 2003).

Recruitment from the more oligotrophic continental shelf spawning grounds through tidal passes into more productive estuarine waters represents an ecologically important change (Raynie and Shaw, 1994). This time period also corresponds to when *B. patronus* larvae transform from selective particulate feeding to omnivorous filter feeding as juveniles (Stoecker and Govoni, 1984; Deegan 1990; Chen et al. 1992; Lozano et al., 2012). This transformation has been reported to begin at approximately 20 mm SL and is completed by approximately 30 mm SL (Hettler, 1984; Warlen, 1988).

Louisiana studies on larval *B. patronus* age and growth have focused on both the offshore (Shaw 1985; Shaw et al. 1988; Warlen, 1988; Raynie and Shaw, 1994) and inshore component of the recruitment corridor (Deegan and Thompson, 1987; Marotz et al. 1990; Raynie and Shaw, 1994). These studies have found growth rates between 0.28 and 0.42 mm·day⁻¹ for the smaller larvae typically encountered on the continental shelf (Deegan and Thompson, 1984; Raynie and Shaw, 1994), and between 0.11 and 0.12 mm·day⁻¹ for larvae collected within Sabine Pass and Fourleague Bay, Louisiana (Warlen, 1988; Raynie, 1991).

Otolith daily growth increments were first described by Pannella (1971, 1974), and have since been confirmed in larval *B. patronus* in laboratory studies (Warlen, 1988). Otolith daily rings can provide information to calculate growth rates and can act as a proxy to identify changes in developmental stages and environment through variability in otolith ring width (Maillet and Checkley 1990; Chambers and Miller, 1995). Analysis of larval otolith structure has been historically done by visual inspection; however, video and digital methodologies have become prevalent with the increase in computing resolution and digital imaging (Ralston and Williams, 1989; Campana, 1992; Morales-Nin et al., 1998). Regardless of what ring counting methodology

is being used, the ring structure must be verified, because the shape and relative size of otoliths are species specific due to genetic control (Schmitt, 1969; Gaemers, 1976; Nolf, 1985; Lombarte and Morales-Nin, 1995; EFAN, 1997; Morales-Nin et al., 1998).

The objectives of this study were as follows. First, to define and determine an iterative digital filtering mechanism to more accurately determine daily increments in larval *B. patronus* otoliths. Secondly, determine the length at age of *B. patronus* for the sampling period. Third, to determine at what age there is a shift in growth rate consistent with the expect shift in feeding strategy from a selective particulate feeder to an omnivorous filter feeder. Fourth, compare otolith microstructure to length at age models for confirmation of growth rate and shift in feeding strategy. Finally, determine the distribution of the spawning period using back calculation of spawning dates from age frequency keys.

5.2 Materials and Methods

5.2.1 Sampling Location

Ichthyoplankton sampling was conducted in Bayou Tartellan, near the Port of Fourchon, Fourchon, Louisiana (Figure 5.1). Bayou Tartellan and Bayou LaFourche are the first major inland channel bifurcations from the connection with the Gulf of Mexico at Belle Pass (29° 5' 53.9" N, 90° 13' 17.8" W). The area represents a well-mixed tidal pass (i.e., little temperature, salinity or dissolved oxygen stratification) having high turbidity, and a relatively small drainage basin contributing a low volume of freshwater input. The sampling site (29° 6' 49" N, 90° 11' 4" W) consisted of a single location where passive plankton net sampling was conducted in approximately 10 meters of water from a dock extending 3.7 meters (12 feet) from the northern bank into an approximately 73 meter wide tidal pass.



Figure 5.1: Map of the study location in relation to the Gulf of Mexico and coastal Louisiana. The points in black represent the sampling location, with the final panel being the sampling location from an aerial photograph of Bayou Tartellan. The X in the last panel marks the location of an extended dock used as a sampling platform and later destroyed by Hurricane Gustav.

5.2.2 Field Sampling Methodology

Ichthyoplankton sampling was conducted using a fixed davit at the end of the dock, which suspended a stainless steel cable from above the sampling deck to the channel bottom. Passive plankton samples were taken using a 60-cm ring net (333 μm mesh, 2 meter length) dyed dark green to minimize visual avoidance and attached to a gimbal with a vane for orientation into the current. A plastic vinyl coated cod-end with 333 μm mesh drainage ports was

attached to the end of the net to facilitate sample collection. A General Oceanics flowmeter (model no. 2030 with slow velocity rotor) was positioned just off center of the ring to determine volume of water filtered.

Ichthyoplankton samples were collected every four hours over a 72-hour period, twice monthly between the months of October and April over a two year period (2006 – 2008), except for December and January, which were only sampled monthly. In addition, there were two sampling efforts made in September 2007. The sampling season was chosen to maximize encounters of wind-dominant meteorological events (i.e., atmospheric cold front passages) from late fall to early spring. Individual sampling dates were chosen to maximize astronomical tidal ranges. During sampling, both a surface and a near-bottom, passive, ichthyoplankton collection was randomly taken. Surface collections were six minutes long, and near-bottom collections were ten minutes to compensate for vertical differences in current speed and ultimately volume of water filtered (i.e., sampling effort). For near-bottom collections, the net mouth was closed on deployment until in position, opened for sampling, and subsequently closed for retrieval to prevent vertical contamination of the sample during transit through the water column. Nets were rinsed and washed down using a freshwater source to avoid sample contamination.

Ichthyoplankton samples were initially preserved in 10% buffered (sodium phosphate, dibasic $\text{NaH}_2\text{PO}_4 \cdot \text{H}_2\text{O}$ and monobasic Na_2HPO_4) formalin for approximately 3.5 hours as a short-exposure, long-term fixative. Samples were then rinsed and switched into a 70% ethanol solution for long-term storage, and later access for larval fish otolith work.

Estuarine hydrographic parameters were measured dockside during each plankton sample using a portable YSI (model no. 85) to record temperature, conductivity (salinity) and dissolved

oxygen. A continuously sampling YSI (model no. 600R) moored on the bottom offshore of the dock, also measured the same parameters. Hydrographic data were periodically downloaded as necessary and archived for storage. Data concerning predicted diurnal tides, measured tide height, and the resulting alteration in the expected tidal prism were from a nearby tide gauge station (Station ID: 8762075) at the Port of Fourchon, Fourchon, Louisiana (29° 6.8' N, 90° 11.9' W).

5.2.3 Laboratory Methodology

In the lab, ichthyoplankton collections with a volume of material greater than 200 mL were split in half using a box plankton splitter, and those with a volume greater than 400 mL were split into quarters. Samples were sorted under a dissecting stereoscope and all ichthyoplankton were removed. A subset of sorted samples was checked for completeness of ichthyoplankton removal by a second party.

Ichthyoplankton were identified to the lowest taxonomic level possible, depending on size of the organism and physical condition. Some larval fish that were difficult to identify were stained using Alizarin blue and Alizarin red to facilitate meristic counts. *Brevoortia patronus* larvae were separated and stored for otolith analysis. Identifications were based on the following literature: Miller and Jorgenson (1973); Fritzsche (1978); Hardy (1978a, 1978b); Johnson (1978); Jones et al. (1978); Martin and Drewry (1978); Colton et al. (1979); Leak (1981); Houde (1982); Stuck and Perry (1982); Fahay (1983); Moser (1984); Ruple (1984); Richards (2006); Fahay (2007).

Brevoortia patronus were subsampled for otolith analysis based on a normal distribution of standard length (SL) of all *B. patronus* larvae collected. Measurement of SL to the nearest 0.1

mm was conducted using a Leica MZ6 stereoscope calibrated against a stage micrometer. *B. patronus* larvae were subsampled from every sampling effort that contained the target species. In samples where three or less *B. patronus* larvae were collected, all larvae were scheduled for otolith removal. In samples that contained greater than three *B. patronus* larvae, three were selected so that the longest SL, shortest SL, and a SL from the normal distribution were scheduled for otolith removal.

5.2.4 Otolith Removal, Preparation, and Interpretation

Removal and preparation of sagittal otoliths from *B. patronus* larvae selected for dissection followed the methodology described by Barbieri et al. (1994a/b). All dissections were conducted using an Olympus SZX12 stereoscope with a 1x objective. Both left and right sagittal otoliths were removed and placed on a slide using Permout[®], with the left otolith cusp side up, and the right otolith cusp side down. Otoliths were polished using 0.3 µm alumina paste and microcloth to reveal the core. Otoliths were etched using a 0.1 N HCL acid for between 10 and 20 s to facilitate reading under a compound stereoscope. Digital images were taken using an Olympus BX41 compound stereoscope, with a phase contrast filter to highlight light and dark ring discontinuity zones, under magnification from 500x to 1250x under oil immersion.

Images were post-processed using Adobe Photoshop CS4[®] (v11.0) to convert the image from color to gray scale, and to enhance differences between light and dark rings by means of increasing the image contrast and improving the illumination. Otolith radii and measurements of grey scale values for each radius were conducted using ImageJ[®] (v1.44p) photo software. Measurement of any radii produces a calibrated length and corresponding grey scale values ranging from 0 (black) to 255 (white) along that radius. A central radius and two radii to the left

and right of the central radii, offset by a single pixel each, were measured. All five radii were averaged to produce the grey scale values used for filter analysis, to avoid the bias that could be introduced by choice of the reading radius and making a reading radius that becomes the average of a 5 pixel radius for any point along the radius (Morales-Nin et al., 1998). Radius length and grey scale data were collected for each otolith that was imaged.

Image data were imported into MATLAB (v7.6.0.324 R2008a) for filtering and age determination. Initial radii measurements were treated as being in the time domain for the purposes of filtering due to the growth of increments being directly related to age in days. Filtering was done using a Fast Fourier Transform (FFT) to determine the appropriate low pass filter structure to exclude high frequency sub-daily discontinuities on the otolith radius. Filter design was based on a low pass filter fit iteratively to the individual otoliths based on the understanding that the nyquist frequency is the daily otolith ring accreted by the larvae. As noted by Morales-Nin et al. (1998) this iterative fitting is done for each otolith due to increments of varying radius length between otoliths, differences in magnification, and variable growth rates for individuals. An Inverse FFT was then done to transform the signal back into the time domain for determination of the location of the sinusoidal peaks, and thus the position and width of the respective rings along the reading radius. There were ten otoliths that were selected at random and ran using this methodology twice, independently, to compare against a traditional eye reading for error and difference in ring count. All ten otoliths showed the same number of rings after both FFT methodology, and only one differed by one ring based on a visual reading of the otolith.

5.2.5 Otolith Ageing and Spawning Dates

Larval gulf menhaden age, recorded in days post spawning (dps), was determined from the increment counts for each otolith radius using the methodology previously described. Daily increment deposition has been confirmed to have an increment count to age regression slope of one for larval *B. patronus* growth (Geffen, 1993). Similar to the methodology used by Raynie (1991), we applied a five day lag for first increment formation post-spawn for *B. patronus* larvae, based on laboratory work (Warlen, 1988). This resulted in a calculation of total age that follows an equation of the form:

$$Age_{dps} = Increments_{total} + \varphi, \quad \text{where } \varphi = 5$$

where Age_{dps} represents the age in days from spawning to collection, $Increments_{total}$ represents the number of increments determined from the digital analysis, and the value of φ is the applied number of days from spawning to the deposition of the initial growth increment. Ages were estimated for larvae not selected for dissection by use of frequency of age at length keys utilizing the FSA package for R Software (v2.14.0).

Determination of spawning dates were calculated for all *B. patronus* larvae, direct calculation was done for those larvae where otolith radii were analyzed and also for those where the age was estimated in the methodology described previously. The spawning date was determined using the following equation:

$$Date_{spawning} = Date_{capture} - Age_{dps}$$

where $Date_{spawning}$ represents the spawning date for that particular larvae, $Date_{capture}$ represents the sample date when that larvae was collected, and Age_{dps} represents the age in days from spawning to collection.

5.2.6 Growth Rates

Distributions of lengths and calculated ages based on otolith extraction were tested for normality using a Shapiro-Wilk's test. Instantaneous larval growth (day^{-1}) is expected to be fastest soon after first feeding, decreasing thereafter, with a large decrease or growth stanza associated with an ontogenetic shift in feeding from selective particulate feeding to omnivorous filter feeding (Deegan 1990; Lozano et al., 2012). To represent this shift in feeding strategy between the larval and juvenile stages, a derivative of the Gompertz model (Gompertz, 1815) was chosen as it highlights this specific pattern of growth. Larval *B. patronus* somatic growth was modeled using only the directly analyzed otolith data by a two-cycle Laird-Gompertz growth model (Laird et al., 1965; Zweifel and Lasker, 1976; Raynie 1991), and fit using R Software (v2.14.0). The two cycle Laird-Gompertz growth model is represented by the following equation:

$$L_t = L_{null} e^{\left[\frac{\gamma(1-e^{-\alpha\Delta_1})}{\alpha} + \frac{\delta(1-e^{-\beta\Delta_2})}{\beta} \right]},$$

$$\Delta_1 = \text{MIN}(t, t^*)$$

$$\Delta_2 = \text{MAX}(t - t^*, 0)$$

where L_t represents the SL (mm) at age t (dps), L_{null} represents SL at hatch for *B. patronus*,

$\gamma = \frac{A}{\alpha}$ and A is the age specific instantaneous growth rate at spawning, α is the rate of

exponential decay in growth rate before t^* , t^* is the time at which there is a shift between

somatic growth stages, $\delta = \frac{B}{\beta}$ and B is the age specific instantaneous growth rate immediately

after the stage shift at $t = t^*$, and β is the exponential decay in growth in B. The length at hatch was estimated, but to increase model speed constrained between 1 and 4 mm based on the

literature reporting L_{null} to be between 2 and 4 mm (Hettler, 1984; Warlen, 1988; Powell, 1994; Raynie and Shaw, 1994). Similarly, t^* was estimated with a lower bound constraint of 20 dps, and an upper bound constraint of 45 dps (Suttkus, 1956; Hettler, 1984; Raynie, 1991). Hind-casting to estimate growth rates for larvae at ages not sampled, due to larvae being offshore at these early ages, can be accomplished using this two cycle Laird-Gompertz growth model (Lozano et al., 2012). The two cycle Laird-Gompertz model was applied to the pooled otolith data, and to each of the two sample years. Comparison between the yearly and poled models was conducted using an F-test in R Software (v2.14.0).

The Laird parameterization of the Gompertz growth model was applied to each of the two developmental stages for groupings based on SL from the distribution of SLs of larvae that had the otoliths removed, and age based on previous literature (Raynie, 1991). The Laird-Gompertz model was fit using R Software (v2.14.0) and took the following form:

$$L_t = L_{null} e^{k(1-e^{-at})}$$

where L_t represents the SL (mm) at age t (days), L_{null} represents SL at hatch for *B. patronus*, a is the rate of exponential decay, and k is a dimensionless parameter so that ka represents the instantaneous growth rate at hatching. Hind-casting can also be used to estimate growth rates for larvae at ages not sampled with this model structure (Lozano et al., 2012).

Mean growth rates and instantaneous growth rates for blocks of 10 dps were calculated. Mean growth rates for the 10 day interval were calculated with the following equation:

$$G_{10} = \frac{(L_{t2} - L_{t1})}{\Delta t}, \quad \text{where } t2 > t1$$

where G_{10} represents the average growth rate for that 10 day interval, L_{t2} represents the modeled SL at some point $t2$, L_{t1} represents the modeled SL at some point $t1$, and Δt is the 10 dps interval. Instantaneous growth rates for the same 10 dps interval rates were then determined from the natural log of the lengths in the following equation:

$$IG_{10} = \frac{(\ln(L_{t2}) - \ln(L_{t1}))}{\Delta t}, \quad \text{where } t2 > t1$$

where IG_{10} represents the average growth rate for that 10 day interval, L_{t2} represents the modeled SL at some point $t2$, L_{t1} represents the modeled SL at some point $t1$, and Δt is the 10 dps interval.

Somatic growth changes were measured using difference in the width of the daily increments and variation in ring distance from the otolith core. Changes in otolith ring width and distance from the core are expected to occur after the change in stage and feeding regimen. Ring width was measured using the digital analysis previously described, and mean ring distance from the core and mean ring width were calculated for both the sampling period from October 2006 to March 2007 and the period from September 2007 to March 2008.

5.3 Results

5.3.1 Hydrographic

Water temperatures based on sampling depth yielded no statistical differences, which is consistent with a vertically well-mixed tidal pass. Water temperatures ($\bar{x} = 20.51^{\circ}\text{C}$) generally had low variability during any sampling effort (Figure 5.2). However, from late November 2006 to early February 2007, recorded temperatures were colder and fluctuations were greater than other sampling efforts. In particular, the January 2007 sampling had a range of 10.2°C during

the 72 hour sampling period. Water temperatures followed the normal seasonal trends, i.e., water was warmer during the early fall (i.e., September and October) and cooled into the winter before rising again during March and April. There was a noticeable drop in temperature during November 2006, and median water temperature remained below 15°C through early February 2007. Although there was also a decrease in water temperature in November 2007, the median water temperature did not fall below 17°C during the remaining sampling year.

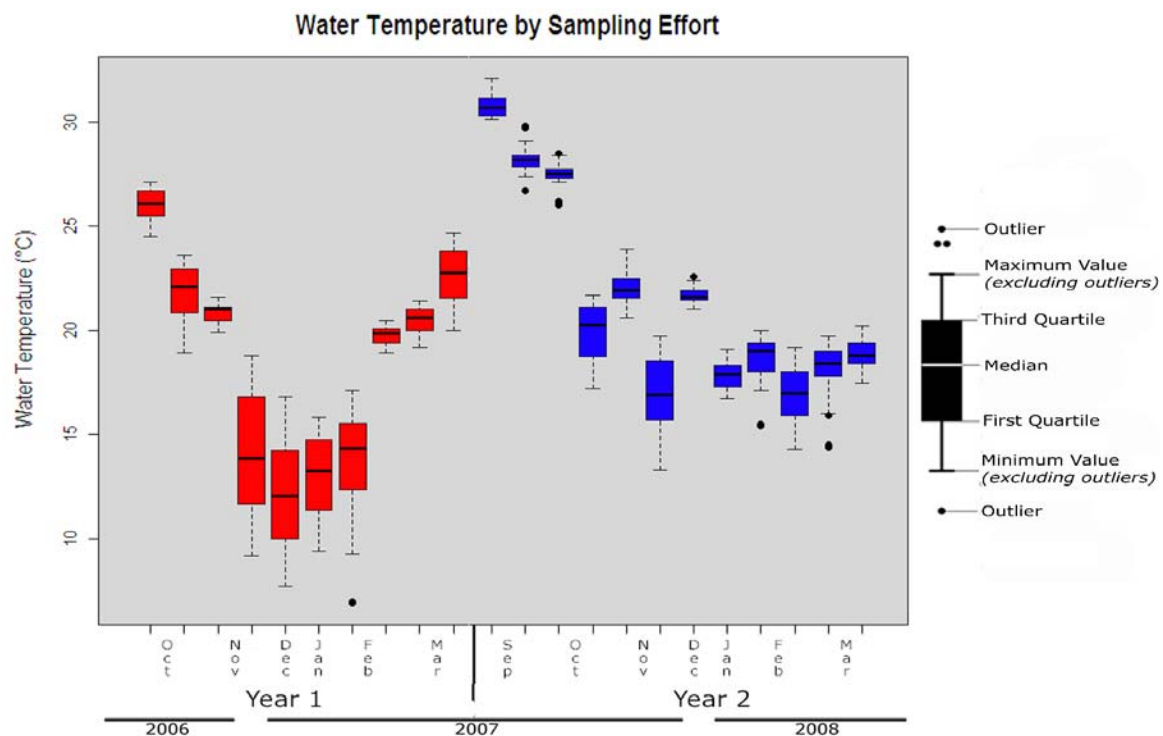


Figure 5.2: Water temperature variations by month across the two years of field sampling, year 1 (red) and year 2 (blue). Both years show a similar trend of decreased temperature from November through early February. Year two was generally warmer, although cooler water lasted into March 2008. High variability occurred during the months with coldest water temperatures.

5.3.2 Larval *Brevoortia patronus* Catches

There were 2,846 *B. patronus* larvae collected in Bayou Tartellan during the sampling efforts from October 2006 to April 2008; 2,158 larvae collected during year one, October 2006 to March 2007, and 688 larvae collected during year two, September 2007 to March 2008. January 2007 accounted for 40% of all larvae collected in the period from October 2006 to March 2007, and 30.3% of the total number of *B. patronus* larvae collected over both years. November 2007 collections had the second highest number of larvae accounting for 26.3% of all *B. patronus* larvae collected in year two, and 6.4% of all larvae collected across both sampling years.

5.3.3 Length, Age, and Spawning Dates

There were a total of 240 *B. patronus* larvae that had sagittal otoliths removed for analysis. Thirty-two otoliths did not produce readable radii and were excluded from the analysis. The length frequency of all larval *B. patronus* that were aged ($N = 208$) was bimodal (Shapiro-Wilk: $p = 1.433e^{-15}$), and as a result, we split the overall distribution into two groups to achieve two distributions that were normal, one of larvae between 5 and 16 mm SL ($\bar{x} = 12.1 \text{ mm}, sd = 3.71$) and the other consisting of larvae greater than 16 mm SL ($\bar{x} = 19.4 \text{ mm}, sd = 1.39$; Figure 5.3). During year one, the mean SL was 14.7 mm ($sd = 4.61$), and for year two, the mean SL was 16.3 mm ($sd = 4.83$) with a slightly larger range (Figure 5.4). Overall, the largest larvae were collected from January through March. In year one, the largest larvae were collected in January 2007 versus in March 2008 for year two. Combining both sample years, larval *B. patronus* had a mean age of 32.3 dps ($sd = 12.15$), a median of 31.5 dps, and a range of 11 to 67 dps. For year one, October 2006 to March 2007, ages were relatively well

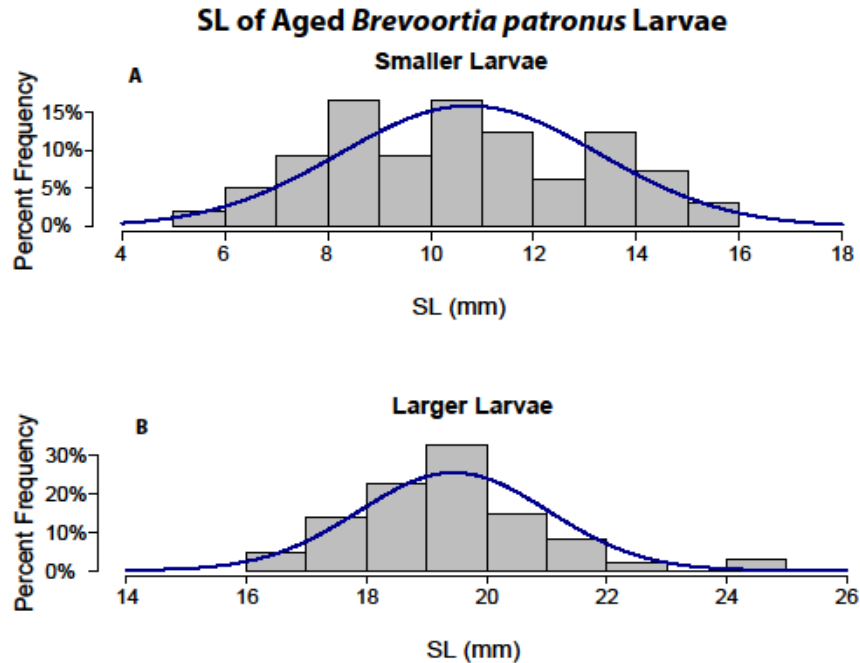


Figure 5.3: Standard length (SL) data for all *B. patronus* larvae used for sagittal otolith analyses, presented as a histogram. (A) Contains all larvae between 5 and 16 mm SL, $\bar{x} = 10.8 \text{ mm}$, $sd = 2.51 \text{ mm}$. (B) Contains all larvae greater than 16 mm SL, $\bar{x} = 19.4 \text{ mm}$, $sd = 1.39 \text{ mm}$. Both histograms were normally distributed ($p > 0.05$, Shapiro-Wilk's test).

distributed across the range of 15 to 67 dps, with a maximum density between 18 and 24 dps.

Also in year one, the oldest larvae were collected in the largest numbers between December 2006 and February 2007 (Figure 5.5). In year two, September 2007 to March 2008, the highest densities were for larvae between 35 and 45 dps, and the overall age distribution was flatter than the previous sample year. Also in year two, the oldest larval *B. patronus* were collected in March 2008.

In both sample years, approximately half of all spawning dates for larvae sampled in Bayou Taretellan occurred in the fall (i.e., before mid-January), with the other half occurring in

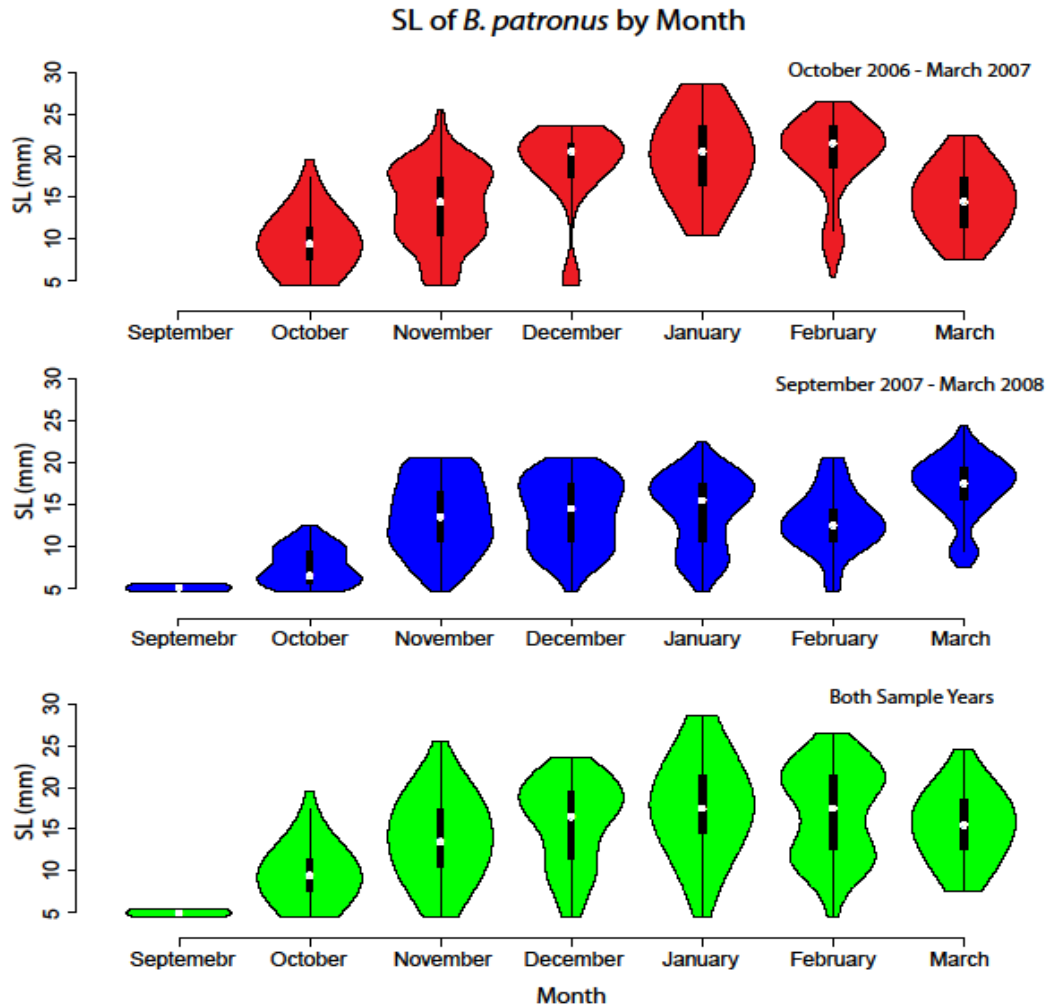


Figure 5.4: Violin plots of larval *B. patronus* SL by month broken down by sampling period for each year and total. Violin plots show the kernel density of lengths as the shape, the mean for each month as the white point, and the 50% center quartile with the thick black bar. October 2006 – March 2007 is provided in red, with $\bar{x} = 14.7 \text{ mm}$, and $sd = 4.61 \text{ mm}$. September 2007 – March 2008 is provided in blue, with $\bar{x} = 16.3 \text{ mm}$, and $sd = 4.83 \text{ mm}$. Pooled data are provided in green, with $\bar{x} = 15.4 \text{ mm}$, and $sd = 4.75 \text{ mm}$.

the spring. In year one, the greatest number of spawning dates occurred during 1-28 February 2007, with a smaller secondary peak occurring in October 2006 (Table 5.1). During year two, the greatest number of spawning dates occurred between 16 January and 15 February 2008, with a second smaller peak in late October/early November 2007.

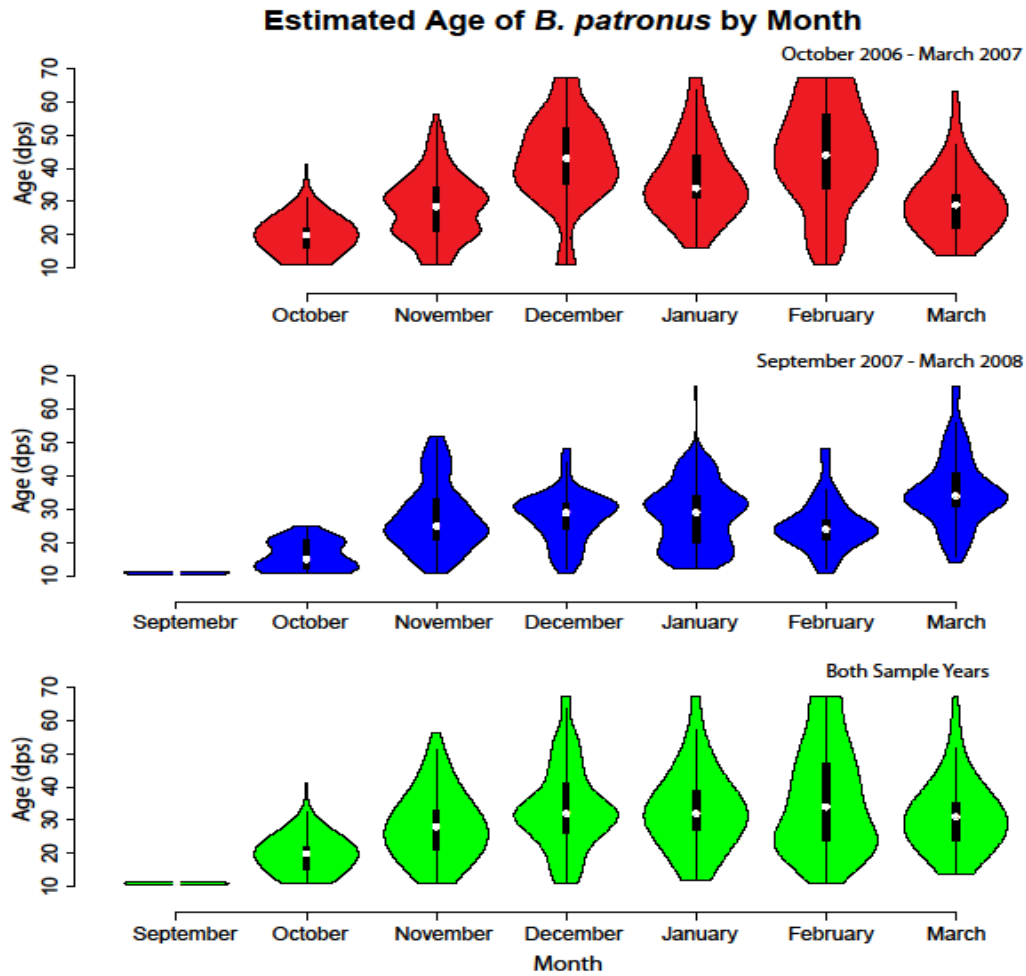


Figure 5.5: Violin plots of larval *B. patronus* age in days post spawning (dps) by month, broken down by sampling period for each year and total. Violin plots show the kernel density of ages as the shape, the mean for each month as the white point, and the 50% center quartile with the thick black bar. October 2006 – March 2007 is provided in red, with $\bar{x} = 30$ dps, and $sd = 13.2$ dps. September 2007 – March 2008 is provided in blue, with $\bar{x} = 29$ dps, and $sd = 11.0$ dps. Pooled data are provided in green, with $\bar{x} = 30$ dps, and $sd = 12.4$ dps.

Table 5.1: Spawning dates for larval *B. patronus* based on back calculated otolith ages and collection dates after application of length frequency keys. Percentages and cumulative percentages are based on half month intervals.

Interval	2006 - 2007		2007 - 2008	
	%	Cumulative %	%	Cumulative %
09/01 - 09/15	0.07	0.07	0.20	0.20
09/16 - 09/30	1.39	1.46	0.40	0.61
10/01 - 10/15	15.28	16.74	1.97	2.58
10/16 - 10/31	8.45	25.19	9.91	12.49
11/01 - 11/15	2.95	28.14	10.12	22.61
11/16 - 11/30	2.49	30.63	4.86	27.47
12/01 - 12/15	6.79	37.42	11.33	38.80
12/16 - 12/31	9.70	47.12	8.50	47.29
01/01 - 01/15	2.49	49.62	5.92	53.21
01/16 - 01/31	6.58	56.20	14.67	67.88
02/01 - 02/15	20.96	77.17	19.47	87.35
02/16 - 02/28	19.13	96.29	7.28	94.64
03/01 - 03/15	2.25	98.54	3.95	98.58
03/16 - 03/31	1.46	100.00	1.42	100.00

5.3.4 Modeled *Brevorttia patronus* Growth Rates

The two cycle Laird-Gompertz growth model provided a good model fit accounting for the faster initial growth rate and for the slower growth rate due to increased sensory, organ, and gill raker development at the onset of the ontogenetic shift in feeding strategy from a selective particulate feeder to an omnivorous filter feeder (Figure 5.6). This shift in growth rate was estimated in the model to occur after 33 dps ($t^* = 33.086$). The model estimated length at hatch was 2.88 mm SL, with a specific growth rate at hatch of $A = 0.00145 \text{ day}^{-1}$. During this larval stage, the maximum growth rate was $0.71 \text{ mm} \cdot \text{day}^{-1}$, with a mean growth rate of $0.45 \text{ mm} \cdot \text{day}^{-1}$. After the start of the developmental shift, at the modeled SL of 18.13 mm, the age specific

growth rate was $B = 0.00060 \text{ day}^{-1}$. The initial portion of this growth stanza, i.e., the transformation to the juvenile stage and switch in feeding strategy, had a maximum growth rate of $0.20 \text{ mm} \cdot \text{day}^{-1}$, with an average growth rate of only $0.10 \text{ mm} \cdot \text{day}^{-1}$.

Two cycle laird-Gompertz models were also fit separately to year one and two, October 2006 to March 2007 and September 2007 to March 2008, respectively. However, these two models did not result in better performance over the pooled model ($p = 0.203$, $F - \text{test}$; Figure 5.6). The two models did not differ in the time of onset of developmental shift, with $t_{\text{YEAR } 1}^* = 33.145 \text{ dps}$ and $t_{\text{YEAR } 2}^* = 33.025 \text{ dps}$. However, year one did have greater instantaneous growths at hatch $A_{\text{YEAR } 1} = 0.0018 \text{ day}^{-1}$ versus $A_{\text{YEAR } 2} = 0.0012 \text{ day}^{-1}$, and after the beginning of the developmental shift $B_{\text{YEAR } 1} = 0.0009 \text{ day}^{-1}$ versus $B_{\text{YEAR } 2} = 0.0004 \text{ day}^{-1}$. For year one, the maximum growth rate for the larval stage was $0.63 \text{ mm} \cdot \text{day}^{-1}$ ($\bar{x} = 0.44 \text{ mm} \cdot \text{day}^{-1}$), and the initial juvenile stage had a maximum growth rate of $0.25 \text{ mm} \cdot \text{day}^{-1}$ ($\bar{x} = 0.12 \text{ mm} \cdot \text{day}^{-1}$). In year two, the maximum growth rate in the larval stage was $0.77 \text{ mm} \cdot \text{day}^{-1}$ ($\bar{x} = 0.47 \text{ mm} \cdot \text{day}^{-1}$), and the initial portion of the juvenile stage had a maximum growth rate of $0.16 \text{ mm} \cdot \text{day}^{-1}$ ($\bar{x} = 0.09 \text{ mm} \cdot \text{day}^{-1}$).

Individual Laird-Gompertz models were fit for pre- and post-metamorphic stages, first where the stages were delineated by age, and secondly where the stages were determined from SL. The breakdown by age between the two Laird-Gompertz models provided better fits in describing the somatic growth during each period versus the grouping determined by SL, due to the increased variability in length at a particular age. The first Laird-Gompertz model for larval stage based on the age grouping had an initial specific growth rate of $ka = 0.075 \text{ day}^{-1}$, with a weaker decay rate of $\alpha = 0.019$. This larval stage had a modeled maximum growth rate of 0.72

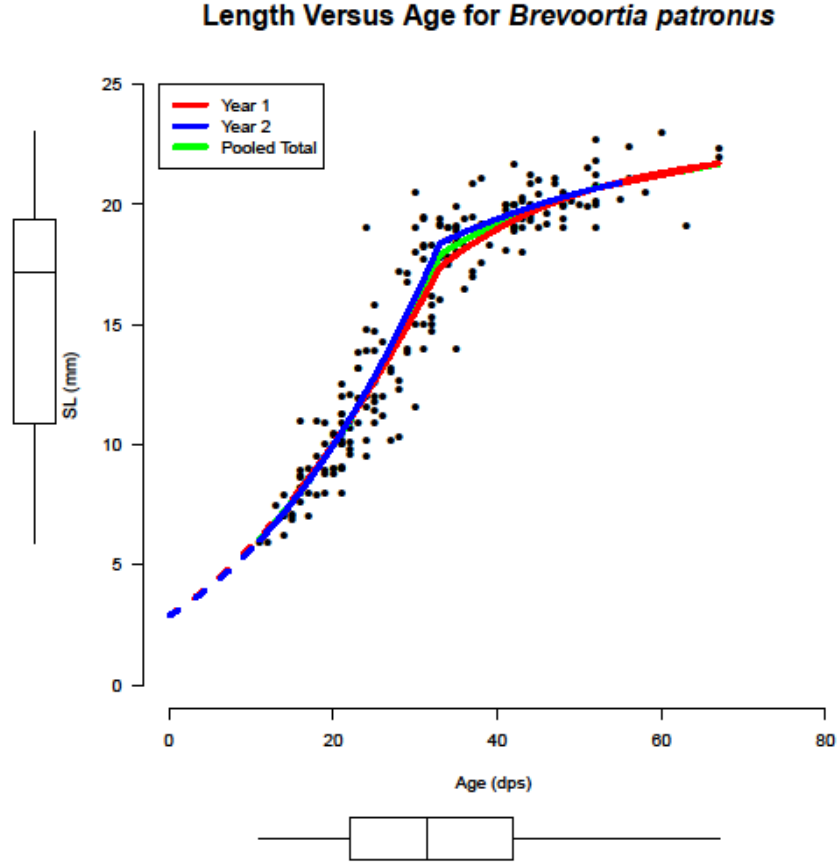


Figure 5.6: Two cycle Laird-Gompertz growth models for each sample year and pooled total of larval *B. patronus* otoliths as SL (mm) versus age in days post spawning (dps). The models are hind casted through the estimated intercept to estimate growth rates of larvae at ages in dps less than the minimum age measured. Boxplots showing the median, 25% and 75% quantiles, 95 percent confidence intervals, and outliers are provided for each axis. The two cycle Laird-Gompertz models for each year are parameterized as:

Year 1

$$SL = 2.881552e^{\left[\frac{0.077875(1-e^{(-0.023201\Delta_1)})}{0.023201} + \frac{0.014877(1-e^{(-0.058754\Delta_2)})}{0.058754}\right]},$$

$$\Delta_1 = \text{MIN}(\text{Age}, 33.145155)$$

$$\Delta_2 = \text{MAX}(\text{Age} - 33.145155, 0)$$

Year 2

$$SL = 2.881552e^{\left[\frac{0.073058(1-e^{(-0.016744\Delta_1)})}{0.016744} + \frac{0.008855(1-e^{(-0.040660\Delta_2)})}{0.040660}\right]},$$

$$\Delta_1 = \text{MIN}(\text{Age}, 33.085634)$$

$$\Delta_2 = \text{MAX}(\text{Age} - 33.085634, 0)$$

mm·day⁻¹, and a mean growth rate of 0.46 mm·day⁻¹ (Figure 5.7A). During the initial portion of the juvenile developmental stage, the decay rate for the age grouped model was $\alpha = 0.063$. This stage in the age grouped model had a maximum growth rate of 0.20 mm·day⁻¹, with an average growth rate of 0.09 mm·day⁻¹. The pre-metamorphic larval stage for the SL grouping had an initial specific growth rate of $ka = 0.090 \text{ day}^{-1}$, with a decay rate of $\alpha = 0.039$. This pre-metamorphic stage had a modeled maximum growth rate of 0.41 mm·day⁻¹, and a mean growth rate of 0.37 mm·day⁻¹ (Figure 5.7B). During the post-metamorphic juvenile developmental stage, the decay rate was $\alpha = 0.015$. The onset of this juvenile development stage had a comparatively lower maximum growth rate of 0.13 mm·day⁻¹, and an average growth rate of 0.11 mm·day⁻¹. Ten day averages of growth rates in dps, i.e., blocks, showed similar rates comparatively to the two cycle Laird-Gompertz and individual grouping Laird-Gompertz models. Overall, the peak growth rate during the initial larval developmental stage was between 20 and 30 dps (0.59 mm·day⁻¹; Table 5.2). The greatest growth rate for each sample year also occurred between 20 and 30 dps, with year one having a rate of 0.55 mm·day⁻¹, and year two having a growth rate of 0.62 mm·day⁻¹. The greatest change in instantaneous growth rates occurred between the 20 to 30 dps block and the 30 to 40 dps block for each year. This period coincides with the ontogenetic change in feeding strategy for a selective particulate feeder to omnivorous filter feeder, and coincides with the model estimated date of approximately 33 dps for the shift in growth stanza.

Otolith microstructure analyses showed changes in both mean ring distance from core as well as mean ring width after 33 dps. Mean ring distance from the otolith core during the initial larval stage was similar for both October 2006 to March 2007 and September 2007 to March 2008. After the modeled ontogenetic shift at approximately 33 dps, otolith growth slowed with

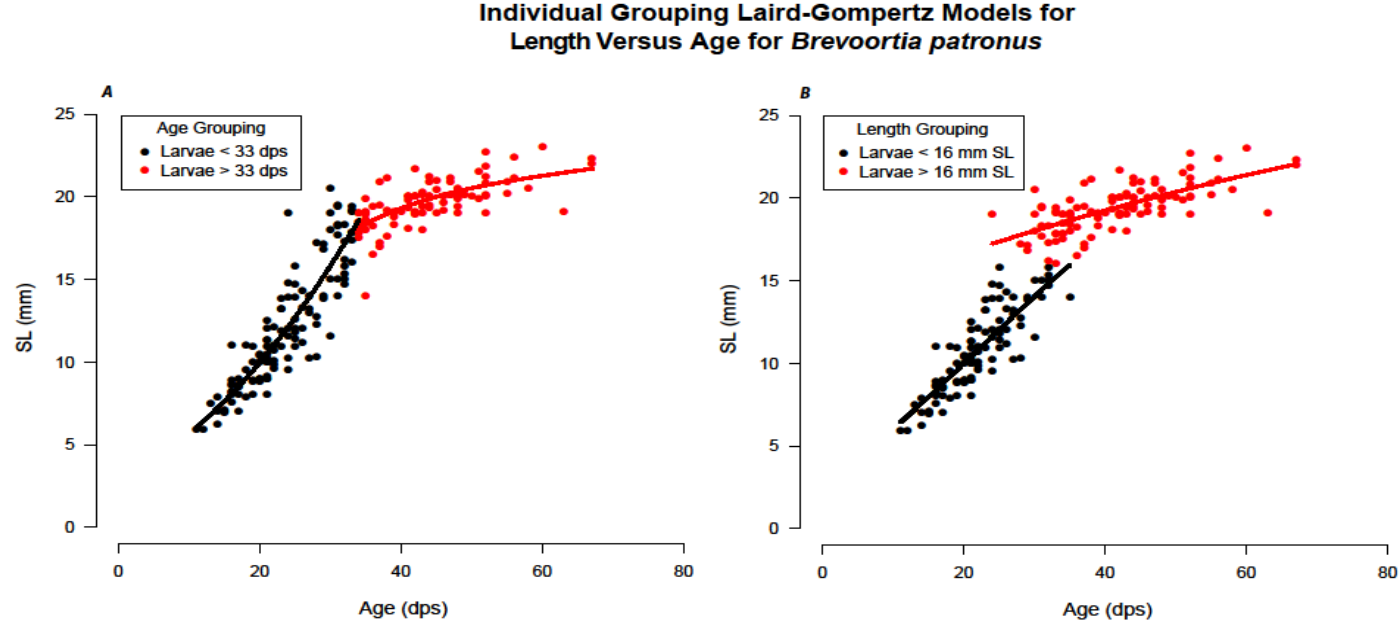


Figure 5.7: Laird-Gompertz growth models of larval *B. patronus* otoliths as SL (mm) versus age (dps) for each of the two individual groupings. (A) In the age grouping, larvae with a measured age less than 33 dps are provided as points in black with the corresponding black model line, and larvae greater than 33 dps are provided as points in red with the corresponding red model line. (B) In the length grouping, larvae with a measured SL less than 16 mm are provided as points in black with the corresponding black model line, and larvae greater than 16 mm SL are provided as points in red with the corresponding red model line.

The two Laird-Gompertz age models are parameterized as:

Larvae < 33 dps (Black)

$$SL = 2.881552e^{3.868674(1-e^{-0.019345Age})}$$

Larvae > 33 dps (Red)

$$SL = 6.54628e^{1.23864(1-e^{-0.05084Age})}$$

The two Laird-Gompertz length models are parameterized as:

Larvae < 16 mm SL (Black)

$$SL = 2.881552e^{2.298079(1-e^{-0.038964Age})}$$

Larvae > 16 mm SL (Red)

$$SL = 13.79161e^{0.74645(1-e^{-0.01480Age})}$$

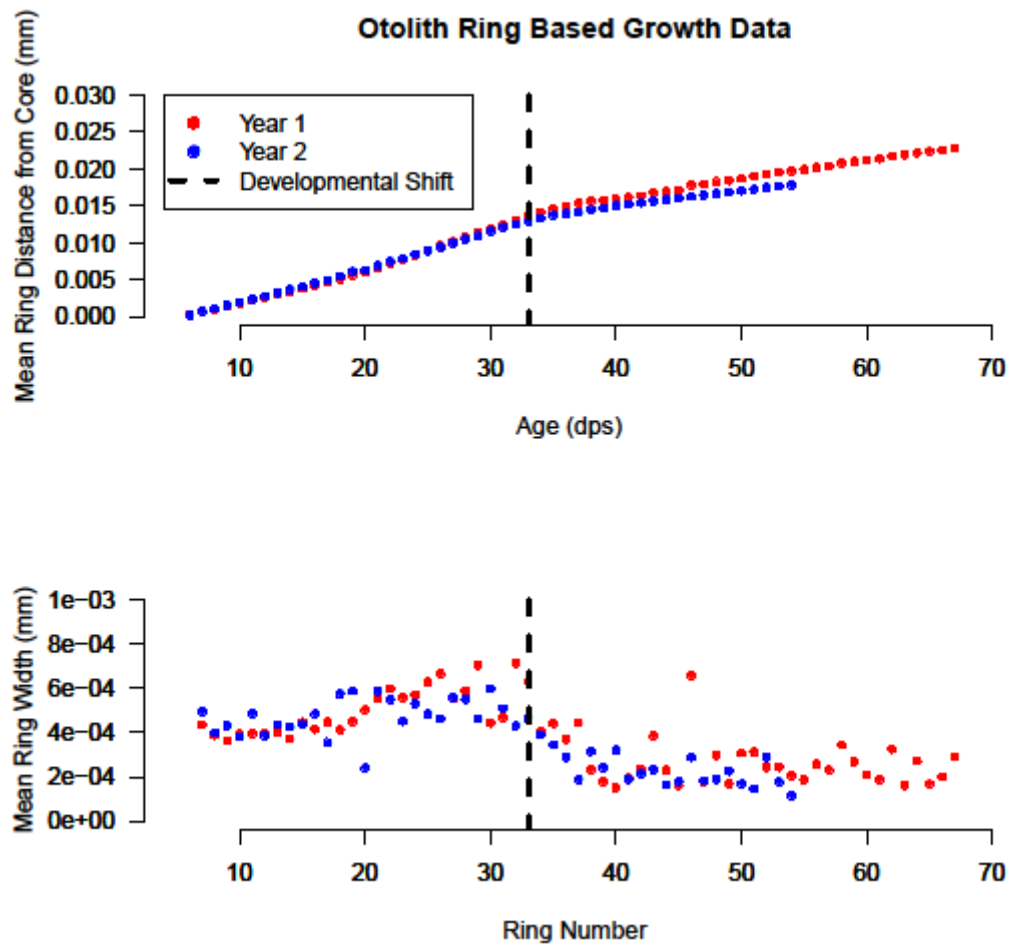


Figure 5.8: (A) Otolith ring mean distance (mm) from the core by sample year. October 2006 to March 2007 are provided in black, and September 2007 to March 2008 are provided in red. The blue dashed line represents the modeled developmental shift at 33 days post spawning (dps) from larvae into the beginning of the juvenile stage. (B) Mean ring width (mm) for individual daily rings from removed and imaged otoliths. October 2006 to March 2007 are provided in black, and September 2007 to March 2008 are provided in red. Decreases in ring width correspond to the modeled developmental shift (blue dashed line) occurring at 33 dps.

limited variability, and year two otolith growth was slower than year one (Figure 5.8A). Mean ring width showed a similar pattern with the decline in ring width occurring after 33 dps, with limited differences between either sampling years. Before the beginning of the ontogenetic shift, ring width for both sample years appeared to increase slightly, correlating to the two-cycle

modeled growth rate being largest prior to the expected shift in feeding morphology/strategy (Figure 5.8B).

Table 5.2: Average growth rates and instantaneous growth rates for larval *B. patronus* based on otolith data, grouped by age blocks of ten days post spawning. Growth rates (g) and instantaneous growth rates (G) are provided for the October 2006 to March 2007 sampling period, the September 2007 to March 2008 sampling period, and the overall combined data.

Blocks (dps)	2006 - 2007		2007 - 2008		Overall	
	g (mm·day ⁻¹)	G (day ⁻¹)	g (mm·day ⁻¹)	G (day ⁻¹)	g (mm·day ⁻¹)	G (day ⁻¹)
0 - 10	0.289	0.070	0.276	0.067	0.281	0.068
10 - 20	0.424	0.055	0.433	0.057	0.428	0.056
20 - 30	0.549	0.044	0.617	0.048	0.586	0.046
30 - 40	0.347	0.020	0.326	0.018	0.338	0.019
40 - 50	0.148	0.008	0.109	0.005	0.128	0.006
50 - 60	0.087	0.004	0.076	0.004	0.081	0.004
60 - 70	0.050	0.002	0.052	0.002	0.050	0.002

5.4 Discussion

Hatch length as calculated by the two-cycle, Laird-Gompertz model was 2.88 mm, which agreed well with previously reported length of approximately 3mm total length reported elsewhere (Hettler, 1984; Warlen, 1988; Powell, 1994; Raynie and Shaw, 1994). Smaller and younger larvae were encountered earlier in the sample period, i.e., September to early October, for both years. September recruitment of *B. patronus* larvae is novel for Louisiana waters (Raynie and Shaw, 1994; Carassou et al., 2012), and the smaller sizes and younger ages suggest a truncated recruitment corridor with spawning occurring earlier than previously reported and within more coastal waters (Shaw et al., 1988). The shorter length of the spawning ground to

estuary recruitment corridor at this time of year may possibly be a result of the GOM hypoxia zone forcing spawning aggregations into a narrow, alongshore corridor (Vaughn et al., 2007). Although there is still much debate on the role hypoxia may play in fisheries production (Chesney and Baltz, 2001; Breitburg, 2002; Diaz and Rosenberg, 2008), such a shortened spawning ground to estuary recruitment corridor may drive earlier estuarine recruitment for larval *B. patronus*, thereby decreasing offshore mortality during larval drift (Cushing, 1974; Letcher et al., 1996).

Spawning dates back calculated from ages (dps) suggested movement of spawning aggregations further offshore the longer the season progressed (Whitehead, 1985; Vaughan et al., 2007). Both sample years had bimodal spawning peaks, with minor differences in the distribution of spawning dates. The fall spawning peak occurred in either October or November, depending on year (Figure 5.5), and was smaller and earlier than the previously reported spawning peaks occurring in late January and February (Shaw et al., 1988; Powell 1994; Raynie and Shaw, 1994; Vaughn et al., 2000). In particular, there were a number of larval *B. patronus* collected in late September to early October 2007 that were 3-5 mm SL. Overall the larvae comprising the smaller fall spawning peak were generally smaller ($\bar{x} = 14 \text{ mm SL}$), and younger (22 dps) than the larger winter peak ($\bar{x} = 19 \text{ mm SL}$, age = 41 dps). The fall peak, however, corresponded to a shorter recruitment corridor and transit time, i.e., approximately 3 weeks, compared to the winter peak with transport times of approximately 6 weeks. The fall transit time, therefore, is much shorter than the 4-10 week transport time estimated by Shaw et al. (1988), but corresponds well with adults being distributed along the coast in nearshore waters

during late summer/early fall before moving further offshore in October (Ahrenholz 1991) and perhaps being constrained by the Louisiana hypoxic zone (Vaughn et al., 2007).

The greatest larval growth rate was determined to occur a few days before the beginning of the ontogenetic transformation from selective particulate feeding to omnivorous filter feeding, with some variability between sampling years. The two cycle Laird-Gompertz model had a maximum growth rate for the initial larval stage ($0.71 \text{ mm} \cdot \text{day}^{-1}$ at 33 dps) similar to the individual age grouped, Laird-Gompertz model ($0.72 \text{ mm} \cdot \text{day}^{-1}$ at 33 dps), and both models had higher maximum growth rates than the SL grouped, Laird-Gompertz model ($0.41 \text{ mm} \cdot \text{day}^{-1}$) or the grouped 10 dps block ($0.586 \text{ mm} \cdot \text{day}^{-1}$ at 20-30 dps). The individual Laird-Gompertz models grouped by SL showed agreement with previous studies for the larval stage growth, with no difference between this study's mean calculated growth ($0.37 \text{ mm} \cdot \text{day}^{-1}$) and previously reported values of $0.36 - 0.37 \text{ mm} \cdot \text{day}^{-1}$ (Warlen, 1988; Raynie, 1991). However, the agreement between the two cycle Laird-Gompertz models in this study, modeled growth by Raynie and Shaw (1994), and the individual Laird-Gompertz models grouped by age suggested the timing of metamorphosis development was tied to age and ultimately upon ontogeny-based, shifting prey fields (Ditty et al., 2003; Ditty and Shaw, 2005). Any differences in length at these ages are likely due to variability in food sources/resources causing differences in the larval growth rate (Warlen, 1988; Lyczkowski-Shultz et al., 1990; Warlen, 1992) during the initial larval stage, when *B. patronus* larvae are selective particulate feeders (Stoecker and Govoni, 1984; Deegan 1990; Lozano et al., 2012) .

Water temperature differences between sampling year one and two supported the slight differences in growth rates and otolith microstructure for both years. In year one, the highest

growth rate was $0.63 \text{ mm} \cdot \text{day}^{-1}$, and was much lower than the maximum growth rate in year two ($0.77 \text{ mm} \cdot \text{day}^{-1}$), when overall warmer water temperatures could have increased somatic growth (Houde, 1987; Heimbuch et al., 2007). However, differences in mean ring distance from otolith core, while small, showed the opposite trend of slightly faster otolith ring growth during year one. Previous work, however, has found similar decoupling between otolith growth and somatic growth (Mosegaard et al., 1988; Fey, 2006). Otolith microstructure for both years showed an increase in otolith ring width before the beginning of the ontogenetic shift from selective particulate feeding to an omnivorous filter feeding. The high growth rate before the shift in feeding strategy is potentially the result of lag time to adjust to new food source/resources, while the appropriate feeding structures finish development (Stoecker and Govoni, 1984; Deegan, 1990; Maillet and Checkley 1990; Lozano et al., 2012).

There was overwhelming agreement between the pooled, two cycle Laird-Gompertz model, the two cycle Laird-Gompertz models fit for each individual years, and the otolith microstructure analysis, for the mean age at which the ontogenetic shift from the larval to a juvenile stage began (33 dps), which coincided with the age previously reported for Fourleague Bay, Louisiana (33.55 dps; Raynie and Shaw, 1994). Otolith mean distance from the core and mean ring width decreased after 33 dps, which probably reflects limited feeding at this point due to the ontogenetic shift (Deegan, 1990; Raynie, 1991; Warlen, 1992; Lozano and Houde, 2013). Ten day blocked averages for growth rate and instantaneous growth rate showed similar agreement with the models for the initiation of transformation, with the greatest decrease in growth rates occurring between 30 and 40 dps. Transforming larvae of this age, which were between approximately 19 and 21 mm SL, may be expending more energy in development of

feeding apparatuses as they change food sources for the juvenile/adult stage (Deegan, 1990; Maillet and Checkley, 1990), and/or in deepening their body rather than increased length (Deegan, 1990, Raynie and Shaw, 1994).

The slower growth rates during the period, when feeding strategy begins to change, were similar across sampling years and modeling technique. The growth rates for the pooled ($0.10 \text{ mm} \cdot \text{day}^{-1}$) and yearly two cycle models ($0.12 \text{ mm} \cdot \text{day}^{-1}$ and $0.09 \text{ mm} \cdot \text{day}^{-1}$, respectively) had strong agreement with the grouped Laird-Gompertz models ($0.11 \text{ mm} \cdot \text{day}^{-1}$ and $0.09 \text{ mm} \cdot \text{day}^{-1}$). Within the 10 day blocking averages, the difference in growth rates between years is minor, and the expected period during onset of the feeding transition showed a similar decrease in growth rates. The switch of feeding from a selective, particulate, zoo-planktivorous strategy to an omnivorous filter feeding strategy likely drove the lower growth rate during this period (Deegan, 1990; Maillet and Checkley, 1990; Chen et al. 1992; Lozano et al., 2012). Moreover, the decrease in otolith ring width showed that although daily rings were still accrued, there was limited growth during this time period. Previously reported growth rates of $0.11 \text{ mm} \cdot \text{day}^{-1}$ (Raynie, 1991) and $0.12 \text{ mm} \cdot \text{day}^{-1}$ (Deegan, 1990) agreed with all models herewithin. Despite this reduction in growth rate during transformation to the juvenile stage, larval *B. patronus* may typically undergo another period of rapid growth after 30 mm SL, when the larvae have acquired fully-developed feeding structures and are able to filter feed effectively, thereby enabling growth rates as high as $0.48 \text{ mm} \cdot \text{day}^{-1}$ (Deegan, 1990).

5.5 Conclusions

In general, the objectives of this study were successfully met. The use of the digital filtering methodology for analyzing *B. patronus* otoliths, combined with modeling and

microstructure analyses, provided an effective tool for analyzing length at age. The use of digital filtering techniques to quickly and objectively determine daily increments in small, fragile larval *B. patronus* otoliths also provided objective measurements of otolith microstructure. Although useful in comparisons to previous work, the individually-grouped, Laird-Gompertz models were less parsimonious and did not capture the ontogenetic shift in feeding strategy from a selective particulate feeder to an omnivorous filter feeder, except through interpretation. Finally, increased water temperature during year two appeared to increase growth rates, but those rates appeared to be decoupled from direct otolith ring depositional width comparisons between years.

The peak spawning period for *B. patronus* estimated from this study was from December to early February in 2006-2007 and from January to February in 2008. However, collection of small (3 – 5 mm SL) and young (7 – 12 dps) larvae in late September - early October had back-calculated spawning dates that suggested a much earlier spawning season (i.e., early September) and a much shorter recruitment corridor than previously reported. Generally, larvae were older and larger the longer the season progressed, consistent with previous literature.

The two cycle Laird-Gompertz models, individually grouped Laird-Gompertz models, ten day blocked averages, and otolith microstructure all show high agreement that the beginning of an ontogenetic shift in feeding strategy occurred at approximately 33 dps. Moreover, all models showed that the greatest growth rate occurred prior to the ontogenetic shift in feeding capability, confirming the accumulative learning curve that larger larvae acquire to effectively select particulate zooplankton from the water column. The decrease in growth rate after the shift in development began was remarkably similar in all modeling analyses, and the growth rate appeared to be relatively constant over both sampling years.

5.6 Literature Cited

- Adobe Photoshop CS4® (v11.0). 2008. Adobe Systems Incorporated.
- Ahrenholz, D.W. 1991. Population biology and life history of the North American menhadens, *Brevoortia* spp. *Mar. Fish. Rev.*, 53: 3-19.
- Barbieri, L.R., M. Chittenden Jr., and S.K. Lowerre-Barbieri. 1994a. Maturity, spawning, and ovarian cycle of Atlantic croaker, *Micropogonias undulatus*, in the Chesapeake Bay and adjacent coastal waters. *Fish. Bull.*, 92(4): 671-685.
- Barbieri, L.R., M. Chittenden Jr., and S.K. Lowerre-Barbieri. 1994b. Age, growth and mortality of Atlantic croaker, *Micropogonias undulatus*, in the Chesapeake Bay region, with a discussion of apparent geographical changes in population dynamics. *Fish. Bull.*, 92(4): 1-12.
- Breitburg, D. 2002. Effects of hypoxia, and the balance between hypoxia and enrichment, on coastal fishes and fisheries. *Estuaries*, 25(4): 767-781.
- Campana, S.E. 1992. Measurement and interpretation of the microstructure of fish otoliths. In: D.K. Stevenson and S.E. Campana, eds., *Otolith microstructure examination and analysis*. *Can. Sp. Pub. Fish. Aqu. Sci.*, 117: 59-71.
- Carassou, L., F.J. Hernandez, S.P. Powers, and W.M. Graham. 2012. Cross-shore, seasonal depth-related structure of ichthyoplankton assemblages in coastal Alabama. *Trans. Am. Fish. Soc.*, 141: 1137-1150.
- Chambers, R.C. and T.J. Miller. 1995. Evaluating fish growth by means of otolith increment analysis: special properties of individual-level longitudinal data. Recent developments in fish otolith research. J.D.Secor & S.E.Campana (eds) *Columbia, SC: University of South Carolina Press*: 155-175.
- Chesney, E.J. and D.M. Baltz, 2001. The effects of hypoxia on the northern Gulf of Mexico coastal ecosystem: A fisheries perspective. pp. 321-354 In: Nancy N. Rabalais and R. Eugene Turner (eds.), *Coastal hypoxia: Consequences for living resources and ecosystems*. Coastal and Estuarine Studies 58, American Geophysical Union, Washington, D.C.
- Chen, W., J.J. Govoni, and S. Wavlen. 1992. Comparison of feeding and growth of larval round herring (*Etrumeus teres*) and gulf menhaden (*Brevoortia patronus*). *Fish. Bull.*, 90:183-189.

- Colton, J.B., W.G. Smith, A.W. Kendall Jr., P.L. Berrien, and M.L. Fahay. 1979. Principal spawning areas and times of marine fishes, Cape Sable to Cape Hatteras. Fish. Bull., 76: 911-916.
- Cushing, D. 1974. The possible density-dependence of larval mortality and adult mortality in fishes. Springer.
- Dahlberg, M.D. 1970. Atlantic and Gulf of Mexico menhadens, genus *Brevoortia* (Pisces: Clupeidae). Bulletin of the Florida State Museum, Biological Sciences 15:91-162.
- Deegan, L.A. 1990. Effects of estuarine environmental conditions on population dynamics of young-of-the-year gulf menhaden. Mar. Eco. Prog. Ser.. Oldendorf **68**:195-205.
- Deegan, L.A., and B.A. Thompson. 1987. Growth rate and early life history of young-of-the-year gulf menhaden as determined from otoliths. Trans. Am. Fish. Soc., 116: 663-667.
- Del Rio, R., S. Bargu, D. Baltz, S. Fire, G. Peterson, and Z. Wang. 2010. Gulf menhaden (*Brevoortia patronus*): A potential vector of domoic acid in coastal Louisiana food webs. Harmful Algae, 10(1): 19-29.
- Diaz, R.J., and R. Rosenberg. 2008. Spreading dead zones and consequences for marine ecosystems. Science, 321(5891): 926-929.
- Ditty, J.G., L.A. Fuiman, and R.F. Shaw. 2003. Characterizing natural intervals of development in the early life history of fishes: An example using blennies (Teleostei: Blennidae). pp. 405-418 In: H.I. Browman and A.B. Skiftesvik (eds.). The Big Fish Bang: Proceedings of the 26th Annual Larval Fish Conference. Institute of Marine Research, Bergen, Norway, (ISBN 82-7461-059-8), 476 pp.
- Ditty, J.G., and R.F. Shaw. 2005. Morphological development in five reef-associated species of blenny. J. Fish Biol. 66: 1261-1284.
- Epifanio, C.E., and R.W. Garvine. 2001. Larval transport on the Atlantic continental shelf of North America: a review. Est., Coast and Shelf Sci., 52: 51-57.
- European Fish Ageing Network (EFAN). 1997. Report of the first plenary meeting. Brest, Belarus, May 1997: 12 p.
- Fahay, M.P. 1983. Guide to the early stages of marine fishes occurring in the western North Atlantic Ocean, Cape Hatteras to the south Scotian Shelf. N. Atl. Fish. Sci., 4: 1-423.

- Fahay, M.P. 2007. Early Stages of Fishes in the Western North Atlantic Ocean: Davis Strait, Southern Greenland and Flemish Cap to Cape Hatteras. Scorpaeniformes Through Tetraodontiformes, Volume 2: Northwest Atlantic Fisheries Organization. 1696 pp.
- Fey, D.P. 2006. The effect of temperature and somatic growth on otolith growth: the discrepancy between two clupeid species from a similar environment. *J. Fish Bio.*, 69(3): 794-806.
- Fritzsche, R.A. 1978. Development of Fishes of the Mid-Atlantic Bight: An Atlas of Egg, Larval and Juvenile Stages. Volume 5, Chaetodontidae through Ophidiidae. FWS/OBS-78/12, U.S. Fish and Wildlife Service, Washington D.C. 237 pp.
- Gaemers, P.A.M. 1976. New concepts in the evolution of the Gadidae (Vertebrata, Pisces), based on their otoliths. *Mededelingen van der Werkgroep voor Tertiaire en Kwartaire Geologie* 13: 3-22.
- Geffen, A. 1993. Validation of otolith increment deposition rate. *Can. Special Pub. of Fish. and Aqu. Sci.*, :101-101.
- Gillanders, B., K.W. Able, J.A. Brown, D.B. Eggleston, and P.F. Sheridan. 2003. Evidence of connectivity between juvenile and adult habitats for mobile marine fauna: an important component of nurseries. *Mar. Eco. Prog. Ser.*, 247:281-295.
- Gompertz, B. 1815. On the Nature of the Function Expressive of the Law of Human Mortality, and on a New Mode of Determining the Value of Life Contingencies. *Philosophical Transactions of the Royal Society of London* 115: 513-585.
- Goode, 1878. *Brevoortia patronus*. *Proceedings of the U.S. Natural Museums*. 1:39.
- Guillory, V., J. Geaghan, and J. Roussel. 1983. Influence of environmental factors on gulf menhaden recruitment. Technical Bulletin No. 37. Louisiana Department of Wildlife and Fisheries. New Orleans, Louisiana. 32 pp.
- Hardy Jr., J.D. 1978a. Development of Fishes of the Mid-Atlantic Bight: An Atlas of Egg, Larval and Juvenile Stages. Volume 2, Anguillidae through Syngnathidae. FWS/OBS-78/12, U.S. Fish and Wildlife Service, Washington D.C. 229 pp.
- Hardy Jr., J.D. 1978b. Development of Fishes of the Mid-Atlantic Bight: An Atlas of Egg, Larval and Juvenile Stages. Volume 3, Aphredoderidae through Rachycentridae. FWS/OBS-78/12, U.S. Fish and Wildlife Service, Washington, D.C. 249 pp.

- Heimbuch, D.G., E. Lorda, D. Vaughan, L.W. Barnthouse, J. Uphoff, W.V. Winkle, A. Kahnle, B. Young, J. Young, and L. Kline. 2007. Assessing coastwide effects of power plant entrainment and impingement on fish populations: Atlantic menhaden example. *N. Am. J. Fish. Man.*, 27(2), 569-577.
- Hettler, W.F. 1984. Spawning and rearing Atlantic menhaden. *Progress in Fishery Culture*, 43(2): 80-84.
- Houde, E.D. 1982. Kinds, distributions and abundances of sea bass larvae (Pisces:Serranidae) from the eastern Gulf of Mexico. *Bull. Mar. Sci.*, 32: 511-522.
- Houde, E.D. 1987. Effects of temperature and delayed feeding on growth and survival of larvae of three species of subtropical marine fishes. *Mar. Bio.*, 26: 271-285.
- Johnson, G.D. 1978. Development of Fishes of the Mid-Atlantic Bight: An Atlas of Egg, Larval and Juvenile Stages. Volume 4, Carangidae through Ehippidae. FWS/OBS-78/12, U.S. Fish and Wildlife Service, Washington D.C. 189 pp.
- Jones, P.W., F.D. Martin, and J.D. Hardy. 1978. Development of Fishes of the Mid-Atlantic Bight: An Atlas of Egg, Larval and Juvenile Stages. Volume 1, Acipenseridae through Ictaluridae. FWS/OBS-78/12, U.S. Fish and Wildlife Service, Washington D.C. 224 pp.
- Laird, A.K., S.A. Tyler, and A.D. Barton. 1965. Dynamics of normal growth. *Growth* 29: 233-248.
- Leak, J.C. 1981. Studies on recruitment process focusing on early life history of the Japanese sardine, *Sardinops melanostictus* (Schlegel). *Bulletin of Natural Resources, Institute of Fisheries Science* 3: 25-278.
- Letcher, B.H., J.A. Rice, L.B. Crowder, and K.A. Rose. 1996. Variability in survival of larval fish: disentangling components with a generalized individual-based model. *Can. J. Fish. Aq. Sci.*, 53:787-801.
- Lewis, R.M., and C.M. Roithmayr. 1981. Spawning and sexual maturity of gulf menhaden, *Brevoortia patronus*. *Fish. Bull.*, 78: 947-951.
- Lombarte, A., and B. Morales-Nin. 1995. Morphology and ultrastructure of secular otoliths from five species of the genus *Coelorincus* (Gadiformes: Macrouridae) from the southeast Atlantic. *J. of Morph.*, 225: 179-192.
- Lozano, C. and E.D. Houde. 2013. Factors contributing to variability in larval ingress of Atlantic menhaden, *Brevoortia tyrannus*. *Est., Coast. and Shelf Sci.*, 118: 1-10.

- Lozano, C., E. Houde, R. Wingate, and D. Secor. 2012. Age, growth and hatch dates of ingressing larvae and surviving juveniles of Atlantic menhaden *Brevoortia tyrannus*. *Journal of Fish Biology* 81:1665-1685.
- Lyczkowski-Shultz, J., D.L. Ruple, S.L. Richardson, J. Cowan, and H. James. 1990. Distribution of fish larvae relative to time and tide in a Gulf of Mexico barrier island pass. *Bull. Mar. Sci.*, 46(3): 563-577.
- Maillet, G.L. and D.M. Checkley Jr. 1990. Effects of starvation on the frequency of formation and width of growth increments in sagittae of laboratory-reared Atlantic menhaden *Brevoortia tyrannus* larvae. *Fish. Bull.*, 88: 155–165.
- MATLAB and Statistics Toolbox Release. V7.6.0.324 R2008a, The MathWorks, Inc., Natick, Massachusetts, United States.
- Marotz, B.L., W.H., Herke, and B.D. Rogers. 1990. Movement of Gulf menhaden through three marshland routes in southwestern Louisiana. *N. Am. J. Fish. Man.*, 10(4): 408-417.
- Martin, F.D., and G.E. Drewery. 1978. Development of Fishes of the Mid-Atlantic Bight: An Atlas of Egg, Larval and Juvenile Stages. Volume 6, Stromateidae through Ogococephilidae. FWS/OBS-78/12, U.S. Fish and Wildlife Service, Washington D.C. 176 pp.
- McCrea-Strub, A., K. Kleisner, U. Sumaila, W. Swartz, R. Watson, D. Zeller, and D. Pauly. 2011. Potential impact of the Deepwater Horizon oil spill on commercial fisheries in the Gulf of Mexico. *Fisheries* 36:332-336.
- Miller, G.L., and S.C. Jorgenson. 1973. Meristic characters of some marine fishes of the western Atlantic Ocean. *Fish.s Bull.*, NOAA 71: 301-312.
- Morales-Nin, B., A. Lombarte, and B. Japon. 1998. Approaches to otolith age determination: image signal treatment and age attribution. *Sci. Mar.*, 62(3): 247-256.
- Mosegaard, H., H. Svedäng, and K. Taberman. 1988. Uncoupling of somatic and otolith growth rates in Arctic char (*Salvelinus alpinus*) as an effect of differences in temperature response. *Can. J. Fish. Aq. Sci.*, 45(9): 1514-1524.
- Moser, H.G. 1984. Ontogeny and Systematics of Fishes. American Society of Ichthyologists and Herpetologists Special Publication No. 1. Allen Press, Lawrence, Kansas. 760 pp.
- Nelson, W. R., and D.W. Ahrenholz. 1986. Population and fishery characteristics of Gulf Menhaden, *Brevoortia patronus*. *Fish. Bull.*, 84(2), 311-325.

- Nelson, J., R. Wilson, F. Coleman, C. Koenig, D. DeVries, C. Gardner, and J. Chanton. 2012. Flux by fin: fish-mediated carbon and nutrient flux in the northeastern Gulf of Mexico. *Mar. Bio.*, 159:365-372.
- Nolf, D. 1985. Otolithi piscium. In: M.P. Schultze, (ed), Handbook of Paleoichthyology Vol. 10. Gustav Fisher Verlag, Stugart, Germany, and New York, USA.
- Pannella, G. 1971. Fish otoliths: daily growth layers are periodical patterns. *Science* 173: 1124-1127.
- Pannella, G. 1974. Otolith growth patterns: an aid in age determination in temperate and tropical fishes. *The Ageing of Fish*, T.B. Bagenel, ed. Unwin Brothers, Ltd., Surrey, England. 28-39.
- Powell, A.B. 1994. Life history traits of two allopatric clupeids, Atlantic menhaden and gulf menhaden, and the effects of harvesting on these traits. *N. Am. J. Fish. Man.*, 14(1): 53-64.
- Pritchard, E.S. 2005. *Fisheries of the United States 2004*. Silver Spring, MD: National Marine Fisheries Service, Office of Science and Technology, pp. 1-19.
- R Development Core Team (v.2.14.0). 2008. R: A language and environment for statistical computing. R Foundation for Statistical Computing, Vienna, Austria. ISBN 3-900051-07-0, URL <http://www.R-project.org>.
- Rasband WS. ImageJ, U.S. National Institutes of Health, Bethesda, Maryland, USA, imagej.nih.gov/ij/, 1997—2012.
- Ralston, S. and H. Williams. 1989. Numerical integration of daily growth increments: An efficient means of aging tropical fishes for stock assessment. *Fish. Bull.*, 87: 1-16.
- Raynie, R.C. 1991. Study of the spatial and temporal ichthyoplankton abundance along a recruitment corridor from offshore to estuarine nursery. MS Thesis. Louisiana State University, Baton Rouge, Louisiana, USA. 115 pp.
- Raynie, R.C., and R.F. Shaw. 1994. Ichthyoplankton abundance along a recruitment corridor from offshore spawning to estuarine nursery ground. *Est., Coast. and Shelf Sci.*, 39(6): 421-450.
- Richards, W.J. 2006. *Early Stages of Atlantic Fishes: An Identification Guide for the Western Central North Atlantic*. Volume I & II. CRC Press, Boca Raton, FL. 2640 pp.

- Ruple, D.L. 1984. Occurrence of larval fishes in the surf zone of a northern Gulf of Mexico barrier island. *Est., Coast. and Shelf Sci.*, 18(2): 191-208.
- Schmitt, W. 1969. The otoliths as a mean for differentiation between species of very similar appearance. *Procedural Symposium on Oceanic Fishes. Resources of Sea Tropical Atlantic. FAO.* 393-396.
- Shanks, A.L., and G.L. Eckert. 2005. Population persistence of California Current fishes and benthic crustaceans: a marine drift paradox. *Eco. Mono.*, 75(4), 505-524.
- Shaw, R.F., B.D. Rogers, J. Cowan, and W.H. Herke. 1988. Ocean-estuary coupling of ichthyoplankton and nekton in the Northern Gulf of Mexico. *Am. Fish. Soc. Symp.* 3: 77-89.
- Shaw, R.F., W.J. Wiseman JR, R.E. Turner, L.J. Rouse Jr, R.E. Condrey, and F.J. Kelly Jr. 1985. Transport of larval gulf menhaden *Brevoortia patronus* in continental shelf waters of western Louisiana: a hypothesis. *Trans. Am. Fish. Soc.*, 114(4): 452-460.
- Simonsen, K.A. and J.H. Cowan. 2013. Effects of an inshore artificial reef on the trophic dynamics of three species of estuarine fish. *Bull. Mar. Sci.*, 89:657-676.
- Stoecker, D. and J. Govoni. 1984. Food selection by young larval gulf menhaden (*Brevoortia patronus*). *Mar. Bio.*, 80:299-306.
- Stuck, K.C. and H.M. Perry. 1982. Ichthyoplankton community structure in Mississippi coastal waters. Pp. VI-I-1 to VI-I-53. *In: Fishery monitoring and assessment completion report, 1 January 1977 to 31 December 1981. Gulf Coast Research Lab, Project No. 2-296-R.*
- Suttkus, R.D. 1956. Early life history of the gulf menhaden, *Brevoortia patronus*, in Louisiana. *Trans. of the N. Am. Wild. Conf.*, 21: 290-307.
- VanderKooy, S. J. and J.W. Smith. (Eds) 2002. The menhaden fishery of the Gulf of Mexico, United States: a regional management plan. *Gulf States Mar. Fish. Com.*, 99: 143 pp.
- Vaughan, D.S., Smith, J.W., and M.H. Prager. 2000. Population characteristics of gulf menhaden, *Brevoortia patronus*. NOAA/National Marine Fisheries Service, NOAA Technical Report NMFS, 149.
- Vaughan, D.S., K.W. Shertzer, and J.W. Smith. 2007. Gulf menhaden (*Brevoortia patronus*) in the U.S. Gulf of Mexico: fishery characteristics and biological reference points for management. *Fish. Res.*, 83:263-275.

- Vaughan, D.S., J.W. Smith, and A.M. Schueller. 2010. Age, growth, and reproduction of gulf menhaden. Southeast data, assessment, and Review SEDAR 27-DW02. 34 pp.
- Warlen, S.M.. 1988. Age and growth of larval gulf menhaden, *Brevoortia patronus*, in the northern Gulf of Mexico. Fish. Bull., 86(1): 77-90.
- Warlen, S.M. 1992. Age, growth, and size distribution of larval Atlantic menhaden off North Carolina. Trans. Am. Fish. Soc., 121:588-598.
- Whitehead, P.J.P., 1985. FAO Species Catalogue. Clupeoid fishes of the world (Suborder Clupeoidei). An annotated and illustrated catalogue of the herrings, sardines, pilchards, sprats, shads, anchovies and wolf-herrings. Part 1 – Chriocentridae, Clupeidae and Pristigasteridae. FAO Fisheries Synopsis, Rome 125(7/2); 305-579.
- Zweifel, J.R., and R. Lasker. 1976. Prehatch and post-hatch growth of fishes – a general model. Fish. Bull., 74: 609-621.

CHAPTER 6. LATERAL DIFFERENCES IN LARVAL DENSITY AND PROBABILITY OF ENCOUNTER USING A ZERO INFLATED NEGATIVE BINOMIAL MODEL WITHIN A VERTICALLY WELL-MIXED TIDAL PASS

Vertically, well-mixed tidal passes and estuaries in the northcentral Gulf of Mexico can present recruitment and retention issues for Ichthyoplankton, since they cannot exploit flow differentials based on depth. Alternatively, lateral flow differences related to edge effects within tidal passes may present opportunities for retention during estuarine outwelling. Densities of larval *Anchoa hepsetus*, *Anchoa mitchilli*, *Brevoortia patronus*, *Sciaenops ocellatus*, *Cynoscion arenarius*, and *C. nebulosus*, were collected at lateral three stations (northern edge, center channel, and southern edge) laterally across a tidal pass, and at two depths (surface, and near-bottom) in Bayou Tartellan, Louisiana, over 72-hour sampling periods in both April and September 2007. A Zero Inflated Negative Binomial (ZINB) model was used to analyze differences in larval density and probability of encounter, while minimizing bias from the large number of samples containing no larvae of a particular species. Results indicated that during inflows on flood tides, most larvae had a higher probability of encounter and higher densities at the surface in the center channel, where currents were strongest. During outwelling flows on ebb tides, larger larvae generally had a higher probability of encounter and higher densities at the natural southern edge of the tidal pass. The anthropogenically-altered (i.e., bulkhead) northern edge of the tidal pass appeared to be limited in both probability of encounter and density for all species considered.

6.1 Introduction

In the northern Gulf of Mexico (GOM), 75% to 95% of the commercial fisheries landings are comprised of estuarine-dependent species, exemplifying the importance of effective estuarine recruitment of offshore-spawned ichthyoplankton through tidal passes into estuarine nurseries (Chambers, 1992; Mann, 2000). Other than the Mississippi and Atchafalya Rivers, most embayments and estuaries in the northcentral GOM have relatively small drainage basins with little freshwater head; are relatively shallow (1 – 3 m); and have a north-south cardinal

orientation which is in alignment with the prevailing wind fields. This is especially true during the late fall through early spring when periodic and energetic atmospheric cold front events occur. Such meteorologically-driven flows have not only been shown to increase vertical mixing (Brown et al., 2004; Li et al., 2009), but to also temporarily override the prevailing diurnal microtides (Rogers et al., 1993; Wang and Craig, 1993; Parker et al., 1995; Park, 2012; Kim and Park, 2012). This wind forcing can be estimated by looking at the overall net transport of water within the tidal pass after filtering the diurnal tidal cycle effects from measured velocities and calculated volume estimates (Stone et al., 2004; Li et al., 2011). Previous northern GOM zooplankton studies along the northern GOM have shown a lack of ichthyoplankton vertical stratification (Lochmann et al., 1995; Holt and Holt, 2000; Kim et al., 2010), which is most probably a reflection of this limited potential for vertical haline stratification (Smith, 1977; Moeller et al., 1993; Cahoon and Reed, 1995; Wang, 1997; Li et al., 2009; Li et al., 2011). The lack of vertical stratification within the water column and ichthyoplankton community diminishes the potential for behaviorally-mediated recruitment strategies such as selective tidal stream transport (STST), which is common in the deep, vertically well-stratified estuaries (i.e., drowned river valleys) of the east coast of the U.S.A. (Arnold and Cook, 1984; Boehlert and Mundy, 1988; Tankersley et al., 1998; Gibson et al. 2001; Criales et al., 2011).

Under vertically well-mixed conditions, flow velocities at discrete depths are somewhat more constant, with the exception of the bottom boundary layer, where friction and vertical eddy diffusion dominate tidal advection (Wang and Craig, 1993; Trowbridge et al., 1999; Wang, 2002). In addition, the shape of the tidal pass and resultant hydrodynamics created from bathymetric variability, branches, and eddies can create environments where flow velocity may

vary laterally during either tidal stage (Kjerfve, 1978; Boon and Byrne, 1981; Wang and Craig, 1993; Li and O'Donnell, 1997). Under such vertically well-mixed conditions, this combination of responses, therefore, may make tidal pass flow velocities more likely to vary in relation to edge distance within tidal stage, than with depth typical of vertically-stratified systems (Whitfield, 1989; Lyczkowski-Shultz et al., 1990; Raynie and Shaw, 1994). For example, within a partially/well-mixed estuary, tidal stage has an asymmetrical effect on the bottom boundary layer, with the “law of the wall” (i.e., average velocity being proportional to the log distance between the point and the wall) being non-existent during ebb tides (Trowbride et al., 1999; Stacey and Ralston, 2005).

Differences in ichthyoplankton densities between flood and ebb tides at the center and edges of tidal passes have been documented in northern GOM studies (Lyczkowski-Shultz et al., 1990; Raynie, 1991; Raynie and Shaw, 1994). In a companion to this analysis (Kupchik, 2014), no statistically significant vertical differences in larval density between surface and near-bottom collections for either tide at a dock sampling station in Bayou Tartellan were found for *Anchoa hepsetus* (broad-striped anchovy), *Anchoa mitchilli* (bay anchovy), *Brevoortia patronus* (gulf menhaden), *Sciaenops ocellatus* (red drum), *Cynoscion arenarius* (sand seatrout), and *Cynoscion nebulosus* (spotted seatrout). A similar lack of differences in vertical densities for *A. hepsetus* and *B. patronus* was reported from the Oyster Bayou tidal pass and its upper estuary, Fourleague Bay, Louisiana (Raynie and Shaw, 1994). However, higher densities of larvae occurred at the edges of Oyster Bayou during strong outflows, versus maximum densities in the center of the channel during flood tides (Raynie, 1991). In Dog Keys Pass, Mississippi Sound, larval densities for *B. patronus* and *C. nebulosus* also showed no vertical differences, but higher densities of

larger larvae were collected near the edge of the tidal pass during strong outflows (Lyczkowski-Shultz et al., 1990). Estuarine-dependent larvae spawned offshore in the northern GOM, therefore, experience effective recruitment by taking advantage of the strongest flooding flows at the center channel or residual inflows due to coastal setup, and effective retention by exploiting differences in flow velocities at different lateral locations within tidal passes, or ultimately recruiting far enough into the estuary to avoid being outwelled during ebb tides (Weinstein et al., 1980; Beckley, 1985; Roper, 1986; Whitfield, 1989; Schultz et al., 2003).

Another difficulty when trying to determine operative transport/recruitment/retention mechanisms for ichthyoplankton is their well-documented spatial heterogeneity in marine environments (Hewitt, 1981; Frank et al., 1993; Letcher and Rice, 1997; Bradbury et al., 2003; Décima, 2010; Leis et al., 2013). Larval fish patch dynamics often result in excess zeroes during sampling above what would be expected for any distribution (Liu, 2009), which can potentially mask differences and may bias analytical results due to unaccounted for sources of variability (Barry and Welsh, 2002; Maunder and Punt, 2004; Minami et al., 2007). When the proportion of zeroes exceeds the number allowed under the distribution, the data set is said to be zero-inflated (Lambert, 1992; Heilbron, 1994; Tu, 2002). Two processes can lead to zero inflation. First, a zero that is a result of ecological processes acting upon the distribution (i.e., “true” zeroes) such as a low frequency of occurrence due to life history strategy (i.e., batch spawning, spawning periodicity, etc.) or strong, periodic physical forcing creating samples with no organisms present (Gaston and McArdle, 1994; Martin et al., 2005). Alternatively, “false” zeroes, the result of sampling and observer errors, can occur from either failure to incorporate appropriate spatial/temporal scales in the study design or failure to encounter a species despite its presence

(MacKenzie et al., 2002; Tyre et al., 2003). Failure to account for either zero generating process will produce bias in parameter estimates and negatively impact the ability to accurately infer relationships between groups of organisms and habitat, or appropriate management strategies (Lambert, 1992; MacKenzie et al., 2003; Field et al., 2005; Rhodes et al., 2005).

This analysis was designed to determine ichthyoplankton distributions and lengths at different locations laterally across the tidal pass, while accounting for hydrodynamic parameters, flow direction, and processes which can lead to zero-inflation. Models were developed individually for *Anchoa hepsetus* (broad-striped anchovy), *Anchoa mitchilli* (bay anchovy), *Brevoortia patronus* (gulf menhaden), *Sciaenops ocellatus* (red drum), *Cynoscion arenarius* (sand seatrout), and *Cynoscion nebulosus* (spotted seatrout), based on differences in life-history strategy.

6.2 Materials and Methods

6.2.1 Sampling Location

Ichthyoplankton sampling was conducted in Bayou Tartellan, near the Port of Fourchon, Louisiana (Figure 6.1). Bayou Tartellan and Bayou LaFourche are the first major inland splits from the connection with the GOM at Belle Pass (29° 5' 53.9" N, 90° 13' 17.8" W). The area represents a well-mixed tidal pass (i.e., little temperature, salinity or dissolved oxygen vertical stratification) having high turbidity, and a relatively small drainage basin contributing a low volume of freshwater input. The sampling site (29° 6' 49" N, 90° 11' 4" W) consisted of three locations where passive plankton net sampling was conducted. The first location was in approximately 10 meters of water from a dock extending approximately 4 meters from the northern bank into a 73 meter wide tidal pass. The second and third sampling locations were

conducted from a moored boat at either the center of the tidal channel, or approximately 10 meters from the southern bank at the channel edge of the naturally sloping bank (Figure 6.1).

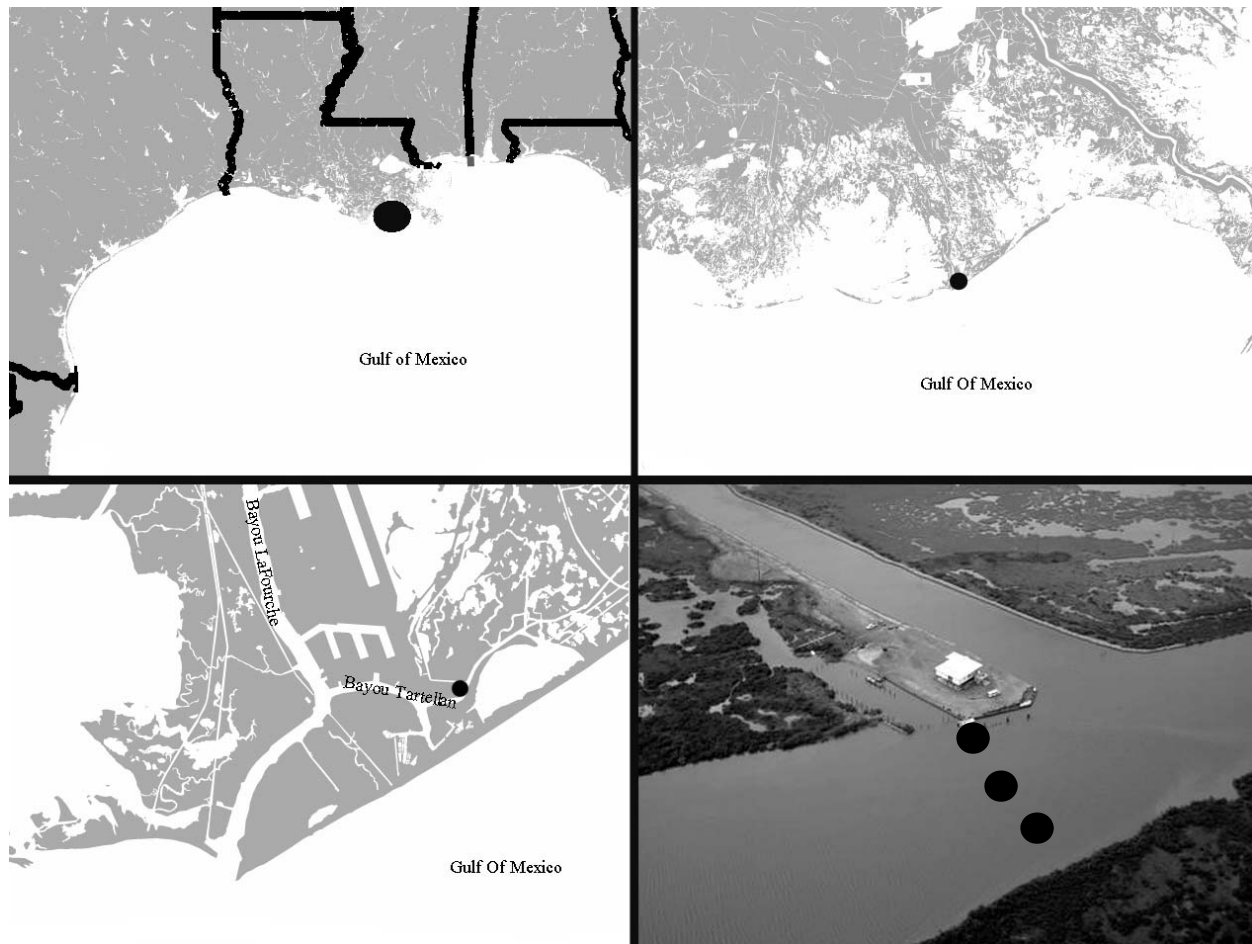


Figure 6.1: Map of the study location in relation to the Gulf of Mexico and coastal Louisiana. The points in black represent the sampling locations, with the final panel being the sampling locations from an aerial photograph of Bayou Tartellan.

6.2.2 Field Sampling Methodology

Ichthyoplankton sampling at the northern edge of the tidal pass was conducted using a fixed davit at the end of the dock, which suspended a stainless steel cable from the channel bottom to above the sampling deck. Boat ichthyoplankton sampling was conducted using a fixed

davit attached to the starboard side, which suspended a winched steel cable from the channel bottom. The boat was repositioned to mooring stations at mid-channel and the southern shore for each sampling effort. For all locations, passive plankton samples were taken using a 60-cm ring net (333 μm mesh, 2 meter length, dyed dark green) attached to a gimbal with a vane for orientation into the current. A plastic vinyl coated cod-end with 333 μm mesh drainage ports was attached to the end of the net to facilitate sample collection. A General Oceanics flowmeter (model no. 2030 with slow velocity rotor) was positioned just off center of the ring to determine volume of water filtered and subsequent calculation of zoo-/ichthyoplankton densities (number of organisms / volume of water).

During sampling, both a surface and a near-bottom, passive, ichthyoplankton collection was taken in random order. Surface collections were six minutes long, and near-bottom collections were ten minutes to compensate for vertical differences in current speed and ultimately volume of water filtered (i.e., sampling effort). For near-bottom collections, the net mouth was closed on deployment until in position, opened for sampling, and subsequently closed for retrieval to prevent vertical contamination of the sample during transit through the water column. Nets were rinsed and washed down from the outside in, to avoid sample contamination.

A minimum of three replicate, ichthyoplankton samples were collected for each combination of tidal and diel stage (i.e., day and night flood, day and night ebb) for each location over a 72 hour period. Two sampling efforts were conducted, 18th - 21st April 2007 and 16th - 19th September 2007. Individual sampling dates were chosen to maximize astronomical tidal ranges.

Ichthyoplankton samples were initially preserved in 10% buffered (sodium phosphate, dibasic $\text{NaH}_2\text{PO}_4 \cdot \text{H}_2\text{O}$, and monobasic Na_2HPO_4) formalin for approximately 3.5 hours as a

short-exposure, long-term fixative. Samples were then rinsed with fresh water and switched into a 70% ethanol solution for long-term storage, and later access for larval fish otolith work.

Meteorological data were collected by accessing an on-site meteorological station that continuously recorded wind speed, wind gust strength, wind direction, barometric pressure, and air temperature, and by using a handheld temperature/pressure integrated anemometer on the dock. The meteorological station was located approximately 20 meters from the dock sampling site, and was at a height of 20 meters to avoid confounding interactions with ground structures. Meteorological data were also incorporated from a station located on Grand Isle (29° 15.8' N, 89° 57.4' W, Station ID: 87161724), approximately 27 kilometers away from the sample site and maintained by the National Oceanographic and Atmospheric Association (NOAA).

Estuarine hydrographic parameters were measured during each plankton sample using a portable YSI (model no. 85) to record temperature, conductivity (salinity), and dissolved oxygen. A continuously sampling YSI (model no. 600R) moored offshore of the dock, also measured the same parameters. Meteorological and hydrographic data were periodically downloaded as necessary and archived for storage. Data concerning predicted diurnal tides, measured tide height, and the resulting difference in tidal prism were from the tide gauge station (Station ID: 8762075) at the Port of Fourchon, Fourchon, Louisiana (29° 6.8' N, 90° 11.9' W).

A bottom-mounted, upward-looking Acoustic Doppler Current Profiler (ADCP, RDI 1200 KHz Broadband Workhorse) was placed in the center of Bayou Tartellan to measure the vertical profile of current velocity and direction. Manned boat and autonomous robotic boat surveys (Weeks et al., 2011) along Bayou Tartellan and Bayou LaFourche out to Belle Pass were also conducted using downward-looking ADCPs. These data provided a correction factor for the

mid-channel stationary upward-facing ADCP, and were used to estimate differences in currents at both edges of the tidal pass. A volume transport (m^3/s) was calculated for Bayou Tartellan from these data. To remove the tidal and inertial effects, a 6th-order 40-hr Butterworth low-pass filter was applied to the raw volume transport to produce a **net water transport** (m^3/s ; NWT). These net transport data effectively show the lower-frequency subtidal oscillations associated with cold front events and other wind forcing, while filtering out the higher frequency diurnal tidal oscillations (Li et al. 2009).

6.2.3 Laboratory Methods

In the lab, zoo-/ichthyoplankton collections with a volume of material greater than 200 mL were split in half using a box plankton splitter, and those with a volume greater than 400 mL were split into quarters. Samples were sorted under a dissecting stereoscope and all ichthyoplankton were removed for identification, measurement and analyzed. A subset of sorted samples was checked for completeness of zooplankton removal by a second party.

Ichthyoplankton were identified to the lowest taxonomic level possible, depending on size of the organism and physical condition. Standard length (SL) of each specimen was measured to prohibit damage to caudal fins biasing results, and recorded for analysis. Some larval fish that were difficult to identify were stained using Alizarin blue and Alizarin red to facilitate meristic counts. Identifications were based on the following literature: Stuck and Perry (1982); Fahay (1983); Moser (1984); Ruple (1984); Richards (2006); Fahay (2007).

6.2.4 Statistical Analysis

As previously mentioned, the large number of zeroes associated with sampling ichthyoplankton presents a source of variability that, if unaccounted for, could bias estimates and

comparisons. To address the large number of zeroes in the dataset, we utilized an approach that combined a generalized linear model allowing for probability estimates of absence in the tidal pass, as well as quantifying the expected ichthyoplankton density at encounter. The statistical analysis was conducted with a zero-inflated negative binomial (ZINB) model, where the mixture distribution is composed of a negative binomial model for the count response and a logistic model for zero inflation. The negative binomial model may contain zeroes, and the logistic model contains only zero responses. The ZINB model is a generalization of the zero-inflated Poisson (ZIP) model originally derived by Lambert (1992). The model was fit using the GENMOD procedure (SAS 9.3) for generalized linear models.

The two data generating processes are related in the following equation, where:

$$y_i \sim \begin{cases} 0, & \text{with probability } \varphi_i \\ g(y_i|\mathbf{X}_i), & \text{with probability } 1 - \varphi_i \end{cases}$$

the zero generating process occurs with probability φ_i , and the process generating the count distribution occurs with probability $1 - \varphi_i$. Bernoulli trials are used to determine which process generates the data. Covariates may be common between the two models, but not necessary, and inference is based off the combination of the two results. Refer to Appendix A for the complete derivation of the zero-inflated negative binomial distribution.

Due to a passive sampling design, the response variable (counts of ichthyoplankton) was standardized to the mean volume of water sampled ($\bar{x} = 15m^3$). The ZINB model contains both continuous and class covariates. The continuous covariates in the model are standard length of the individual larvae (SL), net water transport (NWT), and water density (δ_t). Water density (δ_t), incorporated as a water mass tracer, was calculated using the equation from Gill (1982;

Appendix 3.1). The first class covariate was location (*LS*) within the tidal pass, which had 3 levels: Dock, Channel, and Shore. The second class covariate was depth (*SD*), with two levels: Surface and Near-Bottom. The final class variable was a diel classification (*DN*) with two levels: Day and Night. All model variables are evaluated with a Wald's Chi Square probability (ChiSq).

Minimum sufficient models are created through a forward stepwise procedure with comparison of the generality of models being done using Akaike's Information Criterion (AIC; Akaike, 1974). Models were specified for each species included in the analysis as life history differences dissuade a comprehensive model. The study is focused on the higher-level interaction terms. To investigate whether larger larvae may preferentially use the edges of the tidal pass during outflows and the center channel during inflows, the interaction term of location, SL, and NWT ($NWT \cdot SL \cdot LS$) was used. To investigate any vertical depth usage, the interaction of depth, SL, and NWT ($NWT \cdot SL \cdot SD$) was used. Finally, to investigate if there is diel vertical movement by larvae, the interaction of depth with the diel component ($SD \cdot DN$) was used. For species where higher level terms were not included in the final minimum sufficient model, the focus is on the following model interaction: location of the sample across the tidal pass by NWT ($NWT \cdot LS$).

6.3 Results

6.3.1 General Hydrodynamics

Net water transport effectively showed the lower-frequency subtidal oscillations from wind forcing on the system. During 18-21 April 2007, the oscillations followed fluctuations in wind direction accounting for a lag of a few hours, with no overall trend during sampling (Figure 6.2). There was an overall downward trend in NWT during 16-19 September 2007 (Figure 6.3).

Salinity measurements were overall higher in April ($\bar{x} = 30.6 \text{ ppt}, sd = 1.56, range = 28.4 \text{ ppt} - 33.2 \text{ ppt}$) than in September ($\bar{x} = 26.7 \text{ ppt}, sd = 0.72, ge = 25.1 \text{ ppt} - 28.2 \text{ ppt}$). There were no statistically significant differences between surface and near-bottom

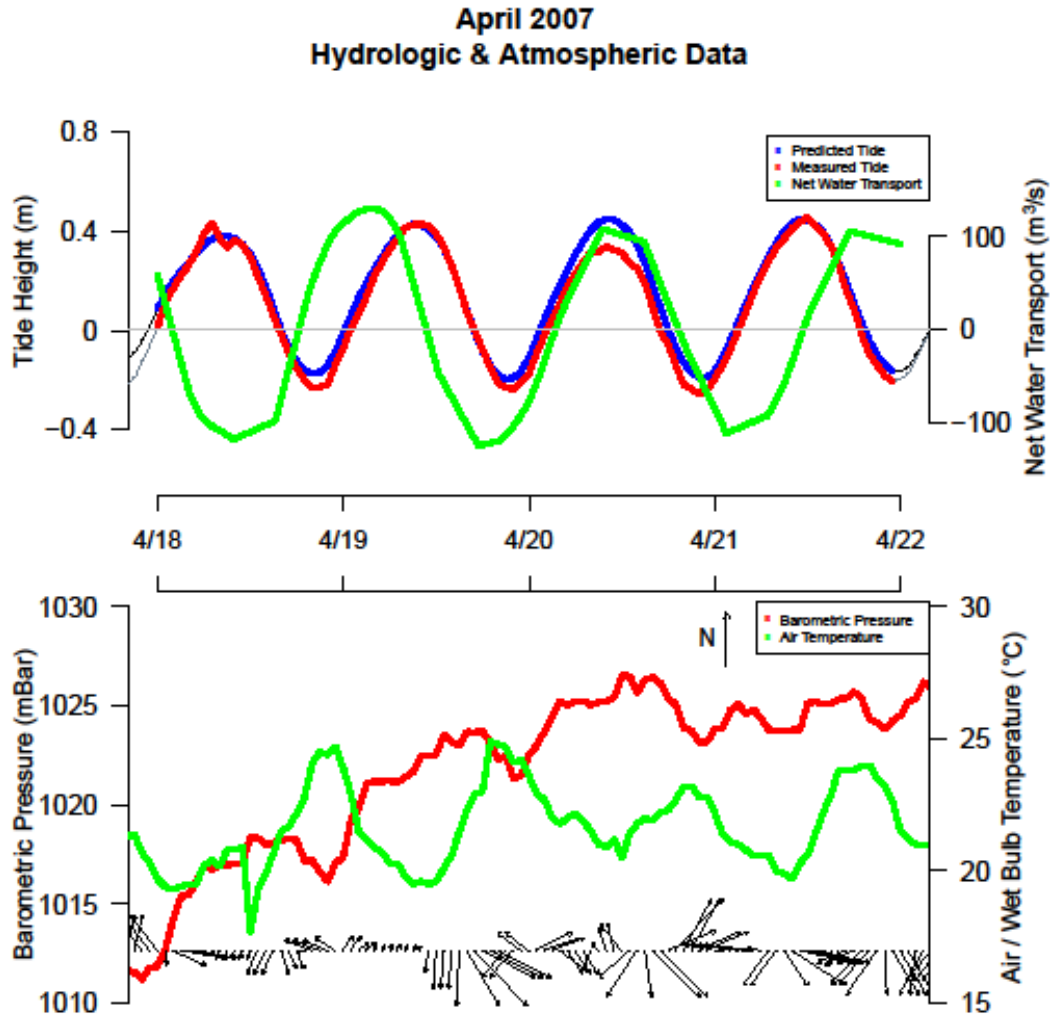


Figure 6.2: The upper graph provides predicted and measured tidal heights and overall net water transport for Bayou Tartellan during 18-22 April 2007. The lower graph provides the atmospheric data, including barometric pressure, air temperature, wet bulb temperature, and wind direction and magnitude for the same time period. For wind speed, every 2 degrees on the temperature scale corresponds to 1 m/s of wind speed.

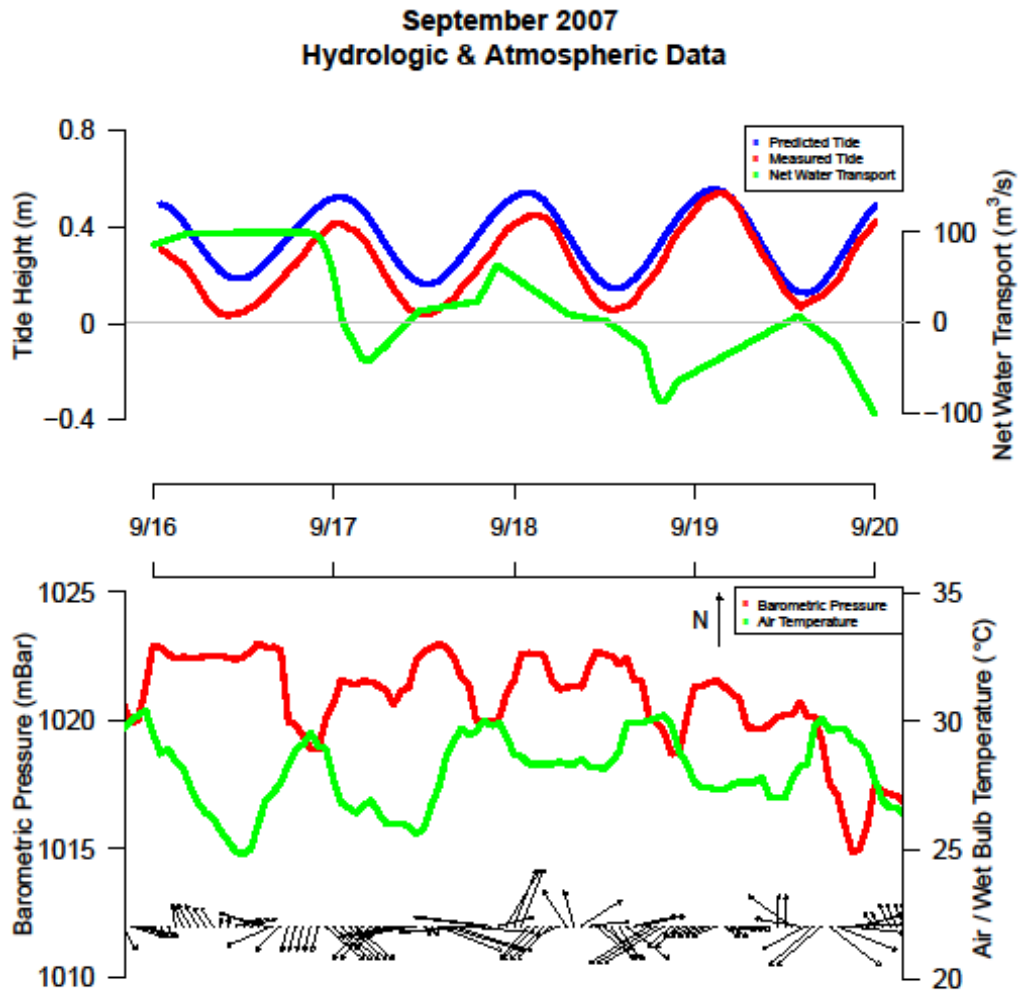


Figure 6.3: The upper graph provides predicted and measured tidal heights and net water transport for Bayou Tartellan during 16-20 September 2007. The lower graph provides the atmospheric data, including barometric pressure, air temperature, wet bulb temperature, and wind direction and magnitude for the same time period. For wind speed, every 2 degrees of temperature corresponds to 1 m/s of wind speed.

salinities for each respective month (April: $p = 0.0953, WMW$; September: $p = 0.5218, WMW$). Mean water temperatures were colder in April ($\bar{x} = 23.0^{\circ}C, sd = 1.46, range = 20.7^{\circ}C - 25.3^{\circ}C$) than mean temperatures in September ($\bar{x} = 28.2^{\circ}C, sd = 0.59, range = 26.7^{\circ}C - 29.8^{\circ}C$). Similar to salinity measurements, there was a lack of significant

difference between surface and near- bottom water temperatures in each month (April: $p = 0.6119$, *WMW*; September: $p = 0.0995$, *WMW*). Higher salinities and lower water temperatures in April led to a higher mean water density ($\bar{x} = 24.0$ σ_t , $sd = 1.7$) than in September ($\bar{x} = 19.1$ σ_t , $sd = 0.7$ ppt).

6.3.2 Cross Channel Hydrodynamics - Northern Dock Edge

The mean NWT from 18-21 April at the northern dock was slightly negative at -3.7 m³/s ($sd = 91.4$), and the distribution was slightly skewed with a median of -1.7 m³/s. The greatest positive NWTs were as high as 121.2 m³/s, with 25% of all calculated NWTs greater than 97.1 m³/s. Net water transports in this range had water mass characteristics of either salinities above 30.5 ppt at temperatures less than 22°C ($\delta_t > 24.3$), indicative of a more coastal-ocean source, or with salinities less than 30.5 ppt at temperatures between 23°C and 24°C ($22.6 < \delta_t < 23.8$). The greatest negative NWT value was -125.7 m³/s, and 25% of the calculated transports were less than -92.0 m³/s. Outwelling from strong negative NWTs had a range of salinities, and the majority of these events were classified as having temperatures consistent with the warmer estuarine water mass, at temperatures above 24°C .

During 16-19 September, the mean NWT at 7.3 m³/s ($sd = 78.2$) was greater than in April, and there was a lack of skewness with a median of 7.4 m³/s. The largest positive NWTs at the dock had magnitudes as great as 121.5 m³/s, and a quarter of the calculated values were above 86.3 m³/s. These strong inflow NWTs had salinities from 25.8 to 28.2 ppt, and a narrow range of water temperatures from 27.8°C to 28.8°C ($18.1 < \delta_t < 20.5$). Maximum negative NWT for September was -98.4 m³/s, with a quarter of all values less than -88.9 m³/s. Strong outwelling from large negative NWTs were associated with salinities less than 26 ppt and

temperatures greater than 28.5°C ($\delta_t < 18.3$), or at temperatures below 27.8°C and salinities below 27.5 ppt ($\delta_t < 20.3$).

6.3.3 Cross Channel Hydrodynamics - Center Channel

The mean NWT in the center channel during 18-21 April was -10.8 m³/s ($sd = 99.2$), and had a heavy skew towards negative NWT values with a median value of -78.6 m³/s. The largest positive NWT was 127.4 m³/s, with a quarter of all NWTs greater than 93.1 m³/s. The highest positive NWTs were characterized by salinities greater than 32 ppt and temperatures below 22°C ($\delta_t > 25.6$), more indicative of a coastal water mass. The largest negative NWT value was -117.4 m³/s, and 25% of all calculated NWTs were lower than -102.4 m³/s. The largest negative NWTs were characterized by salinities between 29.5 and 31.5 ppt and by temperatures from 21.5 to 25.2°C ($22.5 < \delta_t < 25.3$).

The mean NWT in the center channel for 16-19 September was -2.2 m³/s ($sd = 73.1$), with a heavily skewed distribution towards negative NWTs (*median* = -31.0 m³/s). The strongest positive NWTs had a magnitude of 95.3 m³/s, with a quarter of all NWTs being greater than 65.5 m³/s. The strongest positive NWTs were characterized by salinities above 26.7 ppt ($\delta_t > 18.7$) between temperatures of 28.4 and 29.2°C. Maximum negative NWT for September was -93.4 m³/s, with a quarter of all NWTs less than -78.1 m³/s. The strongest negative NWTs, associated with estuarine outwelling, occurred at salinities between 26.5 and 27.2 ppt and temperatures below 28.2°C.

6.3.4 Cross Channel Hydrodynamics - Southern Shore Edge

The mean NWT for 18-21 April at the southern shore edge was 5.5 m³/s ($sd = 97.6$) with a negative skew based on a median NWT of -10.2 m³/s. The greatest NWTs were calculated

to be 129.0 m³/s, with a quarter of all NWTs greater than 110.2 m³/s. The large positive NWTs at the southern shore edge were characterized by salinities greater than 32 ppt and temperatures below 22°C ($\delta_t > 25.6$), indicative of coastal waters. Strong outwelling NWTs had a maximum value of -110.0 m³/s, with a quarter of all NWTs less than -88.8 m³/s. The strongest negative NWTs had salinities between 29.7 and 30.6 ppt at temperatures between 21.5 and 24.4°C ($22.9 < \delta_t < 24.4$).

The mean NWT at the southern edge for 16-19 September was -1.3 m³/s ($sd = 74.3$), and had a positive skew with a median NWT of 22.0 m³/s. The maximum positive NWT was 99.0 m³/s, and a quarter of all calculated NWTs were at least 70.4 m³/s. The strong positive NWTs occurred at salinities above 27.4 ppt and water temperatures between 28.3 and 28.6°C ($\delta_t > 19.5$). The greatest negative NWT was -89.7 m³/s, with a quarter of all calculated NWTs less than -71.3 m³/s. These larger negative NWTs were strongest with water masses that were more estuarine-like with measured salinities of 26.4 ppt and 27 ppt and temperatures less than 28.3°C ($19.0 < \delta_t < 19.5$). Small positive and negative NWTs were more numerous on the southern shore than either the center channel or northern dock edge, and were characterized by a wide range of salinities (26.5-27.7 ppt) and temperatures (17.8-29.06°C) producing a narrow range of water densities ($18.6 < \delta_t < 20.0$).

6.3.5 General Ichthyoplankton

There were 37,433 larval fish representing 19 families and 26 genera collected in both the April and September sampling efforts. In April, 3,069 larval fish representing 15 families and 20 genera were collected, while in September, 34,364 larval fish, 14 families and 15 genera were collected. Positive NWTs had a maximum density of 917 indiv./15m³, with multiple densities

above 400 indiv./15m³. In contrast, there are no densities during negative flows greater than 400 indiv./15m³ (Figure 6.4), except for a single value density of 2300 indiv./15m³. This singular density was collected from near-bottom center channel, and was exclusively composed of *Anchoa* spp., < 4.5 mm SL, and was treated as an outlier for modeling purposes. Statistical analyses were conducted on densities for the following six most abundant species: broad-striped anchovy (*Anchoa hepsetus*), bay anchovy (*Anchoa mitchilli*), gulf menhaden (*Brevoortia patronus*), red drum (*Sciaenops ocellatus*), sand seatrout (*Cynoscion arenarius*), and spotted seatrout (*Cynoscion nebulosus*).

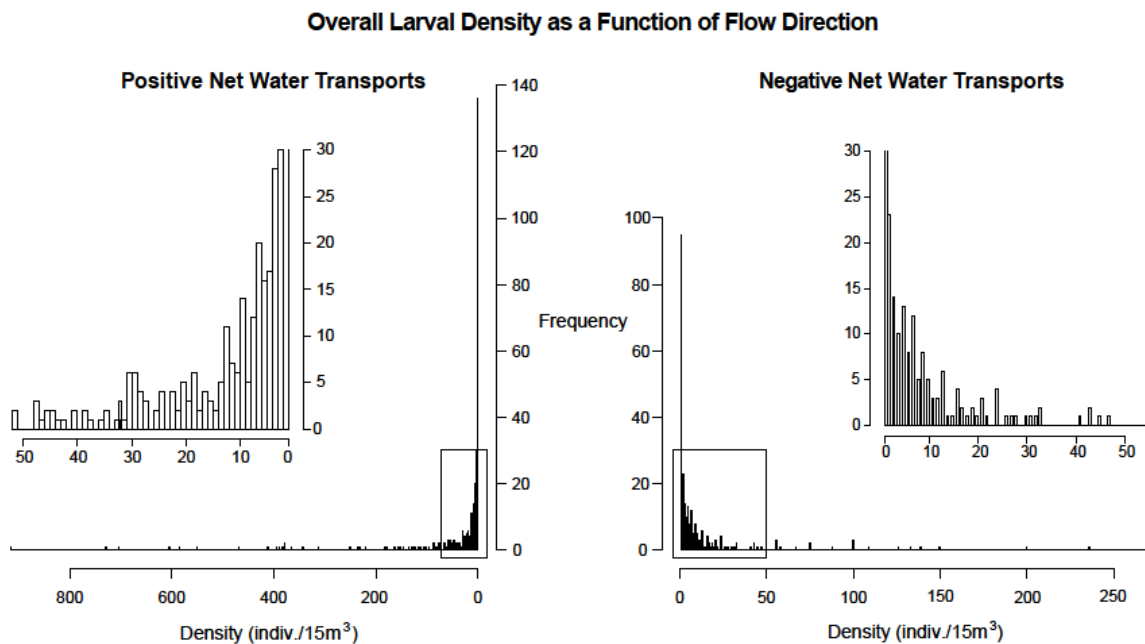


Figure 6.4: Frequency histograms of overall larval density during both positive and negative net water transports. Positive net water transports saw a higher frequency of zero collections, more positive collections overall, and higher maximum densities compared to negative transport events. Areas for the inserts are bounded by the rectangular box, and focus on densities less than 50 indiv./15m³.

6.3.6 *Anchoa hepsetus* (broad-striped anchovy)

Larval *A. hepsetus*, an estuarine-dependent species spawned offshore, were collected in both April ($\bar{x} = 2.02 \text{ indiv./15m}^3, sd = 7.93$) and September ($\bar{x} = 13.5 \text{ indiv./15m}^3, sd = 53.1$). Recruitment was heavily pulsed, with only an overall 24.8% encounter rate. In April, the greatest numbers of larval *A. hepsetus* were within the 12 - 13 mm category, and those greater than 15 mm SL, which were approximately 21% and 24% of all individuals, respectively ($\bar{x} = 11.2 \text{ mm}, sd = 5.75$; Figure 6.5). In September 2007, mean length was 9.37 mm ($sd =$

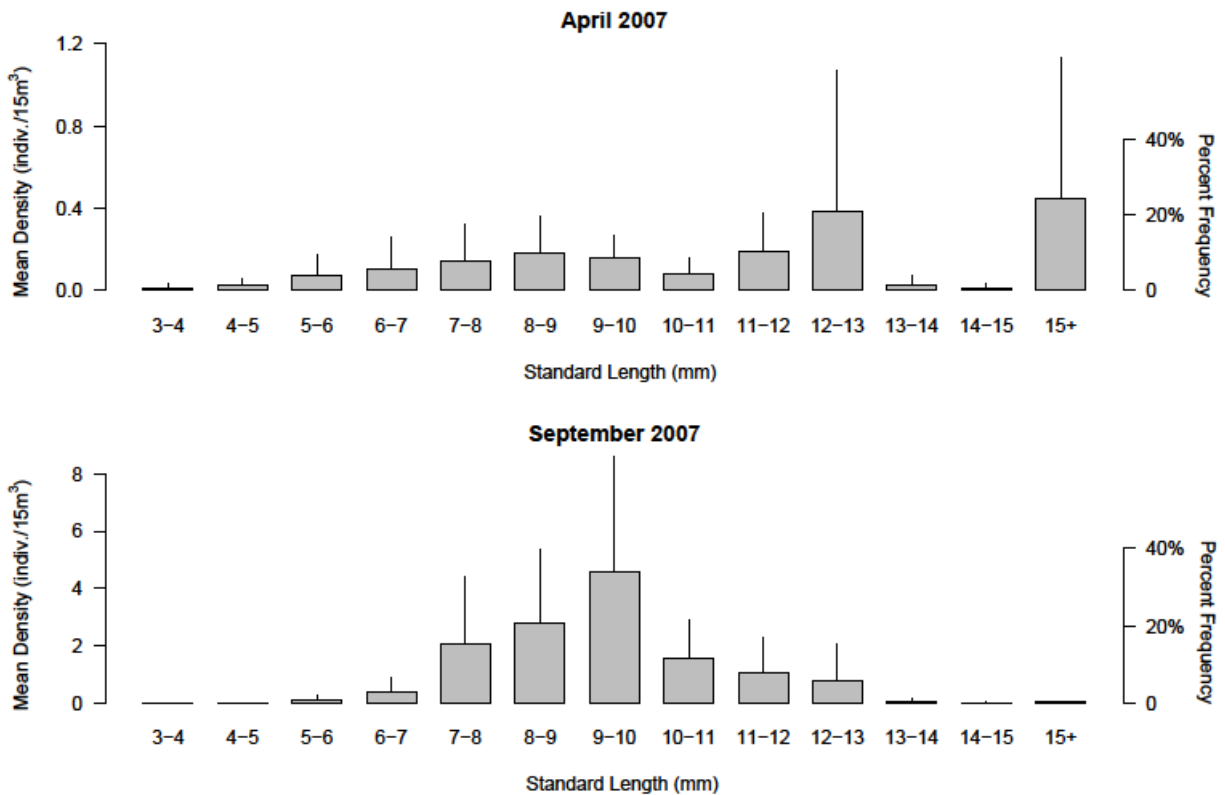


Figure 6.5: Mean density, standard error, and size-class percent frequency histograms for *A. hepsetus* larvae collected in 18-21 April and 16-19 September 2007. In April most of the larvae were greater than 12 mm SL. In September the highest densities of larvae were centered on the 9-10 mm SL size-class.

6.15), and lengths were more normally distributed and centered around the 9-10 mm size class, which represented approximately 34% of all larvae.

Larval densities of *A. hepsetus* were significantly affected by SL and water depth ($p < 0.0001$, Table 6.1). However, the lack of a significant interaction between SL, depth, and NWT suggests STST was not utilized as a recruitment and retention mechanism. Larvae between 6 and 12 mm SL had higher densities near-bottom than at the surface. Surface densities were generally low, with small peaks between 8 and 10 mm SL and for larvae greater than 14 mm SL.

Water density was not significant in the model for describing differences in densities of larval *A. hepsetus* (Table 6.1), despite ranges in water temperature and salinity similar to other species in the analysis. Larvae were collected at a water temperature range of 21.0°C to 28.4°C ($\bar{x} = 25.0\text{ }^{\circ}\text{C}$, $sd = 2.39$), and over a wide range of salinities, i.e., 26.7 ppt to a more shelf-like 33.2 ppt ($\bar{x} = 29.4\text{ ppt}$, $sd = 1.78$). The large range of salinities and water temperatures produced a fairly large range of water densities, where larval *A. hepsetus* were collected ($19.2 < \delta_t < 26.9$, $\bar{x} = 22.4$, δ_t , $sd = 2.20$).

There was an increase in probability of encounter for both the center channel and the southern shore edge as NWT increased ($p < 0.0001$, Table 6.1). There was a net estuarine recruitment of larvae from offshore and coastal spawning grounds because significantly greater chances of encounter were expected during positive NWTs ($p < 0.0001$, Table 6.1), and larval broad-striped anchovy were collected from a large range of NWTs ($-117.4\text{ m}^3/\text{s} < \text{NWT} < 129.0\text{ m}^3/\text{s}$; $\bar{x} = -19.7\text{ m}^3/\text{s}$). During positive NWTs, the center channel had much greater densities ($\bar{x} = 309.6\text{ indiv.}/15\text{m}^3$, $sd = 1387.7$) than either the southern shore edge ($\bar{x} = 0.92\text{ indiv.}/15\text{m}^3$, $sd = 2.21$), or northern dock edge ($\bar{x} = 0.34\text{ indiv.}/15\text{m}^3$, $sd = 0.46$;

Table 6.1: Model terms and associated significance levels for general ichthyoplankton and each species included for the Zero Inflated Negative Binomial Model (ZINB). For all models, terms for both the logistic zero model (ZM) and the negative binomial model (NBM) are provided with the appropriate significance levels. Terms in the models that were significant at $p \leq 0.05$ (Chi-Square) are in bold. Terms that upon stepwise model building were not significant in decreasing AIC, and subsequently excluded from the model, are represented by an x.

		Species			
		<i>Anchoa hepsetus</i>		<i>Anchoa mitchilli</i>	
	Model Terms	ZM	NBM	ZM	NBM
Primary Model Terms	Standard Length (SL)	<0.0001	0.0008	0.1504	0.1429
	Net Water Transport (NWT)	<0.0001	0.0703	0.4932	0.0759
	Water Density (WD)	x	x	<0.0001	0.0267
	Location of Sample (LS)	<0.0001	<0.0001	<0.0001	<0.0001
	Sample Depth (SD)	0.0002	<0.0001	<0.0001	<0.0001
	Diel Classification (DN)	0.8412	<0.0001	<0.0001	0.1107
	Month (M)	x	x	x	x
Interaction Model Terms	NWT * SL	x	0.3878	0.0013	0.3567
	NWT * WD	x	x	x	0.2429
	NWT * LS	<0.0001	<0.0001	<0.0001	0.3422
	NWT * SD	x	0.0897	<0.0001	<0.0001
	WD * SL	x	x	0.0834	0.1635
	M * SL	x	x	x	x
	LS * SL	x	0.1158	0.0071	<0.0001
	SD * DN	<0.0001	0.8648	<0.0001	<0.0001
	SD * SL	x	<0.0001	<0.0001	<0.0001
	NWT * SL * LS	x	0.0036	0.0057	0.2833
	NWT * SL * SD	x	0.1751	<0.0001	<0.0001
Pearson Chi-Square		0.9703		0.9058	

Table 6.1 *Continued*: Model terms and associated significance levels for general ichthyoplankton and each species included for the Zero Inflated Negative Binomial Model (ZINB). For all models, terms for both the logistic zero model (ZM) and the negative binomial model (NBM) are provided with the appropriate significance levels. Terms in the models that were significant at $p \leq 0.05$ (Chi-Square) are in bold. Terms that upon stepwise model building were no not significant in decreasing AIC, and subsequently excluded from the model, are represented by an x.

		Species			
		<i>Brevoortia patronus</i>		<i>Sciaenops ocellatus</i>	
	Model Terms	ZM	NBM	ZM	NBM
Primary Model Terms	Standard Length (SL)	<0.0001	0.0007	0.0001	0.1006
	Net Water Transport (NWT)	x	<0.0001	x	0.0038
	Water Density (WD)	x	x	x	x
	Location of Sample (LS)	0.0051	<0.0001	<0.0001	<0.0001
	Sample Depth (SD)	x	x	x	0.8001
	Diel Classification (DN)	x	x	x	<0.0001
	Month (M)	<0.0001	<0.0001	x	x
Interaction Model Terms	NWT * SL	x	0.0002	x	x
	NWT * WD	x	x	x	x
	NWT * LS	x	0.0001	x	<0.0001
	NWT * SD	x	x	x	x
	WD * SL	x	x	x	x
	M * SL	x	<0.0001	x	x
	LS * SL	x	x	x	x
	SD * DN	x	x	x	x
	SD * SL	x	x	x	x
	NWT * SL * LS	x	0.0001	x	x
	NWT * SL * SD	x	x	x	x
Pearson Chi-Square		1.2257		0.8199	

Table 6.1 *Continued*: Model terms and associated significance levels for general ichthyoplankton and each species included for the Zero Inflated Negative Binomial Model (ZINB). For all models, terms for both the logistic zero model (ZM) and the negative binomial model (NBM) are provided with the appropriate significance levels. Terms in the models that were significant at $p \leq 0.05$ (Chi-Square) are in bold. Terms that upon stepwise model building were no not significant in decreasing AIC, and subsequently excluded from the model, are represented by an x.

		Species			
		<i>Cynoscion arenarius</i>		<i>Cynoscion nebulosus</i>	
Model Terms		ZM	NBM	ZM	NBM
Primary Model Terms	Standard Length (SL)	<0.0001	<0.0001	x	<0.0001
	Net Water Transport (NWT)	<0.0001	<0.0001	x	<0.0001
	Water Density (WD)	<0.0001	x	x	<0.0001
	Location of Sample (LS)	<0.0001	<0.0001	<0.0001	0.0157
	Sample Depth (SD)	x	x	x	x
	Diel Classification (DN)	<0.0001	<0.0001	x	<0.0001
	Month (M)	x	x	x	x
Interaction Model Terms	NWT * SL	x	<0.0001	x	x
	NWT * WD	x	x	x	x
	NWT * LS	0.0191	0.1267	x	0.0006
	NWT * SD	x	x	x	x
	WD * SL	x	x	x	x
	M * SL	x	x	x	x
	LS * SL	x	<0.0001	x	x
	SD * DN	x	x	x	x
	SD * SL	x	x	x	x
	NWT * SL * LS	x	x	x	x
	NWT * SL * SD	x	x	x	x
Pearson Chi-Square		1.2082		0.2402	

Table 6.2). Of most interest is the significant difference of larval *A. hepsetus* densities indicated by the interaction of location across the tidal pass, SL, and NWT ($p = 0.0036$, Table 6.1). At the

northern dock edge, the greatest densities of larvae were found between 0 and 50 m³/s, and were comprised of larvae greater than 12 mm in length ($\bar{x} = 13.2 \text{ mm}, sd = 2.08$; Figures 6.6 and 6.7; Table 6.2). Peak densities of larval *A. hepsetus* in the center channel occurred at between 40 m³/s and greater than 100 m³/s for larvae generally smaller than 10mm in length (Figure 6.6). Lengths of larval *A. hepsetus* in the center channel ($\bar{x} = 10.0 \text{ mm}, sd = 2.38$) and the southern shore edge ($\bar{x} = 9.56 \text{ mm}, sd = 2.73$; Table 6.2) had similar size class distributions, while the northern dock had a larger proportion of larger larvae (Figure 6.7). In contrast, peak densities occurred at the southern shore edge during negative NWTs of approximately -50 m³/s. When compared to densities during positive NWTs, larval densities during negative NWTs increased at the southern shore edge ($\bar{x} = 1.52 \text{ indiv./}15\text{m}^3, sd = 3.71$) and northern dock edge ($\bar{x} = 0.72 \text{ indiv./}15\text{m}^3, sd = 0.12$), whereas larval density decreased in the center channel ($\bar{x} = 3.04 \text{ indiv./}15\text{m}^3, sd = 14.7$; Table 6.2). The SL during negative NWTs increased at the southern shore edge ($\bar{x} = 10.5 \text{ mm}, sd = 3.10$), and decreased at the northern dock edge ($\bar{x} = 10.1 \text{ mm}, sd = 2.72$) and center channel ($\bar{x} = 8.50 \text{ mm}, sd = 2.53$; Table 6.2).

6.3.7 *Anchoa mitchilli* (bay anchovy)

September densities of estuarine-obligate *A. mitchilli* larvae ($\bar{x} = 85.0 \text{ indiv./}15\text{m}^3, sd = 195.5$) were greater than those collected in April ($\bar{x} = 20.0 \text{ indiv./}15\text{m}^3, sd = 46.2$). In September, larval *A. mitchilli* mean SL ($\bar{x} = 8.34 \text{ mm}, sd = 2.97$) was also greater than in April ($\bar{x} = 6.93 \text{ mm}, sd = 2.40$). The greatest densities sampled in September were between 7-10 mm SL and comprised approximately 50% of all sizes. In April, nearly 40% of all

Table 6.2: Larval fish mean densities (LD), probability of encounter (PE), and mean standard length (SL) for all species included in the analysis based on location across the tidal pass and by positive and negative net water transports. LD are provided as a mean and standard deviation in parenthesis, PE is presented as the percent chance of encounter, and SL are presented as the mean and standard deviation in parentheses. Overall LD, PE, and SL are provided for each species across all locations for either all positive transports or all negative transports.

	Species	Northern Dock Edge			Center Channel			Southern Shore Edge			Overall		
		LD	PE	SL	LD	PE	SL	LD	PE	SL	LD	PE	SL
Positive Net Water Transports	<i>A. hepsetus</i>	0.34 (0.46)	2.9%	13.2 (2.08)	309.6 (1388)	55.3%	10.0 (2.38)	0.92 (2.21)	73.6%	9.56 (2.73)	79.8 (714.6)	36.3%	10.1 (2.58)
	<i>A. mitchilli</i>	17.5 (50.9)	14.1%	7.33 (2.55)	8.60 (10.9)	50.0%	7.82 (3.12)	20.9 (38.9)	53.8%	7.58 (2.88)	16.2 (40.9)	34.5%	7.63 (2.91)
	<i>B. patronus</i>	0.40 (1.31)	30.6%	7.17 (7.23)	16.3 (126.9)	30.5%	13.3 (4.92)	0.76 (4.38)	34.2%	13.0 (4.30)	4.57 (64.6)	31.6%	12.1 (5.18)
	<i>S. ocellatus</i>	0.76 (1.29)	2.6%	3.00 (0.58)	1.68 (2.14)	37.2%	4.88 (2.31)	2.77 (3.88)	36.0%	4.08 (1.02)	1.53 (2.58)	20.1%	4.41 (1.86)
	<i>C. arenarius</i>	2.59 (10.2)	52.6%	3.85 (1.28)	2.42 (3.09)	79.1%	5.14 (1.81)	4.18 (7.60)	79.5%	5.03 (1.79)	2.99 (8.17)	67.0%	4.91 (1.77)
	<i>C. nebulosus</i>	0.71 (2.15)	7.2%	3.83 (1.53)	1.03 (3.63)	50.0%	3.32 (0.75)	1.35 (4.88)	52.8%	3.33 (0.83)	0.96 (3.45)	29.9%	3.38 (0.86)
Negative Net Water Transports	<i>A. hepsetus</i>	0.72 (0.12)	54.1%	10.1 (2.72)	3.04 (14.7)	83.1%	8.50 (2.53)	1.52 (3.71)	54.4%	10.5 (3.10)	1.23 (80.6)	61.5%	9.71 (2.90)
	<i>A. mitchilli</i>	8.47 (22.9)	44.8%	6.91 (2.37)	25.4 (56.1)	60.3%	7.36 (2.55)	17.7 (59.2)	55.1%	8.80 (2.83)	15.6 (45.8)	51.9%	7.53 (2.65)
	<i>B. patronus</i>	0.07 (0.22)	30.6%	13.3 (4.83)	0.04 (0.19)	30.8%	16.0+ (0)	0.06 (0.20)	32.6%	16.0+ (0)	0.06 (0.21)	31.2%	14.7 (2.91)
	<i>S. ocellatus</i>	0.03 (0.04)	2.6%	3.17 (0.58)	1.32 (2.42)	37.2%	4.40 (1.20)	0.66 (1.38)	36.0%	4.33 (1.64)	0.53 (1.53)	20.1%	4.22 (1.40)
	<i>C. arenarius</i>	7.57 (27.4)	59.2%	3.11 (1.13)	2.98 (6.11)	67.2%	3.67 (1.31)	2.76 (7.28)	68.4%	3.65 (1.24)	5.01 (19.3)	63.9%	3.51 (1.25)
	<i>C. nebulosus</i>	0.05 (0.13)	7.2%	3.17 (0.82)	1.94 (8.64)	50.0%	3.25 (0.87)	0.65 (3.17)	52.8%	3.28 (0.83)	0.70 (4.81)	29.9%	3.24 (0.81)

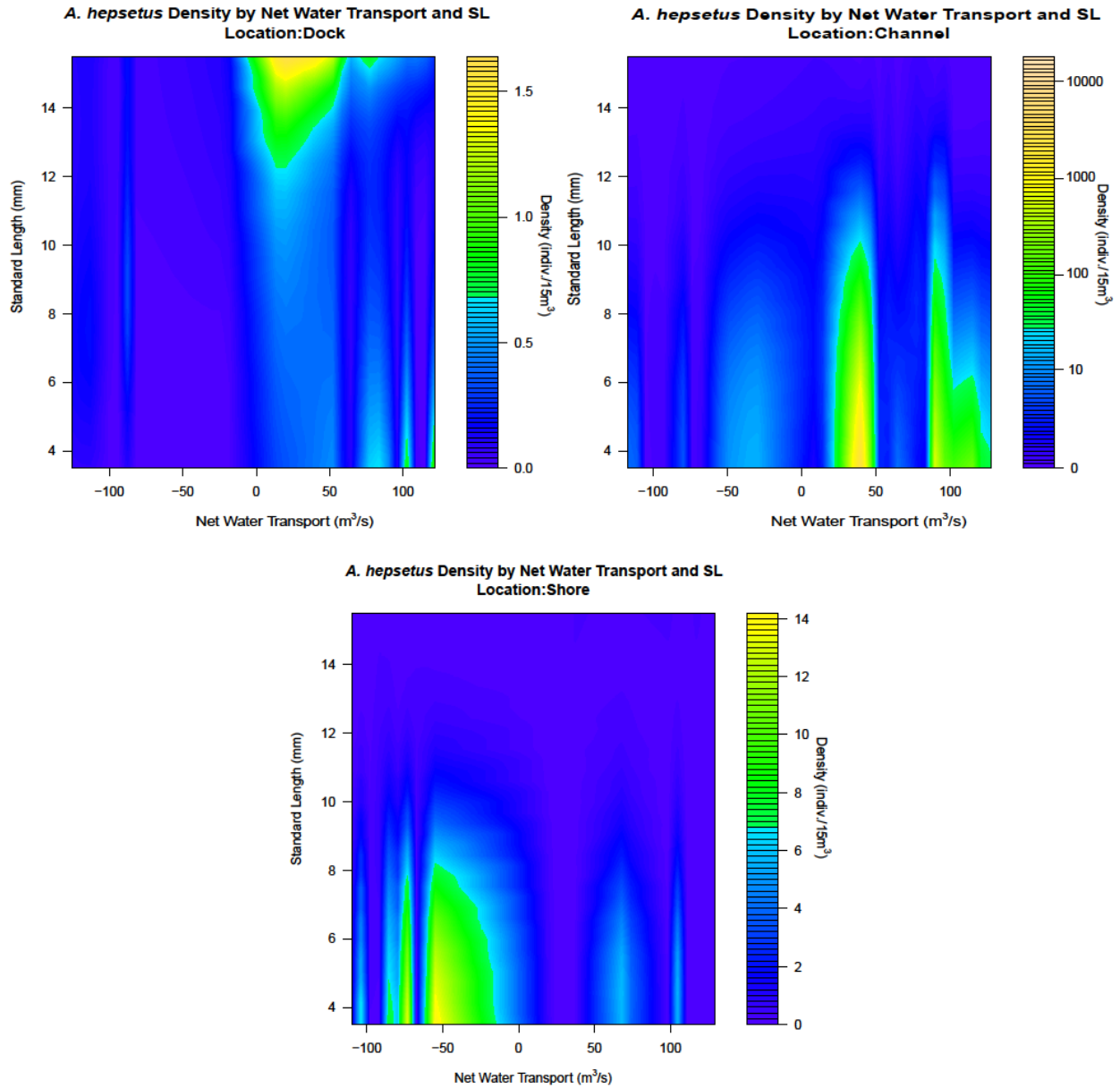


Figure 6.6: Surface plot showing the effect of net water transport and standard length (SL) on modeled densities of larval *A. hepsetus* at the northern dock edge, the center channel, and the southern shore edge. The highest larval densities at the northern dock occurred for larvae greater than 12 mm SL between positive net water transports of 0 and 50 m^3/s , whereas at the center channel it occurred between 40 and 100 m^3/s for larvae less than 10 mm SL, and at the southern shore net water transports of approximately -50 m^3/s for larvae less than 8 mm SL.

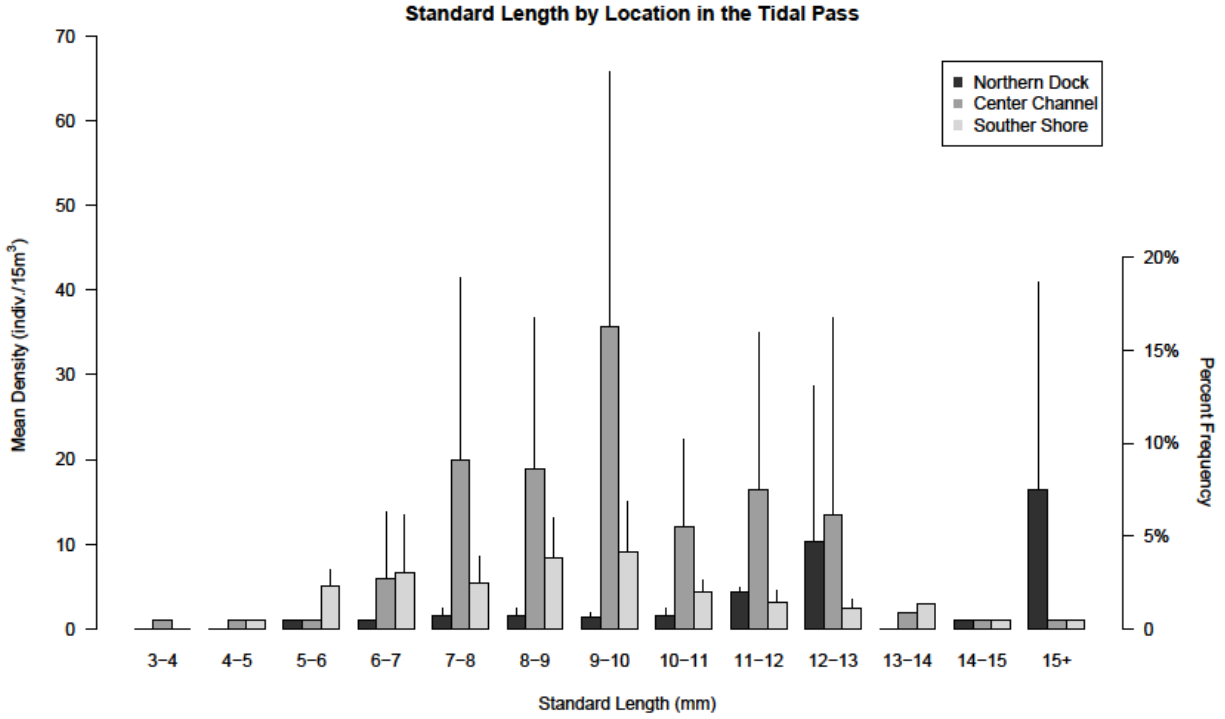


Figure 6.7: Histogram showing the mean density, standard error, and percent frequency of size-classes of larval *A. hepstus* at the three sampling locations across the tidal pass. Larvae greater than 15 mm SL were primarily found at the northern dock edge.

sizes sampled were between 6 and 8 mm SL (Figure 6.8). Over half of all samples contained *A. mitchilli* larvae, with a sample encounter percentage of 53.5%.

Despite larval *A. mitchilli* being more commonly collected within colder, more saline water masses, i.e., larvae more likely encountered at higher water densities ($p < 0.0001$, Table 6.1), large density pulses of *A. mitchilli* were associated with warmer, fresher waters representative of the inner estuary ($\bar{x} = 25.1^{\circ}\text{C}$, $sd = 2.63$, $range: 21.0^{\circ}\text{C}$ to 29.4°C ; $p = 0.0267$, Table 6.1). The maximum recorded salinity was 33.2 ppt, and the lower bound was 25.7 ppt ($\bar{x} = 29.2$ ppt, $sd = 2.07$). The range of salinities and water temperatures produced a fairly large range in water densities for *A. mitchilli* ($18.3 < \delta_t < 26.9$; $\bar{x} = 21.2$ δ_t , $sd = 2.54$).

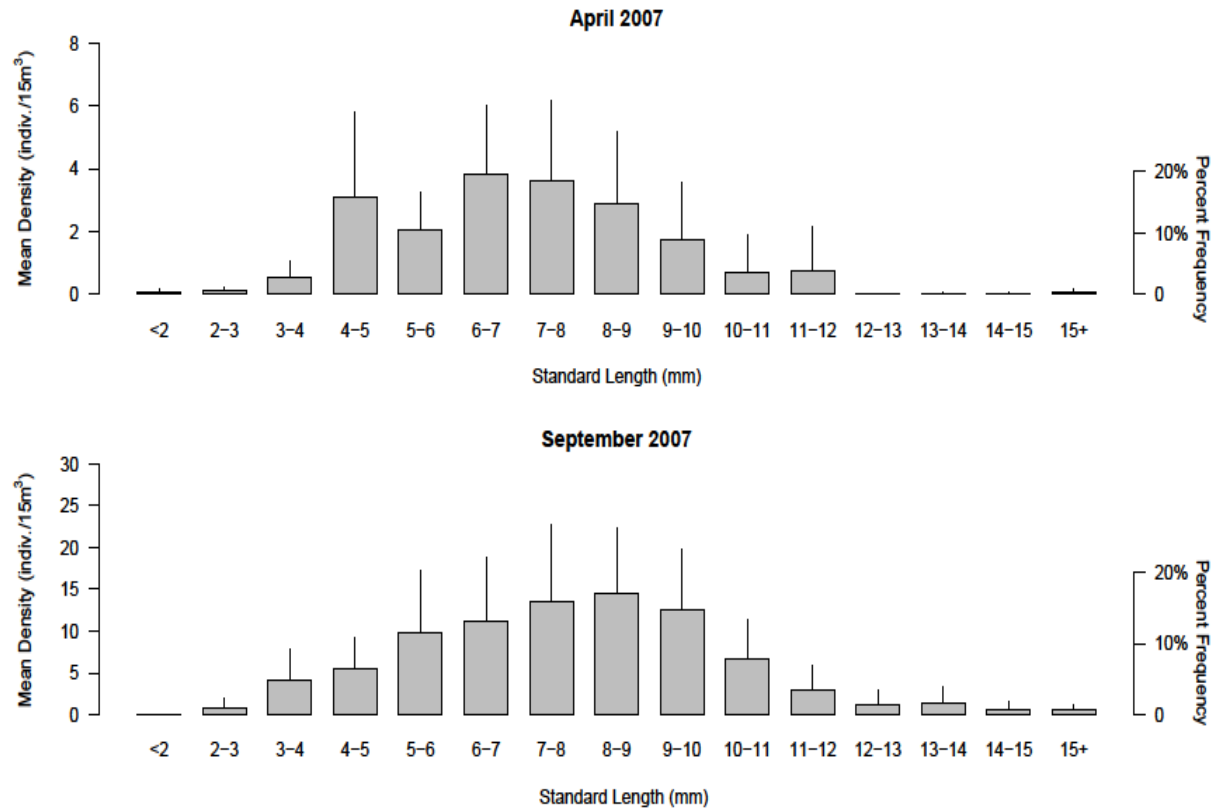


Figure 6.8: Mean density, standard error, and size-class frequency histograms of *A. mitchilli* larvae collected in April and September 2007. In April most of the larvae were between 6 and 8 mm SL. In September the highest densities of larvae were between 7 and 10 mm SL.

The interaction between depth and diel was highly significant in determining probability of encounter and larval *A. mitchilli* densities ($p < 0.0001$, $p < 0.0001$, respectively; Table 6.1). Daytime surface encounters were far less likely to contain larvae than any other depth/diel combination, suggesting visual gear avoidance to be likely despite ambient high turbidity and measures to minimize the optical profile of the gear. However, the surface day combination showed a large increase in the expected density of larval *A. mitchilli*, suggesting that large densities, while rare, were more likely to be encountered at the surface during the day.

The interaction of location across the tidal pass, SL, and NWT is of most interest, but was only significant in determining probability of encounter ($p < 0.0057$, Table 6.1). Also of high interest was the interaction of depth, SL, and NWT which was highly significant in describing probability of encounter and larval density, respectively ($p < 0.0001$, $p < 0.0001$, Table 6.1). Across the range of SLs, the probability of larval fish being present at the northern dock edge was greater than the center channel and southern shore edge with increasing positive NWTs (Figure 6.9). However, during negative NWTs, larger *A. mitchilli* had a slightly greater probability of encounter at the center channel and southern shore edge versus the northern dock. Similar to location, with increasing larval *A. mitchilli* SL and increasing positive NWTs, there were increases in probability of encounter at the surface. There were significant differences in probability of encounter and larval densities by SL between locations ($p < 0.0071$, $p < 0.0001$, Table 6.1), where the center channel had the greatest densities of larger larvae ($\bar{x} = 8.03 \text{ mm}$, $sd = 11.77$), followed by the southern shore edge ($\bar{x} = 7.64 \text{ mm}$, $sd = 11.76$), and the northern dock edge had the smallest lengths and least variability ($\bar{x} = 7.03 \text{ mm}$, $sd = 8.79$; Figure 6.10). At the northern dock edge, there were fairly constant proportions of sizes from 4 to 12 mm. The center channel had a better representation of larger sizes, and had similar proportions for all larvae sampled between 6 and 15 mm SL, with a notable peak in density between 13 and 14 mm SL. During positive NWTs, the southern shore had the highest overall densities ($\bar{x} = 20.9 \text{ indiv./15m}^3$, $sd = 38.9$) followed by the northern dock ($\bar{x} = 20.9 \text{ indiv./15m}^3$, $sd = 38.9$) and center channel ($\bar{x} = 17.5 \text{ indiv./15m}^3$, $sd = 50.9$), with all having similar mean SLs (*range*: 7.33 – 7.82 mm SL). On negative NWTs, the center channel had the overall highest density ($\bar{x} = 25.4 \text{ indiv./15m}^3$, $sd = 56.1$), followed by the southern shore ($\bar{x} =$

17.7 indiv./15m³, $sd = 59.2$) and the northern dock ($\bar{x} = 8.47$ indiv./15m³, $sd = 22.9$), yet the southern shore had the greatest mean SL, i.e., 8.8 mm versus 7.36 mm (center channel) or 6.91 mm (northern dock; Table 6.2). Overall, the highest chance of encountering *A. mitchilli* larvae greater than 6 mm SL was during strong outwelling NWTs.

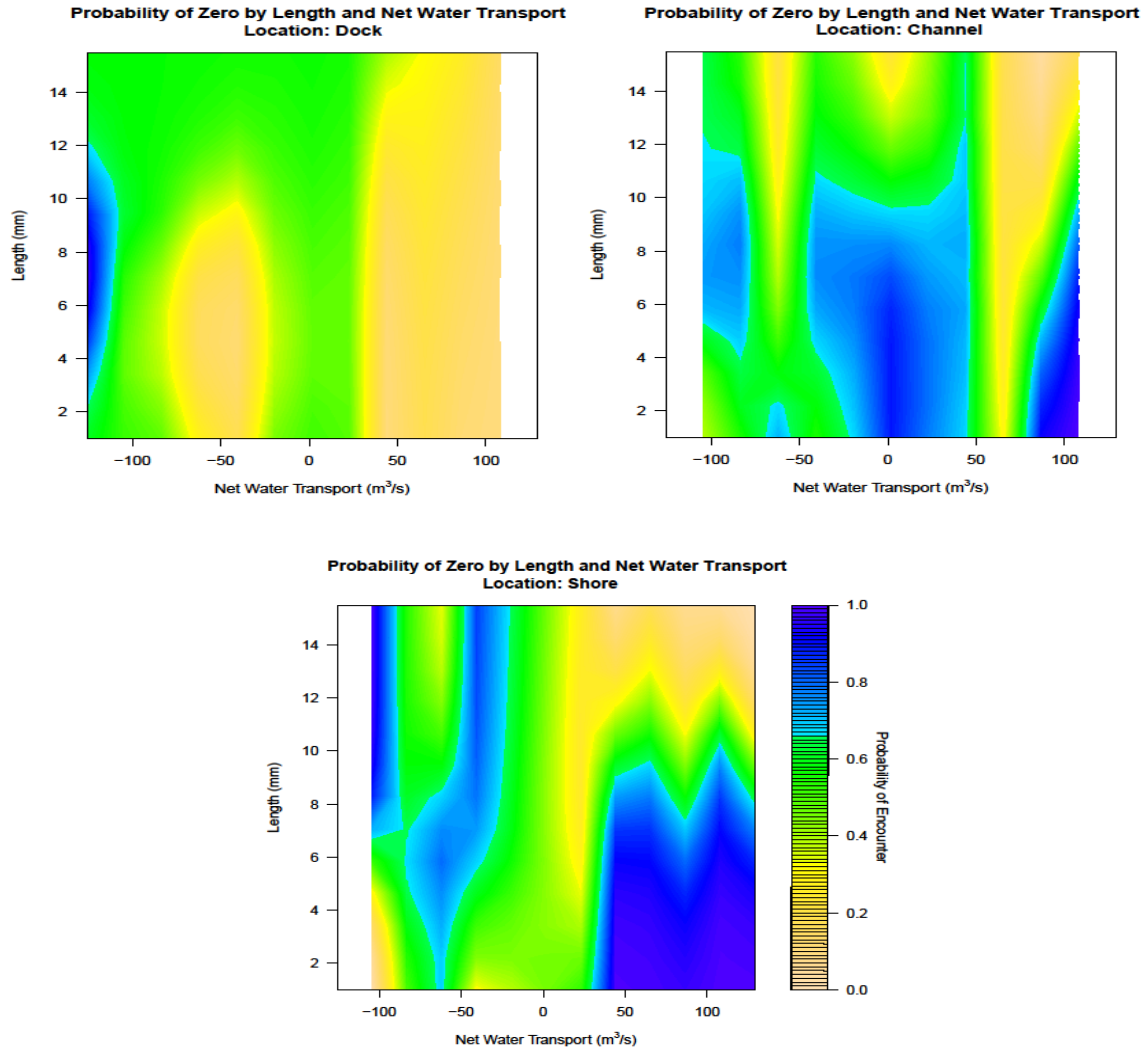


Figure 6.9: Surface plot for probability of encounter for *A. mitchilli* as a function of SL and NWT. Across the range of SLs, the northern dock had high probability of encounter at NWTs greater than 35 m³/s and for smaller larvae at NWTs around -50 m³/s, whereas the center channel, across the range of SLs had the highest probability of encounter at transports greater than 60 m³/s especially for larvae greater than 8 mm SL, and the southern shore at transports greater than 25 m³/s for larvae greater than 10 mm SL.

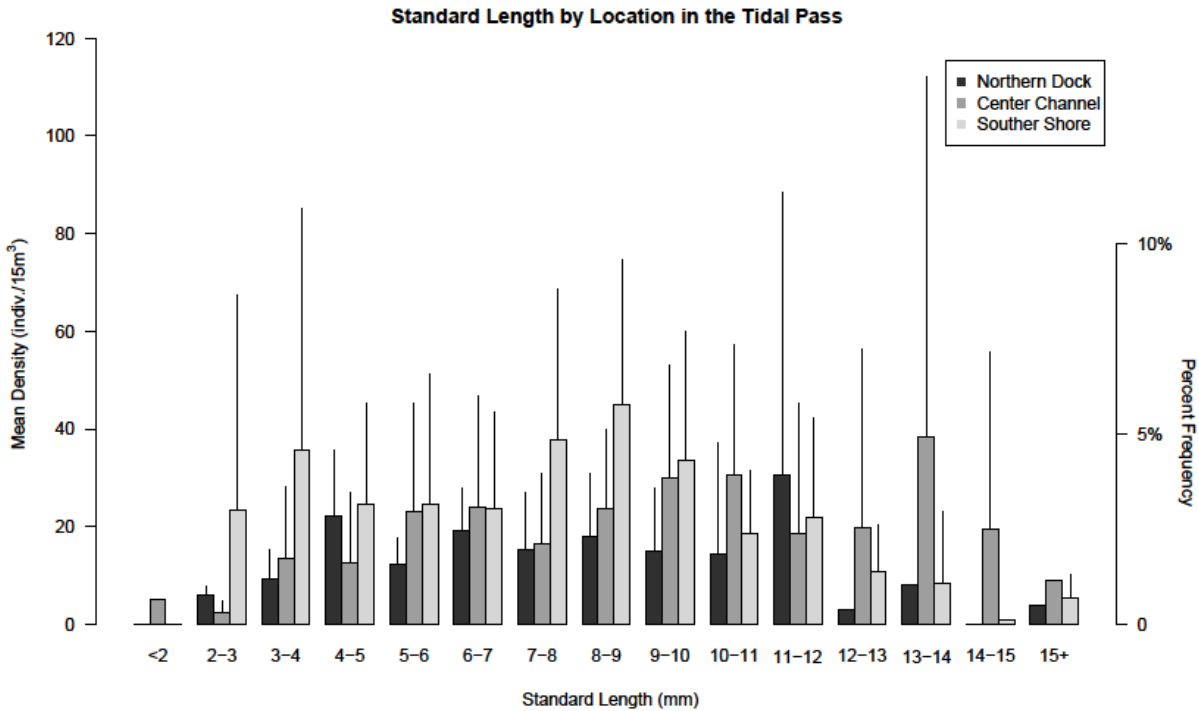


Figure 6.10: Histogram showing the mean density, standard error, and percent frequency of size classes of *A. mitchilli* at the three sampling locations across the tidal pass.

6.3.8 *Brevoortia patronus* (gulf menhaden)

Brevoortia patronus larvae, which are estuarine dependent, had a higher probability of encounter ($p < 0.0001$, Table 6.1) and higher densities ($p < 0.0001$, Table 6.1) in April ($\bar{x} = 2.01 \text{ indiv./15m}^3$, $sd = 5.23$), than September ($\bar{x} = 0.70 \text{ indiv./15m}^3$, $sd = 3.93$). A large portion of samples contained no larval *B. patronus*; with an overall sample encounter percentage of only 20.4%. Densities of larger *B. patronus* in April ($\bar{x} = 15.0 \text{ mm}$, $sd = 1.66$) were significantly greater than in September ($\bar{x} = 3.5 \text{ mm}$, $sd = 0.71$; $p < 0.0001$, Table 6.1). Generally, there was increased probability of encounter and higher densities for larval *B. patronus* with increasing SL ($p < 0.0001$, $p = 0.0007$, Table 6.1). The greatest densities in April were of larvae greater than 15 mm SL, and comprised more than 90% of all sizes sampled

(Figure 6.11). When including the effect of NWT, larger larvae occurred in higher densities on positive flows greater than 50 m³/s ($p = 0.0002$, Table 6.1; Figure 6.12A). In September, 98% of all larvae sampled were between 2 and 5 mm SL, and larvae less than 4 mm in length had peak densities between 50 and 100 m³/s (Figure 6.12B).

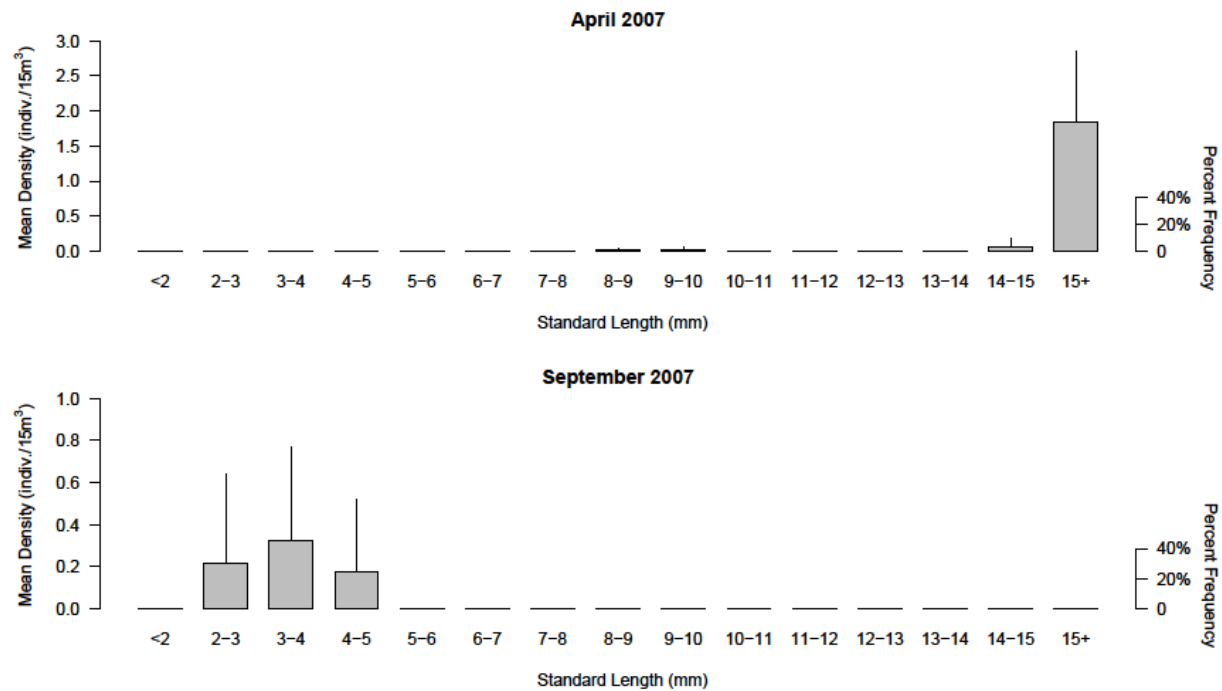


Figure 6.11: Mean density and size-class percent frequency histograms of *B. patronus* larvae collected in 18-21 April and 16-19 September 2007. In April nearly all of the larvae were greater than 14 mm SL. In September all of the larvae were between 2 and 5 mm SL.

The ZINB model results showed significant differences in across channel probabilities of encounter ($p = 0.0051$, Table 6.1). Larval densities as a function of the interaction of location, SL, and NWT ($p = 0.0001$, Table 6.1) were also highly significant. Overall, the highest probability of encounter was along the southern shore edge. There was strong evidence for both

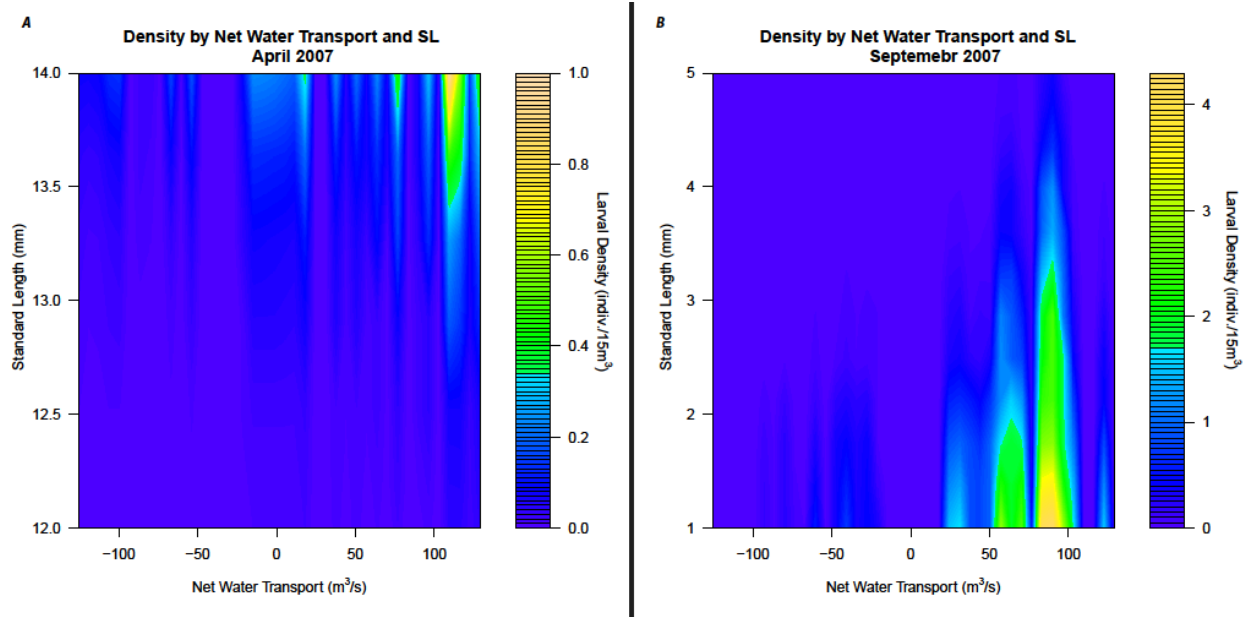


Figure 6.12: Surface plot showing the effect of net water transport and SL on modeled densities for larval *B. patronus* for April (Plot A) and September (Plot B). Plot (A) shows peak densities for larvae with standard lengths from 12 to 14 mm, at positive net water transports greater than $100\text{m}^3/\text{s}$. Plot (B) shows peak densities for shorter larvae occurring between 50 and $100\text{ m}^3/\text{s}$.

effective estuarine recruitment and retention. Positive NWT larval densities were greatest in the center channel ($\bar{x} = 16.3\text{ indiv./}15\text{m}^3, sd = 129.6$), and much greater than either the southern shore edge ($\bar{x} = 0.76\text{ indiv./}15\text{m}^3, sd = 4.38$) or northern dock edge ($\bar{x} = 0.40\text{ indiv./}15\text{m}^3, sd = 1.31$; Table 6.2). In contrast, during negative NWTs, densities for the southern shore edge ($\bar{x} = 0.06\text{ indiv./}15\text{m}^3, sd = 0.20$), the center channel ($\bar{x} = 0.04\text{ indiv./}15\text{m}^3, sd = 0.19$) and northern dock edge ($\bar{x} = 0.07\text{ indiv./}15\text{m}^3, sd = 0.22$; Table 6.2) were all much lower. Larger *B. patronus* were taken at the center channel and southern shore during both positive and negative NWTs (Table 6.2).

6.3.9 *Sciaenops ocellatus* (red drum)

Due to their normal truncated spawning and recruitment season, estuarine dependent *S. ocellatus* larvae were only collected in September ($\bar{x} = 8.76 \text{ n}/15\text{m}^3$, $sd = 17.2$); yet, even with this very short season, there was a large amount of pulsing or patchiness as only 33.8% of the September samples contained larvae. Probability of encounter for larval *S. ocellatus* significantly decreased with increasing SL in Bayou Tartellan ($p = 0.0001$, Table 6.1). Larvae

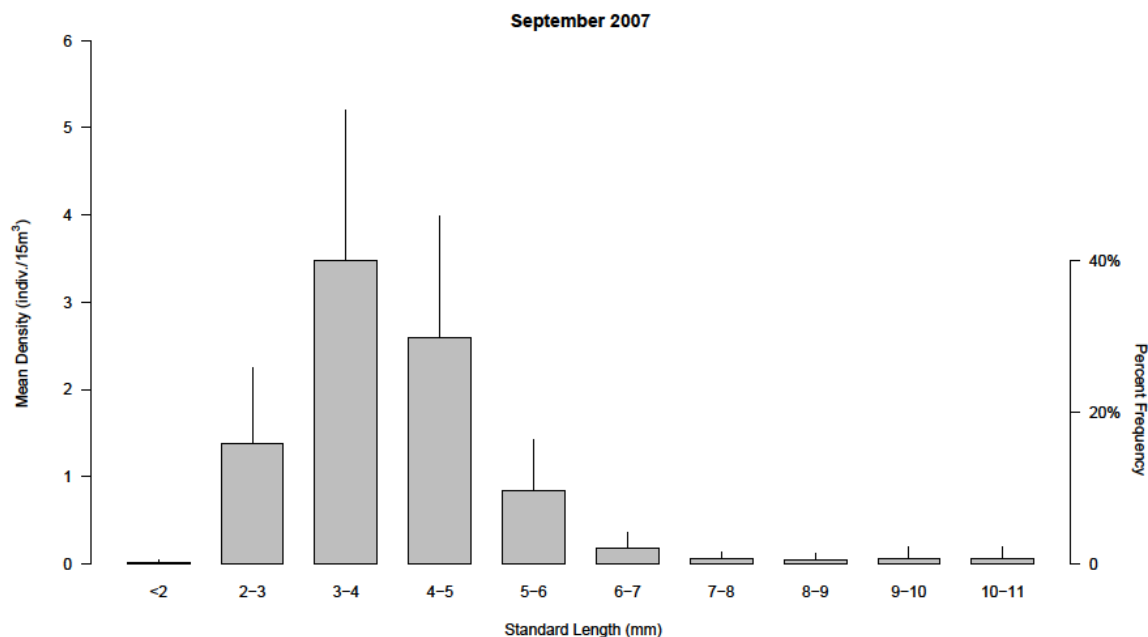


Figure 6.13: Mean density, standard error, and size-class frequency histograms of *S. ocellatus* larvae collected from 16-19 September 2007. The highest mean densities and greatest frequency of larvae were between 3 and 5 mm SL.

had a mean SL of 5.95 mm ($sd = 2.96$, *range*: 1 mm to 10.8 mm SL), and approximately 85% of all larvae were between 3 mm and 5 mm SL (Figure 6.13). Larger densities were sampled at

night ($\bar{x} = 17.3 \text{ indiv./}15\text{m}^3, sd = 21.1$) than day ($\bar{x} = 0.19 \text{ indiv./}15\text{m}^3, sd = 0.62$; $p < 0.0001$, Table 6.1). The lack of a significant depth term or interaction of depth and diel term suggests that perhaps larvae were able to visually avoid the gear during daylight hours.

Location across the tidal pass was significant in determining the probability of encounter and larval density ($p < 0.0001$, $p < 0.0001$, Table 6.1), and the higher level interaction of the location and NWT was also highly significant in describing larval *S. ocellatus* densities ($p < 0.0001$, Table 6.1). Positive NWTs resulted in increasing densities of larvae, and densities decreased to zero with outgoing flow strengths greater than $-50 \text{ m}^3/\text{s}$. When larvae were encountered, the northern dock edge had higher densities; however, the overall likelihood of encounter was significantly less there than either at the center channel or the southern shore. This resulted in overall densities at the northern dock edge ($\bar{x} = 1.81 \text{ indiv./}15\text{m}^3, sd = 6.39$) that were much lower than either the southern shore edge ($\bar{x} = 17.4 \text{ indiv./}15\text{m}^3, sd = 24.6$) or the center channel ($\bar{x} = 13.3 \text{ indiv./}15\text{m}^3, sd = 17.8$), regardless of flow direction. During positive NWTs, densities were highest at the southern shore ($\bar{x} = 2.77 \text{ indiv./}15\text{m}^3, sd = 3.88$), followed by the center channel ($\bar{x} = 1.68 \text{ indiv./}15\text{m}^3, sd = 2.14$), and the northern dock edge ($\bar{x} = 0.76 \text{ indiv./}15\text{m}^3, sd = 1.29$; Table 6.2). During negative NWTs, densities were less at all three locations, supporting estuarine recruitment from offshore. Highest densities were collected at the center channel ($\bar{x} = 1.32 \text{ indiv./}15\text{m}^3, sd = 2.42$) and southern shore ($\bar{x} = 0.66 \text{ indiv./}15\text{m}^3, sd = 1.38$), with very low densities collected at the northern dock edge ($\bar{x} = 0.03 \text{ indiv./}15\text{m}^3, sd = 0.04$; Table 6.2), which were also an order of magnitude lower than during positive NWTs. Mean lengths were slightly larger on negative NWTs at the southern shore and northern dock edge, and slightly shorter within the center channel (Table 6.2).

6.3.10 *Cynoscion arenarius* (sand seatrout)

April densities of estuarine dependent *C. arenarius* larvae ($\bar{x} = 2.78 \text{ indiv./15m}^3$, $sd = 11.0$) were much lower than September ($\bar{x} = 25.4 \text{ indiv./15m}^3$, $sd = 52.3$). Overall, larval *C. arenarius* had a sample encounter percentage of 37.6% during the study. However, April collections had fewer individual pulses, whereas in September pulses or evidence of patchiness were more numerous and contained higher densities. In general for either month, smaller larvae were more numerous and contained higher densities. In general for either month, smaller larvae were more likely to be encountered ($p < 0.0001$, Table 6.1) and were found in higher

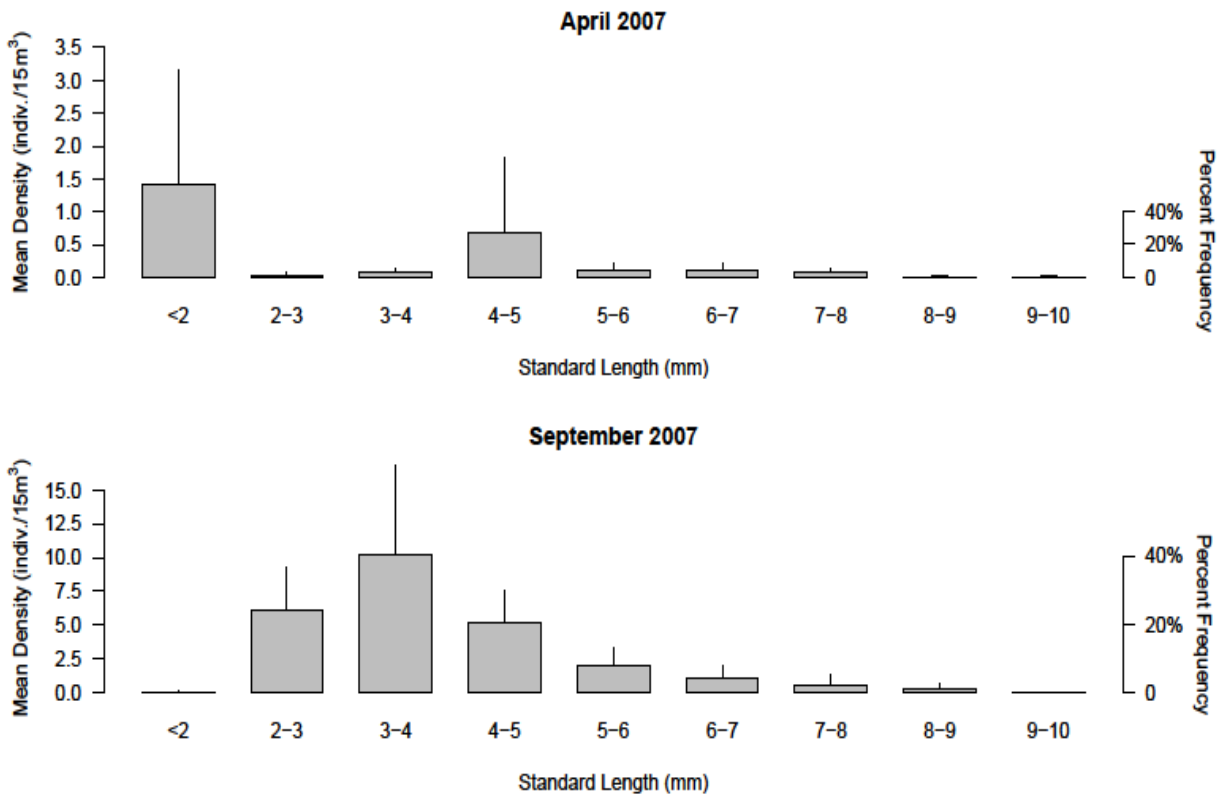


Figure 6.14: Mean density, standard error, and size-class frequency histograms for *C. arenarius* larvae collected in 18-21 April and 16-19 September 2007. In April most larvae were less than 2 mm SL. In September most of the larvae were between 2 and 5 mm SL.

densities ($p < 0.0001$, Table 6.1). No larvae from any location had a length greater than 10 mm SL in either month. April had more larvae less than 2 mm SL (Figure 6.14).

Probability of encounter for larval *C. arenarius* was significantly influenced by water density ($p < 0.0001$, Table 6.1). There was a decrease in probability of encounter up to water densities of approximately $23.5\delta_t$, where there was a leveling off at around a 50% encounter rate, suggesting recruitment from coastal ocean waters or from the deeper channels of the estuary mouth.

There was a significant diel component to predicting probability of encounter and larval density for *C. arenarius* ($p < 0.0001$, $p < 0.0001$, Table 6.1). The probability of encounter was higher during the day, than night. However, densities were much lower during the day ($\bar{x} = 4.27 \text{ indiv./}15\text{m}^3$, $sd = 11.10$) than night ($\bar{x} = 22.71 \text{ indiv./}15\text{m}^3$, $sd = 51.78$). The lack of a significant depth term and interaction term between depth and diel component, points to STST not being a recruitment/retention strategy with limited or no evidence for diel vertical migration within the water column.

The interaction of location and NWT ($p = 0.0191$, Table 6.1) indicated that the probability of encounter was low for all three locations and flow directions, with the northern dock edge always having the lowest probabilities. *Cynoscion arenarius* had significant differences in larval densities based on SL as a function of NWT ($p < 0.0001$) and SL with location across the tidal pass ($p < 0.0001$, Table 6.1). In general, larger larvae, particularly those greater than 6 mm SL, were less likely to be encountered in the tidal pass and had lower overall densities. Positive NWTs had slightly higher densities for larvae greater than 3mm SL ($\bar{x} = 4.91 \text{ mm}$, $sd = 1.77$), and densities were greater at the southern shore and larvae were

larger at the center channel and southern shore (Table 6.2). In contrast, negative NWTs had high densities of larvae less than 3mm SL ($\bar{x} = 3.51 \text{ mm}, sd = 1.25$), and densities were greater at the northern dock, but larvae had larger SLs at the southern shore (Table 6.2). The ZINB modeled the northern dock edge ($\bar{x} = 3.42 \text{ mm}, sd = 1.23$) to have the highest densities of *C. arenarius* larvae <4 mm SL. The southern shore edge ($\bar{x} = 4.55 \text{ mm}, sd = 1.74$) had higher densities of smaller larvae than the center channel ($\bar{x} = 4.49 \text{ mm}, sd = 1.76$), and all locations became similar for larvae over 6 mm SL.

6.3.11 *Cynoscion nebulosus* (spotted seatrout)

Estuarine dependent *C. nebulosus* larvae were only collected in September ($\bar{x} = 3.97 \text{ indiv./}15\text{m}^3, sd = 10.3$), and had an overall sample encounter percentage of 41.9%. Significantly higher densities of *C. nebulosus* larvae were collected as water density increased ($p < 0.0001$, Table 6.1), indicative of spawning in coastal ocean or higher saline tidal pass waters rather than the estuary. There was also a significant diel component ($p < 0.0001$, Table 6.1) to larval *C. nebulosus* densities, with day densities being smaller than night. Although the larvae collected were very small (2-6 mm SL), the disparity in densities between day ($\bar{x} = 0.41 \text{ indiv./}15\text{m}^3, sd = 0.72$) and night ($\bar{x} = 7.54 \text{ indiv./}15\text{m}^3, sd = 13.75$) suggests visual gear avoidance.

Larval densities for *C. nebulosus* significantly varied by SL ($p < 0.0001$), and for the interaction of location across the tidal pass and NWT ($p = 0.0006$, Table 6.1). Peak densities consisted of the 2 to 4 mm SL size classes (September: $\bar{x} = 3.31 \text{ mm}, sd = 0.83$), which comprised over 74% of all larvae sampled (Figure 6.15). In general as larval length increased,

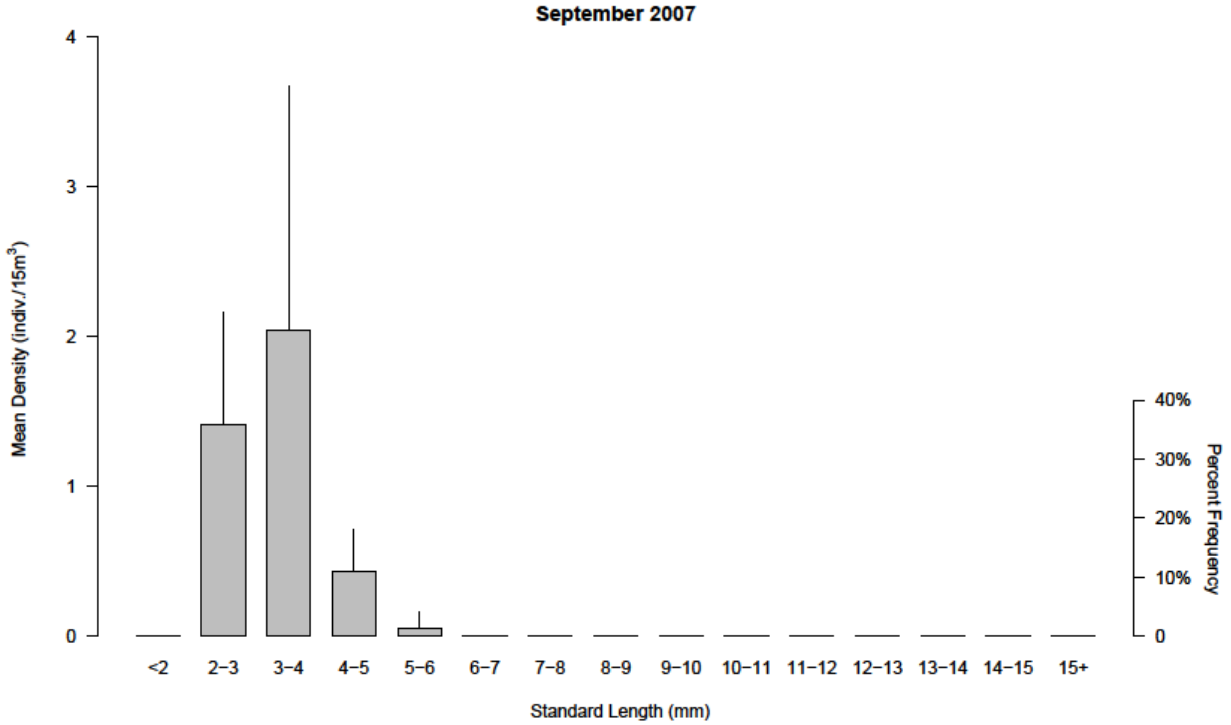


Figure 6.15: Mean density, standard error, and size class frequency histograms of *C. nebulosus* larvae collected in 16-19 September 2007. The highest mean densities and greatest frequency of larvae were between 2 and 4 mm SL.

there was a decrease in expected larval density as very few larvae larger than 17 mm SL were sampled (i.e., $n = 3$ for larvae $15 + \text{ mm SL}$). During positive NWTs, densities were significantly greater at the southern shore ($\bar{x} = 1.35 \text{ n}/15\text{m}^3, sd = 4.88$) and center channel ($\bar{x} = 1.03 \text{ n}/15\text{m}^3, sd = 3.63$) than the northern edge ($\bar{x} = 0.71 \text{ n}/15\text{m}^3, sd = 2.15$; Table 6.2). In contrast during negative NWTs, the center channel had greater densities ($\bar{x} = 1.94 \text{ n}/15\text{m}^3, sd = 8.64$) than the southern ($\bar{x} = 0.65 \text{ n}/15\text{m}^3, sd = 3.17$) or extremely low densities at the northern dock edge ($\bar{x} = 0.05 \text{ n}/15\text{m}^3, sd = 0.13$; Table 6.2).

6.4 Discussion

6.4.1 Hydrography

Bayou Tartellan tidal pass was vertically well-mixed having no statistical difference between surface and near-bottom water temperature, salinity, or water density for either sampling month. The passage of atmospheric cold front passages with associated energetic rotating wind fields would increase vertical mixing in this shallow estuary (Walker and Hammack, 2000). Hydrodynamic differences in this vertically well-mixed system may, therefore, depend more highly on tidal stage, flow magnitude, lateral discontinuities, or edge distance effects within the channel, than on vertical thermohaline stratification (Lyczkowski-Schultz et al., 1990; Maynard, 2006). Observed differences among the northern dock, center channel, and southern shore positive and negative NWTs supports this lateral concept.

The difference in periodicity and trend between NWT, and predicted versus measured tides showed the impact that small-scale, temporal effects like wind events have on the hydrology in the tidal pass, e.g., significant changes in NWT direction and magnitude (Swenson and Chuang, 1983; Chesney et al., 2000; Perez and Day, 2000; Walker and Hammack, 2000; Swenson, 2003; Li, 2011). Specifically in April, NWT was cyclic and driven by the passage of frontal events occurring before and after our four-day sampling period, creating very little change overall in the tidal prism. In September, however, strengthening negative NWTs were related to a deviation in the tidal prism following a frontal event on 15 September, despite predominantly southerly winds during this period. The influence of atmospheric forcing on subtidal oscillations has been shown to be an important driver of estuarine flushing in micro-tidal environments (Bianchi et al., 1997; Chesney et al., 2000; Lipp et al., 2001; Brown et al., 2004).

Variability within hydrodynamics and NWT differed in each of the two sampling months for each of the three sampling locations across the tidal pass. In April, higher salinities and colder water temperatures during positive NWTs were characteristic of coastal-shelf waters, with the greatest positive NWTs in the center channel, lower at the southern shore edge, and lowest at the northern dock edge. Negative NWTs were greatest at the northern dock and lowest at the southern shore, characterized by higher water temperatures and lower salinities more indicative of estuarine waters. In September, all three locations had similar water mass characteristics, where the greatest positive NWTs occurred with high salinity and more consistent with coastal-ocean waters, although temperatures were generally warmer than 28°C. Negative transports had lower salinities indicative of the upper estuary, and cooler temperatures, possibly from a previous passage of a winter frontal event lowering temperatures in this shallow, well-mixed estuary. The negative transports were greatest in the center channel and once again lowest at the southern shore. These lateral hydrodynamic trends, based on location across the tidal pass, are likely influenced by bathymetric variability, distributary branches, and local eddies creating differing flow patterns dependent on the magnitude and directionality of the flow (Wang et al., 1993; Li and O'Donnell, 1997). The asymmetrical relationship between the two edges of the tidal pass likely results from the law of the wall being non-existent during outgoing flows for the northern dock edge, and confounded by a distributary being directly upstream (Trowbridge et al., 1999; Stacey and Ralston, 2005).

6.4.2 *Anchoa* Congenerics

Life history characteristics highlight the difference between an estuarine-dependent species such as *A. hepsetus* (broad-striped anchovy), which spawn near-shore in approximately

10 meters of water or less (Ditty et al., 1988; Lapolla, 2001), and the estuarine-obligate, *A. mitchilli* (bay anchovy), which spawns within the estuary requiring no transport across shelf and through the tidal pass (Zastrow et al., 1991). Although both *A. hepsetus* and *A. mitchilli* were sampled during both study months, September had higher densities than April for both species, which probably reflects a protracted spawning period starting in spring, peaking during mid-summer, and then tapering off during early fall (Castro and Cowen, 1991; Lapolla, 2001; Fahay, 2007). The estuarine-dependent versus estuarine-obligate nature of these two species was clearly seen during both months, when broad-striped anchovy densities peaked during positive NWTs, and bay anchovy densities peaked during negative NWTs and also had more estuarine encounters overall.

Interestingly, during positive NWTs, the southern shore edge had the highest probability of encounter for larval *A. hepsetus* and *A. mitchilli*, while during negative flows, the probability of encounter in the center channel increased for *A. hepsetus* and *A. mitchilli*, and decreased at the southern shore. However, there was a significant increase in the mean length for both *Anchoa* congeners at the southern shore during negative NWTs. Larger *A. hepsetus* and *A. mitchilli* larvae were likely to be found in higher densities at the southern shore edge, particularly at high flow rates around $-50\text{m}^3/\text{s}$, which may help in minimizing being flushed out of the estuary during strong outwelling (Lapolla, 2001; Nieland et al., 2002). Similar findings for increased larval density at the edges of tidal passes versus the center channel during outflows have been documented and postulated as potentially being a retention mechanism in both Louisiana and Alabama (Lyczkowski-Schultz et al., 1990; Raynie, 1991; Raynie and Shaw, 1994). In particular, the extended benthic boundary layer conditions created by the gentler sloping natural shoreline

of the southern shore edge may provide refuge areas of decreased flows more conducive to estuarine retention for larger larvae that can move laterally across the tidal pass thereby encountering less energetic flows (Trowbridge et al., 1999; Lapolla, 2001; Nieland et al., 2002; Wang, 2002). The lack of large densities at the northern dock edge during negative NWTs for either species may reflect the decreasing effect of the law of the wall in providing refuge from outwelling (Trowbridge et al., 1999; Wang, 2002; Stacey and Ralston, 2005).

6.4.3 Other Species

The estuarine-dependent nature of *B. patronus*, *S. ocellatus*, and the two *Cynoscion* congeners was indicated by higher flood densities. Larval *B. patronus* densities were significantly higher during positive NWTs, with higher densities occurring in the center channel at transports greater than 50 m³/s. The spawning season for *B. patronus* has been traditionally reported as being from October to February (Ditty et al., 1988; Barbieri et al., 1994; Hare and Able, 2007; Vaughan et al., 2007; Schaffler et al., 2009; Taylor et al., 2009; Hernandez et al., 2010). However, the small larvae collected in September suggests earlier spawning and estuarine recruitment, and perhaps initial spawning closer to shore than previously reported in Louisiana (Ruple, 1984; Shaw et al., 1985). *Sciaenops ocellatus* and the two *Cynoscion* congeners all showed the same trend of higher densities occurring during positive NWTs.

During positive NWTs, all species in the analysis showed lateral partitioning across the tidal pass in terms of either probability of encounter and/or larval density. Generally, positive NWTs showed the highest probability of encounter and greatest densities to be located in the center channel or southern shore edge of the tidal pass. In addition, mean SLs for all species except *A. hepsetus* and *C. nebulosus* were larger in the center channel, which would provide

larger larvae the maximum tidal excursion up estuary (Beckley, 1985; Whitfield, 1989; Roper, 1986; Schultz et al., 2003). In particular, densities for *A. hepsetus* and *B. patronus* were much greater in the center channel, versus either edge. The other species in the analysis, *A. mitchilli*, *S. ocellatus*, *C. arenarius*, and *C. nebulosus* all had the greatest densities on flood tides at the southern shore edge, and except for *A. mitchilli*, were not significantly different from the center channel.

During negative NWTs, lateral partitioning across the tidal pass in terms of probability of encounter and larval density also occurred. Generally, larger larvae were found at the southern shore edge of the tidal pass, possibly a reflection of size-dependent, behavioral mediation which could result in increased estuarine retention (Fisher 2005; Stanley et al., 2012). The notable exceptions were *S. ocellatus* and *C. nebulosus*, which had the largest larvae in the center channel, although these larvae were relatively small ($< 4.5 \text{ mm SL}$). During outwelling events, the center channel had a higher probability of encounter and smaller SLs for *A. hepsetus*, *A. mitchilli*, and *B. patronus*, which may be a reflection of the strongest currents simply overriding the swimming capabilities of smaller larvae. For example, even though the center channel had high densities for *A. hepsetus*, *A. mitchilli*, and *C. nebulosus*, their mean SLs was significantly smaller than mean SLs at the southern shore edge.

The extended benthic boundary layer conditions and sediment surface variability (e.g., oyster shells) at the natural, gently sloping edge of the southern shore edge of the tidal pass appeared to provide reduced flows and might increase the ability to resist outwelling events for larvae large enough to move horizontally (Wang et al., 1993; Trowbridge et al., 1999; Wang, 2002). At the anthropogenically-altered, northern dock edge, the law of the wall appeared to

have had a diminished effect in moderating outgoing flows during strong negative NWTs (Trowbridge et al., 1999; Wang, 2002; Stacey and Ralston, 2005)

Despite high Louisiana estuarine turbidities (Childers and Day, 1990; Nichol et al., 1994; Lane et al., 2006) and efforts to minimize the visual profile of the passive sampling gear, all species showed model results, which could suggest visual gear avoidance during daylight surface collections. The lack of a significant depth and diel interaction term for all species, except for *B. patrnous*, suggested that vertical stratification or migration is not likely due to the well-mixed nature of this tidal pass. Gulf menhaden larvae, however, did show weak evidence of diel vertical migration, which has been previously reported for similar tidal passes along the northern GOM (Shaw et al., 1988; Raynie, 1991; Govoni, 1997). The lack of any significant interactions linking depth with flow intensity and direction, except for the only estuarine-obligate species, *A. mitchilli*, suggested that STST is not an operative recruitment mechanism in vertically well-mixed estuaries (Whitfield, 1989; Roper, 1986; Schultz et al., 2003; Criales et al., 2011).

6.5 Conclusions

The problems of heterogeneity within larval fish distributions in marine environments, and the resultant patch dynamics often result in excess zeroes above what would be expected for any distribution. Here the use of a ZINB is explored to help deal with that heterogeneity, while providing insight on probabilities of encounter and confidence to the predictions of larval density. The advantage of the ZINB over a simpler negative binomial model is the expressed relation of the covariates to the perfect state, and thus zero generation in the data (Minami et al., 2007). Failing to account for zero generating processes can produce bias in parameter estimates and impact the ability to accurately understand relationships between groups of parameters and

organisms, where simple estimates of larval density may not elucidate horizontal movement, vertical/lateral structure, or recruitment/retention mechanisms.

These ichthyoplankton analyses showed that probabilities of encounter and larval densities can be species specific, size dependent, and be related to the differences in NWT direction and strength across a tidal pass. The center channel had the strongest inflows for positive NWTs, and the greatest chance for estuarine-dependent larvae to successfully recruit far up estuary. At the natural bank of the southern shore edge of the tidal pass, the benthic boundary layer conditions and sediment surface variability appeared to provide reduced flows and an opportunity to resist outwelling events for larger larvae. The bulkheaded northern dock edge did not appear to aid in resisting outgoing flows.

With no significant differences between surface and near-bottom hydrographic measurements and few or no tidal-depth (or diel) interactions, directed vertical movement under STST was not supported for transport through and retention within this vertically well-mixed tidal pass. Virtually all species in the analysis, with the exception of the only estuarine obligate species, *A. mitchilli*, exhibited varying degrees of recruitment pulsing or patchiness. In conclusion, the differences in ichthyoplankton distributions at different lateral locations across the tidal pass, may be enhanced by size-dependent, behaviorally-mediated horizontal movement which could utilize flow differences, micro-eddies and other small-scale circulation patterns, and channel geomorphic structural differences and boundary conditions, to maximize estuarine recruitment and retention.

6.6 Literature Cited

- Akaike, H. 1974. A new look at the statistical model identification. IEEE. Transactions on Automatic Control 19: 716-723.
- Barbieri, L.R., M. Chittenden Jr, and S.K. Lowerre-Barbieri. 1994. Maturity, spawning, and ovarian cycle of Atlantic croaker, *Micropogonias undulatus*, in the Chesapeake Bay and adjacent coastal waters. Fisheries Bulletin 92: 671-685.
- Barry, S.C. and A.H. Welsh. 2002. Generalized additive modeling and zero inflated count data. Ecological Modeling 157: 179-188.
- Beckley, L.E. 1985. Tidal exchange of ichthyoplankton in the Swartkops estuary mouth, South Africa. South African Journal of Zoology 20: 15-20.
- Bianchi, T.S., M. Baskaran, J. DeLord, and M. Ravichandran. 1997. Carbon cycling in a shallow turbid estuary of southeast Texas: The use of plant pigment biomarkers and water quality parameters. Estuaries and Coasts 20: 404-415.
- Boehlert, G.W., and B.C. Mundy. 1988. Roles of behavioral and physical factors in larval and juvenile fish recruitment to estuarine nursery areas. American Fisheries Society Symposium 3(5): 224-227.
- Boon, J.D., and R.J. Byrne. 1981. On basin hyposmetry and the morphodynamic response of coastal inlet systems. Marine Geology 40: 27-48.
- Bradbury, I.R., P.V. Snelgrove, and P. Pepin. 2003. Passive and active behavioural contributions to patchiness and spatial pattern during the early life history of marine fishes. Marine Ecology Progress Series 257: 233-245.
- Brown, C., S. Holt, S. Jackson, D. Brooks, and G. Holt. 2004. Simulating larval supply to estuarine nursery areas: how important are physical processes to the supply of larvae to the Aransas Pass Inlet? Fisheries Oceanography 13: 181-196.
- Cahoon, D.R., and D.J. Reed. 1995. Relationships among marsh surface topography, hydroperiod, and soil accretion in a deteriorating Louisiana salt marsh. Journal of Coastal Research 11: 357-369.
- Castro, L.R., and R.K. Cowen. 1991. Environmental factors affecting the early life history of bay anchovy *Anchoa mitchilli* in Great South Bay, New York. Marine Ecology Progress Series 76: 235-247.

- Chambers, J.R. 1992. Coastal degradation and fish population losses. Stemming the Tide of Coastal Fish Habitat Loss. Marine Recreational Fishery Publication 14: 45-52.
- Chesney, E.J., D.M. Baltz, and R.G. Thomas. 2000. Louisiana estuarine and coastal fisheries and habitats: Perspectives from a fish's eye view. *Ecological Applications* 10: 350-366.
- Childers, D.L., and J.W. Day. 1990. Marsh-water column interactions in two Louisiana estuaries. I. Sediment dynamics. *Estuaries*, 13: 393-403.
- Criales, M.M., M.B. Robblee, J.A. Browder, H. Cardenas, and T.L. Jackson. 2011. Field observations on selective tidal-stream transport for postlarval and juvenile pink shrimp in Florida Bay. *Journal of Crustacean Biology* 31: 26-33.
- Décima, M., M.D. Ohman, and A. De Robertis. 2010. Body size dependence of euphausiid spatial patchiness. *Limnology and Oceanography* 55: 777.
- Ditty, J., G. Zieske, and R. Shaw. 1988. Seasonality and depth distribution of larval fishes in the northern Gulf of Mexico above latitude 26 degree 00'N. *Fisheries Bulletin* 86: 811-823.
- Fahay, M.P. 1983. Guide to the early stages of marine fishes occurring in the western North Atlantic Ocean, Cape Hatteras to the south Scotian Shelf. *North Atlantic Fisheries Science* 4: 1-423.
- Fahay, M.P. 2007. Early Stages of Fishes in the Western North Atlantic Ocean: Davis Strait, Southern Greenland and Flemish Cap to Cape Hatteras. *Scorpaeniformes Through Tetraodontiformes*. Northwest Atlantic Fisheries Organization. 1696 pp.
- Field, S.A., A.J. Tyre, and H.P. Possingham. 2005. Optimizing allocation of monitoring effort under economic and observational constraints. *Journal of Wildlife Management* 69: 473-482.
- Fisher, R. 2005. Swimming speeds of larval coral reef fishes: impacts on self-recruitment and dispersal. *Marine Ecology Progress Series* 285: 223-232.
- Frank, K.T., J.E. Carscadden, and W.C. Leggett. 1993. Causes of spatio-temporal variation in the patchiness of larval fish distributions: differential mortality or behaviour? *Fisheries Oceanography* 2: 114-123.
- Gaston, K.J., and B.H. McArdle. 1994. The temporal variability of animal abundances: measures, methods and patterns. *Philosophical Transactions of the Royal Society of London. Series B: Biological Sciences* 345: 335-358.

- Gibson, R., M. Barnes, and R. Atkinson. 2001. Selective tidal-stream transport of marine animals. *Oceanography and Marine Biology, An Annual Review* 39:305-353.
- Gill, A.E. 1982. *Atmosphere-ocean dynamics*. Academic Press, London. 662 pp.
- Govoni, J.J. 1997. The association of the population recruitment of gulf menhaden, *Brevoortia patronus*, with Mississippi River discharge. *Journal of Marine Systems* 12: 101-108.
- Hare, J.A., and K.W. Able. 2007. Mechanistic links between climate and fisheries along the east coast of the United States: explaining population outbursts of Atlantic croaker (*Micropogonias undulatus*). *Fisheries Oceanography* 16:31-45.
- Heilbron, D.C. 1994. Zero-altered and other regression models for count data with added zeros. *Biometrical Journal* 36:531-547.
- Hernandez Jr, F.J., S.P. Powers, and W.M. Graham. 2010. Detailed examination of ichthyoplankton seasonality from a high-resolution time series in the northern Gulf of Mexico during 2004-2006. *Transactions of the American Fisheries Society* 139: 1511-1525.
- Holt, G.J., and S.A. Holt. 2000. Vertical distribution and the role of physical processes in the feeding dynamics of two larval sciaenids *Sciaenops ocellatus* and *Cynoscion nebulosus*. *Marine Ecology Progress Series* 193: 181-190.
- Kim, C.K., Park, K., Powers, S.P., Graham, W.M., and K.M. Bayha. 2010. Oyster larval transport in coastal Alabama: Dominance of physical transport over biological behavior in a shallow estuary. *Journal of Geophysical Research: Oceans* (1978–2012) 115.
- Kim, C.K., and K. Park. 2012. A modeling study of water and salt exchange for a micro-tidal, stratified northern Gulf of Mexico estuary. *Journal of Marine Systems* 96:103-115.
- Kjerfve, B. 1978. Bathymetry as an indicator of net circulation in well mixed estuaries. *Limnology and Oceanography* 23:816-821.
- Kupchik, M.J. 2014. A study of the temporal and spatial distribution of ichthyoplankton and post-larval penaeids recruiting into a Louisiana tidal pass. PhD Dissertation. Louisiana State University, Baton Rouge, LA, USA. 384 pp.
- Lambert, D. 1992. Zero-inflated poisson regression, with an application to defects in manufacturing. *Technometrics* 34:1-14.

- Lane, R.R., J.W. Day, and J.N. Day. 2006. Wetland surface elevation, vertical accretion, and subsidence at three Louisiana estuaries receiving diverted Mississippi River water. *Wetlands* 26:1130-1142.
- Lapolla, A.E. 2001. Bay anchovy *Anchoa mitchilli* in Narragansett Bay, Rhode Island. II. Spawning season, hatch-date distribution and young-of-the-year growth. *Marine Ecology Progress Series* 217:103-109.
- Letcher, B.H., and J.A. Rice. 1997. Prey patchiness and larval fish growth and survival: Inferences from an individual-based model. *Ecological Modeling* 95(1): 29-43.
- Li, C., and J. O'Donnell. 1997. Tidally-driven residual circulation in shallow estuaries with lateral depth variation. *Journal of Geophysical Research: Oceans* (1978–2012) 102:27915-27929.
- Li, C., E. Weeks, and J.L. Rego. 2009. In situ measurements of saltwater flux through tidal passes of Lake Pontchartrain estuary by Hurricanes Gustav and Ike in September 2008. *Geophysical Research Letters* 36:L19609.
- Li, C., H. Roberts, G.W. Stone, E. Weeks, and Y. Luo. 2011. Wind surge and saltwater intrusion in Atchafalaya Bay during onshore winds prior to cold front passage. *Hydrobiologia*:1-13.
- Lipp, E.K., C. Rodriguez-Palacios, and J.B. Rose. 2001. Occurrence and distribution of the human pathogen *Vibrio vulnificus* in a subtropical Gulf of Mexico estuary. *Hydrobiologia* 460: 165-173.
- Liu, H. 2009. Semiparametric regression analysis of zero-inflated data. Ph.D. Dissertation. University of Iowa, Iowa, USA. 110 pp.
- Lochmann, S.E., R.M. Darnell, and J.D. McEachran. 1995. Temporal and vertical distribution of crab larvae in a tidal pass. *Estuaries* 18: 255-263.
- Lyczkowski-Shultz, J., D.L. Ruple, S.L. Richardson, J. Cowan, and H. James. 1990. Distribution of fish larvae relative to time and tide in a Gulf of Mexico barrier island pass. *Bulletin of Marine Science* 46: 563-577.
- MacKenzie, D.I., J.D. Nichols, J.E. Hines, M.G. Knutson, and A.B. Franklin. 2003. Estimating site occupancy, colonization, and local extinction when a species is detected imperfectly. *Ecology* 84: 2200-2207.
- MacKenzie, D.I., J.D. Nichols, G.B. Lachman, S. Droege, J.A. Royle, and C.A. Langtimm. 2002. Estimating site occupancy rates when detection probabilities are less than one. *Ecology* 83: 2248-2255.

- Mann, K.H. 2000. Ecology of the coastal waters with implications for management. 2nd Edition. John Wiley and Sone, Hoboken, NJ. 410 pp.
- Martin, T.G., B.A. Wintle, J.R. Rhodes, P.M. Kuhnert, S.A. Field, S.J. Low-Choy, A.J. Tyre, and H.P. Possingham. 2005. Zero tolerance ecology: improving ecological inference by modeling the source of zero observations. *Ecology Letters* 8: 1235-1246.
- Maunder, M.N., and A.E. Punt. 2004. Standardizing catch and effort data: a review of recent approaches. *Fisheries Research* 70: 141-159.
- Maynard, S.T. 2006. Evaluation of the micromodel: An extremely small-scale movable bed model. *Journal of Hydraulic Engineering* 132: 343-353.
- Minami, M., C.E. Lennert-Cody, W. Gao, and M. Román-Verdesoto. 2007. Modeling shark bycatch: the zero-inflated negative binomial regression model with smoothing. *Fisheries Research* 84:210-221.
- Moeller, C.C., O.K. Huh, H.H. Roberts, L.E. Gumley, and W.P. Menzel. 1993. Response of Louisiana coastal environments to a cold front passage. *Journal of Coastal Research* 9(2): 434-447.
- Moser, H.G. 1984. *Ontogeny and Systematics of Fishes*. American Society of Ichthyologists and Herpetologists Special Publication No. 1. Allen Press, Lawrence, Kansas. 760 pp.
- Nichol, S.L., R. Boyd, and S. Penland. 1994. Stratigraphic response of wave-dominated Eestuaries to different relative sea-level and sediment-supply histories: Quaternary case studies from Nova Scotia, Louisiana and Eastern Australia. *Special Publication- Society of Economic Paleontologists and Mineralogists* 51: 265-265.
- Nieland, D.L., R.G. Thomas, and C.A. Wilson. 2002. Age, growth, and reproduction of spotted seatrout in Barataria Bay, Louisiana. *Transactions of the American Fisheries Society* 131: 245-259.
- Park, K. 2012. Importance of stratification on mixing and transport in a shallow, micro-tidal northern Gulf of Mexico estuary. *Journal of Geophysical Research: Oceans* 1-7.
- Parker, K.S., T.C. Royer, and R.B. Deriso. 1995. High-latitude climate forcing and tidal mixing by the 18.6-year lunar nodal cycle and low-frequency recruitment trends in Pacific halibut (*Hippoglossus stenolepis*). *Canadian Special Publication of Fisheries and Aquatic Sciences* 121: 447-459.

- Perez, B., and J. Day. 2000. Influence of Atchafalaya River discharge and winter frontal passage on suspended sediment concentration and flux in Fourleague Bay, Louisiana. *Estuarine, Coastal and Shelf Science* 50: 271-290.
- Raynie, R.C. 1991. Study of the spatial and temporal ichthyoplankton abundance along a recruitment corridor from offshore to estuarine nursery. Louisiana State University, Baton Rouge, Louisiana, USA. 136 pp.
- Raynie, R.C., and R.F. Shaw. 1994. Ichthyoplankton abundance along a recruitment corridor from offshore spawning to estuarine nursery ground. *Estuarine, Coastal and Shelf Science* 39: 421-450.
- Rhodes, J.R., C.A. McAlpine, D. Lunney, and H.P. Possingham. 2005. A spatially explicit habitat selection model incorporating home range behavior. *Ecology* 86: 1199-1205.
- Richards, W.J. 2006. Early Stages of Atlantic Fishes: An Identification Guide for the Western Central North Atlantic. Volume I & II. CRC Press, Boca Raton, FL. 2640 pp.
- Rogers, B.D., R.F. Shaw, W.H. Herke, and R.H. Blanchet. 1993. Recruitment of postlarval and juvenile brown shrimp (*Penaeus aztecus* Ives) from offshore to estuarine waters of the northwestern Gulf of Mexico. *Estuarine, Coastal and Shelf Science* 36: 377-394.
- Rooker, J.R., S.A. Holt, M.A. Soto, and G.J. Holt. 1998. Postsettlement patterns of habitat use by sciaenid fishes in subtropical seagrass meadows. *Estuaries and Coasts* 21: 318-327.
- Roper, D. 1986. Occurrence and recruitment of fish larvae in a northern New Zealand estuary. *Estuarine, Coastal and Shelf Science* 22: 705-717.
- Ruple, D.L. 1984. Occurrence of larval fishes in the surf zone of a northern Gulf of Mexico barrier island. *Estuarine, Coastal and Shelf Science* 18: 191-208.
- Schaffler, J.J., C.S. Reiss, and C.M. Jones. 2009. Spatial variation in otolith chemistry of Atlantic croaker larvae in the Mid-Atlantic Bight. *Marine Ecology Progress Series* 382: 185-195.
- Schultz, E.T., K.M. Lwiza, M.C. Fencil, and J.M. Martin. 2003. Mechanisms promoting upriver transport of two species of larval fish in the Hudson River Estuary (USA). *Marine Ecology Progress Series* 251: 263-277.
- Shaw, R.F., J.H. Cowan, and T.L. Tillman. 1985. Distribution and density of *Brevoortia patronus* (gulf menhaden) eggs and larvae in the continental shelf waters of western Louisiana. *Bulletin of Marine Science* 36(1): 96-103.

- Shaw, R.F., B.D. Rogers, J. Cowan, and W.H. Herke. 1988. Ocean-estuary coupling of ichthyoplankton and nekton in the Northern Gulf of Mexico. *American Fisheries Society Symposium* 3: 77-89.
- Smith, N.P. 1977. Meteorological and tidal exchanges between Corpus Christi Bay, Texas, and the northwestern Gulf of Mexico. *Estuarine and Coastal Marine Science* 5: 511-520.
- Stacey, M.T., and D.K. Ralston. 2005. The scaling and structure of the estuarine bottom boundary layer. *Journal of Physical Oceanography* 35: 55-71.
- Stanley, R., P.V. Snelgrove, and R.S. Gregory. (2012). Dispersal patterns, active behaviour, and flow environment during early life history of coastal cold water fishes. *PloS One* 7(9): e46266.
- Stone, G.W., B. Liu, D.A. Pepper, and P. Wang. 2004. The importance of extratropical and tropical cyclones on the short-term evolution of barrier islands along the northern Gulf of Mexico, USA. *Marine Geology* 210: 63-78.
- Stuck, K.C. and H.M. Perry. 1982. Ichthyoplankton community structure in Mississippi coastal waters. Pp. VI-I-1 to VI-I-53. *In: Fishery monitoring and assessment completion report, 1 January 1977 to 31 December 1981. Gulf Coast Research Lab, Project No. 2-296-R.*
- Swenson, E.M. 2003. Assessing the potential climate change impact on salinity in the northern Gulf of Mexico estuaries: a test case in the Barataria estuarine system. *Integrated assessment of the climate change impacts on the Gulf Coast Region. GCRCC & LSU Graphic Series, Baton Rouge, LA: 131-150.*
- Swenson, E.M., and W.S. Chuang. 1983. Tidal and subtidal water volume exchange in an estuarine system. *Estuarine, Coastal and Shelf Science* 16: 229-240.
- Tankersley, R.A., M.G. Wieber, M.A. Sigala, and K.A. Kachurak. 1998. Migratory behavior of ovigerous blue crabs *Callinectes sapidus*: evidence for selective tidal-stream transport. *The Biological Bulletin* 195: 168-173.
- Taylor, J.C., W.A. Mitchell, J.A. Buckel, H.J. Walsh, K.W. Shertzer, G.B. Martin, and J.A. Hare. 2009. Relationships between larval and juvenile abundance of winter-spawned fishes in North Carolina, USA. *Marine and Coastal Fisheries: Dynamics, Management, and Ecosystem Science* 1: 12-21.
- Leis, J.M., J.E. Caselle, I.R. Bradbury, T. Kristiansen, J.K. Llopiz, M.J. Miller, M.I. O'Connor, C.B. Paris, A.L. Shanks, S.M. Sogard, S.E. Swearer, A. Treml, R.D. Vetter, and R.R. Warner. 2013. Does fish larval dispersal differ between high and low latitudes? *Proceedings of the Royal Society, Biological Sciences* 280: 1-10.

- Trowbridge, J., W. Geyer, M. Bowen, and A. Williams III. 1999. Near-bottom turbulence measurements in a partially mixed estuary: turbulent energy balance, velocity structure, and along-channel momentum balance. *Journal of Physical Oceanography* 29: 3056-3072.
- Tu, W. 2002. Zero-inflated data. *Encyclopedia of Environmetrics* 4: 2387-2391.
- Tyre, A.J., B. Tenhumberg, S.A. Field, D. Niejalke, K. Parris, and H.P. Possingham. 2003. Improving precision and reducing bias in biological surveys: estimating false-negative error rates. *Ecological Applications* 13: 1790-1801.
- Vaughan, D.S., K.W. Shertzer, and J.W. Smith. 2007. Gulf menhaden (*Brevoortia patronus*) in the US Gulf of Mexico: Fishery characteristics and biological reference points for management. *Fisheries Research* 83: 263-275.
- Walker, N.D., and A.B. Hammack. 2000. Impacts of winter storms on circulation and sediment transport: Atchafalaya-Vermilion Bay region, Louisiana, USA. *Journal of Coastal Research* 16(4): 996-1010.
- Wang, F. 1997. Dynamics of intertidal marshes near shallow estuaries in Louisiana. *Wetlands Ecology and Management* 5: 131-143.
- Wang, X. 2002. Tide-induced sediment resuspension and the bottom boundary layer in an idealized estuary with a muddy bed. *Journal of Physical Oceanography* 32: 3113-3131.
- Wang, X., and P. Craig. 1993. An analytic model of tidal circulation in a narrow estuary. *Journal of Marine Research* 51: 447-465.
- Weeks, E., C. Li, H. Roberts, R.F. Shaw, and N. Walker. 2011. A comparison of unmanned survey vessel and manned vessels for nearshore tidal current and transport measurements. *Journal of the Marine Technical Society* 45(5): 71-77.
- Weinstein, M., S. Weiss, and M. Walters. 1980. Multiple determinants of community structure in shallow marsh habitats, Cape Fear River Estuary, North Carolina, USA. *Marine Biology* 58: 227-243.
- Whitfield, A.K. 1989. Ichthyoplankton interchange in the mouth of a southern African estuary. *Marine Ecology Progress Series* 54(1-2): 25-33.

Zastrow, C., E. Houde, and L. Morin. 1991. Spawning, fecundity, hatch-date frequency and young-of-the-year growth of bay anchovy, *Anchoa mitchilli*, in mid-Chesapeake Bay. Marine Ecology Progress Series 73: 161-171.

CHAPTER 7. GENERAL SUMMARY AND CONCLUSIONS

This dissertation focused on zoo-/ichthyoplankton recruitment for estuarine-dependent larvae across varying spatial and temporal scales, incorporating both environmental and organismal analyses. It provided an investigation of recruitment in the highly variable environment along a recruitment corridor in the northern Gulf of Mexico (GOM) from inner continental shelf into a Louisiana tidal pass. First, the general vertical structure of zoo-/ichthyoplankton for the inner continental shelf off Louisiana was determined using a mixed Analysis of Variance (ANOVA). Second, the potential effects of winter cold front passages on estuarine recruitment for winter spawning species using a Generalized Additive Model (GAM) were analyzed. Third, to investigate potential growth effects along the recruitment corridor during this transition period from more oligotrophic continental shelf waters to higher productivity and lower salinity estuarine waters for larval *Micropogonias undulatus* and *Brevoortia patronus*, a non-linear growth model and fine-scale measurement of otolith microstructure was used. Finally, potential differences in lateral cross channel probability of encounter and larval densities as they relate to the size of larvae and flow dynamics utilizing a Zero Inflated Negative Binomial (ZINB) model was investigated in an effort to help mitigate problems associated with the patchy distributions of larvae in the tidal pass.

Chapter 1: There was a high percentage of zoo-/ichthyoplankton which had an affinity for surface or upper water column waters on Louisiana's inner continental shelf. This result is even more relevant when considering ichthyoplankton vulnerabilities to potential oil spills in the GOM. Such offshore industrial accidents, like those of the Deepwater Horizon oil spill (2010) and other events, e.g., Taylor Energy Wells Platform 23051 oil spill/leak (ongoing since 1994)

and the gas blowout at the Hercules 265 Rig (2013), could represent significant additional mortality effects on early fishery life history stages already experiencing up to 99% natural mortality.

Chapter 2: The passage of winter atmospheric frontal events was demonstrated to have strong effects on ichthyoplankton estuarine recruitment and retention for two species of offshore-spawned, estuarine-dependent larvae in particular, *Brevoortia patronus* and *Micropogonias undulatus*. Both species had similar life history traits and recruitment dynamics, which were associated with the length of the recruitment/transport corridor, i.e., spawning depth or distance from shore, and potential dependence on astronomical and meteorological forcing. Flood tides during the interim or pre-frontal phase with its dominate southerly wind fields and coastal setup, appeared to be an important enhancement to inshore transport mechanisms and successful estuarine recruitment for *B. patronus* and *M. undulatus*. Both species also experienced high larval densities on flood tides during low-frequency, westerly winds and corresponding low barometric pressures during passage of the front, which may be a result of enhanced inshore transport during the initial length of Bayou Tartellan which has a West-to-East orientation. Interestingly, there was a lack of enhanced estuarine recruitment for both species above the normal tidal component from easterly winds and expected Ekman transport onshore. During ebb tides, both species saw higher larval densities during northerly winds at high and low barometric pressures, creating conditions which would be negative for estuarine retention.

Chapter 3: The problems of heterogeneity within larval fish distributions in marine environments, and the resultant patch dynamics often result in excess zeroes above what would be expected for any distribution. Using a Zero Inflated Negative Binomial (ZINB) model to

control for that heterogeneity provided insight on probabilities of encounter and confidence to the predictions of larval density laterally across Bayou Tartellan. These ichthyoplankton analyses showed that probabilities of encounter and larval densities could be related to differences in net water transport (NWT) direction and strength across a tidal pass, were size dependent, and were species specific. The center channel had the strongest inflows for positive NWTs, and the greatest chance for estuarine-dependent larvae to recruit successfully up estuary. At the natural, gently sloping bank of the southern shore edge of the tidal pass, the benthic boundary conditions and sediment surface variability appeared to provide reduced flows (especially during ebb tides) and an opportunity to resist outwelling events for larger larvae. The bulkheaded northern dock edge did not appear to be an aid in resisting outgoing flows.

Chapter 4: To assess the effects of the recruitment corridor on individuals, instead of from assemblages of ichthyoplankton, otolith microstructure analyses were conducted. In order to provide more resolution on growth rate, across-shelf transport, the timing of estuarine ingress, standard length (SL) at hatch, and rate of growth in the days post hatch (dph), Laird-Gompertz growth models were used larval *Micropogoniasundulatus*. The nature of the model allowed for expression of the limited somatic growth of larvae before recruitment into the lower salinity and more highly productive estuarine system of Bayou Tartellan. Moreover, the growth model also allowed for calculation of instantaneous growth rates that reflect small-scale, daily changes resulting from variable oceanographic conditions within the the recruitment corridor. This approach eliminates the bias introduced from overall growth averages expressed in a linear relationship with a singular rate of $0.2 \text{ mm} \cdot \text{day}^{-1}$, or from bias introduced from groupings of larvae in dph. The model also allowed for an estimation of maximum growth rate, which showed

that maximum fall growth rates with respect to dph occurred later than in the spring. Evidence based on differing growth rates between the fall spawning and recruitment season and the spring recruitment season suggested for the first time in the northern GOM that different spawning subgroups may exist as has been shown within North Carolina waters and the mid-Atlantic bight. This result was confirmed with differences in otolith microstructure between the fall and spring for both years, and the microstructure analysis was able to show different cohorts with variable recruitment corridor lengths possibly due to within year variability in adult batch spawning. The highly significant salinity component in the mixed model relating growth rate to the hydrodynamics in Bayou Tartellan reconfirmed the importance of low salinity and high productivity of estuarine waters for maximizing growth for larval and, ultimately, juvenile *M. undulatus*.

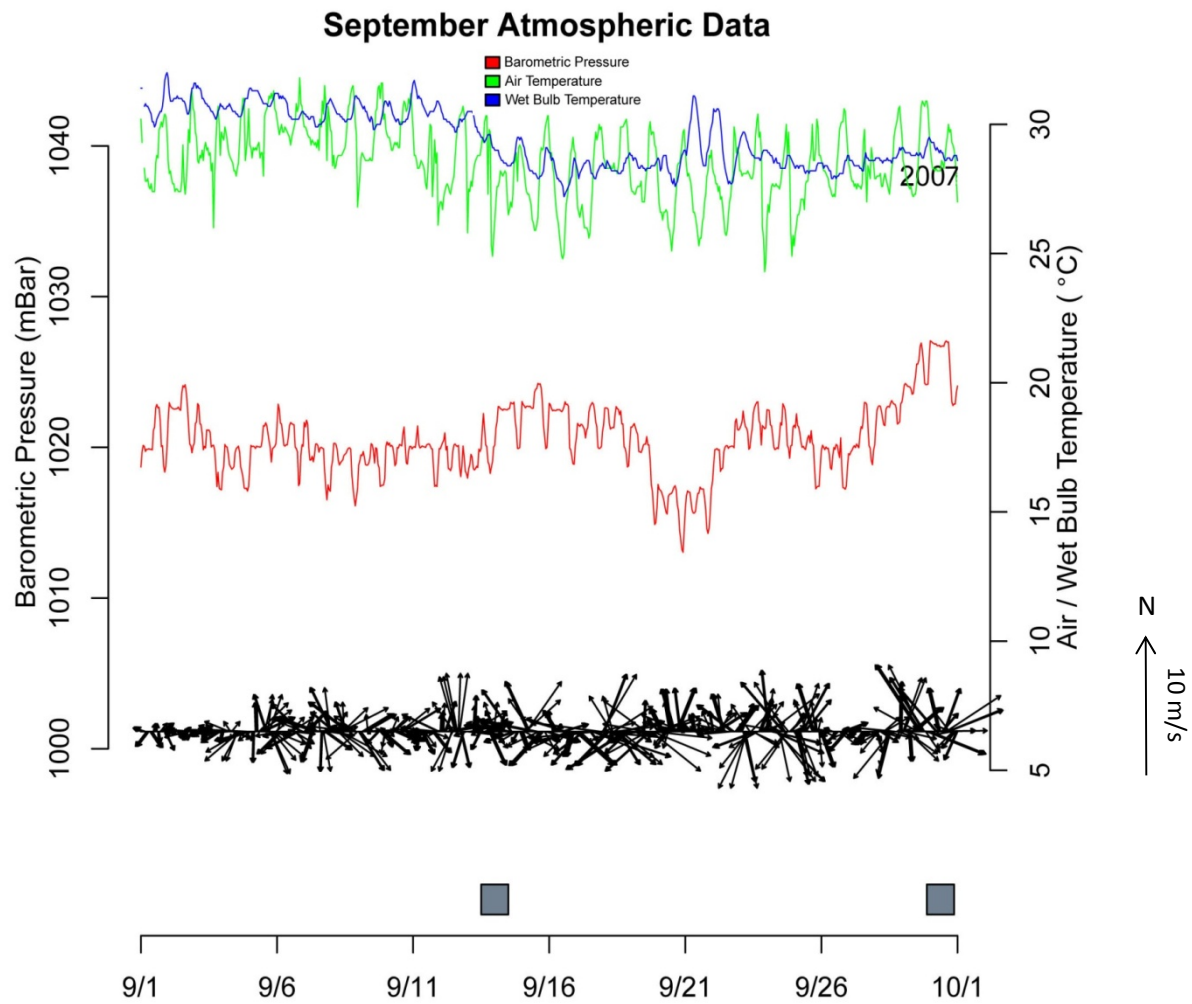
Chapter 5: The peak spawning period for *B. patronus* was estimated to be from December to early February in 2006-2007 and from January to February in 2008. However, collection of small (3 – 5 mm SL) and young (7 – 12 days post spawning; dps) larvae in late September - early October would have back-calculated spawning dates that suggest a much earlier than previously reported spawning season (i.e., early September) and a much shorter recruitment corridor. Generally, larvae were older and larger the longer the season progressed, consistent with previous literature. The two-cycle Laird-Gompertz models, individually grouped Laird-Gompertz models, ten-day blocked growth averages, and otolith microstructures all showed high agreement, and indicated that the beginning of an ontogenetic shift in feeding strategy occurred at approximately 33 dps. Moreover, all models showed that the greatest growth rate occurred offshore and prior to the ontogenetic shift in feeding capability, confirming growth

benefits from the accumulative learning curve that larger larvae acquire to effectively select particulate zooplankton prey items. The decrease in growth rate after the shift in development from a selective particulate feeder to an omnivorous filter feeder was remarkably similar in all modeling analyses, and the growth rate appeared to be relatively constant over both sampling years.

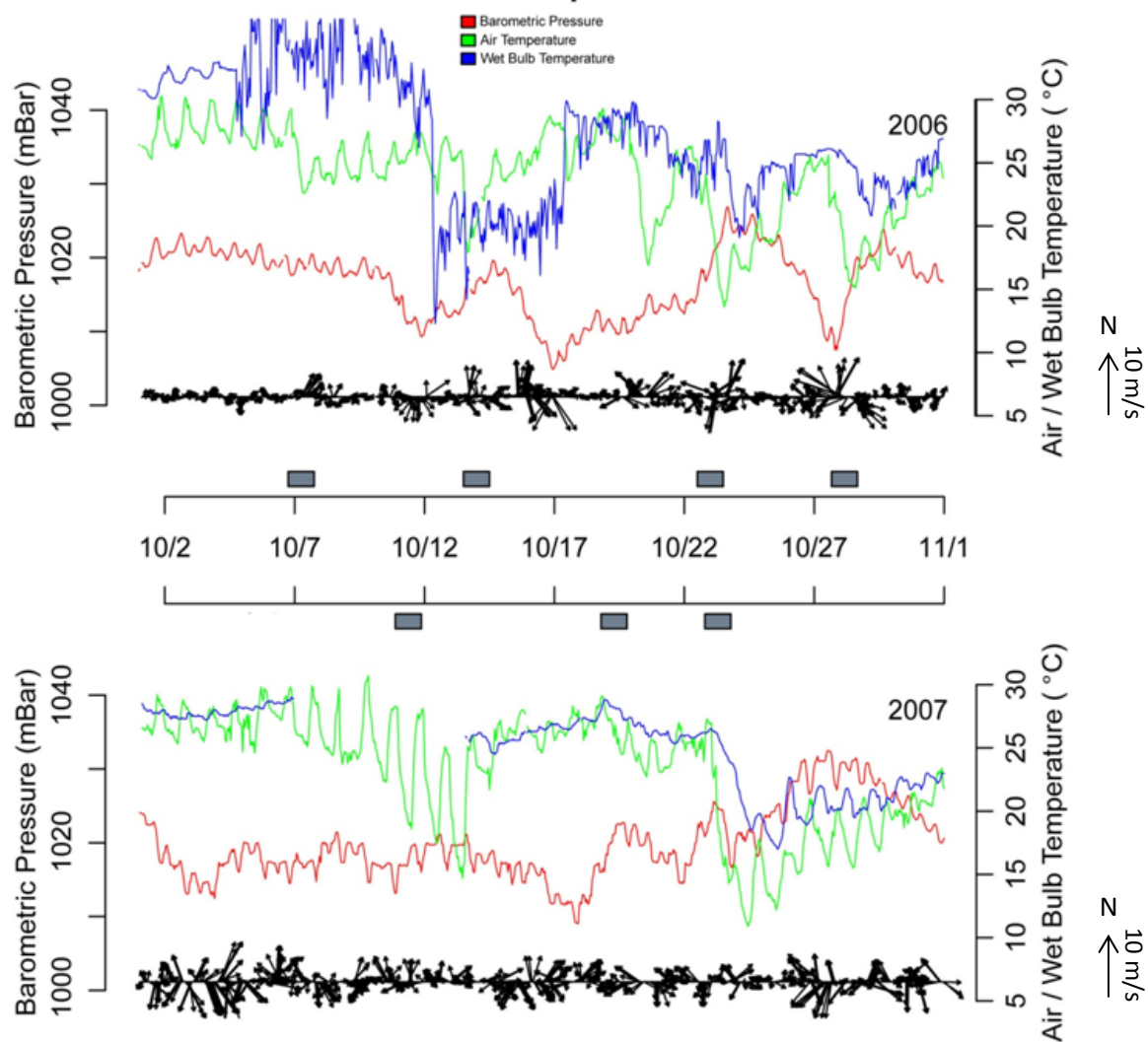
In conclusion, the effects of tides, atmospheric events, life history strategy affecting recruitment corridor length, and hydrologic differences in forcing based on distance to tidal pass edge, all provide insight into the mechanisms that aid and/or hinder recruitment of estuarine-dependent zoo-/ichthyoplankton that spawn offshore and require transport to estuarine nursery grounds. Concentration of larvae on the inner continental shelf off Louisiana in surface waters and the upper water column presents chances for interactions with impacts from the oil/gas industry that may further increase natural mortality. Winter cold front passages acting on the system may present both enhancement for recruitment during southerly winds and coastal setup on flood tides, and negatively impact successful retention during northerly wind enhanced ebb tides for estuarine-dependent species. However, net overall recruitment was clearly indicated by more larvae being collected on inflows versus outflows. The effect of the transition from the more oligotrophic inner continental shelf waters to more productive estuarine waters was evident in growth rates for larval *M. undulatus*. Growth increased upon entering the lower salinity waters of the coastal boundary layer and more productive and less saline estuarine waters, highlighting the importance of successful recruitment from offshore spawning ground into the estuary. Finally, growth rates for larval *B. patronus* showed what appears to be an opposite trend, but the maximum growth rate occurring just before metamorphosis and the ontogenetic shift in feeding

strategy at this time to take advantage of the more productive estuarine waters is likely resulting in the stepped growth relationship. Despite the vertically well-mixed nature of most estuaries in Louisiana including particular Bayou Tartellan, differences in flow velocity near the edges of tidal passes may present areas of reduced flow especially during ebb tides for larvae large enough to actively move laterally where they may encounter these areas, thereby aiding retention.

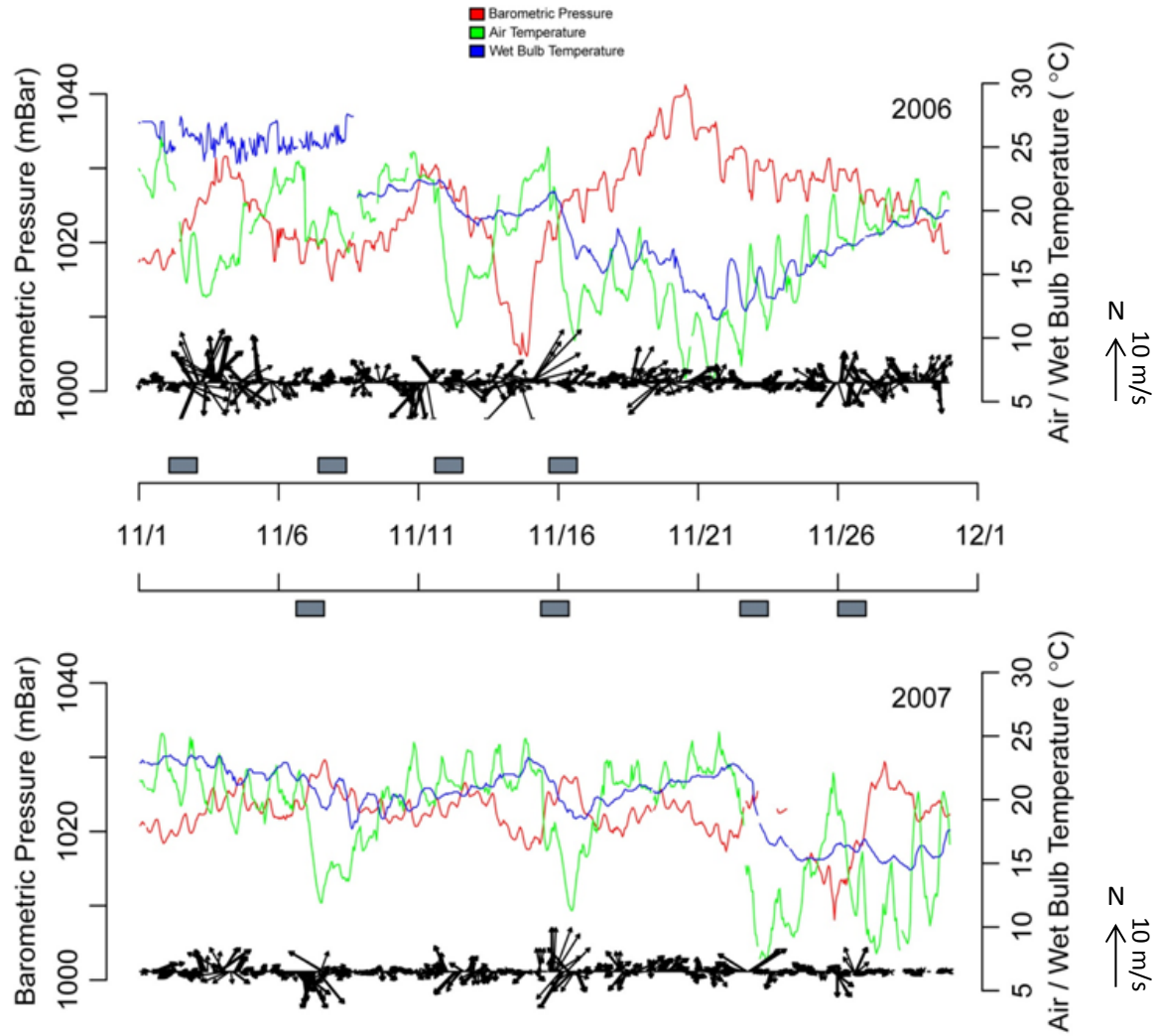
APPENDIX A: ATMOSPHERIC AND TIDAL CHARTS



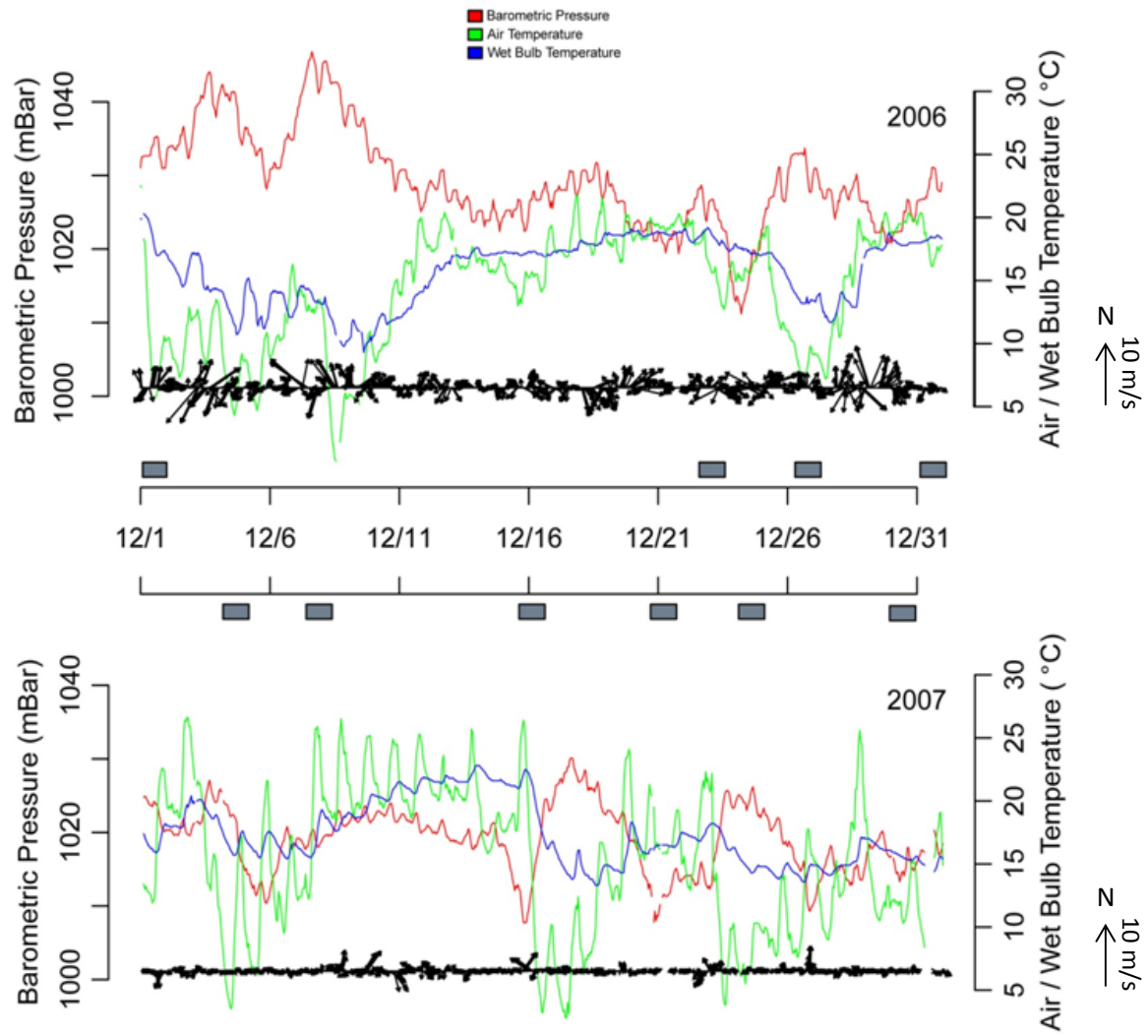
October Atmospheric Data



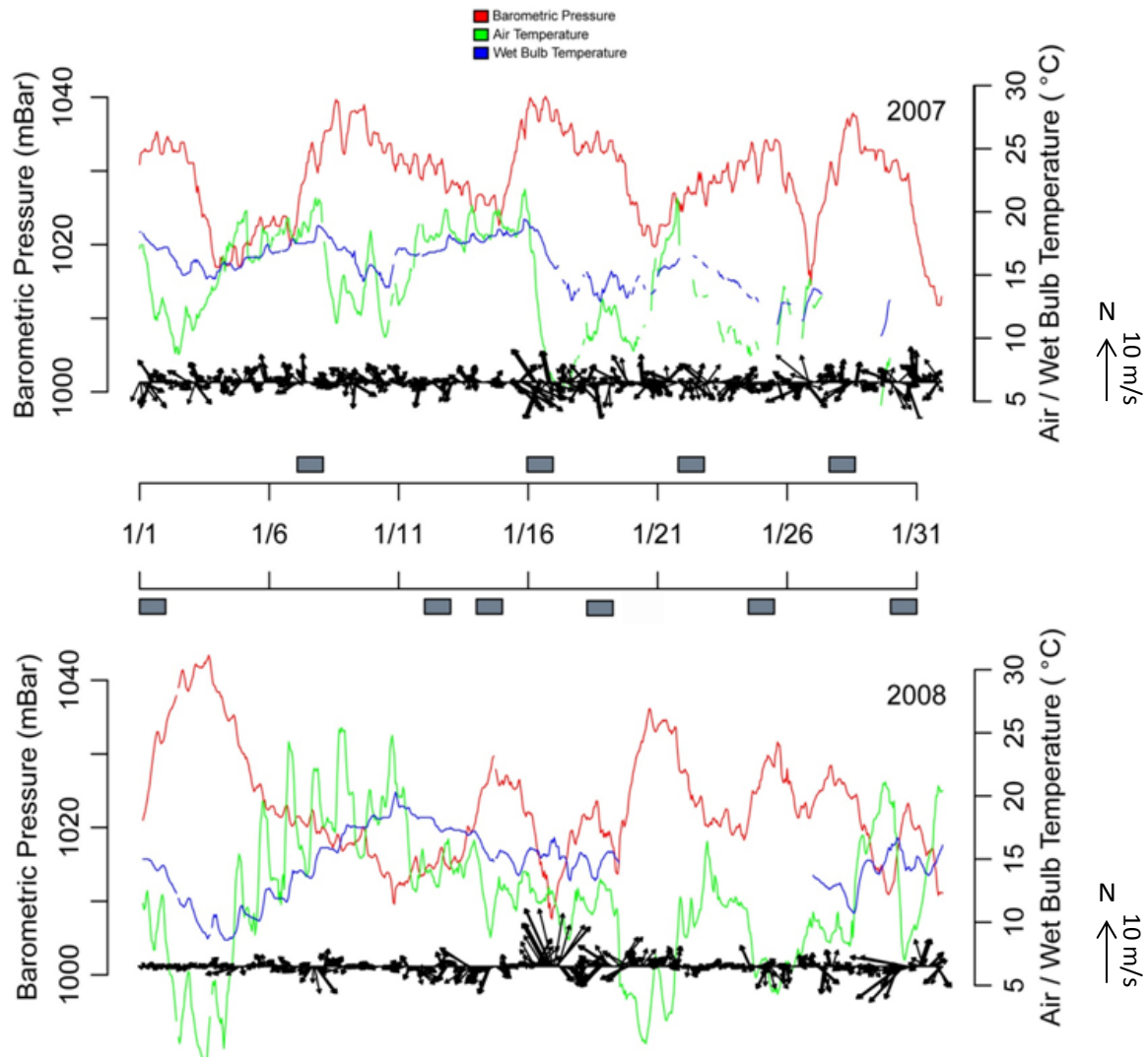
November Atmospheric Data



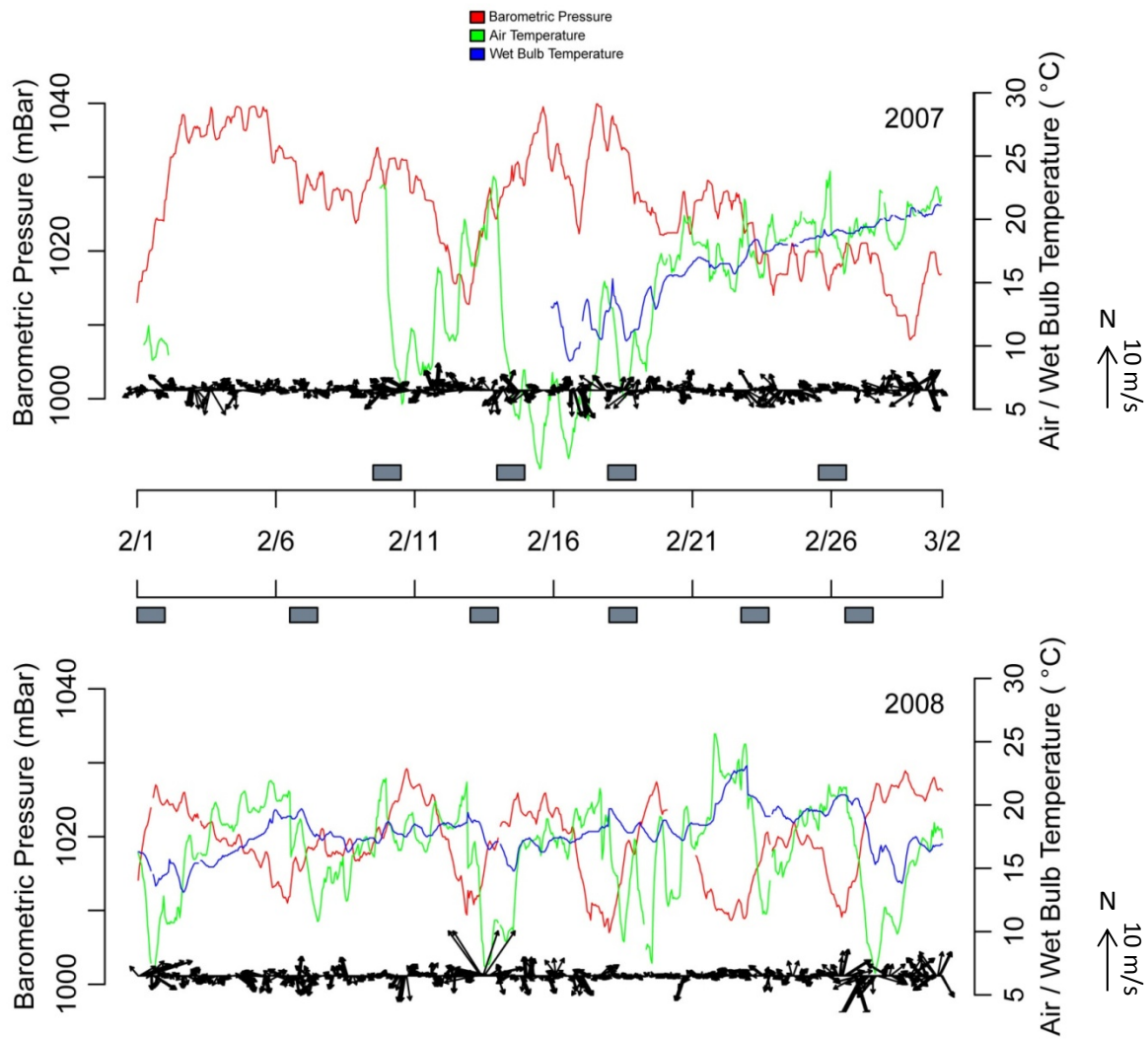
December Atmospheric Data



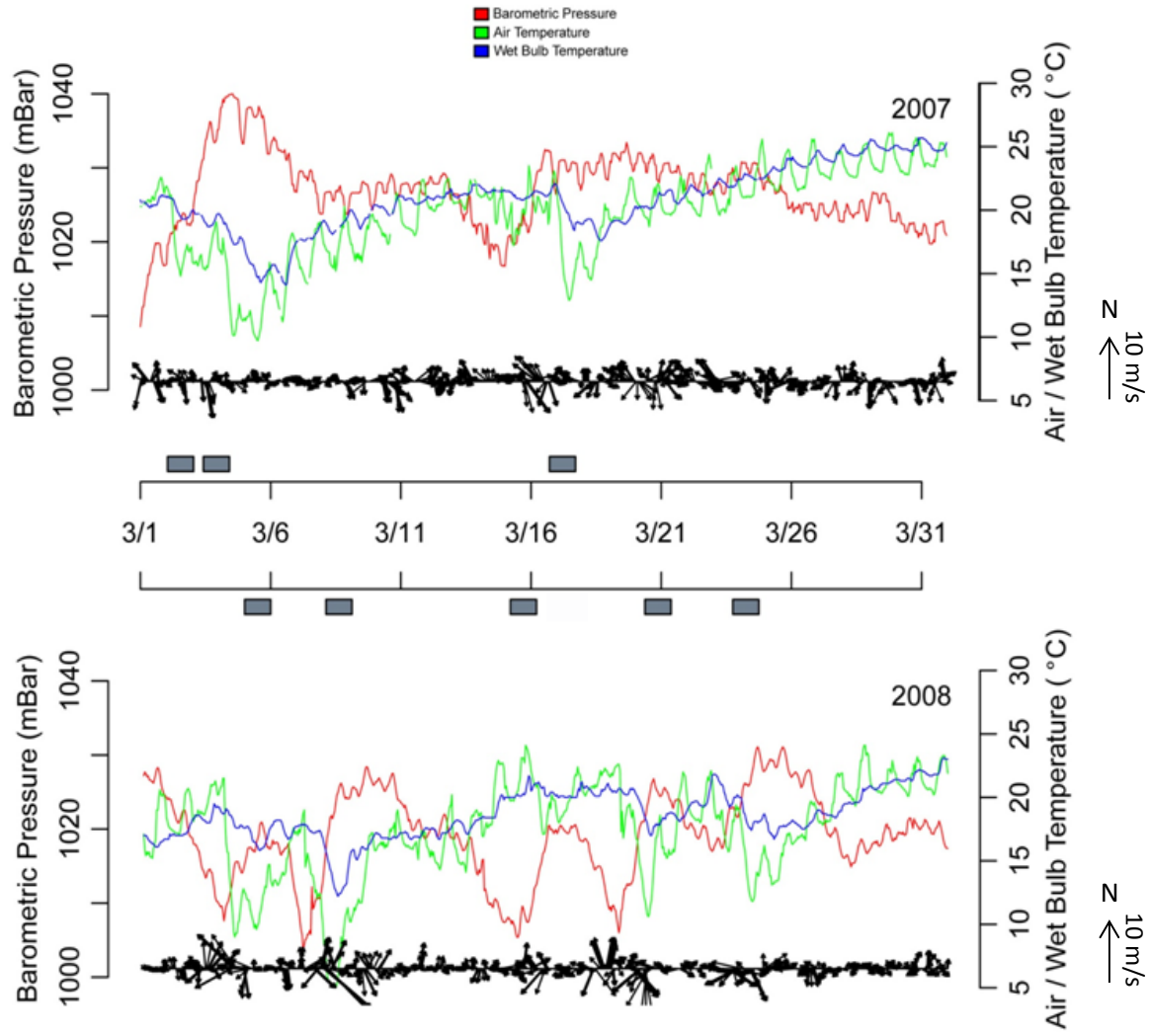
January Atmospheric Data



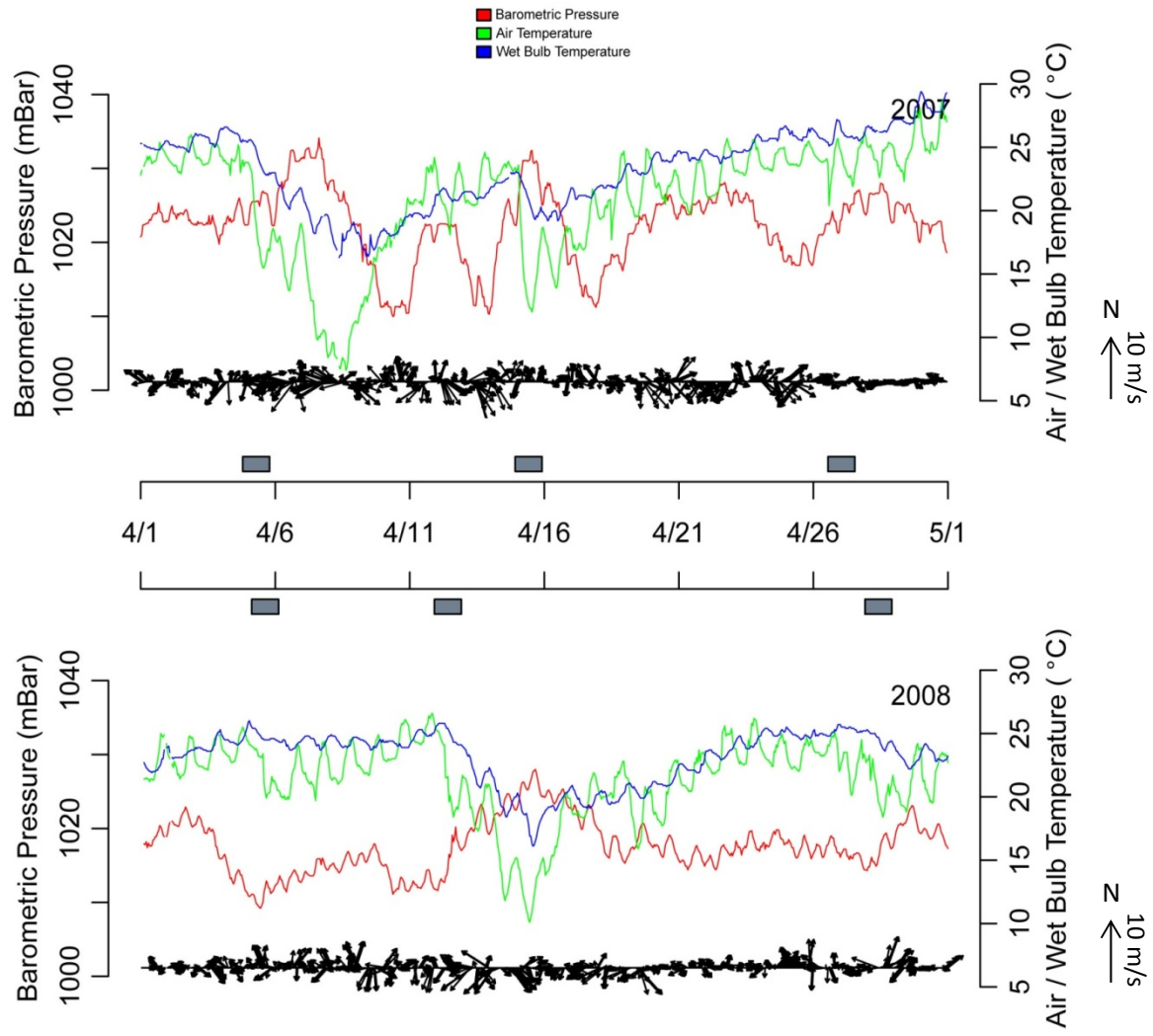
February Atmospheric Data



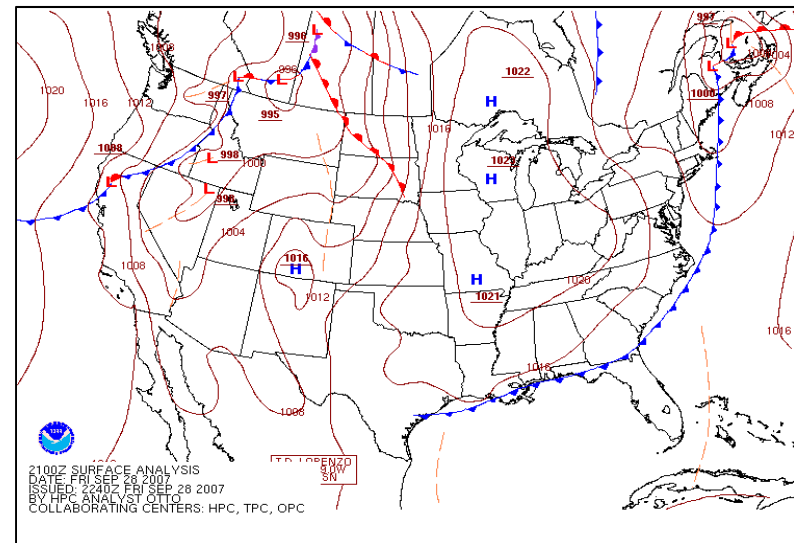
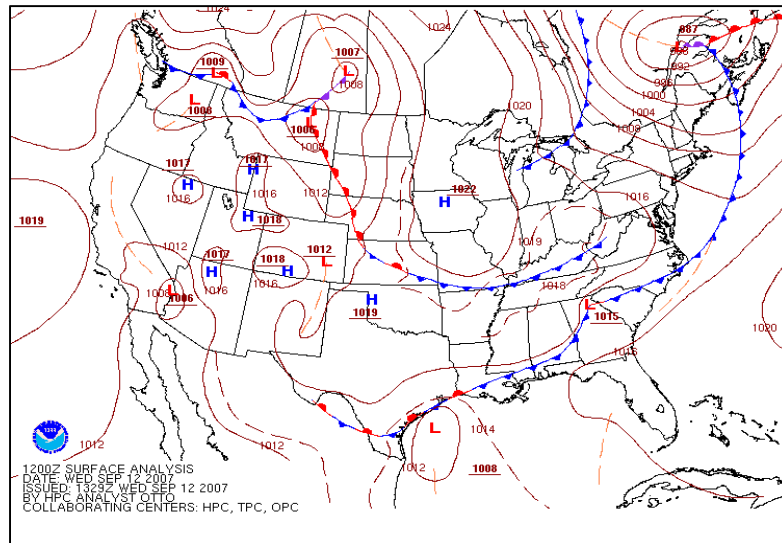
March Atmospheric Data

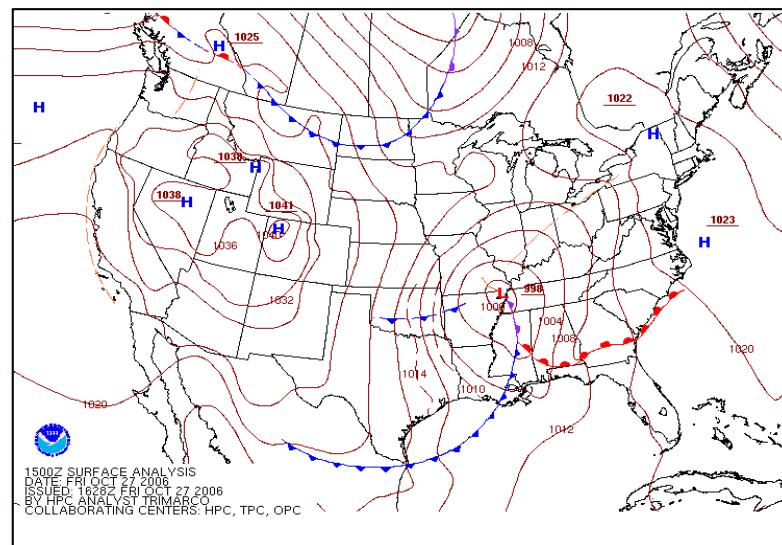
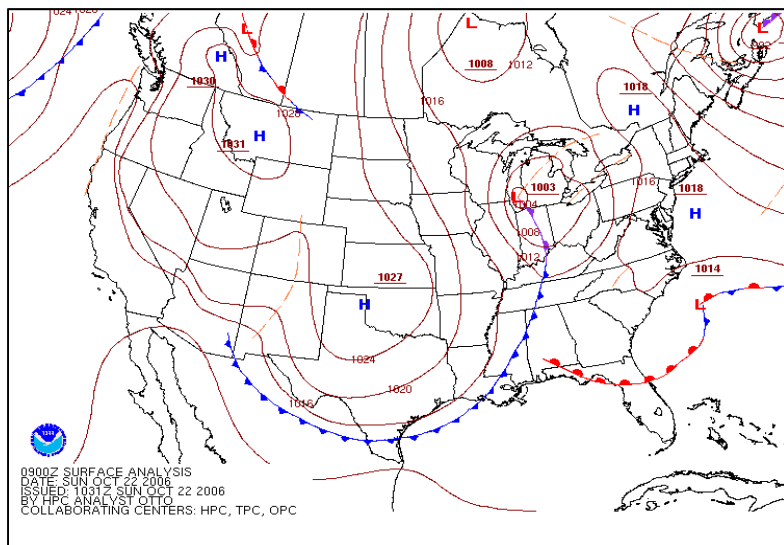
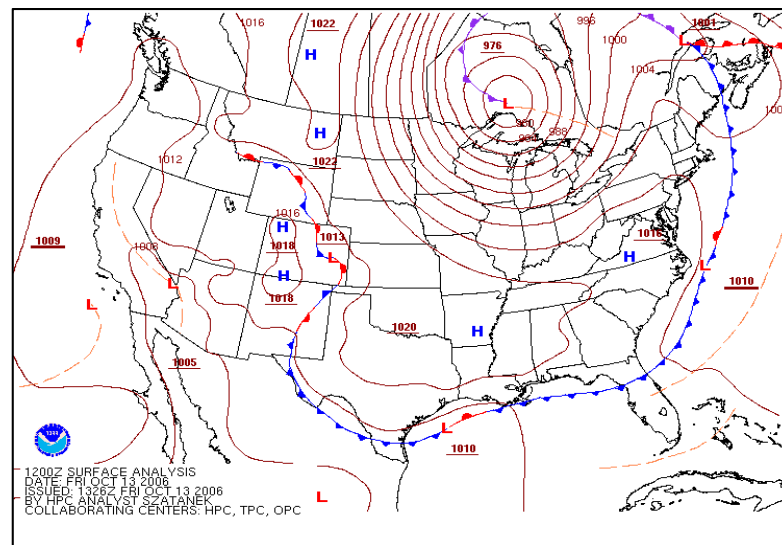
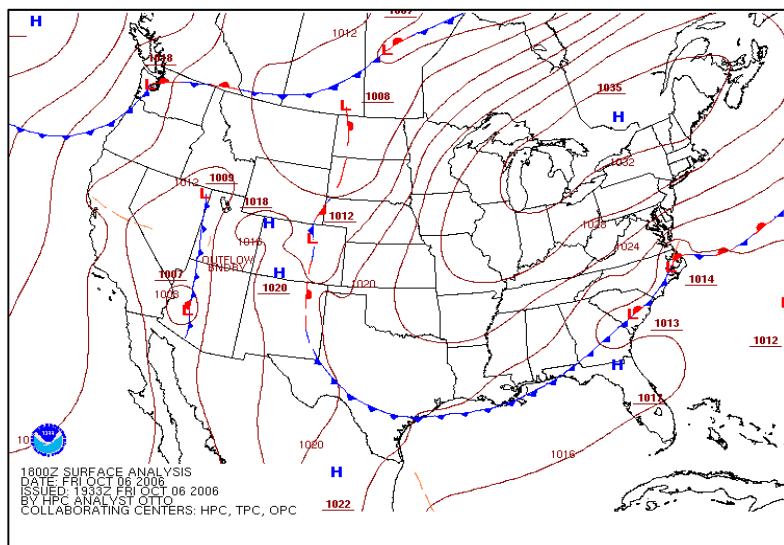


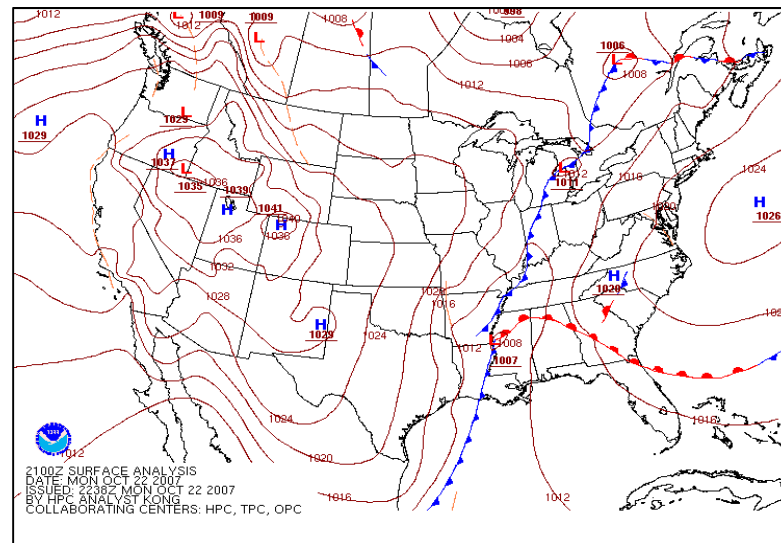
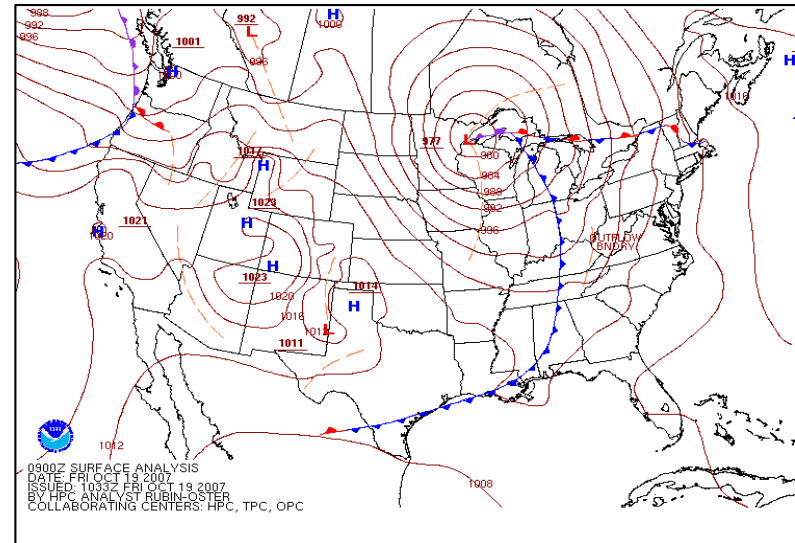
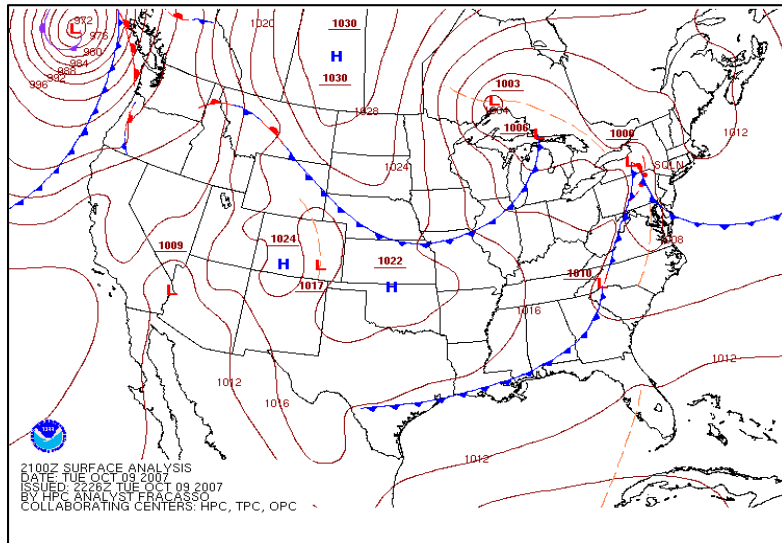
April Atmospheric Data

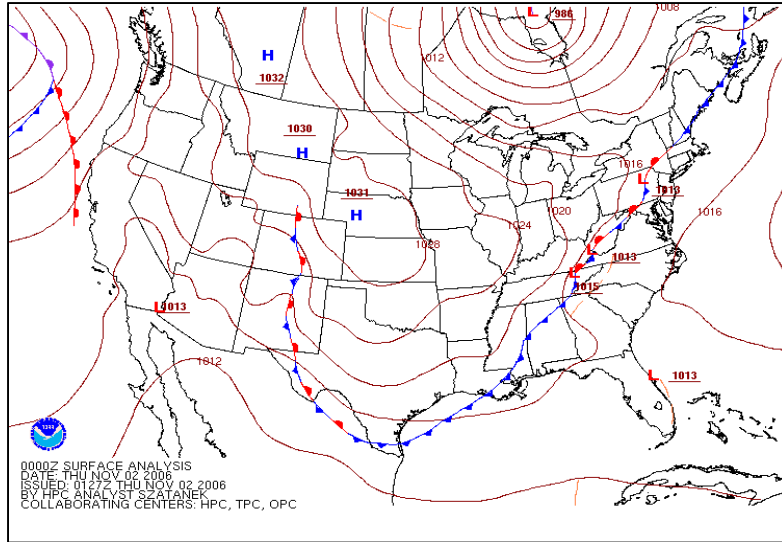


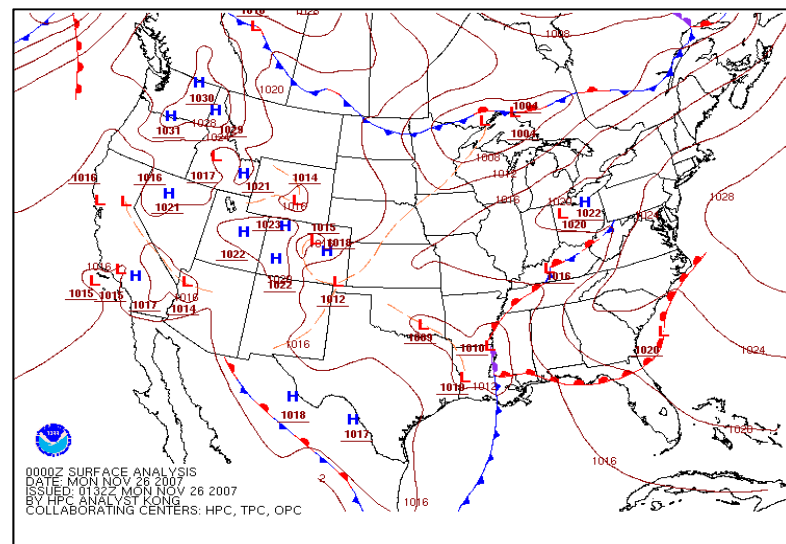
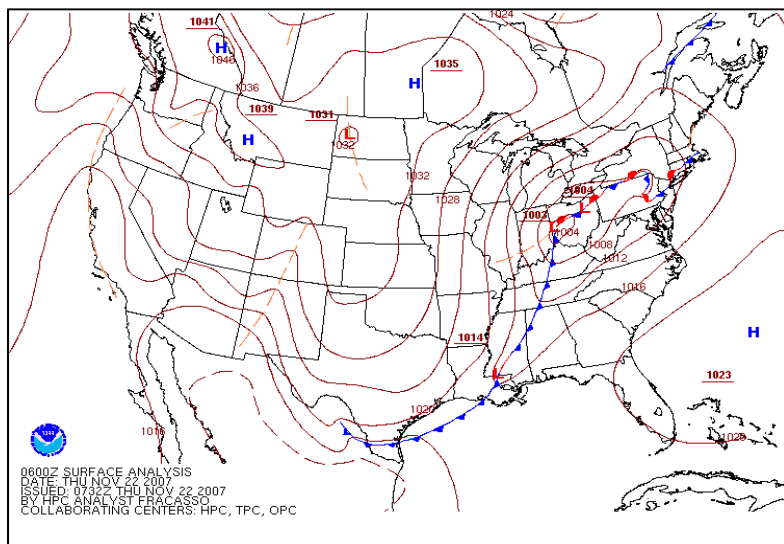
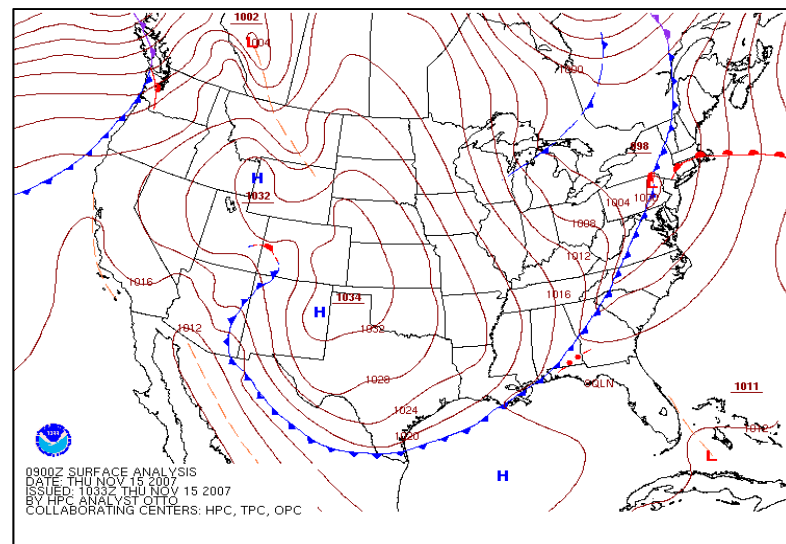
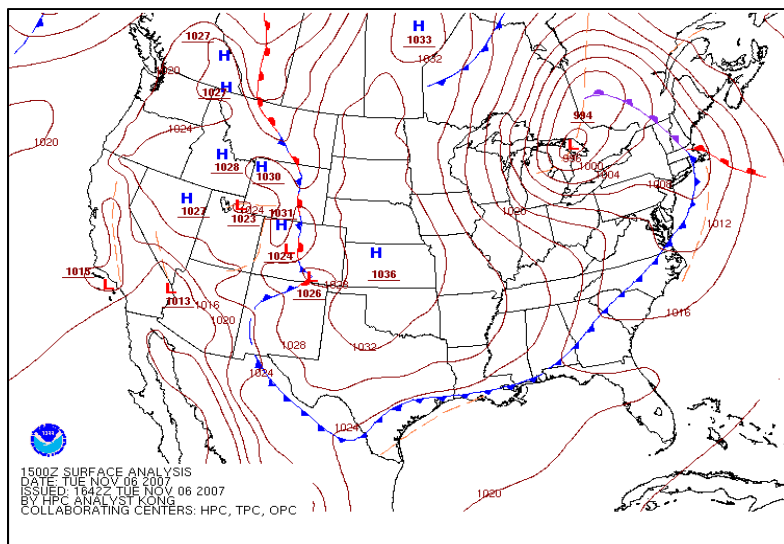
APPENDIX B: WEATHER MAPS FOR COLD FRONTS

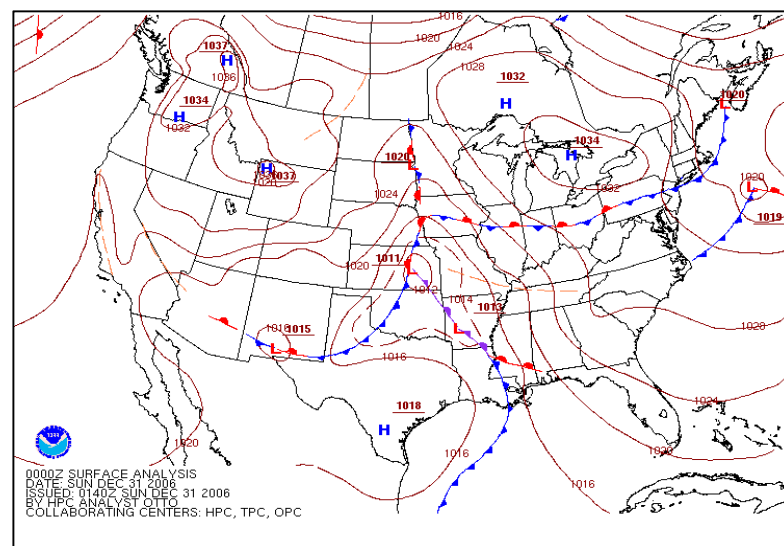
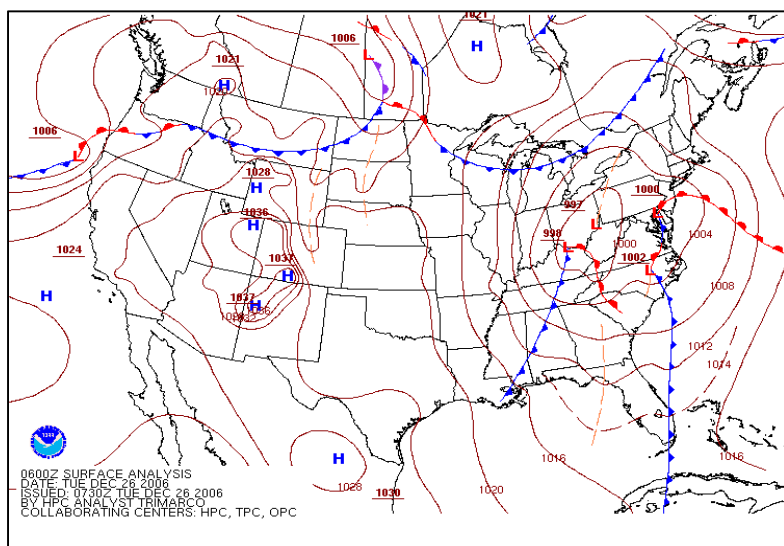
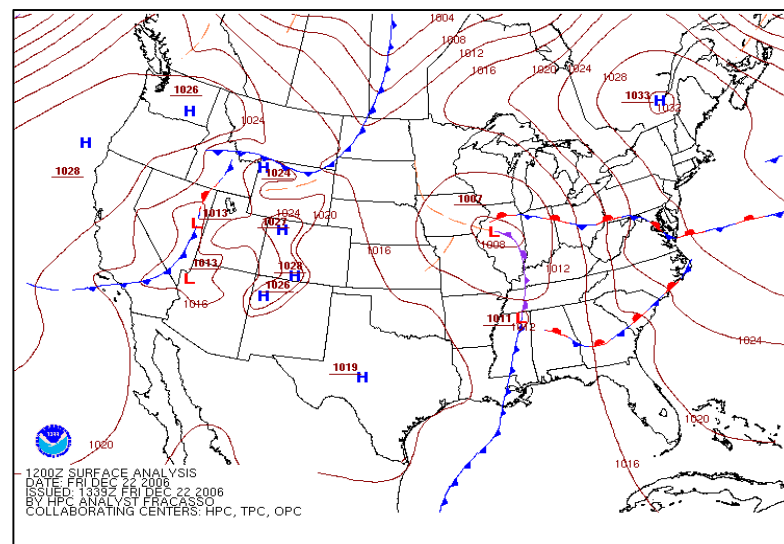
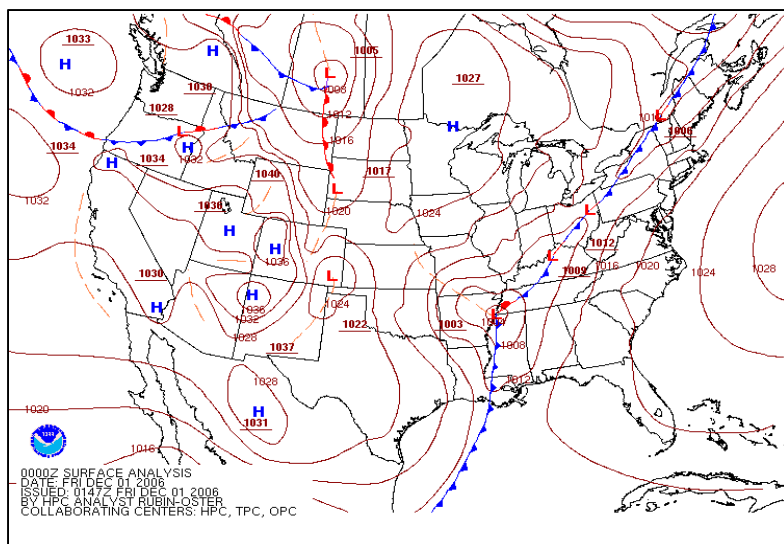


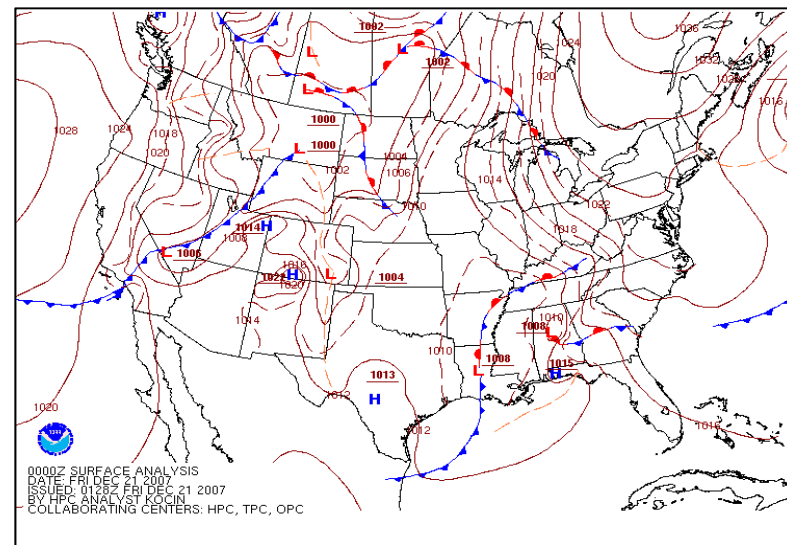
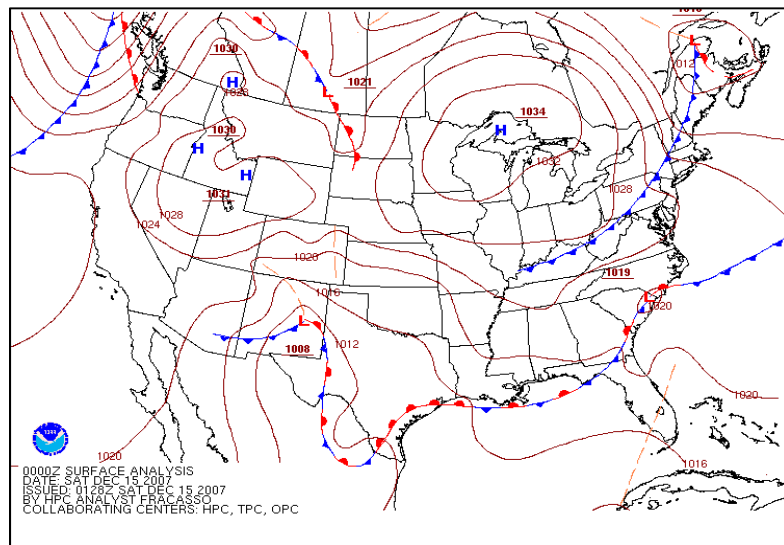
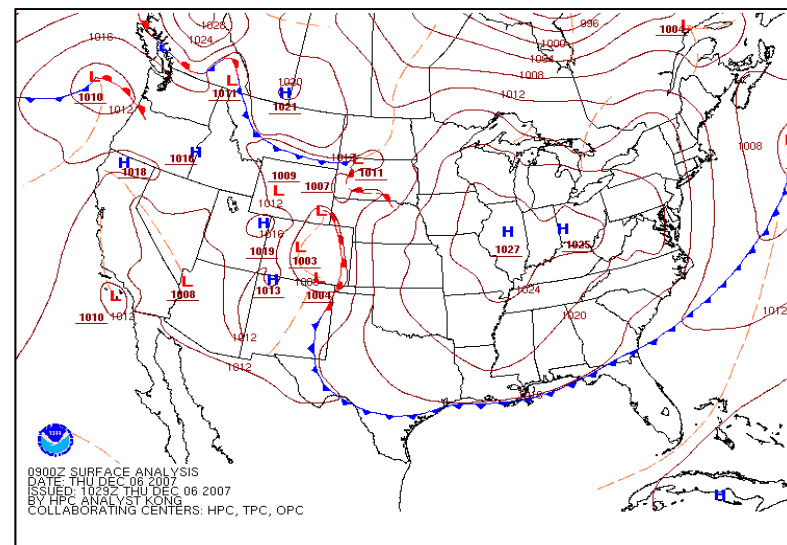
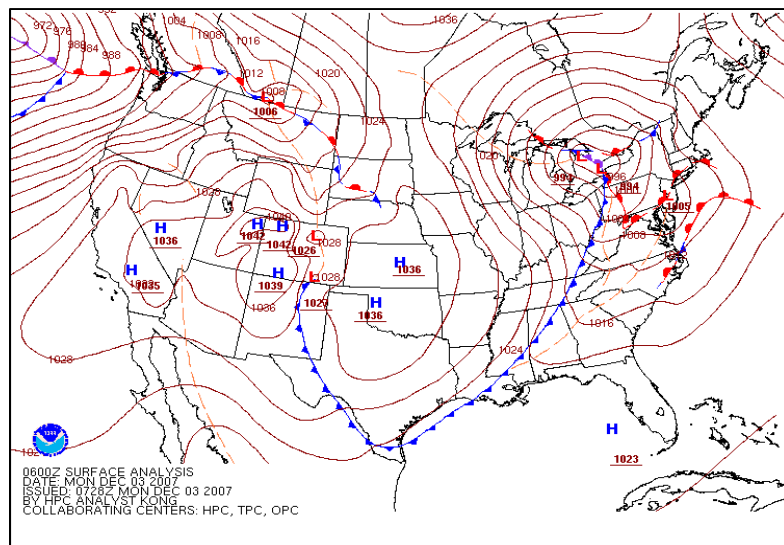


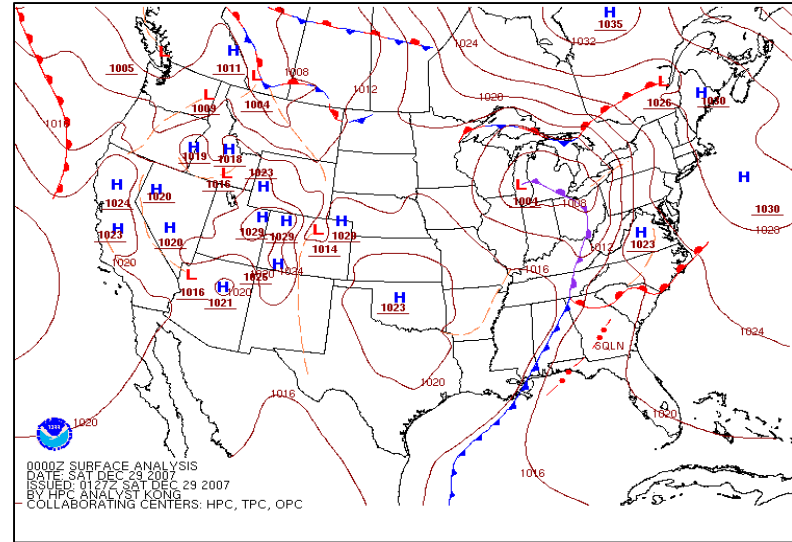
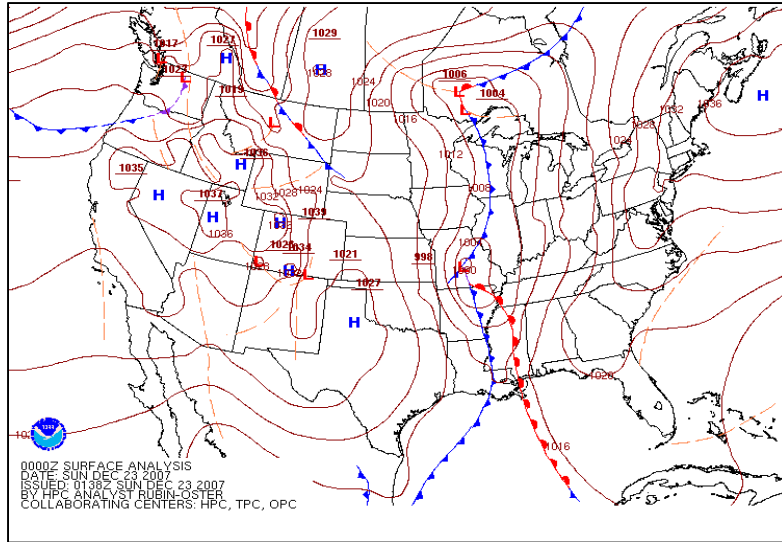


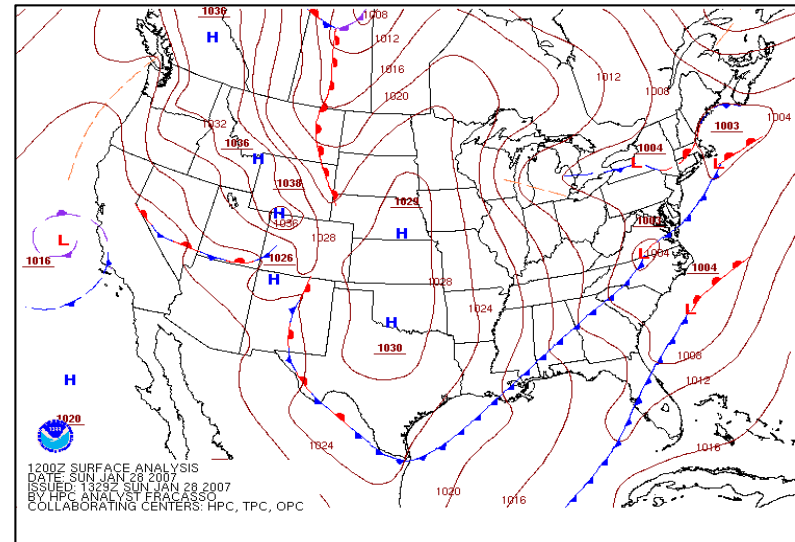
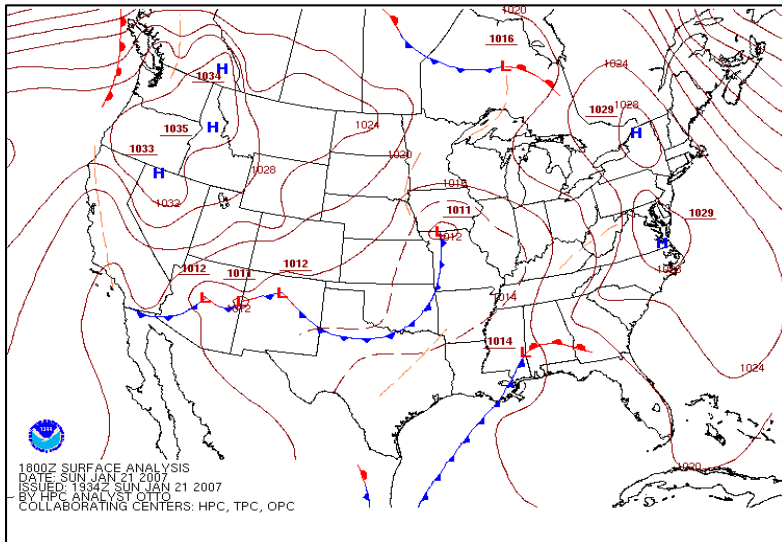
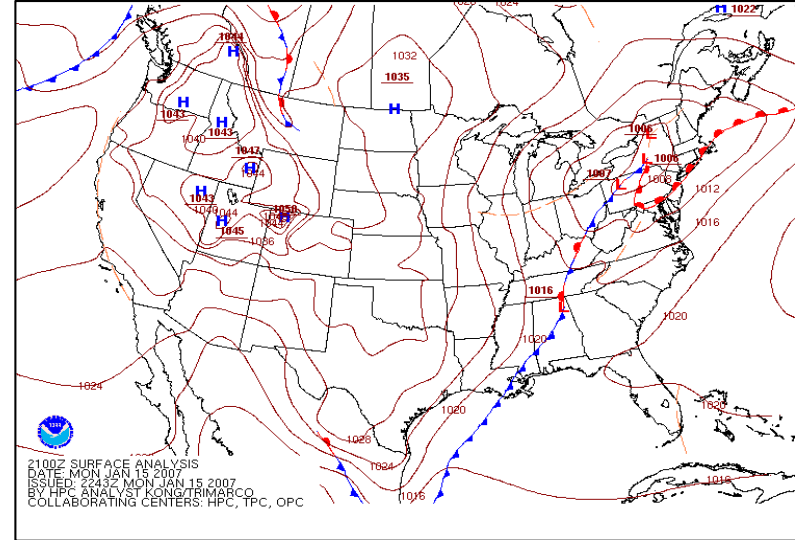
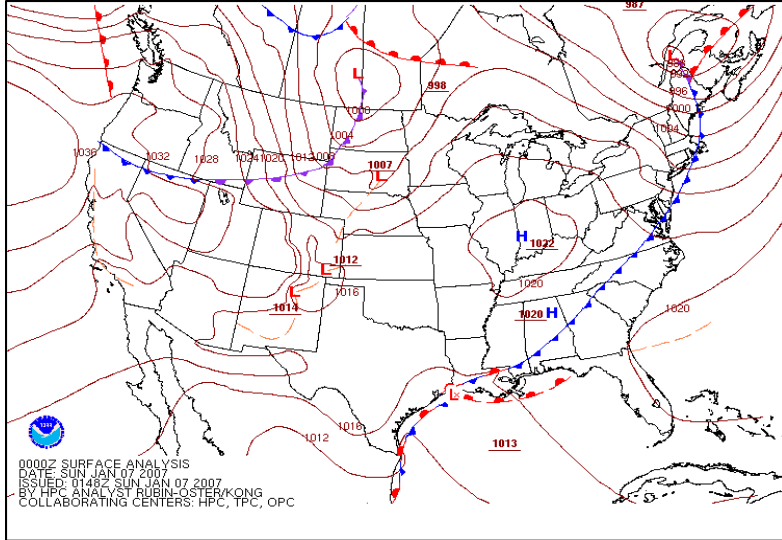


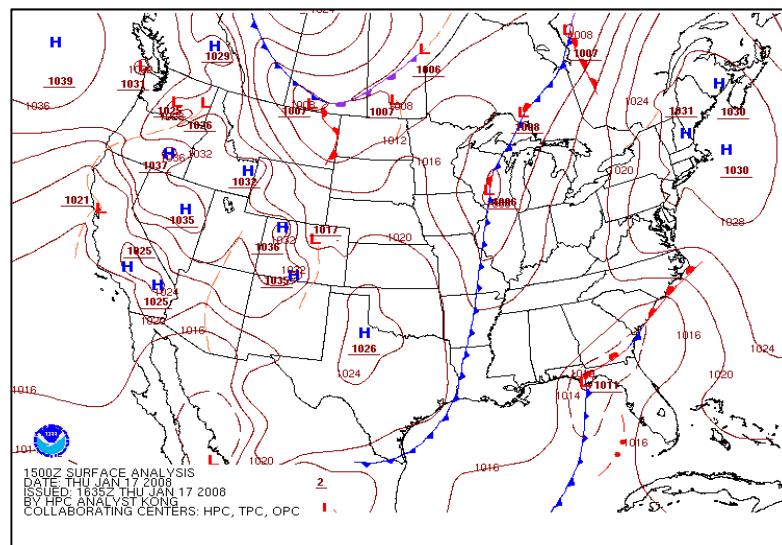
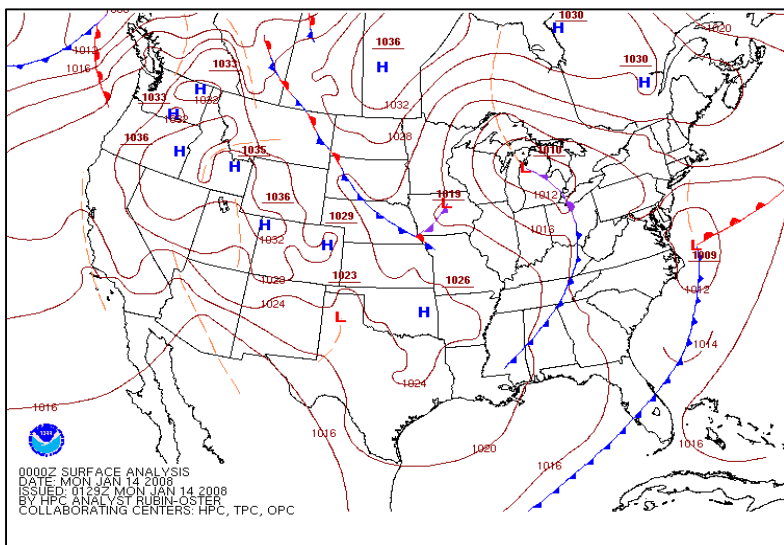
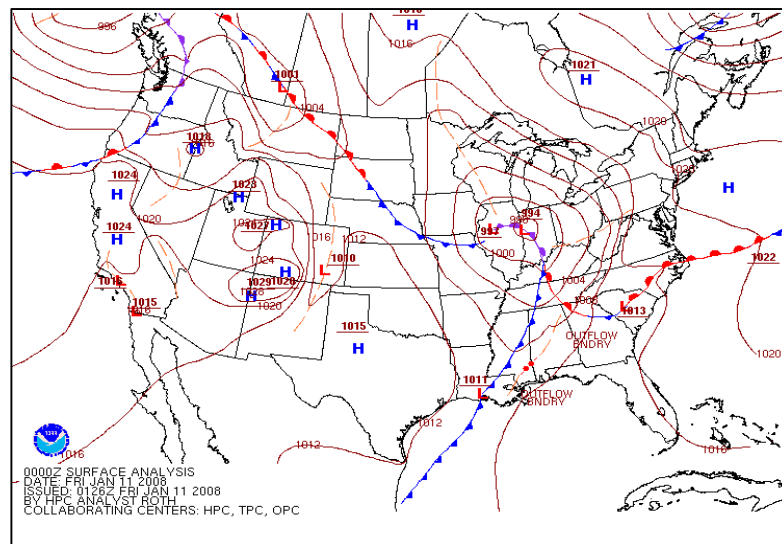
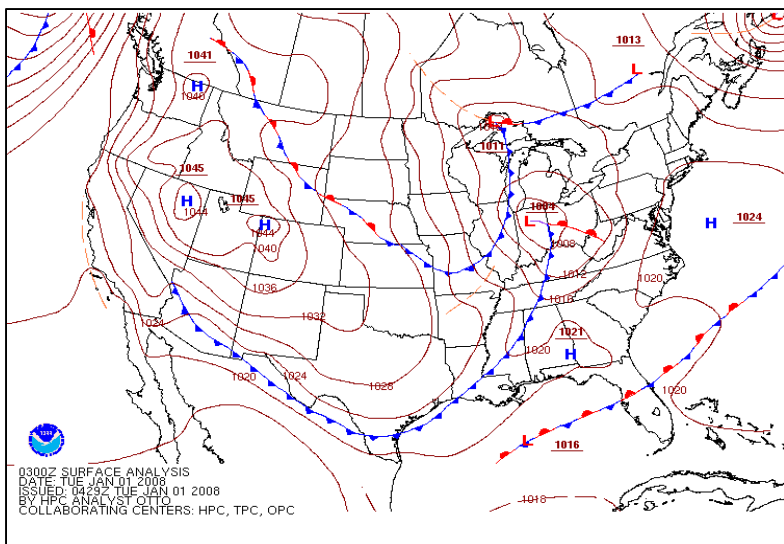


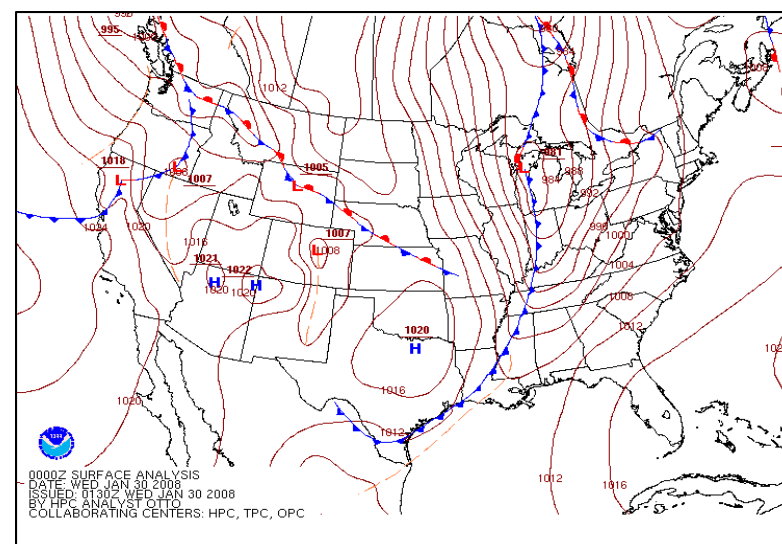
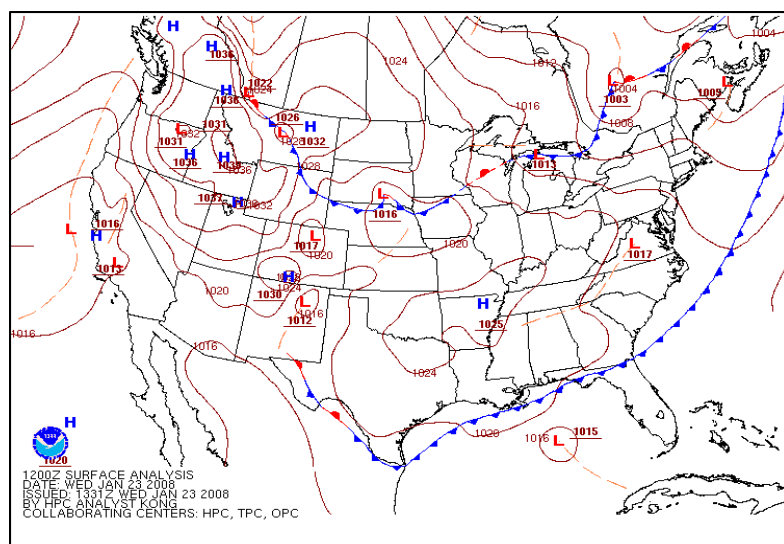


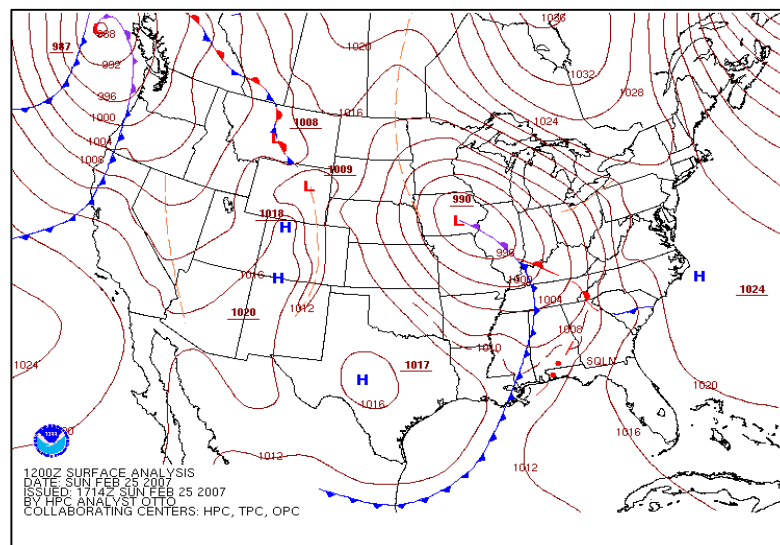
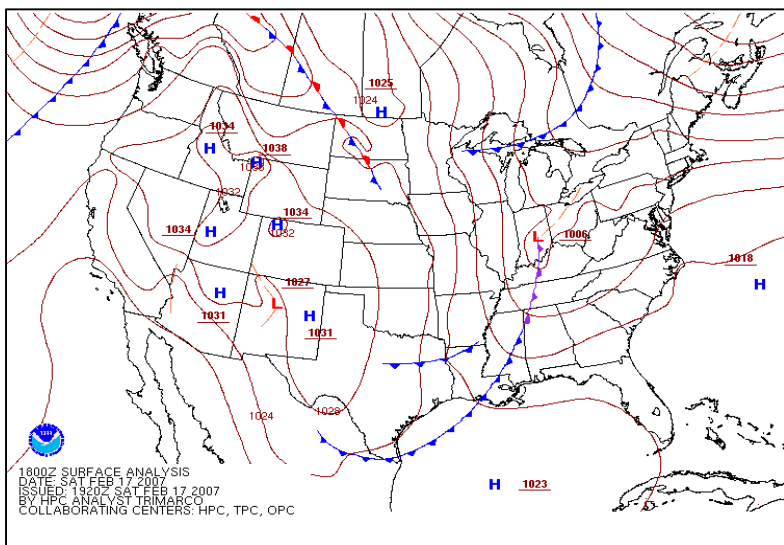
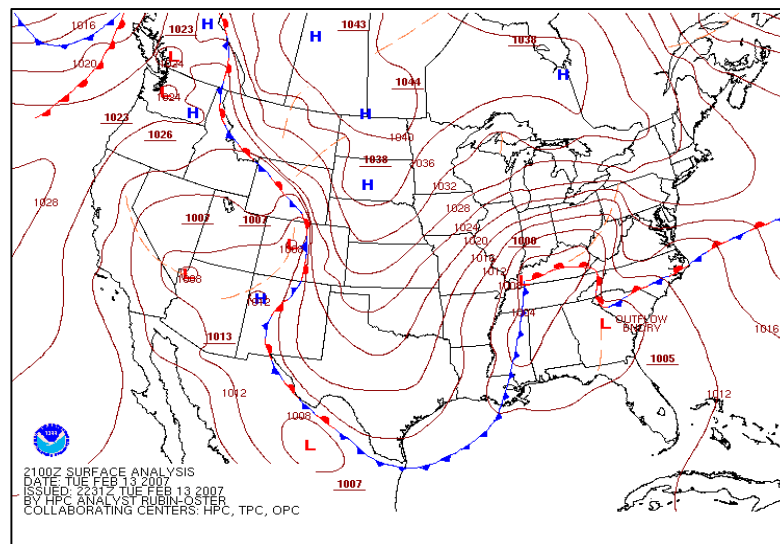
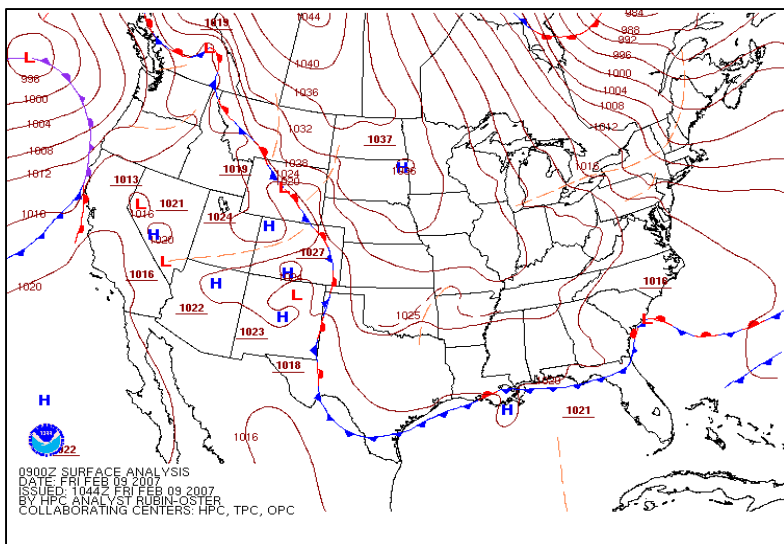


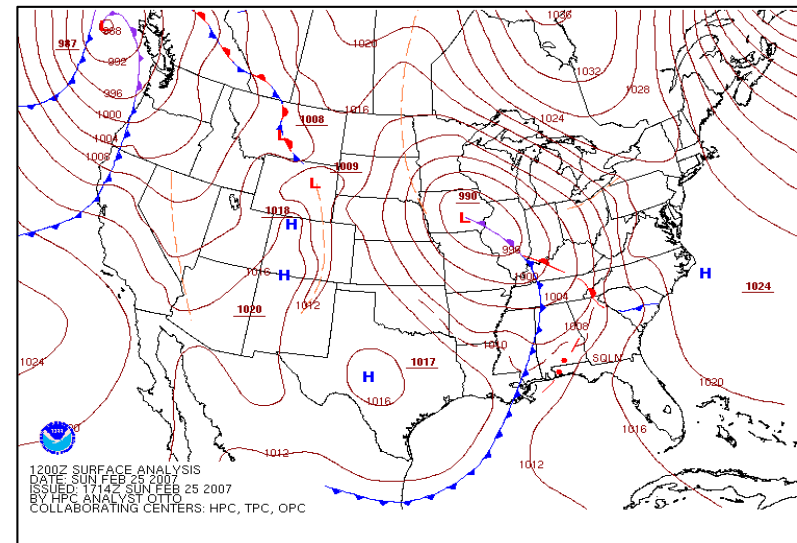
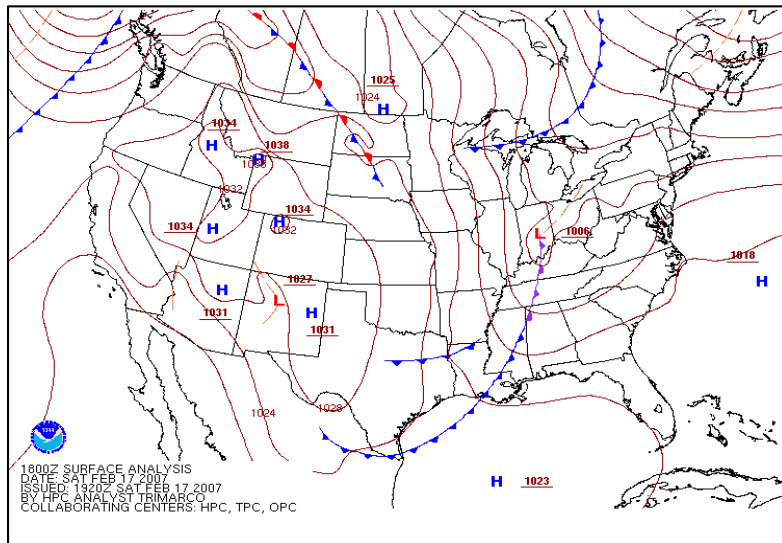
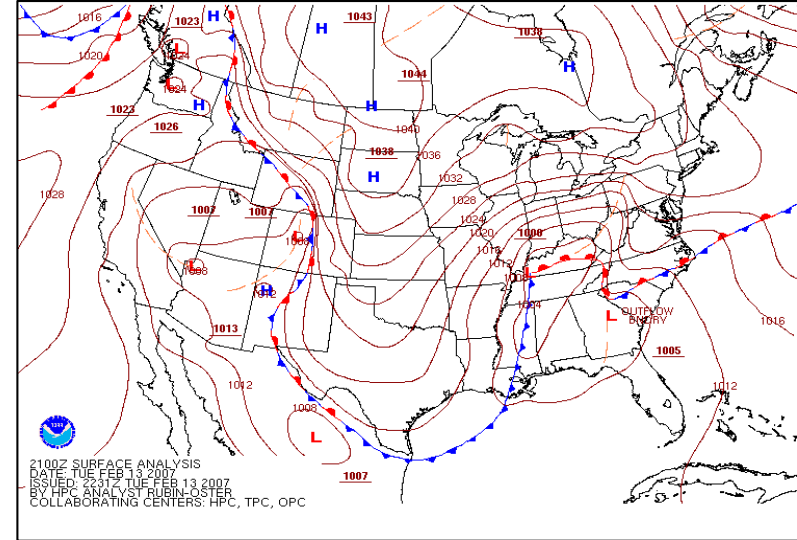
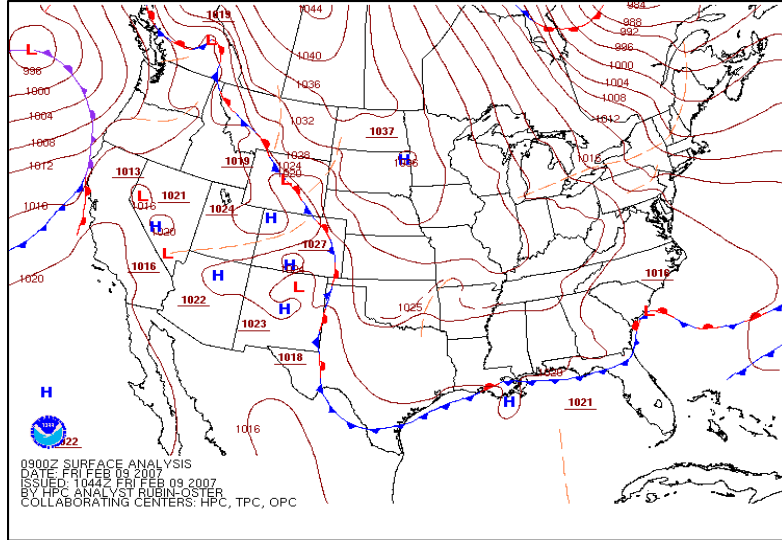


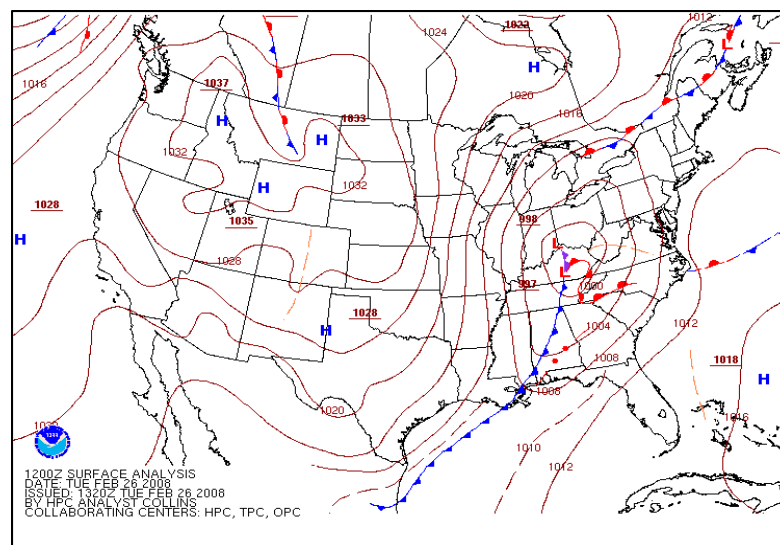
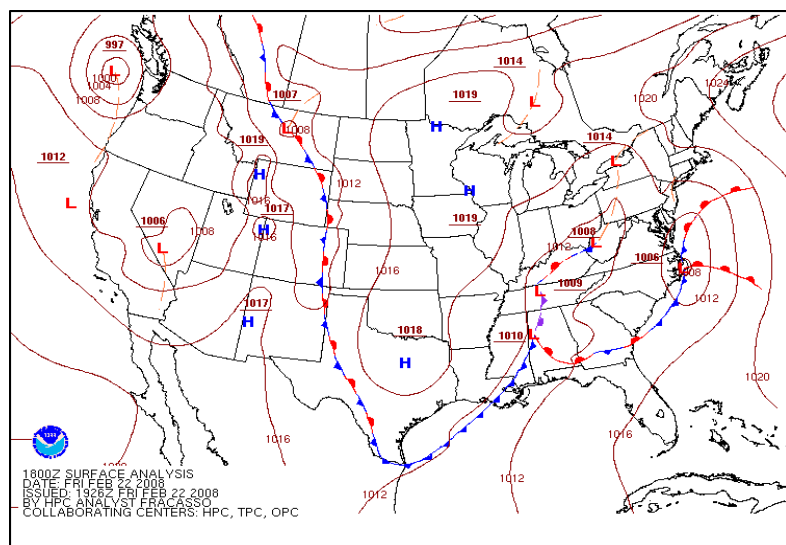


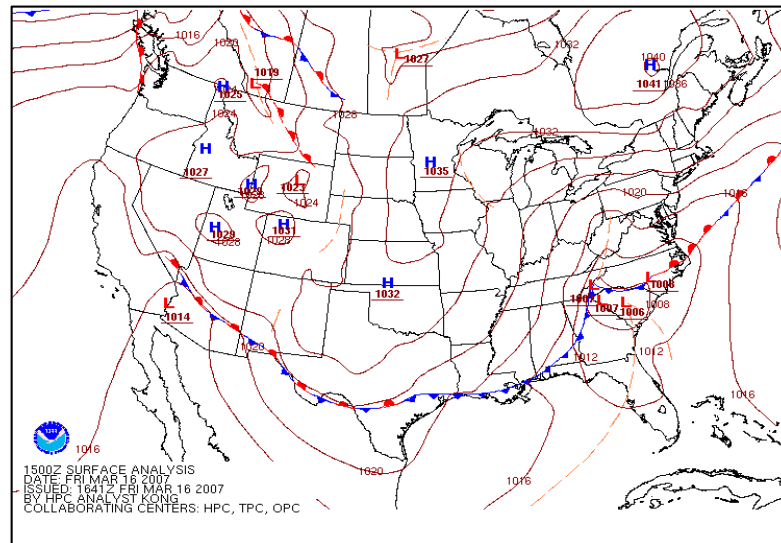
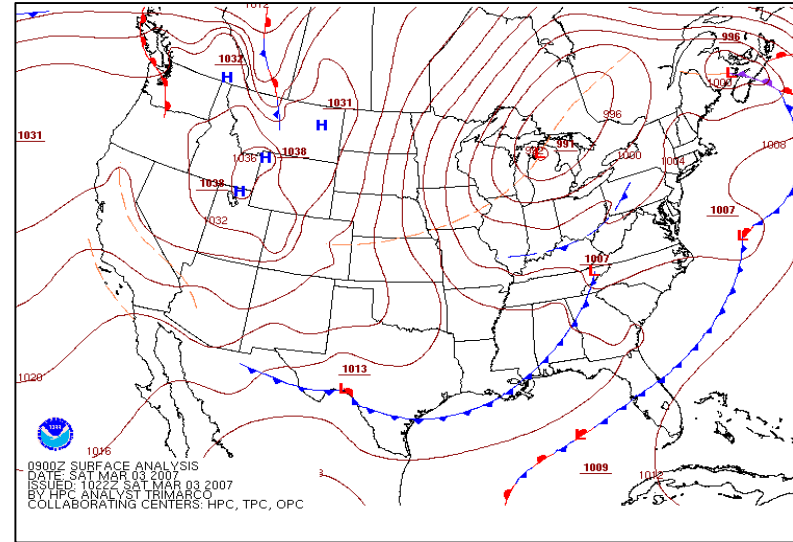
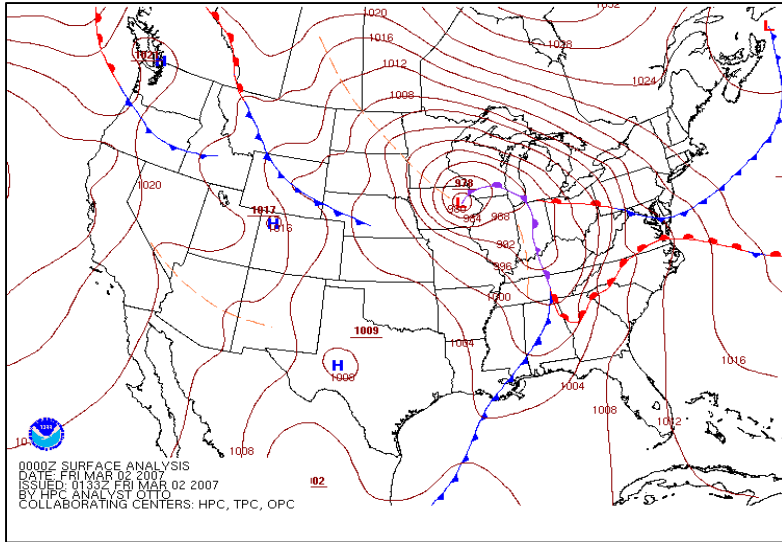


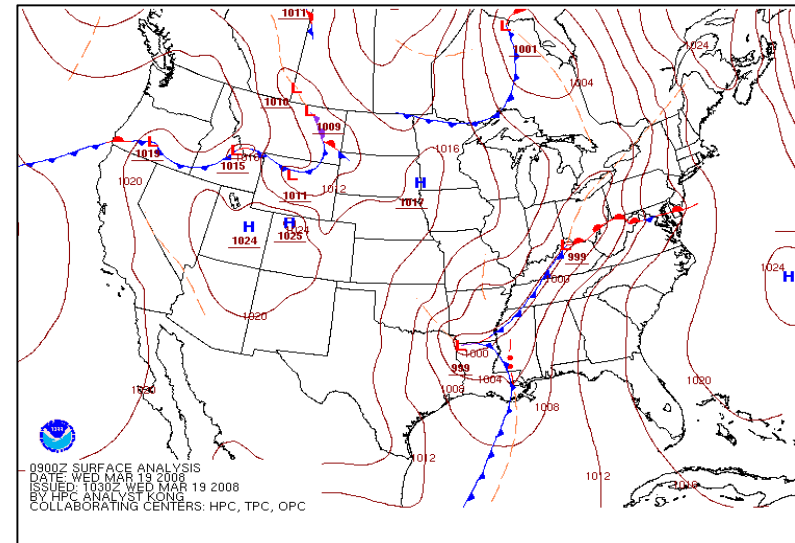
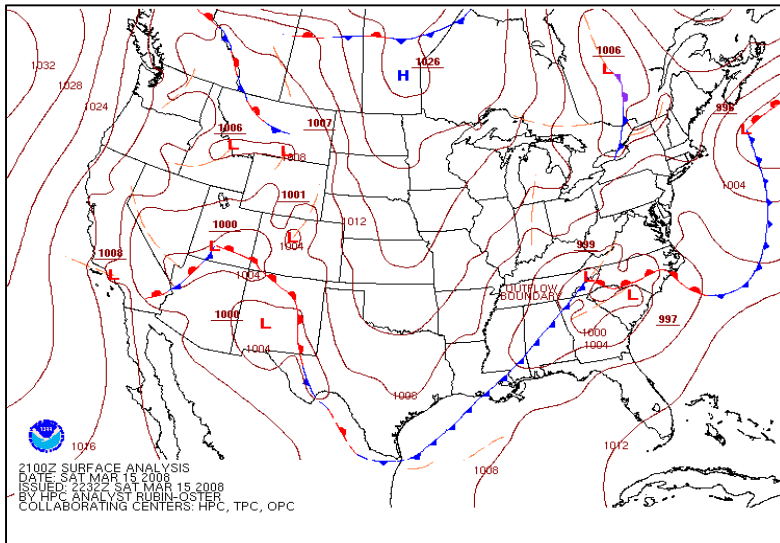
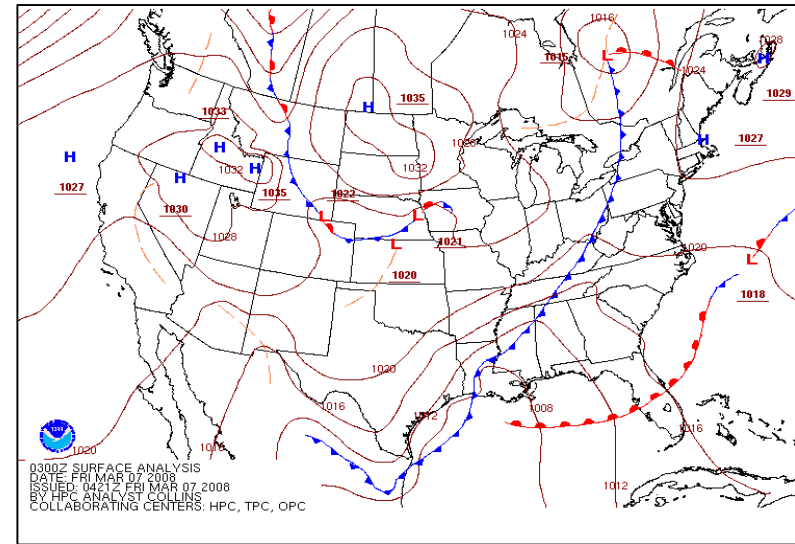
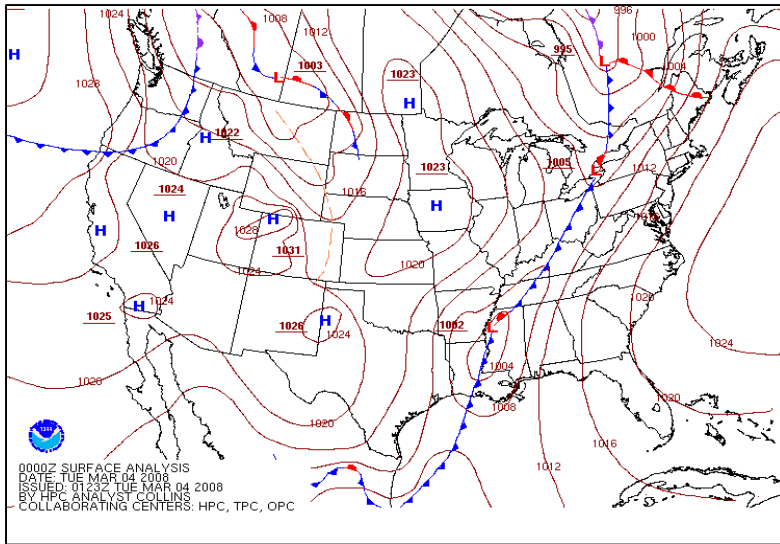


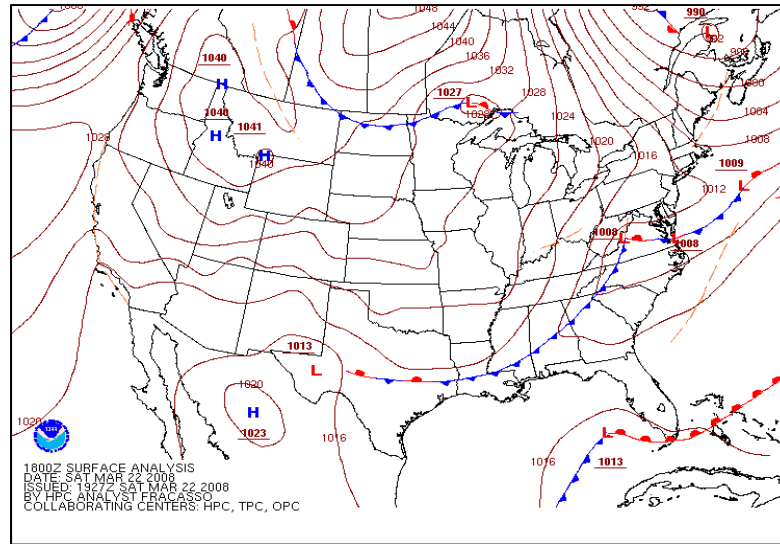


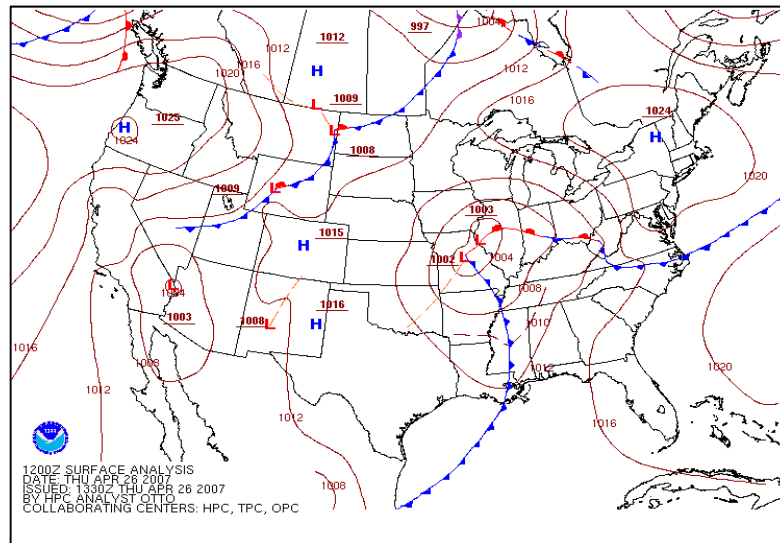
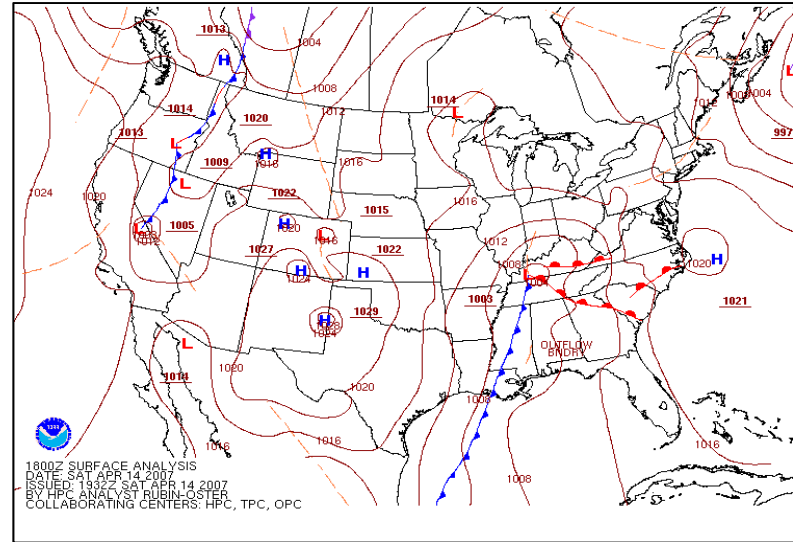
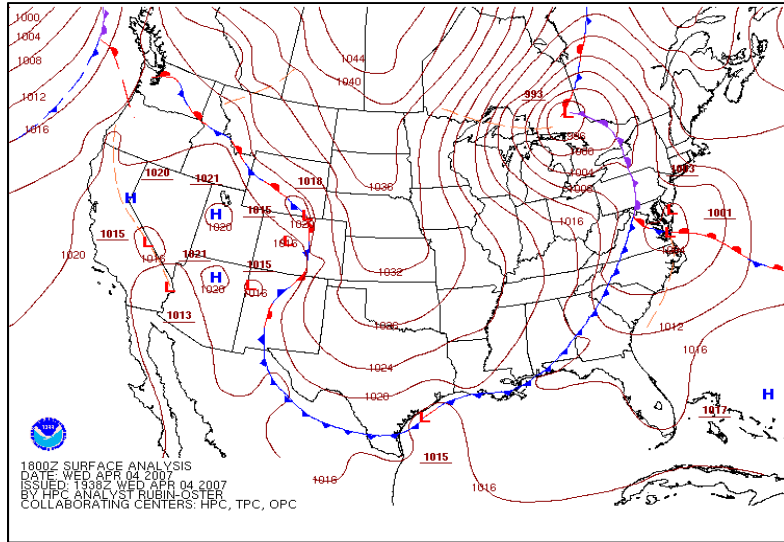


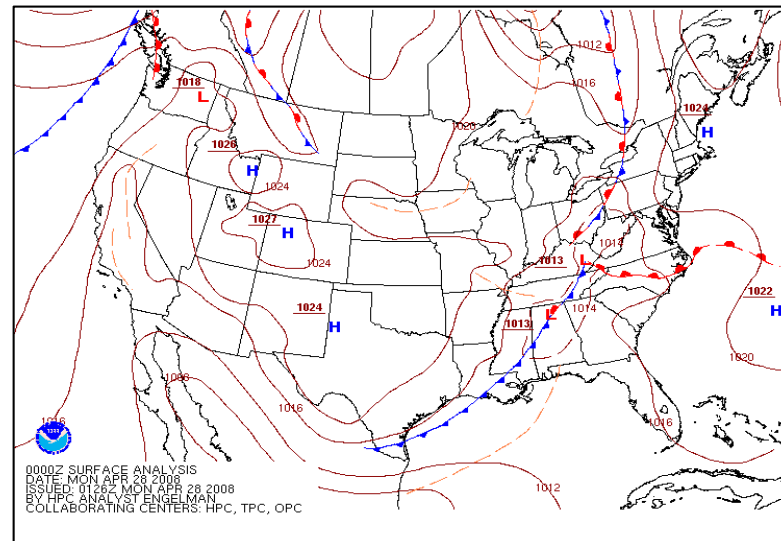
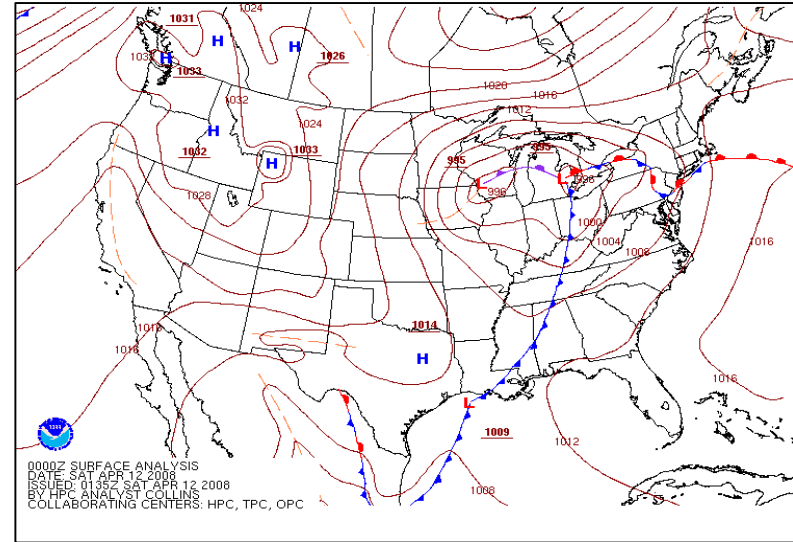
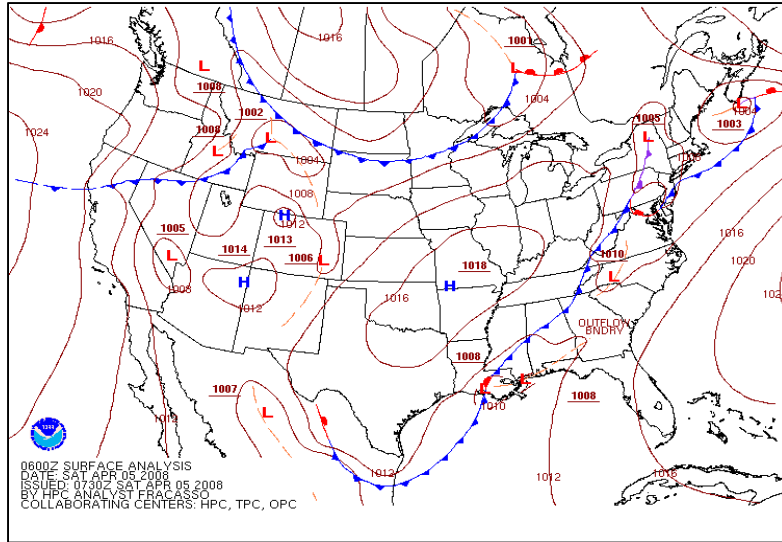












APPENDIX C: DERIVATION OF THE ZERO INFLATED NEGATIVE BINOMIAL

- ❖ Considering a random variable that is discrete (X), which has a maximum that is countable
 - This random variable has a general pmf:

$$P[X = x_i | \theta] = g(x_i, \theta), \quad \text{where } \theta \in \Omega \cup R^S$$

- For the negative binomial distribution that pmf is:

$$g(x, \theta, \beta) = \frac{N\Gamma(N + \beta x)(\theta(1 - \theta)^{\beta-1})^x}{x! \Gamma(N + \beta x - x + 1)(1 - \theta)^{-N}}, \quad x = 0, 1, 2, 3, \dots$$

$$\text{where } 0 < \theta < 1, |\theta\beta| < 1, \beta = 0 \text{ or } \beta \geq 1, \text{ and } N > 0$$

- Define new random variables with the following pmf:

$$f(x, \theta, p) = \begin{cases} (1 - p) + pg(0, \theta), & x = 0 \\ pg(x, \theta), & x = 1, 2, 3, \dots \end{cases} \quad \text{where } 0 < p < 1, \theta \in \Omega$$

- Let (x_1, x_2, \dots, x_n) be a random sample of size n from the pmf of the newly defined random variables. The likelihood function is then determined as:

$$L(\theta, p; \underline{x}) = [(1 - p) + pg(0, \theta)]^{n_0} p^{n-n_0} \prod_{x_i \neq 0} g(x_i, \theta)$$

- The maximum likelihood equations for the estimation of p and θ :

$$\frac{n_0(-1 + g(0, \theta))}{(1 - p) + pg(0, \theta)} + \frac{n - n_0}{p} = 0$$

$$\frac{n_0 p \frac{\partial}{\partial \theta} g(0, \theta)}{(1 - p) + pg(0, \theta)} + \sum_{x_i \neq 0} \frac{\partial}{\partial \theta} \log g(x_i, \theta) = 0$$

- The result of these two equations becomes:

$$\frac{(n - n_0) \frac{\partial}{\partial \theta} g(0, \theta)}{1 - g(0, \theta)} + \sum_{x_i \neq 0} \frac{\partial}{\partial \theta} \log g(x_i, \theta) = 0$$

VITA

Matthew John Kupchik, originally from Berlin, New Jersey, received his bachelor's degree of science in marine science at the Richard Stockton College of New Jersey in December 2004. Following graduation, Matthew worked for ENVIS-One, an environmental consulting firm, before matriculating at Louisiana State University in the fall of 2005. Matthew has had a love of the marine realm since he was a young boy, and knew that his heart was in research of the ocean. Matthew will receive his doctoral degree from the Department of Oceanography and Coastal Sciences at Louisiana State University in May 2014, as well as a master's degree in applied statistics from the Department of Experimental Statistics at Louisiana State University. He will begin work as a postdoc with the Gulf Serpent Project at LSU and has applied for several fellowships.